Vitaly Gurylev

Nanostructured Photocatalyst via Defect Engineering

Basic Knowledge and Recent Advances

Springer

Nanostructured Photocatalyst via Defect Engineering

Vitaly Gurylev

Nanostructured Photocatalyst via Defect Engineering

Basic Knowledge and Recent Advances

Springer

Vitaly Gurylev
National Synchrotron Radiation Research Center
Hsinchu, Taiwan

ISBN 978-3-030-81910-1 ISBN 978-3-030-81911-8 (eBook)
https://doi.org/10.1007/978-3-030-81911-8

This Springer imprint is published by the registered company Springer Nature Switzerland AG
The registered company address is: Gewerbestrasse 11, 6330 Cham, Switzerland

This book is dedicated to Prof. Tsong-Pyng Perng,
who is to me more than just a PhD mentor.

Preface

Utilization of solar energy is considered to be an efficient tool to govern reactions which realization currently is identified to be accessible only under harsh and extreme conditions. For instance, traditional splitting of water into its basic components, namely oxygen and hydrogen, is usually carried out via electrolysis or thermolysis which requires to utilize a tremendous amount of energy and sources and it negatively influences the surrounding environment. In turn, this process could be realized simply via immersion of certain materials called photocatalysts into aqueous media and its subsequent irradiation with light. In this case, the rate of oxygen and hydrogen production is determined mostly by the properties and characteristics of photocatalysis as it should satisfy numerous very strict requirements for efficient absorption and utilization of solar light.

Recent studies discovered that there exist a lot of compounds and structures which could serve this purpose. Yet, to the greatest misfortune, even though they can push forward the photocatalytic reactions, their efficiency is very low as they are unable to advance the transformation of solar to chemical energies at required levels. As an example, TiO_2 and ZnO, the most available and studied photocatalysis, can be activated only by UV light, which is a small portion of solar spectra. As a result, their performance is too low for practical application and industrial implementation. Thus, for creating an effective photocatalytic process, it is necessary to deeply revisit the existing materials and seriously address their most crucial drawbacks.

Defect engineering can perfectly satisfy this role. It provides a unique opportunity to tune and modify various important features of the target materials simply by changing its internal structure, for example, via removal of some of its own atoms, or introduction of new foreign compounds. It results in consequent reconstruction of periodical arrangement and formation of new order within crystal structure as to compensate the occurred changes and restore the equilibrium accompanied by changes in the band structure. Thus, the geometrical and electronic configurations of target materials become ultimately affected. Given the low price, high effectiveness, simplicity, and very small impact on outer compositions and structures of target materials as most of the undergoing adjustments are carried out internally,

this methodology is considered to be a highly promising candidate to build a photocatalyst with characteristics close to ideal. Yet, to be properly applied, it should be studied and addressed in the most practical and adequate way in order to avoid any misinterpretation regarding present progress and escape "trial-and-error" pathways.

This book greatly serves this purpose as it delivers fully organized, detailed, and accessible knowledge regarding the influence of intrinsic and extrinsic defects on the advancement and photocatalytic application of various nanostructured semiconductor materials with critical evaluation of existing contradictions and conflicting trends available in literature. It is believed that various groups of readers would find this book highly useful. For readers not in this profession, it would provide a great chance to get acquainted with the science and technology lying beyond the introduction of defects, while professionals would greatly appreciate the appearance of appropriate and applicable database filled with systematic and reliable information regarding various semiconductor nanomaterials and their defect engineering.

Hsinchu, Taiwan Vitaly Gurylev

Acknowledgments

I want to especially thank Dr. Yu-Jong Wu and members of the AstroChem Lab of the Molecular Science Group, National Synchrotron Radiation Research Center (NSRRC), for creating an exceptional and highly supportive environment and atmosphere to complete this work, and constantly meeting all my requirements and needs for comfort and enjoyable accommodation.

I want to thank the Ministry of Science and Technology (Taiwan) for financially supporting my stay with the Molecular Science Group, which proceeded under assistance and supervision of Dr. Yu-Jong Wu and NSRRC.

I want to thank my best friend Kyle (Chien Jung) Su, who always makes me believe that my future is in my hand as well as my writing.

I want to thank the Nanomaterials and Hydrogen Energy Laboratory in the Department of Materials Science and Engineering, National Tsing Hua University, and its supervisor Prof. T. P Perng – for filling me with required knowledge during my stay there as PhD student and postdoctoral fellow, which became the core of this book.

I want to thank Prof. Artur Useinov for deep and thorough discussions, for always answering my numerous calls and requests for meeting, and providing much-needed advice and comments regarding the process of writing this book.

I want to thank Springer, and especially Michael Luby, for believing in my ideas and offering a chance to accomplish a book, and Olivia Ramya Chitranjan—thank you for guiding me through the whole process of writing and submission, for reviewing and checking chapters, providing feedback to my all questions and queries, and for always being helpful and supportive.

Finally, I want to express my deep and sincere gratitude to my beautiful wife for continuous support, love, care, and understanding—thank you for being patient and always staying beside me during the times when I was fully engaged in writing this book.

About the Book

This book is fully dedicated to reaching complete understanding regarding principles and fundamentals of defect engineering toward realization of an efficient photocatalyst. It consists of two parts, each of which addresses particular types of defects. The first part that makes up most of the book is designed to provide complete perception and full awareness of behavior and nature of intrinsic defects. It is considered that their controlled introduction and consequent manipulation over concentration, distribution, nature, diffusion, etc., are identified as one of the most effective and practical methodologies to modify the properties and characteristics of target photocatalytic materials without sufficient alteration, breakage, or intrusion of overall external structure. As various materials have highly distinguishable particularities and features toward implementation of defect engineering approach to modify them, a selected range of nanostructured photocatalysts, including not only typical wide-band gap metal oxides (TiO_2, ZnO) but also newly discovered visible-light activated compounds (Ta_3N_5, CuO_2, C_3N_4, etc.), is covered in separate and detailed terms in the form of case studies in order to fully access their individual specification and uniqueness. The second part of the book is dedicated to reaching certain perception toward formation of extrinsic defects in the form of metallic and non-metallic dopants and description of their characteristics as this approach is also often used to achieve efficient photocatalyst. It is also of particular interest to understand what are the advantages and disadvantages of both, intrinsic and extrinsic, strategies and compare their outcome in terms of obtained performance.

Contents

About the Author

Vitaly Gurylev holds an MS in chemical engineering from Chung Yuan Christian University, Taiwan, and a PhD in materials science and engineering from National Tsing Hua University, Taiwan. After graduation in 2016, he spent 3 years as a post-doc in the same institution and then relocated to the neighboring National Synchrotron Radiation Research Center to become a part of its Molecular Science Group while continue serving the same position. His research interest is mainly related to defect engineering and its application to build various nanostructured functional materials with tunable properties and characteristics that can be used in photocatalytic processing. Currently, he has published 13 papers in SCI journals of high impact index including 1 review and 1 featured article, 10 of which have designated him as first or corresponding author. Besides, his work has given rise to several prominent contributions to national and international conferences and also invited talks. He also was designated as outstanding reviewer by some SCI journals.

Chapter 1
Photocatalysis: Fundamentals

1.1 Introduction

The increased population of modern society supported by continuous advancement of present technologies requires access to enormous amount of energy to satisfy its basic requirements. Presently, this task is fulfilled via continuous and excessive consumption of fossil fuels through proceeded establishment and realization of chemical, oil, and natural gas industries. Yet, further implementation of this scenario is hardly acceptable as our planet has very limited supply of these fuels which means that their increased depletion might lead to consequent risk of total exhaustion and appearance of serious energy crisis. Another problem lies in their even geographical distribution which limits access to sharing them on an equal basis and makes availability and possession to be regarded as pricey and hardly reachable for certain populations. Finally, the development and adoption of these energy-related fossil fuel-based industries result in ceaseless contamination of surrounding environment as billions of tons of hazardous chemicals released annually to atmosphere and oceans. It is heavily affecting marine life, humans, and plant kingdoms. Thus, there is a strong motivation and powerful stimulus in developing of alternative energy sources that should be characterized by sustainability, renewability, accessibility, and negligible polluting emission.

In this regard, utilization of solar energy has been considered as one of the best approaches to satisfy these requirements. While it can be applied in several competing technologies and processes via continuous conversion into various types of energies such as electrical, thermal, etc., the most exciting and promising application of solar light is the possibility to transform it into chemical-based oxidation and reduction potentials. Thus, it could push forward reactions which under normal situation are hardly considered to occur or require very extreme conditions to become initiated. For instance, degradation of toxic and very stable organic compounds and chemicals such as harmful bacteria or dyes can be realized at ambient temperature

V. Gurylev, *Nanostructured Photocatalyst via Defect Engineering*,
https://doi.org/10.1007/978-3-030-81911-8_1

and pressure via photooxidation process without utilizing any external forces or severe environment [1]. At a relatively low price, it is a non-disposal, efficient, and cost-effective method which could be adopted not only for treatment of wastewater and antimicrobial/antibacterial applications but also for efficient purification of drinking water. In another case, solar light could be utilized to achieve production of high-quality pure hydrogen via photocatalytic water splitting process [2]. It is a sustainable, non-hazardous, and economically valuable process, and it can readily replace current techniques such as natural gas reforming or electrocatalysis which are considered as environmentally unfriendly and/or expensive. Solar energy also can be used for photocatalytic reduction of CO_2 and its consequent transformation into less harmful and value-added compounds such as CH_4, CO, and CH_3OH that could be stored and used later in various supplemented technologies [3]. This process might greatly reduce the impact of global warming on Mother Nature and at the same time provide unlimited supply of sustainable and renewable energy.

Photocatalysis also can be used for opposing processes, e.g., synthesis of complex chemical compounds whose formation requires the consumption of enormous amount of energies, sources, and capitals. For example, ammonia is usually obtained via nitrogen fixation which could only be proceeded at very critical conditions and consequently results in release of large volume of CO_2 into atmosphere. To increase its environmental friendliness, reduce the perplexity of this process, decrease the accompanied overall cost, and fully exclude the utilization of fossil fuels, it could be realized via assistance of solar light [4].

Photocatalysis generally requires the use of semiconductor compound whose ability to produce large amount of charge carriers with different signs under light-irradiation conditions plays a crucial role on promoting the photooxidation and/or photoreduction reactions. It is obvious that the narrower the band gap of semiconductor, the more solar light it can absorb, and the more electrons and holes can be created to initiate the redox reactions. Yet, each particulate photocatalytic processing mentioned above has certain differences and discrepancies, and it dictates the requirements toward development of suitable material that enables not only initiating them but also governing and optimizing their processing. For example, CO_2 photoconversion is more energy demanding than others as, firstly, breakage of O=C=O bond is a highly nontrivial task due to its stability and, secondly, it evolves six- or more-electron transfer process [3]. In turn, realization of water splitting to produce hydrogen can be proceeded via four- or even two-electron pathway, while for successful occurrence of dye degradation, it is simply enough to use only a single-electron transfer [2]. Thus, it is evident the necessity to deeply address precise particularities of each major photocatalytic process. These knowledge are highly essential in reaching the profound and absolute understanding in which direction the development of materials suitable for photocatalysis should be advanced.

1.2 Case Example I: Photocatalytic Degradation of Pollutants in Water

It is well-known that organic dyes and pigments are very hazardous substances whose presence in water sources causes harmful contamination of surrounding environment and seriously influences the living systems inhabiting including humans, animals, and plants. Various methods are used to achieve the removal of these chemicals such as precipitation, adsorption, flocculation, flotation, oxidation, reduction, and also electrochemical, aerobic, anaerobic, and biological treatment. Yet, low degradation efficiency, production of secondary pollutants, and high cost of the accessories and their consequent maintenance lead to their inability to undergo full industrialization in order to become widely available for the modern society. In this regard, there is a need in development and realization of new processes which could be applied with low expense, simple, highly recyclable, and affordable. These requirements can effectively be fulfilled by photocatalysis which in addition to the abovementioned parameters also provides the advantage of environmental friendliness and impressive efficiency.

Photocatalytic degradation of dyes using solar light is defined as heterogeneous oxidation reaction in which highly toxic molecules are subjected to complete transformation into non-hazardous compounds such as carbon dioxide and water. To initiate it, the material which serves as a photocatalyst is exposed to the irradiation of light with energies of photons suitable enough to promote the jumping of electrons toward conductions band (CB), while positive holes remain in the valence band (VB). It is obvious that the better the utilization of light, i.e., the narrower the band gap, the more photons can be absorbed, and thus the higher concentration of charge carriers can be produced. At this step, it is important to avoid their recombination as it might result in sufficient decrease of their presence. Once produced, these photo-induced electrons and holes migrate to the surface of the catalyst where they become involved in oxidation and reduction reactions, respectively, with adsorbed species. It is described as the following [5]: *Firstly*, photogenerated holes that reside in the valence band interact with surface-bound water to generate hydroxyl radicals ($OH^{\bullet}$) (Eq. 1.1) which are very aggressive and strong oxidizing agents and can easily degrade the dye:

$$H_2O(\text{ads}) + H + (\text{VB}) \rightarrow OH^{\bullet}(\text{ads}) + H^{+}(\text{ads}) \tag{1.1}$$

To be more precise, they attack adsorbed organic molecules via extraction of H atoms from C-H bond or through addition to double bonds or aromatic rings leading to appearance of carbon-centered radical species that tends to combine with O_2 to induce transformation into CO_2 [6]. It is interesting to notice that some of ($OH^{\bullet}$) radicals given their extreme activity are able to desorb from the surface of photocatalyst and permeate into surrounding aqueous media thus diffusing all around reaction solution. In this regard, they can initiate oxidation reactions with remote species which are not in direct contact with a photocatalyst and in fact are located at

a certain distance from it [7]. *Secondly*, photogenerated electrons which reside in the conduction band initiate the reduction of surface-bound oxygen to produce superoxide radical anion ($O_2^{\bullet}$) via the following reaction (Eq. 1.2) [5]:

$$O_2 + e - (CB) \rightarrow O_2^{\bullet} (ads) \tag{1.2}$$

This superoxide actively participates in the oxidizing process of dye degradation even though the resulted efficiency is lower than that of ($OH^{\bullet}$). In addition, presence of these species enables to increase the separation rate of charge carriers hence providing additional contribution to the light-induced performance. *Thirdly*, superoxide radicals which avoid participation in the oxidation reaction can easily be converted via proton-coupled electron transfer into hydroperoxyl radicals ($HO_2^{\bullet}$) (Eq. 1.3) and then to hydrogen peroxide (H_2O_2) (Eq. 1.4). The latter compound, in turn, cannot be considered as a stable, and it tends to trap the electron in order to proceed further dissociation into aggressive radical ($OH^{\bullet}$) (Eq. 1.5):

$$O_2^{\bullet} (ads) + H^+ \rightarrow HO_2^{\bullet} \tag{1.3}$$

$$2HO_2^{\bullet} \rightarrow H_2O_2 (ads) + O_2 \tag{1.4}$$

$$2H_2O_2 \rightarrow 2OH^{\bullet} (ads) \tag{1.5}$$

Thus, the higher the concentration of H_2O_2 (or $HO_2^{\bullet}$), the more electrons are trapped, the more ($OH^{\bullet}$) radicals can be produced, and the higher is the charge separation rate and better dye degradation efficiency. Yet, too much of H_2O_2 might negatively influence the photocatalytic performance as it becomes the scavenger for positively charged holes [8]. In addition, excessive concentration of hydroxyl radicals might lead to their partial recombination which undoubtedly decrease the oxidation rate of dye. Briefly, the degradation process is shown in Fig. 1.1.

Comparing the reactions on CB and VB, the single-electron transfer from the former band to dissolved oxygen molecule has been generally recognized as the rate determining step in degrading the pollutant [9]. Simply put, if O_2 is not reduced at a required rate, electrons begin to intensively accumulate on the surface of a photocatalyst which inevitably leads to increased recombination of charge carriers. This process becomes halted once the sum of rates associated with recombination and electron transfer to oxygen approaches the rate that describes the photogeneration of holes. Hence, it becomes evident that the rate of photooxidation equals and, consequently, is limited by the rate of O_2 reduction [10]. This supposition is confirmed by the rate at which electron is transferred to oxygen molecule (this range is usually within several milliseconds) as it is much lower than that of hole transfer (this range is usually within 100 ns) [6].

Not every semiconductor material can be utilized as an efficient photocatalyst for water treatment as strict and very defined requirements toward suitability of their physical and chemical properties as well as basic characteristics to serve this purpose should be fulfilled. It is a highly important step since its correct realization not

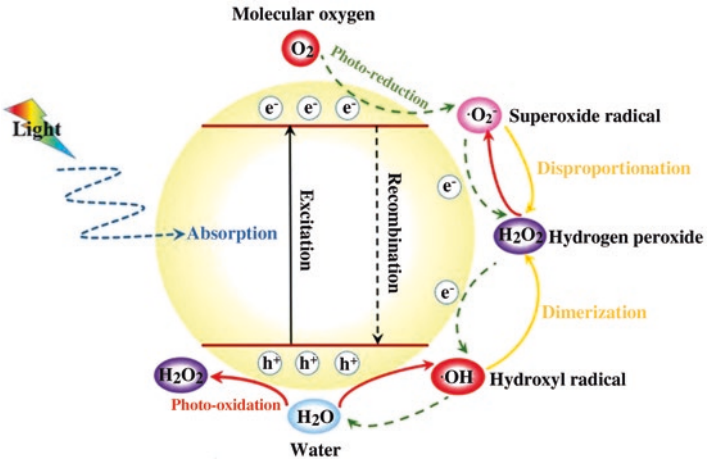

Fig. 1.1 Schematic diagram illustrating principle of dye degradation photocatalyst. (Reprinted from Ref. [1] with permission from *Elsevier*. Copyright 2020)

only governs the quality of photocatalytic performance in terms of tuning its efficiency and stability but also regulates whether the target material can induce it and under which conditions.

Band-gap energy and its position with respect to redox reactions To degrade given pollutant under light irradiation, the conduction band of semiconductor material must be more negative than the reduction potential of the redox couple. At the same time, the valence band is required to be more positive than the relative potential of the oxidation reaction. Simply put, the band-gap position of possible candidate for photocatalysis should be acceptable to initiate the decomposition of the dye. It can be demonstrated based on the following example. It is well-known that redox potentials of RhB dye degradation for reduction and oxidation are laid at −0.16 V vs. NHE and 2.38 eV vs. NHE [11], respectively, which means that the band gap of photocatalyst apart should exceed ~2.54 eV to cover both of them in order to fit the required process. Certainly, it can be even larger, as the more negative the CB and the more positive the VB positions of the semiconductor, the more thermodynamically beneficial becomes the realization of these reactions, respectively, yet this advantage immediately brings into effect another issue that needs to be considered. To be clear, the band gap larger than ~3.0 eV means inability of material to absorb visible light which, in fact, is accounted for sufficient part of solar light spectra. It leads to reduced concentration of absorbed photons that in turn results in sufficient decrease of available photo-induced electron-hole pairs and consequently causes dramatic declining of the photocatalytic performance. For example, band gap of TiO_2 perfectly satisfies the redox potentials of most dyes, and this material is considered to be a strong oxidizing agent which effectively removes most of pollutions from water. Yet, given its wide band gap equaled to ~3.2–3.4 eV, irradiation with UV light only can be used to activate it which makes it is unable to fully utilize solar spectra.

Overall, there are not so many single component materials and compounds whose band-gap position with respect to vacuum level can match both redox reactions. With the greatest regret, sufficient part of them is referred to the same class as TiO_2, e.g., wide band-gap semiconductors that show very low sensitivity toward irradiation with visible light. Thus, their optical characteristics should be modified in order to shift the absorption edge toward longer wavelength. For example, it was reported that formation of oxygen vacancies in ZnO and TiO_2 can be considered as an efficient tool to resolve this problem since introduction of these defects greatly extends utilization of photons with energies up to ~2 eV or even lower [12, 13].

As it is not easy to find materials with suitable band gap that can show desirable optical and electronic characteristics, the dye degradation reaction via some metal oxides can be proceeded using modified reaction pathways. As an illustration, well-known WO_3 whose band gap is ~2.8 eV cannot cause single-electron reduction reaction of O_2 given that its CB is more positive (e.g., +0.5 V vs NHE) than the relevant potential. In this regard, it was generally accepted that this material is unsuitable for utilizing as photocatalyst for efficient oxidative decomposition of organic compounds in air. Thus, to become activated, it should be modified properly via, for example, coupling with other semiconductors, noble metal deposition, etc. [14]. Yet, this position of band gap is highly acceptable for multi-electron reduction of O_2 which occurs via formation of H_2O_2 through the following reaction: $O_2 + 2H^+ + 2e^- \rightarrow H_2O_2$ (aq.) at the potential of +0.682 V that is more positive compared to that of single electron process (+1.23 V). It was reported that loading with noble metals such as platinum increases further the efficiency due to additional supply of electrons [15]. The same concept also is applicable to Ag_3PO_4 whose position of conduction band equaled to 0.45 V (vs. NHE) cannot match the redox potential of $O_2/O_2^{\bullet}$ reaction (0.33 V). Thus, thermodynamically, Ag_3PO_4 cannot initiate the degradation of dye following the route of well-known oxidation process. Instead, the two-electron reaction was reported to be efficiently implemented. This is especially important discovery given that that Ag_3PO_4 is a visible light-induced photocatalyst due to its band gap of ~2.45 eV and thus is considered to be a highly attractive compound [16].

Efficient electron transport It is important to reduce the recombination rate of photo-induced charge carriers and to provide their efficient transportation toward the surface of materials where they can activate redox reactions. For example, TiO_2 has a great potential for photocatalytic water treatment as positions of its bands are highly suitable for both reduction and oxidation reactions. Yet nearly 90% of charge carriers created in the bulk of this material due to the absorption of light are fully annihilated within a very short period of time [17, 18] which means that only remaining 10% is responsible for reaching the surface and interacting with adsorbed species. Thus, low efficiency of photocatalysis often could be observed. In this regard, there are two strategies which can be used to deal with this problem. One is to expand the spectral range of absorbed light that could result in increased concentration of utilized photons and consequently lead to higher availability of photogenerated charge carrier density. Several interest approaches can be suggested

to promote this step. For example, it can be realized via doping with metal/non-metal which can causes the appearance of additional energy levels close to valence or conduction bands. Accordingly, increased sensitivity toward capturing photons with energies laid beyond actual absorption edge can be obtained. Another possibility is to use thin layer of certain and highly specified compound with relatively small band gap to make it cover the surface of target material. Thus, under irradiation with sunlight, photons captured by it could be transferred toward the required direction as to reach balance of their distribution. Also, loading with noble metal nanoparticles can be used to improve the light absorption since at extremely small sizes of several nanometers, they show semiconductor optical characteristics, as a result becoming sensitive to photons with energies close to visible range. Moreover, due to differences in Fermi energies, the transfer of additional electrons occurs toward TiO_2 causing their concentration on its surface to become increased.

In turn, the second strategy for reducing the recombination rate is referred to the overall improvement in utilization efficiency of photogenerated charge carriers following the enhancement of their separation rate. For example, it can be done via decreasing the diffusion lengths due to smaller size or dimension of compound. It allows electrons and holes to escape possibility becoming easily trapped within the bulk of materials and enables them to reach the surface faster and with minimal losses of energies. Moreover, fabrication of multi-component heterojunction also can be considered as optimal choice since isolated accumulation of electrons and holes on the surface of each materials follows the alignment of their band gaps with respect to one another and thus can easily promote effective charge separation.

Photocatalytic materials should be cheap, abundant, environmentally friendly, and biologically and chemically stable. Even though these requirements do not influence much on the real rate of photocatalytic reaction nor its correct proceeding and choice of defined pathway, their implementations are highly important for the future industrialization and all-around world distribution of light-induced technologies as to make them become widely adopted and highly accessible. Accordingly, utilized materials should fully satisfy them. The justification of this concept can be demonstrated based on the following illustration. It is commonly accepted that deposition of noble metals-based nanoparticles on the surface of wide band-gap semiconductor results in enhancement of charge carrier transportation characteristics and appearance of visible light absorption and overall improvement of performance [9]. Hence, this approach might be considered as a great method to extend the efficiency of current photocatalytic processes. Yet, its attractiveness is shadowed by the extreme cost of noble metals and their scarce availability. In another example, CdS or Cu_2O are considered to be optimal materials for dye degradation, as both of them have suitable alignment of band gap and also are able to absorb visible light. However, their stabilities are too low as they become the subject of decomposition during prolonged photocatalytic process which sufficiently decrease the practicability of their usage [19, 20].

Hence, developing efficient material for light-induced dye degradation is a highly nontrivial task even though this process is considered to be one of the simplest forms of photocatalysis as it definitely has much less preconditions and limitations to avoid compared with, for example, solar water splitting and CO_2 conversion processes described below. Yet, it is clear that tremendous efforts are still required in this direction to extend further already achieved progress as currently this technology is not ready for complete and full-scale implementation and consequent adoption due to absence of efficient, affordable, and available materials which can be considered as long-time awaiting answer to the mentioned above requirements.

1.3 Case Example II: Photocatalytic and Photoelectrochemical Water Splitting

Water molecule is a very stable formation whose dissociation into hydrogen and oxygen cannot be proceeded easily as severe conditions are required to break the chemical bonds within it. For example, to realize it via thermolysis, the application of temperature up to several thousands of Kelvins is necessary to obtain only very small fraction (~5%) of dissociated molecules at atmospheric pressure. Thus, the use of sunlight to activate it might become an optimal solution to avoid the external utilization of artificially created energy sources that is based on extensive consumption of electricity and high temperatures. It is especially important given that production of oxygen and hydrogen currently is under extremely high demand as the speed at which the development and implementation of technologies based on application of fuel cell increase greatly in the last decade. Yet, to effectively apply this perspective strategy, numerous challenges should be overcome. *Firstly*, photocatalytic water splitting is not a spontaneous but uphill process which requires positive change of Gibbs energy for 237 kJ mol^{-1} [21]. *Secondly*, there is a high possibility that generated hydrogen and oxygen gas might result in occurrence of reverse reaction to backwardly form H_2O considering its downhill nature. It might inevitably decelerate any photocatalytic activities for water splitting and negatively influence the expected outcome. It is interesting to notice that contrary to general conclusion, some authors praised the appearance of water molecules produced in this way since they can again be reused for oxidation reaction, as it happens, for example, in the case of TiO_2 [22]. *Thirdly*, and most importantly, solar-to-hydrogen energy conversion efficiency for photocatalytic water splitting systems is extremely low and reaches only ~1%. In fact, for its industrialization, the required minimum should become at least ~10–12%. For comparison, the efficiency of photovoltaic-assisted electrolysis can achieve enormous ~30%, and it can cover all additional expenses applied to this process.

The overall reaction of solar water splitting is a multi-electron process whose mechanism is described as follows. In the beginning, light irradiation with energy of photons equaled or higher than width of band gap should be used. It causes electrons to move toward the conduction band while holes are remained in the valence

band. In the next step, these photo-induced charge carriers are transferred to the surface where they are supposed to initiate reactions with adsorbed water molecules. It is crucially important to avoid recombination process as it might sufficiently decrease their availability and to decline the rate and outcome of water splitting. Various methods and strategies are used to achieve it, some of them similar to those mentioned in the previous section such as introduction of intrinsic and extrinsic defects, control over crystalline facets, advancement via surface engineering approach, etc. Yet, the most efficient one currently considered is the deposition of co-catalyst in the form of transition and noble metal or metal oxide nanoparticles. The photogenerated electrons migrate to the surface of the host photocatalyst and become trapped by these metal-based co-catalysts, and it occurs due to differences in Fermi energies between them. Meanwhile, the photogenerated holes stay at the host photocatalyst where they can avoid recombination. For its part, this process can be proceeded in opposite direction when positive charges are transported to the co-catalyst, while negative charges are remained in the host materials. Yet, it is a rare and less investigated phenomenon.

Once electrons and holes become in contact with water molecules whether presented on the surface of photocatalyst or transported into co-catalyst, the following oxidation and reduction reactions are initiated, respectively (Eqs. 1.6, 1.7, and 1.8) [22]:

$$\text{Reduction half reactions}: 2e^- + 2H^+ \rightarrow H_2 \tag{1.6}$$

$$\text{Oxidation half reaction}: H_2O + h \rightarrow O_2 + 2H^+ \tag{1.7}$$

$$\text{Overall reaction}: 2H_2O \rightarrow O_2 + 4H^+_{(aq)} + 4e^- \rightarrow 2H_{2(g)} + O_{2(g)} \tag{1.8}$$

Schematically, this process is demonstrated in Fig. 1.2a. The oxidation reaction which is also called an oxygen evolution reaction (OER) is considered to be the

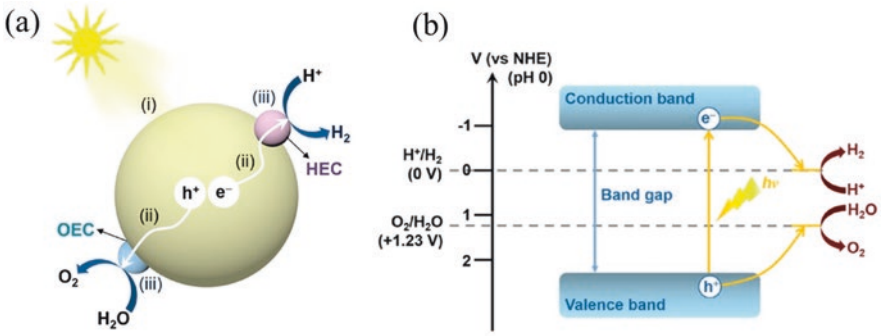

Fig. 1.2 (**a**) Diagram showing the reactions during water splitting on a semiconductor photocatalyst: (i) light absorption, (ii) charge separation and transport, and (iii) redox reactions. (**b**) Energy diagram for photocatalytic water splitting based on one-step excitation. (Reprinted from Ref. [25] with permission *American Chemical Society*. Copyright 2020)

bottleneck of overall water splitting process. The OER involves the formation of double O-O bond via two water molecules which are associated with liberation of four protons accompanied by four electrons. In a further step, once produced, these quadruple compounds become involved into two-electron/two-proton process of hydrogen reduction which is called as hydrogen evolution reaction (HER) [23]. Given that the transfer of electrons within interface occurs via single-electron process, i.e., one electron per time, OER reaction should be taken via multi-step transfer which means that charges are required to be firstly stored and then gradually discharged to realize productive O-O bond forming reaction [23]. Thus, it makes the kinetic of OER become very slow and results in a large overpotential. As this reaction is considered to be a first step in water splitting process, increasing its effectiveness appears to be a key factor toward efficient hydrogen production.

The reaction capabilities of photogenerated electrons and holes, respectively, are determined by the alignment of band gap with respect to defined redox potentials. As it was mentioned briefly above and can be seen from Fig. 1.2b, semiconductor materials enable to perform full cycle of water splitting process via both half-reactions only if its CB is more negative than the redox potential of H^+/H_2 (−0.41 eV vs. NHE at pH 7) and the VB is more positive than the redox potential of O_2/H_2O (−0.82 eV vs NHE at pH 7) [22]. The difference between these two potentials is 1.23 eV, which might bring an illusion that utilization of materials with that band gap is enough to drive both half-reactions. Yet, given multiple reasons such as migration of excited electrons and holes, overpotential due to sluggish OER, difference between HER and OER kinetics, etc., there are certain losses in energy. Accordingly, the real situation is that material with band gap of ~1.8 eV or more can only satisfy these requirements. It has to be noticed that presence of co-catalyst can lower the activation energy/overpotential for surface redox reactions. For example, Pt can be used to decrease the overpotential of both OER and HER, while NiO is exclusively applied for OER reaction only [24].

As it is expected that hydrogen production could be activated by illumination with natural sun, there is also another important issue which needs to be considered: the photocatalyst should absorb visible light. To justify it, the following reasoning is provided [25]: If assuming that materials are only sensitive to ultraviolet (UV) light with wavelength up to 400 nm as it happens, for example, in the case of wide-band-gap TiO_2, and taking into account a quantum efficiency (QE) of 100%, i.e., all photons with these energies are absorbed and become associated with appearance of photo-induced charge carriers, the solar-to-hydrogen (STH) conversion efficiency, defined as the chemical energy of generated H_2 divided by the solar energy of incident light, can be estimated at the limit of ~2%. It is necessary to notice that entropic losses in this case are neglected which definitely cannot occur in real situation. In turn, when the absorption is extended to ~700 nm or even up to ~1000 nm, the STH can reach the values of ~25% and ~47%, respectively. Considering that current target for STH is only ~10%, one can calculate that for achieving this goal, the required material should have absorption edge extended to at least ~520 nm. Definitely, in this case, QE should be considered as 100% [25] which often is hardly possible. To summarize the above, it is clear that efficiency of solar energy conversion becomes

higher for overall water splitting under longer wavelength irradiation, as the number of available photons in the solar spectrum increases which leads to more advanced presence of photo-induced charge carriers. Definitely, it is not easy to find materials whose band gap perfectly suits both oxidation and reduction potentials of water splitting while at the same time absorbs visible light. There are several prominent candidates discovered in recent years that might satisfy these requirements such as Ta_3N_5, Cu_2O, C_3N_4, TaON, etc. Yet, compared with well-known and studied for several decades compounds that have wide band gap such as ZnO and TiO_2, the former ones suffer from various problems such as low chemical or mechanical stability, high cost, low accessibility, and non-friendly influence on the environment. Even though it has no direct relation to their proceeding of light-induced reactions, these influence negatively on the overall performance. Thus, it prevents their extensive use. For example, Ta_3N_5 has perfect band position with respect to both redox reactions and can absorb visible light given its band gap of ~2.1 eV. In this regard, it is expected to show relatively high output in hydrogen production under sunlight. The problem is, however, that this compound has some level of photocorrosion which might result in the degradation of hydrogen production efficiency during extended session of light irradiation [26].

There exist two types of solar water splitting approaches, namely, photocatalytic and photoelectrochemical, which are widely used in literature. As they have certain differences in their fundamental setup, more detailed discussion is required to deeply understand them. The first type, i.e., photocatalysis-related system, is simply based on immersing of target material, usually in the form of nanoparticles or other nanoscale-related structures prepared in powder-shaped arrangement, into aqueous media under agitated conditions, and its consequent illumination with specific light source. It is highly important that the photocatalyst should be homogeneously distributed in the reaction chamber and also to show water miscibility which requires the presence of certain functional groups on its surface [27]. Another important issue is that this suspension is supposed to demonstrate the capability to effectively absorb photons with required energies and additionally also enable them to scatter in various directions thus extending the penetration depth of utilized light [28]. It ultimately results in increasing the overall number of photo-induced charge carriers and positively influences successful processing of both redox reactions. In turn, it is obvious that 0-D structures are more preferable for this type of water splitting process than that of other dimensions. Firstly, it provides shorter diffusion lengths as charge carriers only need to be transported toward the surface-liquid interface. Secondly, with decreasing the size of nanoparticles, their surface area increases sufficiently, and it results in appearance of more reaction sites for absorbed molecules. Thirdly, synthesis of 0-D structures is very simple, and thus their overall cost is extremely low.

Photocatalytic water slitting is classified via one-step and two step (so-called Z scheme) processes [29]. The former setup requires the use of single photocatalyst whose band gap should exactly satisfy reduction and oxidation potentials as it was, for example, in the case of Ta_3N_5 mentioned above, while for the latter one, an electronic mediator is used to connect both redox reactions; thus, their separate

realizations are proceeded by different photocatalysts [30]. This mechanism can be explained using g-C_3N_4/TiO_2 heterojunction as an example [31]. Based on calculation via density functional theory, it was revealed that offsets of valence and conduction bands for this complex structure are ~0.40 and ~0.18 eV, respectively. Thus, interfacial synergy makes the surface of TiO_2 become filled with negative charges, whereas the g-C_3N_4 surface is occupied by positive charges. It leads to the formation of a built-in electric field at the interface. Once the illumination is applied, this field accelerates the transfer of photoexcited electrons residing in the CB of TiO_2 toward the VB of g-C_3N_4 and results in their recombination with holes and consequent annihilation. Following it, photoexcited electrons and holes become naturally accumulated in the CB of g-C_3N_4 and the VB of TiO_2, respectively. Achieved separation of charge carriers by this methodology efficiently prolongs their lifetime thus leading to increased redox capabilities. Following it, the HER reaction occurs on the surface of C_3N_4 given its electrons-filled conduction band, while OER reaction is proceeded by TiO_2 following its holes-filled VB.

It has to be noticed that efficiencies of both setups are still extremely low. Despite numerous efforts applied over the past years, it approaches only the value of STH equaled to ~1%. Yet, several prominent results were reported very recently which allow to consider that it is possible to extend the performance up to the level that is required to achieve for its practical application. For example, it was stated that CoO nanoparticles with sizes of 5–8 nm, even without any co-catalyst deposition, could demonstrate STH as high as 5% under illumination with AM 1.5G solar simulator which represents one of the best ever reported efficiencies for photocatalytic systems [32]. Yet, to the deepest regret, it is rather exemption than a tendency given the wide range of results currently available in literature.

In turn, the second type of water splitting that is referred to photoelectrochemical (PEC) processing involves application of photoactive thin film fabricated on supporting electrode surface in the presence of electrolyte solution. This setup especially is applicable to materials whose band gap and alignment cannot meet the requirements for overall water splitting. For example, valence bands of Si, GaAs, and GaP usually are more negative than the water oxidation potential [33], while in turn, conduction band of WO_3, Fe_2O_3, and MoS_2 is more positive than the potential for hydrogen evolution reaction [29]. Therefore, these semiconductors cannot be used alone for this process as only to perform corresponding half-reactions. Yet, in this role, they also show limited outcome. To be clear, photogenerated electrons or holes which were not consumed due to OER or HER, respectively, tend to find the charges with oppose sign to recombine. Following it, the efficiencies of these compounds are very poor and inacceptable. To resolve abovementioned issues and to assist in proper proceeding of water splitting process, external bias is applied to these semiconductors causing them to become a photoelectrode that can have cathode- or anode-like characteristics depending on the position of the band gap and the type of their own conductivity.

The mechanism of PEC water splitting process is described by taking the photoanode (n-type semiconductor) as an example [29]. After irradiation with photons that have sufficient energies, electrons are generated in it and later become

transferred toward the conducting substrate. Later, they are caught by the external voltage that drifts them to the counter electrode for the reduction reaction. In turn, holes are transported to the surface of photoanode by built-in electric field where they start to evolve into water oxidation. An oppose process is applied once the photoanode is replaced by photocathode. Disadvantages of this setup are as follows: (1) additional electrical energy is consumed to proceed the redox reactions; (2) counter electrode usually is fabricated using noble metal such as platinum; and (3) certain complexity of PEC system compared with that used for simple photocatalytic process.

One should notice that recently it became a very popular strategy to use p-n tandem system for overall water splitting when both electrodes become illuminated with light. In this case, electrons accumulated in the CB of the p-type materials are subjected to transfer toward CB of n-type material, while the hole relocation occurs in the opposite direction between VBs of both materials. It allows to reach very efficient separation of charge carriers when the reduction reaction occurs in the photoanode which represents n-type materials while the oxidation is proceeded on the surface of p-type compound that is ascribed as photocathode. It has to be admitted that the model of charge carrier transport in this case has a lot of similarities to that which is used for the Z-scheme during photocatalytic water splitting with only difference being the former one requires the use of external bias to initiate light-induced process. In addition, utilization of p-n junction in PEC setup also brings another advantage as it allows to apply the materials with smaller band gap which is enough to absorb photons with energies laid in visible range.

1.4 Case Example III: Photoconversion of CO_2

Persistent increase of CO_2 concentration in the atmosphere due to intensive use of fossil fuel and ongoing degradation of forest area around the world as a result of large-scale industrialization negatively affect our planet as it results in increased levels of oceans, causing the rise of temperature all around the globe. To solve this problem, it is highly necessary to develop an alternative source of energy which is unable to produce harmful gaseous compounds and in reverse provides an effective, pollutant-free, and affordable solution to balance CO_2 presence in the atmosphere by reducing its content. Various methodologies are suggested to address the latter demand such as carbon capturing and storage (CCS), electrochemical and thermochemical conversions, biological fixation, etc. Yet, a sufficient part of them suffers from certain problems which prevents their widespread and adoption. For example, CCS is an environmentally unfriendly technology as it might cause the leakage from geological storage. It is also highly expensive given the cost of transportation and compressions [34]. In turn, thermal and catalytic-based procedures require access to high temperatures, pressures, and exothermic reactions whose affordance is questionable for some populations and territories in our planet. Thus, it is not surprising that solar-assisted photoconversion of CO_2 is considered to be one of the

best options due to the following concerns: Firstly, the sun provides access to absolutely free source of energy; secondly, it is an eco-friendly process; thirdly, there is no need for additional extreme expenditure except the initial one that is used to construct the system; and fourthly, it results in transformation of highly toxic CO_2 into hydrocarbon fuel/useful chemicals which later can be applied in various industries and productions.

Basically, photocatalytic CO_2 reduction is described by the following three steps [35]: (1) absorption of light with energies equaled or higher than the band gap; (2) separation of charge carriers and their transportation to the surface of semiconductor material; and (3) realization of redox reactions with adsorbed CO_2 molecule (Fig. 1.3a). Among the above three steps, the first two are the same as those used for solar water splitting mentioned in the previous section. Thus, it is also important to avoid recombination of photogenerated electron-hole pairs and increase of their

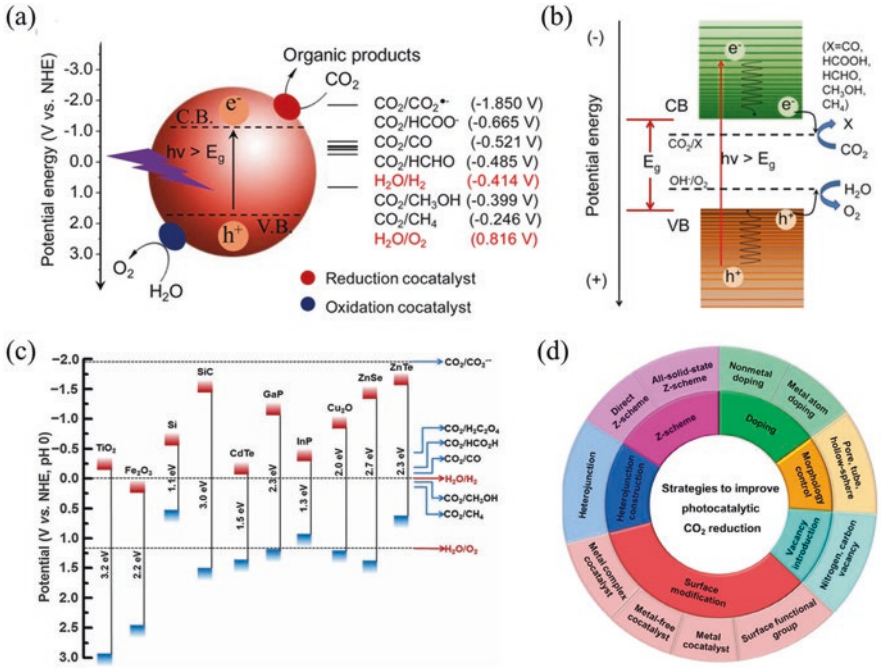

Fig. 1.3 (**a**) Schematic illustration of mechanism and (**b**) relative energy levels of photocatalytic reduction of CO_2 on a semiconductor photocatalyst. (Reprinted from Ref. [35] (https://pubs.acs.org/doi/full/10.1021/acsomega.7b00721) with permission from *American Chemical Society*. Copyright 2017. Further permissions related to the material excerpted should be directed to the ACS) (**c**) Conduction band (red squares) and valence band (blue squares) positions of some candidate semiconductor photocatalysts and the redox potentials versus NHE of CO_2 reduction and water splitting at pH 0. (Reprinted from Ref. [36] with permission from *The Royal Society of Chemistry*. Copyright 2016) (**d**) Strategies employed for improving the photocatalytic CO_2 reduction over metal-free materials. (Reprinted from Ref. [34] with permission from *John Wiley and Sons*. Copyright 2020)

transportation characteristics to escape being captured in bulk. As for the third step, to proceed with the redox reactions, the CO_2 molecule firstly should be adsorbed on the surface of photocatalyst and secondly become activated properly in order to be ready for conversion procedure. It usually occurs through formation of partially charged $CO_2^{\bullet-}$ species which is initiated by interaction of adsorbed CO_2 molecule with surface atoms of photocatalyst. It can be readily demonstrated using TiO_2 as an example. CO_2 molecules are tending to adsorb on defective Ti^{3+} sites, and it initiates transferring of electrons toward them. This protocol leads to oxidation of the Ti^{3+} and its transformation into Ti^{4+}. In turn, original linear symmetry of CO_2 molecule due to additional electron becomes bent and thus leads to lowering of energy barrier for accepting excited electrons given the decreased LUMO level [35, 36]. In a consequent move, to trigger the photoreduction of CO_2, the appearance of H^+ in the system is highly required. It is realized via water oxidation by photo-induced holes. Later, H^+ becomes involved in the CO_2 electron-assisted reduction reaction which is proceeded by breakage of O=C=O bond and arrangement of new C-bonding with different species through series of reactions [37]. Its type and final outcome have clear dependency on the availability of excited electrons. Thus, various reduction products in the form of CO, C_2H_6, CH_3OH, etc. can be obtained. Overall, the following reaction pathways are determined based on the number of electrons involved in the reaction [38] (Table 1.1). It has to be noticed that the concentration of photo-induced electrons which could be used for CO_2 conversion might be seriously limited as hydrogen evolution reaction is proceeded in parallel. Thus, it is clear that recombination rate has a crucial and extreme influence on the obtained outcome as electrons should be shared between two reaction pathways. Given that this process occurs in water, proceeding of HER is more favorable in these conditions and thus

Table 1.1 Common products from CO_2 photoreduction and their simplified redox reactions and redox potential at pH 7

Product	Reaction	E^o redox[a] (V versus NHE)
Oxygen	$H_2O \rightarrow 1/2O_2 + 2H_2 + 2e^-$	0.82
Methane	$CO_2 + 8H^+ + 8e^- \rightarrow CH_4 + 2H_2O$	−0.24
Ethane	$2CO_2 + 14H^+ + 14e^- \rightarrow C_2H_6 + 4H_2O$	−0.27
Carbon monoxide	$CO_2 + 2H^+ + 2e^- \rightarrow CO + 4H_2O$	−0.51
Methanol	$CO_2 + 6H^+ + 6e^- \rightarrow CH_3OH + H_2O$	−0.39
Ethanol	$2CO_2 + 12H^+ + 12e^- \rightarrow C_2H_5OH + 3H_2O$	−0.33
1-Propanol	$3CO_2 + 18H^+ + 18e^- \rightarrow CH_3CH_2CH_2OH + 5H_2O$	−0.31
2-Propanol	$3CO_2 + 18H^+ + 18e^- \rightarrow CH_3CH_2(OH)$ $CH_3 + 5H_2O$	−0.30
Formaldehyde	$CO_2 + 4H^+ + 4e^- \rightarrow HCHO + H_2O$	−0.55
Acetaldehyde	$2CO_2 + 10H^+ + 10e^- \rightarrow CH_3CHO + 3H_2O$	−0.36
Propionaldehyde	$3CO_2 + 16H^+ + 16e^- \rightarrow CH_3CH_2CHO + 5H_2O$	−0.32
Acetone	$3CO_2 + 16H^+ + 16e^- \rightarrow CH_3COCH_2 + 5H_2O$	−0.31
Formic acid	$CO_2 + 2H^+ + 2e^- \rightarrow HCOOH$	−0.58
Acetic acid	$2CO_2 + 8H^+ + 8e^- \rightarrow CH_3COOH + 2H_2O$	−0.31

Reproduced from [38] with permission from The Royal Chemical Society. Copyright 2013

consumed sufficient part of available electrons which leads to a low selectivity for resulted carbonaceous products [36]. Thus, one might consider that directly using H_2 gaseous for proceeding CO_2 conversion is a better option than that of the water as it allows to avoid HER reaction. Yet, the selectivity of this pathway is very low since it mostly results in the appearance of CO as the main outcome, while other reaction products might be less accessible [39].

Numerous efforts have been applied to make the photoconversion of CO_2 sufficiently reliable and compelling and to show high selectivity in final products, yet it is still suffering from poor outcome which is unable to make it become a practically available process. For example, one of the best bias-free photoconversion efficiencies reported in literature up to date is ~1% which was reached via application of reduced blue titania sensitized with bimetallic Cu-Pt nanoparticles [40]. It was discovered that this system enabled to selectively generate a substantial amount of both methane and ethane under artificial sunlight due to the fact that Cu nanoparticles provided sites for CO_2 adsorption, while Pt were used to effectively prevent electron-hole recombination. However, generally reported conversion outcome of CO_2 reduction is much lower and reaches only tens of percent if not less. The following factors could be described as reasons of such unsatisfied performance [36]. Firstly, it is well-known that CO_2 is considered to be a very strong and chemically inactive molecule, and thus, to break the C=O=O bond, one needs an application of massive amount of energy accompanied by the presence of an appropriate catalyst that possesses required characteristics and properties. Simply put, reduction of CO_2 dissolved in H_2O is determined to be an uphill reaction, and to obtain hydrocarbon fuels such as CH_4 or CH_3OH, it requires to make very high positive change in the Gibbs free energy equaled to 818.3 kJ mol^{-1} and 702.2 kJ mol^{-1}, respectively [36]. For comparison, splitting of H_2O molecule into hydrogen and oxygen using standard conditions causes the change in the free energy for "only" 237.2 kJ mol^{-1}. Secondly, the light-induced conversion of CO_2 is a multi-electron process which clearly depended on the availability of charge carriers on the surface of catalyst and presence of protons within the solution. For example, to generate C_2H_6 and C_2H_5OH, it is necessary to succeed in transportation of 16 and 12 electrons, respectively, which is much more difficult than, for example, to initiate two-electron reaction associated with H_2 evolution from H_2O. Thirdly, the material which is going to be used as a photocatalyst should have CB higher than the reduction potential of CO_2 as it facilitates the transfer of electrons, while VB is required to be below the water oxidation potential as it favors the transfer of holes (Fig. 1.3b). In addition, it should absorb visible light as it constitutes a significant part of the solar spectra. Fourthly, CO_2 has poor solubility in water, and thus, its adsorption on the surface of the catalyst and consequent activation via proton-coupled electron transfer is proceeded with certain difficulties [35]. Thus, other processes such as hydrogen evolution reaction [41] become more preferential and dominated for the photo-induced electrons to choose for participation. It results in low selectivity of carbonaceous products.

Definitely, the latter problem could be solved simply by using various additives such as NaOH and Na_2CO_3; however, the negative side of this method is that their presence in solution makes the reduction of bicarbonate and carbonate species more

difficult [35]. Another method to resolve the problem of CO_2 solubility in water is simply to avoid this media by applying gas-phase reduction protocol which is based on mixing the water vapor with CO_2 gas and using it as starting reactants. In fact, it results in higher outcome compared to that of using liquid-phase process. For example, Xie et al. [42] investigated photoconversion of CO_2 by TiO_2 and Pt-TiO_2 catalysis in both setups and discovered that gas-phase reaction causes much higher production activity to obtain CH_4 over that of the liquid phase. Furthermore, the former process initiates better selectivity toward CO_2 rather than water reduction as less hydrogen were detected in the system. In turn, Olivo et al. [43] investigated both processes and confirmed that vapor-phase deoxygenation indeed drives great selectivity toward obtaining methane, whereas in the liquid phase, water dehydrogenation allows to achieve intermediate oxidation state products, i.e., formic acid, formaldehyde, and methanol. The problem is, however, that gas-phase reduction protocol requires a more complex setup that leads to certain difficulties in its adequate realization.

Among various photocatalysis used for reduction of CO_2, TiO_2 has been employed most widely given that its VB and CB positions are suitable to redox reactions (Fig. 1.3c) and in addition, it is also a cheap, abundant, chemically stable, and easy-to-produce material. Yet, it only can be activated under UV light which limits its performance and outcome. Definitely, it is clear that some other materials, in perspective, are suitable to be utilized under solar light for CO_2 conversion as their band gap apart from suiting the redox potentials for both oxidation and reduction reactions also is narrow enough to capture photons with energies of visible light irradiation. However, moving from theoretical estimation to practical utilization, it becomes clear that their efficiencies are extremely low due to other factors which also need to be considered deeply. For example, copper-based semiconductors such as CuO, Cu_2O, and Cu_2S, with band gaps of ~1.7 eV, ~2.2 eV, and ~1.2 eV, respectively, can demonstrate excellent visible light harvesting. Given that they also show good selectivity toward CO_2 reduction whether in the form of single or tandem catalyst, it should be no question for their applications in this photoconversion process. However, the narrow band gap leads to highly limited photocatalytic activity as it causes extremely fast recombination of photo-induced carries [44, 45]. Additionally, these materials suffer from poor chemical stabilities as it was mentioned above. For example, CuO is rather reactant than catalyst during the photoconversion reaction with CO_2, as under interaction with this gaseous compound, it undergoes transformation into copper carbonate [46]. Thus, it is hardly surprising that various approaches are applied to extend the current performance of materials given that their pure forms often could not satisfy even the most basic requirements for stable and efficient reduction of CO_2 (Fig. 1.3d). Among them, doping with metal and nonmetal elements, use of co-catalyst, and application of multicomponent composition such as Z-scheme and heterojunction semiconductors have been investigated the most actively [35]. For example, returning to TiO_2 and its ability to absorb only UV light, it is often combined with other compounds such as CdS, graphene, and GaP [44] which are sensitive to the visible spectra of solar irradiation. Thus, they can accept photons with less energies and consequently transfer them to this material.

Doping also can extend the activity of semiconductor materials as it was shown in the study by Li et al. [47] where N-TiO_2 photocatalyst was able to reduce CO_2 gas under illumination with visible light.

In turn, very recently, a lot of attention was given to the possible role of intrinsic surface defects in increasing the reactivity toward CO_2 photoconversion as they enable to govern adsorption of its molecules and their processing. For example, it was discovered that attraction between oxygen vacancies created on the surface of $SrTiO_3$ and oxygen atoms presented in CO_2 molecules could lower the activation barrier and enhance the availability of trapping sites and their attractiveness [48]. In another study, it was shown that reduction of CO_2 through dissociation of $CO_2^{\bullet-}$ charge species into CO by means of vacancy-induced mechanism could occur even in dark [49]. This discovery allows to consider that realization of this reaction might not be limited only by daily time or cloudless weather but also could be proceeded at night or in rainy days thus creating 24-hour unstoppable cycle.

Overall, it can be said that CO_2 photoconversion using solar light illumination is a very perspective, novel, and highly advanced technology whose proper development and application might provide a great solution to the existed problem of atmosphere pollution and so-called green effect. Furthermore, given the obtained outcome of reduction reaction, it also allows to reach environmentally friendly production of various carbon-containing chemicals that processing by using current industrial technologies is, in fact, expensive, dangerous, and most importantly, results in extreme pollution. Thus, CO_2 photoconversion can feed two birds with one stone. Yet, as it was mentioned above, it is a far-reaching perspective given its current efficiency and selectivity. In light of this, extensive and deep studies are still required to shift it from category of "highly demanded" to "widely accessible."

1.5 Case Example IV: Photocatalytic Nitrogen Fixation

Nitrogen is one of the most important and essential elements to keep the functionality of all biological organisms. It serves as starting blocks for the synthesis of various organic compounds such as amino acid, nucleotides, etc. which highly assist in growing tissues in plants and animals [50]. However, even though the content of nitrogen is extremely high in atmosphere, it cannot be directly utilized by living matters given that the molecular structure of the N_2 molecule is very stable due to the presence of nonpolar energetic N-triple bond [51]. Thus, the consumption of nitrogen is usually proceeded via its assemblance as ammonia. It is determined to be the necessary raw material for fertilizer production. The transformation of N_2 to NH_3 is thermodynamically accessible process as it is supposed to result in release of energy due the following reaction: $N_{2(g)} + 3H_{2(g)} = 2NH_{3(g)}$, $\Delta H_{298K} = 92.2$ kJ mol^{-1} [50]. Yet, its spontaneous proceeding cannot be realized at ambient conditions due to extreme chemical stability and inactivity of nitrogen and also its low proton affinity [52].

Industrial production of ammonia is achieved via well-known Haber-Bosch approach in which high-purity streams of nitrogen and hydrogen are reacted over

metal-based catalyst at high temperature and pressure of ~500 °C and ~250 atm, respectively, which constitute nearly 1% of all-around worldwide fossil energy and result in several million tons of CO_2 emission each year [53]. Such a huge pollution is mostly caused by the presence of hydrocarbons in raw materials that are used to produce pure hydrogen. Thus, in consideration of sustainable development that modern society is required to follow, it is highly desirable and essential to develop and implement more energy-affordable and environmentally friendly strategies which could replace current Haber-Bosch synthesis.

In nature, the nitrogenous enzymes in azobacteries can realize the nitrogen fixation at room temperature and atmospheric pressure without utilizing external forces and sources [51]. Inspired by this biological system and given that Fujishima and Honda [54] reported the first use of semiconductor materials such as TiO_2 for splitting of water into hydrogen and oxygen under UV light, a flurry of research activities has been devoted to the development of accessible photocatalyst which can generate ammonia simply via using water and nitrogen as reagent compounds. Even though the efficiency of this setup is much lower than it is required for even a partial industrialization, its future perspectives as alternative to the mentioned above Haber-Bosch synthesis are obvious.

The overall reaction of photocatalytic nitrogen fixation is considered to have the following form [50]:

$$N_2 + 3H_2O \rightarrow 2NH_3 + 1.5O_2 \tag{1.9}$$

It is a thermodynamically uphill process which is partially described in terms of water splitting and consequently results in appearance of proton H^+ followed by its further interaction with nitrogen through electron-assisted pathway to become assembled into NH_3 (Fig. 1.4a). For clarification of its correct proceeding, the

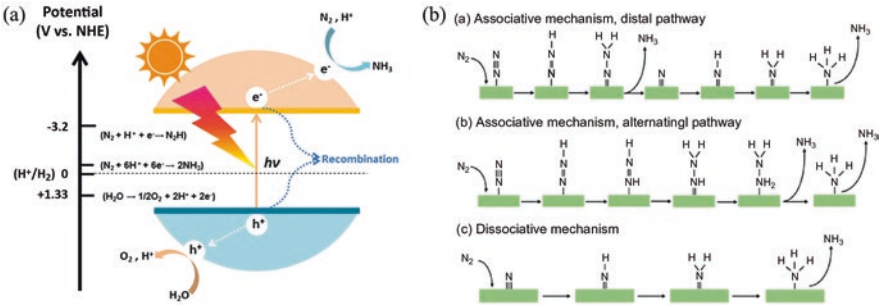

Fig. 1.4 (**a**) Schematic of semiconductor-based photocatalysts used for the conversion of N_2 to NH_3. The redox potentials (V vs. NHE at pH = 0) of water splitting and dinitrogen hydrogenation are marked on the left. (Reprinted from Ref. [50] with permission from *The Royal Society of Chemistry*. Copyright 2018) (**b**) Reaction pathways for the nitrogen reduction reactions by proton-coupled electron transfer, including the dissociative pathway, distal and alternative associative pathway, and enzymatic pathway. (Reprinted from Ref. [56] with permission from *The Royal Society of Chemistry*. Copyright 2019)

following stages are determined: Firstly, the material which is going to be served as photocatalyst is irradiated by photons with energies equaled or higher than its band gap. It initiates gathering of electrons in the conduction band, while holes remain in the valence band. Secondly, given credits to possible partial recombination of photo-induced charge carriers which hardly could be avoided, in the next step, the remaining part migrates to the surface where it will initiate redox reactions with adsorbed species. It has to be noticed that above-described two steps are very similar to that used for other photocatalytic reactions mentioned in previous sections. Thirdly, upon arrival to the surface, the holes begin to proceed oxidation of H_2O, while N_3 tends to be reduced into NH_3 via a series of multi-step insertion of photo-induced electrons and water-derived protons which is also called as the hydrogenation step. The following half-reactions are used to describe this process [55]:

$$Step\,1: 2H_2O + 4h+ \rightarrow O_2 + 4H^+ \tag{1.10}$$

$$Step\,2: N_2 + 6H^+ + 6e^- \rightarrow 2NH_3 \tag{1.11}$$

To make their occurrences become possible, it is essential that VB and CB of the materials are located below and above the redox potentials of the corresponding reactions as shown in Fig. 1.4a. Several words need to say about the actual mechanism of N_2 fixation by photocatalyst. Taking its electrochemical equivalent as example [56], it might be described via successful realization of the next three stages: (1) adsorption of dinitrogen molecules on the surface of semiconductor; (ii) cleavage of the nitrogen triple bonds and hydrogenation of dinitrogen; and (iii) desorption of the as-formed ammonia molecules (or other intermediate products) from the surface of semiconductor. In the case of photocatalyst, the hydrogenation of dinitrogen is accomplished by consecutive proton and electron transfer whose accessibilities are correlated with water reduction and surface of semiconductor, respectively. It is interesting to notice that electrocatalytic nitrogen fixation, which is also extensively investigated as the future technology in comparison to the paralleled photocatalytic process, requires that the protons for the reaction should be taken from electrolyte solution that is used instead of water as an aqueous media where the N_2 is dissolved, while electrons are supplied via external bias.

One might consider that similar to CO_2 photoconversion process, the electrons which appear on the surface of semiconductor materials should be shared between hydrogen evolution and ammonia reduction reactions. Yet, it can easily be avoided, as nitrogen fixation from thermodynamic point of view is more favorable to occur since it has higher-onset potential than that of HER, even though under basic conditions, they are very close [56]. It is important to notice that incomplete reduction of dinitrogen results in appearance of high-energy intermediates. For example, a four- and two-electron pathway leads to generation of hydrazine and diazene, accordingly, by the following reactions [50]:

$$Hydrazine: N_2 + 2H^+ + 4e^- \rightarrow N_2H_4 \tag{1.12}$$

$$Diazene: N_2 + 2H + 2e^- \rightarrow N_2H_2 \tag{1.13}$$

Yet, as both reactions have a highly negative potentials which are equaled to −0.36 V and −1.10 V vs NHE, respectively, it means that they are thermodynamically less favored compared with that of six-electron assisted reaction [56], and thus their occurrence as final products is only possible under extremely non-equilibrium conditions. However, these intermediates are part of proton-coupled transferred mechanism since the formation of NH_3 occurs through them. In turn, the initial step for triggering actual nitrogen fixation is the transfer of the very first electron toward the adsorbed N_2 ad-molecule which resigned on the surface of catalyst [56]. It occurs even in the absence of required proton. The following reactions along with their onset potentials were proposed to describe this process [50]:

$$N_2 + e^- \rightarrow N_2 \quad E^O(V) \text{ vs NHE} - 4.16\,V \tag{1.14}$$

$$N_2 + H^+ + e^- \rightarrow NH_2 \quad E^O(V) \text{ vs NHE is} - 3.2\,V \tag{1.15}$$

As can be seen, highly negative potentials make them very difficult to proceed as large energetic barrier should be overstepped for initiation. Based on this, it was considered that these reactions hamper the overall kinetics of N_2 photocatalytic reduction as in addition to mentioned issues, it is also highly difficult to find the materials whose conduction band would match it.

Depending on different hydrogenation (protonation and reduction) and nitrogen bond cleavage sequences, generally, two types of nitrogen fixation mechanisms are proposed [56]: (i) the dissociative route and (ii) the associative route. In the dissociative route, dinitrogen firstly become adsorbed on the surface of target material followed by nitrogen bond cleavage, leaving two adsorbed N-adatoms, which then are evolved into hydrogenation independently and consequently are released from the catalyst in the form of NH_3. It has to be mentioned that this pathway is more appropriate to electrocatalytic process than the one initiated by irradiation with solar light. As for the associative route, nitrogen bond cleavage and hydrogenation reaction occur simultaneously. Since end-on coordination scheme is by far the most common bonding mode [57] which represents that only single N atom in the dinitrogen molecule interacts with the surface of catalyst, it might be suggested that the association pathway is a more preferable route for photocatalytic reaction. In addition, it can be further categorized into two courses which are called as distal and alternating pathways [58]. In the former one, the proton/election compound is going to reach one of N atoms in the adsorbed dinitrogen molecule and results in full cleavage of the N-N bond followed by release of NH_3. Thus, another N-adatom is left on the surface of the catalyst. It is also hydrogenated subsequently in the latter step. In turn, the alternating pathway results in simultaneous reactions of both nitrogen atoms with respective proton/election compounds, and only after that N-N bond become broken. Then the reduced species are released from the surface of catalyst as separate product. Schematically, these types of photocatalytic nitrogen fixation are shown in Fig. 1.4b.

Unmodified semiconductors with original structurers and properties could hardly meet the standards for correct realization of photocatalytic nitrogen fixation process, given that the position of their conduction band can scarcely reach the negative potentials of solvated dinitrogen anions whose formation is contributed to the N_2 reduction. Another problem is that rarely avoidable recombination of photo-induced charge carriers might become the reasons that a number of available electrons which arrive to the surface simply would not be enough to initiate the hydrogenation of N_2 via six-electron mechanism. Other problems such as insufficient accessibility of favorable spots on the surface where N_2 molecule can be adsorbed or wide band gap of semiconductor photocatalyst and thus limited option of using only UV light also might become a crucial issue in the search for an appropriate material. However, even though proper compounds could finally be synthesized and effectively used, transforming this discovery into successful industrial application might become a nontrivial task given the questions of their abundance, production and utilization cost, chemical stability, and environmentally safety. Thus, to meet all these requirements and to create adequate photocatalytic materials for solar light assisted N_2 fixation, numerous efforts have been applied to properly modify and adjust already existed traditional semiconductors in terms of their electronic, structural, optical, etc. compositions using well-known and widely applied procedures such as doping with metal and non-metal, formation of vacancies, and assemblance with other materials including noble and transitional metals.

Several prominent examples of certain photocatalytic semiconductors adopted for nitrogen fixation are concisely demonstrated below. Yet, it is important to notice that deeper discussion regarding the exact and precise classification regarding the types of applied materials, their elemental composition and diversity of modified geometrical and electronic configurations, as well as detailed description of some specific particularities and features along with identification of clear and individual strategies for their further improvement and advancement is beyond the scope of this chapter as its goal is only to briefly overview photocatalytic nitrogen fixation and its current progress. Interesting readers are asked to search specialized literature such as Ref. [50], for example.

TiO_2-based materials TiO_2 can easily perform the oxidation of water resulting in efficient delivery of proton toward adsorbed N_2 for activating the reduction reaction. Yet, its outcome is considered to be extremely low as TiO_2 suffers from high recombination rate and could only absorb UV light which limits the number of captured photons. Several strategies are applied to make this material become more suitable for N_2 fixation process. For example, it was stated that formation of defects on the surface leads to increased adsorption of N_2 molecules [59], while doping with Fe and Cr results in highly enhanced separation rate of photo-induced charge carriers as iron ions enable the trapping of electrons, while chromium atoms lead to decreased diffusion lengths of minority carriers [60, 61]. These changes have been found to have a profound influence in increasing the overall N_2 reduction efficiency. In turn, similar to Fe, incorporation of other elements such as Co, Mo, Ce, and Ni and also specifically tuned V into TiO_2 was discovered to have highly positive effect

on the light-induced formation of NH_3, while the influence of Cr, Pd, and Cu doping was demonstrated to be less significant [62, 63]. Moreover, noble metal loading including Ru, Pt, and Rh can also be considered as attractive strategy to enhance the productivity toward N reduction as they are able to eject additional electrons into conduction band of TiO_2 [64].

Alternative binary metals Apart from TiO_2, other metal oxide compounds such as iron oxide, tungsten oxide, and zinc oxide [50] also have been studied extensively even though the progress toward their successful realization as an efficient photocatalyst is less prominent than that of TiO_2. Iron oxide originally is unable to show any activity toward light-induced nitrogen fixation, while it is one of the best compounds to be used in the abovementioned Haber-Bosch synthesis. Yet, in combination with other materials such as loading on porous g-C_3N_4 [65] or due to self-modification into amorphous form [66], it could achieve very sufficient photoactivity toward reduction of N_2 under simulated solar and visible lights, respectively. Another discovery regarding iron oxide was made by Khader et al. [67] who successfully prepared a mixture of α-Fe_2O_3 and Fe_3O_4 (90% vs 10%) and demonstrated its effective application to reach continuous production of ammonia for about 580 h under illumination of light with energy greater than 2.3 eV. Tungsten oxide is also actively used for photocatalytic fixation of N_2. For example, Li et al. [68] reported that carbon-tungstic-acid hybrids in the form of C-WO_3-H_2O enable to show significant performance toward generation of NH_3 under irradiation with Xe lamp. It was stated that photoactive $WO_3 \cdot H_2O$ guaranteed the supply of electrons and protons for subsequent hydrogenation, while presence of carbon atoms in this hybrid resulted in strengthening of reduction reaction. In turn, it was reported [69] that introduction of Mo species into defect-rich $W_{18}O_{49}$ ultrathin nanowires can be considered as an excellent approach for extending photocatalytic production of ammonia. The observed Mo-W centers serve as active sites for chemisorbing N_2 molecules. At the same time, the enhanced metal-oxygen covalency in lattice of this photocatalyst activates the electron transfer. In turn, doped Mo species elevate the defect band center toward the Fermi level securing more energy in terms of photoexcited electrons which can be further used for reduction reaction.

Overall, it has to be noticed that even though great and really impressive progress is reached toward developing a suitable compound to serve for photocatalytic N_2 reduction, the demonstrated NH_3 conversion efficiency is still extremely low and cannot be viewed for any practical application yet. To be clear, current production is estimated in terms of "mmol/g," while for any serious consideration, it should become at least "mol/g." Thus, the present goal is to make the photocatalytic yield reaching the minimum required level which might provide some hope that this process would have perspectives to be adopted for industrial facilities. In such course of action, it might speed up the progress of improving its practical reliability and accessibility. Hence, it is important to continuously apply all current efforts in reaching it through further development of appropriate and correct semiconductor materials with required band-gap value, position, and stability. Overall, there is a strong belief that solar energy conversion of nitrogen might initiate a revolution of

renewable and sustainable energy sector which can bring numerous benefits to the present environmental and economic situation around the globe.

1.6 Other Photocatalytic Reactions

Apart from the abovementioned well-known photocatalytic reactions whose wide investigation deserved numerous attentions in literature, there exist other less studied but nevertheless also highly important light-induced processes which deserved to be mentioned and discussed briefly.

1.6.1 Photocatalytic Reduction of Cr (VI)

Hexavalent chromium known as Cr (VI) is extensively applied in various industrial applications such as pigmenting, metal plating, and leather tanning [70]. Yet, there is a huge concern that their realization might result in appearance of liquid waste whose inappropriate processing and inadequate storage make possible the development of unexpected leakages thus leading to heavy chromium contamination of nearby soil, ground, and surface waters [71]. As hexavalent chromium is determined to be one of the most dangerous pollutants due to its high toxicity to humans, animals, and plants, there is an urgent need in proper treatment of this compound via environmentally friendly, affordable, and cost-effective strategy as existing methods such as chemical precipitation, ion exchange, filtration, etc. suffer from low effectiveness, complexity of the operation procedures, and high cost.

In this regard, photocatalytic reduction attracts serious interest among the scientific community as it only requires utilization of solar light to drive the reaction, hence, can be considered as highly accessible approach. To proceed it, the conduction band of applied semiconductors is required to be located more negatively than the reduction potential of Cr (VI) which however is not easy to be identified as it has clear dependency on the acidity or basicity of an aqueous solution. At pH value less than 2.0, Cr (VI) existed as H_2CrO_4, while higher pH results in its transformation into CrO_4 structure. Potentials for both compounds were identified as ~1.35 V vs. NHE and −0.13 V vs. NHE, respectively [72] (Fig. 1.5a, b). Thus, the reduction of Cr (VI) can be proceeded by one of both pathways (Eqs. 1.16 and 1.17) depending on the conditions of surrounding aqueous media [71]:

$$Low\ pH: \mathrm{HCrO_4^-} + 7\mathrm{H^+} + 3\mathrm{e^-} \rightarrow \mathrm{Cr^{3+}} + 4\mathrm{H_2O} \tag{1.16}$$

$$High\ pH: \mathrm{CrO_4^{2-}} + 4\mathrm{H_2O} + 3\mathrm{e} \rightarrow \mathrm{Cr(OH)_3} + 5\mathrm{OH^-} \tag{1.17}$$

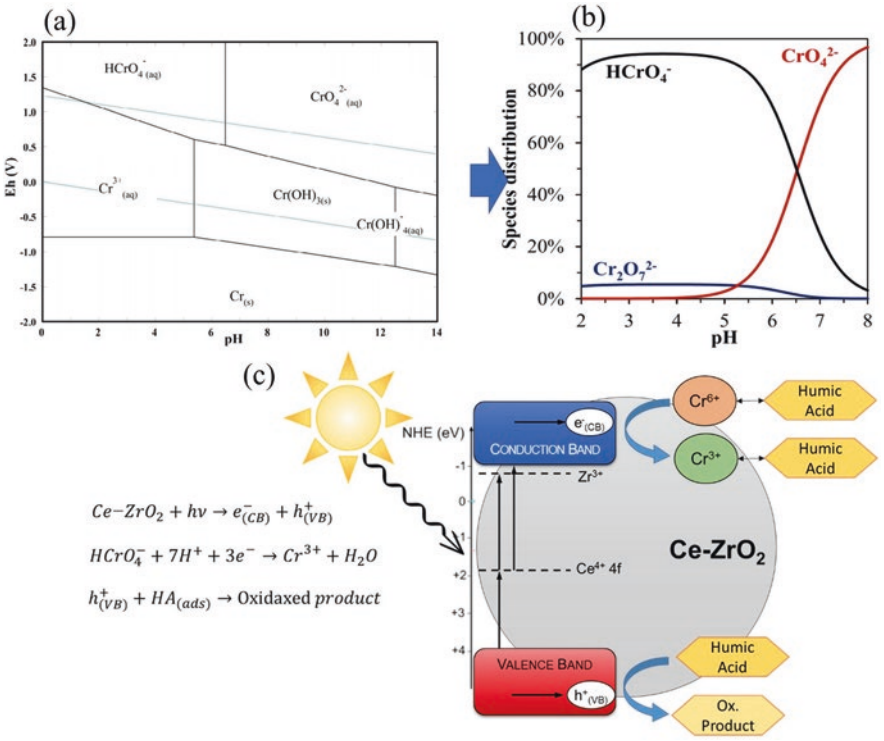

Fig. 1.5 (**a**) Potential with respect to the standard hydrogen electrode versus pH diagram of Cr-H_2O system at 25 °C, (**b**) Cr (VI) species distribution diagram, and (**c**) proposed mechanism for the photocatalytic reduction of Cr (VI) in the presence of humic acid using Ce-ZrO_2 catalyst under visible light irradiation. (Reprinted from Ref. [71]. Copyright 2018 MDPI. Available under the Creative Commons Attribution 4.0 Generic License, https://creativecommons.org/licenses/by/4.0/)

It has to be noticed that Cr (VI) photocatalytic reduction is controlled by a surface-reaction step which means that lowering the pH favors the adsorption and consequent activation of this compound. Yet, certain photocatalytic materials at these conditions show degradation of their intrinsic properties which might neutralize all advantages of low pH. For example, TiO_2 at extreme acidic conditions has accumulation of positive charges on its surface which recombines with photogenerated electrons resulting in almost complete absence of charge carriers that disable the reduction of Cr (VI) [73]. In addition, as can be seen from the above, this reaction also involves proton-coupled electron transfer mechanism similar to that observed in previously discussed photocatalytic processing. The presence of H^+ is usually achieved via water oxidation reaction whose realization is determined by photogenerated holes residing in the valence band. In turn, the electrons located in the conduction band participate in the reduction process. Comparing both half reactions, which occurred during the photocatalytic conversion of Cr (VI) in water in the absence of any additional hole scavengers, water oxidation is regarded as a more

complicated process that involves four-electron transfer, while reduction is limited by three-electron processing, and thus the former is considered as rate determining step. In this regard, to increase the efficiency of the photocatalytic reduction of Cr (VI) in water, certain organic compounds are added to serve as hole scavengers.

Various materials were reported to be applied for degrading this harmful compound including well-known oxides such as CdS, ZnS, WO_3, TiO_2, ZnO, and ZrSe. Each of them has its own kinetics and specification which influence the proceeding of reaction, its outcome, and, most importantly, efficiency.

Titanium dioxide TiO_2 was considered to be one of the most intensively studied catalyses given its abundance, availability, and environmental friendliness. It is suitable for water oxidation, yet given the position of its conduction band which is located at −0.42 V vs NHE, reduction of Cr (VI) can only be activated at the neutral conditions [71]. Even though the potential of this harmful compound in theory can be shifted to more positive values via introduction of highly acidic conditions, the advantage of this step might simply be neglected by largely reduced charge transfer characteristics of TiO_2 as it was mentioned above. In addition, low photocorrosion results in significant shortening of the operation time. Furthermore, holes which were not consumed during water oxidation likely cause the formation of $OH^{\bullet}$ radicals on the surface of TiO_2 and assist in oxidation of Cr (III) back to Cr (VI), thus hampering the overall conversion efficiency. Another problem which should be faced is that this material is mostly activated by UV light given its wide band gap which limits the concentration of photo-induced carriers. Various approaches can be applied to solve these problems. For example, combining TiO_2 with other materials, such as titanite nanotubes results in increasing rate of Cr (VI) reduction up to 50% [74], while coupling with noble metals such as Ag greatly benefits charge separation efficiency and shifts the absorption of light toward visible spectra. Furthermore, it was reported that Ag-TiO_2 enable to achieve the processing of this photocatalytic reaction even in dark conditions [75].

Ce-doped zirconium oxide The advantage of this material compared with TiO_2 is that it might be activated under visible light and thus enable to access solar spectra. Also, it has a great stability toward acidic conditions and thus can be easily applied at pH values lower than two [71]. Given that Cr (VI) at these conditions exist in the form of $HCrO_4^-$, which has a higher reduction potential and can be less repulsed by zirconia surface, it results in great conversion efficiency. Furthermore, immobilization of this photocatalyst on SiC support as well as addition of electron-reach humic acid (HA) into aqueous solution could be used to further extend the performance of Zr-based catalyst. For example, it was reported that 36% of Cr (VI) was reduced to Cr (III) in the presence of HA, whereas this value reaches only 25% without HA. It was explained by scavenging holes on VB via HA-related mechanism (Fig. 1.5c) [71].

Carbon nitride This material is able to absorb visible light given its band gap of 2.7 eV and suitable position of conduction band, yet it has low productivity for Cr (VI) reduction due to very fast recombination of photogenerated electrons and holes and other less discussed problems. Various approaches are applied to solve this

problem and extend the photocatalytic efficiency further such as soaking of g-C_3N_4 in HNO_3 or HCl aqueous solution [76]. It resulted in larger specific surface area and appearance of positive surface charges which contribute to water oxidation and higher adsorption capacities for Cr (VI). Another approach to improve the efficiency of C_3N_4 was demonstrated by Dong et al. [77] via self-doping mechanism.

1.6.2 Photocatalytic Reduction of Other Toxic and Nontoxic Metals

There are numerous hazardous metallic compounds which can be found in wastewater such as silver Ag(I), copper Cu (II), mercury Hg (II), uranium U (VI), and Zn (II). As reported by Wahyuni and Aprilita [78], (1) silver contamination might be due to its usage in the electronic industry; (2) copper is caused by disposal from electroplating and electrical stuffs; (3) mercury originated by gold recovery and incinerator in hospitals; (4) uranium purification or extraction from its respected mineral leads to appearance of uranium (VI) ion; and (5) the detection of zinc metals in wastewater can be explained by its usage in various types of industries such as mining and coal and waste combustion processing not mentioning nanoscale technologies and devices.

It was reported that common photocatalyst such as TiO_2 can effectively reduce those metals by transforming into less harmful compounds via the following reactions [78]:

$$Ag^{+} + e^{-} \rightarrow Ag^{0} \qquad E^{0} = 0.79\,V \tag{1.18}$$

$$Cu^{2+} + e^{-} \rightarrow Cu^{+} \text{ or } Cu^{2+} + 2e^{-} \rightarrow Cu^{0} \qquad E^{0} = 0.153\,V \text{ vs.} E^{0} = 0.34\,V \tag{1.19}$$

$$H_g^{2+} + 2e^{-} \rightarrow Hg^{0} \qquad E^{0} = 0.85\,V \tag{1.20}$$

$$UO_2^{2+} + e^{-} \rightarrow UO^{+} \qquad E^{0} = 0.63\,V \tag{1.21}$$

$$Zn^{2+} + 2e^{-} \rightarrow Zn^{0} \qquad E^{0} = 0.76\,V \tag{1.22}$$

It has to be noticed that reduction reaction activated by light irradiation also can be used to deposit the target metal compound on the specific substrates. For example, chemical-based formation of noble metal nanoparticles, especially platinum, and their consequent light-supported loading on semiconductor surfaces is an established practice in photocatalysis. In turn, preparation of catalytically active non-precious metal nanoparticles via photo-reduction also became possible recently. As an illustration, it was demonstrated that TiO_2 could effectively transform $CuSO_4$ into well-dispersed Cu_2O or Cu nanoparticles with highly defined sizes using only visible light [79].

1.6.3 Photocatalytic Hydrogen Peroxide Production

Hydrogen peroxide (H_2O_2) is one of the most demanded and utilized chemicals around the world as it is very efficient in assisting in development of various chemical reactions and processes and has one of the highest contents of active oxygen. Oxidation of anthraquinone (AQ) is the major process used for industrial-based production of H_2O_2. Yet it requires the application of complex multi-step reactions accompanied by large supply of energy and also creates a lot of wastewater and solid compounds followed by generation of exhaust gases negatively affecting Mother Nature. Thus, an alternative to this processing is in high demand. Most recently, photocatalytically activated production of H_2O_2 has been receiving certain attention among scientists as it allows to avoid the use of explosive H_2 and only requires the application of water and O_2 as starting materials, while the energy to initiate necessary reactions can be supplied by sunlight. Most importantly, any pollutions are completely absent during the overall process.

Typically, reactions on the surface of photocatalysts include several steps which mostly are similar to other types of light-induced processes and briefly described as follows: (1) absorption of photons with energy equaled or higher than band gap of semiconductor materials used as catalyst and consequent generation of photo-induced charge carriers; (2) their transport to the surface; and (3) redox reactions with adsorbed species from surrounding media. As the first two steps were discussed numerously in previous sections with certain details, here the main attention is devoted exclusively to the occurrence of the third step. The H_2O_2 photocatalytic reaction is considered to have an uphill character with a standard Gibbs free energy change of 117 kJ mol^{-1} and thus cannot occur spontaneously [80]. Its proceeding is usually realized through either an indirect sequential two-step single-electron or two-electron reduction which is developed through the formation of intermediate oxygen radical or via direct transformation of O_2 [81]. A schematic illustration of both pathways for photocatalytic H_2O_2 production is shown in Fig. 1.6a, b). As can be seen, holes residing in VB tend to advance water oxidation, while electrons from CB are responsible for the reaction with adsorbed O_2 to generate the final produce of H_2O_2.

For more concrete and precise illustration, indirect sequential two-step single-electron pathway of reduction process is demonstrated by Eqs. (1.23, 1.24, 1.25, and 1.26), and it is described by the following sequence [82]: (1) one-electron reduction of O_2 and appearance of superoxide radical $O_2^{\bullet}$ (Eq. 1.23); (2) $O_2^{\bullet}$ reacts with H^+ to become reconstructed into $HO_2^{\bullet-}$ radical (Eq. 1.24); (3) this radical is subjected to the second one-electron reduction (Eq. 1.25) to become transformed into $HO_2^{\bullet}$; and (4) its reaction with H^+ to form the final product of H_2O_2 via Eq. (1.26). In turn, one step two-electron process is described by only single transformation (Eq. 1.27) as O_2 directly reacts with two H^+ for the conversion into H_2O_2 [82]. It was demonstrated that out of two pathways, the one-electron route has negative effect on efficiency of H_2O_2 production, thus, two-electron route is more preferential [81].

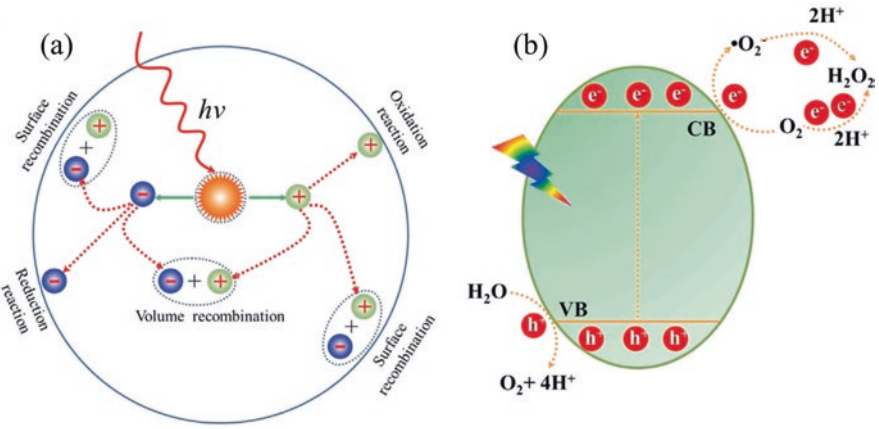

Fig. 1.6 (**a**) Photoexcitation and charge-decay pathway in a photocatalyst. (**b**) Schematic representation of the photocatalytic system for the production of H_2O_2. (Reprinted from Ref. [82] with permission from *John Wiley and Sons*. Copyright 2019)

$$One \quad electron\,route: \qquad O_2 + e^- \rightarrow O_2^{\bullet} \tag{1.23}$$

$$O_2^{\bullet} + H^+ \rightarrow HO_2 \tag{1.24}$$

$$HO_2 + e^- \rightarrow HO_2^{\bullet} \tag{1.25}$$

$$HO_2^{\bullet} + H^+ \rightarrow H_2O_2 \tag{1.26}$$

$$Two \quad electrons\,route: \qquad O_2 + 2H^+ + 2e^- \rightarrow H_2O_2 \tag{1.27}$$

As the photocatalytic H_2O_2 production meets almost the same challenges and problematic issues as other related processes such as photoreduction of CO_2 or solar water splitting, relatively similar approaches are applied to increase the performance of utilized catalytic materials whose range include but not limited to the following semiconductors: TiO_2, g-C_3N_4, metal-organic compounds, etc. Overall, the greatest attention is granted to the next strategies: (1) modification of morphology and structure in terms of introducing various types of defects including vacancies and interstitials. It influences positively charge recombination rate as presence of intrinsic imperfections results in higher capability to separately trap photo-induced electrons and holes and tune their diffusion lengths. Defects also can alter the energy levels of the conduction and valence bands and cause the narrowing of the band-gap energy, thereby leading to the extended absorption of visible light. (2) Formation of various complexes based on mesoporous or hierarchical 1D/3D composition enables to increase specific surface area and improve scattering of light photons to make them become easily trapped within these structures. (3) Loading with noble metal nanoparticles enables to improve charge carrier transportation, enhancing optical characteristics, and also suppress the decomposition of H_2O_2. In addition, utilization

of this architecture also might lead to appearance of surface plasmon resonance effect which highly contributes to the enhanced efficiency of photocatalytic processing. (4) Doping with metal and non-metal compounds which is an excellent tool to improve the charge carrier mobility and concentration, tune the position of both CB and VB in a similar manner to that realized by intrinsic defects, or adjust inner electronic structure to make it become more suitable for oxidation and reduction reactions.

Although some very promising and intriguing results have been demonstrated, the overall efficiency of H_2O_2 photocatalytic production is still extremely low and cannot satisfy even the most basic requirements and precondition of industrially approved practical applications. Thus, it is required to expand further continuous adjustment and improvement of this process since its improvement could be achieved only by developing a proper and suitable catalyst able to overcome all difficulties and drawbacks. It is expected that efficient photocatalytic formation of H_2O_2 in the nearest future might become more than just a far-reaching dream and would be transformed into something real and concrete.

1.6.4 Biomass Treatment: Photocatalytic Oxidation of Glucose

The transformation of renewable biomass into useful chemicals has received great attention in recent years since it can be considered as an attractive alternative to the utilization of various fossil fuel-based processes. For example, glucose as the main component of biomass can be selectively oxidized into carboxylic acids such as glucaric acid, gluconic acid, levulinic acid, etc. This reaction is especially attractive since these products can be applied in certain industries. Apart from well-known chemical transformation used for this reaction, it was reported recently that it could also be accessed via route of photocatalytic process. For example, recently, Iervolino et al. [83] demonstrated that light-induced conversion of glucose into hydrogen fuel can be realized in aqueous solution through employment of TiO_2 particles modified by simultaneous presence of fluorine and platinum. The only disadvantage of using this compound is that it requires prevailed use of UV-light source to initiate the reaction given the wide band gap of TiO_2. In this regard, Cheng et al. [84] reported that by applying ZnO/CoPzS8 composite, it was possible to achieve photocatalytic oxidation of glucose in pure water under simulated sunlight irradiation without adding any acid or base. The following value-added chemicals were detected as result of this reaction: gluconic acid, arabinose, glycerol, and formic acid. As a final word, it is believed that employment of green photocatalytic process for transforming cheap and abundant biomass feedstocks, in this case glucose, into value-added chemicals is a very promising pathway. Yet, the same problem as for other photocatalysis also is raised here: low conversion efficiency and insufficient selectivity. Thus, continuous efforts are in need to further extend present knowledge regarding this reaction.

1.6.5 Several More Examples of Photocatalytic Reactions

Overall, it has to be noticed that various photocatalytic processes are presented in the literature regarding transformation of certain chemicals into desired compounds. Below, only some of most prominent examples are mentioned since it is impossible to cover them all at a satisfied depth. Given that this chapter only serves as introductory to this topic, interesting readers are suggested to address specific literature for more precise details.

1. Methane can be converted by photocatalytic steam reforming to hydrogen following the reaction of $CH_4 + 2H_2O \rightarrow 4H_2 + CO_2$ or can undergo photocatalytic total oxidation in the form of $CH_4 + 2O_2 \rightarrow CO_2 + 2H_2O$ [85].
2. Photocatalytic reduction of nitrobenzene *to aniline* was reported by Jensen et al. [86] who demonstrated that this process can be realized under visible light irradiation using CdS quantum dots. Yet, it requires six sequential photo-induced proton-coupled electron transfers which makes it rather complicated and thermodynamically demanded.
3. The photocatalytic reduction of nitrous oxide is commonly proceeded via various transition- and noble-metal-exchanged zeolites such as the ones filled with Co, Pr, Fe, Cu, and Ag ions given their high reactivities [87].

1.7 Final Remarks on Photocatalysis

Solar irradiation provides access to extremely clean, abundant, endless, and renewable source of energy that meets current criteria and needs of human society development. To convert this energy into useful outcome which can be applied in various demanding processes, the proper materials which serve as photocatalyst are required to be used. Thus, it became possible to catch, convert, and utilize this enormous photon-based energy in the way and direction following the desirable goal. For example, sunlight allows to reach dissolution of harmful CO_2, production of hydrogen fuel, and removal of harmful, dangerous, and toxic pollutants from water, to convert certain chemicals into more valuable and wanted compounds. It is believed that in the far perspective, the chemical industry might become a more environmentally friendly sector and would not cost so harm to our planet as most of the processes in their facilities could be realized via exposing certain setup and aqueous media under the sun and simply awaiting the result. It is very attractive and bright future as photocatalytic-based technology are only in child-birth age which might be the reason why light-induced conversion efficiency is still too low to be considered seriously. Yet, 40 years ago, no one could even consider that these reactions are possible. Thus, it is only in our hands to make the reality that we want to be part of our coming future.

References

1. Z. Long, Q. Li, T. Wei, G. Zhang, Z. Ren, Historical development and prospects of photocatalysts for pollutant removal in water. J. Hazard. Mater. **395**, 122599 (2020). https://doi.org/10.1016/j.jhazmat.2020.122599
2. D. Sudha, P. Sivakumar, Review on the photocatalytic activity of various composite catalysts. Chem. Eng. Process. **97**, 112–133 (2015). https://doi.org/10.1016/j.cep.2015.08.006
3. J. He, C. Janáky, Recent advances in solar-driven carbon dioxide conversion: Expectations versus reality. ACS Energy Lett. **5**, 1996–2014 (2020). https://doi.org/10.1021/acsenergylett.0c00645
4. R. Shi, Y. Zhao, G.I.N. Waterhouse, S. Zhang, T. Zhang, Defect engineering in photocatalytic nitrogen fixation. ACS Catal. **9**, 9739–9750 (2019). https://doi.org/10.1021/acscatal.9b03246
5. A. Ajmal, I. Majeed, R.N. Malik, H. Idriss, M.A. Nadeem, Principles and mechanisms of photocatalytic dye degradation on TiO_2 based photocatalysts: A comparative overview. RSC Adv. **4**, 37003–37026 (2014). https://doi.org/10.1039/C4RA06658H
6. H. Park, H. Kim, G. Moon, W. Choi, Photoinduced charge transfer processes in solar photocatalysis based on modified TiO_2. Energy Environ. Sci. **9**, 411–433 (2016). https://doi.org/10.1039/C5EE02575C
7. W. Kim, T. Tachikawa, G. Moon, T. Majima, W. Choi, Molecular-level understanding of the photocatalytic activity difference between anatase and rutile nanoparticles. Angew. Chem. Int. Ed. **53**, 14036–14041 (2014). https://doi.org/10.1002/anie.201406625
8. A. Touati, L. Jlaiel, W. Najjar, S. Sayadi, Photocatalytic degradation of sulfur black dye over Ce-TiO_2 under UV irradiation: Removal efficiency and identification of degraded species. Euro-Mediterr. J. Environ. Integr. **4**, 4 (2019). https://doi.org/10.1007/s41207-018-0086-5
9. X. Li, J. Yu, M. Jaroniec, Hierarchical photocatalysts. Chem. Soc. Rev. **45**, 2603–2636 (2016). https://doi.org/10.1039/C5CS00838G
10. C.M. Wang, A. Heller, H. Gerischer, Palladium catalysis of O_2 reduction by electrons accumulated on TiO_2 particles during photoassisted oxidation of organic compounds. J. Am. Chem. Soc. **114**, 5230–5234 (1992). https://doi.org/10.1021/ja00039a039
11. M.A. Basith, R. Ahsan, I. Zarin, et al., Enhanced photocatalytic dye degradation and hydrogen production ability of $Bi_{25}FeO_{40}$-rGO nanocomposite and mechanism insight. Sci. Rep. **8** (2018). https://doi.org/10.1038/s41598-018-29402-w
12. V. Gurylev, C.-Y. Su, T.-P. Perng, Hydrogenated ZnO nanorods with defect-induced visible light-responsive photoelectrochemical performance. Appl. Surf. Sci. **411**, 279–284 (2017). https://doi.org/10.1016/j.apsusc.2017.03.146
13. S.G. Ullattil, S.B. Narendranath, S.C. Pillai, P. Periyat, Black TiO_2 nanomaterials: A review of recent advances. Chem. Eng. J. **343**, 708–736 (2018). https://doi.org/10.1016/j.cej.2018.01.069
14. J.C. Murillo-Sierra, A. Hernández-Ramírez, L. Hinojosa-Reyes, J.L. Guzmán-Mar, A review on the development of visible light-responsive WO_3-based photocatalysts for environmental applications. Chem. Eng. J. Adv. **5**, 100070 (2021). https://doi.org/10.1016/j.ceja.2020.100070
15. R. Abe, H. Takami, N. Murakami, B. Ohtani, Pristine simple oxides as visible light driven photocatalysts: Highly efficient decomposition of organic compounds over platinum-loaded tungsten oxide. J. Am. Chem. Soc. **130**, 7780–7781 (2008). https://doi.org/10.1021/ja800835q
16. M.A. Morales, I. Fernández-Cervantes, R. Agustín-Serrano, S. Ruíz-Salgado, M.P. Sampedro, J.L. Varela-Caselis, R. Portillo, E. Rubio, Ag_3PO_4 microcrystals with complex polyhedral morphologies diversity obtained by microwave-hydrothermal synthesis for MB degradation under sunlight. Results Phys. **12**, 1344–1356 (2019). https://doi.org/10.1016/j.rinp.2018.12.082
17. L. Zhang, H.H. Mohamed, R. Dillert, D. Bahnemann, Kinetics and mechanisms of charge transfer processes in photocatalytic systems: A review. J. Photochem. Photobiol. C **13**, 263–276 (2012). https://doi.org/10.1016/j.jphotochemrev.2012.07.002
18. N. Serpone, D. Lawless, R. Khairutdinov, E. Pelizzetti, Subnanosecond relaxation dynamics in TiO_2 colloidal sols (particle sizes Rp = 1.0-13.4 nm). Relevance to heterogeneous photocatalysis. J. Phys. Chem. **99**, 16655–16661 (1995). https://doi.org/10.1021/j100045a027.W

19. H. Yu, X. Huang, P. Wang, J. Yu, Enhanced photoinduced-stability and photocatalytic activity of CdS by dual amorphous cocatalysts: Synergistic effect of Ti(IV)-hole cocatalyst and Ni(II)-electron cocatalyst. J. Phys. Chem. C **120**, 3722–3730 (2016). https://doi.org/10.1021/acs.jpcc.6b00126
20. C.-L. Huang, W.-L. Weng, Y.-S. Huang, C.-N. Liao, Enhanced photolysis stability of Cu_2O grown on Cu nanowires with nanoscale twin boundaries. Nanoscale **11**, 13709–13713 (2019). https://doi.org/10.1039/C9NR01406C
21. S. Chen, T. Takata, K. Domen, Particulate photocatalysts for overall water splitting. Nat. Rev. Mater. **17**, 17050 (2017). https://doi.org/10.1038/natrevmats.2017.50
22. N. Fajrina, M. Tahir, A critical review in strategies to improve photocatalytic water splitting towards hydrogen production. Int. J. Hydrog. Energy **44**, 540–577 (2019). https://doi.org/10.1016/j.ijhydene.2018.10.200
23. Y. Surendranath, D.G. Nocera, Oxygen evolution reaction chemistry of oxide-based electrodes, in *Progress in Inorganic Chemistry*, (Wiley, 2011), pp. 505–560. https://doi.org/10.1002/9781118148235.ch9
24. X. Hu, X. Tian, Y.-W. Lin, Z. Wang, Nickel foam and stainless steel mesh as electrocatalysts for hydrogen evolution reaction, oxygen evolution reaction and overall water splitting in alkaline media. RSC Adv. **9**, 31563–31571 (2019). https://doi.org/10.1039/C9RA07258F
25. Q. Wang, K. Domen, Particulate photocatalysts for light-driven water splitting: Mechanisms, challenges, and design strategies. Chem. Rev. **120**, 919–985 (2020)
26. Y. He, J.E. Thorne, C.H. Wu, P. Ma, C. Du, Q. Dong, J. Guo, D. Wang, What limits the performance of Ta_3N_5 for solar water splitting? Chem **1**, 640–655 (2016). https://doi.org/10.1016/j.chempr.2016.09.006
27. H. Wu, H.L. Tan, C.Y. Toe, J. Scott, L. Wang, R. Amal, Y.H. Ng, Photocatalytic and photoelectrochemical systems: Similarities and differences. Adv. Mater. **32**, 1904717 (2020). https://doi.org/10.1002/adma.201904717
28. X. Wu, G.Q. (Max) Lu, L. Wang, Shell-in-shell TiO_2 hollow spheres synthesized by one-pot hydrothermal method for dye-sensitized solar cell application. Energy Environ. Sci. **4**, 3565–3572 (2011). https://doi.org/10.1039/C0EE00727G
29. G. Ma, T. Hisatomi, K. Domen, Semiconductors for photocatalytic and photoelectrochemical solar water splitting, in *From Molecules to Materials: Pathways to Artificial Photosynthesis*, ed. by E. A. Rozhkova, K. Ariga, (Springer International Publishing, Cham, 2015), pp. 1–56. https://doi.org/10.1007/978-3-319-13800-8_1
30. W.-P. Hsu, M. Mishra, W.-S. Liu, C.-Y. Su, T.-P. Perng, Fabrication of direct Z-scheme Ta_3N_5-$WO_{2.72}$ film heterojunction photocatalyst for enhanced hydrogen evolution. Appl. Catal. B Environ. **201**, 511–517 (2017). https://doi.org/10.1016/j.apcatb.2016.08.060
31. J. Liu, B. Cheng, J. Yu, A new understanding of the photocatalytic mechanism of the direct Z-scheme g-C_3N_4/TiO_2 heterostructure. Phys. Chem. Chem. Phys. **18**, 31175–31183 (2016). https://doi.org/10.1039/C6CP06147H
32. L. Liao, Q. Zhang, Z. Su, Z. Zhao, Y. Wang, Y. Li, X. Lu, D. Wei, G. Feng, Q. Yu, X. Cai, J. Zhao, Z. Ren, H. Fang, F. Robles-Hernandez, S. Baldelli, J. Bao, Efficient solar water-splitting using a nanocrystalline CoO photocatalyst. Nat. Nanotechnol. **9**, 69–73 (2014). https://doi.org/10.1038/nnano.2013.272
33. X. Li, J. Yu, J. Low, Y. Fang, J. Xiao, X. Chen, Engineering heterogeneous semiconductors for solar water splitting. J. Mater. Chem. A **3**, 2485–2534 (2015). https://doi.org/10.1039/C4TA04461D
34. H. Shen, T. Peppel, J. Strunk, Z. Sun, Photocatalytic reduction of CO_2 by metal-free-based materials: Recent advances and future perspective. Solar RRL **4**, 1900546 (2020). https://doi.org/10.1002/solr.201900546
35. S.R. Lingampalli, M.M. Ayyub, C.N.R. Rao, Recent progress in the photocatalytic reduction of carbon dioxide. ACS Omega **2**, 2740–2748 (2017). https://doi.org/10.1021/acsomega.7b00721

36. X. Chang, T. Wang, J. Gong, CO_2 photo-reduction: Insights into CO_2 activation and reaction on surfaces of photocatalysts. Energy Environ. Sci. **9**, 2177–2196 (2016). https://doi.org/10.1039/C6EE00383D
37. N. Shehzad, M. Tahir, K. Johari, T. Murugesan, M. Hussain, A critical review on TiO_2 based photocatalytic CO_2 reduction system: Strategies to improve efficiency. J. CO2 Util. **26**, 98–122 (2018). https://doi.org/10.1016/j.jcou.2018.04.026
38. J. Hong, W. Zhang, J. Ren, R. Xu, Photocatalytic reduction of CO_2: A brief review on product analysis and systematic methods. Anal. Methods **5**, 1086–1097 (2013). https://doi.org/10.1039/C2AY26270C
39. K. Teramura, T. Tanaka, H. Ishikawa, Y. Kohno, T. Funabiki, Photocatalytic reduction of CO_2 to CO in the presence of H_2 or CH_4 as a reductant over MgO. J. Phys. Chem. B **108**, 346–354 (2004). https://doi.org/10.1021/jp0362943
40. S. Sorcar, Y. Hwang, J. Lee, H. Kim, K.M. Grimes, C.A. Grimes, J.-W. Jung, C.-H. Cho, T. Majima, M.R. Hoffmann, S.-I. In, CO_2, water, and sunlight to hydrocarbon fuels: a sustained sunlight to fuel (Joule-to-Joule) photoconversion efficiency of 1%. Energy Environ. Sci. **12**, 2685–2696 (2019). https://doi.org/10.1039/C9EE00734B
41. M.G. Walter, E.L. Warren, J.R. McKone, S.W. Boettcher, Q. Mi, E.A. Santori, N.S. Lewis, Solar water splitting cells. Chem. Rev. **110**, 6446–6473 (2010). https://doi.org/10.1021/cr1002326
42. S. Xie, Y. Wang, Q. Zhang, W. Deng, Y. Wang, MgO- and Pt-promoted TiO_2 as an efficient photocatalyst for the reduction of carbon dioxide in the presence of water. ACS Catal. **4**, 3644–3653 (2014). https://doi.org/10.1021/cs500648p
43. A. Olivo, E. Ghedini, M. Signoretto, M. Compagnoni, I. Rossetti, Liquid vs. gas phase CO_2 photoreduction process: which is the effect of the reaction medium? Energies **10**, 1394 (2017). https://doi.org/10.3390/en10091394
44. Y. Gao, K. Qian, B. Xu, Z. Li, J. Zheng, S. Zhao, F. Ding, Y. Sun, Z. Xu, Recent advances in visible-light-driven conversion of CO_2 by photocatalysts into fuels or value-added chemicals. Carbon Resour. Convers. **3**, 46–59 (2020). https://doi.org/10.1016/j.crcon.2020.02.003
45. J.-Y. Li, L. Yuan, S.-H. Li, Z.-R. Tang, Y.-J. Xu, One-dimensional copper-based heterostructures toward photo-driven reduction of CO_2 to sustainable fuels and feedstocks. J. Mater. Chem. A **7**, 8676–8689 (2019). https://doi.org/10.1039/C8TA12427B
46. A.E. Nogueira, J.A. Oliveira, G.T.S.T. da Silva, C. Ribeiro, Insights into the role of CuO in the CO_2 photoreduction process. Sci. Rep. **9**, 1316 (2019). https://doi.org/10.1038/s41598-018-36683-8
47. X. Li, Z. Zhuang, W. Li, H. Pan, Photocatalytic reduction of CO over noble metal-loaded and nitrogen-doped mesoporous TiO_2 . Appl. Catal. A Gen **429–430**, 31–38 (2012). https://doi.org/10.1016/j.apcata.2012.04.001
48. K. Xie, N. Umezawa, N. Zhang, P. Reunchan, Y. Zhang, J. Ye, Self-doped $SrTiO_{3-\delta}$ photocatalyst with enhanced activity for artificial photosynthesis under visible light. Energy Environ. Sci. **4**, 4211–4219 (2011). https://doi.org/10.1039/C1EE01594J
49. L. Liu, C. Zhao, Y. Li, Spontaneous dissociation of CO_2 to CO on defective surface of Cu(I)/TiO_{2-x} nanoparticles at room temperature. J. Phys. Chem. C **116**, 7904–7912 (2012). https://doi.org/10.1021/jp300932b
50. X. Chen, N. Li, Z. Kong, W.-J. Ong, X. Zhao, Photocatalytic fixation of nitrogen to ammonia: State-of-the-art advancements and future prospects. Mater. Horiz. **5**, 9–27 (2018). https://doi.org/10.1039/C7MH00557A
51. X. Xue, R. Chen, C. Yan, P. Zhao, Y. Hu, W. Zhang, S. Yang, Z. Jin, Review on photocatalytic and electrocatalytic artificial nitrogen fixation for ammonia synthesis at mild conditions: Advances, challenges and perspectives. Nano Res. **12**, 1229–1249 (2019). https://doi.org/10.1007/s12274-018-2268-5
52. H.-P. Jia, E.A. Quadrelli, Mechanistic aspects of dinitrogen cleavage and hydrogenation to produce ammonia in catalysis and organometallic chemistry: Relevance of metal hydride bonds and dihydrogen. Chem. Soc. Rev. **43**, 547–564 (2013). https://doi.org/10.1039/C3CS60206K

53. L. Wang, M. Xia, H. Wang, K. Huang, C. Qian, C.T. Maravelias, G.A. Ozin, Greening ammonia toward the solar ammonia refinery. Joule **2**, 1055–1074 (2018). https://doi.org/10.1016/j.joule.2018.04.017
54. A. Fujishima, K. Honda, Electrochemical photolysis of water at a semiconductor electrode. Nature **238**, 37–38 (1972). https://doi.org/10.1038/238037a0
55. M. Cheng, C. Xiao, Y. Xie, Photocatalytic nitrogen fixation: The role of defects in photocatalysts. J. Mater. Chem. A **7**, 19616–19633 (2019). https://doi.org/10.1039/C9TA06435D
56. W. Guo, K. Zhang, Z. Liang, R. Zou, Q. Xu, Electrochemical nitrogen fixation and utilization: Theories, advanced catalyst materials and system design. Chem. Soc. Rev. **48**, 5658–5716 (2019). https://doi.org/10.1039/C9CS00159J
57. C.-F. Huo, T. Zeng, Y.-W. Li, M. Beller, H. Jiao, Switching end-on into side-on C⋮N coordination: A computational approach. Organometallics **24**, 6037–6042 (2005). https://doi.org/10.1021/om0505054
58. J.S. Anderson, J. Rittle, J.C. Peters, Catalytic conversion of nitrogen to ammonia by an iron model complex. Nature **501**, 84–87 (2013). https://doi.org/10.1038/nature12435
59. H. Hirakawa, M. Hashimoto, Y. Shiraishi, T. Hirai, Photocatalytic conversion of nitrogen to ammonia with water on surface oxygen vacancies of titanium dioxide. J. Am. Chem. Soc. **139**, 10929–10936 (2017). https://doi.org/10.1021/jacs.7b06634
60. J. Soria, J.C. Conesa, V. Augugliaro, L. Palmisano, M. Schiavello, A. Sclafani, Dinitrogen photoreduction to ammonia over titanium dioxide powders doped with ferric ions. J. Phys. Chem. **95**, 274–282 (1991). https://doi.org/10.1021/j100154a052
61. L. Palmisano, V. Augugliaro, A. Sclafani, M. Schiavello, Activity of chromium-ion-doped titania for the dinitrogen photoreduction to ammonia and for the phenol photodegradation. J. Phys. Chem. **92**, 6710–6713 (1988). https://doi.org/10.1021/j100334a044
62. G.N. Schrauzer, T.D. Guth, Photolysis of water and photoreduction of nitrogen on titanium dioxide. J. Am. Chem. Soc. **99**, 7189–7193 (1977). https://doi.org/10.1021/ja00464a015
63. O.A. Ileperuma, C.T.K. Thaminimulla, W.C.B. Kiridena, Photoreduction of N_2 to NH_3 and H_2O to H_2 on metal doped TiO_2 catalysts (M = Ce, V). Sol. Energy Mater. Sol. Cells **28**, 335–343 (1993). https://doi.org/10.1016/0927-0248(93)90121-I
64. K.T. Ranjit, T.K. Varadarajan, B. Viswanathan, Photocatalytic reduction of dinitrogen to ammonia over noble-metal-loaded TiO_2. J. Photochem. Photobiol. A Chem **96**, 181–185 (1996). https://doi.org/10.1016/1010-6030(95)04290-3
65. S. Liu, S. Wang, Y. Jiang, Z. Zhao, G. Jiang, Z. Sun, Synthesis of Fe_2O_3 loaded porous g-C_3N_4 photocatalyst for photocatalytic reduction of dinitrogen to ammonia. Chem. Eng. J. **373**, 572–579 (2019). https://doi.org/10.1016/j.cej.2019.05.021
66. K. Tennakone, S. Wickramanayake, C.a.N. Fernando, O.A. Ileperuma, S. Punchihewa, Photocatalytic nitrogen reduction using visible light. J. Chem. Soc., Chem. Commun., 1078–1080 (1987). https://doi.org/10.1039/C39870001078
67. M.M. Khader, N.N. Lichtin, G.H. Vurens, M. Salmeron, G.A. Somorjai, Photoassisted catalytic dissociation of water and reduction of nitrogen to ammonia on partially reduced ferric oxide. Langmuir **3**, 303–304 (1987). https://doi.org/10.1021/la00074a028
68. X. Li, W. Wang, D. Jiang, S. Sun, L. Zhang, X. Sun, Efficient solar-driven nitrogen fixation over carbon-tungstic-acid hybrids. Chem-Eur J. **22**, 13819–13822 (2016). https://doi.org/10.1002/chem.201603277
69. N. Zhang, A. Jalil, D. Wu, S. Chen, Y. Liu, C. Gao, W. Ye, Z. Qi, H. Ju, C. Wang, X. Wu, L. Song, J. Zhu, Y. Xiong, Refining defect states in $W_{18}O_{49}$ by Mo doping: A strategy for tuning N_2 activation towards solar-driven nitrogen fixation. J. Am. Chem. Soc. **140**, 9434–9443 (2018). https://doi.org/10.1021/jacs.8b02076
70. L.B. Khalil, W.E. Mourad, M.W. Rophael, Photocatalytic reduction of environmental pollutant Cr(VI) over some semiconductors under UV/visible light illumination. Appl Catal B **17**, 267–273 (1998). https://doi.org/10.1016/S0926-3373(98)00020-4

71. F.E. Bortot Coelho, V.M. Candelario, E.M.R. Araújo, T.L.S. Miranda, G. Magnacca, Photocatalytic reduction of Cr(VI) in the presence of humic acid using Immobilized Ce–ZrO_2 under visible light. Nanomaterials (Basel) **10** (2020). https://doi.org/10.3390/nano10040779
72. Y. Liu, S. Xin, B. Jiang, The enhanced effect of oxalic acid on the electroreduction of Cr(VI) *via* formation of intermediate Cr(VI)-oxalate complex. Environ. Technol. **41**, 430–439 (2020). https://doi.org/10.1080/09593330.2018.1499815
73. Z. Zhao, H. An, J. Lin, M. Feng, V. Murugadoss, T. Ding, H. Liu, Q. Shao, X. Mai, N. Wang, H. Gu, S. Angaiah, Z. Guo, Progress on the photocatalytic reduction removal of chromium contamination. Chem. Rec. **19**, 873–882 (2019). https://doi.org/10.1002/tcr.201800153
74. W. Liu, J. Ni, X. Yin, Synergy of photocatalysis and adsorption for simultaneous removal of Cr(VI) and Cr(III) with TiO_2 and titanate nanotubes. Water Res. **53**, 12–25 (2014). https://doi.org/10.1016/j.watres.2013.12.043
75. Y. Choi, M.S. Koo, A.D. Bokare, D. Kim, D.W. Bahnemann, W. Choi, Sequential process combination of photocatalytic oxidation and dark reduction for the removal of organic pollutants and Cr(VI) using Ag/TiO_2. Environ. Sci. Technol. **51**, 3973–3981 (2017). https://doi.org/10.1021/acs.est.6b06303
76. Y. Zhang, Q. Zhang, Q. Shi, Z. Cai, Z. Yang, Acid-treated g-C_3N_4 with improved photocatalytic performance in the reduction of aqueous Cr(VI) under visible-light. Sep. Purif. Technol. **142**, 251–257 (2015). https://doi.org/10.1016/j.seppur.2014.12.041
77. G. Dong, K. Zhao, L. Zhang, Carbon self-doping induced high electronic conductivity and photoreactivity of g-C_3N_4. Chem. Commun. **48**, 6178–6180 (2012). https://doi.org/10.1039/C2CC32181E
78. E.T. Wahyuni, N.H. Aprilita, *Photoreduction Processes over TiO_2 Photocatalyst, Photocatalysts - Applications and Attributes* (2018). https://doi.org/10.5772/intechopen.80914
79. S. Cao, C.-J. Wang, G.-Q. Wang, Y. Chen, X.-J. Lv, W.-F. Fu, Visible light driven photoreduction of Cu^{2+} to Cu_2O to Cu in water for photocatalytic hydrogen production. RSC Adv. **10**, 5930–5937 (2020). https://doi.org/10.1039/C9RA09590J
80. Y. Shiraishi, T. Takii, T. Hagi, S. Mori, Y. Kofuji, Y. Kitagawa, S. Tanaka, S. Ichikawa, T. Hirai, Resorcinol–formaldehyde resins as metal-free semiconductor photocatalysts for solar-to-hydrogen peroxide energy conversion. Nat. Mater. **18**, 985–993 (2019). https://doi.org/10.1038/s41563-019-0398-0
81. Y. Sun, L. Han, P. Strasser, A comparative perspective of electrochemical and photochemical approaches for catalytic H_2O_2 production. Chem. Soc. Rev. **49**, 6605–6631 (2020). https://doi.org/10.1039/D0CS00458H
82. H. Hou, X. Zeng, X. Zhang, Production of hydrogen peroxide by photocatalytic processes. Angew. Chem. Int. Ed. **59**, 17356–17376 (2020). https://doi.org/10.1002/anie.201911609
83. G. Iervolino, V. Vaiano, J.J. Murcia, L. Rizzo, G. Ventre, G. Pepe, P. Campiglia, M.C. Hidalgo, J.A. Navío, D. Sannino, Photocatalytic hydrogen production from degradation of glucose over fluorinated and platinized TiO_2 catalysts. J. Catal. **339**, 47–56 (2016). https://doi.org/10.1016/j.jcat.2016.03.032
84. M. Cheng, Q. Zhang, C. Yang, B. Zhang, K. Deng, Photocatalytic oxidation of glucose in water to value-added chemicals by zinc oxide-supported cobalt thioporphyrazine. Cat. Sci. Technol. **9**, 6909–6919 (2019). https://doi.org/10.1039/C9CY01756A
85. X. Yu, V. De Waele, A. Löfberg, V. Ordomsky, A.Y. Khodakov, Selective photocatalytic conversion of methane into carbon monoxide over zinc-heteropolyacid-titania nanocomposites. Nat. Commun. **10**, 700 (2019). https://doi.org/10.1038/s41467-019-08525-2
86. S.C. Jensen, S. Bettis Homan, E.A. Weiss, Photocatalytic conversion of nitrobenzene to aniline through sequential proton-coupled one-electron transfers from a cadmium sulfide quantum dot. J. Am. Chem. Soc. **138**, 1591–1600 (2016). https://doi.org/10.1021/jacs.5b11353
87. W.-S. Ju, M. Matsuoka, M. Anpo, The photocatalytic reduction of nitrous oxide with propane on lead (II) ion-exchanged ZSM-5 catalysts. Catal. Lett. **71**, 91–93 (2001). https://doi.org/10.1023/A:1016612626475

Chapter 2
General Principles of Defect Engineering

2.1 Introduction

Successful implementation of photocatalyst can be realized via fulfillment of several important requirements. *Firstly*, the target material should absorb visible light to promote the formation of charge carriers, namely, electron in the conduction band and holes in the valence band as it allows to utilize photons with a wide range of energies. *Secondly*, these photo-induced charge carriers are supposed to avoid recombination with each other in order to be transferred toward the surface for activating redox reactions with outer media and their consequent processing in a smooth and efficient way. *Thirdly*, the energy position of band gap should be properly aligned with respect to potentials of each redox reaction; otherwise, they cannot be initiated. Furthermore, it is necessary to consider the problem of industrialization so that photocatalysis becomes available to mass production in order to be easily implemented in each household. In this case, the materials used for it should be cheap, environmentally friendly, abundant, chemically stable, non-hazardous, etc. Thus, it is not a trivial and simple task to find a suitable candidate which can satisfy all these conditions. For example, most semiconductors suffer from deficiency to fully utilize solar light due to broadness of their band gap, extremely high rate of electron-hole recombination rate, insufficient charge transport, poor activation capabilities toward the adsorbed molecules, and consequently low outcome of redox reactions whether oxidation or reduction type or even both in terms of their efficiencies and stabilities. To increase them, it was suggested that coupling of several materials, surface sensitization with organic dye, or decoration with noble metals can be applied. Undoubtedly, these strategies are very promising, and several quite important and distinguished milestones in photocatalytic processing have been reached via adopting them, yet, they also have some serious problems which should be considered deeply and addressed properly. *Firstly*, they are resource-dependent and could lead to risks associated with progressive exhaustion and unavailability of

V. Gurylev, *Nanostructured Photocatalyst via Defect Engineering*,
https://doi.org/10.1007/978-3-030-81911-8_2

critical elements; *secondly*, their implementation results in increased complexness of experimental procedure and consequently leads to higher production and utilization cost; and *thirdly*, given that combined materials have different chemistry and electronic and geometrical compositions, it might cause the appearance of more perplexes and knotted pathways for the redox reactions to occur as well as to bring additional difficulties in keeping them at certain desirable levels for specific duration of time. For example, noble nanoparticles during photocatalytic reaction tend to agglomerate, and thus efficiency of their usage becomes critically degraded. In this case, pure semiconductors are still considered as a more preferential choice for taking the role of optimal photocatalysts as they can be easily applied and adopted for everyday use. Yet, to practically realize their potential, it is important to seriously address most crucial drawbacks associated with their electronic structure and at the same time preserve their genuine constitution and compositions which means that their changes could be allowed to occur only within proper and designated range. Thus, it is necessary to develop a simple and effective methodology which could be used to successfully modify most demanding properties causing their enhancement regardless the nature and composition of target material.

Defect engineering can perfectly satisfy these requirements. It provides a unique opportunity to tune and modify various important features of the target material simply by adjusting its internal constitution via, for example, removal of some of its own atoms, or their replacement with newly arrived foreign elements. It results in reorganization and consequent establishment of more advanced order within internal periodic arrangement that enables to compensate the occurring changes and restore the once broken equilibrium. Thus, geometrical and electronic structures within localized areas become ultimately affected. Given the affordance and accessibility, high effectiveness, simplicity, and almost negligible impact on outer composition and morphology of target materials as most of transformations and adjustments are proceeded within the internals, this methodology is considered to be a highly promising candidate to assist in building photocatalyst with characteristics close to ideal. Yet, to be properly applied, it should be studied and addressed in the most practical and adequate way as to avoid any misconception and false interpretation and also escape "trial-and-error" pathways. And firstly, a basic understanding of various structural defects and their most fundamental characteristic is required to be apprehended.

2.2 Defect Engineering: Fundamentals

Persistent existence of various types and families of defects in materials is a very common and highly recognizable phenomenon which hardly could be escaped as ideal composition cannot exist in principle. For example, ZnO always demonstrate the presence of hydrogen impurities within its structure, and their unintentional introduction is usually associated with non-optimal conditions of synthesis or consequent treatment protocol. The same also could be referred to the constant availability of zinc and oxygen vacancies in this semiconductor as their appearances

even within the lowest limit could hardly be avoided despite using the most perfect and highly equilibrium fabrication routes. Traditionally, defects were considered as an unwanted element for photocatalytic applications since their occurrence only causes the disruption of regular periodic arrangement of crystal lattice which eventually leads to the breakage of local thermodynamic equilibrium and consequent deterioration of compositional and band structures. Thus, it is supposed to result in worsening and degradation of effective electron transport, reduced range of light absorption, chemical instability, etc. For instance, defects might act as recombination centers for charge carriers via capturing and annihilating free electrons and holes, thus sufficiently decreasing the rate of their delivery to the surface of catalyst. As a result, the number of adsorbed species which can be oxidized or reduced becomes much lower. In another example, defects can be considered as scattering centers that enable to slow down transport of charges and decrease their diffusion length. Their negative role was especially emphasized with decreasing the size and dimension of materials and approaching nanoscale level given the changes in volume-to-surface ratio. Thus, for a long time, it was commonly accepted that to increase the photocatalytic and photoelectrochemical performances of target compound, the formation of defects within its volume should be avoided at best efforts or at least decreased sufficiently. In this regard, reaching the highest perfectness of crystal lattice became an ultimate goal which was considered as an effective pathway for acquiring the desired level of light-induced activity.

However, in some cases, it appears that this strategy might not work well since numerous efforts applied in pursuing the absolute structure and improved performance often could not be associated with appearance and accessibility of required characteristics and desired features. Defects are still observed in materials at any account, and their disorganized, chaotic, and uncoordinated presence often becomes a prominent factor to camouflage most of applied efforts in achieving so awaiting perfectness. Thus, it was considered that instead of struggling with nature, it might be useful to "turn lemon into lemonade" and look deeply into "defect engineering" as an efficient tool and methodology to realize previously inaccessible yet highly solicited and appealed properties. Following this trend, recent studies provided several essential and crucial evidences to confirm the ground for this thought. The main discovery was that under certain conditions, the intentionally introduced defects, in fact, are highly expected, prominent, and necessary features in materials. To be clear, it was demonstrated that achieving precise and accurate control over their nature, concentration, distribution, transformation, and behavior is the key factor which determines the effectiveness of the concept of "defect engineering." Once applied properly and adequately, it can be used not only to greatly improve already existing properties but also to cause the appearance of new and unexpected yet highly attractive characteristics. For example, introduction of intrinsic defects in the form of surface oxygen vacancies into wide band-gap materials such as TiO_2 ($E_g \sim 3.4$ eV) or Ta_2O_5 ($E_g \sim 3.8$ eV) can greatly improves utilization of UV light and also expands the absorption edge toward visible light spectrum. In another case, correct positioning of extrinsic defects in ZnO such as hydrogen or nitrogen atoms that demonstrate donor- or acceptor-like characteristics results in advancing its electronic structure due to increased concentration and mobility of certain type of charge carriers and appearance of relevant energy levels within the band gap.

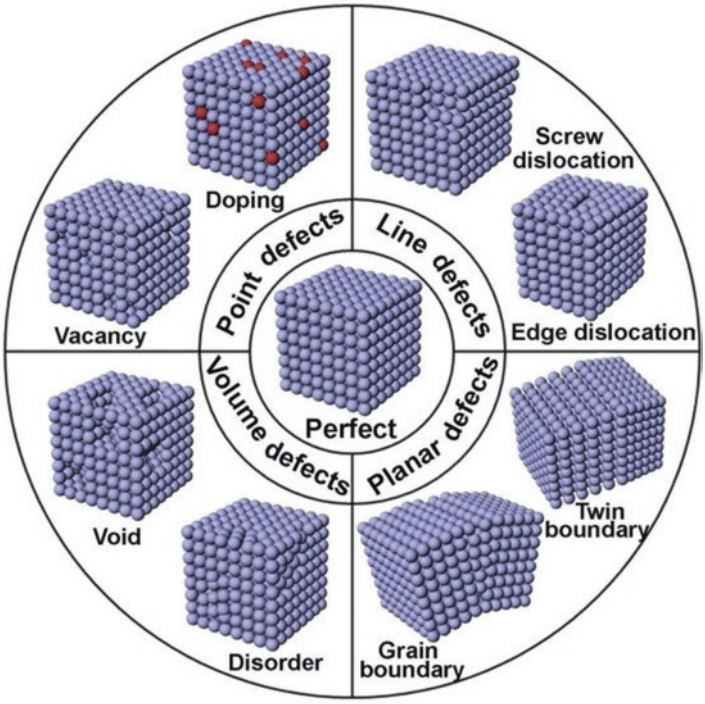

Fig. 2.1 Types of common defects in photocatalytic materials (Reprinted from Ref. [1] with permission from *Elsevier*. Copyright 2018)

Generally, defects can be classified according to their atomic structure or considering their precise and concrete localization within the semiconductor materials. Given the first description, structural imperfections and irregularities have the following categories: 0-D point defects which represent, for example, vacancies and doping; 1-D line defects which represent, for example, screw and edge dislocations; 2-D planar defects which represent, for example, twin and grain boundaries; and 3-D defects which represent, for example, lattice disorder and voids [1] (Fig. 2.1). In turn, based on the position of defects within the semiconductors, they are divided into bulk and surface defects. The latter classification is described more detailed in the next chapter.

2.3 Point Defects

2.3.1 Brief Overview

Point defects are defects whose appearances are limited by the absence of lattice extension in any direction and dimension. Their sizes have no specific definition as they are usually confined within the range of several atomic radii. These defects are

classified as intrinsic and extrinsic types where the former one is referred to deviations of the lattice structure from its ideal composition without adding any foreign atoms or ions. It categorizes as "vacancies" and "self-interstitials." In turn, extrinsic defects are generated due to the presence of impurity or intentional introduction of dopant compounds into the materials and can be divided into "substitutional type" and "interstitials type" (Fig. 2.2). Depending on the treatment method, ionic radius, electronegativity, etc., they might reside in various positions within crystal lattice causing very different influence on the properties and characteristics of the host material. It has to be noticed that, for simplicity, in this and other chapters, the word "atom" with regard to external defects would mean both neutral and ionized species. For more precise identification, the reader should follow the context.

Intrinsic Defects

Vacancies. If a particular atom has kinetic energy higher than its neighbors, it can break the potential barrier and escape position in periodic crystal which it occupies at normal conditions. The remained empty spot is called a vacancy. It is formed more easily on the surface of materials given that the atom there requires less energy to be removed due to weakened bonding. Thus, nanoscale compounds have more defects than their bulk counterparts given the differences in surface-to-volume ratio. After formation, the vacancy can move deeper inside materials due to overall diffusion of atoms toward the surface. Yet, it also can proceed in opposite direction if additional treatment is applied to the surface thus decreasing its energy and creating potential gradient toward it from bulk. Non-specified, random, and often accidental appearance of vacancies usually results in breakage of local electrical neutrality. Thus, to balance it, vacancies with opposite sign (cation or anion, depending on the type of vacancy which was introduced initially) are required to be created. This vacancy pair is called a Schottky defects (Fig. 2.2a), and their presence is a very general phenomenon for various binary semiconductors such as TiO_2, ZnO, Ta_3N_5,

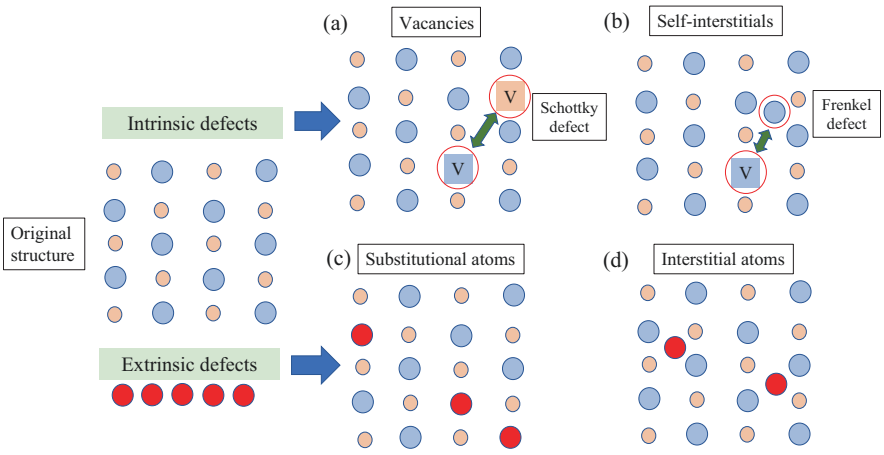

Fig. 2.2 Schematic representation of intrinsic and extrinsic types of point defects

Ta_2O_5, etc. For example, TiO_2 in neutral state has one titanium vacancy to balance two oxygen vacancies, while in the case of Cu_3N, one copper vacancy can be neutralized by consequent formation of three nitrogen vacancies. Following it, Schottky defect has no influence on the stoichiometry of the materials as the chemical balance remains the same since vacancies of both elements are created. The only outcome of this type of defects is that it decreases the density of materials due to released atoms.

Self-interstitials. When the atom resides in a random position within the crystal lattice which is normally supposed to be unoccupied and empty from any intruders, this atom is called as self-interstitial. Typically, within a close-packed solid compound, interstitial sites are small, and formation of this type of defect requires an application of larger energy than that used to make a vacancy. Yet, their appearance can be caused by similar reasons, and thus there often occurs a phenomenon that these two defects are developed simultaneously or even has a clear and distinguish connection, i.e., the same atoms which are evacuated from periodic array and leave behind a vacancy instead of escaping the materials oppositely continue its stay within the crystal lattice and instead take the interstitial position. In this case, this pair of defects, vacancy/self-interstitial, is called a Frenkel defect (Fig. 2.2b). Depending on the nature of atoms which cause such a perturbation and rearrangement of crystal lattice, the Frenkel defect can be classified as anion and cation types. To illustrate it, we can again consider TiO_2. Once the O^{2-} ion moves from a normally occupied lattice position to a vacant interstitial site, the Frenkel defect has an anion type. In turn, when the movement is realized by Ti^{4+} ions, cation Frenkel defects are formed. Finally, one should notice that self-interstitial atoms have a high mobility and can easily move around crystal lattice as what happens, for example, in the case of Ag^+ ions that can easily jump from one interstitial site to a neighboring unoccupied interstitial site [2].

Extrinsic Defects

Interstitial defect. The intrusion of external atom might lead to its residing in the interstitial site that is considered as normally unoccupied position in crystal lattice (Fig. 2.2c). To fit it, the "intruder" should be smaller in size compared with that of surrounding atoms in the host material. Given that availability of "emptiness" within crystal lattice is very limited in terms of its dimensionality, the presence of interstitials defects usually leads to certain compression and distortion of near-neighbor periodical arrays.

Substitutional defect. The formation of this defect happens once the original atom in the lattice site of a crystalline solid becomes replaced by an external atom (Fig. 2.2d). This process does not occur instantly as this particular external atom firstly is supposed to occupy any empty spots within the crystal lattice and only then to be transported around it in order to exchange its position with atom of host material. It is also often the case that the host material already has a certain presence of vacancy spots, and thus the external atom can directly reside there without extra move. This process is energetically more favorable as it does not require additional break or reforming of original bonds within the lattice. Overall, introduced external

atoms can have higher or lower radii than those of host atoms, yet it is suggested that this deviation should not exceed the difference of 30–40%. To adapt these changes, crystal lattice usually undergoes expansion or shrinkage procedure. It is necessary to mention that atoms from foreign dopant and introduced impurity can exist not only as isolated and fully independent point formation, but they also enable to interact with each other or neighboring intrinsic defects to form various perplexing complexes which can trap charges. It might lead to increasing the overall volume of available defects and their consequent transformation into enlarger planar faults and voids [3].

2.3.2 Intrinsic and Extrinsic Defects: Difference and Particularities

As mentioned above, intrinsic defects are created as a result of deviation and transformation that originally balanced and relatively perfect crystal structure undergoes due to a certain input of external energy into the system, while extrinsic defects are fully based on introduction of foreign atoms into host material and their consequent localization within regular periodic arrangement at substitutional or interstitial positions. Both types of defects are considered to have a point-like feature, and thus certain characteristics are common for them such as inability to show any extension in the lattice and spatial dimension within several atomic radius. Yet, they also demonstrate some very unique particularities which differentiate them in terms of specific influences on the structure and stoichiometry of host materials.

Intrinsic defects Formation of vacancies due to evacuation of specific type of atoms usually leads to appearance of non-stoichiometric domains within semiconductor that tends to affect the chemical composition of surrounding crystal lattice. The more vacancies are formed, the higher is the level of observed non-stoichiometry. For instance, Zhang et al. [4] discovered that by releasing oxygen atoms in ZnO, it was possible to reach the formation of ZnO_{1-x} compound where x had a clear relationship with the number of created empty vacancy spots. In addition, presence of these defects can be used to adjust the reconstruction of the surface accompanied by subsequent increase of roughness or porosity [5]. It could be explained as follows. The free energy of domain with missed atoms is different from that of neighboring fully stoichiometric lattice; thus, their appearance leads to the distortion and even breakage of localized thermodynamic equilibrium. To compensate it and to minimize the total free energy of the system, the remaining atoms are required to relax their position with respect to the newly formed vacancies and to adopt more favorable arrangement. It is usually proceeded with redistribution of mass, i.e., mass flow between surface and bulk or mass perturbations beneath the surface. The optimal reconstruction is established when the lowest surface energy is reached. In addition, the formation of vacancies also causes development of locations filled with certain disorder since the evacuation of atoms decrements the quality of crystal lattice.

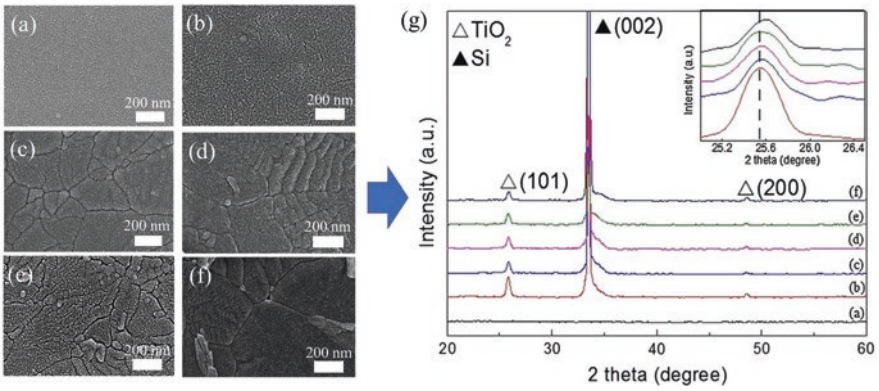

Fig. 2.3 SEM images of TiO_2 thin films deposited by ALD with thickness of ~22 nm and thermally treated in proper gaseous environment. (**a**) As-deposited, this sample is determined to be amorphous and (**b**) annealed in air at 500 C; this sample is considered to be a fully stoichiometric compound and is regarded as a standard to compare and anneal in hydrogen at (**c**) 350 °C, (**d**) 400 °C, (**e**) 450 °C, and (**f**) 500 °C. Hydrogenation was applied to introduce oxygen vacancies (V_O); the higher the temperature of the treatment, the more V_O are created. (**g**) Corresponding XRD pattern of these samples. The inset is the enlargement of a major anatase peak of TiO_2. (Adapted from Ref. [5] with permission from Elsevier. Copyright 2015)

Overall, it can be said that the more vacancies are produced, the higher is the level of reconstruction, and the more distorted the structure becomes (Fig. 2.3).

In turn, self-interstitial defect has much less influence on stoichiometry of semiconductor materials given that the overall number of atoms within the lattice remains unaltered as the changes occur only in their disposition and consequent relocations. As for the structural composition, its adjustment is proceeded with very minor changes given that self-interstitial atoms cannot cause much deviation of the energy within its surrounding near-neighbor atoms. It is explainable by the fact that equilibrium concentration of self-interstitials is lower than that of vacancies due to higher formation energy of the former, and thus in most cases, they are unable to contribute for any sufficient reconstruction of crystal lattice if only to initiate large distortion. Overall, their influences often are shadowed by that of vacancies [6].

Extrinsic defects These defects have very crucial influence on structural arrangement of host materials as the intrusion of foreign compounds inevitably results in breakage of established equilibrium within crystal lattice which requires searching of new preferred orientation in order to minimize the newly available free energy. It usually occurs via perturbation of surface mass and consequent adjustment of new metastable order. Thus, it might lead to increased roughness of surface or appearance of porous structure within the host material or oppositely decreased level. Needless to say, by thermodynamic point of view, this process is very similar to that which is realized due to formation of intrinsic defects, specifically vacancies. In addition, introduction of foreign compounds into semiconductor materials inevitably results in changes of its chemical compositions that often are accompanied by

undesirable and desirable shift in stoichiometry. It is usually proceeded via two scenarios which are described as follows, respectively: The first one refers to nucleation and growth of a new phase within host materials associated with various transitions due to poor solubility of doped element. It causes overall deviation of its composition which consequently becomes transformed into a new compound, whether partially of fully. For metal and oxide-based dopants due to their limited solubility, these adjustments and further reconstructions might be more pronounced than that which occurs with the use of non-metal elements. Thus, too high fraction of introduced metal-based element is more relevant for achieving alloying rather than to realize adequate doping process even though the former term is more adapted for metals and less for semiconductor materials. For instance, filling of TiO_2 with 4% of Ni or 6% of Fe results in transformation of this binary compound into ternary one in the form of $NiTO_3$ and $FeTiO_3$, respectively [7]. To make the metallic dopants become soluble in absolute or close to it terms, so that they could become the part of chemical composition in host material, thus playing the role of substitutional or interstitial defect, the second scenario is usually implemented. It requires the use of their much lower concentration to reach it. For instance, to produce ($Z_{1-x}OAl_x$) solid solution, it was reported that presence of Al with only ~2% is enough [8]. In turn, non-metal doping is almost always realized via second scenario as it rarely causes the appearance of new phase or development of unexpected configurations or compounds within the target material even at extremely high accumulation and assemblance. As an example, Ng et al. [9] investigated nitrogen-incorporated ZnO with atomic fraction of doping up to 30%, and it only led to detection of chemical composition in the form of $ZnO_{1-x}N_x$ due to replacement of oxygen by diffused N ions, while no additional external phases were discovered.

For its part, doping also can be used to create intrinsic defects in the target materials. It is usually proceeded via two routes. One of them is related to charge accumulation and compensation processes as introduction of aliovalent dopants increases the concentration of defects with opposite charge in order to maintain already broken electrical neutrality [10]. This process satisfies so-called first law of doping [11]. As for another route, it is referred to as consequent reconstruction and adjustment of crystal lattice structure as introduction of foreign atoms into target material often leads to appearance of additional stress within host crystal lattice given differences in atomic radii between two compounds. Hence, to release it, and to compensate energy deviation, formation of vacancies is highly required [12].

Several words also should be said about influence of both types of point defects on electronic structure of the material where they are introduced. Intrinsic and extrinsic defects equally enable to increase the concentration and mobilities of charge carriers with n-type and p-type characteristics, whether in separate or combined accounts, thus leading to strengthening of original conductivity or creating its transition. It also can cause the formation of additional mid-gap levels within the band gap that contribute to more effective transitions and positioning of charge carriers and also provide effective tool to control their presence and availability by changing the level of Fermi energy. In addition, some of these defects within certain

limits of their presence, distribution, and other related characteristics enable to shift valence or conduction bands up and down, respectively, thus lowering the band gap of material and making it more suitable for absorption of visible light.

However, apart from the advantages which both types of point defects can initiate, their presence also is associated with appearance of certain drawbacks that negatively influence abovementioned improvements. For example, doped elements that have been introduced via improper synthesis route or post-synthesis treatment protocol might become itself an additional unexpected new phase, as it was mentioned above, which have different types, concentrations, or mobility of charge carriers, thus, to be less conductive and even represents insulator characteristics. In this case, it is considered not as dopant but rather as unwanted impurity that seriously limits effective transfer of photo-induced electron and holes toward the surface. By turns, intrinsic defects such as vacancies can serve as trapping centers for charge carriers with both signs accelerating their recombinations. For better clarification, each type of point defects is discussed below in more precise details with special emphasis on their origin and classification.

2.3.3 Intrinsic Defects

2.3.3.1 Anion Vacancies

As relatively low formation energy is required for their formation, to introduce anion vacancies is much easier compared with that of cation vacancies. Generally speaking, as these defects are considered to be low-valence and electron-abundant centers, their presence can effectively modify electronic structure, energy band configuration, and optical properties of target materials increasing its usefulness and practicability as photocatalysts [13]. Among several types of anion vacancies reported in literature, oxygen vacancies (V_O) have been implemented and studied most extensively given that a sufficient part of semiconductor materials applied in solar light processing represents metals oxide. In addition, other anion vacancies such as nitrogen, carbon, and sulfite vacancies have very high resemblance with V_O in terms of structural and electronic particulates. Thus, the main focus in this chapter is given to understanding of V_O which is accounted as projection of typical anion vacancy.

Considering various semiconductor oxides, it might become obvious that Ti-, Zn-, and Fe- based structures are one of the most utilized compounds that are used for V_O-associated photocatalysis. The evacuation of oxygen atoms from their crystal lattice causes the breakage of energy equilibrium which needs to be compensated by two processes. *Firstly*, there is a filling of generated vacancy spot with electrons whose localizations are supported by Madelung potential. It prevents them to be equally spread around the crystal lattice [14]. *Secondly*, to compensate the disruption of total free energy within the system and to minimize its value, the neighboring atoms are required to relax their positions with respect to the newly formed vacancy and to accept more advanced arrangement. It allows to strengthen and

stabilize their linkages with the rest of crystal lattice at a certain extent and to cover the disappearance of one of their bonding [15]. It should be noticed that formation of V_O often cannot be considered as a single process since metal atoms which surround it can also be reduced and transformed into interstitial compounds due to decreased number of chemical bonding or accepted electrons. It happened, for example, in TiO_2, where Ti^{4+} can easily become Ti^{+3} as a result of oxygen deficiency. In fact, its presence in quantitative terms can even follow the concentration V_O at a certain yet very specific range [16].

There are several factors which influence the formation and specific patterning of oxygen vacancies within the material. One of them is related to preferred orientation of the crystal lattice as even within the same oxide material due to the presence of facets with different crystallographic directions, the arrangement of atoms which surrounding V_O might have some particularities. As an illustration, Li et al. [17] investigated BiOCl with two contrasting surfaces such as close packed [001] and open channel [010]. It was revealed that appearance of V_O in the former resulted in its bonding to two Bi^{2+} and four O atoms with the changed of Bi-O bond length from 2.28 to 2.36 Å. In contrast, oxygen vacancies created within [010] facet were connected to three Bi^{2+} and two Cl. Thus, Bi-O and Bi-Cl bond lengths were changed from 2.39 to 2.33 Å and 2.93 to 2.82 Å, respectively. Besides, the release of electrons from defective BiOCl [010] could be proceeded much easier as it requires overstepping lower-energy barrier than that of BiOCl [001]. It is a highly important discovery as electrons play an essential role in light-induced oxidation reactions. In turn, it was also realized that orientation of crystal lattice can as well be used to control the concentration and distribution of produced anion vacancies. For instance, Li et al. [18] investigated the presence of V_O in ZnO synthesized with different ratios of polar [002] and nonpolar [100] crystallographic planes and established that "samples with large polar planes generally contain more oxygen vacancies."

Moreover, anion vacancies might have a profound effect on adjusting the band structure of the host material. Their formation often is accompanied by the appearance of mid-gap states whose existence allows the use of photons with energies lower than actual band gap. Thus, the excited electrons can jump between these levels as a step to travel from the valence to conduction bands. Due to this, defective semiconductors materials can show shifting of absorption edge toward visible spectra which often can be detected even by naked eyes as it is correlated with change of its color. For example, TiO_2 is a white color compound which, however, becomes black with the presence of V_O [19] (Fig. 2.4a, b). A similar effect is also observed in ZnO where introduction of V_O changes original color from white to black too [20] (Fig. 2.4c).

2.3.3.2 Cation Vacancies

Cation vacancies is another type of intrinsic defects which is widely investigated in terms of their application to improve the photocatalytic activity of semiconductor materials. However, given their formation which requires more utilization of higher energy compared with that of anion vacancies and also considering better stability

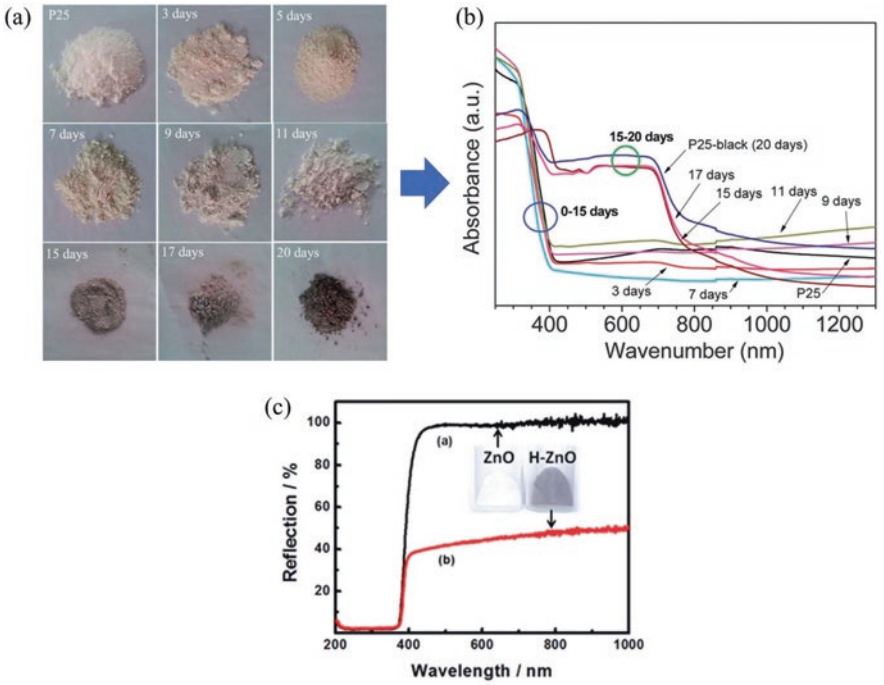

Fig. 2.4 (**a**) Photographic images of P25 (commercial TiO_2 nanoparticles composted of anatase and rutile phases) treated under hydrogen for 0–20 days at 35 bar hydrogen atmospheres at room temperature and (**b**) corresponding UV-vis spectra. (Reprinted from Ref. [19] with permission from The Royal Chemical Society. Copyright 2019) (**c**) UV-visible reflectance spectra of pristine and hydrogenated ZnO nanoparticles. (Reprinted from Ref. [20] with permission from The Royal Chemical Society. Copyright 2014)

of this type of defect within crystal lattice of host materials [21] as to modify or remove them the access to very specific synthesis or treatment protocol is required, there are still some existing challenges in reaching precise control over their manipulation and characteristics. In fact, it is much easier to create conditions during experimental procedures which favor the formation of anion vacancies such as oxygen deficiencies in TiO_2 and ZnO or nitrogen deficiency in Ta_3N_5 rather than generating Ti and Zn vacancies or Ta vacancies, respectively. Yet, apart from differences in synthesis, the processes which occur inside the materials during formation of cation vacancy and have impact on its properties and features are very similar to those assigned for the appearance of anion vacancy with only small correction: that its electronic structure allows to identify it as rather acceptor-like defects. For example, taking ZnO as illustration, it can be said that evacuation of Zn atom leads to binding of localized hole to each of the four nearest-neighbor O ions which are inevitably accompanied by their consequent relaxation in order to adjust symmetry according to new arrangement.

Following it, one might realize that cation vacancies could be used to change the type of dominated charge carriers as often their extended introduction in n-type materials, which in fact represents the majority of applied semiconductor photocatalysis, is associated with the conversion of their conductivity toward p-type. For example, this concept was perfectly confirmed by works of Wang et al. [22] and Pan et al. [23] who demonstrated that generation of Ti and Zn vacancies in TiO_2 and ZnO, respectively, resulted in highly effective $n \rightarrow p$ transition. Moreover, if anion vacancies are also co-presented in material beyond reasonable limit, i.e., with concentration higher than those required for equilibrium existence, thus, given their generally accepted donor-like characteristics, it becomes possible to create highly localized and clearly distinguished and confined domains filled with only particular type of defects which establish their prevailed type of conductivity. For instance, Gurylev et al. [24] applied this principle through formation of intrinsic p-n homojunction within ZnO thin film whose realization was achieved by controlled coexistence of zinc and oxygen vacancies, respectively. This structure can be regarded as very perspective for photocatalytic application since it does not require utilization of additional materials or compounds neither application of external sources to be fabricated. However, to make the appearance of this geometry become available in other binary semiconductors, both cation and anion vacancies should be shallow rather than deep defects which means that positions of their mid-gap energy levels are supposed to be developed in very close distance to the conduction and valence bands [6]. Only in this case, these vacancies enable to produce electrons and holes to contribute for transition of conductivity into the opposite type. Otherwise, they only serve as compensation center for strengthening corresponding original n- and p-type conductivities, respectively.

It is however often the case that cation vacancies might negatively impact the properties of target material as it is very different from that of anion vacancies which mostly are considered to be a positive contribution to the host material. It can be explained simply by the fact that cation vacancies generally are ascribed to the absence of metal atoms from the crystal lattice which, in fact, results in degradation of the so-called overall metallic portion. The resulting structure begins to show more insulating characteristics which are associated with worsening of charge transportation properties and other related phenomena. For example, Stampfl and Freeman [25] investigated introduction of Ta vacancies in TaN_x via density functional calculation (DFT)-based simulation model and revealed that "presence of Ta vacancies reduces the density of states around the Fermi level" which led to lowering of free elector density and "result[ed] in an increased resistivity and a reduction in conductivity compared to stoichiometric TaN." Thus, it was concluded that regions of Ta-deficient structures were primary responsible for the metal-to-insulator transition. Experimental evidence obtained by the same group during investigation of TaN_x grown by high-vacuum sputtering system using different nitrogen pressures in order to control its stoichiometry was in line with that conclusion [26].

Thus, combining together both phenomena described above, the introduction of cation vacancies inevitably results in appearance of two competing processes within the semiconductor material such as increasing of conductivity following the supply

of positively (negatively) charged carriers and accompanied transformation into more intrinsic form due to lowering of overall metal presence in its structure. It has to be noticed that formation of anion vacancies in turn can hardly lead to this phenomenon as changes in their presence generally result only in variation of concentration and mobility of charge carriers within reasonable limits as the material still maintains its semiconductor nature even though it might become degenerated.

2.3.4 Extrinsic Defects

2.3.4.1 Metal Doping

Metal doping is a widely applied approach to modify the properties and structure of target semiconductor materials. *Firstly*, it results in increased photonic efficiency as the optical response is shifted toward higher wavelength due to appearance of mid-gap energy states within the band gap, and *secondly*, it also can be used to improve the separation rate of electron-hole pairs since the equilibrium concentration of charge carriers becomes shifted. Besides it, other characteristics such as surface area, presence of pores and their dimensions, and reconstruction of morphology which have an impact on photoefficiency can also be controlled by the presence of these defects. Finally, introduction of dopants whose Fermi levels located close to valence or conduction bands of the target semiconductor can be used to increase the supply of minor carriers in the form of supplementary holes and electrons depending on the original type of conductivity in target materials. Thus, it enables realization of transitions such as $n \rightarrow p$ or $p \rightarrow n$. This processing is similar to that which can be proceeded during utilization of intrinsic defects. Yet, it is incorrect to think that these positive changes are very common and unavoidable and simply can be connected to doping with all metallic compounds. In fact, it is often the case that metal ions are introduced into target materials, even though they have clear cation-related characteristics, serve opposite role, and result in lowering of charge concentration and mobility, thus acting as electron and hole trap centers. For example, Carey and McKenna [27] performed extended DFT calculation and revealed that this scenario exactly applies to the mission of V, Sb, and Sn dopants in TiO_2, while Hf and Zr ions have been determined to be a highly positive inclusion.

Metal elements once presented in semiconductor material can occupy both interstitials and substitutional sites depending on their concentration and natures. It results in crucial alteration of crystal lattice due to appearance of significant strain caused by doping which consequently initiates structural disorder and degradation of crystallinity within semiconductor materials accompanied by the changes in chemical composition. Taking ZnO as example, it can be demonstrated that its substitutional doping occurs once the introduced metal atoms match those of Zn^{2+} in terms of their electronegativity and ionic radius [28]. In turn, interstitial doping is achieved if only the ionic radius becomes smaller, while electronegativity remains the same level. As for the larger ionic radius and higher or lower electronegativity,

even though the doping occurs and the metal ions might take in perspective interstitials positions, it is considered to be a very restricted process due to low solubility of dopant in this case. Thus, substitutional doping is more accessible. In addition, following Hume-Rothery rule, valences of both doped and host materials are also an important factor which needs to be considered as the higher the difference between these two values, the more difficult for the introduced foreign atoms to be properly resided in target crystal lattice [29]. One should notice that in analogy to Schottky defects, cation or anion vacancy might be created due to doping with metals as to keep the electrical neutrality. For instance, filling of ZnO with negatively charged Al atoms results in appearance of acceptor-like V_{Zn} [30].

Solubility of introduced metal atoms in semiconductor is a very important parameter that is necessary to be considered. It determines whether it is possible to create solid solution in the form of $A_{1-x}BC_x$ where AB represents the structure of original binary semiconductor and C is a metal atom to be doped. The following characteristics can influence the smooth occurrence of this process: size of particles, ratio of ionic radius between dopant and doped compound, and the metal oxidation state [28]. To be clear, at too high concentration, the metal dopants cannot be fully dissolved within the target material, and it leads to lateral segregation of its excess volume at the surface [31] and assemblance as external separately localized composition. Another possibility is that due to low solubility of dopant, it can result in arrangement of ternary phase which is completely different from that of binary one and is considered as newly created compound with totally different properties and characteristics. For example, synthesis of ZnO doped with only 1% of Fe results in appearance of small fraction of $ZnFe_2O_4$ compounds within it whose presence as neighbor becomes higher with increased concentration of Fe in ZnO and reached almost 50% at doping with only 10% of Fe [32]. Thus, importance of solubility in utilizing proper concentration of introduced atoms to realize correctly proceeded metal doping cannot be overestimated.

Several words need to be said about the specific influence of extrinsic cation deficiency on particulate semiconductor materials such as TiO_2, ZnO, Ta_3N_5, WO_3, Fe_2O_3, etc. which are widely investigated as great candidates for various photocatalytic processes mentioned in Chap. 1, yet their efficiencies are much lower than that of expected ones due to wide band gap, high charge recombination rate, etc. Doping with metal atoms can be considered as a great pathway to sufficiently improve their already existing properties or cause the appearance of new and extraordinary yet highly desirable characteristics which can be used to serve as sufficient contribution to their photoefficiency. For example, anatase form of TiO_2 is more effective in light-induced reactions than that of rutile yet thermal annealing with temperatures over 600 °C results in phase transformation which means that, for example, application of post-synthesis treatment to increase the presence of oxygen vacancies might be very challenging. Doping with metal ions such as Zr^{4+} which substitutes Ti^{4+} can stabilize the anatase phase at high temperatures making its transition into rutile to become more difficult [33]. Accordingly, it was also reported that metal doping in the form of Nb atoms can be used to adjust the crystal phase and morphology of synthesized TiO_2 without additional treatment protocol [34] (Fig. 2.5). Simply put,

low niobium concentration enables to form one-dimensional rutile nanorods, while increase of its presence leads to synthesis of two-dimensional anatase nanosheets. Also, apart from governing the properties and characteristics of target material which has direct influence on the efficiency of photocatalytic reaction such as band-gap width, optical absorption of visible light, or improved charge separation rate, metal doping can also be used to solve other less discussed problems which however also at certain extend might influence the photocatalytic efficiency. For instance, Ta_3N_5 suffers from low photocorrosion and thus show reduced applicability to proceed solar-based reactions for extended time. Doping with Mg is a great approach in facing this problem as in addition to "unprecedented PEC water splitting activity," the Mg-Ta_3N_5 also demonstrated stable performance for over 1 h [35].

Thus, metal doping is a very effective technique to enhance the performance of photocatalysis. Yet, due to the problem of low solubility, inability for doped element to properly match the lattice structure of host materials following the difference in ionic radius or other reasons, and high possibility to co-form various intrinsic defects for covering thermodynamic loses of equilibrium, this approach has certain limitations in choosing the correct metal element to be applied as effective dopants. Nevertheless, continuous efforts are still in progress.

2.3.4.2 Non-metal Doping

One of the first report which demonstrated that doping with non-metal elements is an effective strategy to extend the photocatalytic activity of the target semiconductor materials is referred to the work of Asahi et al. [36] who used nitrogen atoms to modify the structure of TiO_2 in order to make it sensitive toward absorption of visible light. Following it, this approach became a very popular topic toward application in various semiconductor materials as it provides promising results regarding

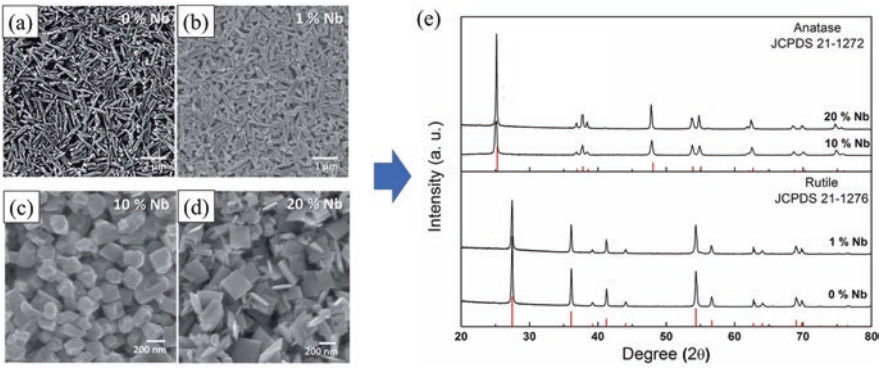

Fig. 2.5 (**a**–**d**) Morphological and structural information of Nb-doped TiO_2 nanostructures and (**e**) corresponding XRD pattern. (Reprinted from Ref. [34] with permission from The Royal Chemical Society. Copyright 2015)

the improved outcome of photocatalytic reactions. Doping with anion elements is mostly referred to their replacement of non-metal atoms in target material. For example, in the case of ZnO, introduction of nitrogen, sulfur, carbon, or any other related elements results in their substitution of oxygen atoms. Thus, the finalized solid solution is usually presented in the form of $ZnO_{1-x}N_x$ where N represents the dopant. As can be seen, it is very similar to that observed during metal doping with the only difference being oxygen its substitutional element. Definitely, residence of anion elements in target material also can be proceeded as interstitial defects, yet it is a rather rare and less investigated phenomenon. Nevertheless, a more detailed discussion about it is provided below. It has to be noticed that screening through literature might arise conclusion that some non-metals have very poor solubility in semiconductor. Thus, to achieve their homogeneous distribution within whole body of target materials, their relatively high concentration or utilizing special treatment is required. For example, to realize nitrogen incorporation into TiO_2 thin film, Franco et al. [37] used doping concentration of ~18% which is much higher than that mentioned above for the employment of metal elements. At these conditions, the only observed phase was attributed to the slightly modified TiO_2. Yet, this scheme provides certain difficulties toward its proper implementation and also requires to utilize huge amount of chemicals. Thus, it is suggested that applying non-metal doping as only to assist in modifying the surface of semiconductor since it is usually realized at its lower concentration might be a more attractive option. In this regard, higher flexibility in controlling the parameters of this process including solubility and distribution and also the presence and behavior of introduced atoms as their formation in bulk is neglected can be achieved. It is especially important given that photocatalytic processing is usually occurred via surface reaction, and thus its current conditions and states play a crucial role in governing it. For instance, Feng et al. [38] reported that doping with only 2–3% of boron was enough to create B-doped TiO_2 with sufficient amount of B atoms residing on the surface. In turn, it also can be accomplished by employment of non-metal dopant in the form of solid compound and applying certain thermal treatment to activate its diffusion. Particularly, Gurylev et al. [39] reported that during deposition of TiO_2 on the surface of carbon nanotubes (CNTs) and consequent annealing at moderate temperatures, the intrusion of carbon atoms into the surface of former compound was observed leading to their substitution of oxygen species and formation of Ti-C bonds.

In order to make extrinsic anion defect become perfectly coupled with target materials, it is important to reach the balance arrangement within it in the absence of much degradation in surrounding crystal lattice and consequent appearance of disordering [40]. This task is much easier to achieve than in the case of previously discussed cation doping as non-metal chemical elements which are used for this purpose mostly represent the first row in the periodic table that have relatively small atoms, especially in their neutral form. It allows them to effectively diffuse through the lattice of target material and later become bonded to atoms in regular arrays through residing in interstitials or substitutional positions. From the structural point of view, the latter type of defect requires less adjustments and relaxation of surrounding neighbors than that of the former one as it only results in elongation of

newly established bonds with nearest metal atoms in crystal lattice of semiconductor. For instance, doping of TiO_2 with substituted carbon leads to appearance of Ti-C bonds (2.008 and 2.217 Å) with length slightly different from that of the original Ti-O bonds (1.942 and 2.002 Å) [41]. Thus, it is a more applicable process, and most of the reports regarding non-metal doping demonstrate the formation of this type of defect. In turn, foreign atoms at the interstitial position are supposed to establish new bonding with nearest anion atom in periodical array in order to become full member of crystal lattice as what happened, for instance, in the case of nitrogen-doped TiO_2 which demonstrated formation of -N-O bonds [42]. The appearance of this type of defects is reported to a lesser extent.

It is also important to discuss the electronic nature of both types of non-metal defects and their influence on the transport characteristics of charge carriers. To make this discussion more illustrated, TiO_2 is considered as an example given that this material is the most widely applied photocatalyst [43]. For a particular dopant element such as B or C, the DFT simulation discovered that substitutional species (with respect to O atoms in TiO_2 lattice) are supposed to proceed self-reduction as they grab non-excited electrons residing in valence band, while interstitial species are found to be oxidized since they donate electrons to nearest-neighbor Ti^{3+} species [43]. Overall, the resulting mid-gap energy states appearing in the band gap of the materials in association with each of these defects represent, therefore, very distinct particularities. *Firstly*, their existence are determined by the electronegativity of introduced anion elements as it should have this value lower than that of oxygen [44]. *Secondly*, substitutional dopants have strong acceptor-like characteristics as the resulting mid-gap states usually locate near the valence band. *Thirdly*, the interstitial dopants initiate the appearance of donor-like features in the material since they create mid-gap states that lay higher in band gap and also often are accompanied by the formation of various intrinsic defects which have positions of their energy levels close to the conduction band [43]. Experimental evidence available in literature generally support this conclusion. For example, Peng et al. [45]. investigated TiO_2 doped with nitrogen and determined that mid-gap levels created by its atoms residing at substitutional and interstitial sites are located at 0.14 eV and 0.73 eV, respectively, from the maximum of valence band. Based on this description, it should be noticed that when both types of defects are simultaneously introduced into the material, they might involve into intensive interaction with each other which eventually leads to changes in charge transfer, and thus it contributes to their additional stabilization [43]. Yet, it is a very rare phenomenon as their co-existence can be realized only during very particular synthetic conditions and highly specific treatment protocol. For instance, Di Valentin et al. [41] investigated TiO_2 via DFT simulation and revealed that application of oxygen-poor conditions can favor the inclusion of C atoms in positions normally occupied by lattice O, i.e., substitutional defects. In this case, the formation of oxygen vacancies is highly necessary as their presence reduces the overall energy cost of this processing. This mechanism, in fact, also can be applied to other non-metal elements such as nitrogen of sulfide [43]. In turn, a stoichiometric TiO_2 sample whose existence satisfies fully oxidizing

surrounding environment enables managing the residing C atoms in both interstitial and substitutional positions at once [41].

Thus, given that introduction of non-metal elements into semiconductor material is usually proceeded in oxygen-poor atmosphere or within the environment which only support its limited supply such as thermal treatment in gaseous ambient, vapor-phase synthesis, bombardments with high-energy particles or the growth in chemical solution filled with proper anion compound, etc., it results in dominated formation of substitutional defects over that of interstitials. However, it cannot be considered as optimal choice since non-metal compounds residing in interstitial positions might induce better photocatalytic efficiency of wide band-gap materials under visible light compared with that of substitutional which can be explained by higher position of their mid-gap states within band gap [45]. Yet, to make these defects become the dominated type, application of special treatment is required.

2.4 Line Defects

Viewing with the naked eye the surface of a single crystal that has a metallic nature would reveal a very clear and smooth structure with the absence of any imperfections or defects. Once we use optical microscopy and apply certain magnification, it becomes evident that the surface in fact is very populated. It exists in the form of granular composition filled with regions of separated crystallinity that are confined by highly distinguished boundaries. These boundaries are called dislocations, and they represent one-dimensional or line defects [46]. For simplicity, dislocations are ascribed as a sudden abruption of atomic periodic array along their continuous extension. Occurrences of these defects usually are proceeded in two cases, firstly, if the crystallographic plane represents incomplete row of atoms and becomes stressed between two absolutely perfect planes and, secondly, if distribution of vacancies is realized in single and focused direction following the orientation of periodic arrangement. This type of defect can easily move within crystal lattice, and this process is usually accompanied by the appearance of a phenomenon called a slip which represents a sliding of atomic planes. The slip can occur in both horizontal and vertical direction which makes it called a glide and climb, respectively. In this regard, a dislocation may be defined as a line that forms a boundary within a slip plane separating a region that has slipped and the one that is remained preserved. It is generally accepted that vacancies are required to be presented in crystal lattice as their diffusion sufficiently facilitates the motion of dislocation. Furthermore, with vacancy concentrations far from equilibrium, the resulting dislocation motion can cause the increase of their presence as more incomplete crystallographic planes are formed via activation of Bardeen-Herring sources [47].

Dislocations occur in high densities and traditionally are considered to be the main contributor to almost all mechanical properties of material. Their formation is usually achieved via plastic deformation and phase transformation such as solidification or as a result of thermal stresses caused by rapid cooling. Dislocations are

characterized by Burger vector which is determined as a benchmark of the lattice distortion caused by the introduction of these defects. It also can be used to show the amount and direction in which the slip occurs due to their movement. Overall, there are two types of dislocations which can be observed in materials, namely, edge and screw dislocations. Both of them can be ascribed by Burger vector, which is parallel and perpendicular, respectively, to their dislocation line. Their existence as separated species are very limited as most dislocations are present in the assembled form. More details regarding these types are given below.

Edge dislocation An edge dislocation which also sometimes is called as Taylor-Orowan dislocation represents a defect that occurs when an extra plane(s) of atoms is inserted into the regular crystal, disturbing nearby atomic planes. In this regard, atoms above the dislocation line become squeezed together which is equaled to state of compression, while atoms below are forced to be apart which is correlated with application of tensile stresses. Following it, edge dislocation is regarded as positive and negative when compressive stresses present above and below the dislocation line, respectively. Yet, it should be noted that differentiation between two dislocations is very formal as simple rotation of the crystal to 180° either clockwise or anticlockwise transforms a positive dislocation into a negative one and backward.

Screw dislocation A screw dislocation which is also called sometimes as Burger dislocation represents more complicated nature than that of edge dislocation. It can be illustrated by cutting a crystal along a plane and shearing its upper front portion by one atomic distance to the left (or right) with regard to the lower front portion. The designation "screw" for this defect is considered from the fact that lattice planes of the crystal spiral the dislocation line (inner part of cut) [48]. This type of dislocation also can have positive and negative directions which are equal to lattice spirals of upper part in right-hand and left-hand fashions, respectively. A screw dislocation has an absence of preferred slip plane compared with that of edge dislocation and thus can perform cross-slip via transferring into another plane due to local stresses thus realizing non-planar movement. Yet, screw dislocation cannot climb, as it is adopted only for horizontal move and it makes their spreading around crystal lattice more limited than that of edge dislocation which, in turn, is opened for movement toward both vertical and horizontal directions [49].

It should be mentioned that a dislocation cannot be restricted by the position only within the materials inside. This is because a dislocation is an example of the boundary between a slipped area and non-slipped area as it was mentioned above. If the slipped area does not spread up to the surface of materials, then its boundary becomes continuous, and the dislocation is transformed into a closed loop. Only when the slipped area extends to materials surface is it possible for a single dislocation to have a point where it has ended [48].

2.5 Planar Defects

Planar defects are considered as imperfections with a thickness of only several atomic layers whose existence and continuous evolution within the material are enveloped and restricted by the presence of nearest-neighborhood perfect crystalline structure. There are existing internal and external planar defects classified as follows: grain boundaries, stacking faults, and gain interfaces are referred to the former type, while surfaces are ascribed to the latter type. The existence of these imperfections cannot be considered as thermodynamically favorable since they represent meta-stable states similar to that of dislocations. Their appearance are determined by the assemblance of the line defects into a two-dimensional structure [50]. Each type of planar imperfections is briefly described below.

Grain boundaries Grain boundaries represent the interface between two single-crystal grains which possess different crystallographic orientations. The normal atomic bonding that is used in grains is less applicable within the range of grain boundary as more loosely bound atoms prevail at this region which makes them more energetically active compared to those located within the grain interior. As a result, the grain boundary becomes a heterogeneous region where various atomic reactions and processes related to movement and transformation of atoms such as solid-state diffusion, phase transformations, impurity segregation, mechanical relaxation, etc. are more favorable to be developed from thermodynamic position [51] (Fig. 2.6a). In addition, grain boundaries cause very serious scattering of electrons which negatively affect their transport characteristics and also critically degrade the overall conductivity. Overall, it might lead to the increase of charge recombination in semiconductors [52]. Grain sizes in nanoscale materials such as thin films are typically in the range of ~1 μm and are much smaller than common grain sizes which existed in their bulk counterparts [53] (Fig. 2.6b). Thus, it is expected that the former ones tend to have higher reactivity as photocatalysts than that of the latter ones.

Several words need to say about special type of gran boundaries which is called a *twin boundary*. It represents highly defined lattice symmetry where atoms on one side of the boundary are arranged in mirror-image positions with respect to atoms on the other side. The grain which is “squeezed” between these boundaries is appropriately determined as twin. The appearance of this structure results from atomic displacements which are produced due to applied mechanical shear forces (mechanical twins) and also during annealing or heat treatments that follow the deformation (annealing twins) [54].

Stacking faults Stacking faults are anomalies in the stacking sequence of crystal planes that abrupt the continuity of a perfect lattice [55]. They can be easily illustrated taking silicon film [111] and particularly its first several atomic layers as an example. Each of these planes is considered to be a close-packed array filled with atoms, and each successive layer fits into the interstices of the previous layer. Thus, atoms in the second layer (B) are supposed to nest in one set of interstices of the first

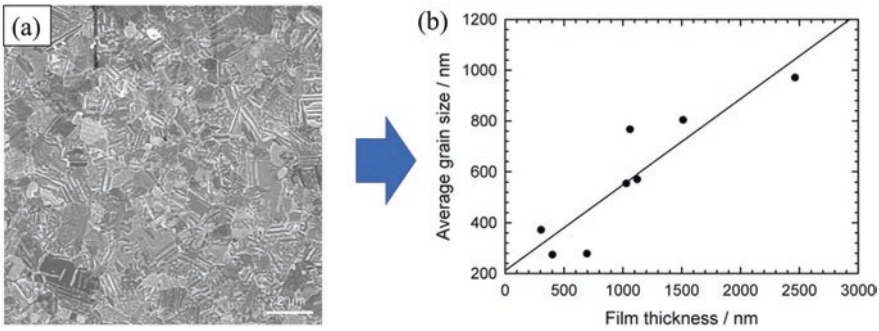

Fig. 2.6 (**a**) Microstructure of a 1-mm-thick copper film after removal of the native oxide by FIB (focused gallium ion beam) sputtering. (**b**) Grain size as determined from FIB cross sections as a function of film thickness. (Reprinted from Ref. [53] with permission from Taylor & Francis. Copyright 2012)

(A) layer, while atoms in the third layer (C) perform the same action with interstices of the second layer. In this case, a perfect structure in the form of ABCABCABC is preserved. If, however, a plane of atoms is missing from the normal sequence, e.g., ACABCABC, or a plane of atoms has been inserted ahead of its order, e.g., ABCBABCABC, it is called a stacking fault defect [56]. Their appearances are a very common phenomenon during epitaxial growth of semiconductor films as it is hard to proceed correct and consistent filling of atomic layers given non-equilibrium conditions and high temperature used during this process. For example, Yang et al. [57] identified that stacking faults are the dominant defect in the annealed ZnO thin films grown on c-plane sapphire by atomic layer deposition.

Phase interfaces Phase interfaces which also sometimes are called as phase boundaries are the junction of two crystals within the materials which have certain differences in lattice structure and composition [58]. One of particularities identified with regard to this type of defect is that its position has a high level of migration since it follows the development and transformation of relevant phases. For example, Li et al. [59] investigated reduction of CuO into Cu_2O via thermal treatment in vacuum at temperatures up to 670 °C and discovered that level of oxygen out-diffusion control the movement of phase boundary between two compounds, and thus it can be used to adjust the presence and distribution of Cu_2O grains within the CuO matrix.

Surfaces These defects also can be called as “free surfaces “or “external surfaces” since they represent the most top atomic array of any solid compound. To be clear, the arrangement of atoms at the surface in most solids always has certain differences and mismatches in atomic configuration compared to that of the bulk. It is explained by the fact that surface atoms only bonded in one side; thus, they have similar crystal structure but at a slightly different lattice parameter than the atoms located deeper. For example, Gallego et al. [60] investigated Pt (111) and revealed that the first and second topmost surface layers exhibited an expansion and contraction,

respectively, within the same value of 0.9%. Yet, it has to be noticed that this analysis was performed in deep vacuum at a pressure of ~3×10^{-10} Torr. In a typical condition, the structure of free surfaces is much complicated due to various processes such as chemical changes within the top of atomic plane due to exposure to air, presence of dangling bonds, adsorption of certain species such as oxygen and nitrogen, and also contamination which cannot be avoided. Overall, it increases the difference between arrangement of atoms allocated on the surface and in the bulk.

2.6 Volume Defects

Apart from abovementioned defects, other imperfections exist in all solid materials which are much larger in size and therefore sometimes even called bulk defects. They are classified as precipitates, dispersants, inclusions, and voids [61]. *Precipitates* are assemblance of impurity atoms or accumulated elements that introduction into target materials is proceeded via solid-state reaction. They contribute to increasing its strength as they sufficiently decrease the migration of dislocation acting as barrier for the movement. The efficiency of precipitate is determined by its size, concentration, and distribution within crystal structure of materials as well as elemental composition. *Dispersants* take role of the second phase which is introduced into the materials to accurately tune and adjust the behavior of primary phase. They are presented as large particles with sizes ranging from 10 to 100 μm. It has to be noticed that properties of this multiphase structure such as thermal and electrical conductivities are usually considered as a combined average of properties associated with each phase. *Inclusions* are foreign particles or large precipitations and are considered to be undesired features whose intrusion and consequent presence decline useful features of materials. For example, dust and dirt negatively influence the fabrication of nanoelectronic devices as they prevent proper transportation of charge carriers. Thus, this type of defect should be avoided. *Voids* appear due to vacancy aggregation or existence of gas bubbles which are trapped during solidification. These defects have highly negative effects on the characteristics and performance of materials. For instance, due to them, the mechanical strength becomes weaker [61, 62].

2.7 Defects in Semiconductor Nanomaterials: Current Progress

2.7.1 General Methods to Produce Defects

In this chapter, only methods which are used to form point defects since are demonstrated since presence of their other types such as line, planar, and volume is more appropriate for metallic compounds and less observable and applicable in

semiconductor materials. Thus, for more detailed information regarding their appearances, it is suggested to request proper literature. Point defects as mentioned above can be categorized into intrinsic and extrinsic types, and methods used to synthesize them in most cases are relatively similar. The only difference is that to create intrinsic deficiency, it is required to realize conditions which favor the ejection of certain portions of original atoms from the structure, while for the extrinsic deficiency, oppositely, the surrounding should serve as a source of foreign atoms that are required to be introduced into the materials. Thus, each fabrication technique has a very peculiar and specific adjustment regarding some of its parameters as to make it become suitable for formation of each types of defects. Below, some of them are discussed briefly as to get general acquaintance and to provide very basic ideas about their processing. As for the more detailed description, it can be accessed in the proper sections of this book as to follow each particulate material and its unique characteristics.

Vapor-phase techniques Vapor-phase techniques include mostly chemical and physical- vapor deposition synthesis that are widely applied to create nanoscale defective materials since both of them are considered as bottom-up approaches which allow to achieve precise accuracy. For instance, to introduce intrinsic defects, it is enough to decrease the content of proper gaseous precursors to be supplied into the reaction chamber. It can be realized, for example, simply by reducing its pressure or concentration. Subsequently, newly arrived atoms cannot fully fill the periodic array within the crystal lattice of fabricated materials, thus, leading to appearance of vacancies. As an illustration, Heo et al. [63] demonstrated the applicability of this approach to generate oxygen- and zinc-deficient ZnO using molecular-beam epitaxy. Definitely, other parameters of vapor-phase synthesis also can be employed to proceed required changes in stoichiometry such as temperature of reaction, type of substrate, etc., yet it is less influential and controllable compared with the effects created by playing with precursor characteristics and more applicable for very precise tuning of various features in already created defects. In turn, this synthesis route can be utilized to produce extrinsic deficiency that is ascribed via doping with required elements simply by allowing them to access the reaction chamber as one of precursor or through addition to original ones and thus been allowed to participate chemical or physical reactions assisting in material fabrication. It is especially important to notice that metal elements which are supposed to serve as dopants should be presented in the form of vapor-phase that is achieved usually via application of high temperature during synthesis and consequent evaporation or through using them in the form of preliminary prepared gaseous chemical compound. For example, Potter et al. [64] applied additional supply of aluminum chloride at temperature of 450 °C to create Al-doped ZnO thin film via CVD.

Chemical methods These methods include various fabrication strategies where certain substances and compounds are combined together via specifics chemical reactions to be served as building blocks leading to fabrication of target materials. These reactions are usually proceeded at the conditions which cannot be called as

extreme as there is no need to apply high temperatures or use, for example, special gas ambient. The resulting product is usually presented in the powdered form that at higher magnification might be identified as various complex 1-D and 3-D and simpler 0-D and 2-D structures as well as their combinations and derivatives. Overall, these chemical methods include but are not limited to the followings approaches: solgel synthesis, hydrothermal method, precipitation, and co-precipitations methods, spray-pyrolysis method, etc. Thus, to create intrinsic deficiency, it is generally proceeded via inclusion of certain chemical compound into reaction solution that might serve as electron or hole donors depending on the desirable goal to create anion or cation vacancies, respectively. Control over the time, temperature, and other related parameters of reaction as well as concentration of this chemical can be used to suppress or oppositely enhance the presence of vacancies in resulted product. In turn, to achieve the extrinsic deficiency, it is required that materials which serve as doping element is included into synthesis route in the form of chemical compound or element to become a part of finalized chemical reactions.

Mechanical synthesis This method is usually realized by application of high-energy ball milling (BM) process which demonstrated to be a highly effective and simple technique for reaching fabrication of nanocrystalline powders with desired specifications. In a BM process, the friction and collision of ball could create temperatures over 1000 °C at a highly localized area of ~1 μm^2 within a short period of 10^{-3}–10^{-4} seconds [65]. Specifically, to achieve the formation of intrinsic deficiency which is mostly proceeded via development of anion vacancies given that their formation requires less energy than that of cation vacancies, it is sufficiently enough to just throw the target materials into planetary ball mill and use proper time and rotating speed of its consequent treatment. As for the extrinsic deficiency, it can be reached by additional introduction of required elements into the ball grinder as what happened, for example, in a study by Shatnawi et al. [66] where the formation of Mn-doped ZnO nanocrystalline particles in the form of $Zn_{1-x}Mn_xO$ was achieved via solid-state reaction by simultaneous milling of both ZnO and MnO powders for 5 h. The resulting structure preserved almost similar morphology to that of pristine ZnO, yet its optical properties were highly enhanced (Fig. 2.7). It has to be noticed that doping with non-metal compounds also can be realized using this technique, yet its precursors should be used in a solid form as it was demonstrated by Lu et al. [67] who fabricated N-doped ZnO by applying urea ($CO(NH_2)_2$) as precursors.

2.7.2 Manipulation and Control of Defects

It is very easy to introduce defects into materials, but to tune and make them to become adjusted the way which is necessary to achieve the best performance requires application of additional efforts. It can be proceeded usually via two routes where one of them is based on manipulating the parameters of material synthesis during which the introduction of desirable structural and compositional changes

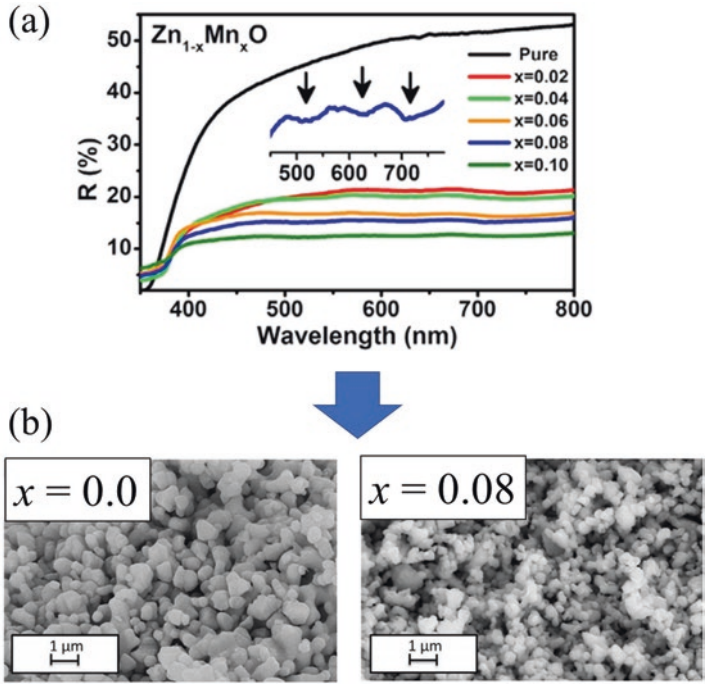

Fig. 2.7 (**a**) UV-vis diffuse reflectance spectra for representative samples of $Zn_{1-x}Mn_xO$ with different percentage of Mn content. The inset shows the broad reflection minima in the visible range for the samples with 0.08% Mn. (**b**) SEM images of $Zn_{1-x}Mn_xO$ with x = 0.0 and x = 0.08. (Reprinted from Ref. [66] with permission from Elsevier. Copyright 2016)

occurs, while another one is attributed to the post-synthesis treatment that in fact is more difficult to accomplish since it requires application of additional sources, efforts, and energies.

Shifting discussion toward the first route, and taking vapor synthesis techniques as example, formation of defects, regardless whether intrinsic or extrinsic, within specific and defined concentration can easily be governed by managing the characteristics of used precursors or varying the temperature within the reaction chamber, as it was mentioned above. Furthermore, playing with these paraments can also be used to adjust other more complicated features of introduced defects such as their distribution, migration, and assemblance and also subsequent transformation onto more complex and extended forms. For its part, chemical methods provide much wider spectrum of tools which can be used to govern the existence of both types of defects. For instance, simply by playing with nature of compounds which are applied to induce the chemical reaction as well as varying its fraction or operating lower or higher temperatures during its mixing, drying, etc. can be considered as a perfect pathway to control certain properties of doped atoms or vacancies within the finalized materials. As for mechanical synthesis, application of proper conditions for this process is also highly crucial to achieve the precise accuracy over presence of

desirable defects in terms of their localized appearances. For instance, Kaftelen et al. [68] reported that by employing the freezing conditions of 77 K, it becomes possible to reach the generation of ZnO filled with surface and bulk defects, while realization of this processing at room temperature led to assemblance of composition where bulk defects were dominated. Thus, one cannot say that formation of defects during synthesis of materials is a granted and unalterable phenomenon which cannot be properly tuned and adjusted. In fact, oppositely, it provides a lot of tools to make this process more operational and manageable so that introduction of required changes in structure and composition of target materials could follow very specific pathways toward achieving their desirable specifications.

The same also can be said regarding application of post-synthesis protocol. For instance, utilization of hydrogenation treatment to TiO_2 and ZnO is a well-established process to create oxygen vacancies. The higher the temperature of treatment, the more advanced their concentration becomes, the more uniformly they are distributed, and the more pronounced the effect on photocatalytic performance [5, 69] (Fig. 2.8). In succession, incorporation of foreign atoms into target materials especially in the form of non-metal elements also can be realized under thermal treatment with proper ambient such as nitrogen or sulfur. By adjusting the flow rate or pressure, purity of these gases, and direction of stream, it is possible to determine the level of their assemblance and its allocation, i.e., whether on the surface or in bulk of target material, as well as tune their concentration and possible interaction

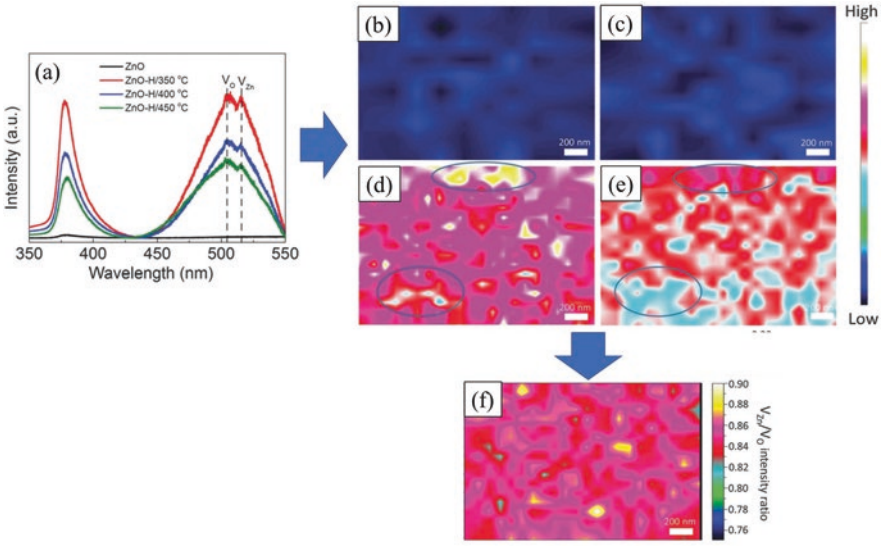

Fig. 2.8 (**a**) PL spectra of as-deposited and hydrogenated ZnO thin films. Two-dimensional spatial maps of PL intensities of defect emissions located at 504 nm and 520 nm for ZnO films. (**b**) As-deposited, 504 nm; (**c**) as-deposited, 520 nm; (**d**) hydrogenated at 400 °C, 504 nm; (**e**) hydrogenated at 400 °C, 520 nm; and (**f**) intensity ratio of defect emissions (V_{Zn}/V_O) from (**d**) and (**c**). (Reprinted from Ref. [69] with permission from the *PCCP Owner Societies.* Copyright 2016)

with various intrinsic defects. As for metal doping, it can be proceeded simply via placing both materials (the one which is going to be doped and the one which serves as dopant) apart inside reaction tube and subjecting it to annealing with accompanied supply of certain ambient into reaction chamber which makes the interaction become activated by the diffusion. In fact, this approach has certain similarities to that of non-metal doping described above, as it uses solid compound instead of gases to develop the incorporation of foreign atoms. By varying the distance at which materials are placed into tube, temperature of treatment, its duration, both heating and cooling rates, etc., it is possible to govern the doping characteristics with very defined accuracy. Yet, one should notice that it is hardly possible to adjust the level of solubility within the target materials and thus, even though so many parameters can be applied to make the implementation of extrinsic deficiency become a smooth process, it is much difficult to reach their high processing effectiveness compared to that achieved during formation of their intrinsic counterparts. Overall, this discussion is continued in more precise terms in the following sections of this book as to make better apprehension, the association with unique specifications and characteristics of each particular material is highly necessary.

2.7.3 Materials Properties vs Defect Presence: Positive and Negative Sides

The presence of defects allows to govern and manage various properties and features of materials so as to transform them into highly reliable compounds which can satisfy the strictest requirements to become an efficient photocatalyst. Yet, it is not always the case, as incorrect handling of defects and inability to clearly understand and adequately control their nature and behavior might become factors which restrict the expected improvements since under improper handling, they enable to bring clear deterioration of materials properties and degrade its performance. In this section, we briefly review what the negative and positive sides are of defect engineering as recognizing them allows to consider what to expect from employment of this methodology.

2.7.3.1 Positive Contribution of Defect Engineering

There are a huge number of papers and technical reports appearing in the literature in recent years regarding the application of defect-based approach to modify semiconductor in order to increase their photocatalytic-related performances. Based on this, it is clear that presence of defects can do almost impossible as to make the materials which initially was determined to be absolutely unsuitable for

solar-induced reaction, in contrary, shows highly impressive outcome. To be more specific, defects influence the following characteristics:

Optical properties Defect can decrease the width of band gap by shifting up or down the valence and conduction bands, respectively. Another mechanism which is responsible for increasing the absorption of photons with energies lower than band gap is that both intrinsic and extrinsic defects introduce mid-gap energy states within band gap which can be used by electrons as steps to jump from valence to conduction band. Finally, the original absorption efficiency can also be improved sufficiently as what happened, for example, for TiO_2 whose utilization of UV light became extended due to the presence of oxygen vacancies on its surfaces [5, 19].

Electrical and electronic properties Defects are usually regarded as belonging whether to n-type or p-type conductivities; thus, it is inevitable that their introduction increases the presence of corresponding charge carriers in the materials via rising their concentrations and mobilities and thus enhancing the original conductivity or realizing its transition into opposite type. Higher availability of charge carriers also often leads to improved separation rate which contributed to their enhanced transportation characteristics thus allowing them to reach surfaces more efficient to activate light-induced reactions with adsorbed molecules. One should notice that defects also can assist in extending lifetimes of electrons and holes by taking the role of individual trap centers for each of them. More detailed descriptions of these phenomena are provided in other chapters.

Structural characteristics Presence of defects can be used to extend the current morphology of materials to the new level, making it more advanced and prosperous toward application in photocatalytic processing. For example, the formation of surface-located defects results in partial reconstruction of surrounding crystal lattice which causes consequent increase of roughness. It correlated with enhanced specific surface area, formation of an additional micro-mesoporous features, and better porosity [70]. In turn, doping also can be used to advance the surface characteristics of target materials as what happened, for instance, in the case of Na-doped TiO_2 [71], where the introduction of this elements at atomic concentration of ~3.9%, ~7.8%, and ~9.8% resulted in respective improvement of specific surface area, volume, and diameter of pores. In another side, presence of various elements in the target materials can increase its chemical and mechanical stabilities thus leading to advancement of overall photocorrosion. It allows to extend the operation under light-irradiated conditions toward much longer time.

2.7.3.2 Negative Contribution of Defect Engineering

To be honest, there are much less available reports in recent years which demonstrated that presence of defects is a very undesirable phenomenon, and it is suggested to be avoided at any cost as they decline most important characteristics and properties of materials to some extent. Below are some particular examples provided and discussed.

Optical properties Defects enable to increase the width of band gap and consequently shift the absorption edge toward lower wavelength. It is called a Burstein-Moss effect, and it is explained as follows. With the increase in concentration of defects, more and more donor states are produced, and it pushes Fermi level higher in energy until it lies inside the conduction band above the occupied donor states [72]. Thus, the excited electrons are required to jump there to be resided in conduction band instead of simply reaching its lowest edge which is located closer. For example, reduced V_2O_5 nanostructures showed the increase of band gap from 1.95 to 2.45 eV due to presence of delocalized and injected electrons [73]. In turn, Al-doped ZnO also can demonstrate negative changes in optical properties, compared with undoped ZnO; particularly, transparency range increased from ~3.0 to ~3.25 eV, respectively [74].

Electrical and electronic properties Defects can serve as recombination centers as instead of trapping the electrons or holes on separate occasion, thus increasing their lifetimes just like in vacancies, or by scattering them as realized via doped atoms, they behave as locations where or near which both charge carriers become combined, and thus, it leads to their self-annihilations. For example, Xu et al. [75] investigated CdS nanorods for photocatalytic application and discovered that their improved crystallinity highly benefits the performance as the more light-induced electrons and holes could reach the surface joining the corresponding reactions without being trapped in defects. In turn, Larumbe et al. [76] determined that doping of TiO_2 with Fe might be considered as a less optimal pathway to improve its properties, as the resulting compounds demonstrated low photoefficiency which was mostly ascribed to increased ratio of charge recombination.

Structural characteristics Presence of defects on the surface of materials usually results in certain mass perturbation and its subsequent recontribution in searching of a new minimum of energy. In most cases, these changes are positively influence the morphology as the overall specific surface area, level of mesoporousity etc. increase sufficiently. Yet, there are available reports where, oppositely, it leads to deteriorating structural characteristics as established metastable thermodynamic equilibrium matches highly unfavorable arrangement of surface atoms. Furthermore, these negative changes also can be correlated with post-synthesis treatment used to introduce defects due to its extreme conditions, as it was demonstrated, for instance, by Leshuk et al. [77] who applied annealing at 450 °C in H_2 for 24 h to create oxygen vacancies in TiO_2. The resulting structure showed reduced specific surface area for more than ~3 times compared with that of pristine sample.

2.7.4 Current Challenges and Future Perspectives

Defect engineering provides a great potential for improving the performance of various semiconductors in terms of their solar energy conversion-related applications. To be precise, it allows to modify their light absorption, improve charge separation, optimize surface compositions, etc. Yet, although great and impressive achievements have been demonstrated in this direction in recent years, there are still several crucial challenges that require urgent solutions as current outcome of photocatalysis is still far from expected.

Firstly, it is important to reach clear and deep understanding regarding the rational structures and characteristics of defects within the materials since it might be considered as a crucial pathway to avoid their negative influence. This step is especially important, given the number of contradictive studies regarding it that are currently available in literature. *Secondly*, based on this knowledge, it is essential to design materials filled with defects under deep consideration of their types, nature, and behavior. *Thirdly*, the current fabrication techniques are required to be adapted more properly as to realize the formation of defects with more precise control over their characteristics. For instance, thermal treatment as a method to create vacancies in semiconductor can also influence its phase composition or even deteriorate surface morphology since it requires the use of high temperatures. Thus, an alternative to this method is required to be developed. *Fourthly*, it is out of importance that materials filled with defects are supposed to show also certain stability as required addition to their high efficiency so that they can be used for longer time making the utilization more practicable. The example of Mg-doped Ta_3N_5 mentioned above [35] is a great example on how it could be effectively applied in reality.

2.8 Final Remarks on Defect Engineering

Defect engineering is a new subject whose development became possible only recently when advanced analyzing techniques were utilized to demonstrate that presence of defects in fact is responsible for various important phenomena. It brings a novel concept which means that instead of avoiding them at any cost as undesirable features which deteriorate properties and characteristics of materials, they can be applied efficiently to make them become more advanced. It is considered to be a very attractive strategy, as defects always exist, and the ideal materials simply cannot be created within the scope of presence technologies and sources. Thus, even though synthesis of highly perfect compounds was reported in literature, they surely have a small fraction of defects which slip the detection and identification, and thus it builds an impression of their absence. To create this “ideality,” however, various complicated treatment procedures are required, and consequent analysis should be performed under extreme vacuum. Thus, under normal conditions, defects usually are present in very considerable amount and all we can do is to accept that they are

the unseparated part of materials that can assist in reaching our purposes and goals. However, to do so, it is necessary to get acquainted with them and their most basic characteristics so as to understand what they are and how they behave. This chapter provides such an opportunity as here each type of defects including zero-dimensional, one-dimensional, two-dimensional, and three-dimensional is described in precise details in the purpose of providing the most essential knowledge about them. In the following chapters, it is shown how this knowledge can be applied in practice to fabricate certain specific materials with desirable features which can demonstrate outstanding performance.

References

1. S. Bai, N. Zhang, C. Gao, Y. Xiong, Defect engineering in photocatalytic materials. Nano Energy **53**, 296–336 (2018). https://doi.org/10.1016/j.nanoen.2018.08.058
2. C. Wagner, Point defects and their interaction. Annu. Rev. Mater. Sci. **7**, 1–24 (1977). https://doi.org/10.1146/annurev.ms.07.080177.000245
3. E.G. Seebauer, M.C. Kratzer, Extrinsic defects, in *Charged Semiconductor Defects: Structure, Thermodynamics and Diffusion*, (Springer, London, 2009), pp. 233–289. https://doi.org/10.1007/978-1-84882-059-3_8
4. C. Zhang, X. Geng, J. Li, Y. Luo, P. Lu, Role of oxygen vacancy in tuning of optical, electrical and NO_2 sensing properties of ZnO_{1-x} coatings at room temperature. Sensors Actuat. B Chem **248**, 886–893 (2017). https://doi.org/10.1016/j.snb.2017.01.105
5. V. Gurylev, C.Y. Su, T.P. Perng, Surface reconstruction, oxygen vacancy distribution and photocatalytic activity of hydrogenated titanium oxide thin film. J. Catal. **330**, 177–186 (2015). https://doi.org/10.1016/j.jcat.2015.07.016
6. A. Janotti, C.G. Van de Walle, Native point defects in ZnO. Phys. Rev. B **76**, 165202 (2007). https://doi.org/10.1103/PhysRevB.76.165202
7. K. Murugan, J. Joardar, A.S. Gandhi, B.S. Murty, P.H. Borse, Photo-induced monomer/dimer kinetics in methylene blue degradation over doped and phase controlled nano-TiO_2 films. RSC Adv. **6**, 43563–43573 (2016). https://doi.org/10.1039/C6RA03738K
8. M. Ohtaki, T. Tsubota, K. Eguchi, H. Arai, High-temperature thermoelectric properties of $(Zn_{1-x}Al_x)O$. J. Appl. Phys. **79**, 1816–1818 (1996). https://doi.org/10.1063/1.360976
9. Z.-N. Ng, K.-Y. Chan, S. Muslimin, D. Knipp, P-type characteristic of nitrogen-doped ZnO films. J. Electron. Mater. **47**, 5607–5613 (2018). https://doi.org/10.1007/s11664-018-6468-2
10. J.H. Park, Y.J. Lee, J.-S. Bae, B.-S. Kim, Y.C. Cho, C. Moriyoshi, Y. Kuroiwa, S. Lee, S.-Y. Jeong, Analysis of oxygen vacancy in Co-doped ZnO using the electron density distribution obtained using MEM. Nanoscale Res. Lett. **10**, 186 (2015). https://doi.org/10.1186/s11671-015-0887-2
11. R. van de Krol, Principles of photoelectrochemical cells, in *Photoelectrochemical Hydrogen Production, Electronic Materials: Science & Technology*, ed. by R. van de Krol, M. Grätzel, vol. 102, (Springer US, Boston, 2012), pp. 13–67. https://doi.org/10.1007/978-1-4614-1380-6_2
12. S. Kumar, N. Tiwari, S.N. Jha, S. Chatterjee, D. Bhattacharyya, A.K. Ghosh, Structural and optical properties of sol-gel derived Cr-doped ZnO diluted magnetic semiconductor nanocrystals: An EXAFS study to relate the local structure. RSC Adv. **6**, 107816–107828 (2016). https://doi.org/10.1039/C6RA15685A
13. C. Mao, J. Wang, Y. Zou, H. Li, G. Zhan, J. Li, J. Zhao, L. Zhang, Anion (O, N, C, and S) vacancies promoted photocatalytic nitrogen fixation. Green Chem. **21**, 2852–2867 (2019). https://doi.org/10.1039/C9GC01010F

14. M. Krzywiecki, L. Grządziel, A. Sarfraz, D. Iqbal, A. Szwajca, A. Erbe, Zinc oxide as a defect-dominated material in thin films for photovoltaic applications - experimental determination of defect levels, quantification of composition, and construction of band diagram. Phys. Chem. Chem. Phys. **17**, 10004–10013 (2015). https://doi.org/10.1039/C5CP00112A
15. A. Janotti, C.G. Van de Walle, Oxygen vacancies in ZnO. Appl. Phys. Lett. **87**, 122102 (2005). https://doi.org/10.1063/1.2053360
16. H. Liu, H.T. Ma, X.Z. Li, W.Z. Li, M. Wu, X.H. Bao, The enhancement of TiO_2 photocatalytic activity by hydrogen thermal treatment. Chemosphere **50**, 39–46 (2003). https://doi.org/10.1016/S0045-6535(02)00486-1
17. H. Li, J. Shang, H. Zhu, Z. Yang, Z. Ai, L. Zhang, Oxygen vacancy structure associated photocatalytic water oxidation of BiOCl. ACS Catal. **6**, 8276–8285 (2016). https://doi.org/10.1021/acscatal.6b02613
18. G.R. Li, T. Hu, G.L. Pan, T.Y. Yan, X.P. Gao, H.Y. Zhu, Morphology-function relationship of ZnO: Polar planes, oxygen vacancies, and activity. J. Phys. Chem. C **112**, 11859–11864 (2008). https://doi.org/10.1021/jp8038626
19. H. Lu, B. Zhao, R. Pan, J. Yao, J. Qiu, L. Luo, Y. Liu, Safe and facile hydrogenation of commercial Degussa P25 at room temperature with enhanced photocatalytic activity. RSC Adv. **4**, 1128–1132 (2013). https://doi.org/10.1039/C3RA44493G
20. T. Xia, P. Wallenmeyer, A. Anderson, J. Murowchick, L. Liu, X. Chen, Hydrogenated black ZnO nanoparticles with enhanced photocatalytic performance. RSC Adv. **4**, 41654–41658 (2014). https://doi.org/10.1039/C4RA04826A
21. E. Olsson, X. Aparicio-Anglès, N.H. de Leeuw, Ab initio study of vacancy formation in cubic $LaMnO_3$ and $SmCoO_3$ as cathode materials in solid oxide fuel cells. J. Chem. Phys. **145**, 014703 (2016). https://doi.org/10.1063/1.4954939
22. S. Wang, L. Pan, J.-J. Song, W. Mi, J.-J. Zou, L. Wang, X. Zhang, Titanium-defected undoped anatase TiO_2 with p-type conductivity, room-temperature ferromagnetism, and remarkable photocatalytic performance. J. Am. Chem. Soc. **137**, 2975–2983 (2015). https://doi.org/10.1021/ja512047k
23. L. Pan, S. Wang, W. Mi, J. Song, J.-J. Zou, L. Wang, X. Zhang, Undoped ZnO abundant with metal vacancies. Nano Energy **9**, 71–79 (2014). https://doi.org/10.1016/j.nanoen.2014.06.029
24. V. Gurylev, A. Useinov, P.Y. Hsieh, C.Y. Su, T.P. Perng, Hydrogenated ZnO thin film with p-type surface conductivity from plasma treatment. J. Phys. D. Appl. Phys. **50**, 24LT02 (2017). https://doi.org/10.1088/1361-6463/aa6e91
25. C. Stampfl, A.J. Freeman, Metallic to insulating nature of TaN_x: Role of Ta and N vacancies. Phys. Rev. B **67**, 064108 (2003). https://doi.org/10.1103/PhysRevB.67.064108
26. L. Yu, C. Stampfl, D. Marshall, T. Eshrich, V. Narayanan, J.M. Rowell, N. Newman, A.J. Freeman, Mechanism and control of the metal-to-insulator transition in rocksalt tantalum nitride. Phys. Rev. B **65**, 245110 (2002). https://doi.org/10.1103/PhysRevB.65.245110
27. J.J. Carey, K.P. McKenna, Screening doping strategies to mitigate electron trapping at anatase TiO_2 surfaces. J. Phys. Chem. C **123**, 22358–22367 (2019). https://doi.org/10.1021/acs.jpcc.9b05840
28. M.D. Hernández-Alonso, Metal doping of semiconductors for improving photoactivity, in *Design of Advanced Photocatalytic Materials for Energy and Environmental Applications*, ed. by J. M. Coronado, F. Fresno, M. D. Hernández-Alonso, R. Portela, (Springer, London, 2013), pp. 269–286. https://doi.org/10.1007/978-1-4471-5061-9_13
29. J.H.W.F. Smith, *Foundations of Materials Science and Engineering*, 4th (fourth) edn. (McGraw-Hill Companies, The, 2005). New York, NY 10019 (USA)
30. H. Rotella, Y. Mazel, S. Brochen, A. Valla, A. Pautrat, C. Licitra, N. Rochat, C. Sabbione, G. Rodriguez, E. Nolot, Role of vacancy defects in Al doped ZnO thin films for optoelectronic devices. J. Phys. D. Appl. Phys. **50**, 485106 (2017). https://doi.org/10.1088/1361-6463/aa920b
31. T. Tabata, J. Aubin, K. Huet, F. Mazzamuto, Segregation and activation of Ga in high Ge content SiGe by UV melt laser anneal. J. Appl. Phys. **125**, 215702 (2019). https://doi.org/10.1063/1.5096889

32. S. Karamat, R.S. Rawat, P. Lee, T.L. Tan, R.V. Ramanujan, Structural, elemental, optical and magnetic study of Fe doped ZnO and impurity phase formation. Prog. Nat. Sci. **24**, 142–149 (2014). https://doi.org/10.1016/j.pnsc.2014.03.009
33. M.D. Hernández-Alonso, I. Tejedor-Tejedor, J.M. Coronado, J. Soria, M.A. Anderson, Sol-gel preparation of TiO_2-ZrO_2 thin films supported on glass rings: Influence of phase composition on photocatalytic activity. Thin Solid Films **502**, 125–131 (2006). https://doi.org/10.1016/j.tsf.2005.07.256
34. H.-Y. Wang, J. Chen, F.-X. Xiao, J. Zheng, B. Liu, Doping-induced structural evolution from rutile to anatase: Formation of Nb-doped anatase TiO_2 nanosheets with high photocatalytic activity. J. Mater. Chem. A **4**, 6926–6932 (2016). https://doi.org/10.1039/C5TA08202A
35. L. Pei, Z. Xu, Z. Shi, H. Zhu, S. Yan, Z. Zou, Mg-doped Ta_3N_5 nanorods coated with a conformal CoOOH layer for water oxidation: Bulk and surface dual modification of photoanodes. J. Mater. Chem. A **5**, 20439–20447 (2017). https://doi.org/10.1039/C7TA06227C
36. R. Asahi, T. Morikawa, T. Ohwaki, K. Aoki, Y. Taga, Visible-light photocatalysis in nitrogen-doped titanium oxides. Science **293**, 269–271 (2001). https://doi.org/10.1126/science.1061051
37. A.L.M. Franco, G. Zambrano, M.E. Gómez, E. Camps, L. Escobar-Alarcón, Photocatalytic activity of nitrogen-doped and undoped titanium dioxide sputtered thin films. Superf. y Vacio. **25**, 161–165 (2012). http://www.scielo.org.mx/scielo.php?script=sci_abstract&pid=S1665-35212012000300003&lng=es&nrm=iso&tlng=es
38. N. Feng, A. Zheng, Q. Wang, P. Ren, X. Gao, S.-B. Liu, Z. Shen, T. Chen, F. Deng, Boron environments in B-doped and (B, N)-codoped TiO_2 photocatalysts: A combined solid-state NMR and theoretical calculation study. J. Phys. Chem. C **115**, 2709–2719 (2011). https://doi.org/10.1021/jp108008a
39. V. Gurylev, T.-K. Chin, A. Useinov, Charge transfer and field emission characteristics of TiO_2@CNTs nanocomposite: Effect of TiO_2 crystallinity. J. Alloy Compd. **157598** (2020). https://doi.org/10.1016/j.jallcom.2020.157598
40. R. Portela, Non-metal doping for band-gap engineering, in *Design of Advanced Photocatalytic Materials for Energy and Environmental Applications*, Green Energy and Technology, ed. by J. M. Coronado, F. Fresno, M. D. Hernández-Alonso, R. Portela, (Springer, London, 2013), pp. 287–309. https://doi.org/10.1007/978-1-4471-5061-9_14
41. C. Di Valentin, G. Pacchioni, A. Selloni, Theory of carbon doping of titanium dioxide. Chem. Mater. **17**, 6656–6665 (2005). https://doi.org/10.1021/cm051921h
42. Y. Hu, H. Liu, X. Kong, X. Guo, Effect of calcination on the visible light photocatalytic activity of N-doped TiO_2 prepared by the sol-gel method. J. Nanosci. Nanotechnol. **14**, 3532–3537 (2014). https://doi.org/10.1166/jnn.2014.8021
43. C. Di Valentin, G. Pacchioni, Trends in non-metal doping of anatase TiO_2: B, C, N and F. Catal. Today **206**, 12–18 (2013). https://doi.org/10.1016/j.cattod.2011.11.030
44. G. Liu, L. Wang, H.G. Yang, H.-M. Cheng, G.Q. (Max) Lu, Titania-based photocatalysts-crystal growth, doping and heterostructuring. J. Mater. Chem. **20**, 831–843 (2010). https://doi.org/10.1039/B909930A
45. F. Peng, L. Cai, H. Yu, H. Wang, J. Yang, Synthesis and characterization of substitutional and interstitial nitrogen-doped titanium dioxides with visible light photocatalytic activity. J. Solid State Chem. **181**, 130–136 (2008). https://doi.org/10.1016/j.jssc.2007.11.012
46. S.R. Bare, G.A. Somorjai, Surface chemistry, in *Encyclopedia of Physical Science and Technology*, ed. by R. A. Meyers, Third edn., (Academic, New York, 2003), pp. 373–421. https://doi.org/10.1016/B0-12-227410-5/00757-2
47. Z. Chen, B. Ge, W. Li, S. Lin, J. Shen, Y. Chang, R. Hanus, G.J. Snyder, Y. Pei, Vacancy-induced dislocations within grains for high-performance PbSe thermoelectrics. Nat. Commun. **8** (2017). https://doi.org/10.1038/ncomms13828
48. R. Abbaschian, R.E. Reed-Hill, *Physical Metallurgy Principles*, 4th edn. (Cengage Learning, Stamford, 2008)
49. S.V. Kailas, "Imperfections in solids," Lecture notes, Dept. of Mechanical Engineering, Indian Institute of Science, Bangalore. https://www.kluniversity.in/physics/pdfs/cripdf.pdf

50. L.E. Murr, *Handbook of Materials Structures, Properties, Processing and Performance* (Springer International Publishing, 2015). https://www.springer.com/gp/book/9783319018140
51. M. Ohring, Chapter 1 - A review of materials science, in *Materials Science of Thin Films*, ed. by M. Ohring, Second edn., (Academic, San Diego, 2002), pp. 1–56. https://doi.org/10.1016/B978-012524975-1/50004-5
52. F. Warkusz, The scattering of electrons on grain boundaries: Electrical conductivity. Thin Solid Films **161**, 1–11 (1988). https://doi.org/10.1016/0040-6090(88)90230-1
53. B. Merle, E.W. Schweitzer, M. Göken, Thickness and grain size dependence of the strength of copper thin films as investigated with bulge tests and nanoindentations. Philos. Mag. Let. **92**, 3172–3187 (2012). https://doi.org/10.1080/14786435.2012.685773
54. A.K. Batra, M.D. Aggarwal, Crystal twins and stacking faults, in *Field Guide to Crystal Growth*, (Spie Press Book, 2018). https://doi.org/10.1117/3.2309590.ch16
55. S. Sturm, B. Jančar, Chapter 8 - Microstructure characterization of advanced ceramics, in *Advanced Ceramics for Dentistry*, ed. by J. Z. Shen, T. Kosmač, (Butterworth-Heinemann, Oxford, 2014), pp. 151–172. https://doi.org/10.1016/B978-0-12-394619-5.00008-0
56. M. Ohring, Chapter 8 - epitaxy, in *Materials Science of Thin Films*, ed. by M. Ohring, Second edn., (Academic, San Diego, 2002), pp. 417–494. https://doi.org/10.1016/B978-012524975-1/50011-2
57. S. Yang, C.C. Kuo, W.-R. Liu, B.H. Lin, H.-C. Hsu, C.-H. Hsu, W.F. Hsieh, Photoluminescence associated with basal stacking faults in c-plane ZnO epitaxial film grown by atomic layer deposition. Appl. Phys. Lett. **100**, 101907 (2012). https://doi.org/10.1063/1.3692730
58. M. Enomoto, 5 - Structure, energy and migration of phase boundaries in steels, in *Phase Transformations in Steels*, ed. by E. Pereloma, D. V. Edmonds, (Woodhead Publishing, 2012), pp. 157–183. https://doi.org/10.1533/9780857096104.1.157
59. J. Li, S.Q. Wang, J.W. Mayer, K.N. Tu, Oxygen-diffusion-induced phase boundary migration in copper oxide thin films. Phys. Rev. B **39**, 12367–12370 (1989). https://doi.org/10.1103/PhysRevB.39.12367
60. S. Gallego, C. Ocal, F. Soria, Surface and bulk reconstruction of Pt(111) 1 × 1. Surf. Sci. **377-379**, 18–22 (1997). https://doi.org/10.1016/S0039-6028(96)01320-9
61. S. Pal, B.C. Ray, B.C. Ray, Structural description of materials, molecular dynamics simulation of nanostructured materials, 1–71 (2020). https://doi.org/10.1201/9780429019845-1
62. L.E. Murr, Volume defects: 3D imperfections in crystals, in *Handbook of Materials Structures, Properties, Processing and Performance*, ed. by L. E. Murr, (Springer International Publishing, Cham, 2015), pp. 313–324. https://doi.org/10.1007/978-3-319-01815-7_17
63. Y.W. Heo, D.P. Norton, S.J. Pearton, Origin of green luminescence in ZnO thin film grown by molecular-beam epitaxy. J. Appl. Phys. **98**, 073502 (2005). https://doi.org/10.1063/1.2064308
64. D.B. Potter, I.P. Parkin, C.J. Carmalt, The effect of solvent on Al-doped ZnO thin films deposited via aerosol assisted CVD. RSC Adv. **8**, 33164–33173 (2018). https://doi.org/10.1039/C8RA06417B
65. K. Ralphs, C. Hardacre, S.L. James, Application of heterogeneous catalysts prepared by mechanochemical synthesis. Chem. Soc. Rev. **42**, 7701–7718 (2013). https://doi.org/10.1039/C3CS60066A
66. M. Shatnawi, A.M. Alsmadi, I. Bsoul, B. Salameh, M. Mathai, G. Alnawashi, G.M. Alzoubi, F. Al-Dweri, M.S. Bawa'aneh, Influence of Mn doping on the magnetic and optical properties of ZnO nanocrystalline particles. Results Phys. **6**, 1064–1071 (2016). https://doi.org/10.1016/j.rinp.2016.11.041
67. J. Lu, Q. Zhang, J. Wang, F. Saito, M. Uchida, Synthesis of N-doped ZnO by grinding and subsequent heating ZnO-urea mixture. Powder Technol. **162**, 33–37 (2006). https://doi.org/10.1016/j.powtec.2005.12.007
68. H. Kaftelen, K. Ocakoglu, R. Thomann, S. Tu, S. Weber, E. Erdem, EPR and photoluminescence spectroscopy studies on the defect structure of ZnO nanocrystals. Phys. Rev. B **86**, 014113 (2012). https://doi.org/10.1103/PhysRevB.86.014113

69. V. Gurylev, C.-Y. Su, T.-P. Perng, Distribution pattern and allocation of defects in hydrogenated ZnO thin films. Phys. Chem. Chem. Phys. **18**, 16033–16038 (2016). https://doi.org/10.1039/C6CP01768A
70. H. Yuan, S.A.A.A. Aljneibi, J. Yuan, Y. Wang, H. Liu, J. Fang, C. Tang, X. Yan, H. Cai, Y. Gu, S.J. Pennycook, J. Tao, D. Zhao, ZnO Nanosheets abundant in oxygen vacancies derived from metal-organic frameworks for ppb-level gas sensing. Adv. Mater. **31**, 1807161 (2019). https://doi.org/10.1002/adma.201807161
71. I. Singh, B. Birajdar, Synthesis, characterization and photocatalytic activity of mesoporous Na-doped TiO_2 nano-powder prepared via a solvent-controlled non-aqueous sol-gel route. RSC Adv. **7**, 54053–54062 (2017). https://doi.org/10.1039/C7RA10108B
72. S.N. Svitasheva, A.M. Gilinsky, Influence of doping level on shift of the absorption edge of gallium nitride films (Burstein-Moss effect). Appl. Surf. Sci. **281**, 109–112 (2013). https://doi.org/10.1016/j.apsusc.2013.02.094
73. Q. Wang, M. Brier, S. Joshi, A. Puntambekar, V. Chakrapani, Defect-induced Burstein-Moss shift in reduced V_2O_5 nanostructures. Phys. Rev. B **94**, 245305 (2016). https://doi.org/10.1103/PhysRevB.94.245305
74. N. Azizah, S. Muhammady, M.A.K. Purbayanto, E. Nurfani, T. Winata, E. Sustini, R. Widita, Y. Darma, Influence of Al doping on the crystal structure, optical properties, and photodetecting performance of ZnO film. Prog. Nat. Sci. **30**, 28–34 (2020). https://doi.org/10.1016/j.pnsc.2020.01.006
75. M. Xu, L. Jiang, J. Wang, S. Feng, P.-L. Tremblay, T. Zhang, Efficient photocatalytic hydrogen evolution with high-crystallinity and noble metal-free red phosphorus-CdS nanorods. Int. J. Hydrog. Energy **45**, 17354–17366 (2020). https://doi.org/10.1016/j.ijhydene.2020.04.200
76. S. Larumbe, M. Monge, C. Gómez-Polo, Comparative study of (N, Fe) doped TiO_2 photocatalysts. Appl. Surf. Sci. **327**, 490–497 (2015). https://doi.org/10.1016/j.apsusc.2014.11.137
77. T. Leshuk, R. Parviz, P. Everett, H. Krishnakumar, R.A. Varin, F. Gu, Photocatalytic activity of hydrogenated TiO_2. ACS Appl. Mater. Interfaces **5**, 1892–1895 (2013). https://doi.org/10.1021/am302903n

Chapter 3
Bulk vs Surface Defects

3.1 Introduction

The presence of defects in semiconductor materials plays a crucial role in determining their photocatalytic performances as it can result in positive as well as negative outcome. There are many factors which affect this influence. Considering vacancy-type defects in a binary material such as ZnO as an example, it can be said that, *firstly*, they might have neutral, single, double charge states. It regulates the positions of its nearest-neighbor atoms in terms of consequent relaxation and reaching newly established thermodynamic equilibrium with minimum energy. *Secondly*, presence of vacancy creates specific mid-gap levels inside of band gap whose localization, however, is not fixed as they can be shifted up and down given the differences in arrangement of these defects and also due to changes in the transition levels between charge states. It has to be noticed that the same processes also can lead to rising up or lowering down the edges of valence and conduction bands, respectively, thus resulting in narrowing or oppositely increasing the width of band gap. *Thirdly*, introduction of vacancies might be accompanied by the formation of other related intrinsic defects such as self-interstitials or antisites (it is ascribed as atoms of Zn occupy positions of oxygen atoms) and their accompanied assemblance into more complex defect structures. Furthermore, there is also a need to acknowledge the type of vacancy, e.g., whether it has anion or cation character, as inaccurate management of defect formation due to nonrelevant synthesis procedure or improperly applied post-synthesis treatment might cause an unexpected transformation of ZnO from semiconductor to absolute insulator with extremely low charge concentration of carriers and absolute inability to show any photoactivity. In reverse, it also might become a highly degenerated compound with sharp metallic behavior. Thus, it is clear that formation of defects requires control at very challenging levels as not only their various characteristics should be deeply considered, such as formation energy, relaxation of surrounding crystal lattice, etc., but also it is necessary to always keep

V. Gurylev, *Nanostructured Photocatalyst via Defect Engineering*,
https://doi.org/10.1007/978-3-030-81911-8_3

in mind the nature and specifications of material system which is served as a host for them. For instance, taking nitride and oxide structures as illustration, introduction of anion vacancies might have some differences within these structures given the dissimilarities in particularities of oxygen and nitrogen vacancies, respectively.

However, there exist another parameter that can be used to govern the influence of intentionally introduced defects on photocatalytic performance which is very unique as manipulation over them can be realized not only through dismissing their own particulate characteristics but also regardless the type of employed semiconductor. This parameter is explained as follows: Given that much of the material that is utilized in light-induced reaction is supposed to have certain dimensions and volume, thus, depending on the experimental processing and its accompanied conditions used to create defects, there often happens a situation when their appearance is designated to be specifically distributed within the regions regarded as surface- or bulk-related. Given that host atoms within both of them have certain dissimilarities in their arrangements, it drastically affects the structure of defects residing there and also influences their localized environment including relaxation of nearest-neighbor chemical bonding and modification and perturbation of electronic structures within surrounding crystal lattice. It inevitably correlates with the level of material performance during photocatalytic activity. This concept is perfectly applied to both intrinsic and extrinsic deficiencies as it was demonstrated, for example, by Kong et al. [1] and Chang and Liu [2] respectively. In the first report, TiO_2 nanocrystals were synthesized with tunable surface/bulk defects using vapor-induced hydrothermal hydrolysis. It was discovered that "decreasing the relative concentration ratio of bulk defects to surface defects… significantly improve the separation efficiency of photogenerated electrons and holes, thus… enhancing the photocatalytic efficiency." In turn, the authors of second study revealed that uneven doping of vanadium ions within the surface layer of TiO_2 improves the photocatalytic performance; in contrast, bulk doping has detrimental effects.

Yet, to apply this methodology correctly, there appears a question whose importance cannot be overestimated, i.e., at what depth the particulate defect can change its status transforming from surface species into the bulk ones? Before starting this discussion, it is necessary to notice that typical nanostructured materials except the ones whose sizes are extremely small and in the range of sub-nanometer scale have several regions within them which can be described as surface, sub-subsurface, and bulk. It is, however, very common that subsurface layer is recognized as a part of surface composition and frequently is disregarded to have a clearly defined presence within the material. It happens through several reasons. *Firstly*, it simplifies the understanding of photocatalytic processing given that defects can be introduced whether into the surface or in the bulk, and thus it is much easier to follow their behavior and related characteristics. *Secondly*, to identify the existence of subsurface states, application of more advanced and complex analyzing protocol is required such as ion beam etching during XPS measurement, which, in turn, might not be a suitable option for delicate compositions as it also can generate vacancies and thus add additional difficulties in interpreting the structure. *Thirdly*, as individual thickness of surface layer without referring to subsurface is regarded in the

range of ~0.5 nm or even several atomic layers, it might be challenging to determine anything within it. Thus, in order to make its analysis to become more adequate, its range should be extended deeper inside the material reaching at least a dimension of several nanometers. Yet, to be honest, it is not easy to distinguish the extent of these "several nanometers," as it might depend on the proportion of materials or its structure. As an illustration, for TiO_2 thin film with thickness of ~22 nm, the definition of surface has a range of depth equal to ~12 nm [3], while for TiO_2 nanorods with diameter of ~25 nm, it was stated that its limitation reaches only ~4 nm [4]. It is evident that such a discrepancy might bring additional difficulties in interpretation of results as based on it, each material and composition reported in literature are regarded to have its own self-determined definition and extension of surface which however might not be applied toward other related structures even within similar materials system. Thus, it is not practically useful, and another approach to distinguish bulk and surface layers should be considered. It might be suggested that detecting the appearance of defects using analyzing techniques whose penetration depth lays within the range of several nanometers such as XPS, UPS, and Auger electron spectroscopy (AES) results in referring to them as surface-based states. In turn, using the analysis which can probe whole composition of target materials regardless its thickness or size such as XRD, EPR, and Raman spectroscopy results in classifying the detected defects as bulk-based states. This methodology was comparatively applied, for example, by Wu et al. [5] while investigating TiO_2 NPs. However, even though it allows to realize which one is dominated specie in sample and also to understand its role during light-induced application, the disadvantage of this approach is that it cannot be used to directly compare concentration of both types of defects. Thus, the provided above definitions of bulk and surface defects should be taken with certain cautions as the depth at which their mutual boundary is supposed to be located might be very conditional.

3.2 Bulk Defects

Usually, it is often considered that bulk deficiency, both intrinsic and extrinsic, is a highly undesirable feature since their presence only leads to unfavorable effects lowering the range of expected advancement in terms of photocatalytic performance. At the same time, an opposite opinion also existed in literature which clearly defines that bulk defect can bring certain usefulness to the materials. Below, a brief explanation of their structure and particular characteristics is provided to figure out how they influence characteristics of host semiconductors during photocatalytic processing.

Intrinsic defects As it was generally accepted, intrinsic bulk defects usually are present in the form of trap centers for light-induced electrons and holes which sufficiently decrease their lifetimes. In addition, their existence also degrades transport characteristics of remained charge carriers negatively affecting diffusion toward sur-

face thus reducing overall light-induced output. Yet, it would be incorrect to say that simply by eliminating any bulk defects and leaving only those located in the surface, the efficiency of target material becomes abruptly increased. In fact, bulk defects also play a certain role in contributing and consequently governing photocatalytic processing, but it is usually proceeded via their combined presence with surface defects which results in appearance of consequent synergetic effect. The study by Hou et al. [6], for example, clearly confirms this concept. The authors investigated the changes in solar hydrogen production of TiO_2 as a function of concentration ratio between bulk single-electron-trapped oxygen vacancies (V_O) and surface-located counterparts (Fig. 3.1). It was determined that occurrence of former defects within certain quantity was highly necessary in order to obtain the most optimal performance of TiO_2 as even though they play the role of recombination centers for charge carriers thus decreasing the overall concentration of available light-induced electrons and holes, they contribute at some extent into shifting of absorption edge toward longer wavelength due to formation of mid-gap states that localize under the conduction band of TiO_2. These defects also are important when it is necessary to play with electrical characteristics of materials, for example, to perform the $n \rightarrow p$

(a)

Samples	τ_1 [ps]	τ_2 [ps]	I_1 [%]	I_2 [%]	I_1/I_2	Rate/H_2 (mmol g^{-1} h^{-1})
TiO_2-R10(8:1)	189	322	46.33	53.67	0.86	16.4
TiO_2-R10(4:1)	206	336	56.58	43.42	1.30	22.5
TiO_2-R10(2:1)	208	341	60.03	39.97	1.50	20.6
TiO_2-R50(2:1)	211	345	61.74	38.26	1.61	16.5

(b)

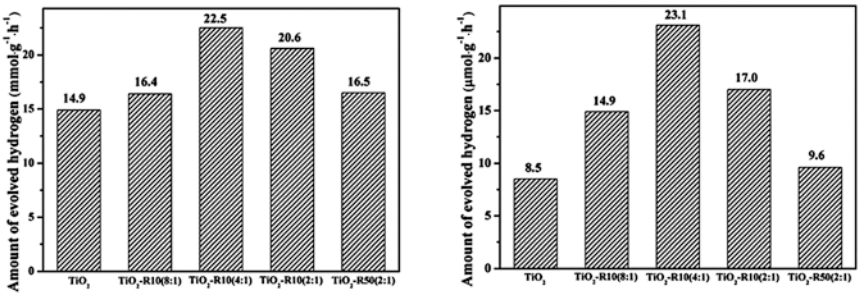

Fig. 3.1 (**a**) Positron lifetime, relative intensities, and production H_2 rates of the prepared samples. The lifetime components (τ_1) and (τ_2) qualitatively reveal the bulk and surface oxygen vacancies, receptively. I_1 and I_2 represent their relative intensities, and the intensity (I) embodies the relative concentration of the bulk or surface oxygen vacancies. (**b**) Effect of photocatalytic activity on the H_2 production rate of the samples (left image, under UV-vis light irradiation; right image, under visible light irradiation). Clarification of sample names is as follows. As samples were prepared via mixing TiO_2 and $NaBH_4$ using thermal treatment at Ar for calcination at 300 °C, labelling them as TiO_2-Rx(y) represents that x is the calcination time and *y* is the mixed mass proportion of TiO_2 and $NaBH_4$. (Reprinted from Ref. [6] with permission from *The Royal Chemical Society*. Copyright 2018)

transition within TiO_2 [7] or strengthening its conductivity [8] since they allow to reach higher uniformity of charge distribution by filling more volume.

As for achieving the precise understanding regarding the structure of bulk defects, it is explained in the following terms. Considering heavily packed crystal lattice, the number of enveloping chemical bonds and consequent presence of nearest-neighbors around atoms located deep inside materials is higher than those at the surface. Thus, realization of intrinsic bulk deficiency such as formation of vacancies or self-substitutional usually is ascribed via higher formation energy which is accompanied by relaxation of surrounding crystal lattice at much shorter distances [9]. It defines their lower stability than that of surface defects. In this regard, it is obvious that to create them, the application of severe synthesis protocol or more intense treatment procedure is required. For example, ion sputtering of ZnO with the energies at the range of 1–2 keV only resulted in exclusive appearance of defects located at the surface, and their presence could only be detected within topmost several atomic layers [10]. To make them become extended deeper into materials, it is required to increase the energy of this treatment up or even over ~90 kEv [11]. In this case, the presence of newly created defects in ZnO could be clearly identified by X-ray diffraction analysis and Raman scan which stated that their introduction reached the bulk of material. Thus, one may conclude that formation of defects in the bulk is often accompanied by the presence of surface-based deficiency, but not vice versa considering difference in applied energies and efforts.

Extrinsic defects Bulk doping often is regarded as an unattractive method to extend the photoactivity of desired compounds given several reasons. *Firstly*, introduction of foreign elements into surface layer is more energetically favorable and requires less formation energy [12, 13], similar to that of intrinsic deficiency. *Secondly*, bulk doping usually leads to development of structural defects and compositional disorders within the material structure as foreign atoms in order to advance their positioning deeply inside crystal lattice should "struggle" their way there causing along paved pathway the distortion and deformation of enclosing arrays of atoms resided in neighboring periodical arrays. Yet, it cannot be said that bulk doping should be completely abandoned and avoided since several reports that are available in literature demonstrated that its effectiveness in terms of charge separation rate and consequent photocatalytic performance can be, in fact, even higher than that of its surface counterpart. For example, Wang et al. [14] compared surface and bulk doping of WO_3 with Na and discovered that using former strategy resulted in more intense shifting up of Fermi level position and longer lifetime of electrons which highly contributed to the improved visible-light-driven (>420 nm) photodegradation of methyl blue. It was explained by more uniform spreading of Na ions within TiO_2 which allowed to reach increased mobility of charge carriers in "localized states."

3.3 Surface Defects

Intrinsic defects Surface intrinsic defects such as Ti^{3+} and oxygen vacancies in TiO_2 or oxygen and zinc vacancies in ZnO are considered to be efficient trapping centers which greatly contribute to the enhanced charge transportation and thus lead to increase of overall photocatalytic performance. Also, their presence can efficiently expand the absorption range toward visible light which is especially important for the materials that only are sensitive to UV light. It is correlated with the formation of localized energy levels within the band gap which allow to transfer electrons from valence to conduction band by utilizing photons with much lower energies. Experimental evidence determined that this process is more related to shallow trapping that is usually associated with introduction and presence of surface defects [15]. Furthermore, given that these defects often represent donor- and acceptor-like characteristics, respectively, they also effectively increase the concentration of relevant charge carriers as well as improve their mobility thus expanding overall lifetime and also sufficiently enhancing light-induced activity. In turn, numerous theoretical simulations confirmed reliability of this conclusion. For example, Alexandrov et al. [16] investigated $SrTiO_3$ via first principle calculation and determined that neutral surface oxygen vacancies turn out to be a much "more shallow defect than that in the bulk." In this regard, it was concluded that their defect level resulted in degenerating the conduction band which led to locally enhanced electrical conductivity since the number of charge carriers that were available over nearest ions became increased. As a result, semiconductor-based surface was transformed into "practically metallic" state, while its bulk counterpart remained to keep the original characteristics.

Thus, it represents that applying surface deficiency toward semiconductor materials might not only sufficiently improve already existing properties but also lead to appearance of new and unexpected features which are unusual for this concrete material, yet are highly useful and desirable in terms of their contribution into photocatalytic activity toward processing various reactions including decomposition organic pollutants and generation of hydrogen via water splitting. For example, Lv et al. [17] annealed ZnO under hydrogen flow at 455–475 °C for 1–9 h and discovered that formation of surface oxygen vacancies makes this wide band-gap semiconductor to become sensitive toward irradiation with visible light which resulted in enhanced photocatalytic performance. It was explained by increased width of valence band whose expansion was enough to promote the transport of electrons toward the conduction band by utilizing photons with energies lower than original band gap of ZnO, e.g., ~3.4 eV (Fig. 3.2). It is interesting to notice that when these defects were introduced mostly into the bulk of ZnO due to longer treatment or using higher temperature, no visible light photoactivity was observed despite enhanced absorption characteristics even though the overall improvement of performance under solar irradiation was reported.

As for the structure of intrinsic surface defects, they have much lower formation energy compared with that of the bulk ones. It is partially explained by more

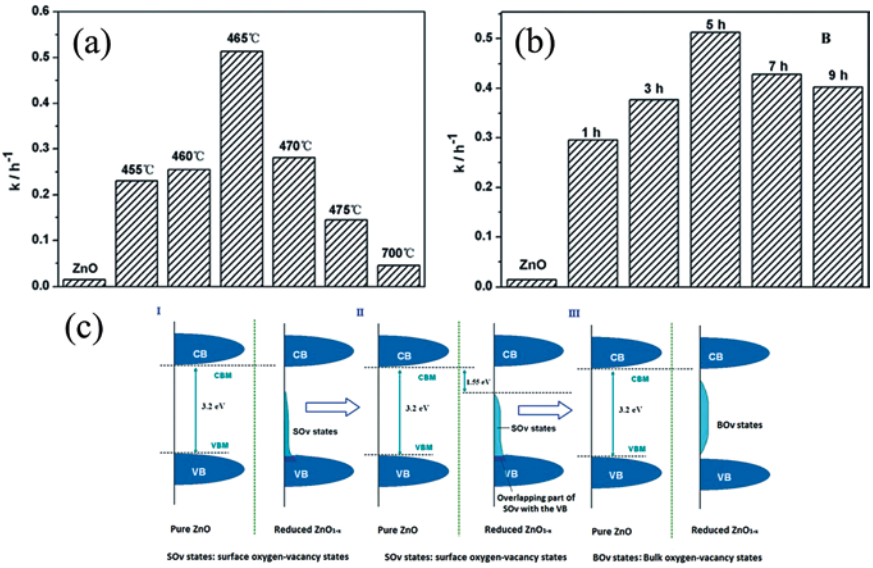

Fig. 3.2 A comparison of the visible photocatalytic activity of the untreated ZnO and ZnO after H_2 reduction treated with (**a**) various temperatures for 5 h and (**b**) various times at 465 °C on the degradation of MB, respectively (visible-light region in the range of 400–800 nm). (**c**) The schematic diagram of the energy band structure and the DOS of the pure ZnO and reduced ZnO_{1-x} illustrates the evolution of the DOS with the increase of oxygen vacancy concentration (from I to III). (Reprinted from Ref. [17] with permission from *The Royal Chemical Society*. Copyright 2013)

loosened structure of atoms at the surface which means that their evacuation requires the breakage of a smaller number of surrounding chemical bonding. In addition, relaxation of remaining atoms to adjust their positions with respect to newly formed defect can be proceeded with higher level of self-government and autonomy given much less influence by nearest-neighbor species. It means that stability of surface defects is very high and, at equilibrium conditions, it is more energetically favorable for atoms to leave the surface than struggle their way out from the bulk. This concept can be addressed to both cation- and anion-based vacancies as it happened, for example, in the case of ZnO [9].

Extrinsic defects Surface doping is regarded to be a very controversial approach to improve the photocatalytic efficiency as compared to the intrinsic deficiency, it might not always guarantee that resulting composition would show the expected performance or other related features and characteristics. The main challenge is that it requires to achieve uniform distribution of doped elements in the surface layer as to make locally relaxed and perturbated geometrical and electronic structures, respectively, become equally extended within crystal lattice thus realizing efficient and stable charge transportation. In this regard, bulk doping might become a more prevailed choice since its parameters are much easier to control due to larger volume and more homogeneous compositions. Thus, with certain rate of success, it enables to show better correlation with improved photoactivity.

Surface doping is usually realized via various approaches such as chemical synthesis, which is especially applicable to introduction of metal elements or by using thermal treatment in the defined and specially adjusted gas ambient at moderate temperature which, in turn, is more suitable for filling with non-metal elements. For example, Bjelajak et al. [18] applied annealing in NH_3 to TiO_2 which resulted in surface chemisorbed N species. However, these methods in certain terms are non-ideal as they can also lead to simultaneous doping of bulk. In turn, it was reported that using the deposition of thin layers or uniformly spread nanoparticles on the surface of target materials followed by consequent thermal treatment step might be an attractive approach to activate interdiffusion and realize doping within only the topmost surface layer. For instance, Oztel et al. [19] used sputtering to cover the surface of SnO_2 with Pt nanoparticles and later subjected to annealing at 600 °C to activate the doping procedure. The presence of Pt in SnO_2 was adjusted by the change of sputtering time as it allows to control the diameters of its nanoparticles. This approach has several important advantages. *Firstly*, it provides high flexibility in choosing the concentration and even depth at which the foreign atoms might be penetrated within the host crystal lattice; *secondly*, it can be applied to most of structures regardless their morphologies and compositions; and *thirdly*, it can be used for the elements and compounds whose level of solubility is extremely small due to large ionic radii and cannot be increased without forming additional phases and structures.

Special words need to be addressed for describing the nanolamination process via atomic layer deposition (ALD) or chemical vapor deposition (CVD), since it was discovered recently that this method can efficiently increase uniformity and solubility level of both surface and bulk doping. Its methodology is explained as follows: During growth of materials, a specified portion of doped element is introduced repeatedly into reaction chamber within fixed cycle number or moment of time for ALD and CVD, respectively. The higher the frequency of this introduction, the greater and the more uniform is the level of doping. After completion of deposition, the following thermal treatment usually is applied in order to activate interdiffusion thus making doped elements spread homogeneously. The temperatures that are used during this step are usually relatively lower than those applied for realizing conventional processing. For example, Su et al. [20] demonstrated that nanolamination protocol can be used to increase surface and bulk doping of Zn in TiO_2 from usually reported ~2% to impressive ~16% and ~8%, accordingly. This structure demonstrated highly increased photocatalytic activity as such a high concentration of Zn caused the appearance of additional electrons to be transferred in the direction of conduction band, thus increasing the density of surface reaction sites where molecules from surrounding media can be adsorbed. In another example, formation of Al-doped TiO_2 could only be activated at temperatures over 1200 K, while nanolamination-supported fabrication route allows to reduce it down to 450 °C. In this regard, the level of achieved bulk and surface doping was estimated as ~7% and ~16%, much higher than the standard one [21].

Thus, as can be seen, surface doping provides great opportunity to reach solubility of compounds whose ionic radii cannot allow them to be introduced in target

materials. Thus, it can be applied to a wide range of structures and compounds compared with that of bulk doping, making it an extremely attractive approach to create structures which under normal circumstance were hardly considered to be realized.

3.4 Distribution, Concentration, and Diffusion of Defects: Why Is It Important

The presence of defects in materials, whether intrinsic or extrinsic, is described by various characteristics such as concentration, distribution, nature, and migration or diffusion whose proper adjustment plays a crucial role in tuning their usefulness and applicability toward improved photocatalytic performance. Here, some of these characteristics are described in specific details in order to understand their importance and also to provide reliable mechanism of their proper control and adjustment within the materials.

3.4.1 Distribution of Defects

Intentional introduction of surface intrinsic defects, such as oxygen vacancies in $TiO_{2,}$ results in formation of localized regions around them which are usually described by increased density of charge carriers or, specifically, as in this case, donors. Thus, one can easily understand that if there is uneven distribution or improper assemblance and agglomeration of these defects in the form of separate clusters or islands, it might cause imbalanced charge transportation between localized regions between them which, in turn, lower mobility of charge carrier, thus making them trapped and consequently becoming recombined much easier. As a result, it leads to a critically declined rate of photocatalytic efficiency. Furthermore, presence of vacancies is greatly beneficial for attracting molecules from the surrounding media since they not only serve as their absorbing sites but also sufficiently contribute to their proper activation toward redox reactions. For example, Huygh et al. [22] investigated adsorption, dissociation, and diffusion of CO_2 on both fully oxidized and reduced anatase (001) surfaces using density functional theory calculation. It was revealed that processing of CO_2 molecules was completely unfeasible on the stoichiometric surface, while introduction of oxygen vacancy defects gave rise to new highly stable adsorption configurations with a stronger activation of the C-O bonds which results in exothermic dissociation of CO_2. These results were also confirmed by several experimental evidence such as those reported by Tan et al. [23]. Thus, it is evident that reaching only a partial coverage of surface with these defects states sufficiently lessens the expected outcome of photocatalytic reactions. In turn, once the formation of oxygen vacancies is properly harmonized

in order to make them become available in relatively uniform compositions with equal concentration all around surface or bulk areas, it leads to opposing results, as in additions to greatly stabilized and homogeneous migration and conformity of charge carriers, it also sufficiently increases the number of adsorbed molecules to be evolved into light-induced reduction and oxidation reactions in a simultaneous and efficient manner. Thus, it is unsurprising that distribution of defects, especially in the form of vacancies, has a clear linear dependency with the photoactivity of host material, i.e., the more uniform and continuous it is, the higher the performance as it was shown, for instance, by Gurylev et al. [3]. However, it also has certain limitations as once the surface is covered in absolute and equable term, the only parameter which continues to rise is the concentration of defects which might overcome saturation point and bring a negative impact.

Furthermore, the concept related to regular and continuous presence of defect is also highly important to realize their correct analysis and estimation via proper and reliable approach. Simply put, at their existence in the form of separated clusters and islands, the application of instruments which use point-based assessment such as X-ray photoelectron or Raman spectroscopies is assumed to be very tricky as accidently picking up the locations that are only covered partially or even absolutely free from any defects could provide incorrect information of their insufficient presence or even give a false impression of their complete absence, respectively. In this case, only mapping-based analyzing protocol might be regarded as a source of reliable information for them. For example, Gurylev et al. [24] investigated distribution of oxygen and zinc vacancies in hydrogenated ZnO via microzone photoluminescence spatial mapping procedure and defined that their appearances on the surface of hydrogenated ZnO occur in the form of separated islands with very random distribution and casual densities. Furthermore, it was determined that their localized appearances were closely linked to each other and thus both types of defects could not be considered as separated and individually existed species. Later, thus, knowledge was applied to fabricate ZnO filled with both oxygen and zinc vacancies which showed improved absorption in UV/vis spectra and enhanced photoelectrochemical efficiency under solar and visible lights [25]. The same methodology could also be realized using microzone Raman spatial mapping which along with providing clear and defining data regarding the disposition of intrinsic defects such as oxygen vacancies in TiO_2, in addition, can serve as a tracking tool to follow their evolution with regard to continuous advancement of applied treatment protocol [3] (Fig. 3.3).

As for extrinsic defects, their uniform and optimal distribution in the target material is usually defined by the absence of detecting any unnecessary and unexpected phases which could be interpreted as equalized spread of doped elements within crystal lattice without much accumulation and assemblance. However, it is a very relative estimation, as the precision and reliability of this observation are often correlated with the specification of technique which was applied to analyze the sample. Simply put, by checking X-ray diffraction, one might conclude that bulk structures have relatively uniform presence of dopants, yet, it does not mean that composition of surface layer should inevitably follow it as utilization of more surface-sensitive analysis is required to confirm it. This mechanism also works vice versa.

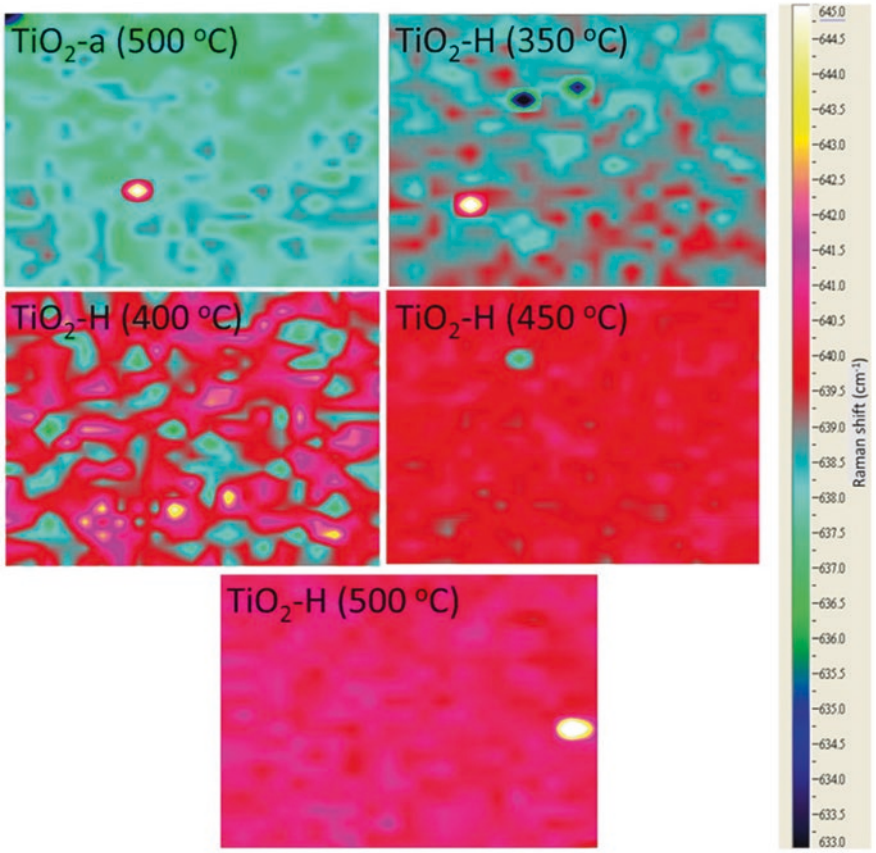

Fig. 3.3 Spatial two-dimensional color-coded mapping images of corresponding peak shift of main E_g Raman mode ranging from 633 to 645 cm^{-1} for TiO_2 thin films annealed in air at 500 C and annealed in hydrogen at 350–500 °C. For clarification, the more positive the position of this peak, the more oxygen vacancies are formed in TiO_2. (Adapted from Ref. [3] with permission from *Elsevier*. Copyright 2015)

Furthermore, one should become fully aware that during doping of small-scaled nanostructures, the introduced foreign atoms usually diffuse toward the surface, thus making the appearance of doping gradient in the material. This processing is called as "self-purification mechanism," and it was observed, for example, during introduction of Fe atoms into 20 nm-sized TiO_2 nanocrystals with atomic ratios ranging from 1% to 25% [26]. It results in uneven distribution of doped elements which in turn sufficiently reduces charge transportation, making the delivery of photo-induced electrons and holes to the surface more difficult. Thus, it is evident that reaching uniform spreading of dopants within the target materials is a challenging task. Even though several analyzing techniques might show that this target is reached, in fact, their concrete assemblance or accumulation might be beyond their

detection limit and is thus remained in shadow. To resolve it, it is suggested to use post-doping thermal treatment as to allow introduced foreign elements to be diffused around their host materials in a more proper way in order to reach better homogeneity, as it was shown, for example, in studies by Su et al. [20, 21].

In turn, it is interesting to notice that non-uniform doping can be used by some authors as a method to create *pn*-junction within the target material. For example, Zhang et al. [27] created thin film-related composition via assemblance of two structures where the bottom one represents a layer of TiO_2 doped with addition of Mn, while the upper one which is close to the surface remains to be undoped TiO_2. The authors stated that Mn^{4+} in the bottom layer becomes the electron acceptor and the photon-generated electrons transferred from surface-located layer toward them leaving behind holes. Thus, thin film-related composition was considered to contain n-type and p-type conductive bottom and upper layers, respectively. This structure showed much higher photocatalytic efficiency than that of uniformly doped TiO_2 when Mn additions were spread equally within both layers.

3.4.2 Concentration of Defects

One might consider that concentration of introduced defects, whether intrinsic or extrinsic, and photocatalytic activity has a clear correlation, i.e., the greater their presence and the more they are introduced into materials, the higher their influence in terms of increased donor and acceptor densities and improved charge separation efficiency, and also, the more mid-gap states are created with the band gap, the better is the absorption of light, and the more evident is the outcome in the form of enhanced light-induced performance. Yet, it works only till reaching a certain saturation point of defect concentration, as it was briefly mentioned above, beyond which their increments would only lead to gradual self-annihilation of associated localized charge carriers given their excessive presence or appearance of other negative effects. Thus, there always exists an optical concentration of defects which are associated with best light-induced performance. It has a clear relation with size, morphology, and type of target material. Considering TiO_2 as an illustration, Su et al. [28] investigated the behavior of this material under hydrogenation at 300, 400, 500, and 600 °C. It was revealed that the higher the temperature of treatment, the more oxygen vacancies were produced, and the more enhanced the donor density became (Fig. 3.4a, b). The best photoelectrochemical performance, however, was achieved by TiO_2 after hydrogenation at 300 °C (Fig. 3.4c). It was stated that at these conditions, oxygen vacancies reached a specific saturation point which satisfied the most balanced presence of donors. In turn, Gurylev et al. [3] applied relatively similar treatment with a slightly different temperature range of 350–500 °C and demonstrated that 500 °C, in fact, is the point at which the saturation of oxygen vacancies occurs, and thus it corresponds to the most favorable concentration of donors. Such a discrepancy might in part be explained by the fact that the former

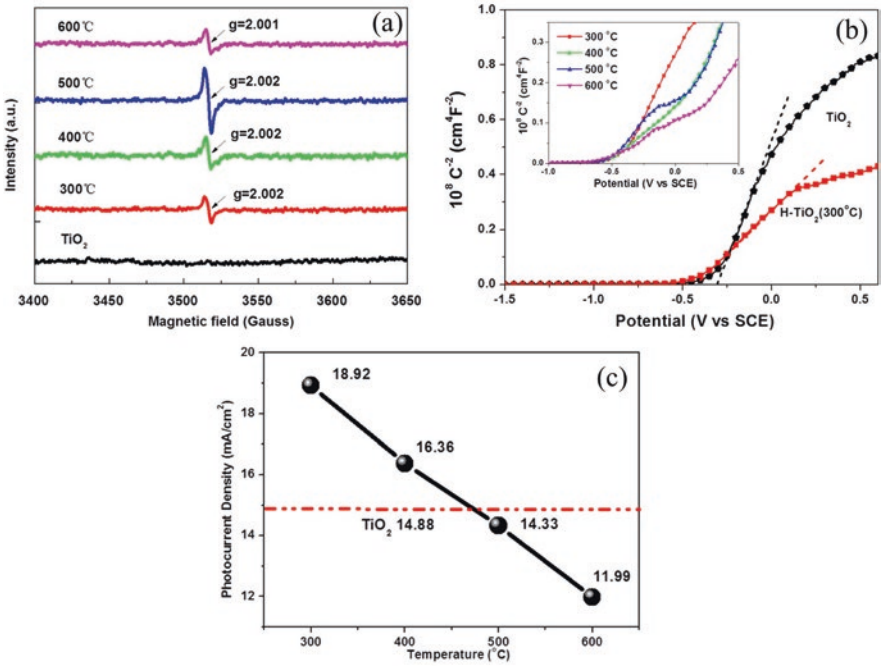

Fig. 3.4 (**a**) EPR spectra recorded at 300 K for TiO_2 and H-TiO_2 samples prepared at different temperatures. Signals at g = 2.002 and g = 2.001 are attributed to the defects like oxygen vacancy (with one electron). It is seen that the density of oxygen vacancy reaches saturation point on the surface of H-TiO_2 at 500 °C. (**b**) Mott-Schottky plots collected in the dark for the TiO_2 and the H-TiO_2 samples. Inset represents Mott-Schottky plots of H-TiO_2 prepared at 300, 400, 500, and 600 °C, which was collected under the same conditions. Smaller positive slope indicated higher donor density. (**c**) Photocurrent density of TiO_2 and H-TiO_2 measure using dye-sensitized solar cells setup. (Reprinted from Ref. [28] with permission from *American Chemical Society*. Copyright 2015)

study used nanoparticles with a dimension of ~300 nm, while in the latter case, thin film with thickness of ~22 nm was applied.

3.4.3 Diffusion of Defects

Diffusion of defects, especially intrinsic ones such as zinc and oxygen vacancies in ZnO, is determined by the energy of their migration barrier which they should overcome in order to become mobile so that they can become moveable within crystal lattice of target materials. Various parameters influence it, in particular, the type of defects, charge state, method which was used to create them, the nature of material that they belong to, etc. The last one is especially important as, for example, oxygen vacancies in TiO_2 and ZnO cannot be compared given differences in compositions

of both semiconductors, even though these defects have very similar descriptions, and thus each one should be regarded as a unique and separate case. Once the migration barrier is overpassed, the following outcomes usually occur as a result of defect diffusion:

1. Localized displacement of their position when a nearest-neighbor cation or anion atom moves into the vacant site leaving a vacancy behind. It usually occurs in order to reach the minimization of energy distribution due to appearance of defect.
2. Long-range motion when bulk defects tend to migrate toward the surface. This process despite its seeming simplicity has certain complications depending on the size and dimension of materials. Thus, it might lead to a different outcome. For example, Deng et al. [29] investigated migration of oxygen vacancies (V_O) in ZnO nanowires and determined that the smaller the wire was, the higher the ratio of surface unsaturated bonds versus internal bonds, the higher the bonding strength, and thus, the greater the barrier for V_O diffusion which prevented them from reaching the surface. On the other hand, the smaller wire possesses a lower rigidity of the lattice and hence could be relaxed more freely which decreases barrier for V_O diffusion, making its delivery to designated locations more accessible. Thus, due to this competition, only part of available oxygen vacancies might reach the surface even though migration barriers can be overpassed by all of them. It has to be noticed that diffusion also can be proceeded in an opposite direction, i.e., from bulk to surface, yet it is a rare phenomenon.
3. Bind with other defects and impurities creating associated complexes. This pathway has certain handicaps as the target defect instead of searching for right partner to be combined and thus increasing its feasibility might do this with its reverse equivalent and simply become annihilated completely as it happened, for example, during uniting of zinc interstitials and zinc vacancy in ZnO.
4. Removal of defect from materials via their out diffusion. Migration barrier determines which amount of additional energy should be introduced into the system in order to initiate this process. For example, ZnO crystals implanted with N^+, O^+, and Al^+, and co-implanted with O^+/N^+ and Al^+/N^+ ions, had to be subjected to temperatures above 800 °C to restore its original structure [30].

It has to be noticed that diffusion of doped elements into target materials is the main pathway to create extrinsic defects as they firstly need to be introduced into its surface by using doped-based sources such as surrounding gas phase or certain chemical and then under-applying external stress or via introducing additional energy making their way deeper into the bulk. In this processing, the doping concentration decreases gradually from the surface, and it is usually followed by accompanied formation and consequent migration of intrinsic defects which serve as compensation of introduced foreign elements. In this regard, there are two types of diffusion which can be applied to this process, namely, intrinsic and extrinsic diffusion. The first one is used when the dopant concentration is low compared to the intrinsic carrier concentration; thus, the diffusion coefficient is constant with respect to the dopant concentration, and it was observed, for example, in the study by

Shirasaki et al. [31] who investigated doping of $BaTiO_3$ with La and determined that this process is accompanied by the formation of Ba- and T- vacancy sites. In turn, during extrinsic diffusion, dopant concentration exceeds the intrinsic carrier concentration, which leads to appearance of electric field that assists in diffusion of doped elements deeper into the materials, thus making it called as concentration enhanced process. For instance, Radecka and Rekas [32] reported that incorporation of Nb into TiO_2 at a temperature range of 900–1300 K occurred by extrinsic diffusion mechanism governed via motion of titanium vacancies.

3.5 Defect Engineering of 0-D, 1-D, 2-D, and 3-D Materials

3.5.1 Brief Overview

Deep understanding of fundamentals regarding formation of intrinsic as well as extrinsic defects in semiconductors provides a great tool to achieve precise and accurate control over their various properties including electrical, electronic, and optical characteristics which are highly important in constructing functional and operational nanoscale photocatalysts that can show the required and practically applied efficiency. As it was mentioned above, defects result in both positive and negative developments as what happened with introduction of oxygen vacancies in n-type materials which in dependence of certain conditions might take the role of deep or shallow donors; thus, their presence has a significant influence on the intrinsic conductivity of materials, yet with different effect. Considering firstly the behavior of deep donors, it might take the function of annihilation centers for charge carriers thus leading to consequent gradual decrement of conductivity, while shallow-type defect, in turn, always behaves oppositely as their presence greatly contributes to its enhancement via creating additional electrons and assisting in supplying them toward the conduction band. Hence, one might consider that knowing how to introduce defect, to control their basic features and also in which particular way to keep their characteristics within the range of boundaries that determine their usefulness and practicability is enough to become aware of correct applying most essential principles of defect engineering making its practical coverage to reach the highest effectiveness.

Yet, it would be correct to say that this approach has limitation in applicability since the behavior of defects in various low-dimensional nanostructured materials cannot be accounted as similar and an absolutely identical process. In fact, it is highly influenced by particulate individualities of each of these materials such as morphologies, structures, and accompanied characteristics and might be different even within the same elemental systems. For example, in three-dimensional (3-D) materials, large structural distortion results in high formation enthalpy of specific defect, while in lower-dimensional counterparts, due to existence of voids or some kind of gaps between layers or ribbons, structural deformation can be accomplished

without applying significant energy penalty [33]. Thus, depending on the structural type of materials, the following phenomenon might be observed regarding the existence of defects and roles they take: low or high formation energies [9], ultra-long migration [34], changing role from charge dopants to the effective trap centers [35], etc. Furthermore, in some low-dimensional materials due to asymmetric coordination environment, the same atom can occupy several (or more) inequivalent lattice sites, thus causing distinctive defect properties which results in highly complicated chemistry even for simple binary composition compounds [33]. Finally, it is also important to consider that dimension of materials regulates the appearance of electron confinement and delocalization effects within it which might crucially influence the characteristics of introduced defects, or in reverse, likely to become the subject of defects' affection. Thus, it is important to address in specific and separate terms all types of low-dimensional materials with regard to particularities of concrete defect formation in them and consequent influences on modification of characteristics. Obtaining this knowledge would allow to understand which methodology is required to be applied to each of them in order to reach the expected outcome.

3.5.2 Defects in 0-D Materials

Zero-dimensional (0-D) materials belong to a class of materials where all three dimensions have a range within nanoscale limit of 1–100 nm (Fig. 3.5a). They usually exist in the form of quantum dots, particles, or spheres. For simplicity and convenience of discussion, in this section, we only consider quantum dot (QD) structures as they represent the most interesting, attractive, and fast-developing class of 0-D materials given their intensive application in electronics and energy devices. Formation of defects in them has certain particularities.

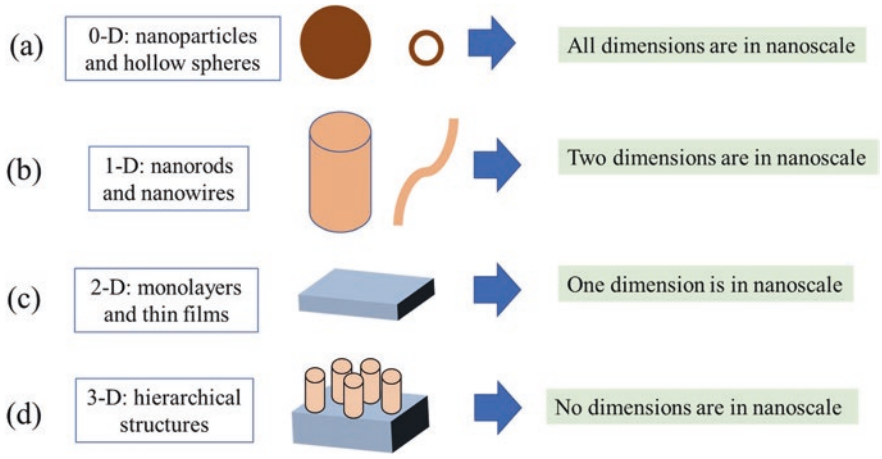

Fig. 3.5 Schematic illustration of low-dimensional nanomaterials

Firstly, taking into attention that their sizes usually are extremely small, it results in very high surface-to-volume ratio, thus causing a significant enlargement of surface deficiency ratio over that of bulk deficiency. *Secondly*, given that there is a clear contraction in any direction and dimension, it cases the appearance of very distinct quantum confinement effect which is associated with limited movement of both positive and negative charge carriers and is independent on the original type of conductivity. This effect occurs when the size of quantum dots is comparable or smaller than the exciton Bohr radius. For example, lead sulfide (PbS) has an exciton Bohr radius of 18 nm which represents that nanoparticles below this size should exhibit significant quantum effects. In case of TiO_2, this radius is only 1.5 nm, and one might suggest that consequences of quantum confinement effects are less likely to be observed in this material [36]. Overall, during its appearance, excitons gain additional energy which can be used as theoretical basis for increasing the band gap, thus leading to often observed blue shift in the absorption edge [37]. In this regard, introduction of defects such as donor-like vacancies into n-type materials results in strengthening of electron confinement within the QD where the holes, in fact, are also confined. Thus, due to the extreme localization of the electrons at the defect site, their k-vector becomes distributed in momentum space following description of Heisenberg's uncertainty principle. In this way, the Γ-point contributions of the electronic wave functions give rise to optically direct and, consequently, more efficient radiative transitions described as recombination of electron-hole pairs to release the photons [38]. As a result, there is sufficient reduction of effective concentration of available charge carriers, and consequently the outcome of photocatalytic reactions becomes declined. *Thirdly*, electronic levels of intrinsic defects may also experience influence of the confinement effect. For instance, green photoluminescence emission appeared at ~524 nm, and associated with oxygen vacancies or zinc interstitials is only weakly observed in the bulk ZnO but significantly visible in QDs [39]. *Fourthly*, doping of QDs with various useful impurities is an extremely challenging task. To be clear, incorporation of even a single impurity atom into a semiconductor nanocrystal with diameter of ~5 nm is equivalent to a dopant concentration of 10^{19} cm^3 which is likely the limit of extremely heavy doping in the case of a bulk semiconductor [26, 40]. This concept can be perfectly illustrated by comparing the study of Sun et al. [41] who reported filling of ZnO QD by La with molar mass ranging from 5% to 50% and to that of Pascariu et al. [42] who demonstrated that La concentration of only 0.02–4% was sufficiently enough to dope ZnO fibers with diameters of ~600 nm. Furthermore, it was also suggested that even though impurity atoms can easily become resided on the surface of nanocrystals, only the dopants which penetrated deeply inside it might play an important role in determining the electronic properties of their host [26, 43]. In particular, Andersen et al. [44] investigated doping of CdSe QD with indium atoms via simulation approach and determined that only after placing them exactly in the center of QD, the appearance of electrically active impurity states within band gap of CdSe was identified, while surface doping failed to achieve it. It was suggested that formation of these states either at or just above the highest occupied energy level was expected to contribute toward enhanced transportation characteristics within this particular material

system. However, realization of bulk doping of QD is a highly challengeable and nontrivial task given that only a small fraction of the added dopants is incorporated into the crystal lattice, as it is more energetically favorable to have them remain on the surface via forming clusters, segregating into a separate phase, or simply be adsorbing on the host [45]. *Fifthly,* precise and concrete localization of vacancies significantly influences on determining their role for governing optical properties of QD. For example, Pimachev et al. [46] used combined experimental and theoretical approaches to investigate spatial distribution of Zn vacancies in ZnS quantum dots and revealed that when Zn vacancies are located on the QD surface as a spot rather than being uniformly distributed over the surface and the core, the shift in absorption spectra toward the lower energies (about 0.1 eV) was observed.

Thus, it is evident that introduction of defects whether in the form of intrinsic or extrinsic, into QD and other 0-D nanomaterials, is considered to be a difficult task as it has great chance to lead for completely opposite results, and instead of expecting an increase of photocatalytic activity, one might observe its sufficient decrements or even disappearance. Following it, very careful strategy should be applied as to find the optimal balance between existence of defects and their influence in the electronic structure of their host materials as it was, for example, perfectly demonstrated in a study by Han et al. [47] who fabricated oxygen vacancy-rich SnO_2 quantum dots which showed nearly ~260 times higher efficiency in degradation of methylene blue under visible light.

3.5.3 Defects in 1-D Materials

One-dimensional (1-D) materials belong to class of materials where one dimension is beyond the nanoscale range (Fig. 3.5b). They usually exist in the form of nanotubes, nanowires, and nanorods. Charge carriers are confined within two dimensions, indicating that they can move freely only in one direction which usually represents the growth orientation. Formation of intrinsic and extrinsic defects in these structures was considered to have mostly positive impact since they cause the appearance of mid-gap states in the forbidden zone which not only increases the carrier concentration but also highly improves transition of electrons toward the conduction band. Besides, other characteristics such as mechanical strength, absorbance edge, higher surface area, etc. might be also extended as well. For instance, Park et al. [48] demonstrated fabrication of oxygen-vacancy-modified brookite TiO_2 nanorods to serve as visible-light-responsive photocatalyst, while Sutka et al. [49] reported that this goal could be achieved by ZnO nanorods via doping with Co. Furthermore, 1-D materials due to extremely large specific surface area and great chemical stability also can be used as a substrate for other nanostructures representing very attractive basis for depositing various metal and metal oxide nanoparticles and thus creating more complex compositions with advanced properties. In this case, intentionally introduced defects such as zinc and oxygen vacancies in ZnO nanorods provide a strong driving force for accommodating much larger number of

external atoms than that of the perfect surface resulting not only in selective loading and better interaction of these nanostructures but also effectively suppressing their consecutive sintering and accumulation which positively influence photocatalytic activity toward various reaction [50, 51]. Yet, it is incorrect to think that deficiency and improved characteristics of 1-D materials inevitably follow each other as positive outcome is not always possible. The reasons are that specific particularities regarding them in terms of both electronic and geometrical structures need to be taken into deep considerations.

Firstly, the mobility of electrons at certain conditions has a strong linear correlation with changing the diameter of 1-D materials, i.e., the larger their width, the more efficient transportation characteristics it has. As an example, Ford at el [52]. observed this phenomenon on InAs nanowires within the radius range of ~7–18 nm, Fig. 3.6a, b. Several mechanisms were suggested to explain it. Simply put, shrinking the width of 1-D structures leads to increasing the role of surface atomic roughness thus resulting in enhanced scattering of charge carriers, therefore effectively lowering their mobility. Furthermore, electron effective mass is likely to increase with the

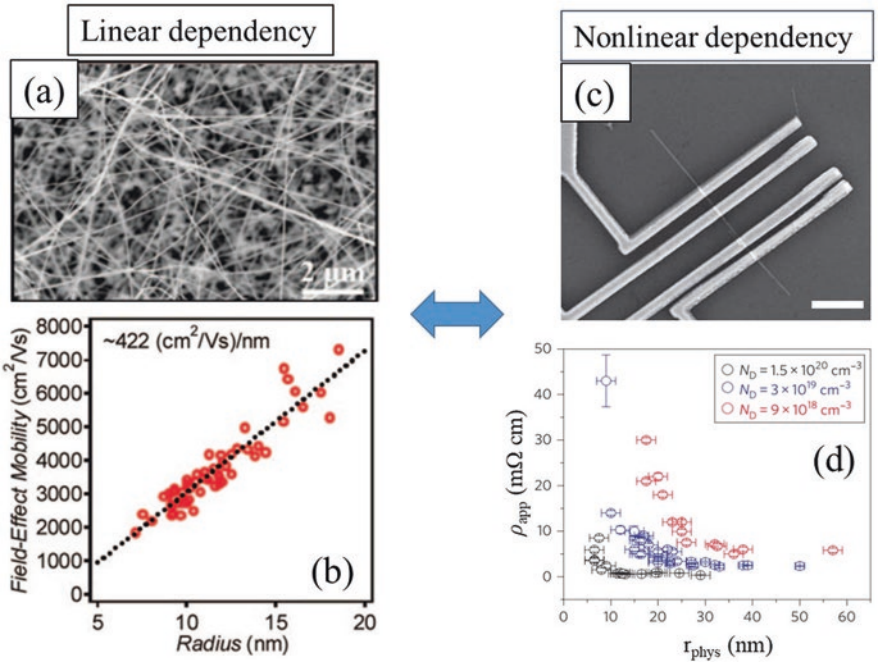

Fig. 3.6 (**a**) Electron microscopy characterization of InAs NWs. (**b**) Peak field-effect mobility as a function of radius for more than 50 different devices with NWs ranging from 7 to 18 nm in radius post oxide subtraction. (Reprinted from Ref. [52] with permission from *American Chemical Society*. Copyright 2009) (**c**) Scanning electron micrograph of a silicon nanowire contacted by metal electrodes in a multi-terminal layout. Scale bar, 1 mm. (**d**) Apparent resistivity of nanowires as a function of physical radius $r_{phys,}$ for various donor densities N_D. (Reprinted from Ref. [53] with permission from *Springer Nature*. Copyright 2009)

diameter miniaturization which provides additional difficulties in their effective transportation. Creating defects in these thin 1-D materials would only worsen electronic properties, making it much poorer than that of their thicker counterpart. To some extent, it also could be explained by the quantum confinement effect as with increased concentration of charge carriers, they become localized more extremely due to inability to move freely, thus forcing them to be recombined. This phenomenon is more associated with intrinsic deficiency and usually is referred to 1-D materials with diameters up to 10–15 nm. As for the extrinsic deficiency, it was reported recently that negative impact of doping on the characteristics of these structures exceeds that of intrinsic deficiency and can be extended to a diameter even up to 30 nm. Given that at this size the impact of quantum confinement or other related effect associated with miniaturization on electronic structure of 1-D materials is almost negligible, alternative mechanisms were suggested to explain the damaging role of dopants. For instance, Björk et al. [53] investigated phosphorous-doped Si nanowires and demonstrated that instead of expected increase of conductivity, contrary different phenomena were onserved, namely, increased resistivity (Fig. 3.6c, d). It was referenced to the deactivation of doping atoms that occurred due to dielectric mismatch imposed by the transition from a silicon nanowire to air (through a 1-nm native oxide), which affects the ionization energy of donors inside the nanowire. The lower the donor concentration, the higher resistivity observed during doping, and the thicker the diameter of nanowires at which the negative impact of dopants began to appear. It is necessary to notice that theoretical models developed in earlier studies predicted that this mechanism could only be applied to nanowires surrounded by a low dielectric constant medium [54]. Yet, Björk et al. [53] stated in contrary that "doping deactivation… is a general effect for all doped semiconductor materials." *Secondly,* it is not easy to achieve uniform introduction of foreign elements into 1-D structures as often their dense forest composition, extremely high-aspect ratio morphology, and profound layered thickness become very huge obstacles for diffusion. Thus, more complex and advanced strategies such as atomic layer deposition should be applied in order to cover full length and scale of these structures. *Thirdly*, since most 1-D materials are typically grown vertically on the substrate, it is natural to define doping profiles vertically, in contrast to traditional planar devices. Yet, vertical geometry provides additional challenges for diffusion and ion implantation, the two currently dominating doping methods for planar structures and devices [55].

Thus, introduction of both intrinsic and extrinsic defects in 1-D materials might be regarded as not an easy task despite those numerous data which were reported in literature. In fact, very careful strategy should be used instead as to consider and estimate all particularities associated with various aspects of these structures including their charge carriers transport, quantum confinement effect, and, especially, the influence of their diameter and length.

3.5.4 Defects in 2-D Materials

Two-dimensional (2-D) materials are those made up entirely of their surface and are often only a several atomic layers thick (Fig. 3.5c). Each layer in these materials is atomically thin with semi-infinite lateral dimensions, and the layers are separated by an opening referred to as a van der Waals gap due to the type of bonding that holds the layers together [56]. Electrons in these materials can freely move in x and y directions, but they have restricted extension in the third z direction. Owing to their atomically layered structure, 2-D materials commonly exhibit some very unique features, including extremely high electric conductivity, unprecedented flexibility, greatly enhanced mechanical strength, and superior surface area. For example, taking graphene as a representative, its carrier mobility is ~250,000 $cm^2\ V^{-1}\ s^{-1}$ at room temperature, a good optical transparency of ~97.7%, and its theoretical surface area is 2630 $m^2\ g^{-1}$ [57]. Defects in 2-D materials can have more far-reaching effects than in other related low-dimensional counterpart. This is because nearly all its atoms are located on the surface, especially in the case of monolayers, as there are no bulk parts in these materials. Thus, alteration of the surface atomic arrangements due to defects can change certain properties dramatically. For example, band gap can be precisely tuned via changing orientations of grain boundaries and their consequent displacement. It is also possible to create additional optical peaks in the visible light range [58]. In turn, it was also reported that introduction of vacancy defects can decrease the Young's modulus making the materials softer, and the consequent vacancy reconstruction can stabilize it. This approach could be applied not only to the well-known 2-D materials such as graphene [59], but it has also found application in accessing topmost surface of some semiconductor materials such as ZnO [24].

As in other low-dimensional materials, formation of defects in 2-D materials has certain particularities which need to be addressed. *Firstly*, given its monolayer structures where it consists of only surface atoms, it is much easier to achieve control over manipulation and arrangement of defects with precision of atomic resolution. For example, knock-on damage threshold is dependent on chemical composition and atomic configuration [60]. Taking h-BN as an illustration, the threshold for removing N (84 kV) is higher than that of B (74 kV), and thus, the selective formation of B vacancies can be realized by irradiating this material with e-beam at energies of ~80 keV. These boron monovacancies induce the instability of neighboring atoms, resulting in capability to tune their presence and concentration. In turn, the relatively stable nitrogen atoms remain along the edge of these vacancy clusters having zigzag structure; thus, the defects are shaped into triangular-shaped holes [61]. *Secondly*, defects can result in very serious structural changes such as transition from a crystalline structure to a state approaching a random network or appearance of already amorphous composition [60]. *Thirdly*, extremely high impact of substrate on 2-D materials due to its low thickness makes the doping process a very challengeable task. Unlike bulk semiconductors, where the initial several tens of angstroms (Å) of material can be discarded, the doping of 2-D layers usually occurs

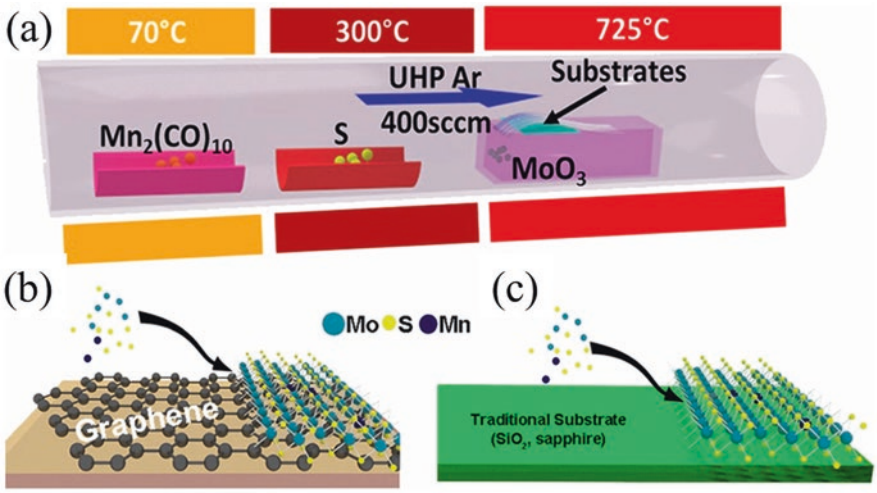

Fig. 3.7 Synthesis of pristine and manganese-doped MoS_2 is achieved using (**a**) traditional powder vaporization techniques. Dimanganese decacarbonyl ($Mn_2(CO)_{10}$) and sulfur (S) are located upstream of the hot zone, and molybdenum trioxide (MoO_3) and growth substrate are located in the hot zone during synthesis. The utilized substrates are (**b**) graphene and (**c**) traditional insulating substrates (sapphire and SiO_2). (Reprinted from Ref. [62] with permission from *American Chemical Society*. Copyright 2015)

within <7 Å of the 2-D/substrate interface [56]. For instance, Zhang et al. [62] reported that introduction of Mn into MoS_2 could only be realized with solid-source CVD when graphene is applied as the substrate instead of conventionally used SiO_2 or sapphires (Fig. 3.7) which provides many limitations in analyzing and application of this structure. *Fourthly*, there is absence of currently a universal standard to identify the defect concentration including both intrinsic and extrinsic types like that used for traditional semiconductor research as various methodologies and analyses are usually applied to achieve it [56]. In some cases, X-ray spectroscopy is employed to calculate their relative concentration, while in other cases cases, visualization images obtained via high-resolution transmission electron microscopy (HRTEM) are exploited to count how many atoms were removed or replaced. While doing these measurements, it is also highly important to understand what the role of the substrate is in the obtained data as often the signal depth from analyzing equipment has much higher depth resolution than the thickness of 2-D material.

In addition, 2-D materials provide unique opportunity to access the mechanism of defect-induced process via in situ visualization using common experimental techniques such as scanning tunneling microscopy or HRTEM. For example, Kurasch et al. [63] stated that "investigating the underlying mechanism of boundary migration in a 3-D material… reserved for computer simulation or analytical theory, as capturing the dynamics of individual atoms in the core region of a GB is well beyond the spatial and temporal resolution limits of current characterization techniques." However, these limits can be overcome "by investigating a 2-D material,

polycrystalline graphene, in an aberration-corrected transmission electron microscope, exploiting the energy of the imaging electrons to stimulate individual bond rotations in the GB core region." Thus, it allows to determine certain particularities of defect formation in these materials which also with certain reservation might be applied to other low-dimensional structures, compositions, and systems.

3.5.5 Defects in 3-D Materials

Three-dimensional (3-D) materials represent the class of materials that are not limited to the range of nanoscale in any dimension and direction (Fig. 3.5d). They can be introduced in the form of hierarchical structures, accumulation of nanoparticles, bundles of nanowires, nanotubes, or nanorods such as nanotrees or nanobushes, etc. Compared to other low-dimensional systems, 3-D materials provide a unique morphology, which is expected to have a larger surface area and thus to contribute effectively in more efficient transport of reactants and products, so that photocatalytic performance can be greatly improved. As there is no quantum confinement, the electrons are fully delocalized, indicating that their movement has no restrictions and can be proceeded in any direction and dimension. It is very similar to that observed for bulk materials; thus, 3-D structures are often called bulk nanomaterials, e.g., bulk-sized composition that constitutes of combined presence of nanoscale-based elements.

Fabrication of 3-D materials can be realized via assembling compounds with lower dimensions into more complex compositions. For example, Sridhar et al. [64] created three dimensional "graphene-nanotube-palladium nanostructure" that consists of carbon nanotubes vertically standing on graphene sheets with direct covalent bonding and palladium nanoparticles attached at the top of the carbon nanotubes. The resulting structure accumulates the positive properties of each of its compound as it showed an ultrahigh redox capacitance due to high porosity, extreme surface-to-volume ratio, and redox response of the palladium nanoparticles. Application of defect engineering not only plays a significant role in extending the properties of these 3-D structures further but also contributes strongly to their successful and smooth synthesis. For example, considering the abovementioned study of Sridhar et al. [64], it should be noticed that when carbon nanotubes (CNTs) became synthesized, different imperfections, which can be classified as point defects, dislocations, or plane defects are assisted in activating the growth of catalytic metal nanoparticles serving as their nucleation sites. Furthermore, intentionally designed defects can be introduced either in CNTs or graphene in order to increase the strength between them to make their sharing of charge carriers more effective and uniform.

However, formation of defects in 3-D materials cannot be considered to be only as positive contribution as it is also accompanied by certain particularities which need to be considered in order to reach correct projecting of their role and function. *Firstly*, due to composite structures, the general strategy to introduce intrinsic and extrinsic deficiency cannot be applied here, and each building block of 3-D materials

should be subjected to special treatment protocol supported by carefully designed and implemented conditions and requirements. Overall, it creates additional complexness to the experimental procedures and increases its cost and time consumption. *Secondly*, the development of 3-D materials implies the existence of some challenges in applying fundamental and traditional physics toward understanding the incorporation and activation of dopants as well as developing the metrics which can be used to assess the appropriateness of the created profiles. In addition, it is required to formulate new standards to be employed for quantifying them [65]. To be clear, focusing on small area analysis and very confined volume hardly can provide correct information regarding distribution of dopants and their precise positions in 3-D materials as due to their uneven spreading, it might bring erroneous conclusion regarding their presence. It is especially relevant given possible multilayered or hierarchical composition of these materials. The same as well can be addressed to introduction of intrinsic defects as their uniform coverage of extremely large surface area might not be advanced smoothly simply due to the fact that some of its regions have absence of direct contact with surrounding environment as what happened, for example, in the case of porous or mesoporous compositions. It requires to create additional diffusion of reactive compounds toward them to activate the desired processing such as initiating the evacuation of atoms and consequent formation of vacancies. Another problem is that target nanostructures often represent relatively non-similar materials system which respond differently for the same experimental condition. *Thirdly*, it is not easy to probe the introduction and consequent evolution of intrinsic defects as their clear detection might be challenging given that analyzing signal might not penetrate deep enough to estimate hidden areas or, oppositely, if it is multilayered or hierarchal composition or synchronously detect several materials making the interpretation of resulted signal more complicated.

3.6 Final Remarks on Defect Localization

Compositions and structure of materials is a very useful tool to achieve precise and accurate control over defect formation. It can also be used for consequent manipulation of their positioning, distribution, concentrations, and other related parameters, thus enabling them to be transformed into highly useful additions which are able to extend further the existing characteristics of the host materials, transforming it into strong photocatalysts. For example, localizing defects within bulk volume or surface layer compounds sufficiently influence their ability to govern the transportation of charge carriers. In the former case, it can be greatly deteriorated as defects that reside deeply into materials serve as recombination centers, while in the latter case, it oppositely sufficiently improved this feature since defects contribute to the enhancement of electron-hole separation rate, making them available for reaching the adsorbed molecules in a much higher quantity. In turn, changing the dimension, structure, or morphology of the materials where defects can be created also might be considered as a very attractive choice to precisely adjust their useful features. As

an illustration, it is obvious that, within the same level of doping or introduction of certain fixed concentrations of vacancies into 1-D and 3-D materials, they would serve completely different roles in adjusting their geometrical and electronic compositions given their certain structural particularities and morphological features. To be more precise, in 1-D materials, these defects have an ability to cause either positive or negative consequence depending, for example, on the diameter of nanowires or nanorods where they are going to be introduced as it brings into play the quantum confinement effect. For its part, in 3-D materials, the incorporated foreign atoms might be non-uniformly distributed within its structure making their presence hardly detectable and thus less influential or oppositely concentrated in very particular and the most exposed location within it creating undefined doping gradient. In another example, introduction of very low quantity of intrinsic defects in 2-D materials is highly sufficient to turn it into a very efficient compound given that all its atoms are located in the surface, and recombination process occurring in bulk can be simply avoided due to its absence as physical matter. In exchange, presence of vacancies or self-interstitials in 0-D materials is determined by their positioning whether on their surface or in its center where the latter location was discovered to be more influential than the former one in terms of further advancement in materials properties.

Thus, based on these examples, it is obvious that successful application of defects engineering cannot be considered without its close correlation with basic principles of material design and synthesis as not only defect itself determines their own functionality, usefulness, and practicability but also the type of structure or compositions where they are introduced, and their precise locations within them also plays an important and crucial role. Yet, in order to efficiently apply this strategy, deep knowledge and clear understanding of the defect positions, its spatial spreading, and correlation with internal atoms of host compound should be realized as without it, the attempts become more similar to try-and-error pathway. Another issue which needs to be considered is that analysis of defects often cannot be promoted correctly given the difficulties of accessing materials with certain morphologies and structures. In this case, application of more simplified constitution (only in terms of their morphologies leaving aside physical, chemical, and other related characteristics) might perfectly satisfy these requirements as, for instance, what happens via using 2-D structures whose planar and open spacing along with localization of all atoms at the range of visuality allows to clearly observe almost all processes happening within it. Later, it can be projected on more complex and advanced structures such as 1-D and 3-D materials.

References

1. M. Kong, Y. Li, X. Chen, T. Tian, P. Fang, F. Zheng, X. Zhao, Tuning the relative concentration ratio of bulk defects to surface defects in TiO_2 nanocrystals leads to high photocatalytic efficiency. J. Am. Chem. Soc. **133**, 16414–16417 (2011). https://doi.org/10.1021/ja207826q
2. S. Chang, W. Liu, Surface doping is more beneficial than bulk doping to the photocatalytic activity of vanadium-doped TiO_2. Appl Catal B **101**, 333–342 (2011). https://doi.org/10.1016/j.apcatb.2010.09.035

3. V. Gurylev, C.-Y. Su, T.-P. Perng, Surface reconstruction, oxygen vacancy distribution and photocatalytic activity of hydrogenated titanium oxide thin film. J. Catal. **330**, 177–186 (2015). https://doi.org/10.1016/j.jcat.2015.07.016
4. Z. Li, F. Wang, A. Kvit, X. Wang, Nitrogen doped 3D titanium dioxide nanorods architecture with significantly enhanced visible light photoactivity. J. Phys. Chem. C **119**, 4397–4405 (2015). https://doi.org/10.1021/jp512622j
5. Z. Wu, S. Cao, C. Zhang, L. Piao, Effects of bulk and surface defects on the photocatalytic performance of size-controlled TiO_2 nanoparticles. Nanotechnology **28**, 275706 (2017). https://doi.org/10.1088/1361-6528/aa7374
6. L. Hou, Z. Guan, M. Zhang, C. He, Q. Li, J. Yang, Adjusting the ratio of bulk single-electron-trapped oxygen vacancies/surface oxygen vacancies in TiO_2 for efficient photocatalytic hydrogen evolution. Cat. Sci. Technol. **8**, 2809–2817 (2018). https://doi.org/10.1039/C8CY00644J
7. S. Wang, L. Pan, J.-J. Song, W. Mi, J.-J. Zou, L. Wang, X. Zhang, Titanium-defected undoped anatase TiO_2 with p-type conductivity, room-temperature ferromagnetism, and remarkable photocatalytic performance. J. Am. Chem. Soc. **137**, 2975–2983 (2015). https://doi.org/10.1021/ja512047k
8. A. Klasen, P. Baumli, Q. Sheng, E. Johannes, S.A. Bretschneider, I.M. Hermes, V.W. Bergmann, C. Gort, A. Axt, S.A.L. Weber, H. Kim, H.-J. Butt, W. Tremel, R. Berger, Removal of surface oxygen vacancies increases conductance through TiO_2 thin films for perovskite solar cells. J. Phys. Chem. C **123**, 13458–13466 (2019). https://doi.org/10.1021/acs.jpcc.9b02371
9. D.Q. Fang, R.Q. Zhang, Size effects on formation energies and electronic structures of oxygen and zinc vacancies in ZnO nanowires: A first-principles study. J. Appl. Phys. **109**, 044306 (2011). https://doi.org/10.1063/1.3549131
10. A. Sulyok, M. Menyhard, J.B. Malherbe, Stability of ZnO{0001} against low energy ion bombardment. Surf. Sci. **601**, 1857–1861 (2007). https://doi.org/10.1016/j.susc.2007.02.011
11. J. Lv, C. Li, J.J. BelBruno, Defect evolution on the optical properties of H^+-implanted ZnO whiskers. CrystEngComm **15**, 5620–5625 (2013). https://doi.org/10.1039/C3CE40655E
12. J. Simfukwe, R.E. Mapasha, A. Braun, M. Diale, Density functional theory study of Cu doped {0001} and {01 2} surfaces of hematite for water splitting. MRS Adv. **3**, 669–678 (2018). https://doi.org/10.1557/adv.2018.180
13. M. Wu, D. Sun, C. Tan, X. Tian, Y. Huang, Al-doped ZnO monolayer as a promising transparent electrode material: A first-principles study. Materials **10**, 359 (2017). https://doi.org/10.3390/ma10040359
14. X. Wang, L. Pang, X. Hu, N. Han, Fabrication of ion doped WO_3 photocatalysts through bulk and surface doping. J. Environ. Sci. **35**, 76–82 (2015). https://doi.org/10.1016/j.jes.2015.04.007
15. V. Jovic, S. Moser, A. Papadogianni, R.J. Koch, A. Rossi, C. Jozwiak, A. Bostwick, E. Rotenberg, J.V. Kennedy, O. Bierwagen, K.E. Smith, The itinerant 2D electron gas of the indium oxide (111) surface: Implications for carbon- and energy-conversion applications. Small **16**, 1903321 (2020). https://doi.org/10.1002/smll.201903321
16. V.E. Alexandrov, E.A. Kotomin, J. Maier, R.A. Evarestov, First-principles study of bulk and surface oxygen vacancies in $SrTiO_3$ crystal. Eur. Phys. J. B. **72**, 53–57 (2009). https://doi.org/10.1140/epjb/e2009-00339-4
17. Y. Lv, W. Yao, X. Ma, C. Pan, R. Zong, Y. Zhu, The surface oxygen vacancy induced visible activity and enhanced UV activity of a ZnO_{1-x} photocatalyst. Cat. Sci. Technol. **3**, 3136–3146 (2013). https://doi.org/10.1039/C3CY00369H
18. A. Bjelajac, R. Petrović, M. Popović, Z. Rakočević, G. Socol, I.N. Mihailescu, D. Janaćković, Doping of TiO_2 nanotubes with nitrogen by annealing in ammonia for visible light activation: Influence of pre- and post-annealing in air. Thin Solid Films **692**, 137598 (2019). https://doi.org/10.1016/j.tsf.2019.137598
19. S. Oztel, S. Kaya, E. Budak, E. Yilmaz, Influences of platinum doping concentrations and operation temperatures on oxygen sensitivity of Pt/SnO_2/Pt resistive gas sensors. J. Mater. Sci. Mater. Electron. **30**, 14813–14821 (2019). https://doi.org/10.1007/s10854-019-01854-4

20. C.-Y. Su, C.-C. Wang, Y.-C. Hsueh, V. Gurylev, C.-C. Kei, T.-P. Perng, Enabling high solubility of ZnO in TiO_2 by nanolamination of atomic layer deposition. Nanoscale **7**, 19222–19230 (2015). https://doi.org/10.1039/C5NR06264K
21. C.-Y. Su, C.-C. Wang, Y.-C. Hsueh, V. Gurylev, C.-C. Kei, T.-P. Perng, Fabrication of highly homogeneous Al-doped TiO_2 nanotubes by nanolamination of atomic layer deposition. J. Am. Ceram. Soc. **100**, 4988–4993 (2017). https://doi.org/10.1111/jace.15044
22. S. Huygh, A. Bogaerts, E.C. Neyts, How oxygen vacancies activate CO_2 dissociation on TiO_2 anatase (001). J. Phys. Chem. C **120**, 21659–21669 (2016). https://doi.org/10.1021/acs.jpcc.6b07459
23. X. Tan, G. Qin, G. Cheng, X. Song, X. Chen, W. Dai, X. Fu, Oxygen vacancies enhance photocatalytic removal of NO over an N-doped TiO_2 catalyst. Cat. Sci. Technol. **10**, 6923–6934 (2020). https://doi.org/10.1039/D0CY01394C
24. V. Gurylev, C.-Y. Su, T.-P. Perng, Distribution pattern and allocation of defects in hydrogenated ZnO thin films. Phys. Chem. Chem. Phys. **18**, 16033–16038 (2016). https://doi.org/10.1039/C6CP01768A
25. V. Gurylev, C.-Y. Su, T.-P. Perng, Hydrogenated ZnO nanorods with defect-induced visible light-responsive photoelectrochemical performance. Appl. Surf. Sci. **411**, 279–284 (2017). https://doi.org/10.1016/j.apsusc.2017.03.146
26. S. Manu, M.A. Khadar, Non-uniform distribution of dopant iron ions in TiO_2 nanocrystals probed by X-ray diffraction, Raman scattering, photoluminescence and photocatalysis. J. Mater. Chem. C **3**, 1846–1853 (2015). https://doi.org/10.1039/C4TC02362E
27. K. Zhang, W. Xu, X. Li, S. Zheng, G. Xu, Effect of dopant concentration on photocatalytic activity of TiO_2 film doped by Mn non-uniformly. Open Chem. **4**, 234–245 (2006). https://doi.org/10.2478/s11532-006-0010-8
28. T. Su, Y. Yang, Y. Na, R. Fan, L. Li, L. Wei, B. Yang, W. Cao, An insight into the role of oxygen vacancy in hydrogenated TiO_2 nanocrystals in the performance of dye-sensitized solar cells. ACS Appl. Mater. Interfaces **7**, 3754–3763 (2015). https://doi.org/10.1021/am5085447
29. B. Deng, A.L. da Rosa, T. Frauenheim, J.P. Xiao, X.Q. Shi, R.Q. Zhang, M.A.V. Hove, Oxygen vacancy diffusion in bare ZnO nanowires. Nanoscale **6**, 11882–11886 (2014). https://doi.org/10.1039/C4NR03582H
30. Z.Q. Chen, M. Maekawa, A. Kawasuso, R. Suzuki, T. Ohdaira, Interaction of nitrogen with vacancy defects in N^+-implanted ZnO studied using a slow positron beam. Appl. Phys. Lett. **87**, 091910 (2005). https://doi.org/10.1063/1.2037847
31. S. Shirasaki, M. Tsukioka, H. Yamamura, H. Oshima, K. Kakegawa, Origin of semiconducting behavior in rare-earth-doped barium titanate. Solid State Commun. **19**, 721–724 (1976). https://doi.org/10.1016/0038-1098(76)90905-4
32. M. Radecka, M. Rekas, The studies of high-temperature interaction of Nb□TiO_2 thin films with oxygen. J. Phys. Chem. Solids **56**, 1031–1037 (1995). https://doi.org/10.1016/0022-3697(95)00033-X
33. R. Kondrotas, C. Chen, X. Liu, B. Yang, J. Tang, Low-dimensional materials for photovoltaic application, J. Semicond. 41 (2020) en/article/id/3a2b181b-c0aa-4536-84d3-f4af6345b09e
34. Q. Chen, H. Li, S. Zhou, W. Xu, J. Chen, H. Sawada, C.S. Allen, A.I. Kirkland, J.C. Grossman, J.H. Warner, Ultralong 1D vacancy channels for rapid atomic migration during 2D void formation in monolayer MoS_2. ACS Nano **12**, 7721–7730 (2018). https://doi.org/10.1021/acsnano.8b01610
35. J.-Y. Noh, H. Kim, Y.-S. Kim, Stability and electronic structures of native defects in single-layer MoS_2. Phys. Rev. B **89**, 205417 (2014). https://doi.org/10.1103/PhysRevB.89.205417
36. K.J. Balkus, Chapter 9 - Metal oxide nanotube, nanorod, and quantum dot photocatalysis, in *New and Future Developments in Catalysis*, ed. by S. L. Suib, (Elsevier, Amsterdam, 2013), pp. 213–244. https://doi.org/10.1016/B978-0-444-53874-1.00009-3
37. S. Repp, S. Weber, E. Erdem, Defect evolution of nonstoichiometric ZnO quantum dots. J. Phys. Chem. C **120**, 25124–25130 (2016). https://doi.org/10.1021/acs.jpcc.6b09108

38. M. Brehm, M. Grydlik, Site-controlled and advanced epitaxial Ge/Si quantum dots: Fabrication, properties, and applications. Nanotechnology **28**, 392001 (2017). https://doi.org/10.1088/1361-6528/aa8143
39. D. Haranath, S. Sahai, A.G. Joshi, B.K. Gupta, V. Shanker, Investigation of confinement effects in ZnO quantum dots. Nanotechnology **20**, 425701 (2009). https://doi.org/10.1088/0957-4484/20/42/425701
40. R.A. Abram, G.J. Rees, B.L.H. Wilson, Heavily doped semiconductors and devices. Adv. Phys. **27**, 799–892 (1978). https://doi.org/10.1080/00018737800101484
41. L.-W. Sun, H.-Q. Shi, W.-N. Li, H.-M. Xiao, S.-Y. Fu, X.-Z. Cao, Z.-X. Li, Lanthanum-doped ZnO quantum dots with greatly enhanced fluorescent quantum yield. J. Mater. Chem. **22**, 8221–8227 (2012). https://doi.org/10.1039/C2JM00040G
42. P. Pascariu, M. Homocianu, C. Cojocaru, P. Samoila, A. Airinei, M. Suchea, Preparation of La doped ZnO ceramic nanostructures by electrospinning–calcination method: Effect of La^{3+} doping on optical and photocatalytic properties. Appl. Surf. Sci. **476**, 16–27 (2019). https://doi.org/10.1016/j.apsusc.2019.01.077
43. D. Mocatta, G. Cohen, J. Schattner, O. Millo, E. Rabani, U. Banin, Heavily doped semiconductor nanocrystal quantum dots. Science **332**, 77–81 (2011). https://doi.org/10.1126/science.1196321
44. K.E. Andersen, C.Y. Fong, W.E. Pickett, Quantum confinement in CdSe nanocrystallites. J. Non-Cryst. Solids **299-302**, 1105–1110 (2002). https://doi.org/10.1016/S0022-3093(01)01132-2
45. M. Makkar, R. Viswanatha, Frontier challenges in doping quantum dots: Synthesis and characterization. RSC Adv. **8**, 22103–22112 (2018). https://doi.org/10.1039/C8RA03530J
46. A. Pimachev, V. Proshchenko, S. Horoz, O. Sahin, Y. Dahnovsky, The effect of spatial distribution of Zn vacancies in ZnS quantum dots on optical absorption spectra. Solid State Commun. **257**, 47–49 (2017). https://doi.org/10.1016/j.ssc.2017.04.004
47. X. Han, J. Zhao, L. An, Z. Li, Y. Xin, One-step synthesis of oxygen vacancy-rich SnO_2 quantum dots with ultrahigh visible-light photocatalytic activity. Mater. Res. Bull. **118**, 110486 (2019). https://doi.org/10.1016/j.materresbull.2019.05.011
48. S. Park, S. Baek, D.-W. Kim, S. Lee, Oxygen-vacancy-modified brookite TiO_2 nanorods as visible-light-responsive photocatalysts. Mater. Lett. **232**, 146–149 (2018). https://doi.org/10.1016/j.matlet.2018.08.086
49. A. Šutka, T. Käämbre, R. Pärna, I. Juhnevica, M. Maiorov, U. Joost, V. Kisand, Co doped ZnO nanowires as visible light photocatalysts. Solid State Sci. **56**, 54–62 (2016). https://doi.org/10.1016/j.solidstatesciences.2016.04.008
50. M.-H. Liu, Y.-W. Chen, X. Liu, J.-L. Kuo, M.-W. Chu, C.-Y. Mou, Defect-mediated gold substitution doping in ZnO mesocrystals and catalysis in CO oxidation. ACS Catal. **6**, 115–122 (2016). https://doi.org/10.1021/acscatal.5b02093
51. M.B. Boucher, S. Goergen, N. Yi, M. Flytzani-Stephanopoulos, 'Shape effects' in metal oxide supported nanoscale gold catalysts. Phys. Chem. Chem. Phys. **13**, 2517–2527 (2011). https://doi.org/10.1039/C0CP02009E
52. A.C. Ford, J.C. Ho, Y.-L. Chueh, Y.-C. Tseng, Z. Fan, J. Guo, J. Bokor, A. Javey, Diameter-dependent electron mobility of InAs nanowires. Nano Lett. **9**, 360–365 (2009). https://doi.org/10.1021/nl803154m
53. M.T. Björk, H. Schmid, J. Knoch, H. Riel, W. Riess, Donor deactivation in silicon nanostructures. Nat. Nanotechnol. **4**, 103–107 (2009). https://doi.org/10.1038/nnano.2008.400
54. M. Diarra, Y.-M. Niquet, C. Delerue, G. Allan, Ionization energy of donor and acceptor impurities in semiconductor nanowires: Importance of dielectric confinement. Phys. Rev. B **75**, 045301 (2007). https://doi.org/10.1103/PhysRevB.75.045301
55. J. Wallentin, M.T. Borgström, Doping of semiconductor nanowires. J. Mater. Res. **26**, 2142–2156 (2011). https://doi.org/10.1557/jmr.2011.214
56. K. Zhang, J. Robinson, Doping of two-dimensional semiconductors: A rapid review and outlook. MRS Adv. **4**, 2743–2757 (2019). https://doi.org/10.1557/adv.2019.391

57. L.-Z. Guan, L. Zhao, Y.-J. Wan, L.-C. Tang, Three-dimensional graphene-based polymer nanocomposites: Preparation, properties and applications. Nanoscale **10**, 14788–14811 (2018). https://doi.org/10.1039/C8NR03044H
58. Q. Li, X. Zou, M. Liu, J. Sun, Y. Gao, Y. Qi, X. Zhou, B.I. Yakobson, Y. Zhang, Z. Liu, Grain boundary structures and electronic properties of hexagonal boron nitride on Cu(111). Nano Lett. **15**, 5804–5810 (2015). https://doi.org/10.1021/acs.nanolett.5b01852
59. N. Jing, Q. Xue, C. Ling, M. Shan, T. Zhang, X. Zhou, Z. Jiao, Effect of defects on Young's modulus of graphene sheets: A molecular dynamics simulation. RSC Adv. **2**, 9124–9129 (2012). https://doi.org/10.1039/C2RA21228E
60. J. Jiang, T. Xu, J. Lu, L. Sun, Z. Ni, Defect engineering in 2D materials: precise manipulation and improved functionalities. Research **2019** (2019). https://doi.org/10.34133/2019/4641739
61. T. Xu, Y. Zhou, X. Tan, K. Yin, L. He, F. Banhart, L. Sun, Creating the smallest BN nanotube from bilayer h-BN. Adv. Funct. Mater. **27**, 1603897 (2017). https://doi.org/10.1002/adfm.201603897
62. K. Zhang, S. Feng, J. Wang, A. Azcatl, N. Lu, R. Addou, N. Wang, C. Zhou, J. Lerach, V. Bojan, M.J. Kim, L.-Q. Chen, R.M. Wallace, M. Terrones, J. Zhu, J.A. Robinson, Manganese doping of monolayer MoS_2: The substrate is critical. Nano Lett. **15**, 6586–6591 (2015). https://doi.org/10.1021/acs.nanolett.5b02315
63. S. Kurasch, J. Kotakoski, O. Lehtinen, V. Skákalová, J. Smet, C.E. Krill, A.V. Krasheninnikov, U. Kaiser, Atom-by-atom observation of grain boundary migration in graphene. Nano Lett. **12**, 3168–3173 (2012). https://doi.org/10.1021/nl301141g
64. V. Sridhar, H.-J. Kim, J.-H. Jung, C. Lee, S. Park, I.-K. Oh, Defect-engineered three-dimensional graphene-nanotube-palladium nanostructures with ultrahigh capacitance. ACS Nano **6**, 10562–10570 (2012). https://doi.org/10.1021/nn3046133
65. W. Vandervorst, C. Fleischmann, J. Bogdanowicz, A. Franquet, U. Celano, K. Paredis, A. Budrevich, Dopant, composition and carrier profiling for 3D structures. Mat. Sci. Semicon. Proc. **62**, 31–48 (2017). https://doi.org/10.1016/j.mssp.2016.10.029

Chapter 4
Analysis of Defects

4.1 Introduction

In the last years, photocatalysis has been regarded as sustainable, pollution-free, relatively cheap, and accessible technique which can achieve reactions that previously were considered to be proceeded mostly under highly extreme and very specific conditions such as dye degradation, water splitting, CO_2 reduction, nitrogen fixation, etc. Their industrial-supported realization currently results only in very low effectiveness and leads to consumption of enormous amount of external energy. However, despite very bright perspectives of this light-inducing processing and those numerous efforts which are applied worldwide to implement it practically, it is not easy to find the materials which can be used to govern photocatalytic reactions at sufficient and expected level as certain requirements need to be fulfilled to make its application feasible and reliable. For example, TiO_2 due to its nontoxicity, low cost, chemical stability, and strong capability to perform various redox reactions is considered to be one of the most promising semiconductors to be used. Yet, it also suffers from serious drawback such as inability to absorb visible light or extremely high recombination rate of photo-induced charge carriers. As it was demonstrated in previous chapters, employment of defect engineering might be a very attractive tool to resolve these problems and to make TiO_2 not only achieve a desirable level of photocatalytic performance but also sustain it for a determined and prolonged period of time. Simply put, adjusting and altering its morphology, composition, and specific structural particularities via introduction of certain defects brings sufficient modification and evolution of its geometrical and electronic configurations. Yet, to effectively realize this processing and make its optimization become practically feasible and productive, there is a strong need in the search for optimum access toward tracing and identifying changes which brings the introduction of intrinsic or extrinsic defects into it but also to identifying their concrete and precise presence of, including fixed position, concentration, and other related characteristics, so as to

V. Gurylev, *Nanostructured Photocatalyst via Defect Engineering*,
https://doi.org/10.1007/978-3-030-81911-8_4

understand in which direction the experimental proceeding and its accompanied theoretical assessment is supposed to be pushed forward in order to reach the designated goals toward further advancing of photocatalytic performance.

In fact, it is a very nontrivial and challengeable task since detecting various defect-related configuration and compositions might be very tricky and difficult due to their elusive and extremely diluted nature such as that which possesses oxygen vacancies created in metal oxides [1]. Thus, several well-established methodologies are usually applied to probe their existence and presence. *Firstly*, it is very common and acceptable that evidences of defect introduction especially the ones which have intrinsic nature can be obtained via indirect measurements, particularly following changes in various characteristics of material including its optical, electrical, magnetic, etc. properties. For instance, introduction of oxygen and zinc vacancies in ZnO causes extension of absorbance edge toward visible wavelength and also increases the number of photons with energies of UV range which can be caught. In turn, the presence of these defects also can be identified via shifts in conductivity of ZnO given that oxygen vacancies have clear donor-like features, while zinc vacancies demonstrate very pronounced acceptor-like behavior. Though this methodology is widely used, it cannot be considered as the most optimal choice since these changes often are hardly possible to be attributed as has been caused by only defect formation and also might be reasoned though occurrence of other processes happening within material. Returning back to the above example regarding ZnO, to create vacancies, it is required to use a very defined treatment protocol such as thermal annealing in hydrogen or vacuum at 300–400 °C which likely also influences the appearance of self-interstitials or other types of imperfections, not mentioning the changes in morphology or structure due to thermal stress. Thus, they also might contribute to the alternation of electrical or optical properties. *Secondly*, another approach to detect the presence of defects is related to direct analysis of their presence via specialized instruments and techniques. Even though it has advantages over that of indirect measurement, it also cannot be considered as totally ideal approach due to existence of some substantial drawbacks which put very specific restrictions on complete and full assessment of obtained data and its correct interpretation. As an illustration, spectroscopic analysis can be used not only to probe existence of intrinsic defects but also to access their concentration whether via counting related chemical bonding as it is realized by X-ray spectroscopy analysis (XPS) or by qualitative estimation of the influence caused by their appearance on rearrangement of surrounded atoms as it proceeded in case of Raman spectroscopy. However, this information often cannot be delivered in absolute values as those instruments rather taking the role of matching tools which are used to make comparison with original defectless sample and thus are more suitable for relative identification. In another case, direct visualization can be realized via microscope analysis, and it allows to clearly identify the existence of defects and even trace their motions and consequent evolution, yet it has very distressing limitation. Simply put, this approach only enables to be used within the range of highly localized domain due to small area of analysis and it leaving aside most of sample's volume thus making it less suitable for non-homogeneous compounds and compositions.

Following it, in this section, extensive overview of available instruments and techniques used to detect defects in semiconductor is provided in order to reach full understanding on which requirements need to be applied to create the conditions of analysis that allow to achieve proper access to desired dataset and its consequently correct interpretation. It has to be noticed that the main focus of this chapter is mostly dedicated to the description of only those techniques whose recognition and constant application transformed them into very common and readily available instrumentations that allow delivery of information easily accessible by most of the scientific community. Definitely, identification of defects in terms of applied instruments and techniques which is laid beyond those criteria such as thermal analysis is also represented, yet in very brief basis. It is explained, simply, by the fact that their adoption for widely spread utilization and/or the data they provided might not reach the levels that make them become broadly recognized as effectively operative tools. In addition, one also needs to consider that certain restrictions such as complexness, price, limit of accessibility in certain areas, and research groups also have very specific impact in their less frequent appearances in reported literature.

4.2 Electron Microscopy, Surface Scan, and Visualization Techniques

4.2.1 Transmission Electron Microscopy

Transmission electron microscopy (TEM) can directly imagine atoms by transmitting electrons through a specimen at high resolutions given that their de Broglie wavelength reaches down to 0.01 nanometers for relatively manageable speeds. Out of several types of TEM, spherical aberration corrected high-resolution transmission electron microscopy (Cs-corrected HRTEM) and spherical aberration corrected scanning transmission electron microscopy (STEM) deserve great attention and became the most widely applied techniques. In this regard, the latter technique can be used with different detectors to obtain high-angle annular dark-field (HAADF), annular bright-field (ABF), and annular dark-field (ADF) STEM images, all of which are highly effective and demonstrate better image resolution, sensitivity, and improved signal-to-noise ratios as compared with conventional TEM and high-resolution TEM [2]. Figure 4.1a shows Cs-corrected TEM image of rutile TiO_2 and its reduced analogy where small black and large white dots are considered to be the positions at which individual atoms of titanium and oxygen, respectively, are resigned. The formation of oxygen vacancies was regarded as missed white dots [3]. Following it, one might notice that titanium oxide that is available in the form of Ti_nO_{2n-1} is often called as Magneli phase [1].

It would be inaccurate to think that other types of TEM cannot be used to trace the formation of defects even though it provides certain complications in their correct identification as additional manipulation over obtained data is required. For

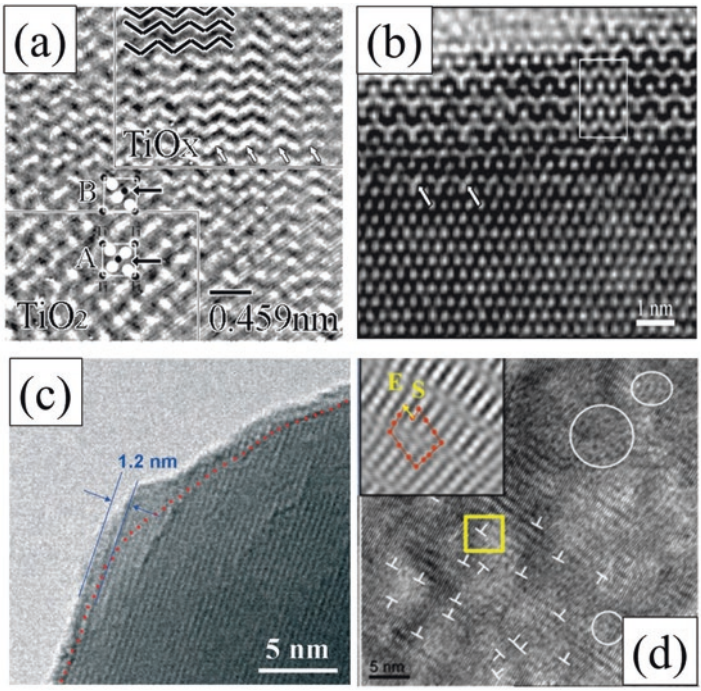

Fig. 4.1 (**a**) Experimental image of TiO_2 and a reduced titanium oxide (TiO_x) area. The upper right is a TiO_x phase, and the lower left is TiO_2. (Reprinted from Ref. [3] with permission from *IOP Publishing*. Copyright 2006) (**b**) HRTEM image of ZnO nanobelt. The inset is a simulated image. White arrowheads show defect area induced by zinc vacancies. (Reprinted from Ref. [4] with permission from *Elsevier*. Copyright 2006) (**c**) HRTEM images of the reduced ZnO_{1-x} showing existence of amorphous shell. (Reprinted from Ref. [5] with permission from *The Royal Chemical Society*. Copyright 2013) (**d**) HRTEM image of Zn-doped TiO_2 nanotubes. Inset is the enlarged Fourier reconstructed lattice image of the area marked by the yellow square. White circles show amorphous packets, while "⊥" symbols are designated for trapped dislocations. (Reprinted from Ref. [6] with permission from *The Royal Chemical Society*. Copyright 2015)

example, Ding et al. [4] performed the analysis of ZnO nanobelts and discovered the existence of black spots within the crystal lattice. To determine whether it belongs to zinc or oxygen vacancies, real HRTEM image had to be combined with the simulated one based on atomic model of superstructure. It was revealed that the "contrast change is only sensitive to the missing Zn ions" (Fig. 4.1b). As for indirect measurement, TEM can allow to evidence the defect-induced lattice distortion such as appearance of amorphous shell with a thickness of ~1–2 nm around the crystallite core due to presence of oxygen vacancies (Fig. 4.1c) [5] or existence of amorphous packets caused by accumulated dislocation as a results of metal doping (Fig. 4.1d) [6]. In addition, this analysis also can be utilized to monitor not only the increase/decrease of lattice constant which can serve as evidence for the shrinkage or

expansion of crystal lattice due to introduction of foreign atoms but also to follow the overall quality of crystal lattice via construction of diffraction pattern as it is inevitably related to changing the level of introduced deficiency.

4.2.2 Scanning Probe Microscopy (SPM)

4.2.2.1 Brief Overview of SPM Techniques

Recent achievements in scanning probe microscopy (SPM) have triggered extensive interest for this technique to be actively applied for investigation of atomic-scale defects and their influences on structural changes in morphology and various features. Generally, the mechanism of using SPM is fully reliant on quantum tunneling effect which allows electrons to escape from the tip in order to be directly transferred or "tunneled" toward the surface of target material where they can resign in the regions of space that originally are not permitted for them based on rules and concepts of classical physics. The probability of finding such tunneling electrons has exponentially inverse proportionality to the distance from the surface, i.e., the farer the surface, the lower is the current and opposite. Thus, changes in morphology, even within the sub-nanometer scale, have very determined influence on the strength and quality of the current. In this regard, this technique allows to trace atomic arrangement of the surface with precise accuracy. It is also necessary to notice that the sharper the tip, the more efficient is the emission of electrons, and the higher is the resolution of obtained images. There are several modes of SPM measurement which include contact, non-contact, and semi-contact types. These naming determines their basic principles of operation which define the type of tip interaction with the surface of sample during analysis. Following it, in this chapter, we only consider those of non-contact mode, as the other two might in some degree influence the shape and forms of morphological features and its partial deformation which is likely to lead to appearance of additional unrecognized and unexpected outcomes. Out of various SPM techniques reported in literature, scanning tunneling microscopy, atomic force microscopy, Kelvin probe microscopy, and conductive force microscopy deserved special attention as they often are used to determine presence of defect via direct and indirect measurements thus providing valuable information regarding their localized appearances and consequent influences in the specific characteristics of materials. Yes, this methodology is only applied to the topmost surface a depth of several atomic layers which in some cases can be considered as advantage and disadvantage depending on the goal of analysis and structure which it is subjected for. More details are provided below as they should be specified for each of the SPM types.

4.2.2.2 Scanning Tunneling Microscopy (STM)

Scanning tunneling microscopy (STM) is considered to be a highly unique tool to define the structure and compositions of intrinsic defects such as vacancies via straightforward observation of changes within the surface as it has integration of atomic scale resolution with localized spectroscopic potential. It is also can be used to visualize the presence of doped elements and to follow their distribution and consequent influence on changes of crystal lattice via accompanied processing such as formation of intrinsic defects, lattice distortion, etc. [7]. Furthermore, this technique allows to create defects such as oxygen vacancies in TiO_2 with very high precision and then realize their diffusion and desorption simply by applying various types and duration of pulse on sample [8]. Overall, numerous works currently available in literature, for example, review article by Diebold [9] and references there, demonstrate that successful application of SPM to detect various types of surface defects in semiconductor materials is a great methodology to investigate deeply their related characteristics and behavior and to understand how the morphological composition becomes altered following their existence and possible evolution.

Yet, despite these great achievements, realization of successful STM analysis might not be an easy task due to several limitations which need to be seriously considered in the course of its proceeding. *Firstly*, it is only applicable to materials whose conductivity is defined as sufficient enough to allow the quantum tunneling. *Secondly*, the interpretation of STM experimental results is often complicated given the fact that tunneling current has dependency not only on the topography of the surface but also on the local electronic structure as its variation is correlated with certain unexpected phenomenon such as presence of reconstruction sites or existence of various in-gap surface states with defined energies [10]. *Thirdly*, it is often complicated to define the nature of observable defects, i.e., whether it is intrinsic or extrinsic type, as they have very close resemblance during actual STM measurement despite their absolutely opposite origins that cause to initiate them. Taking CeO_2 as illustration [11], it was discovered that observed oxygen vacancies have high similarity to fluorine impurities and hydroxyl groups that are available on its surface in sufficient quantity and, therefore, are difficult to be distinguished based only on their visualization alone. Thus, additional approach is supposed to be used for defining their separate and unique existences which is usually relied on understanding the differences in their mobilities, relative concentrations in the surface and sub-surface layers, and tendency to form clusters in the surface layer. For example, STM measurements can be inevitably accompanied by theoretical simulation which highly assists in correct and adequate interpretation of atomically resolved images. The successful application of this methodology was demonstrated by Cui et al. [12] who investigated Mo-doped CaO film and determined by means of DFT calculations that experimentally observed defect features were connected to typical point defects in the CaO lattice. *Fourthly*, STM investigations are only meaningful for so-called model systems, i.e., well-characterized, usually single-crystalline surfaces, and under tightly controlled environments, normally in ultrahigh vacuum (UHV) [13]. Thus, additional checking is required to access the applicability of

these results to the real systems which are often kept under standard conditions of ambient pressure. *Fifthly*, analyzed defects due to their positions within proximity of the surface might have certain and very specific particularities which often create some difficulties in describing them as very unique surface-based features since they also often have partial or even full resemblance to that localized in bulk composition [14]. Overall, it can be said that this analyzing tool is very attractive as it provides direct observation defects. Yet, to achieve its high precisions and applicability to real systems requires additional efforts.

4.2.2.3 Atomic Force Microscopy (AFM)

The atomic force microscope (AFM) is a respected member of the family of scanning probe microscopes, and it is able to measure surface characteristics of various materials such as morphology and mechanical properties at nanoscale or even subnanoscale level without relying on their conductivity as it happened in the case of abovementioned STM. Compared with conventionally used scanning electron microscopy, AFM has the following advantages: more accurate topographical contrast, direct height measurement and unobscured view of surface features, and needlessness of any additional coating [15]. Another important feature of this instrument is that it can be used to quantitatively access the surface morphology in terms of its roughness, depth profile, etc. thus making the comparison between samples to be more correct and accurate as it does not rely only on visual observation.

In the non-contact mode and its improved version called tapping mode, the cantilever is held in the order of tens to hundreds of angstroms from the sample surface, and the interatomic forces between the cantilever and the sample are determined as a result of the long-range van der Waals interactions. The difference between these analyses is that while for original non-contact mode, the oscillations are usually limited solely by attractive force and are very low in frequency, in turn, during tapping, the cantilever has closer presence to sample surface and higher frequency of oscillations; thus, it might also cause the appearance of repulsive forces, so the tip intermittently touches or taps the surface [16]. Tapping mode has advantages over that of original non-contact mode which is that it provides improved lateral resolution of soft samples [15]. In addition, during AFM measurement, regardless the used mode, it is possible to obtain phase imaging which demonstrates differences in surface properties based on variation of composition, elasticity, adhesion, friction, electrical characteristics, and magnetism [17]. Therefore, this mode can give valuable information about existence of several different compounds within the composition of investigated materials even though its height analysis shows very uniform distribution of roughness profile.

AFM analysis is often used to indirectly access the formation of defects, as their introduction often causes the disruption of surface and leads to increased roughness profile as what happened, for example, in the study by Gurylev et al. [18], who investigated the formation of oxygen vacancies in TiO_2 thin films via hydrogenation at temperature range of 350–500 °C. It was discovered that roughness became

higher following the gradual escalation of the temperature during thermal treatment. This process is likely governed by continuous minimization of energy and consequent searching of new equilibrium that can only be realized via mass perturbations. In turn, phase imaging also might be used to understand the presence of defects especially the ones which are categorized as doping. Following the contrast, it is possible not only to trace the appearance of new phase, its spreading across the sample surface, and localized concentrations but also to reach some control over its development via external treatment procedure [19]. Yet, correct interpretation of phase images remains to be difficult. Simply put, often, it is not easy to verify that transformation of original homogeneity into heterogeneity can be directly attributed to the intrinsic or extrinsic deficiency as other related and non-related effects also should be considered.

4.2.2.4 Kelvin Probe Force Microscopy (KPFM)

Kelvin probe force microscopy (KPFM) was firstly demonstrated in 1991, and it is an imaging approach based on atomic force microscopy combined with well-known Kelvin probe method which is a vibrating capacitor technique. KPFM permits to analyzing the contact potential difference (CPD) between two materials at the nanoscale that are placed in parallel and to obtain a quantitative measurement of the surface potential with lateral resolution below 50 nm and potential resolution below 10 mV [20]. Thus, unlike other detection methods, KPFM enables characterization of local electrical properties at subtle and complex areas such as interfaces in nanomaterials and junctions in semiconductor devices and almost has no limitation regarding specifications and particularities of morphology. Utilization of a conducting cantilever with an extremely sharp tip ranging from 10 to 25 nm in radius allows to achieve it [21].

The principle of KPFM operation is as follows [22]. When an AFM tip is brought close to the surface of sample, an electrical force is generated between them as a result of difference in their Fermi energy levels. To establish the equilibrium, it is required that these Fermi levels become aligned at steady state, which can only be proceeded by means of electron tunneling between sample surface and tip. It is usually realized upon applying electric contact, at which point the electrons begin to flow in the direction of the lower to the higher Fermi level, and the system finally arrives to equilibrium state. As a result, the tip and sample surface getting charged and contact potential difference (V_{CPD}) appear, i.e., the difference in work functions of the tip and the sample which is formed due to non-similarity of their vacuum energy levels even though the positions of Fermi levels become aligned [22]. It has to be noticed that external bias can be applied between tip and sample to cancel the V_{CPD}. Schematically, this processing is shown in Fig. 4.2 where work functions of the sample and tip are designated as φ_s and φ_t, respectively. Since the work function of commercially available tips is already known, the work function of the sample can easily be collected from the Kelvin method. It is important to notice that the bias (V_{DC}) is applied to the sample (+) or the tip (−) has different signs.

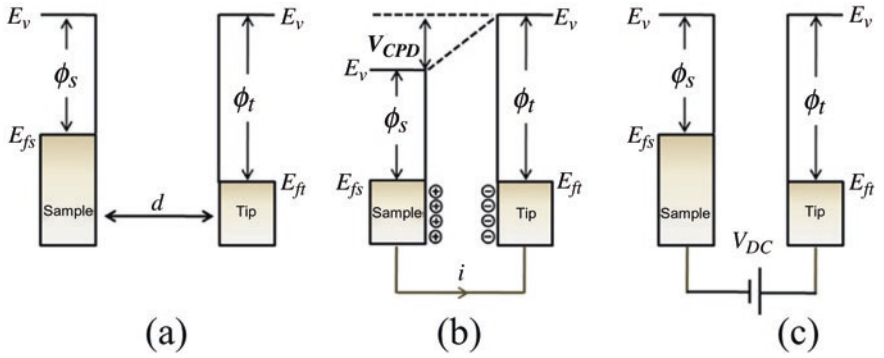

Fig. 4.2 Electronic energy levels of the sample and AFM tip for three cases: (**a**) tip and sample are separated by distance d with no electrical contact, (**b**) tip and sample are in electrical contact, and (**c**) external bias (V_{dc}) is applied between tip and sample to nullify the CPD and, therefore, the tip-sample electrical force. E_v is the vacuum energy level. E_{fs} and E_{ft} are Fermi energy levels of the sample and tip, respectively. (Reprinted from Ref. [22] with permission from *Elsevier.* Copyright 2011)

As measured value of V_{CPD} represents the statistical distribution of electrons in quantum states, and given its direct proportionality to the donor concentration [23], KPFM is often used to analyze the relative or absolute concentrations of not only already existing charge carriers but also the ones which were added into material via external processing or pathways due to introduction of intrinsic or extrinsic defects. Furthermore, their distribution, transfer characteristics, recombination rate, and lifetimes could also be accessed easily and, in addition, correlated with changes in surface morphology and accompanied variation of phase composition. Following it, commonly applied KPFM instrumentation is considered as an important tool to indirectly measure the presence, nature, availability, and distribution of defects in surface via probing its electronic properties. For example, Tosun et al. [24] investigated WSe_2 treated by mild plasma treatment (He or H_2) and discovered through measuring surface potential that energy balance was broken and Fermi level shifted toward conduction band for 200 mEv which corresponded to increasing the electron doping concentration by ~2200. These perturbations were attributed to the dominated formation of selenium vacancies. Later, this supposition was fully confirmed by other analysis. In turn, it also can be applied to measure how the work functions and, thus, the concentration of charge carriers is shifted due to the doping as it was demonstrated by Ben et al. [25] who determined that its value in As-doped ZnO nanorod is ~95 meV higher than that of undoped ZnO nanorods. Furthermore, based on quantitative estimations, KPFM also can be used to calculate the doping concentration and its type and also provide spatial resolved distribution map that shows localized residence of foreign atoms and its resolution depth are only dependent on the quality of measurement [26].

Several words need to say about direct visualization of defects via KPFM. Even though, it might become a powerful tool to detect their electrical characteristics, this analysis could be proceeded only via specially designed atomic-resolution imaging

and requires utilization of ultrahigh vacuum setup. Thus, it is practically a more complex process and might not suit well for a variety of materials. For comparison, measuring of surface potential in Refs. [23] and [25] was performed at room temperature and atmospheric conditions which makes accessibility of this analysis for everyday use highly attractive.

4.2.2.5 Conductive Force Microscopy (C-AFM)

Conductive atomic force microscopy (C-AFM) is based on the setup of AFM with only significant particularity being that the applied tip usually is covered with layer of conducting material such as $PtIr_5$, Pt, etc. Thus, when the tip-surface nanojunction is subjected to voltage difference, current flows through both metal-coated tip and the conducting sample, and it is used to construct charge distribution profile of the surface [27]. For clarification and simplified interpretation, the value of this current is considered as proportional to the surface conductivity or surface density of states and can be used as comparison between various samples given that the applied voltage is the unchanged. At the same time, AFM can still be utilized in its standard modification by vibrating the tip synchronously along with conducting mode to perform the topographical projection. It allows to compare and correlate variations in strength of current signal with surface-based morphological particularities and features on the basis of one to one. It is important to notice that two different analysis systems are used to perform both of these modes, i.e., pre-amplifier is employed to obtain current imaging and piezoelectric sensor attached to the cantilever allows to trace the morphology [27]. It is more an advantageous strategy than that used, for example, in STM, where both images are constructed via similar processing, namely, current appeared between tip and sample. However, while STM is well-known for many years to provide true atomic resolution on oxides, the resolution of C-AFM very seldom enables to overcome the limitation of nanoscale range. In addition, c-AFM allows to be used not only in imaging mode but also as a tool applicable for spectroscopic analysis as it can proceed with the creation of corresponding I-V curves at designated location of surface.

Application of this instrument to detect formation of defects mostly relies on the indirect measurement where the areas with higher or lower conductivities within 2-D/3-D mapping are usually attributed to the presence of intrinsic or extrinsic deficiencies. Comparing to topographical images allows to estimate their localization and spreading intensities within the compositions and structure of samples thus providing an access to control over them via changing the morphological characteristics. For example, Zhang et al. [28] investigated Cu-doped NiO via c-AFM. It was discovered that average current of samples increased following the rising of Cu content and reached the values of 2 nA, 14.1 nA, 47.6 nA, and 43.1 nA for pure, 1 mol %, 5 mol %, and 10 mol % doped NiO, respectively, under the bias of 1 V.

In turn, given that c-AFM usually accesses the topmost surface of samples at the depth of only several atomic layers, its combination with KPFM which also possesses very similar characteristics of measurement can be used to probe and verify

surface conductivity in terms of charge carrier concentration and its type via non-contact approach. It is especially important given that this kind of examination is highly demanded as currently the only available option is to use bulk analysis which definitely has certain limitations in providing access to systematic investigation of surface. For instance, the measurement achieved by Hall effect to determine the type of conductivity and calculate the concentration of charge carriers is relevant only to the whole body of structure and, hence, could hardly be used to achieve any valuable information regarding the processes occurred within the surface layer. Another example of bulk analysis which is widely employed to detect the electrical properties including the sign of detected charge carriers is the use of back-gate field-effect transistors. Yet, this approach is unable to determine whether the detected signal is coming from bulk or surface which sufficiently restricts its application due to sensitivity issue. Besides, it is important to state that both analyzing techniques should have a direct contact with the sample in order to be proceeded correctly, and it might seriously deviate the absolute values of surface conductivity and result in incorrect data acquisition given that possible destruction and damage of certain morphological features are likely to occur. In this regard, Gurylev et al. [23] investigated ZnO exposed to hydrogen plasma using combination of c-AFM and KPFM observations and discovered that average current increases following the treatment time, while its Fermi level shifts to valence band. Interpretation of this data led to the conclusion that increased conductivity can be referred to the proportionally raised concentration of holes due to dominated presence of acceptor centers, which transformed the surface of ZnO from n-type to p-type. Given that the both KPFM and c-AFM techniques as mentioned above can only probe the topmost surface at a depth of only several atomic layers, the bulk of the film remained to be n-type. It was discovered that appearance of acceptor-like zinc vacancies might be the main reason of observed $n \rightarrow p$ transition.

4.2.3 Another Microscopy Analysis

Apart from the abovementioned well-known microscopic techniques whose wide applications deserved numerous attentions in literature, there exist other less utilized but nevertheless also highly important visualized methodologies which deserved to be mentioned and shortly discussed.

(a) *Peak-force tunneling AFM (PF-TUNA) mode.* This type of measurement is exclusively delivered by Bruker Corporation and is based on quantitate acquirement of various important mechanical properties such as adhesion, modulus, deformation, and dissipation during analysis of current imaging within surface profile. The constructed maps are treated as conventional AFM channels and can be displayed and analyzed together with topography [29]. Given that the formation of defects usually results in degradation of crystal quality and its consequent “softening,” it is possible to use these mechanical characteristics to

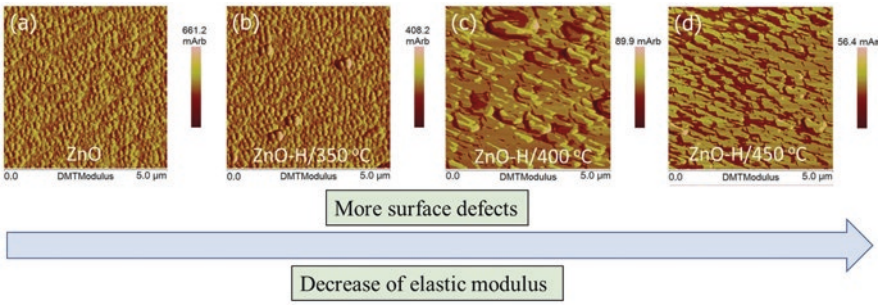

Fig. 4.3 Two-dimensional distribution of elastic moduli (**a**)–(**d**) of as-deposited and hydrogenated ZnO thin films. The higher is the temperature of treatment, the more surface defects are produced, and the softer the materials become. (Adapted from Ref. [30] from with permission from *PCCP Owner Societies*. Copyright 2016)

access localized appearances of intrinsic or extrinsic deficiencies with a depth resolution of only several atomic layers. For example, this strategy was successfully applied by Gurylev et al. [30] who employed variation of surface elastic modulus to visualize the distribution of accumulated defects on the topmost surface of ZnO and demonstrated that correlation between the surface morphology and their densities could be established (Fig. 4.3).

(b) *Confocal fluorescence microscopy.* This technique provides images of sufficient resolution and contrast to visually observe defects and enables to construct three-dimensional projections via combining a series of two-dimensional images of cross sections through an object [31]. For instance, Ameloot et al. [32] utilized this approach to detect defect formation in metal polycarboxylate metal-organic framework during synthesis.

4.3 Spectroscopy Techniques

4.3.1 Electron Paramagnetic Resonance (EPR)

Electron paramagnetic resonance (EPR) also regarded as electron spin resonance (ESR) spectroscopy is an extremely important and effective analysis to probe materials which demonstrate the existence of unpaired electrons. The basic concepts of this technique are very similar to that used by nuclear magnetic resonance spectroscopy, but instead of exciting the spins of atomic nuclei, in EPR, this action is applied to electron spins. Simply put, with applying the external magnetic field at a strength of B_0 to the materials that have unpaired electrons, it leads to their splitting for lower and upper states that possess magnetic spin quantum numbers (m_s) of $\pm 1/2$, and it depends on the alignment of the electron spin, S, either parallel (high-energy) or antiparallel (low-energy) to the magnetic field direction [33]. Both states are

separated by energy difference of $\triangle E = E_{+\frac{1}{2}} - E_{-\frac{1}{2}} = g\mu_B B_0$ in which g is the Landệ factor and μ_B is the Bohr magnetron equaled to 5.788×10^{-5} eV/T. As can be seen, splitting of electrons follows the increased strength of external magnetic field. This physical phenomenon is called as "Zeeman effect." To make their transition from the lower to the upper level, it is necessary to introduce photons with required energy (the conditions of $\triangle E = h\upsilon$ should be fulfilled) into the system and to make them become absorbed by these separated electrons. It also works vice versa as the emission of photons with similar energies can make electrons "fall down" from upper to lower level. Thus, the fundamental equation of EPR could be rewritten in the form of $h\upsilon = g\mu_B B_0$ where h represents Plank constant. It is very commonly accepted that the first derivative of the EPR signal is reported for the analysis.

A lot can be said about sensitivity of detection. It is proposed that the minimum detectable number of electron "spins" is proportional to $\upsilon^{(-7/2)}$. Yet, in real experimental systems, the maximum operating frequency is limited by more practical features such as availability of large enough magnetic fields, its homogeneity over the whole volume of a measurable sizes and dimension within the sample, etc. [34]. EPR spectrometers usually operate at several frequencies among which the following are considered to be the ones most applicable: K-band at 24 kMc/sec (GHz), 8 kG; Q-band at 34 kMc/sec (GHz), 12 kG; X-bands at 9.5–9.8 kMc/sec (GHz), and 3.3. kG. Other bands and specifications are also sometimes utilized depending on the target of analysis. Thus, it is evident that EPR technique is considered to be a branch of microwave spectroscopy. Yet, application of these frequencies imposes certain limitation in using EPR toward materials with volumetric sizes within nanoscale and sub-nanoscale ranges. For example, traditional employing of waveguide X-band results in inductive detection sensitivity reaching only range of 10^{11} spins at ~9 GHz at room temperature [35]. Bearing in mind that spin density is directly proportional to the amount of analyzed materials, it is obvious that this technique is mostly applicable for analysis of powders and film with high thickness and can hardly be used to probe thin film. This concern can be supported by the following estimation. For example, the spin density of amorphous TiO_2 is ~4.5×10^{16}/cm^3 as it was reported in Ref. [36]. The EPR analysis usually requires the minimum spot area of ~2×10 mm^2 to make signal become fully absorbed by sample. A simple calculation reveals that in order to obtain useful information from EPR analysis, the minimal thickness of TiO_2 thin film in this case should be within ~110 nm or higher.

The features of an EPR spectrum which yield useful information that can be applied in evaluation of the materials is collected under two main headings which are:

(a) g-factor—determines the value of the magnetic field at which the resonance might be observed for a designated operating frequency. It is very general that experimentally observed g-factors for defective materials usually lie in the range of ~1.7 to ~2.

(b) Intensity—the integrated intensity of a spectrum observed in EPR is directly proportional to the number of paramagnetic complexes participating in the resonance process [34].

The identification of defects regardless of their existence as intrinsic or extrinsic natures is perhaps one of the most interesting and studied applications of EPR, and in many cases, it is able to yield valuable information regarding their nature, concentration, positioning, and consequent evolution with changing of applied conditions. For example, Stefan et al. [37] investigated Mn-doped ZnO and revealed via EPR that localization of Mn ions in ZnO is realized in the form of three different configurations. Furthermore, it was also possible to quantitatively calculate the ratio of Mn ions in each of them. In turn, EPR also can be used to detect intrinsic defects such as oxygen vacancies in ZnO [5].

Yet, it is important to notice that EPR as analysis tool has certain drawbacks toward probing some specific materials which need to be mentioned as ignoring them might lead to incorrect interpretation of obtained result. For example, mentioned above ZnO are three different types of oxygen vacancies (V_O), i.e., with neutral, +1, and +2 charge states, and it is evident that only V_O with +1 charge could be detected by EPR as this defect has a paramagnetic nature and perfectly suit a band at g-factor of ~ 1.99 [38]. In turn, theoretical calculations demonstrated that oxygen vacancies in ZnO are only stable in +2 or neutral charge states, while charge +1 was determined to be thermodynamically unstable [39]. To generate them, highly metastable conditions should be realized. Once produced and detected, V_o^+ remains certain time within the ZnO and later gradually decays into +2 or neutral charge states [38]. Thus, it might be challenging to say that only a certain fraction of oxygen vacancies exist in ZnO based solely on EPR analysis as it cannot detect their more stable majority due to paired electron configurations.

Finally, it is necessary to comment very popular claim in literature that distribution of surface vacancies can be easily identified by EPR spectroscopy [40]. In fact, to realize this scenario, the use of probe molecules is highly required as only due to this it allows to make this measurement become surface sensitive [41]. Yet, its application was seldom mentioned. In the absence of it, the employment of EPR in its standard setup is limited by examining the condition of whole sample. It means that it allows to verify the presence of defects without straightforward interpretation of their positioning whether in surface or in bulk if only other instruments and techniques were used to identify with precise accuracy the attribution of particulate signal.

4.3.2 Positron Annihilation Spectroscopy (PAS)

Positron annihilation spectroscopy (PAS) is a well-established nondestructive high-sensitivity approach for selective detection and quantification of open volume sites in semiconductors presented in the form of voids, vacancies, and dislocations. During analysis, the sample is irradiated by a radioactive source, such as ^{22}NaCl,

which emits high-energy electrons with positive charges e^+, called positrons. It has to be noticed that maximum penetration depth of such positrons is within the range of ~0.1 mm; thus, this analysis hardly can be attributed to the surface-based approach as it mostly provides information about the bulk composition. Once the positron is penetrated into solid, it rapidly loses a sufficient part of its kinetic energy, making its motion similar to the diffusion of free particle until it comes in the immediate vicinity of an electron. The electromagnetic interaction between them results in complete annihilation of e^+-e^- pair leading to release of gamma photons which than can be detected [42]. Thus, the positron lifetime can be estimated as the difference between its birth and death, and it usually equals to the range of 100–400 ps (10^{-12} s) for crystalline solids, but exact value is strongly influenced by the localized electronic environment around it [43]. To be clear, its trapping in the vacancy sites can lead to the appearance of two phenomenon influencing standard annihilation process: (1) the average lifetime of the positrons can be prolonged, and (2) the energy spectrum of the emitted gamma rays can demonstrate certain variations [44]. Simply put, vacancy represents a region with lower electronic density which means that probability to encounter electrons there is much lower compared with that of defect-free areas. Thus, the existence of positron can be extended for longer duration. Furthermore, their lifetime is sensitively dependent on the size and even the configurational structure of the vacancy clusters as they have clear correlation with each other, i.e., the larger the size of vacancy, the more dissipated is its electron density, and the longer is the lifetime of positron [45]. In turn, the effect on the gamma spectrum is ascribed to the electron momentum distribution around the positron. The velocity of the electrons affects the gamma ray spectrum by the Doppler effect [44]: faster electrons result in larger Doppler broadening of the annihilation line in the gamma spectrum, while slower electrons only lead to reduce its width. Following it, application of PAS toward investigation of defects is usually realized via two major setups perfectly satisfying the representation of these effects: positron annihilation lifetime spectroscopy (PALS) and Doppler broadening spectroscopy (DBS).

It is interesting to notice that theoretically, PAS can only detect neutral or negatively charged defects, while their positive charged counterparts could not effectively trap positrons during their lifetime in a semiconductor [46]. Following it, it is very common to use this approach for investigation of acceptor-like vacancies which mostly represent metallic nature. For example, PAS enabled to demonstrate the existence of gallium vacancies in Ga_2O_3 given that they are generally available in the charge state of -2 [47]. Yet, it would be incorrect to say that probing anion vacancies is completely forbidden by this analysis as their presence in some semiconductors such as TiO_2 and ZnO can be realized in neutral form [38]. Hence, it becomes possible not only to identify them but also to quantitatively access their concentration and distribution. Importantly, the influence of negative and neutral vacancies on broadening of annihilations lines regardless of their attribution to anion or cation types is different. Taking bulk (defect-free) compound as a standard, it was discovered that appearance of former ones crucially changes their shapes, while the detection of latter one only results in detection of very slight variations [46]. Thus, it is very easy to distinguish existence of both types of defects in

materials, as it was, for example, demonstrated by Tuomisto et al. [48] who recognized simultaneous presence of zinc and oxygen vacancies in ZnO by using PAS.

Moreover, under certain conditions, existence of positively charged vacancies still can be detected by PAS, for example, when they present in very high concentrations, i.e., in the order of 10^{-2} atom^{-1} or more, and using the temperature of measurement over ~300 K. In this case, their positron trapping rate eventually can exceed typical positron annihilation rate in non-defective semiconductors which is of the order of ~5×10^9 s^{-1} [46], and, thus, certain information regarding introduction of positively charged vacancies into semiconductor materials can be obtained. Another approach which is commonly used is that formation of cation vacancies is often accompanied by the consequent appearance of anion vacancies in order to maintain structural stability and electrical neutrality. Thus, it is possible to use very approximate values for estimating relevant ratios of both types of vacancies with respect to each other.

Finally, it should be noticed that PAS is able to identify the existence and concentration of defect in terms of their residence whether in the surface or in bulk despite its high depth penetration. However, it is only applicable if structural characteristics and charge states of these defects are relatively same and thus cannot influence on the difference in signals in both localizations and also has no affection toward acquiring the parameters that are taken into consideration. To be clear, defects of small size are mainly available in the bulk, while their larger-sized projections are preferred to concentrate within the surface. It means that at *comparative and the only* assessment, the positron arrived to the bulk should be annihilated at much faster time and rate than those injected into the surface layer.

4.3.3 X-ray Photoelectron Spectroscopy (XPS)

X-ray photoelectron spectroscopy (XPS), also regarded as electron spectroscopy for chemical analysis (ESCA), is used to determine quantitative atomic composition and stoichiometry and provide deep understanding about the chemistry of materials. It is achieved via irradiating the sample with monochromatic X-rays and measuring the kinetic energy of emitted electrons. This energy usually depends on binding strength between electrons and nuclei and has clear relation to the structure of electron shell and the surrounding environment of atoms and thus is unique for each chemical element. XPS is a surface analysis technique with depth resolution reaching approximately ~10 nm and therefore is capable of providing information only about the outer layers completely excluding influence of underneath bulk. As an alternative, XPS also can be utilized to probe deeper layers which is proceeded via etching of surface by argon ion bombardment. Atoms of each elements except hydrogen have characteristic peaks in the XPS spectrum with specifically designated binding energies and intensities which enable their correct identification and consequent quantification. It usually occurs via measuring their broadening or shift, either positive or negative, as well as application of curve-fitting procedures such as

deconvolution and subtracting. In addition, it is also possible to determine chemical-related information of the detected elements, as, for example, to distinguish the oxidation state of metal compounds in binary structure or to realize whether the elements exist as a single component or it appears as a part of chemical compositions which stoichiometry, in turn, also can be recognized.

By considering its application to defect engineering, specifically introduction of extrinsic deficiencies, XPS can be used to reach the following goals: (1) define the successfulness of doping either by metal or non-metal elements and (2) in which form they are presented (chemical states); (3) specify the type of their chemical bonding with surrounding atoms in crystal lattice of host materials, i.e., whether it has substitutional or interstitials character; and (4) provide information regarding compositional atomic ratios of the surface in absolute and relative values. Example of this methodology can be found in Ref. [49] where XPS analysis of ZnO after doping with Mn demonstrated clear appearance of additional Mn 2p and Mn 3p peaks (Fig. 4.4a). Their analysis specified that a sufficient part of introduced Mn existed in

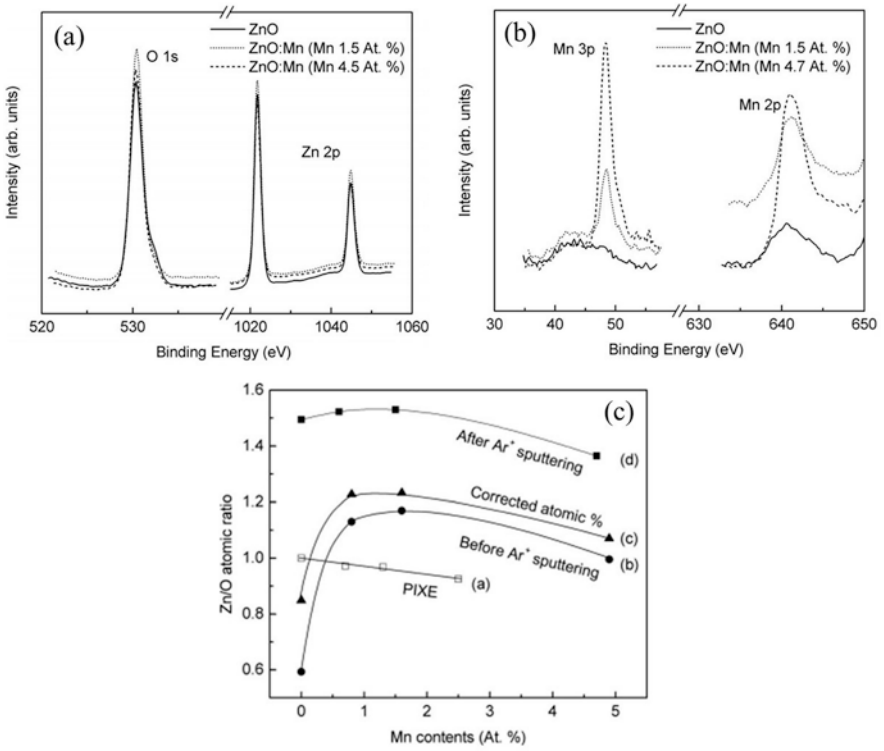

Fig. 4.4 (**a**) XPS spectra for ZnO and ZnO:Mn films (Mn regions). (**b**) XPS spectra for ZnO and ZnO:Mn films (Zn and O regions). (**c**). The ratio of zinc to oxygen, as a function of Mn content, where lines designated as (**a**) are from the PIXE (proton-induced X-ray emission) technique, (**b**) from XPS, (**c**) from XPS after correcting for hydrocarbon peaks in the spectrum, and (**d**) from XPS after Ar^+ ion sputtering. (Reprinted from Ref. [49] with permission from *AIP Publishing*. Copyright 2009)

2+ oxidation state. Furthermore, analysis of Zn 2p and O 1s XPS peaks revealed that ratios of their intensities remained to be the same before and after doping which means that Zn:O stoichiometry did not change due to the presence of foreign atoms (Fig. 4.4b). On its part, employment of XPS to define intrinsic deficiency leads to reaching very similar information regarding their chemical characteristics with only difference that it is mostly applied to determine presence and composition of vacancies, especially those of non-metal elements in binary compounds, while detection of self-interstitials atoms has been reported in much less extent. Moreover, as the existence of these defects might lower the level of crystallinity, XPS in addition can be used to indirectly probe the quality of crystal lattice within the surface layer. Another important particularity of analyzing intrinsic deficiency via this technique is that access to stoichiometry of target surface might be used to calculate with precise accuracy the concentration per unit area which also can be called as their density thus making comparison with defect-free compound more reliable. As an illustration, Gurylev et al. [23] demonstrated the employment of this concept in their work where exposure to hydrogen plasma was implemented to introduce zinc vacancies into ZnO which transformed it into $Zn_{0.86}O$, $Zn_{0.83}O$, and $Zn_{0.72}O$ following the treatment time. The concentrations of zinc vacancies in these samples were estimated as 5.74×10^{21} cm^{-3}, 6.97×10^{21} cm^{-3}, and 1.15×10^{22} cm^{-3}, respectively.

Finally, several words need to say about application of argon sputtering to create depth profile in terms of its influence on the variation of chemical stoichiometry as its consequence often has more disastrous outcome compared with that of materials where doping was considered as target of analysis (Fig. 4.4c). Simply put, Ar sputtering can cause very serious damage within the structure of some metastable compounds resulting in appearance of additional intrinsic defects and even partial reduction and thus degeneration of semiconductor features as what happened, for instance, in the case of InAs [50], where formation of metallic indium after this process was readily visible even by the naked eye. In another example, it was discovered that Ar sputtering of WS_2 might lead to certain desorption of sulfur atoms and consequent detection of metallic tungsten phase. In addition, removal of a small oxidizing fraction naturally existed in WS_2 and caused by non-ideal conditions of synthesis, consequent treatment or further storage was also observed [51]. Thus, one should be extremely cautious to use XPS depth profile measurement to analyze the distribution of intrinsic defects within different layers of materials as it might bring highly contradictive outcomes which provide very little information about real surface- and bulk-residing chemical compositions.

4.3.4 Valence Band X-ray photoelectron spectroscopy (VBXPS)

Valence band X-ray photoelectron spectroscopy (VBXPS) which also is recognized as ultraviolet photoelectron spectroscopy (UPS) has very similar principle of operation to that which is applied during XPS with only difference that it utilizes photons

with much reduced energies such as He^{I} (21.2 eV) and He^{II} (40.8 eV). Thus, their interaction is only proceeded with electrons having low binding energies that are mostly located at the valence band. It allows not only to deeper the understanding of electronic geometry within this band as, for example, to quantitatively access it shifting up due to appearance of additional tail but also to precisely estimate various important parameters such as work function, Fermi level, and, most importantly, absolute positions of both conduction and valence bands with respect to vacuum level. The latter is extremely important as it determines whether the material is suitable to perform given photocatalytically activated redox reactions. The introduction of defects usually results in certain deviations and changes of these characteristics which is considered as indirect proof of their introduction and can be further used for achieving proper analysis to identify their nature, concentration, and other related features with certain accuracy. Finally, the VBXPS also can be employed to confirm the formation of defect-supported mid-gap states and to provide access to their exact positions in terms of calculated distances from the valence band which is very evident in their presence compared with those parameters discussed above. As additional remark, it has to be noticed that as the energies of photons used in this instrumentation are very short, their penetration depth is much smaller than that of XPS and reaches only several tens of angstroms or even less. In view of that fact, VBXPS can find great application, for example, in accessing various extremely thin-layered compositions such as 2D structures as it allows to avoid substrate contribution into obtained response. At the same time, it provides additional difficulty in preparing sample surface as even atomic-scale contamination or accidentally adsorbed foreign molecules might disrupt this analysis.

Xu et al. [52] used VBXPS to investigate the bad-gap structure of BOCl without and with vacancies and determined that introduction of these defects results in appearance of valence band tail which shifted up its maximum from 2.16 to 1.76 eV. Thus, it leads to narrowing of band gap width from 3.25 to 2.91 eV making BOCl visible-light-sensitive materials. In another example, Su et al. [53] applied VBXPS to calculate the work function (Φ) of TiO_2 without and with doping with Zn using equation of $\Phi = h\nu - E_{cut} + E_{onset}$, where $h\nu$ (21.22 eV) represents the incident photoenergy from excitation source, E_{cut} is the cutoff region of the secondary electron, and E_{onset} is the onset of the Fermi edge (Fig. 4.5). It was discovered that Zn presence decreased the value of Φ in TiO_2 from 4.51 to 4.25 eV which meant that Fermi level was shifted toward conduction band; thus, it led to increased accumulation of charge carriers with donor-like characteristics.

A lot can be said about the comparison of analysis performed via VBXPS and KPFM toward evaluation of work function and Fermi levels as several importance dissimilarities existed between these two methods. *Firstly*, VBXPS is required to use ultrahigh vacuum, while KPFM can be performed at ambient conditions. Definitely, in the latter case, it might lead to certain deviation of acquired data, yet it also decreases complexness of measurement, its cost, and time consumption. *Secondly*, compared with VBXPS, KPFM provides the results of analysis mostly in relative units as it estimates work function difference with respect to specific reference sample, and additional efforts are required to transform it into absolute values.

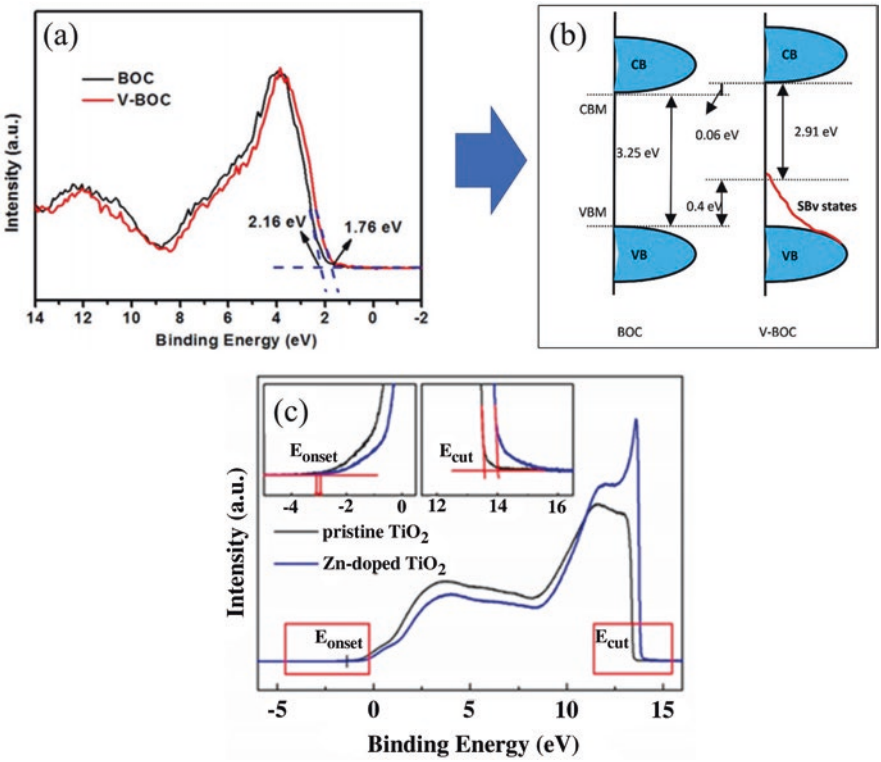

Fig. 4.5 (**a**) Valence-band XPS spectra of the BOC and V-BOC samples. (**b**) Schematic diagram of the positions of valence and conduction bands of BOC and V-BOC. (Reprinted from Ref. [52]. Copyright 2016, *Springer Nature*. Available under the Creative Commons Attribution 4.0 International License, https://creativecommons.org/licenses/by/4.0/) (**c**) UPS spectra of pristine and Zn-doped TiO_2. (Reprinted from Ref. [53] with permission from *American Chemical Society*. Copyright 2018)

Thirdly, KPFM allows to create spatial mapping of work function distribution and compare it with morphological features, while VBXPS is a point analysis which can only probe very localized regions at the surface.

4.3.5 Fourier Transform Infrared Spectroscopy (FTIR)

Atoms in molecule cannot be considered as static objects since they constantly vibrate around their equilibrium positions with specific frequencies which largely depend on various parameters such as their masses, quality of bonding established with other nearest-neighbor atoms, etc. For simplicity, it is generally considered that each vibration whether in the form of rotation or stretching occurs independently with respect to other similar motions around it. In this regard, Fourier transform

infrared (FTIR) uses infrared region of electromagnetic spectrum to measure how much light is absorbed by chemical bonds of these vibrating molecules. It works only if molecules of the sample undergo dipole moment change during vibration which is required to be nonzero [54]; otherwise, two bond dipoles simply cancel each other out, and no detection and analysis is possible. As for more details, the operation principles of FTIR are described as follows. When the monochromatic light with different wavelength is passed through the sample, the chemical bonding within the molecule is able to absorb the portion of it but only those where the frequency of irradiated photons is in a perfect alignment with their own frequencies. Thus, less light is transmitted, and the detector compares its intensity passing through the sample with that of light passing through the reference. As a result, identification of particular frequency at which the vibration of chemical bonding is proceeded serves as unique molecular fingerprint which not only allows to identify its nature but also can be used to determine in relative unit the concentration and proportions of various organic and inorganic compounds within the sample. It is necessary to notice that during FTIR measure, the frequency usually is expressed as a wavenumber (cm^{-1}), and it is defined as the inverse of the wavelength in centimeters. Thus, the higher the wavenumber, the higher the frequency, and the higher the energy of IR carriers, and the higher the penetration depth which can be analyzed within sample. In this regard, using IR with low wavenumber makes it more surface sensitive.

The introduction of extrinsic and intrinsic deficiencies crucially influences the vibration characteristics of chemical bonding within chemical composition of host material, as it results in their intensifying or, oppositely, slowing down. The evidence of this processing is usually received via estimating shift of main peaks in FTIR spectra toward higher or lower wavenumbers depending on the type of defects. For example, when a metal doping with elements which has lower oxidation rate is applied to TiO_2 in terms of substitutional defects, the reduced mass of newly created bonds such as M-O where M represents atoms from introduced metals dopants becomes higher than that of originally existing one which leads to negative shift in wavenumber during FTIR analysis [1]. For instance, Choudhury and Choudhury [55] reported that Ti-O vibration mode originally observed at 454 cm^{-1} for pristine TiO_2 was discovered to be relocated to 425 cm^{-1} after introduction of cobalt ions. This phenomenon also works vice versa as lower reduced mass of substitute-based bonds result in the shift of FTIR peaks toward opposite, positive, direction. The same mechanism is also applicable to the introduction of vacancies as released atoms also cause the decrease of the reduced mass. Finally, apart from the abovementioned detection of extrinsic deficiencies, it has to be noticed that FTIR can provide clear and direct evidence about actual formation of chemical bonding based on introduction of doped elements and its positioning in the crystal lattice of host material. As an example, Ntwaeaborwa et al. [56] demonstrated that after filling of ZnO with Eu, "broad absorption band around 451 cm^{-1} which might be assigned to Eu-O stretching mode confirming that some Eu^{3+} ions were introduced in the Zn^{2+} sites" was observed.

4.3.6 Raman Spectroscopy

4.3.6.1 Brief Overview

Raman spectroscopy is a vibrational technique that can provide information about chemical compositions of target solid samples following an analysis of its vibrational, rotational, and other low-frequency modes. It is based on detecting inelastic scattering produced by molecules through irradiation with monochromatic light with very specific wavelength and energy. As for a more detailed mechanism, it is explained as follows. Most of the light which goes through the material is supposed to be scattered elastically (Rayleigh scattering), which represents that its wavelength remains to be the same before and after interaction. In turn, very small fraction of photons such as one out of million more or less is scattered inelastically due to exchange of energy during interaction with molecules [57] which means that their wavelength becomes higher or lower compared with that of original wavelength. These changes are directly proportional to the vibrational and rotational characteristics of the molecule with which it has interaction as lowering or increasing of their intensities and frequencies, respectively, identifies the quality and level of scattering. Such an inelastic scattering is called to be Raman scattering, and the shifts of energy that incident photons are subjected after scattering is ascribed as Raman shift [58]. It can be used to characterize the nature and features of molecules within the materials which undergo interaction with light given that mentioned vibrational or rotational energies are very specific to each individual chemical bond or chemical component. Thus, it can serve as unique "fingerprint" to identity compositions of target structure, its particulates, as well as presence of impurities and contamination in it and thus can be effectively applied to perfectly suit the role of tracing intrinsic and extrinsic deficiencies.

There are now more than 25 different types of known Raman spectroscopy techniques [59], such as spontaneous Raman, hyper-Raman scattering, Fourier transform Raman scattering, Raman-induced Kerr-effect spectroscopy, and stimulated/coherent Raman scattering. Yet, most of them are often used in biological and medical sampling, and their application to defect engineering might be a nontrivial issue which requires additional understanding. In turn, another classification can be used to fulfill current purpose which make less complication in its access and thus more applicable. Simply put, given the low Raman scattering efficiency of most materials which means that it is not always easy to distinguish Raman peaks from the so-called background generated by the surrounding environment of the sample [58], the lamp-based systems that are commonly applied in fluorescence analysis, in turn, cannot be used here. Following it, a coherent laser source is often a necessary aspect to obtain detectable Raman scattering. In this regard, the choice of the laser(s) and its consequent wavelength is highly important, as it is affecting the outcome of the Raman spectrum in terms of its intensity, absence of noise, or other artefacts, and most importantly, it defines penetration depth and the ability to clearly detect designated vibrational modes assigned to specific chemical bonding. There are huge

numbers of various laser sources available currently such as helium-cadmium laser (325 nm), argon ion laser (364 nm, 488 nm and 514.5 nm), krypton ion laser (530.9 nm and 647.1 nm), helium-neon (632.8 nm), etc. Based on these types and comparing their wavelength to the electronic stricture of semiconductors, Raman spectroscopy analysis can be divided into resonance and non-resonance approaches whose main difference is that the former one results in better sensitivity and much higher intensity of resulting signal in obtained spectra which means that it can be used to analyze the materials at low concentration and density. In turn, the latter approach provides more information regarding the processes occurring within bulk which results in appearance of additional peaks in obtained spectra that are invisible by applying resonance conditions. As for more precise description, recognition and determination of both Raman scatterings for concrete semiconductor are usually proceeded by projecting the wavelength of incident laser to its absorption edge or band-gap value. For example, taking TiO_2 as illustration, it has a distance between valence and conductions bands of 3.2 eV (~390 nm), thus, the lasers whose wavelengths higher than ~400 nm are considered to produce non-resonance analysis, while those with wavelengths lower than that value results in measuring within resonance conditions. More details are provided below regarding both of these approaches in order to reach a deeper understanding on how their particularities and specification influence the detection of defects.

4.3.6.2 Non-resonance Raman Spectroscopy

In non-resonance Raman scattering (RS), where the photon energy of the laser is small compared to the energy of any electronically excited state, all molecular states participate in the scattering process and thereby contribute to the intensity of a particular Raman line in the spectrum. This type of Raman spectroscopy is considered to be classical one which is commonly applied in various fields as it does not require special preparation and setup to be used. It is usually assigned as bulk-sensitive techniques given that its penetration depth can overcome the dimension of analyzed materials; thus, it hardly can provide any valuable information regarding the conditions of the surface. The following illustration of this concept can be taken to demonstrate it. It is well-known that band gap of TiO_2 is ~3.2 eV which means that photons with this or higher energies could be effectively absorbed by it, while photons with lower energies (i.e., higher wavelength of incident laser) would be ballistically transmitted through this material in order to be absorbed by the substrate. Thus, TiO_2 structures with dimensions of several tens of nanometers simply cannot be detected. This concept was perfectly demonstrated by Gurylev et al. [18] who showed that TiO_2 thin film with thickness of ~22 nm was absolutely invisible during Raman analysis that used laser irradiation with wavelength of 512 nm. In fact, it resulted only in appearance of Si peaks served as a substrate (Fig. 4.6a, b).

Both intrinsic and extrinsic deficiencies can be effectively studied by RS given that their introduction usually leads to clearly defined modifications within local structure of target material supported by consequent rearrangement of

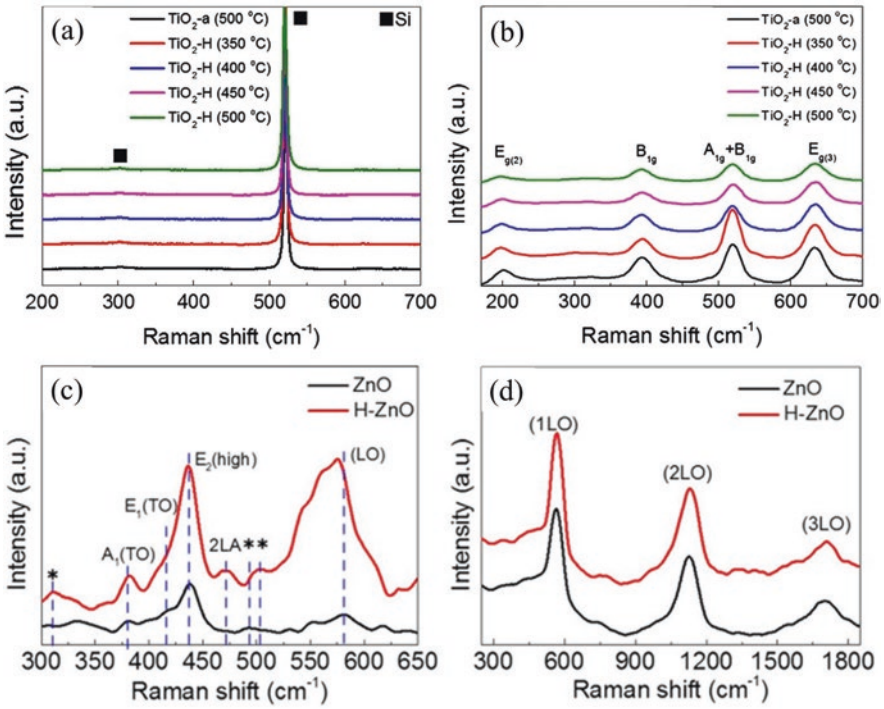

Fig. 4.6 (**a**) Visible (non-resonant) and (**b**) resonance Raman spectra of TiO_2 thin films annealed in air at 500 °C and in hydrogen at 350 °C, 400 C, 450 °C, and 500 °C. Thickness of film is 22 nm. All peaks in (**b**) belong to TiO_2. (Adapted from Ref. [18] with permission from *Elsevier*. Copyright 2015) (**c**) Visible (non-resonant) and (**d**) resonance Raman spectra of as-grown and hydrogenated ZnO nanorods. The assignment of each peak accompanied by the detailed descriptions can be found in original publication. (Reprinted from Ref. [61] with permission from Elsevier. Copyright 2017)

nearest-neighbor atoms in order to compensate the appeared difference in energy. As a result, new thermodynamic equilibrium is established which causes re-calibration of vibrational and rotational characteristics of molecules in order to reflect and compensate these changes. Thus, the positioning, intensity, and width of obtained Raman peaks become influenced. For example, Dhanalakshmi et al. [60] reported Raman spectra analysis of TiO_2 before and after doping with different ratios of Ce. The Raman spectra of all samples showed the appearance of well-resolved peaks assigned as $E_{g(2)}$, B_{1g},A_{1g} + B_{1g}, $E_{g(3)}$, and $E_{g(1)}$ modes which are considered to be characteristics of anatase phase. Out of them, the A_{1g}, B_{1g}, and E_g represent asymmetric bending vibration, symmetric bending vibration, and symmetric stretching vibration of the O-Ti-O bonds in TiO_2, respectively. As the weight percentage of Ce increases, the intensity of all the peaks decreases, and the highly intense Raman peak (E_g) becomes slightly shifted toward the longer wavenumbers. Furthermore, given the mismatch of ionic radius between Ce and Ti, the inclusion

of Ce distorts the lattice structure of TiO_2 by entering into interstitial site and generates oxygen vacancies. Their appearances also contribute to the mentioned shift of $E_{(g)}$ mode given their negative influence on the crystal quality. It has to be noticed that in some materials, such as ZnO, oxygen vacancies or other projection of defective structure might appear as newly formed peaks, and it is also explained by overall degradation of crystal lattice accompanied by its following disordering [61]. Furthermore, several words need to mention about the controversy of using Raman spectroscopy to probe the defect states due to existed inconsistency of available data in literature and inability to currently compare it. Taking as example the formation of oxygen vacancies in TiO_2, one might discover that it is supposed to result in positive shift of Raman peaks similar to that mentioned above, but there are several reports where Raman peaks remain almost the same or even shift to the negative side [18]. This disparity is likely explained by the fact that Raman spectroscopy is a point analysis, and it cannot cover equally the whole material. Given that defects are localized non-uniformly, there is a great chance that their concentration might be low in particulate analyzed sites.

4.3.6.3 Resonance Raman Spectroscopy

Resonance Raman scattering occurs when the incident radiation is at a frequency close to that of an electronic transition of the molecule which is going to be probed. As a result, it provides enough energy to excite the electrons toward a higher electronic state. The major advantages of RRS include the following [62]:

(a) It improves the sensitivity, which allows to detect samples at micromolar concentration, whereas FTIR and conventional Raman require millimolar concentration.
(b) The state of the sample required for RRS can be either solid, fiber, gel, or solution.
(c) The time scale is on the order of 10^{15}–10^{14} s, which is too short, and it is in the order of molecular vibrations.
(d) No additional probes are required for analysis.
(e) It can be used to analyzed surface layer of bulk samples due to low penetration depth which reaches, for example, nearly 20 nm for CeO_2 and ~12 nm for TiO_2.

There are, however, several disadvantages of RRS which need to be considered deeply. *Firstly*, it might lead to strong heating due to parameters of laser light used for excitation and thus can cause damage of the sample surface. *Secondly*, it is not easy to interpret the resulting Raman spectra given that there are much smaller number of available studies to compare the obtained data but also considering the fact that along with consideration of resonance-related effects, one should additionally count the influence of surface states due to low penetration depth of signal.

Similar to RS, RRS also can access both intrinsic and extrinsic deficiencies whose occurrence becomes visible due to changes in shape, intensity, and positioning of peaks. The only difference, as mentioned above, is that it is more surface

based; thus, the obtained data cannot be attributed to the bulk. Yet, it gives another advantage, namely, combined implementation of both RS and RRS analysis might be used to fully investigate the target materials and separate phenomenon that occurred in its bulk and surface in order to deeper understand their origins. This approach, for example, was perfectly applied by Gurylev et al. [61] who used Raman spectroscopies excited by 325 nm and 534 nm to study formation of oxygen and zinc vacancies in ZnO nanorods after hydrogenation (Fig. 4.6c, d). Finally, it has to be noticed that RRS often can serve as a perfect tool to investigate direction of crystallographic axis within the target materials which might be considered as indirect evidence of defect formation. Simply put, in this case, orientations of some crystallites tend to be tilted to a certain degree with respect to the main axis in order to minimize the free energy of the lattice and to balance it. Such a perturbation usually results in changing the nature of crystal lattice toward polycrystallinity, as what happened in ZnO where oxygen vacancies cause appearance of *a*-axis in addition to already established c-axis.

4.3.7 Photoluminescence (PL) and Cathodoluminescence (CL) Spectroscopies

Photoluminescence (PL) and cathodoluminescence (CL) spectroscopies are well-known, important, and highly necessary tools to study various chemical and physical properties of metal oxide semiconductors which also can be used to access the introduction of intrinsic and extrinsic deficiencies. Analysis of data obtained via them allows to achieve clear understanding regarding not only the actual presence of these defects, their concentration and distribution, doping profiles, and quality of crystal lattice, but also it provides access toward changes in electronic structures such as the rate of charge carriers separation, appearance of additional mid-gap states, and availability of self-trapped excitons. Furthermore, given that both PL and CL techniques are nondestructive and contact-free and have high selectivity, their application recently becomes highly necessary to deeper the investigation of defect formation in the target material as it can add great clearness to understanding of their correlation with improvement or declining the resulted photocatalytic efficiency.

As for more details, PL is an optical phenomenon which is referred to the irradiation of semiconductors by light at certain wavelength and its consequent absorption which leads to pushing the electrons toward higher-energy states. The absorbed energy is then released out as the electrons return back to its original state occupied originally. In turn, during CL measurement, almost similar processing is applied to liberate photons with only difference is that instead of optical excitation, high-energy electrons contribute to the irradiation step. It is interesting to notice that their characteristics are the same to that used, for instance, in scanning electronic microscopy or tunneling electronic microscopy. However, unlike photoexcitation, which

can be tuned into resonance with the transitions of the sample, electron excitation is non-selective and non-resonant. In addition, electron injection is weak, resulting in low luminescence yield and resolution [63]. Thus, PL is more preferable choice to be used. Following it, in this section, the main attention is attributed to this approach given that it is utilized much more in studies related to defect engineering than that of CL. Yet, it has to be noticed that appearance of peaks within PL spectra and consequent correlation of their existence with formation of defects also can be applied to CL in almost similar terms as it follows the same mechanism of identification and analysis of intrinsic and extrinsic deficiencies.

Continuing the discussion, it is often not easy to interpret the obtained PL spectra and assign the detected or deconvoluted peaks to certain types of defects as very often several opposing opinions existed in literature on their identifications, and thus various aspects should be considered before finalizing assignment. This concept can be readily demonstrated using PL spectra of ZnO nanorods before and after hydrogenation that is shown in Fig. 4.7a as example [30]. Accordingly, a near-band sharp emission (NBE) peak at 380 nm is attributed to the free excitons, while broad visible emission peak is ascribed to the donor (related to oxygen vacancies)-acceptor (related to zinc vacancies) transition. Annealing in a hydrogen atmosphere results in significant enhancement of both emissions and appearance of two clearly distinguished peaks at 504 nm (2.46 eV) and 520 nm (2.38 eV) which are assigned to oxygen and zinc vacancies (V_O and V_{Zn}), respectively. The following explanation can be provided for their attribution [30]. *Firstly*, transition level of V_{Zn} lies between the 1 and 2 charge states which occur at around 1 eV above the valence band, and it justifies the emission at 2.38 eV. In turn, it was stated that oxygen vacancies do not show any transition at this energy. Yet, it contradicts with the work of Vijayaprasath et al. [64] who assigned it to V_O. *Secondly*, the peak at 2.46 eV (504 nm) can be considered to have great matching with the +2/+ or +2/0 transition level of oxygen vacancies as it matches greatly the outcome of theoretical simulations [30]. In turn, Lv et al. [65] reported that this peak also is supposed to have a certain contribution

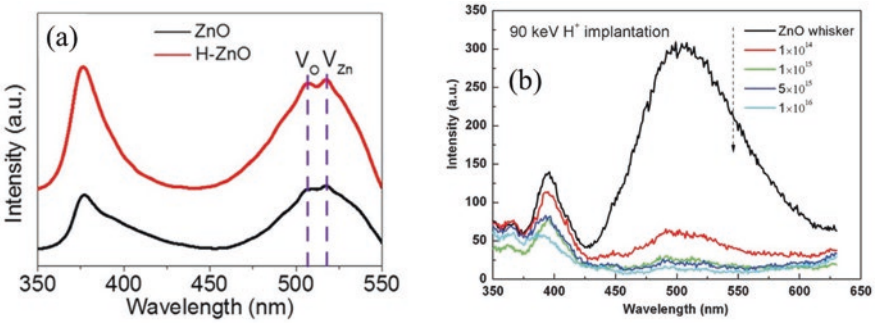

Fig. 4.7 (**a**) PL spectra of as-grown and hydrogenated ZnO nanorods. (Reprinted from Ref. [61]. with permission from *Elsevier*. Copyright 2017) (**b**) PL spectra of the pristine ZnO whiskers and H^+-implanted ZnO samples. (Reprinted from Ref. [65] with permission from *The Royal Chemical Society*. Copyright 2013)

from V_{Zn} even though V_O still might play a dominant role in its appearance (Fig. 4.7b). Thus, as can be seen, even though PL provides exclusive knowledge about formation of defects, to determine their nature requires employment of very deep awareness and caution in order to identify correct attribution to certain type. In addition, it is necessary to notice that often the wavelength at which those peaks are detected might be interpreted as exact position of defect-based energy state within the band gap of target material, and it also shows in which direction the transition of electrons should be proceeded. The same mechanism as well can be applied to identify the existence and position of mid-gap energy state created by doped elements which can serve as "fingerprint" to estimate their existence, nature, concentration, and distribution.

It is also often the case that changing of overall intensity of PL spectra can serve as evidence of certain fluctuation within separation rate of charge carriers and often is used as indicator to access and even compare, yet in relative units only, their lifetimes within various defective materials or with regard to certain standard. Simply put, recombination of electrons and holes usually proceeded via radiative pathway which is described by the release of photons that, in turn, contribute to the increased intensity of PL. Thus, the more charge carrier becomes ceased to existence, the more photons are released, and the higher is the intensity. In turn, the presence of defects often results in longer lifetime of charge carriers given that, *firstly*, they serve as scattered centers lowering their mobility thus making the recombination time to increase and, *secondly*, they take the role of trap centers which makes separation of electrons and holes more efficient. Hence, they have less chance to meet, and it leads to lowering the intensity of PL as there is no contribution to its enhancement due to absence of released photons. One should notice that recombination process definitely also might be proceeded via non-radiative pathway without releasing of photons as the liberated energy is transformed into heat and it is spreading within the crystal lattice. This type of recombination cannot be detected by PL as other measurements are required to access it such as analysis of charge carrier concentration and their mobility. Following it, it is assumed that by utilizing PL, the recombination rate is usually limited by its only radiative form.

4.3.8 Transient Absorption Spectroscopy (TAS)

Various defects such as vacancies and doped elements can significantly influence the behavior of charge carriers including their kinetics, transportation characteristics, and consequent recombination. Generally, defects create additional mid-gap states within the band gap which serve as trap centers for photo-induced electrons and holes thus increasing their separation and leading to the extension of their lifetimes. Yet, it is not always the case as similar defects in certain conditions also can be used in opposite roles and facilitate charge recombination efficiently with consequent decreasing concentrations of available charge carriers. Transient absorption spectroscopy (TAS) is a versatile tool that can analyze photogenerated carriers

within a very short time after initiating their existence via light irradiation, and it provides important information about direct influence of mentioned mid-gap states on their dynamics and consequent relaxation processing. This information allows to estimate the lifetimes of these photogenerated carriers and to realize which factors affect them and can be used to extend their durations [66]. This approach is applicable to both intrinsic and extrinsic deficiencies even though the majority of available literature is concentrated on the former topic.

The principle of TAS instrumentation is explained as follows. Absorption of ultrashort laser pulse, that is also called a pump, by semiconductor brings the increase of energy levels within certain molecules from the ground to the excited state potential. The evolution of this change is monitored by means of a second very similar ultrashort laser pulse called the probe that interrogates the ensemble excited by the pump pulse and whose time delay with respect to the latter can be continuously tuned to follow the dynamics [67]. The information content of a transient absorption spectrum directly follows the frequency of the probe light [68]. For instance, using X-ray or extreme UV portion of the spectrum provides information about how the electronic structure of individual lattice ions changes upon photoexcitation by examining transitions between core and valence electronic states. In turn, utilizing UV, visible, or near-infrared parts of the spectrum can give access to knowledge that are highly applicable for investigation of semiconductor materials, such as [68]:

(a) Band-gap transitions which allow to transport electron from the valence band to the conduction band
(b) Sub-band-gap transitions appeared between localized mid-gap trap states and the conduction or valence band
(c) Intra-band transitions of excited electrons and holes in the conduction band and valence band, respectively. The amplitudes of these features facilitate access to availability of excitons or free electrons and holes.

For the illustration of TAS employment to investigate the influences of defects on the recombination and separation processing of charge carriers in semiconductor materials, the study of Hoch et al. [66] can be considered as example. In their work, relaxation dynamics of $In_2O_{3-x}(OH)_y$ nanoparticles whose band gap was determined as 2.9 eV (~425 nm) were investigated with varying concentrations of defects such as oxygen vacancies and hydroxyl groups using two different excitation energies corresponding to above band gap (318 nm) and near band gap (405 nm). It was demonstrated that both types of defects play a significant role in the excited-state charge relaxation pathways. Simply put, the higher the defect concentrations, the more electrons and holes become trapped, and the longer excited-state lifetimes were detected. It resulted in highly improved separation of charges that could correlate well with observed trends in the photocatalytic activity.

Transient absorption spectroscopy also can be used to understand the precise and definite influence of doped elements on the dynamics of charge carriers and to provide clear understanding on whether the improved photocatalytic activity can be attributed to reducing the recombination rate of electron-hole pairs or other

mechanisms responsible for it. For example, Ichihara et al. [69] investigated La- and/or Cr-doped $SrTiO_3$ and determined that the former compound increases the lifetimes of photoexcited charge carriers, while the latter one acts as recombination center, and its presence, oppositely, effectively decreases their concentration.

4.3.9 X-ray Absorption Spectroscopy (XAS)

X-ray absorption spectroscopy (XAS) is a technique that can deliver the bulk measurement of the elemental and chemical compositions by estimating X-ray absorption coefficient of a material as a function of energy. Each element provides a set of characteristic absorption edges (e.g., dramatic increase in the absorbed X-rays) which is correlated with different binding energies of its electrons providing XAS high sensitivity toward identifying itself and related particularities [70]. Furthermore, this measurement has no dependency on the crystallinity of materials, making it one of the few structural analyses which can be used to evaluate the chemical compositions of fully amorphous and highly disordered compounds or presented in forms of liquid or gaseous phases. To evaluate the sample, XAS uses high intensity, coherent X-ray beam which has great tunability over a wide range of energy, and therefore a synchrotron radiation source is required to perform this analysis [71]. In this regard, it is considered to be highly specific technique yet with very limited accessibility around various research groups.

The X-ray absorption spectrum is typically classified into two regimes: X-ray absorption near-edge spectroscopy (XANES) and extended X-ray absorption fine-structure spectroscopy (EXAFS). Even though both of them have the same physical origin and realized within the same instrumentation setup, the interpretation of obtained results due to differences in energies of related spectral features makes them highly distinguished [71, 72]. For instance, XANES investigates appearance of various particularities within the range of 50–100 eV above the edge and thus probes unoccupied electronic densities located higher than the Fermi level. The results obtained via this analytical method is difficult to analyze, as correct assignment of the observed transitions and proper interpretation of their energy and intensities might be a nontrivial and even somehow challengeable task. In fact, it is often the case that simulation is used in parallel to experimental observations to conform correct identifications of observed peaks and features [73]. In turn, XANES, however, can provide very clear information regarding the oxidation state and coordination number of the absorbing atoms. On the other hand, EXAFS with more subtle spectral features presented at energies up to ~500 eV or greater above the edge serves as a source of information about interatomic distances, coordination numbers of shells surrounding the absorbing atom, and distribution of cation sites within the spinel structure [71, 72].

The introduction of intrinsic and extrinsic defects changes chemical composition of material structure by altering its various parameters such as bond length, coordination numbers, atoms rearrangement, localization and delocalization of electrons,

etc. Hence, both of these XAS-based analytical methods are very useful techniques to investigate the formation of defects and understand what changes occurred within chemical compositions due to their influences. For example, Hsu et al. [74] demonstrated that formation of oxygen vacancies in Co-doped ZnO could be effectively traced by XANES as annealing in reduced atmosphere led to appearance of additional peak in its spectra (peak C in Fig. 4.8a). This peak was attributed to oxygen vacancies, and applied simulation model greatly confirmed this conclusion. Furthermore, it was revealed that the higher the oxygen deficiency, the higher the intensity of this peak. Alternatively, Liu et al. [75] utilized EXAFS to investigate filling of Ta_2O_5 with nitrogen and discovered that originally, Ta-O bonding had a distance of 1.47 Å, and it increased to 1.56 Å after doping. As the Ta-N bond length of pure TaN was near 2.20 Å, it was concluded that the peak shift of 0.09 Å indicated that some of oxygen ions were substituted by nitrogen ions (Fig. 4.8b). Such a small change in interatomic distance is hardly detectable by any other techniques including X-ray analysis which is going to be discussed below or HRTEM mentioned above.

4.4 X-ray Diffraction Analysis (XRD)

X-ray diffraction (XRD) is an extremely important nondestructive relatively inexpensive and easily accessible technique for characterizing crystal composition of materials in quantitative and qualitative manner. It does not require the use of vacuum, as well as application of special protocol to prepare samples, and can be employed to various types and forms of materials regardless of their nature with the only requirement being that it should be presented in the form of solid composition. Overall, XRD analysis can be used to obtain various information which is not

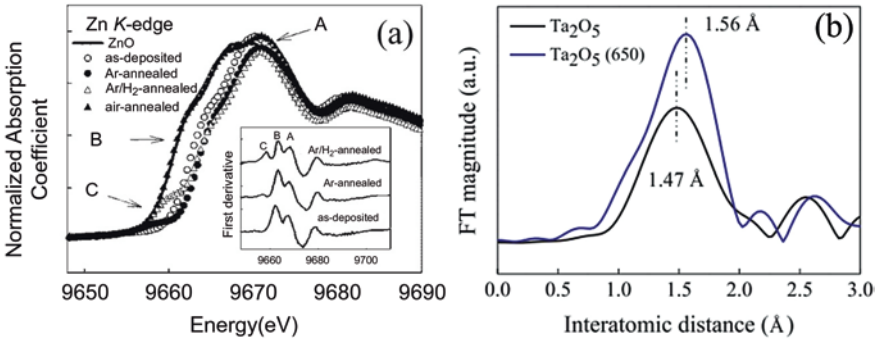

Fig. 4.8 (**a**) The Zn K-edge XANES for the ZnO (500 Å), as-deposited, and annealed films. The inset shows the first derivative of XANES for these films. (Reprinted from Ref. [74] from *AIP Publishing*. Copyright 2006) (**b**) Fourier transforms of k3-weighted EXAFS spectra of pure Ta_2O_5 and N-Ta_2O_5 fabricated via annealing at 650 °C in NH_3. (Reprinted from Ref. [75] with permission from *Elsevier*. Copyright 2018)

limited by probing only the level of crystallinity but also includes identifying the presence of particular phases and preferred crystal orientations (texture) and their ratios and in addition provides access to other structural characteristics such as evaluations of grain size; interatomic distance and lattice parameters; presence of strain and identification of its form, nature, and origin; existence of various intrinsic crystal defects; and tracing the introduction of doped elements in terms of their residing whether in interstitials or substitutional positions, as well as calculating their concentration and other related features and even determination of length of chemical bonding.

The mechanism laid beyond XRD analysis is based on constructive interference of X-ray monochromatic beam scattered at specific angles from each set of lattice planes in a sample, and it results in appearance of diffraction peaks [76]. Their intensities and positioning can be used to analyze the atomic configuration and its periodic arrangement within the lattice planes. Standard database for X-ray powder diffraction patterns which is available online not only is used to quickly check the nature of material subjected to this analysis but also can serve as a reference to access its specific structural particularities. There are several types of XRD analysis that are frequently applied for research purposes, and they are mostly classified by their sensitivity toward assessing presence of materials and depth at which the X-rays can penetrate. For example, traditionally used powder XRD is employed to probe the bulk compositions and only be applied to materials whose amount is sufficient enough to be detected. This requirement makes it to be hardly utilized for analyzing nanoscale compounds if only the latter is presented in the form of accumulated particles, thin film with relatively high thickness, bundle of nanowires or nanotubes, etc. In turn, more advanced grazing incidence XRD allows can fulfill this task as it enables to probe very small volumes such as 10-nm-thick layer of TiO_2 deposited on Si [77]. Furthermore, under certain conditions, it also can be applied to trace changes in structure and crystallinity at the depth of only several atomic layers and thus is highly suitable to examine 2-D materials.

Considering the above, XRD is perfectly suitable for detection of defect formation and their related particularities, as it can trace changes in the quality of crystal lattice. As an illustration, appearance of vacancies very often results in shrinkage of d-spacing which results in positive shift of corresponding diffraction peaks as it follows the famous Bragg law. This processing also often is accompanied by reduction of their intensities since the levels of crystallinity decrease with evacuation of atoms. In turn, during doping, especially substitutional, the XRD peaks might also shift in both directions depending on the ionic or atomic radii of doped element compared to that of atoms within crystal lattice of host materials which are subjected for replacement. For instance, Samsudin et al. [78] investigated F-doped TiO_2 and discovered that as the F- ions have radii of 0.119 nm and 0.116 nm depending on their coordination numbers, they are going to substitute O^{2-} ions with radii of 0.126 nm and 0.122 nm. Thus, a slight shift of anatase (1010) peak toward higher angels was observed after F-doping compared to pristine TiO_2. Overall, it can be said that the higher the concentration of intrinsic or extrinsic defects, the more obvious the shift becomes.

Definitely, it is often the case that XRD is unable to identify the presence of defective compositions or trace changes in their concentration, as what happened, for example, in the work of Liu et al. [79] who reported N-doped TiO_2 prepared via thermally activated nitridation and revealed that with changing the conditions of treatment, the lattice constant of TiO_2 remained the same. Apart from other reasons mentioned in those work, it might be said that this phenomenon is likely attributed to the low sensitivity of general XRD instrumentation which cannot detect small deviation in presence of N_2. Thus, it is strongly suggested that other analysis should be also taken for confirmation as to make a more supportive conclusion on the presence of defects.

Finally, one should mention that alternation of preferred orientation or increasing the polycrystallinity of structure also might serve as evidences of changes in atomic arrangement of crystal lattice following the defect introduction. As an illustration, Kim et al. [80] synthesized *a*-axis oriented ZnO nanorods by hydrothermal method and subjected them to thermal treatment in vacuum at temperatures from 500 to 900 °C. It led to increasing the number of crystallites with *a*-axis preferred orientations and their consequently raised domination over that of crystallites with c-axis orientations. The following mechanism can be used to explain it. Formation of defects results in degradation of crystal quality which forces the orientations of some crystallites to be tilted to a certain degree with respect to the main crystal axis as to minimize the free energy of the lattice and to balance it. Thus, it allows the appearance and consequent detection of others energetically less favorable crystal orientations.

4.5 Other Analyzing Techniques

Apart from the abovementioned well-known techniques to probe the defect formation whose wide investigation deserved numerous attentions in literature, there exist other less frequently applied but nevertheless also highly important analyzing tools which also deserved to be mentioned and discussed briefly.

(a) *Thermal analysis*. Thermal analysis includes a series of techniques which are used to measure the changes of materials properties in terms of their dependency on the change of temperatures. Among them, the most widely applied ones are considered to be differential scanning calorimetry and thermal gravimetric analysis that investigate how the loss of weight correlates with increase of temperature. Simply put, the formation of defects such as vacancies results in reduced density and consent lowering of the overall material mass; thus, it can be used as indirect evidence of their existence.

(b) *Therma-programmed desorption*. Temperature-programmed desorption is applied to measure the desorption rate of surface-located atoms and molecules from the materials as a function of temperature and/or interactions with compounds absorbed for surrounding environment. Its application allows to understand various parameters accompanying this process, such as activation

energy, rate constant, reaction order, Arrhenius pre-exponential factor, etc. Thus, it is an important tool which enables to provide highly useful information regarding the formation of vacancies or possible existence of various impurities and doped elements. For example, Kim et al. [81] used this analysis to reveal the appearances of oxygen and zinc vacancies in ZnO after hydrogenation as this process was associated with release of H_2O molecule and Zn reduced atoms, respectively (Fig. 4.9).

(c) *Rutherford backscattering spectrometry.* Rutherford backscattering spectrometry (RBS) is an ion scattering technique which is extensively utilized to probe compositions of film-like structures. During this analysis, He^{2+} ions penetrate into the sample, and the energy distribution along with yield of the backscattered He^{2+} ions within specific angle becomes captured. Since the backscattering cross section for each element is a well-known value, quantitative compositional depth profile from the RBS spectrum could be readily available. This method analyses doping and contamination level within samples as well as provides quantitative access to its intrinsic deficiency by calculating elemental compositions with very precise accuracy. The main drawback of this approach, however, is that it has low sensitivity toward light elements such as carbon and oxygen [82]. In addition, irradiation of heavy ions causes significant damage of sample surface [83] which might bring certain difficulties to correctly access its chemistry.

As a final word, it has to be noticed that there are great numbers of various instrumentation and approaches can be used to obtain required information about introduction of defects in the materials whether directly or indirectly. It is practically impossible not only to cover them all in depth but also simply mentioning them. For clarity, this chapter only serves to be introductory for immersing in this topic, and interested readers are suggested to address specific literature for more precise details.

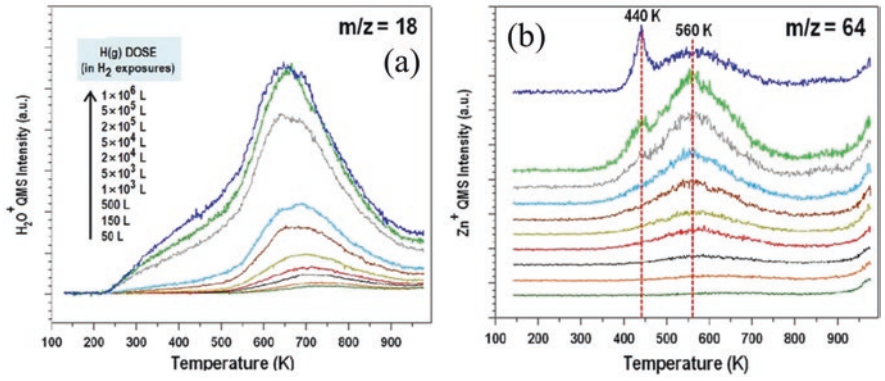

Fig. 4.9 TPD spectra of (**a**) water (m/z = 18) and (**b**) zinc (m/z = 64) from ZnO nanowires pre-exposed to various doses of atomic H(g). (Reprinted from Ref. [81] with permission from *American Chemical Society*. Copyright 2012)

4.6 Final Remarks on Various Analysis Tools and Methods

Current developments in proper identification and detection of intrinsic and extrinsic deficiencies reach great levels as it allows to precisely determine their various features such as positioning, whether they are located in the surface layer or deeply in the bulk, concentration, distribution, and their accompanied gradient profiles in both quantitative and qualitative accounts and also traces their influence on various important characteristics of material including changes in electrical, structural, optical, and other properties, modification of morphology, adjustment of chemical composition, etc. Furthermore, many advanced techniques, particularly KPFM, TAS, etc., also can be used to reach these goals without additional treatment protocol or in the absence of any specific requirements regarding the dimension and conditions of the measured samples making the results of their probing more realistic. Thus, to enable these advantages to be implemented in the most efficient way, not only the proper choice of analyzing tools should be proceeded but also accurate understating and clear awareness of their basic principles, and most practical and fundamental functionalities are highly required and even necessary in achieving the designated results. In fact, various types of instrumentations serve different goals such as (1) to probe the nature and types of defects and also to verify their very specific particularities via direct or non-direct measurements and (2) to obtain the required information of structural and electronic changes within the materials along with their consequence influences on other characteristics. Proper collecting and critical evaluation of these data are highly required to making it serve as an important support and valuable addition to fabricate efficient photocatalytic performance. Overall, combining the abovementioned, it might become evident that this is a very nontrivial and highly challengeable task. Indeed, incorrect application of certain instruments and analysis or inadequate realization and improper interpretation of its findings might lead to appearance of certain misconceptions regarding the composition and structure of target materials as its consequent comparison with that reported in literature likely results in certain mismatches which arise not from differences in utilized experimental approaches but due to contrast in accessing similar analysis and its outcome. For example, Gurylev et al. [18] in their work demonstrated very perfectly that it might have happened even during application of well-known techniques, such as Raman spectroscopy which is considered to be simple enough to be utilized as a routine tool, thus making the consequence of inaccuracy in its correct accessing even more serious. Overall, in their work, it was stated that its "use… to probe the defect states in modified TiO_2" results in "inconsistency of available data" as their appearances led to not only "positive shift of Raman peaks" but also making them be "almost the same… or even shift to negative side." After profound investigation, these inconsistencies were explained as a result of "irregular distribution of oxygen vacancies." Thus, as traditional Raman spectroscopic analysis is a "point scan and cannot analyze the whole area," they might not be detected in a proper way, and certain awareness is required [18].

Considering the abovementioned, the purpose of this chapter can be determined as follows. *Firstly*, it defines major types of instrumentation used to analyze the introduction of various types of defect within the materials with special emphasis toward proper understanding of their fundamentals so that it allows to reach the definite perception how it can be utilized and which dataset is expected to be obtained. *Secondly*, it provides some very recent examples based on reports available in literature about correct applications of those analysis and consequent interpretation of the obtained results. It is believed that described concepts might serve a positive role not only in continuous expanding of the existed knowledge regarding various analysis but also making them to act as a stepping point for continuous development and advancement of current theory applied within certain instrumentations in terms of improving further the available processing, deepening, and widening their presence assessment, etc., as complete and full comprehension of defect structure is still far from full and satisfied accessibility. Adequate implementation of these strategies might sufficiently contribute to speeding up successful application of defects engineering in existing industrial technologies.

References

1. A. Sarkar, G.G. Khan, The formation and detection techniques of oxygen vacancies in titanium oxide-based nanostructures. Nanoscale **11**, 3414–3444 (2019). https://doi.org/10.1039/C8NR09666J
2. Z. Su, J. Liu, M. Li, Y. Zhu, S. Qian, M. Weng, J. Zheng, Y. Zhong, F. Pan, S. Zhang, Defect engineering in titanium-based oxides for electrochemical energy storage devices. Electrochem. Energ. Rev. **3**, 286–343 (2020). https://doi.org/10.1007/s41918-020-00064-5
3. K. Yoshida, T. Kawai, T. Nambara, S. Tanemura, K. Saitoh, N. Tanaka, Direct observation of oxygen atoms in rutile titanium dioxide by spherical aberration corrected high-resolution transmission electron microscopy. Nanotechnology **17**, 3944–3950 (2006). https://doi.org/10.1088/0957-4484/17/15/056
4. Y. Ding, R. Yang, Z.L. Wang, Ordered zinc-vacancy induced $Zn_{0.75}O_x$ nanophase structure. Solid State Commun. **138**, 390–394 (2006). https://doi.org/10.1016/j.ssc.2006.03.032
5. Y. Lv, W. Yao, X. Ma, C. Pan, R. Zong, Y. Zhu, The surface oxygen vacancy induced visible activity and enhanced UV activity of a ZnO_{1-x} photocatalyst. Cat. Sci. Technol. **3**, 3136–3146 (2013). https://doi.org/10.1039/C3CY00369H
6. C.-Y. Su, C.-C. Wang, Y.-C. Hsueh, V. Gurylev, C.-C. Kei, T.-P. Perng, Enabling high solubility of ZnO in TiO_2 by nanolamination of atomic layer deposition. Nanoscale **7**, 19222–19230 (2015). https://doi.org/10.1039/C5NR06264K
7. A. Sasahara, M. Tomitori, XPS and STM study of Nb-doped TiO_2 (110)-(1 × 1) surfaces. J. Phys. Chem. C **117**, 17680–17686 (2013). https://doi.org/10.1021/jp4057576
8. T. Minato, M. Kawai, Y. Kim, Creation of single oxygen vacancy on titanium dioxide surface. J. Mater. Res. **27**, 2237–2240 (2012). https://doi.org/10.1557/jmr.2012.157
9. U. Diebold, The surface science of titanium dioxide. Surf. Sci. Rep. **48**, 53–229 (2003). https://doi.org/10.1016/S0167-5729(02)00100-0
10. S. Urazhdin, D. Bilc, S.H. Tessmer, S.D. Mahanti, T. Kyratsi, M.G. Kanatzidis, Scanning tunneling microscopy of defect states in the semiconductor Bi_2Se_3. Phys. Rev. B **66**, 161306 (2002). https://doi.org/10.1103/PhysRevB.66.161306

11. M.J. Wolf, C.W.M. Castleton, K. Hermansson, J. Kullgren, STM images of anionic defects at CeO_2(111)—a theoretical perspective. Front. Chem. **7** (2019). https://doi.org/10.3389/fchem.2019.00212
12. Y. Cui, X. Shao, S. Prada, L. Giordano, G. Pacchioni, H.-J. Freund, N. Nilius, Surface defects and their impact on the electronic structure of Mo-doped CaO films: An STM and DFT study. Phys. Chem. Chem. Phys. **16**, 12764–12772 (2014). https://doi.org/10.1039/C4CP01565G
13. M. Setvín, M. Wagner, M. Schmid, G.S. Parkinson, U. Diebold, Surface point defects on bulk oxides: Atomically-resolved scanning probe microscopy. Chem. Soc. Rev. **46**, 1772–1784 (2017). https://doi.org/10.1039/C7CS00076F
14. R.B. Capaz, K. Cho, J.D. Joannopoulos, Signatures of bulk and surface arsenic antisite defects in GaAs(110). Phys. Rev. Lett. **75**, 1811–1814 (1995). https://doi.org/10.1103/PhysRevLett.75.1811
15. K.C. Khulbe, C.Y. Feng, T. Matsuura, *Synthetic Polymeric Membranes: Characterization by Atomic Force Microscopy* (Springer, Berlin Heidelberg, 2008). https://doi.org/10.1007/978-3-540-73994-4
16. A. Kühle, 7 - calibration procedures for atomic force microscopes, in *Advanced Techniques for Assessment Surface Topography*, ed. by L. Blunt, X. Jiang, (Kogan Page Science, Oxford, 2003), pp. 175–194. https://doi.org/10.1016/B978-190399611-9/50007-4
17. J. Zhong, J. Yan, Seeing is believing: Atomic force microscopy imaging for nanomaterial research. RSC Adv. **6**, 1103–1121 (2015). https://doi.org/10.1039/C5RA22186B
18. V. Gurylev, C.-Y. Su, T.-P. Perng, Surface reconstruction, oxygen vacancy distribution and photocatalytic activity of hydrogenated titanium oxide thin film. J. Catal. **330**, 177–186 (2015). https://doi.org/10.1016/j.jcat.2015.07.016
19. L. Qiu, J. Liu, R. Alessandri, X. Qiu, M. Koopmans, R.W.A. Havenith, S.J. Marrink, R.C. Chiechi, L.J.A. Koster, J.C. Hummelen, Enhancing doping efficiency by improving host-dopant miscibility for fullerene-based n-type thermoelectrics. J. Mater. Chem. A **5**, 21234–21241 (2017). https://doi.org/10.1039/C7TA06609K
20. C. Manfredotti, Chapter 11 - Imaging at the nanoscale: Scanning probe microscopies applied to semiconductors, in *Characterization of Semiconductor Heterostructures and Nanostructures*, ed. by C. Lamberti, G. Agostini, Second edn., (Elsevier, Oxford, 2013), pp. 467–507. https://doi.org/10.1016/B978-0-444-59551-5.00011-X
21. H. Lee, W. Lee, J.H. Lee, D.S. Yoon, Surface potential analysis of nanoscale biomaterials and devices using Kelvin probe force microscopy. J. Nanomater. **2016**, e4209130 (2016). https://doi.org/10.1155/2016/4209130
22. W. Melitz, J. Shen, A.C. Kummel, S. Lee, Kelvin probe force microscopy and its application. Surf. Sci. Rep. **66**, 1–27 (2011). https://doi.org/10.1016/j.surfrep.2010.10.001
23. V. Gurylev, A. Useinov, P.Y. Hsieh, C.Y. Su, T.P. Perng, Hydrogenated ZnO thin film with p-type surface conductivity from plasma treatment. J. Phys. D: Appl. Phys. **50**, 24LT02 (2017). https://doi.org/10.1088/1361-6463/aa6e91
24. M. Tosun, L. Chan, M. Amani, T. Roy, G.H. Ahn, P. Taheri, C. Carraro, J.W. Ager, R. Maboudian, A. Javey, Air-stable n-doping of WSe_2 by anion vacancy formation with mild plasma treatment. ACS Nano **10**, 6853–6860 (2016). https://doi.org/10.1021/acsnano.6b02521
25. C.V. Ben, H.D. Cho, T.W. Kang, W. Yang, Surface potential measurement of As-doped homojunction ZnO nanorods by Kelvin probe force microscopy. Surf. Interface Anal. **44**, 755–758 (2012). https://doi.org/10.1002/sia.3867
26. C. Baumgart, M. Helm, H. Schmidt, Quantitative dopant profiling in semiconductors: A Kelvin probe force microscopy model. Phys. Rev. B **80**, 085305 (2009). https://doi.org/10.1103/PhysRevB.80.085305
27. C. Pan, Y. Shi, F. Hui, E. Grustan-Gutierrez, M. Lanza, History and status of the CAFM, in *Conductive Atomic Force Microscopy*, (Wiley, 2017), pp. 1–28. https://doi.org/10.1002/9783527699773.ch1
28. Y. Zhang, J. Zuo, Y. Gao, P. Li, W. He, Z. Zheng, Investigation on the nanoscale electric performance of NiO thin films by C-AFM and KPFM: The effect of Cu doping. J. Phys. Chem. Solids **131**, 27–33 (2019). https://doi.org/10.1016/j.jpcs.2019.03.013

29. C. Li, S. Minne, B. Pittenger, A. Mednick, Simultaneous electrical and mechanical property mapping at the nanoscale with PeakForce TUNA, Bruker Application Note, #132, 2011
30. V. Gurylev, C.-Y. Su, T.-P. Perng, Distribution pattern and allocation of defects in hydrogenated ZnO thin films. Phys. Chem. Chem. Phys. **18**, 16033–16038 (2016). https://doi.org/10.1039/C6CP01768A
31. C. Serre, Defects visualized in porous solids. Nature **493**, 313–314 (2013). https://doi.org/10.1038/493313a
32. R. Ameloot, F. Vermoortele, J. Hofkens, F.C. De Schryver, D.E. De Vos, M.B.J. Roeffaers, Three-dimensional visualization of defects formed during the synthesis of metal-organic frameworks: A fluorescence microscopy study. Angew. Chem. Int. Ed. **52**, 401–405 (2013). https://doi.org/10.1002/anie.201205627
33. N. Senesi, G.S. Senesi, Electron-spin resonance spectroscopy, in *Encyclopedia of Soils in the Environment*, ed. by D. Hillel, (Elsevier, Oxford, 2005), pp. 426–437. https://doi.org/10.1016/B0-12-348530-4/00209-5
34. G. Lancaster, Electron paramagnetic resonance (a review). J. Mater. Sci. **2**, 489–495 (1967). https://doi.org/10.1007/BF00562955
35. K. Lips, M. Fehr, J. Behrends, Electron-spin resonance (ESR) in Hydrogenated amorphous silicon (a-Si:H), in *Advanced Characterization Techniques for Thin Film Solar Cells*, (Wiley, 2016), pp. 299–342. https://doi.org/10.1002/9783527699025.ch12
36. S. Ogawa, K. Mori, H. Natsuhara, T. Ohashi, R. Sakakiyama, T. Itoh, N. Yoshida, S. Nonomura, M. Fukawa, K. Sato, Optical properties of TiO_2 thin films estimated by photothermal deflection spectroscopy. Rev. Sci. Instrum. **74**, 863–865 (2003). https://doi.org/10.1063/1.1517149
37. M. Stefan, D. Ghica, S.V. Nistor, A.V. Maraloiu, R. Plugaru, Mn^{2+} ions distribution in doped sol-gel deposited ZnO films. Appl. Surf. Sci. **396**, 1880–1889 (2017). https://doi.org/10.1016/j.apsusc.2016.02.167
38. A. Janotti, C.G. Van de Walle, Native point defects in ZnO. Phys. Rev. B **76**, 165202 (2007). https://doi.org/10.1103/PhysRevB.76.165202
39. A. Janotti, C.G. Van de Walle, Oxygen vacancies in ZnO. Appl. Phys. Lett. **87**, 122102 (2005). https://doi.org/10.1063/1.2053360
40. X. Yu, B. Kim, Y.K. Kim, Highly enhanced photoactivity of anatase TiO_2 nanocrystals by controlled hydrogenation-induced surface defects. ACS Catal. **3**, 2479–2486 (2013). https://doi.org/10.1021/cs4005776
41. K. Suriye, R.J. Lobo-Lapidus, G.J. Yeagle, P. Praserthdam, R.D. Britt, B.C. Gates, Probing defect sites on TiO_2 with $[Re_3(CO)_{12}H_3]$: Spectroscopic characterization of the surface species. Chem.-Eur. J. **14**, 1402–1414 (2008). https://doi.org/10.1002/chem.200701514
42. C.P. Poole, H.A. Farach, R.J. Creswick, R. Prozorov, 17 - Spectroscopic properties, in *Superconductivity*, ed. by C. P. Poole, H. A. Farach, R. J. Creswick, R. Prozorov, Second edn., (Academic, Amsterdam, 2007), pp. 531–582. https://doi.org/10.1016/B978-012088761-3/50039-9
43. J. Gubicza, Chapter 2 - Characterization methods of lattice defects, in *Defect Structure and Properties of Nanomaterials*, ed. by J. Gubicza, Second edn., (Woodhead Publishing, 2017), pp. 27–57. https://doi.org/10.1016/B978-0-08-101917-7.00002-5
44. A. Somoza, A. Dupasquier, 14 - Vacancies in aluminium and solute-vacancy interactions in aluminium alloys, in *Fundamentals of Aluminium Metallurgy*, ed. by R. Lumley, (Woodhead Publishing, 2011), pp. 386–421. https://doi.org/10.1533/9780857090256.2.386
45. B. Viswanathan, Microscopic, spectroscopic, and physical techniques, in *Encyclopedia of Materials: Science and Technology*, ed. by K. H. J. Buschow, R. W. Cahn, M. C. Flemings, B. Ilschner, E. J. Kramer, S. Mahajan, P. Veyssière, (Elsevier, Oxford, 2001), pp. 5661–5666. https://doi.org/10.1016/B0-08-043152-6/00986-4
46. M.J. Puska, C. Corbel, R.M. Nieminen, Positron trapping in semiconductors. Phys. Rev. B **41**, 9980–9993 (1990). https://doi.org/10.1103/PhysRevB.41.9980
47. M.D. McCluskey, Point defects in Ga_2O_3. J. Appl. Phys. **127**, 101101 (2020). https://doi.org/10.1063/1.5142195

48. F. Tuomisto, K. Saarinen, D.C. Look, Irradiation-induced defects in ZnO studied by positron annihilation spectroscopy. Phys. Status Solidi (a) **201**, 2219–2224 (2004). https://doi.org/10.1002/pssa.200404809
49. W.M.H. Oo, L.V. Saraf, M.H. Engelhard, V. Shutthanandan, L. Bergman, J. Huso, M.D. McCluskey, Suppression of conductivity in Mn-doped ZnO thin films. J. Appl. Phys. **105**, 013715 (2009). https://doi.org/10.1063/1.3063730
50. A.J. Barlow, J.F. Portoles, P.J. Cumpson, Observed damage during argon gas cluster depth profiles of compound semiconductors. J. Appl. Phys. **116**, 054908 (2014). https://doi.org/10.1063/1.4892097
51. J. Sundberg, R. Lindblad, M. Gorgoi, H. Rensmo, U. Jansson, A. Lindblad, Understanding the effects of sputter damage in W-S thin films by HAXPES. Appl. Surf. Sci. **305**, 203–213 (2014). https://doi.org/10.1016/j.apsusc.2014.03.038
52. J. Xu, Y. Teng, F. Teng, Effect of surface defect states on valence band and charge separation and transfer efficiency. Sci. Rep. **6**, 32457 (2016). https://doi.org/10.1038/srep32457
53. C.-Y. Su, L.-C. Wang, W.-S. Liu, C.-C. Wang, T.-P. Perng, Photocatalysis and hydrogen evolution of Al- and Zn-doped TiO_2 nanotubes fabricated by atomic layer deposition. ACS Appl. Mater. Interfaces **10**, 33287–33295 (2018). https://doi.org/10.1021/acsami.8b12299
54. A. Majid, A. Jabeen, S.U.-D. Khan, S. Haider, First principles investigations of vibrational properties of titania and zirconia clusters. J. Nanopart. Res. **21**, 20 (2019). https://doi.org/10.1007/s11051-019-4461-1
55. B. Choudhury, A. Choudhury, Luminescence characteristics of cobalt doped TiO_2 nanoparticles. J. Lumin. **132**, 178–184 (2012). https://doi.org/10.1016/j.jlumin.2011.08.020
56. O.M. Ntwaeaborwa, S.J. Mofokeng, V. Kumar, R.E. Kroon, Structural, optical and photoluminescence properties of Eu^{3+} doped ZnO nanoparticles. Spectrochim. Acta A Mol. Biomol. Spectrosc. **182**, 42–49 (2017). https://doi.org/10.1016/j.saa.2017.03.067
57. M.E. Brezinski, 13 - Other tehcnologies, in *Optical Coherence Tomography*, ed. by M. E. Brezinski, (Academic, Burlington, 2006), pp. 353–368. https://doi.org/10.1016/B978-012133570-0/50015-9
58. A.K. Adya, E. Canetta, Chapter 14 - Nanotechnology and its applications to animal biotechnology, in *Animal Biotechnology*, ed. by A. S. Verma, A. Singh, (Academic, San Diego, 2014), pp. 247–263. https://doi.org/10.1016/B978-0-12-416002-6.00014-6
59. R.R. Jones, D.C. Hooper, L. Zhang, D. Wolverson, V.K. Valev, Raman techniques: Fundamentals and frontiers. Nanoscale Res. Lett. **14**, 231 (2019). https://doi.org/10.1186/s11671-019-3039-2
60. J. Dhanalakshmi, S. Iyyapushpam, S.T. Nishanthi, M. Malligavathy, D.P. Padiyan, Investigation of oxygen vacancies in Ce coupled TiO_2 nanocomposites by Raman and PL spectra. Adv. Nat. Sci. Nanosci. Nanotechnol. **8**, 015015 (2017). https://doi.org/10.1088/2043-6254/aa5984
61. V. Gurylev, C.-Y. Su, T.-P. Perng, Hydrogenated ZnO nanorods with defect-induced visible light-responsive photoelectrochemical performance. Appl. Surf. Sci. **411**, 279–284 (2017). https://doi.org/10.1016/j.apsusc.2017.03.146
62. N. John, S. George, Chapter 5 - Raman spectroscopy, in *Spectroscopic Methods for Nanomaterials Characterization*, ed. by S. Thomas, R. Thomas, A. K. Zachariah, R. K. Mishra, (Elsevier, 2017), pp. 95–127. https://doi.org/10.1016/B978-0-323-46140-5.00005-4
63. M. Nayfeh, ed., Chapter 7 - Characterization and simulation technologies of nanomaterial, in: Fundamentals and Applications of Nano Silicon in Plasmonics and Fullerines, Elsevier, 2008: pp. 153–167. https://doi.org/10.1016/B978-0-323-48057-4.00007-4
64. G. Vijayaprasath, R. Murugan, S. Asaithambi, G.A. Babu, P. Sakthivel, T. Mahalingam, Y. Hayakawa, G. Ravi, Structural characterization and magnetic properties of Co co-doped Ni/ZnO nanoparticles. Appl. Phys. A Mater. Sci. Process. **122**, 122 (2016). https://doi.org/10.1007/s00339-016-9655-0
65. J. Lv, C. Li, J.J. BelBruno, Defect evolution on the optical properties of H^+-implanted ZnO whiskers. CrystEngComm **15**, 5620–5625 (2013). https://doi.org/10.1039/C3CE40655E

66. L.B. Hoch, P. Szymanski, K.K. Ghuman, L. He, K. Liao, Q. Qiao, L.M. Reyes, Y. Zhu, M.A. El-Sayed, C.V. Singh, G.A. Ozin, Carrier dynamics and the role of surface defects: Designing a photocatalyst for gas-phase CO_2 reduction. PNAS **113**, E8011–E8020 (2016). https://doi.org/10.1073/pnas.1609374113
67. M. Chergui, 1.19. Ultrafast structural dynamics of biological systems, in *Comprehensive Biophysics*, ed. by E. H. Egelman, (Elsevier, Amsterdam, 2012), pp. 398–424. https://doi.org/10.1016/B978-0-12-374920-8.00123-5
68. K.E. Knowles, M.D. Koch, J.L. Shelton, Three applications of ultrafast transient absorption spectroscopy of semiconductor thin films: Spectroelectrochemistry, microscopy, and identification of thermal contributions. J. Mater. Chem. C **6**, 11853–11867 (2018). https://doi.org/10.1039/C8TC02977F
69. F. Ichihara, F. Sieland, H. Pang, D. Philo, A.-T. Duong, K. Chang, T. Kako, D.W. Bahnemann, J. Ye, Photogenerated charge carriers dynamics on La- and/or Cr-Doped $SrTiO_3$ nanoparticles studied by transient absorption spectroscopy. J. Phys. Chem. C **124**, 1292–1302 (2020). https://doi.org/10.1021/acs.jpcc.9b09324
70. J. Abraham, B. Jose, A. Jose, S. Thomas, Chapter 2 - Characterization of green nanoparticles from plants, in *Phytonanotechnology*, ed. by N. Thajuddin, S. Mathew, (Elsevier, 2020), pp. 21–39. https://doi.org/10.1016/B978-0-12-822348-2.00002-4
71. K.M. Tripathi, M. Castro, J.-F. Feller, S.K. Sonkar, Chapter 3 - Characterization of metal, semiconductor, and metal-semiconductor core–shell nanostructures, in *Metal Semiconductor Core-Shell Nanostructures for Energy and Environmental Applications*, ed. by R. K. Gupta, M. Misra, (Elsevier, 2017), pp. 51–77. https://doi.org/10.1016/B978-0-323-44922-9.00003-X
72. I.F. Cruz, C. Freire, J.P. Araújo, C. Pereira, A.M. Pereira, Chapter 3 - Multifunctional ferrite nanoparticles: from current trends toward the future, in *Magnetic Nanostructured Materials*, ed. by A. A. El-Gendy, J. M. Barandiarán, R. L. Hadimani, (Elsevier, 2018), pp. 59–116. https://doi.org/10.1016/B978-0-12-813904-2.00003-6
73. R.M. Ormerod, Surface chemistry: electron yield spectroscopy, in *Encyclopedia of Materials: Science and Technology*, ed. by K. H. J. Buschow, R. W. Cahn, M. C. Flemings, B. Ilschner, E. J. Kramer, S. Mahajan, P. Veyssière, (Elsevier, Oxford, 2001), pp. 9006–9008. https://doi.org/10.1016/B0-08-043152-6/01623-5
74. H.S. Hsu, J.C.A. Huang, Y.H. Huang, Y.F. Liao, M.Z. Lin, C.H. Lee, J.F. Lee, S.F. Chen, L.Y. Lai, C.P. Liu, Evidence of oxygen vacancy enhanced room-temperature ferromagnetism in Co-doped ZnO. Appl. Phys. Lett. **88**, 242507 (2006). https://doi.org/10.1063/1.2212277
75. W.-S. Liu, S.-H. Huang, C.-F. Liu, C.-W. Hu, T.-Y. Chen, T.-P. Perng, Nitrogen doping in Ta_2O_5 and its implication for photocatalytic H_2 production. Appl. Surf. Sci. **459**, 477–482 (2018). https://doi.org/10.1016/j.apsusc.2018.07.185
76. R. Kohli, K.L. Mittal, eds., Chapter 3 - Methods for assessing surface cleanliness, in: Developments in Surface Contamination and Cleaning, Volume 12, Elsevier, 2019: pp. 23–105. https://doi.org/10.1016/B978-0-12-816081-7.00003-6
77. V. Gurylev, M. Mishra, C.-Y. Su, T.-P. Perng, Enabling higher photoelectrochemical efficiency of TiO_2 via controlled formation of a disordered shell: An alternative to the hydrogenation process. Chem. Commun. **52**, 7604–7607 (2016). https://doi.org/10.1039/C5CC10610A
78. E.M. Samsudin, S.B.A. Hamid, J.C. Juan, W.J. Basirun, A.E. Kandjani, S.K. Bhargava, Effective role of trifluoroacetic acid (TFA) to enhance the photocatalytic activity of F-doped TiO_2 prepared by modified sol–gel method. Appl. Surf. Sci. **365**, 57–68 (2016). https://doi.org/10.1016/j.apsusc.2016.01.016
79. K.-I. Liu, C.-Y. Su, T.-P. Perng, Highly porous N-doped TiO_2 hollow fibers with internal three-dimensional interconnected nanotubes for photocatalytic hydrogen production. RSC Adv. **5**, 88367–88374 (2015). https://doi.org/10.1039/C5RA16492C
80. M.S. Kim, S.-H. Lee, H. Yoon, J.H. Jung, J.-Y. Leem, Effects of post-annealing on structural and optical properties of a-axis oriented ZnO nanorods. J. Nanosci. Nanotechnol. **13**, 6236–6239 (2013). https://doi.org/10.1166/jnn.2013.7688

81. W. Kim, G. Kwak, M. Jung, S.K. Jo, J.B. Miller, A.J. Gellman, K. Yong, Surface and internal reactions of ZnO nanowires: Etching and bulk defect passivation by H atoms. J. Phys. Chem. C **116**, 16093–16097 (2012). https://doi.org/10.1021/jp304191m
82. I. Stensgaard, Surface analysis | ion scattering, in *Encyclopedia of Analytical Science*, ed. by P. Worsfold, A. Townshend, C. Poole, Second edn., (Elsevier, Oxford, 2005), pp. 487–495. https://doi.org/10.1016/B0-12-369397-7/00597-5
83. K. Kimura, Rutherford backscattering spectroscopy, in *Encyclopedia of Analytical Chemistry*, ed. by D. Pappas, Y. Ozaki, (Wiley, 2006), pp. 1–15. https://doi.org/10.1002/9780470027318.a6215

Chapter 5
Case Study I Defect Engineering of TiO_2

5.1 TiO_2: Fundamentals

Titanium dioxide (TiO_2) is available in many polymorphs, among which anatase and rutile phases received the most attention since they are widely present in nature and can be easily realized in the laboratory. There also exist other well-known forms of TiO_2 such as brookite and monoclinic phase, yet, they are more difficult to synthesize and thus are less studied. Following it, this chapter is concentrated only on rutile and anatase forms of TiO_2. In additional, amorphous-structured TiO_2 also is discussed given the raised interest to its characteristics in recent years.

Typically, anatase represents metastable composition which can be easily transformed into more thermodynamically stable rutile by thermal treatment at temperatures over ~600 °C. The crystal lattices of these two polymorphs follow differently arranged octahedral TiO_6 formed by Ti^{4+} ions surrounded by six O^{2-} ions. Particularly, in anatase, each octahedron has contact with eight neighbors, and it results in formation of tetragonal structure. The bond lengths between oxygen atoms in the equatorial plane are the same, and these bonds form four edges that are shared with other octahedra, and it defines crystal composition of anatase [1]. In turn, the rutile also is attributed to the tetragonal structure; however, it is based on octahedral lattice with shared edges, i.e., each octahedron is in contact with ten neighbors in a linear chain disposition [2]. The density and hardness of rutile are higher than that of anatase. In turn, Ti-Ti and Ti-O bond distances are longer and shorter in anatase than in rutile, respectively. As for the optical properties, titanium dioxide has a direct and indirect band gaps of 3.2 eV and 3.0 eV for anatase and rutile, respectively, which means that both of them are unable to absorb visible light and only are sensitive to UV light illumination. In this regard, it has to be noticed that anatase represents colorless compound, while rutile is usually found to have dark red appearance.

V. Gurylev, *Nanostructured Photocatalyst via Defect Engineering*,
https://doi.org/10.1007/978-3-030-81911-8_5

5.2 Intrinsic Defects in TiO_2

5.2.1 Introduction

Owing to its highly attractive properties, such as low cost, exceptional stability, high chemical inertness, bio-compatibility, and nontoxicity, TiO_2 has been recognized widely as an efficient photocatalyst material for various processes such as purification of water, degradation of dyes and pesticides, CO_2 reduction, water splitting, etc. However, this material possesses certain drawback which makes practical and efficient realization of its photoactivity to be a challengeable task. For example, as mentioned above, it cannot absorb visible light. Given that UV light represents only 4–5% of solar spectra, the efficiency of TiO_2 as photocatalyst under sunshine is insufficient. In addition, extremely high recombination of photo-induced charge carriers crucially influences their transportation toward the surface, and thus, the processing of redox and oxidation reactions becomes highly limited. Following it, to fully realize the potential of TiO_2 and to make its implementation into photocatalytic and photoelectrochemical systems to be more feasible and productive, numerous approaches have been used to modify its composition and structure such as coupling with another semiconductor materials, surface sensitization with organic dyes, decoration with noble metals, etc. Yet, most of them require the use of external sources in the form of additional materials or compounds. In turn, it was demonstrated recently that improvement of TiO_2 characteristics could be achieved via self-doping with various intrinsic defects which provide great alternative to abovementioned methods. Simply put, controlled introduction of certain imperfections within crystal lattice of TiO_2 and manipulation over their features and particularities not only can be used to adjust the band gap and provide required configuration of electronic and geometrical structures but also lead to increasing the concentration, mobility, and transportation of charge carriers. Thus, sufficient improvement of various important properties can be achieved.

In this regard, non-stoichiometric TiO_2 has a great potential for application in solar light-based devices. Yet, to fully realize this strategy, a deep understanding regarding its intrinsic defect engineering in terms of synthesis approaches, correlation with improved characteristics, and consequent influence on the photocatalytic applications should be achieved. Below, these topics are discussed in full regard and with deep awareness.

5.2.2 Defect Chemistry of TiO_2

5.2.2.1 Brief Overview

Checking the available reports in literature on non-stoichiometric TiO_2, it is very easy to come to a conclusion that existence of intrinsic defects in it is mostly considered in terms of oxygen vacancies (V_O). Definitely, this type of defect is the

dominant one in TiO_2, and its appearance often is the most favorable and evident under various non-equilibrium conditions. Yet, it would be incorrect to ignore other minor-type defects which also often occur in TiO_2 whether in the form of independent species or as accompanies to the oxygen vacancies. Their presence even in very low concentration has a profound influence on properties of this material and thus cannot be ignored.

In general, apart from oxygen vacancies (V_O) which is defined as missing of oxygen ion from the lattice site (Fig. 5.1a), three other types of defects exist in TiO_2 [3]:

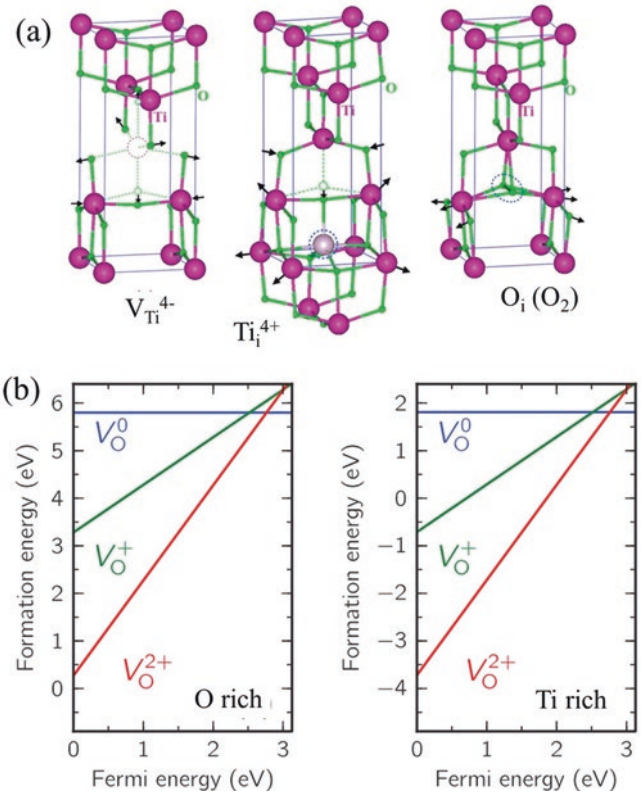

Fig. 5.1 (**a**) Atomic structures of titanium vacancy (V_{Ti}^{4-}), titanium interstitial (Ti_i^{4+}), and oxygen interstitial ($O_i(O_2)$). The large spheres are the Ti atoms, and the small spheres are the O atoms. Relaxation directions of neighboring atoms are selectively indicated by arrows. In some cases, ideal positions of the atoms before relaxation or removal are shown by dashed circles. (Adapted from Ref. [3] with permission from *American Physical Society*. Copyright 2006) (**b**) Calculated formation energies of oxygen vacancies in rutile TiO_2 plotted as functions of Fermi level (E_F) in oxygen-rich and titanium-rich growth conditions. (Reprinted from Ref. [5] with permission from *American Physical Society*. Copyright 2014)

(a) Titanium vacancies (V_{Ti}): Ti ion is missing from its lattice site.
(b) Titanium interstitials (Ti_i): Ti ion is located in an interstitial site.
(c) Oxygen interstitials (O_i): Oxygen ion is located in an interstitial site.

Oxygen vacancies and titanium interstitials are donors of electrons and their presence shifts Fermi level toward conduction band thus increasing the n-type conductivity of TiO_2 as they provide additional electrons and/or serve as compensating centers. In contrast, titanium vacancies and oxygen interstitials are considered as a source of holes given their acceptor-like characteristics, and thus their introduction serves absolutely an opposite role to that of V_O and Ti_i interstitials reducing the number of available electrons. In fact, their increased presence might even lead to appearance of n → p transition within TiO_2.

5.2.2.2 Oxygen Vacancies

Formation of V_O results in relaxation of its nearest-neighbor Ti atoms toward remaining O neighbors, which in turn, also move slightly inward to compensate the broken electrostatic equilibrium [3]. As for the electronic geometry, oxygen vacancies in TiO_2 have three charge states, namely, the doubly ionized oxygen vacancy (V_O^{2+}) which cannot capture any electrons, the singly ionized oxygen vacancy V_O^{1+} which captures only one electron, and, finally, the neutral oxygen vacancy V_O^{x} which can capture two electrons. Theses charge states are also sometimes called as F-color centers. Theoretical calculation determined that V_O represents negative U center, as it is only stable in +2 or neutral charge states, while V_O^{1+} was generally determined to be thermodynamically metastable [4], and highly non-equilibrium conditions should be used to initiate it. Based on this, V_O in TiO_2 is considered to be a double donor. Concrete position of Fermi energy (E_F) within band gap dictates the type of dominated charge state of this defect: as it was revealed by Malashevich et al. [5], if E_F is lower than ~2.8 eV, oxygen vacancies are in the charge state of +2, while E_F over that value represents that oxygen vacancies become stable in the neutral charge state (Fig. 5.1b). It is interesting to notice that it refers to existence of O-rich and O-poor environment, respectively. The position of energy level created by V_O^{2+} is very close to conduction band which provided sufficient evidence to consider this defect as a shallow donor. Thus, it has crucial contribution to the unintentional n-type conductivity of TiO_2. In turn, the positioning of energy levels of other types of V_O assigns them as deep donors. For example, Chen et al. [6] demonstrated that the energy levels of V_O with charges of +2, +1, and neutral were calculated to be located at distances of ~0.20 eV, ~1.78 eV, and ~0.87 eV from the bottom of conduction band, respectively. Their appearance often is accompanied by the reduce Ti^{3+} species due to supplied electron to Ti sites.

5.2.2.3 Titanium Vacancies

Formation of Ti vacancy results in outward relaxation of surrounding O atoms, each to a point approximately halfway between its two remaining Ti neighbors resulting in reduction of Ti-O distances and consequent increasing of O-O distances [3]. Ti vacancy is an acceptor-type defect which has the charge states of 0, −1, −2, −3, and −4 depending on the level of its ionization, e.g., the number of accepted electrons from host material [7]. Furthermore, the higher the positioning of Fermi energy within the band gap and the more evident is the n-type conductivity, the higher is the charge state of V_{Ti} as it changes from neutral to −2 and −4 [8]. Given their nature, these defects play as compensating centers for oxygen vacancies. For example, under O-rich conditions, V_{Ti}^{4-} begins to compensate V_O^{2+} at ~2.28 eV above the valence band maximum (VBM) trapping the Fermi level around this point, while under Ti-rich/O-poor conditions, it occurs at ~0.06 eV below the conduction band minimum (CBM) [9].

However, there is an uncertainty in literature, whether to consider this type of defect enable causing the appearance of p-type conductivity in TiO_2. As an illustration, Na-Phattalung et al. [3] based on DFT calculation stated that V_{Ti} is a quadruple shallow acceptor, and its formation energy under O-rich conditions is negative once E_F becomes higher than ~1.46 eV. This means that V_{Ti} is spontaneously formed, and it pushes down the E_F toward valence band until it reaches the level below the 1.46 eV. As this value is lower than half band gap of TiO_2 (~3.2 eV), it results in changing the role of dominated charge carriers from electrons to holes. Experimental studies confirmed that V_{Ti} indeed can initiate the p-type conductivity in TiO_2 in the absence of any external contribution [10]. Yet, several authors strongly oppose this conclusion. For instance, Boonchun et al. [8] stated that "V_{Ti} …[is] deep acceptor" and "even under extreme oxygen-rich conditions… p-type conductivity can never be realized… without external doping." Thus, whether titanium vacancies initiate the transition of conductivity is still under debate. As a final remark, it is necessary to notice that under the Ti-rich condition, V_{Ti} is a low-energy defect and hence acts as a leading native acceptor [3].

5.2.2.4 Titanium Interstitials

When a Ti is placed on the octahedral interstitial site, one of O neighbors moves considerably toward it. The surrounding Ti atoms are also slightly relaxed outward, due to the electrostatic repulsion between positively charge Ti ions [3]. Ti interstitials (Ti_i) have charge states (+4, +3, +2, +1, 0) which are mostly located very close or above CBM and are determined by the number of acquired elections. It represents that this type of defect is a shallow donor which enables to make contribution for intrinsic n-type conductivity. Theoretical calculation determined that Ti_i^{4+} interstitial has the lowest formation energy in Ti-rich conditions among the defects examined over a wide range of Fermi energies, while for O-rich conditions, it is limited by the position of Fermi level from valence band to ~1.5 eV [8]. This

outcome is mainly due to the energy gain from a transfer of four electrons to the low E_F level [3]. However, at very high Fermi energy and when it is pinned, when it approached conduction band, the formation energy of V_O became slightly lower than that of Ti_i [8]. It has to be noticed that anatase structure contains a lot of open space which can accommodate interstitial atom without much strain; thus, this phase shows higher attractiveness for this defect to appear compared with that of rutile [3] even though some authors argue it [11].

Finally, Ti_i^{4+} is considered to have the highest probability to be formed compared with all other types of Ti interstitials. It simply can be proceeded by the diffusion of Ti ion out of its original position under equilibrium conditions and without applying any additional external stimulus. Furthermore, as it has negative formation energy for a very wide range of Fermi energy in Ti-rich conditions, thus, it is a highly spontaneous process [3, 8]. In turn, for O-rich conditions, it only occurs once the Fermi level is in the lower part of the band gap [8] or close to valence band [3]. It is necessary to notice that appearance of Ti interstitials with other charge states requires that Ti_i^{4+} firstly becomes reduced, and then it can be moved through the crystal. Thus, it is very common that oxygen vacancies are often accompanied by the appearance of Ti_i^{3+} due to supply of electron toward Ti sites which decreases its oxidation state, and then they become kicked out to become self-interstitial species. It has to be noticed that in further discussions, Ti_i^{3+} as well as reduced Ti^{3+} would be referred for simplicity as Ti^{3+} centers as this abbreviation often is used in literature.

5.2.2.5 Oxygen Interstitials

Compare with other abovementioned defects, charge states of oxygen interstitials not only determine its electronic structure but also influence its geometrical arrangement. According to Lee et al., [12], a neutral O_i is the most stable across most of the range of Fermi energies, and it creates a dumbbell O-O bonded ion with an oxygen residing in the lattice, and this configuration is considered as substitutional O_2 molecule. In the −1 charge state, it also results in formation of similar configuration, yet with slightly longer O-O bond. In contrast, O_i^{2-} represents a structure which contains only individually existed ion. Thus, restoration of broken equilibrium due to appearance of this defect requires only very slight relaxation of Ti atoms outward [8]. Substitutional O_2 has a bond length of 1.46 Å which is longer than that which existed in an isolated (free) O_2 molecule (1.21 Å) [3]. The transition level (+2/0) of O_i was determined to be located ~0.81 eV above the VBM [8], indicating that it is a deep rather than shallow acceptor and thus cannot contribute to p-type conductivity and only serve as compensating center, thus resulting in annihilation of donor-like defects. Under applied Ti-rich condition, O_i has formation energy much higher than that of other defects and is hence unlikely to exist in any considerable amount. However, utilizing O-rich condition, its formation energy is reasonably low, making it an important defect [3]. Finally, it noted that this defect cannot be formed spontaneously regardless the position of Fermi level or utilizing any other related factors, as its formation energy is always positive.

5.2.3 How to Create Defects?

5.2.3.1 Hydrogenation

Hydrogenation treatment of TiO_2 has attracted great attention in recent decade as an effective method to introduce various defects. During thermal treatment, hydrogen atoms interact with lattice oxygen in TiO_2 not only located at surface but also in bulk due to interdiffusion resulting in appearance of oxygen vacancies, often accompanied by Ti interstitials and supplemented introduction of lattice disorder. Needless to say, these defects positively influence various important characteristics of TiO_2. The interaction between H_2 and TiO_2 is usually described to occur via three steps [13]. *Firstly*, with annealing temperature exceeding 300 °C, electrons set out to transfer from hydrogen atoms toward internal composition of TiO_2. The vacancies are formed once oxygen atoms create connection with arrived hydrogen atoms and consequently leaving the surface of TiO_2 in the form of H_2O. When the temperature is further increased up to 450 °C, the interaction between H_2 and TiO_2 becomes more intensive, and it results in electron transfer from oxygen vacancies to nearest-neighboring Ti^{4+} ions, transforming them into Ti^{3+} centers. Further increase of temperature above 560 °C leads to higher transfer of thermal energy, and the electrons located within oxygen vacancy states are driven away to be transported to Ti^{4+}. As a result, concentration of oxygen vacancies becomes lower, while more Ti^{3+} begins to appear [13]. Yet, this temperature might induce transformation of anatase into rutile, and thus formation of Ti^{3+} centers via this approach might not be suitable for the former phases which means that it is more conductive for introduction of oxygen-deficient compositions.

As for the amorphous TiO_2, it is suggested that due to the absence of atomic periodical arrangement, both types of defects can be easier to form there compared with that of crystalline phase. As a final remark, it is necessary to mention that as interstitial Ti are formed under more severe conditions (i.e., higher temperature, higher pressure of hydrogen), the formation of oxygen vacancies is easier to reach and thus is more attractive [14].

5.2.3.2 High-Energy Particles Bombardment

Electron bombardment In order to minimize unnecessary influence of high-temperature environment and avoid consumption of excessive energy during H_2-gas thermally activated process, alternative approaches are required for the formation of defective TiO_2. One of those method can be considered as application of electron irradiation which effectively modifies the surface of TiO_2 resulting in appearance of oxygen vacancies or relevant defect complexes and even can be used to realize the existence of Mangeli phase. This process usually occurs via displacement and/or evacuation of O atoms from the TiO_2 surface as a result of electron stimulated desorption that is based on Knotek and Feibelman model [15]. In general terms, it

is explained as follows: electron transfer occurs between oxygen and titanium (to be more precise, 3p holes are created in Ti atoms, and their decay can be realized via interatomic Auger process from a neighboring O atom) which results in transformation of originally negative oxygen species (O^{2-}) into neutral (O^{o}) or positively charge (O^{+}) oxygen ion. Thus, it leads to appearance of Coulomb repulsion from the surrounding Ti^{4+} which kicks out O^{+} leaving behind a vacancy spot. In turn, it was also suggested that removal of some oxygen atoms might occur via so-called site-specific desorption probability that enables to form one-dimensional arrays of V_O [16].

As a conclusion, it has to be noticed that parameters of electron bombardment should be adjusted very accurately. Definitely, the energy of irradiation is supposed to be sufficient enough to overcome the potential barrier of surface bonding, yet, it also cannot be too high as instead of desorbing the target atoms or compounds, it would result in damaging the surface and even its partial etching occurred via uncontrolled collision of fast-electrons with O and Ti atoms.

Ion implantation Ion sputtering using various species also can be used to reproducibly generate atomic level defects and nanometer-scale vacancy clusters in a controlled manner within TiO_2. However, there are several particularities which make its application different from that of electron irradiation, and thus they should be considered deeply in the course of its utilization. *Firstly*, ion sputtering can transfer much larger momentum to the surface, and therefore induced changes are extended deeper inside the material and even reach the range of several tens of nanometers. For example, Majumder et al. [17] revealed that once TiO_2 nanodots are subjected to treatment with Ar^{+} ions, formation of a 45-nm-thick Ti-rich surface layer was observed. Furthermore, by changing the energy of irradiated ions, it is possible to control up to which depth the presence of defects can be extended. *Secondly*, the produced defects have higher stability and cannot be removed simply by exposing TiO_2 to oxygen at low temperature [18]. *Thirdly*, ion sputtering can be used to selectively create Ti- or O-deficient regions within TiO_2 depending on its fluence. Simply put, the evacuation of atoms from its position within crystal lattice is determined by displacement threshold energy which was calculated to be around ~40 eV for oxygen and ~105 eV for titanium [19]. Thus, lower fluence ion irradiation leads to dominated formation of V_O in TiO_2, while its increase can be used to realize the domination of V_{Ti}. *Fourthly*, treatment with ions of certain element along with introduction of defects also likely results in their accompanied intrusion into TiO_2 which might be considered as undesired doping that has a certain degree of influence on its specific characteristics.

Plasma treatment Plasma treatment using various reducing atmospheres is also often applied to realize the appearance of deficient TiO_2. It has several important advantages. *Firstly*, playing with its parameters, such as electric field strength (power), time of exposure, pressure within chamber, temperature, etc., determines the frequency and energy of collisions and thus can provide precise control over the level of introduced non-stoichiometry. *Secondly*, the nature of this processing allows

to achieve the formation of defects exclusively in the surface of TiO_2 leaving aside bulk compositions. Thus, plasma treatment is considered to be a highly desirable and demanding technique. As an example, Li et al. [20] reported that non-thermal dielectric barrier discharge (DBD) plasma with various working gases, including Ar, H_2, and NH_3, was used to desorb oxygen from the titania nanosheets which resulted in formation of crystalline core/amorphous shell structure in the form of $TiO_2@TiO_{2-x}$. Yet, despite its advantages, there still exist certain drawbacks limiting its application which need to be addressed properly. For instance, plasma processing also suffers from unexpected doping, as it happened in the abovementioned study [20] where the treatment with NH_3 resulted in incorporation of nitrogen atoms into TiO_2 that occurs accompanied with the appearance of oxygen vacancies and Ti^{3+} centers. In another case, it is mostly used to achieve the formation of oxygen-deficient TiO_2, and thus, production of other types of defects such as titanium vacancies is hardly possible.

5.2.3.3 Thermal Treatment in Reducing Atmosphere

Oxygen and titanium vacancies also can be created by annealing of pure TiO_2 at elevated temperatures (generally above ~200 °C) in oxygen-poor or oxygen-rich environment, respectively. To reach the ambient with low presence of oxygen, it is very common to apply vacuum condition or use specific neutral gases such as Ar, He, and N_2 or their combinations [14]. Alternately, to activate generation of titanium vacancies, it was suggested to apply pure O_2 gas [21]. The conditions of this processing such as the type of surrounding environment, time of treatment, temperature, etc. can be used to determine the level of deficiency, its distribution, or specific accumulation whether in surface or in bulk [22]. However, there is always the need to remember that thermally activated processing often is employed to improve the crystallinity of target compositions which might effectively shadow the introduction of defects or even completely remove them thus restoring the original stoichiometry. This concept can be perfectly illustrated based on the work of Ghosh and Nambissan [21] who annealed TiO_2 in oxygen-rich atmosphere and discovered that formation of V_O, V_{Ti}, and various defects complexes occurred only at temperatures below or equal to 300 °C. Its increasing, in turn, resulted in gradual out-diffusion of defects which became a dominating process as it prevailed over their generation (Fig. 5.2). Thus, increased quality level of crystal lattice was observed.

5.2.3.4 Vapor-Phase Synthesis

Physical vapor depositions Physical vapor deposition (PVD) such as sputtering and evaporation has been extensively applied to grow defective TiO_2 nanostructures filled mostly with oxygen vacancies. Comparing the basic principles of both of these techniques, it is evident that sputtering provides much higher flexibility in controlling the stoichiometry of deposited structure as it requires the use of plasma

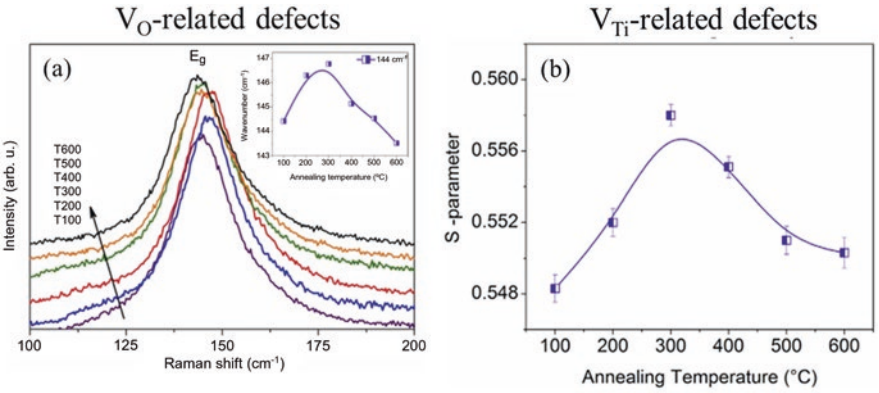

Fig. 5.2 (**a**) Positioning of Raman active mode (at ~144 cm^{-1}) of annealed TiO_2 sample. Inset shows the plot of peak position with respect to temperature of thermal treatment. This mode originated from stretching vibrations of oxygen atoms in O-Ti-O bond, and the presence of oxygen vacancies (V_O) usually results in its shifting toward higher wavenumber side. (**b**) Analysis of defect presence in annealed TiO_2 using Doppler broadening spectroscopy performed via detecting the dependence of the line-shape parameter, *S*, from the temperature of thermal treatment. The increase of *S*-parameter indicates the rise of concentration of V_{Ti} defect or associated defect-combinations. (Reprinted with permission from Ref. [21] with permission from *Elsevier.* Copyright 2019)

for delivering vaporized sources (often presented in the form of TiO_x) to the substrate. Furthermore, Ti metal also can be used as a target material. In this case, reactive ions from plasma apart from serving as transportation tool take the additional role of oxidants actively transforming Ti atoms into TiO_2 molecule followed by their deposition. Accordingly, one might arrive to conclusion that simply by adjusting the parameters of plasma source, it is possible to control the introduction of defects in finalized compositions. For example, Tomaszewski et al. [23] investigated TiO_2 prepared by DC magnetron sputtering and discovered that its oxygen deficiency follows the concentration of O_2 in sputtered gas mixture. In turn, it was also demonstrated that temperature of sputtering plays a crucial role in appearance of various defects in deposited TiO_2, as its increase minimizes the availability of V_O, while concentration of Ti^{3+} surprisingly becomes higher [24].

Chemical vapor deposition Chemical vapor deposition (CVD) is a well-known and widely established technique which allows to reach highly effective fabrication of TiO_2 in various stoichiometries and morphologies depending not only on the particular conditions of this processing such as temperature and pressure inside the reaction chamber or concentration and nature of utilized vapor precursors, their chemical compositions, and flow rate and duration of exposure but also even by applying certain types of utilized substrate. For example, Zhang and Li [25] investigated fabrication of TiO_2 via mist CVD and discovered that concentration of TTIP,

the chemical that served as one of precursors for reaction, plays a crucial role in varying the ratio of oxygen vacancies. Furthermore, it is also possible to employ plasma source during CVD which can serve as supplementary tool [26] to add more accuracy in precise adjustment of the deficiency ratios within the deposited materials simply by avoiding unnecessary and even sometimes harmful influence of high temperatures that accompany the growth process. There are various types of CVD which can be applied for fabrication of non-stoichiometric TiO_2. Apart from the abovementioned mist and plasma-assisted chemical vapor depositions, metal-organic chemical vapor deposition (MOCVD) [27] and other types were also reported among others. As a final word, it has to be noticed that most of literature regarding the formation of TiO_2 by CVD techniques focuses mostly on the fabrication of oxygen-deficient rather than titanium-deficient composition. Apart from the fact that O atoms have lower displacement energy than that of Ti, there is also a need to notice that CVD synthesis often occurred at oxygen-poor environment, i.e., vacuum, which is highly favorable for the release of oxygen atoms. In fact, unexpected formation of V_O in TiO_2 during this processing might become a serious problem as it rarely could be avoided.

Atomic layer deposition Atomic layer deposition of TiO_2 allows to reach precise control down to sub-nanometer level over the defect type, their concentration, and distribution during fabrication process. Synthesis of materials is realized as formation of layered structure where appearance of each layer is determined as a result of self-limiting reaction between two precursors. Overall, it is characterized as one cycle of ALD. Thus, changing the number of cycles inside the reaction chamber can be used to reach the required thickness and structure of composition which, in turn, have great correlation with controlling the behavior and nature of defects within it. It is also necessary to mention that similar to CVD mentioned above, the influence of substrate also often plays a crucial role in this processing. These concepts could perfectly be illustrated based on the work of Chang et al. [28] who investigated fabrication of TiO_2 thin film (Si or quartz substrate) and nanotubes (anodized aluminum oxide was used as a template) via ALD with cycle numbers of 50–700 cycles (growth rate was 0.058 nm/cycle and ~0.050 nm/cycle, respectively). It was discovered that appearance of oxygen deficiency in these structures follows absolutely opposite trends. Particularly, for TiO_2 thin film, the higher concentration of V_O was observed with respect to the increased number of deposition cycles, while for TiO_2 nanotube arrays, this tendency was opposite, i.e., the lower the cycle number, the less V_O were formed. Another parameter of ALD process which can be used to adjust the presence of defects in deposited structure is the temperature inside the reaction chamber. For instance, Wei et al. [29] investigated fabrication of TiO_2 by plasma-assisted ALD with thickness of ~20 nm and temperatures ranging from 100 to 300 °C. It was discovered that formation of oxygen-reach structure became possible once the temperature of deposition exceeded 200 °C.

5.2.3.5 Chemical-Based Approaches

Chemical oxidation method Chemical oxidation reaction to prepare defective TiO_2 compositions usually is proceeded via increasing the oxidation number of Ti through its association with oxygen atoms available as a separate compound or as a part of more complex chemicals. Another option is to use certain chemicals that assist in gaining the oxygen from surrounding media thus facilitating the reaction. It is often the case that thermal treatment should accompany this process serving as additional input of energy to make it speed up. Control over the level of oxidation is realized via adjusting the processing parameters and choosing correct chemicals to join the reaction. Thus, desired defects with clearly defined concentrations and distributions can be easily introduced into resulting compositions. Yet, due to the nature of this process, these defects mostly refer to oxygen vacancies and reduced Ti and Ti interstitials. Simply put, advancing incomplete filling of oxygen atomic positions within newly generated TiO_2 crystal lattice can be used to form V_O. In turn, the appearance of Ti^{3+} centers is realized by limiting the transformation of Ti only to the oxidation state of 3+. For example, Liu et al. [30] prepared reduced TiO_{2-x} nanoparticles by oxidizing TiH_2 powder in H_2O_2 solution (at 160 °C for 20–27 h). It was discovered that the longer the time of treatment, the higher the concentration of defects detected in the bulk and surface.

Chemical reduction method The formation of defects also can be conducted via reduction reaction which proceeding usually is achieved through interaction of TiO_2 with various specified chemicals presented in the form of metallic, organic, and inorganic compounds without/with assistance of thermally activated environment. During this reaction, a certain part of oxygen atoms is effectively evacuated from crystal lattice of TiO_2 leaving behind V_O in a manner very similar to that which occurred during reduction by hydrogenation described above, while oxidation state of Ti due to acquisition of an additional electron transformed from 4+ to 3+ oxidation state and thus led to appearance of highly useful Ti^{3+} centers. In fact, oxidation state can even be lowered down more even though it is a rare phenomenon. Thus, the parameters of reduction reaction should be considered with care as their unproper adjustment might result in appearance of opposite effect, i.e., oxidation of newly created oxygen vacancies and thus decreasing the overall level of deficiency. This concept could be perfectly demonstrated using work of Kang et al. [31] as example. It was reported that synthesis of reduced black TiO_2 nanotubes was reached by dipping them into 0.1 M $NaBH_4$ for different times at room temperature. Further analysis revealed that applying this treatment within the range of 40 min could lead to effective generation of V_O, while extending this time further resulted in their gradual filling by adsorbed O_2.

Solgel method Solgel synthesis is based on the hydrolysis/condensation of a titanium precursor to produce a sol and then a gel, which after drying to remove solvent undergoes heat treatment to stabilize the obtained structure and eject unreacted chemicals [32]. The formation of defects within it is usually determined not only by

the choice of precursors employed in synthesis, their nature, concentrations, and utilized fractions but also by conditions of hydrolysis that play a crucial role. Moreover, specifications of consequent thermal treatment such as temperature, durations, and gas ambient also are applicable to adjust the level of deficiency in TiO_2 with high accuracy. The advantage of this technique is that it enables to introduce wider-range defects than those mentioned above including not only well-known oxygen vacancies and titanium interstitials but also, for example, titanium vacancies, which have very high formation energy and thus are challengeable to appear. In fact, as solgel synthesis often is accompanied by oxygen-reach conditions, definitely, formation of V_{Ti} might be very favorable and even dominated over that of other intrinsic defects. For example, Grey and Wilson [33] demonstrated that Ti-deficient TiO_2 can be achieved via controlled hydrolysis of titanium isopropoxide and further treatment at 80 °C or by neutralization at 0 °C of a solution of $TiCl_4$ in dilute HCl with NH_4OH. Thus, flexibility of solgel method in choosing the type of defect to produce along with its simplicity allows it to become a highly applicable methodology. Definitely, fabrication process can be modified to obtain other defects too.

Hydrothermal method The hydrothermal method is a very promising and fascinating route for the synthesis of nanostructured TiO_2 as it allows not only to realize various complex morphologies including nanosheets, nanoribbons, spheres, nanocorals, and nanorods via very simple route [34] but also have a great influence on their chemical compositions. Its proceeding has very high resemblance to that of solgel as often almost similar chemicals are used to create initial solution. Yet, application of hydrothermal method is described by its own unique pathway which includes the very important and often finalized step of placing this solution into the autoclave to be subjected for treatment at certain temperatures (usually within the range of ~100–300 °C) and within designated durations of time. Due to non-equilibrium conditions created during this process, i.e., presence of high pressure activated by thermally driven energy, the fabricated structures often demonstrate the existence of various defects within its surface or bulk compositions such as oxygen vacancies and Ti interstitials. Their concentrations, distribution, and interactions with each other depend on the applied parameters and used chemicals during this processing. For example, Yu et al. [35] demonstrated the formation of bimodal nanocrystalline mesoporous TiO_2 powders by a hydrothermal method applying tetrabutyl orthotitanate as precursor and made a treatment at 180 °C for 1, 10, and 24 h. It was revealed that the longer the time of synthesis, the lower the presence of oxygen within the surface of fabricated TiO_2.

Other chemical based methods The abovementioned methods to prepare defective TiO_2 present only a small part of chemical-based approaches available in literature as this route is very popular among the scientific community due to its simplicity, accessibility, low cost, and precise control over parameters of fabrication. As it is impossible to introduce them all in details, a brief description of only some of them

is provided below as to give a very general idea of their specific particularities and unique features.

(a) Solvothermal method. The solvothermal method is almost identical to the hydrothermal route with the only exemption being that the solvent used here is non-aqueous which means that there is no need to consider its boiling point. Thus, it is possible to apply much higher temperature of synthesis. It provides very precise control over the morphology and stoichiometry of obtained TiO_2, very similar to that which could be reached during hydrothermal fabrication given their similarity. For example, Song et al. [36] applied solvothermal method to prepare Ti^{3+} self-doped TiO_2 nanoparticles with fusiform-like morphology which demonstrated excellent visible-light photoactivity.

(b) *Spray pyrolysis*. Spray pyrolysis method is based on forming an aerosol from various precursor solutions and their consequent transfer toward heated substrate where they are subjected to certain reactions in order to be transformed into desired compound. For instance, Dwivedi et al. [37] used titanium isopropoxide at concentration of 0.1 M to be sprayed on substrate kept within different zones under the temperatures of 400–850 °C to fabricate TiO_2 nanoparticles with black, green, and white colors (Fig. 5.3). This variation of colorization was mostly attributed to the difference in appearance of Ti^{3+} centers and oxygen vacancy defects within the samples as it follows the changes in the temperature of substrate.

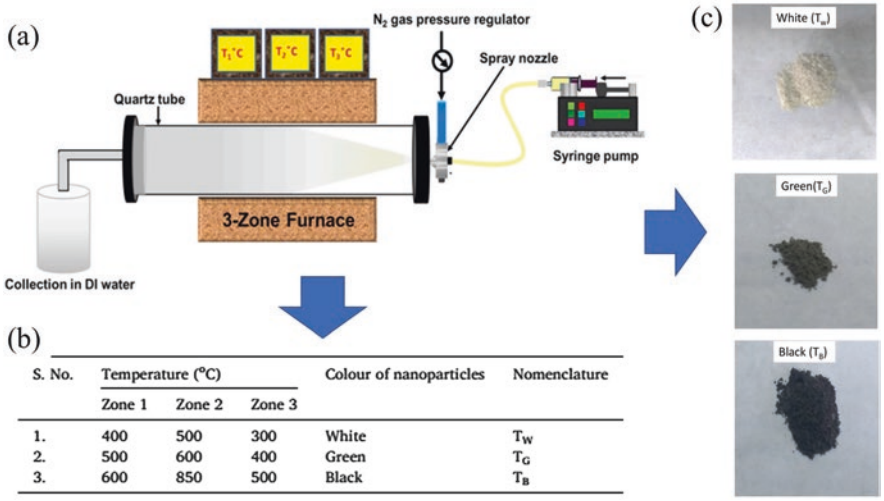

(b)

S. No.	Temperature (°C)			Colour of nanoparticles	Nomenclature
	Zone 1	Zone 2	Zone 3		
1.	400	500	300	White	T_W
2.	500	600	400	Green	T_G
3.	600	850	500	Black	T_B

Fig. 5.3 (**a**) Schematic diagram of continuous spray pyrolysis technique. (**b**) Effect of zone temperatures on the color of the TiO_2 nanoparticle. (**c**) Images of white, green, and black TiO_2 nanoparticles. (Adapted from Ref. [37] with permission from *Elsevier*. Copyright 2020)

5.2.3.6 Electrochemical Methods

Electrochemical reduction In general terms, the electrochemical reduction to fabricate defective TiO_2 is very similar to that of chemical process with only difference being that the former method requires utilization of electric energy to make the reaction occur, while in the latter one, it is pushed forward by difference in chemical potentials between participated substances. Thus, the compositions which is going to be reduced is considered as cathode during this process, while anode often represents Pt electrode. In this way, various parameters such as voltage, duration of treatment, the type of electrolyte solution, and its molar ratio determine the concentration, distribution, and nature of introduced defects. For instance, Xu et al. [38] demonstrated the application of this method to reduce titania nanotubes prepared via AAO template method by using voltage of 5 V for the duration of 5–40 s. The aqueous solution of 0.5 M Na_2SO_4 was used at room temperature as electrolyte. It was revealed that concentration of oxygen vacancies increases following the time of treatment. In another example, Zhou and Zhang [39] investigated the influence of various voltages on the quality of reduced TiO_2 nanotubes. It was determined that cathodic current passes the tubes, and it dramatically increases with the used potential. Thus, higher negative potentials, such as -1.6 V and -1.8 V, resulted in expanding of TiO_2 lattice to such an extent that nanotubes were destroyed due to generation of cracks. In turn, a moderate potential of -1.4 V proved to be sufficient for introducing oxygen vacancies and preserving the structure.

Electrochemical oxidation Electrochemical oxidation which also sometimes is referred as anodization is recognized as a fast and effective method to modify the composition and structure of anode material usually represented in the form of metallic Ti foil or other related composition and morphologies by applying an external voltage between it and cathode. As for the mechanism, it is explained as follows: OH^- and O_2^- ions widely presented in the electrolyte solution usually move toward Ti and react with Ti^{4+} whose dominated appearance on its surface is catalyzed by the current passing through it during anodization. Thus, the formation of TiO_2 layers is observed. The growth of oxide on Ti has a strong dependency on the presence of available oxygen content in the electrolyte (i.e., H_2O concentration). To be clear, its limitation results in generation of unsaturated oxide state according to the following reaction, $Ti^{4+}+xO^{2-} \rightarrow TiO_X + 2xe^-$ [40], where TiO_x is considered to have a certain degree of oxygen deficiency compared with fully stoichiometric TiO_2. The reliability of this strategy was perfectly illustrated, for example, by Tsui et al. [41]. Particularly, it was shown that water content in electrolyte solution influences crucially on the introduction of oxygen vacancy in anodized TiO_2 nanotubes and thus can be used as effective tool to govern their concentrations. It is necessary to mention that the role of NH_4F in creating pores that lead to tubular structure during oxidation is left aside as its description is beyond the scope of this chapter.

Electrochemical deposition Electrochemical deposition or electrodeposition is a greatly accessible method for preparation of metal oxides on conductive substrates.

Its experimental setup has certain similarities to that used to perform electrochemical reduction and oxidation processes described above as all of them utilize applied voltage. Electrodeposition is usually defined by two pathways [42], namely, a cathodic route which is based on using TiO^{2+} solution and anodic route where the formation of TiO_2 is realized by employing $TiCl_3^-$. The resulting composition usually is amorphous and requires additional thermal treatment to transform it into crystal phase. Control over the concentration ratios of species used in electrodeposition, pH of the chemical bath, and range of cathodic-anodic scan provide extremely high flexibility in application of this method to fabricate TiO_2 with desired morphology ad stoichiometry. For example, Ertekin et al. [43] demonstrated electrodeposition of TiO_x film which contained various Magnéli phase titanium suboxides such as Ti_2O_3, T_4O_7, etc. under different applied potentials. Titanyl sulfate saturated solution was used as source compound. It was discovered that appearance of oxygen deficiency and its level were correlated with water insufficiency in supporting electrolyte, while control over suboxide formation was reached via adjusting the value of applied potential.

5.2.3.7 Mechanical Methods

High-energy ball milling (BM) is considered to be an effective and accessible approach for the synthesis of nanocrystalline powders with desired and controlled characteristics and features. In a BM process, the friction and collision of ball could lead to appearance of high temperature usually above 1000 °C at highly localized region within ~1 μm^2 for extremely short time of 10^{-3} to 10^{-4} s [44]. Application of these conditions to TiO_2 as well as to other binary oxides usually results in formation of oxygen vacancies and other related defects such as distortion of lattice and generation of disorder phases. It has to be noticed that this method usually causes the dominated appearance of defects in the bulk of materials. Their concentration and consequent accumulations could be easily controlled by playing with rotating speeds, temperatures, and durations at which the BM is applied. For example, Rajender and Giri [45] used commercial TiO_2 powder (~80 nm) to make it ball-milled under 350 rpm for 40 h using small ZrO_2 balls. It was revealed that increasing the time of this treatment resulted in more evident transformation of TiO_2 into Ti_3O_5 compound that was considered to be "an oxygen deficient phase." Its appearance was related to the "presence of oxygen vacancy (O_v) defects in milled TiO_2 powder."

5.2.3.8 Alternative Methods

Fabrication of defective TiO_2 can be realized via numerous strategies which, however, cannot be discussed fully here due to the limitation of pages. Nevertheless, the main purpose of this section is to provide general idea where the current progress in synthesis of this compound is forwarding. As for more detail discussion, readers are suggested to search for appropriate literature.

Ultrasonication method Ultrasonication enables to make significant changes in morphological, optical, and surface characteristics of solution-dispersed TiO_2 nanoparticles, and thus it is often used to create various defects within its structure including oxygen vacancies and Ti^{3+} centers. Their formation is explained as follows. Ultrasound can generate high-speed inter-particle collisions which lead to extreme heating at the point of impact and effective local melting [46]. Thus, the stoichiometry of surface is effectively disturbed. For example, Osorio-Vargas et al. [47] demonstrated that V_O could be successfully created in commercial TiO_2 by utilization of ultrasonic bath consisting of a direct immersion of ultrasonic horn operating at 20 kHz with an acoustic intensity of 1.2 W mL^{-1} for 6 h. Their appearance resulted in extended optical characteristics of TiO_2.

Microwave/UV-light irradiation method Synthesis of various 0-D TiO_2 structures including, for example, hollow nanospheres or nanoparticles, with controlled sizes and stoichiometries, can be realized simply by placing the prepared reaction solution into microwave oven and its consequent irradiation with designate time and power. The appearance of TiO_2 as specified phase usually is proceeded via precipitation reaction [48] which is advanced by consequently increased temperature within solution. Thus, under certain conditions, it is possible to reach non-complete filling of oxygen or titanium atomic sites within crystal lattice during the process of TiO_2 formation. In turn, microwave irradiation also can be used to treat already prepared TiO_2 structures creating certain defects within it. For example, Horikoshi et al. [49] reported that subjecting well-known commercial P25 powder to microwaves source for 10 min resulted in "additional defect sites such as anion and cation vacancies… produced in the lattice and subsequently at the surface." In turn, UV irradiation also can be used to introduce various defects in TO_2, yet due to its particularity, it is more suitable to treat already synthesized compositions than to be a part of fabrication route. Specifically, low-power UV light is capable to create V_O and Ti^{+3}. The mechanism of their appearances can be described as follows. Illumination with photons with energies higher than band gap generates electron-hole carriers in TiO_2. Thus, some of the holes which were not recombined with their counterparts can react with lattice oxygen leading to its partial removal and formation of surface oxygen vacancies; in turn, some of the electrons react with lattice metals (Ti^{4+}) to make it reduced into Ti^{3+}defective sites.

Ionothermal method Ionothermal method is based on the use of ionic liquids (IL) as both the solvent and potential template or structure-directing agent in the formation of solids [50]. This approach is very similar to that of hydrothermal synthesis where the water is considered as solvent, yet with only difference that, as IL has low vapor pressure, it does not require the use of autoclave, and the reaction is easily proceeded even in a very simple container. Thus, heating of the solution can be advanced even by using, for example, abovementioned microwave irradiation. Li et al. [51] reported the fabrication of black Ti^{3+}-doped anatase TiO_2 single-crystal by treating Ti foil in 1-methyl-imidazolium tetrafluoroborate ionic liquid containing acetic acid (HAc), N,N-dimethylformamide (DMF), and lithium acetate (LiAc) at 200 °C. In addition, it was also stated that oxygen vacancies were produced as well too.

Solgel combustion method Solgel combustion method identified as solution combustion synthesis is a mixture of chemical gelation procedure and combustion process. To be more precise, the proceeding pathway involves an exothermic decomposition reaction of an aqueous gel and a thermally induced anionic redox reaction [52]. Their correct realization can be used to obtain various nanoscale powdered structures and compositions at relatively low temperatures with controlled agglomerations, sizes, and distributions as well as designated presence of certain defects. For example, Xiao et al. [53] used this method to prepare Sm^{3+}-doped TiO_2 nanocrystalline via baking precursor gel contained titanium isopropoxide ($Ti(OC_2H_5)_4$) and $Sm(NO_3)_3$ along with required solvents at 150 °C in muffle furnace followed by auto-ignition at about 250 °C. The resulting compositions contained 0.5%, 1.0%, and 1.5% of Sm. It was demonstrated that content of surface oxygen vacancy had a strong dependency to presence of doped ions and reached highest degree as concentration of Sm in TiO_2 equaled to 0.5 mol%.

Rapid quenching after thermal annealing Annealing of TiO_2 in air at temperatures approaching 1000 °C results in appearance of certain concentration of oxygen vacancies and Ti^{3+} centers given that they have specific activation energy barrier. However, due to gradual cooling, some of these defects if not all were filled with oxygen from the surrounding thus resulting in their partial and even sometimes full annihilation. To solve this problem, Liu et al. [54] demonstrated the use of rapid quenching in the form of direct throwing of annealing samples into ice-water media which resulted in freezing of defects. It allows them to stay in crystal lattice after cooling down and be easily detectable. Furthermore, it was revealed that the higher the temperature of annealing, the more defects could be detected after freezing (Fig. 5.4).

5.2.3.9 Influence of TiO_2 Crystallinity and Phase on the Formation of Defects

TiO_2 has two main crystal phases, namely, anatase and rutile (brookite is deliberately excluded given the number of published works regarding it), which have some differences in their structural characteristics and arrangement of atoms as well as physical and chemical properties. Thus, formation of defects in each of them is determined by certain particulates and very defined restrictions that should be taken into consideration during fabrication process or consequent treatment steps as their incorrect interpretations might result in unexpected outcome. Simply put, the process, which is applicable to anatase, in some cases cannot be utilized under the same conditions with regard to rutile and opposite. In turn, level of crystallinity also plays a crucial role in introduction of defects into TiO_2. For example, fully crystallized and partially or completely amorphous compositions have different activation energy barriers which should be effectively overcome as to make TiO_2 become deficient. More details are provided below regarding these topics. For simplicity and compactness, the discussion mostly refers to the hydrogenation process which

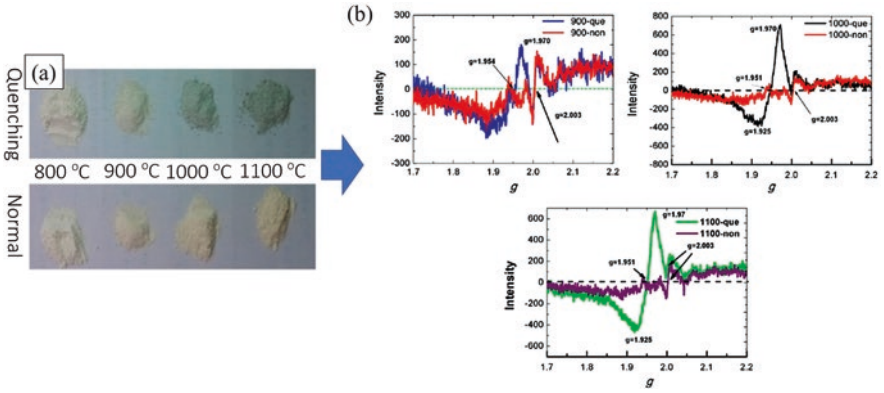

Fig. 5.4 (**a**) Digital pictures of q-TiO_2 (quenched) and n-TiO_2 (normally cooled) samples prepared from the commercial P25 powders after being subjected to different temperature of pre-annealing. Quenched samples have pale blue color, while normally cooled down, white color. (**b**) EPR spectra recorded at 100 K for a-TiO_2 and q-TiO_2 after pre-annealing at different temperatures. Signals at $g \approx 1.95$ and $g = 2.003$ demonstrate the appearance of Ti^{3+} interstitials and V_O in quenched samples. The higher their intensities, the more defects are produced. (Reprinted from Ref. [54] with permission from *American Chemical Society*. Copyright 2017)

usually results in changing the color of TiO_2 from white to gray or black due to formation of disordered compositions and appearance of oxygen vacancies/Ti^{3+} centers. It necessary to notice that the same descriptions with slight modification and certain reservation might also be applied to other processing.

Anatase phase Anatase is low-temperature crystalline phase of TiO_2. The following specifications regarding its defective engineering are required to be brought into attention during hydrogenation. *Firstly*, formation of defects in anatase can be realized only at temperatures up to 600 °C as its further increasing would result in appearance of rutile phase. *Secondly*, the higher the temperature, the more advanced is the concentration, and the more uniform is the spread of oxygen vacancies, the better is the photocatalytic/photoelectrochemical response of TiO_2 [55]. *Thirdly*, anatase originally has higher Urbah energy than that of rutile due to lower coordination between octahedra [56], which represents that within equivalent conditions, it possesses more disorder states and/or accommodated defects. *Fourthly*, DFT calculation showed that anatase has lower formation energy of V_O compared with that of rutile [11]. *Fifthly*, allocation of V_o defects in anatase follows homogeneous distribution, making the maximum possible distance from one another [57]. *Sixthly*, in anatase, V_O is more stable on the surface than underneath it, which is opposite to rutile [4].

Rutile phase In opposition to anatase, rutile is considered to be a high-temperature stable phase of TiO_2 as its appearance occurs after thermal treatment at temperatures over 600 °C. It is also possible to use direct fabrication via hydrothermal, solgel, or other related experimental approaches to initiate it. The following particularities of defect formation are connected with this phase with regard to hydrogenation. *Firstly*,

its most optimal concentration and distribution of defects usually can be reached at temperature much lower than that of anatase. For example, if anatase requires hydrogen-supported thermal treatment at ~550 °C to have an optimal presence of defects, it is enough to use only 350 °C for rutile to reach it [55]. *Secondly*, appearance of Ti interstitials in rutile requires application of lower formation energy than that of anatase [11] which makes their presence more favorable than that of V_O, yet it is debatable [3]. *Thirdly*, hydrogenation leads to higher photoelectrochemical efficiency of rutile than that of anatase taken in absolute values considering the comparison of samples after their introduction to most optimal conditions of treatment [55]. *Fourthly*, it was discovered that after hydrogenation and introduction of defects, conduction band of black rutile becomes higher in energy than that in black anatase by ~0.4 eV. It has to be noticed that before treatment, it had difference of only ~0.1 V [58]. *Fifthly*, the distribution of oxygen vacancies is heterogeneous in rutile [57]. *Sixthly*, band gap of rutile is lower than that of anatase (3.0 eV vs 3.2 eV). Thus, as defects create mid-gap energy levels within the band gap, their locations with respect to CBM and VBM can be different depending on crystalline form. *Seventhly*, change of valence band minimum, or appearance of band tail due to introduction of oxygen vacancies, is less evident in the case of rutile compared with that of anatase [58].

Mixed phase It is very easy to obtain mixed phase composition of TiO_2 (mixed TiO_2) as annealing at temperatures of 650–700 °C of pure anatase structure is simply enough to reach it. Compared with pure TiO_2 existing in anatase or rutile forms, its mixed phase composition has some particularities which makes introduction of defects there a highly specific process. *Firstly*, its response to hydrogenation treatment is very similar to that of anatase phase, yet it cannot be said that due to presence of rutile, the optimal temperature can be extended beyond 550–600 °C [55]. Anatase, in fact, should always be presented in mixed TiO_2 as it is considered to be a dominated phase to make the introduction of defect more feasible and to keep high photocatalytic efficiency. *Secondly*, formation of oxygen vacancies can accelerate the phase transformation and the formation of Ti interstitials oppositely suppressing it [59]. Thus, temperature of hydrogenation should be chosen carefully. *Thirdly*, once two phases combined together and form heterojunction, they usually are electronically coupled. Presence of defects results in increasing or lowering the charge dynamic between phases, depending on which type of defect is introduced, where it is located, and its concentration. For example, it was reported that if V_O is introduced into the interface, it has no influence on electron transfer and only governs the activity of holes [60]. *Thirdly*, ratio of rutile to anatase can influence the introduction of defects and their characteristics given that each phase has its own particularities. For example, anatase-rich compositions show longer photo-induced carrier lifetime compared to that of rutile-rich mixed phase [61]. *Fourthly*, rutile and anatase combined together can behave differently toward introduction of defects and even serve as compensating counterparts neglecting positive impacts to each other. It might result in various controversial and even negative phenomenon, including, for instance, non-uniform appearance of disordered structure or opposite trends in

advancing the morphology due to changes in surface free energy [62]. *Fifthly*, and most importantly, mixed-phase TiO_2 before and after hydrogenation always shows higher photoefficiency than that of pure rutile and anatase phases [55].

Partly crystallized TiO_2 The above discussion regarding various phases of TiO_2 was attributed mostly to fully crystallized TiO_2. In turn, it is necessary to say several words about its partly crystallized form as introduction of defects in it has one important difference. Theoretical calculation performed by Pham et al. [63] demonstrated that formation energy of oxygen vacancy is significantly reduced down to several eV upon introduction of amorphization into crystalline structure. Furthermore, it was also suggested that at Fermi levels near the VBM, the V_O with charge states of +1 and +2 could form spontaneously in amorphous TiO_2. It could be attributed to the weakening of intrinsic bonding and decaying strong periodic arrangement which leads to appearance of "loosen structure," thus making the escape of atom to be realized as lower energy cost. It also leads to higher-level structural disordering compared with fully crystallized TiO_2.

5.2.4 Properties of Defective TiO_2

5.2.4.1 Structural Properties

Structural properties of defective TiO_2 are mostly governed by two types of defects, namely, oxygen vacancies and Ti interstitials. Particularly, the introduction of oxygen vacancies in TiO_2 modifies its geometric structure due to the atomic rearrangement. Removal of O atom results in outward relaxation of three nearest Ti atoms in order to strengthen their bonding with the rest of the lattice. It decreases the overlap between the three Ti dangling bonds and leads to reducing the length of the Ti-O bond length [14]. This result is confirmed by lowering the lattice dimension of oxygen-deficient TiO_2 detected by X-ray diffraction analysis [64]. In turn, the formation of Ti interstitials which occur due to inter-diffusion of Ti atoms usually leads to lattice expansion. Following it, one might notice that simultaneous presence of both mentioned types of defects TiO_2 likely results in appearance of compensating effect, and thus any significant changes in lattice parameters could hardly be observed [37].

Furthermore, it was revealed that formation of these defects within the surface induces to increased roughness of the TiO_2. The origin of this phenomenon could be explained based on example of V_O [64] (Fig. 5.5). Since it is considered to be a low-energy bulk defect, its appearance on the surface of TiO_2 results in distortion of its free energy. Thus, the search for new local thermodynamic equilibrium can only be proceeded by mass redistribution. The preferred reconstruction is established when the lowest energy is reached. The higher concentration of oxygen vacancies leads to more dramatic change of the surface roughness. In addition, introduction of V_O and accompanied Ti^{3+} centers often results in appearance of disordered shell around the

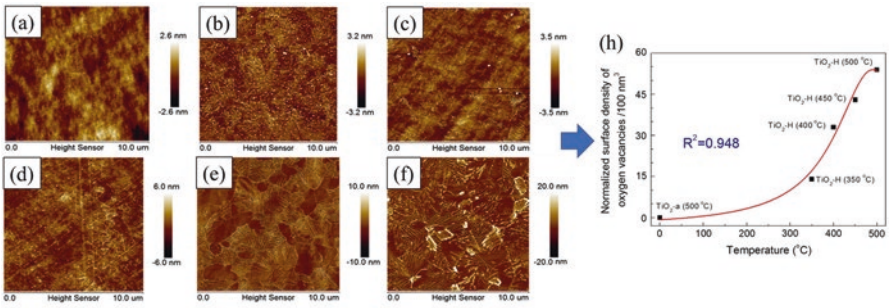

(g) Roughness values R_a and R_q (nm) for TiO_2 thin films.

Sample	R_a	R_q
As-deposited TiO_2	0.44	0.57
TiO_2-a (500 °C)	0.54	0.85
TiO_2-H (350 °C)	0.59	0.85
TiO_2-H (400 °C)	0.88	1.14
TiO_2-H (450 °C)	1.53	2.01
TiO_2-H (500 °C)	3.48	4.86

Fig. 5.5 (**a**) Two-dimensional AFM images of TiO_2 thin films. (**a**) As-deposited, (**b**) annealed in air at 500 °C, and annealed in hydrogen at (**c**) 350 °C, (**d**) 400 °C, (**e**) 450 °C, and (**f**) 500 °C. As-deposited sample represents amorphous structure. Annealing in air for 500 °C was done to make it serve the role of control sample. Annealing in hydrogen, in turn, was used to introduced V_O. (**g**) Roughness values R_a and R_q (nm) for TiO_2 thin film. (**h**) Normalized surface density of oxygen vacancies in hydrogenated TiO_2 thin films with reference to the sample annealed in air at 500 °C. (Reprinted from Ref. [64] with permission from *Elsevier*. Copyright 2015)

crystalline core or on the surface of thin film [14]. Its thickness as well as stoichiometric compositions and level of amorphization can be easily adjusted by conditions of post-synthesis treatment, yet precision of this tuning is still far from required. It was revealed that the higher the thickness of disordered layer, the higher the amount of newly created intrinsic defects.

5.2.4.2 Optical Properties

Introduction of oxygen vacancies and Ti^{3+} centers into TiO_2 usually results in formation of localized energy states within the band gap. It not only enables to increase the overall absorption in parallel but also allows to reduce the band gap and thus to extend the absorption edge toward visible and even infrared wavelength. Thus, the electron firstly jumps from the valence band to the oxygen vacancy or reduced Ti centers or its interstitial which serves as an intermediate transition level, and later it is transferred further toward the conduction band. These V_O- and Ti^{3+}-induced defective states are supposed to locate mostly near the conduction bands given their donor-like characteristics. Particularly, DFT calculation revealed that various configurations of Ti^{3+} resulted in appearance of states within ~0.3–0.8 eV under conduction band [65], while those of oxygen vacancies were determined to exist at a distance of ~0.75–1.18 eV from it [14]. Furthermore, formation of two additional groups of mid-gap states created at about ~1.8 eV and ~3.0 eV was revealed, where

the former one was derived from the Ti 3d orbitals, while the latter was hybridized from O 2p and Ti 3d orbitals and mainly caused by the disordered states [66]. The level at ~1.8 eV was accounted for blue shift of valence band edge and extending the absorption far beyond UV spectra. In addition, as TiO_2 becomes sensitive to visible light, its color is often changed from original white to yellow-green [20], gray [22], or black [26], depending on the nature, concentration, and distribution of newly created defects, their arrangement whether on the surface or in bulk, and methods used to introduce them. In turn, it has to be noticed that titanium vacancies and oxygen interstitials are seldom used as contributors to the changes in optical properties as their formation in TiO_2 is considered to be unfavorable due to acceptor-like characteristics, and application of strong O-rich conditions is required to initiate them.

5.2.4.3 Chemical Modifications

Formation of various defects often leads to serious chemical changes in TiO_2 which influence crucially on its initial compositions. For example, oxygen deficiency might lead to transformation of TiO_2 into one of its suboxides, which are called Magneli phases and represent the form of Ti_nO_{2n-1}. In turn, as defective TiO_2 often is created by hydrogenation process whether in the course of thermal treatment or due to exposure to plasma, it often results in introduction of H atoms into it and consequent formation of energetically stable Ti-OH bonds and Ti-H groups that also have certain influences on various characteristics of reduced TiO_2 and thus cannot be ignored. In turn, the appearance of Ti vacancies would result in formation of substoichiometric compound present in the form of $Ti_{1-n}O_2$.

5.2.4.4 Electronic Properties

Formation of intrinsic defects in TiO_2, specifically, oxygen and Ti vacancies, has a crucial effect on electronic configuration of its band gap due to appearance of additional mid-energy levels close to conductions and valence bands, respectively. As for more detailed discussion, V_O appears in the form of +2 as it is found to be the most stable and energetically favor charge state in neutral TiO_2 [5]. Due to its shallow nature, it serves as the source of n-type conductivity, and increase of its concentration results in increasing the ratio of available electrons. It leads to appearance of polarons characterized by localization of an electron on a particular Ti site, changing its oxidation state from +4 to +3 [67]. Following it, the polaronic states are determined to reside at ~0.94 and ~1.3 eV below the conduction band in addition to that of V_O, with the two electrons having the same spin; they localize in separated Ti atoms. Polarons also can be caused by lattice distortion such as appearance of disordered states that often accompanied the formation of V_O [68]. Similar to that of Ti^{3+} and V_O, they also can have their own energy states within the band gap. When the Fermi level is shifted upward over ~2.8 eV due to increased concentration of donor-like charge carriers and their continuous advancement over that of their

acceptor-like analogies, the dominated charge state of V_O is transformed into neutral [5], which cannot contribute anymore to strengthening of n-type conductivity [69]. Electrons, oppositely, localize in its own vacancy site [14] which likely becomes a trapping center for them. One of those electrons can possibly join Ti site to reduce the oxidation state from +4 to +3. In turn, V_{Ti} takes positions near valence band and plays the role of compensating center for negatively charged carriers declining their concentration. Thus, the more V_{Ti} is proceeded, the more downward is the shift of Fermi level which results in dominated appearance of positively charged carriers.

5.2.4.5 Electrical Properties

TiO_2 in n-type semiconductor and due to its wide band gap of ~3.2–3.4 eV has low electrical conductivity and is unable to realize efficient charge transport which makes it sometimes utilized as insulator layer for various nanoscale devices such as field-effect transistors [70]. To enhance its characteristics in terms of concentration and mobility of charge carriers, defect engineering is considered to be a highly effective tool. Simply put, as oxygen vacancies and Ti^{3+} centers have clearly defined donor-like characteristics, their introduction into TiO_2 results in increased concentration of electrons accompanied by upward shifting of Fermi level toward conduction band. Moreover, it was discovered that resistivity might increase with decreasing the temperature down to freezing conditions [71] which is a very similar behavior of metals and represents the departure of defective TiO_2 from its insulating features. In fact, Smith et al. [72] stated that conductivities of TiO_2 suboxides, i.e., Magneli phases, are comparable to that of graphite. In turn, Ti vacancies due to their shallow nature and acceptor-like characteristics can be used to reach dominated presence of positively charged carriers in TiO_2. Thus, their successful introduction (in this case, the presence of Ti vacancies is expressed in absolute values) or reaching the excess of oxygen (in this case, the presence of Ti vacancies is expressed in relative values) can be used to transform this semiconductor into p-type compound.

5.2.4.6 Other Properties

Apart from the abovementioned characteristics, formation of defects in TiO_2 can influence other properties which are briefly discussed here.

(a) *Ferromagnetism*. It was reported that oxygen vacancy with the charge state of +1 enables induction of room temperature ferromagnetism in TiO_2. Several origins of its appearance were proposed in literature including strong hybridization between the O 2p states and the Ti 3d states [73], presence of lattice distortion and consequent redistribution of charges [74], Stoner exchange splitting of the Ti 3d band [75], etc. In turn, titanium vacancies also can lead to formation of magnetic moment in TiO_2 which could be explained via asymmetry of O 2p states due to electron transfer from nearby Ti atoms [73].

(b) *Thermal conductivity*. Increased concentration of point defects results in interruption of homogeneous thermal carrier propagation and development of local hotspots that may lead to increased possibility of device fail and breakage. Following it, one might consider that the more defects introduced into TiO_2 such as oxygen and titanium vacancies, the lower the value of its thermal conductivity becomes. In addition, it should be mentioned that dimension of produced defects also plays a role. As it was shown by Ok et al. [76], planar defects have higher impact on phonon scattering as compared to the point defects.

5.2.5 Defective TiO_2 via Theoretical Simulations

5.2.5.1 Various Simulation Models and Their Outcome

The main tool which is used to reproduce formation of defects in TiO_2 via theoretical modeling is the density functional theory (DFT) whose wide application is determined by low cost of its accessibility and appropriate accuracy of resulting outcome assuming that correct choice of exchange-correlation energy functionals was realized. To be clear, these functionals, in fact, play the most important and crucial role not only in correct representation of TiO_2 structure but also in proper descriptions of processes happening within it. Various types of them are presented in literature including well-known local density approximations, generalized gradient approximation, etc. Yet, their application might not be considered as the best option as they cause the appearance of self-interaction error (SIE) whereby an electron spuriously interacts with its own density [77]. It has crucial impact on understanding the depth of defect states in TiO_2 as it results in underestimation of the *d* electron localization and the amount of lattice distortions at vacancies [4]. In this case, hybrid DFT realized via selective incorporation of the Hartree-Fock theory into standard functional could be considered as attractive alternative. It resulted in development of the following functionals: B3LYP, the Heyd, Scuseria, Erzernhof (HSE) functional, screened exchange function, PBE0, etc. They all have been found great application toward investigating TiO_2 as they allow to estimate its intrinsic defects in terms of their various characteristics and particularities including formation energies, transitions levels, and geometrical relaxation with accuracy very close to that obtained via experimental approaches. In addition, it needs to mention that Hubbard "+U" correction often is used as external feature to correct SIE within standard DFT calculation. Its employment to oxygen-deficient TiO_2 encourages localization of excess electronic charge with the qualitative distribution depending on the choice of its value [78]. Finally, GW (Green function) perturbation method is also often applied to calculate various parameters of defects in TiO_2. Its correction of DFT eigenvalues takes care of self-energy and self-interaction errors and resolves the problem of band-gap underestimation [5].

5.2.5.2 Comparison with Real Experimental Studies

Estimation of computation modeling only becomes reliable if its outcome can find the reflection in the experimental data and vice versa. Simply put, it is important that theory and practice follow each other as to contribute equally into further advancement of current knowledge regarding the structure and properties of defective TiO_2 following mutual correlation and consequent relevance. For example, previously, it was a huge problem of DFT calculation to correctly introduce band gap of TiO_2 as without it, the obtained values of defect transition levels, as well as the values of their formation energies, could hardly be applied to real samples. With development of more advanced simulation methodologies, this problem and some other less evident mismatches were effectively solved which brings into effect the possibility to accurately predict, estimate, and explain the defective TiO_2 and thus to serve as visualization tool to understand what happens inside it during actual experimental procedure. In fact, it became very common recently to combine together both theoretical and practical approaches as to confirm the reliability of the obtained results. For example, both of them demonstrate that black TiO_2 as a result of hydrogenation is mainly formed due to appearance of mid-gap states that make upward shift of valence band [66]. Yet, the limitation of computing simulation is very evident as, for example, it cannot be applied to absolutely any really existed material systems since additional complexness and multi-structure composition might become a huge obstacle for correct evaluation of its defectiveness. Thus, it is very common that DFT calculations mostly are referred to flat 2-D compositions of TiO_2, while its other forms such as 0-D (i.e., decahedral faceted nanoparticles, hollow spheres), 1-D (i.e., nanowires and nanorods), and 3-D structures (i.e., hierarchical compositions, mesoporous materials) deserved much less attention. It is out of question that formation of defects in any of them would follow absolutely different scenarios in terms of charge localization and redistribution given the existence of quantum confinement effect. Thus, development of theoretical modeling is continued in order to make its capability satisfy the needs in simulating current experimental outcome.

5.2.5.3 Current Challenges

Theoretical simulation has challenges which need to be overcome as to make the estimation of materials structure, in our case, defective TiO_2, highly reliable, efficient, and, most importantly, realistic. Some of them are described below; however, it is impossible to cover them in sufficient detail here, and thus interested readers are suggested to address proper literature for more details. *Firstly*, as DFT calculations traditionally determine the properties at $T = 0$ K unless others are specified, the reported conclusions might require additional verifications to match the real experimental measurement which is mostly performed at ambient conditions or in extreme environments. Definitely, finite temperature approach has been already developed and successfully applied, yet its complexness limits its wide spreading. *Secondl*y, the terms such as “O-poor” and O-reach conditions” are often mentioned during

simulations modeling. Yet, in each experimental setup, they can be defined differently in terms of applied pressure or used ambient as well as concentration of oxygen in it, and it might influence the behavior of defects. *Thirdly*, for DFT approach, defects are usually considered to exist within a clearly defined cluster which contains a very specific number of atoms. Yet, it might be the case that in real situation, various clusters within the same materials have different synergies and thus behave differently. *Fourthly*, there always might be impurities which likely interact with defects. For example, formation of V_O in TiO_2 can be realized by Ar^+ ion sputtering that, in turn, also leads to their doping into surface and bulk layers [79] (Fig. 5.6). To remove them, additional thermal treatment is required. *Fifthly*, it is often assumed that TiO_2 initially has full stoichiometry which is changed only after appearance of intentionally introduced defects. However, in reality, TiO_2 is usually prepared by non-equilibrium synthesis such as vapor-based methods and thus already becomes filled with certain defects, for example, oxygen or titanium vacancies, upon end of fabrication that causes localized distortion of crystal lattice and influence the stoichiometry.

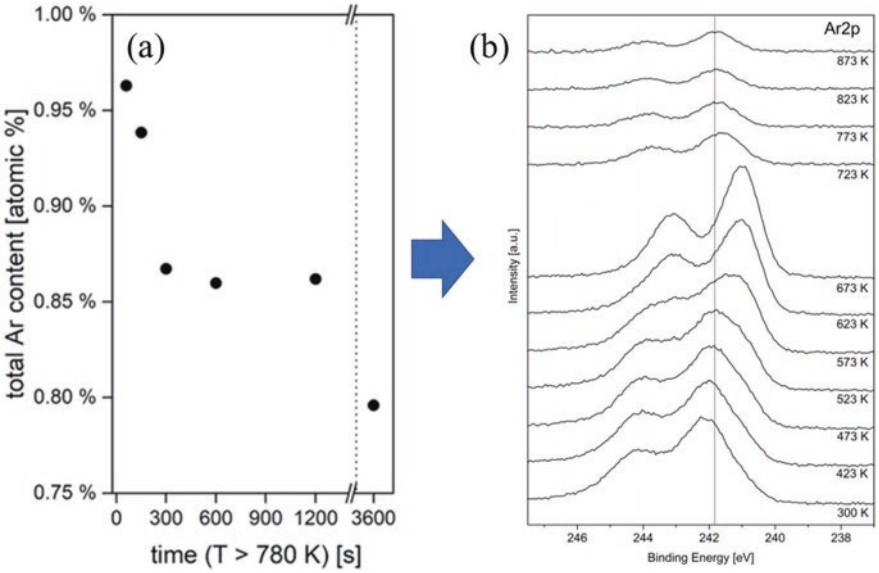

Fig. 5.6 (**a**) Total argon content in a rutile TiO_2 (110) crystal after argon ion bombardment as a function of annealing time. (**b**) Temperature-dependent X-ray photoelectron spectra of the Ar 2p region obtained from a rutile TiO_2 (110) single crystal after 20 min argon-ion bombardment and subsequent annealing at the given temperatures. (Reprinted from Ref. [79] with permission from *American Chemical Society*. Copyright 2019)

5.2.6 *Application of Defective TiO_2 as Photocatalyst*

5.2.6.1 Brief Overview

Given its exceptional properties, such as high stability, resistance to chemical corrosion, low-price, compatibility with most of biological organisms available in our planet, and nontoxicity, titanium dioxide has been investigated widely as an effective photocatalytic material for various applications such as degradation of harmful dyes, nitrogen fixation, production of hydrogen via water splitting, reduction of CO_2, etc. However, the accomplishment of these processes at sufficiently high level is restricted by certain particularities of TiO_2 given its wide band-gap nature which represents inability to absorb visible light and extremely high recombination rate of photogenerated electron/hole pairs. Numerous attempts have been made to overcome these problems including decoration with noble metal, co-catalyst immobilization, and controlled faceting. Intrinsic defect engineering can be considered as attractive alternative to them since it changes the properties and characteristics of TiO_2 through modification of its own compositional structure without use of any external materials or chemical. As it was shown above, it can be used to extend its absorption profile toward visible-light region and increases the concentration of available charge carriers as to make them serve the purpose of enhancing the rate of redox reactions with adsorbed molecules. A more detailed discussion of application of defective TiO_2 to each photocatalytic process is provided below.

5.2.6.2 Photocatalytic and Photoelectrochemical Water Splitting

Producing hydrogen from water using solar light irradiation is considered to be a perspective sustainable and environmentally friendly solution to currently used technologies. Defective TiO_2 due to its unique characteristics not only enables to initiate this process but also sufficiently contributes to improving its effectiveness and steadiness. The conduction band minimum of the defective TiO_2 is thermodynamically and kinetically favorable for water reduction. For example, Chen et al. [66] discovered that hydrogenated black TiO_2 nanoparticles obtained by treating at 200 °C for 5 days under 20 bar H_2 could produce nearly 0.2 mmol of hydrogen gas per hour under simulated solar light which is two orders of magnitude greater than the yields of most semiconductor photocatalysts reported previously. Furthermore, throughout 15 testing cycles in 15 days, the high H_2 yield kept unchanged without catalyst degradation, demonstrating an excellent stability for the black TiO_2. In turn, it was reported that hydrogenated TiO_2 nanotubes prepared via electrochemical method displayed improved photocurrent of 0.65 mA/cm^2 which was nearly two times higher than that of their untreated analogies (0.29 mA/cm^2) [38]. Yet, it has to be noticed that often the mismatch between the amount of increased absorption or band-gap narrowing and the corresponding photocatalytic performance was detected. To be clear, even though absorption in the visible spectra might be extended

due to the presence of defects, visible-light-driven reaction activity simply is absent, and the overall enhancement of solar light-induced performance is only realized via increased utilization of UV light and/or higher concentration of available charge carriers accompanied by lower recombination rate of electron-hole pairs [71]. One of the reasons of this behavior might be referred to the positioning of energy levels created by V_O in the band gap, as their localization below the reduction potentials of H_2O might result in the inability to contribute electrons residing there to the hydrogen evolution reaction. Finally, one should notice that there exists an optimized concentration of defects, which results in greatest photocatalytic/photoelectrochemical performance. Its overpassing might cause the declining of efficiency.

5.2.6.3 Light-Induced Water Purification

Photocatalytic degradation of dyes using solar light is defined as a heterogeneous oxidation process in which highly toxic molecules undergo complete transformation into non-hazardous compounds such as carbon dioxide and water. Defective TiO_2 due to its unique characteristics can sufficiently contribute to the enhancement of its efficiency. For example, Chen et al. [66] investigated degradation of methylene blue under solar light irradiation using fully stochiometric (white) and defective (black) TiO_2. For the former compound, complete removal of this dye from solution was observed after 1 h, while for the latter, it was reached within only 8 min which revealed nearly ~7 times higher efficiency. The more vacancies produced, the better the efficiency of photocatalytic degradation, yet it only works till their concentration reaches saturation [64] (Fig. 5.7a, b). Compared with hydrogen production, this processing also can be effectively and, most importantly, much easier to be realized under visible light as it has less restrictions toward positioning of mid-gap levels with respect to potentials of redox reactions.

5.2.6.4 Photoconversion of CO_2

Photocatalytic reduction of CO_2 with water to produce solar fuels is an attractive approach to lower the negative impact of greenhouse gases and also to produce various valuable carbon-neutral fuels. Defective TiO_2 due to its unique characteristics can sufficiently contribute to the successful realization of this processing *due* to the following particularities [80]. *Firstly*, oxygen-deficient surface is thermodynamically more favorable to adsorb CO_2 than a defect-free surface. *Secondly*, defect sites contribute to the dissociation of H_2O into OH which assist in chemisorption of CO_2 and formation of biocarbon and CO_2^- species. *Thirdly*, defect sites benefit the absorption and dissociation of water on the surface of TiO_2. *Fourthly*, electrons trapped on the surface V_O can help CO_2 adsorption, activation, and dissociation even in dark. For example, Liu et al. [81] realized helium pretreatment of as-prepared TiO_2 at a moderate temperature which resulted in the formation of surface V_O and Ti^{3+} centers on anatase, brookite, and rutile. Compared to the un-pretreated samples,

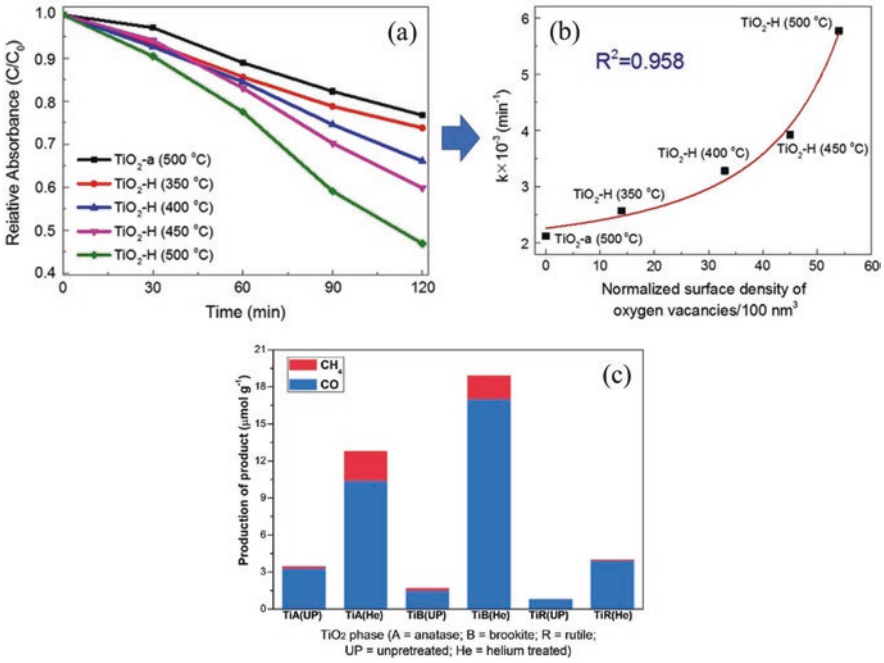

Fig. 5.7 (**a**) Photocatalytic degradation of aqueous methylene blue under simulated sunlight in the presence of TiO_2 thin films, annealed in air at 500 °C or in hydrogen at 350 °C, 400 °C, 450 °C, and 500 °C. (**b**) Kinetic rate constants of TiO_2 thin films vs. normalized surface densities of oxygen vacancies. (Reprinted from Ref. [64] with permission from *Elsevier*. Copyright 2015). (**c**) Production of CO and CH_4 on the three un-pretreated and He pretreated TiO_2 polymorphs for a period of 6 h photoillumination. (Reprinted from Ref. [81] with permission from *American Chemical Society*. Copyright 2012)

the activity of the He-pretreated samples to photoreduce CO_2 was enhanced by 2.2, 10.3, and 3.9 times for CO production and by 13.3, 8.2, and 5.5 times for CH_4 production, respectively (Fig. 5.7c). Finally, there is a need to notice that performance of TiO_2 often starts to drop after a few hours during the reaction of CO_2 photoreduction with H_2O vapor, which is likely due to the competition between adsorption of H_2O and CO_2 [80]. As defective TiO_2 dissociates H_2O into OH, it might contribute to enhancing the stability of this processing.

5.2.6.5 Other Applications

Apart from the abovementioned well-known photocatalytic reactions where defective TiO_2 can be used, it also can be applied successfully in other less studied but nevertheless also highly important light-induced processes.

(a) Nitrogen fixation. Zhang et al. [82] reported that optimized V_O concentration in TiO_2 can result in significant activation toward processing of N_2 molecules that leads to detection of photofixation rate at 324.86 mmol h^{-1} g^{-1} (full spectrum). In turn, the corresponding apparent quantum yield (AQY) under 365 nm illumination reaches ~1.1%. It is considered to be a relatively high level compared to other reports in the literature. Authors demonstrated that V_O coordinate charge separation efficiency, dissociative adsorption capacity, and activation of N_2 molecules.
(b) *Photoreduction of nitric oxide*. According to Wu and van de Krol [83], Fe-stabilized oxygen vacancies in nanosized TiO_2 might serve as active centers for the photocatalytic reduction of nitric oxide into N_2 and O_2 and assist in their spontaneous desorption from the surface. In turn, photoreduction via fully stochiometric TiO_2 which resulted in appearance of nitrate species makes them stay on the surface thus deactivating the catalyst. Thus, presence of V_O also can assist in suppressing the formation of undesired NO_2 from photooxidation of NO.

5.2.6.6 Current Challenges and Future Perspectives

Although great progress has been achieved in realization of efficient light-induced processing using defective TiO_2, there is still a long way ahead before their practical application becomes real in terms of both economic and environmental benefits. To achieve this goal, the following challenges need to be addressed in the future. *Firstly*, it is important to make photocatalytic reactions occur under visible-light illumination, especially the ones which are in a high demand now, i.e., water splitting and CO_2 reduction. It is often the case that increased absorption beyond wavelength of ~400 nm or narrowed band gap has almost no contribution to the efficiency of solar light-induced processes. *Secondly*, the mechanism of some of the above-mentioned photocatalytic reactions that are proceeded by application of defective TiO_2 is still far from understanding even though great progress has been made in recent years. For example, reaction pathways of CO_2 photoreduction are very complicated, and the knowledge about evolution of oxygen vacancies and Ti^{3+} centers during their realization in terms of diffusion, interaction with each other, and changes of charge states might sufficiently contribute to enhanced effectiveness and stability of this reaction. *Thirdly*, it is highly necessary to create more efficient fabrication processing or treatment protocol which can lead to controlled introduction of defects. Currently available approaches are often suffering from inability to precisely tune the distribution, concentration, or nature of intrinsic defects and thus still practically implacable for full industrial implementations.

5.2.7 *Amorphous TiO_2: Alternative to Defective TiO_2*

5.2.7.1 Introduction: Amorphous TiO_2 vs Crystalline TiO_2

Most of the research and investigation dedicated to TiO_2 in the last decades have been fully concentrated on its crystalline phases, while amorphous form (a-TiO_2) remained to be less studied given that it contains disorder composition accompanied by almost constant presence of various intrinsic defects which were considered to have negative influence on the performance of photocatalytic systems. Yet, with developing of defect engineering and its application to various semiconductor materials, recently, this view was completely changed as it was determined that these features, in fact, oppositely, are highly desirable and can be used to control physical and chemical characteristics of TiO_2. In particular, it was determined that amorphization and the favorable formation of the oxygen vacancy in a-TiO_2 could promote the appearance of hole transfer channel at about 1–1.5 eV above the valence band maximum which is responsible for good conductivity [63]. It can provide additional contribution to the enhancing the efficiencies of photochemical reactions. Thus, it is obvious that very unusual electronic structure and disorder atomic arrangements make a-TiO_2 much different from that of crystalline phases, and it allows to demonstrate very unique physical and chemical properties. Based on this, it was determined that this compound can be applied in the following roles during light-induced processing [84]: (i) amorphous TiO_2 can act as an active component to promote light harvesting in UV, visible, and near-infrared regions owing to the lattice disorder, and (ii) amorphous TiO_2 can serve as a protection layer for coating conventional photoelectrodes for corrosion protection in photo-induced water splitting.

5.2.7.2 How to Fabricate Amorphous TiO_2: Morphology-Controlled Synthesis

0-D structures Formation of amorphous TiO_2 in the form of 0-D structures allows to obtain this compound with high specific surface area which apart to already existed disordering and presence of various defects, is considered to be an additional contribution to the enhanced performance of photocatalytic systems. Simply put, this geometry provides higher number of reactive sites, and also enables to increase the concentration of absorbed photons. The synthesis procedure is usually realized via chemical-based route since it allows to achieve precise control over the size and morphology of 0-D structures. The difference between fabrication of amorphous and crystalline forms of TiO_2 usually only refers to the absence of post-synthesis thermal treatment step requirement or its careful utilization but at very low temperatures in the former case. For example, Vargas et al. [85] demonstrated solgel synthesis of amorphous TiO_2 nanoparticles with diameters of ~100 nm, which kept its original structure during post-synthesis treatment up to 350 °C. The formation of amorphous TiO_2 hollow spheres via hydrolysis was also reported, with

shell thickness of ~5–25 nm and overall diameter of ~80 nm [86]. It is interesting to notice that presence of cracks on the shell increased the specific surface area up to ~115 m^2/g, while without them, it was equalized only to ~45 m^2/g.

1-D structures Formation of amorphous TiO_2 as 1-D nanostructures is usually proceeded in the form of nanotubes following the use of anodic aluminum oxide (AAO) as a template. In this case, porous structure is firstly produced from AAO layer via application of certain voltage for concrete duration of time at designated temperature and specific electrolyte which allows to adjust their diameters and lengths. In the second step, various vapor synthesis-based techniques such as CVD, ALD, etc. are used to cover its surface with layers of amorphous TiO_2. Changing parameters during depositions provide great and precise control over the thickness of tube walls. Once core-shell structure is formed, AAO template is removed via immersing into NaOH solution. It has to be noted that ALD allows the formation of multiwalled composition of amorphous nanotubes as combinations of TiO_2 and Al_2O_3 layers could be alternately deposited into AAO pores. As a result, the effective surface increases sufficiently compared with single-walled composition. For example, Chang et al. [87] demonstrated that TiO_2 nanotubes with a length of 600 nm, an average outer diameter of 125 nm, wall thickness of 5.5 nm, and gap span of 20.0 nm have the following surface areas for single-, double-, and triple-walled formations: 4.61×10^5 nm^2, 7.11×10^5 nm^2, and 7.72×10^5 nm^2, respectively. As nanorods are determined to have structure very close to that of nanotubes with only difference is that its end is closed, the same authors reported that ALD also allows to create related compositions with required structure. Another route to generate amorphous TiO_2 nanotubes is to apply anodization of Ti foil in oxidative electrolyte. It results in appearance of porous structures very close to that of AAO. Similar, its characteristics could be controlled via various parameters. This method was described above in more details.

2-D structures A typical method for synthesis of amorphous TiO_2 thin films is the use of ALD techniques at temperatures lower than 200–150 °C. It provides control over the thickness of deposited composition and also allows to adjust its stoichiometry in terms of regulated introduction of oxygen and titanium vacancies. Thus, it is possible to tune its various features such as optical absorption, electrical conductivity, electronic structures, surface roughness, etc. with very precise flexibility and extreme accuracy. For example, with increasing the thickness of deposited film, the concentration of oxygen within it decreases sufficiently [88]. In addition, it is accessible via wide range of precursors in terms of both metallic and nonmetal compounds whose correct choice also influences the finalized composting of the deposited films. It has to be noticed that other vapor base techniques also can grow amorphous TiO_2 films such as radio-frequency sputtering or chemical vapor deposition. Yet, the quality of finalized structures is likely not good as in the case of ALD since it might have pinholes or too high roughness and undesirable non-uniformity of surface. In addition, these techniques cannot be used to fabricate ultrathin within thickness of several nanometer films.

3-D structures Amorphous TiO_2 in the form of 3-D structures also can be fabricated via various approaches even though there are much less number of reports available in literature regarding it compared with other forms of this material. It is mostly realized via template-assisted method. For example, Jiang et al. [89] demonstrated synthesis of amorphous mesoporous titania nanoparticles with 3-D netlike pores within a range of 2–3 nm via solgel route using triblock copolymer F127 as a template. In turn, vapor-based methods also can be effectively employed to create mesopore structures. In this case, a thin layer of amorphous TiO_2 is deposited on designated templates such as multiwalled polysulfone fibers that have high porosity [90]. It provides impressive flexibility in controlling their morphology and architecture. However, in this case, it might be challengeable to remove these templates as annealing at relatively high temperatures up to 400–500 °C is required and it might transform the deposited amorphous TiO_2 into anatase form.

5.2.7.3 Properties of Amorphous TiO_2

Structural properties The structural compositions of a-TiO are very similar to that of its crystalline counterparts. According to Yang et al. [91], it mostly comprises of octahedral sixfold coordinated Ti atoms that are connected through their corners by threefold coordinated atoms. It was also proposed that starting from this base topology, a-TiO_2 exhibits a large degree of structural elasticity due to great number of coordination defects. In addition, it should be noticed that amorphous forms of TiO_2 also likely have a certain concentration of structural defects such as oxygen vacancies and Ti^{3+} centers which cause the lowering of overall stichometry. Their formation might be referred to non-equilibrium conditions during synthesis that induces non-uniform fill of atomic positions In turn, amorphization of TiO_2 structure reduces the formation energy of V_O making its appearance become more evident [63]. Consequent annealing in air result in crystallization of amorphous phase that is also accompanied by “healing” of these defects.

Optical properties As for optical properties, a-TiO_2 in general form has absorption characteristics very close to that of anatase given that band gaps of both compounds are ~3.1 eV–3.2 eV, thus it cannot be sensitive to photons with energies equaled to wavelength of visible light [92]. In turn, a-TiO_2 deposited as a thin shell on crystalline core allow it to serve as an active component for enhancing light harvesting in UV and other regions owing to its lattice disorder [93]. It is interesting to notice that deliberate and highly controlled amorphization of already crystalline TiO_2 might result in appearance of lattice disorder states that enable to extend the light absorption toward near-infrared wavelength due to appearance of additional energy level [66, 94].

Electronic properties Electronic structure of amorphous TiO_2 is far from understandings as various perspectives, sometimes even strongly contradicted, available in literature. For example, Kaur and Singh [95] revealed via DFT calculation that

"electronic structure of [amorphous TiO_2] is similar to that of crystalline electronic structure," while "the valence and conduction tail states result from the positional disorder of O and Ti atoms, respectively." In turn, Pham et al. [63] via molecular dynamic method demonstrated that "long-range disorder and imperfect coordination of Ti and O do not induce defect states in the band gap but have effects on the localization of band edge states." As for the experimental data, Pan et al. [94] revealed that amorphization of TiO_2 resulted in appearance of intermediate energy levels lying within ~1.6 eV from valance band that was notoriously assigned to the "lattice disorder." For comparisons, Chen et al. [66] also stated that lattice disorder enables the formation of energy levels within ~1.8 eV from valence band which initiates its upshift. Moving the discussion forward, amorphous TiO_2 also possess a very unique feature which cannot be found in its crystalline counterpart, namely, hole diffusion across its thin layers which occurred "preferentially *via* the defect states instead of by the valence band" [96]. Following it, a-TiO_2 was designated to have an electronically defective composition, and it enables to show high conductivity. However, the question is raised, which defect states are reasonable for it? It was firstly proposed that defect states created by oxygen vacancies laid at ~1–1.5 eV from valence band are responsible for the appearance of this phenomenon [63]. Yet, later, Guo et al. [97] argued that formation of V_O in amorphous TiO_2 is unfavorable, and instead, O-O peroxy linkages upon injection of excess holes, with an associated defect level lying at ~1.25 ± 0.15 eV above the valence band, can be used to explain it. Thus, based on the above, it is evident that straightforward interpretation of electronic stricture of amorphous TiO_2 is still far from reaching full agreement, and additional efforts are necessary to fully realize it.

5.2.7.4 Application of Amorphous TiO_2 as Photocatalyst

Amorphous TiO_2 as independent compound Amorphous TiO_2 without special treatment or controlled introduction of highly defined defects or specifically designed disordered states usually represents very poor photocatalytic activity for almost any process. For example, Huang et al. [98] stated that "pure amorphous TiO_2 film prepared [magnetron sputtering] was… inactive for photo-decomposing methylene blue and rhodamine B aqueous solutions [under UV lamp]." In turn, Beranek et al. [99] investigated photoelectrochemical characteristics of amorphous and anatase TiO_2 nanotubes under Xe lamp and discovered that the former ones showed very unsatisfied performance which was in times lower than that of the latter structures. It is interesting to notice that photocurrent from amorphous TiO_2 nanotubes was mostly localized in their bottom layer which led to poor transportation of charge carriers. Thermal treatment and conversion into anatase resulted in their more uniform spread which signaled appearance of photocurrent signal from walls of nanotubes.

Amorphous TiO_2 coupled with crystalline TiO_2 Coupling of amorphous TiO_2 with its crystalline counterpart often can result in sufficient improvement of photo-

catalytic photoelectrochemical characteristics. Yet, it is necessary to be aware of various parameters during fabrication and the overall dimension and composition of resulting structure and positioning of amorphous TiO_2 with respect to crystalline phase as its incorrect design might often lead to opposite effect, i.e., degradation of efficiency. This concept can be perfectly demonstrated using work of Gurylev et al. [93] as example (Fig. 5.8). It was shown that photoelectrochemical performance of 10 nm anatase thin film could be improved by covering it with amorphous overlayer prepared by ALD with the thicknesses of ~1.3 nm and ~2.5 nm that possessed very unique characteristics such as presence of lattice distortions and appearance of oxygen vacancies and Ti^{3+} interstitials. Thus, it can serve the same role as that of disordered layer prepared via hydrogenation process [66]. Yet, with increasing the thickness of amorphous TiO_2 up to 5 nm which was considered to be nearly half of that of anatase film, the efficiency of the composite sharply decreased.

Amorphous TiO_2 as a passivation layer for other materials There are several semiconductors such as GaAs, GaASp, and CuO_2 whose band gap makes them highly suitable materials for performing an efficient photoelectrochemical or photocatalytic reactions including water splitting, CO_2 reduction, etc. Yet, their instability in aqueous media considers them as poor candidates to realize these processing since they only enable to show the required performance for a certain period of time. Deposition of protection layer on their surface is determined to be an efficient method to prevent their corrosion and dissolution thus forcing them to be active far beyond their original limit of stability. In this case, amorphous TiO_2 thin film prepared by ALD was discovered to be one of the most optimal choices to fulfil this

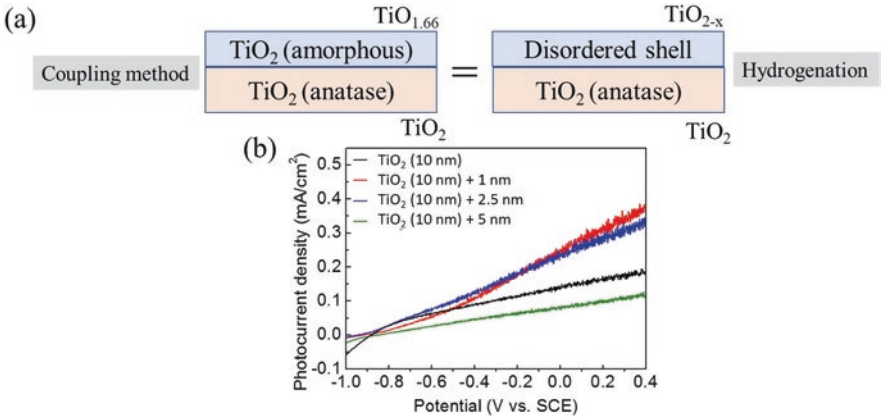

Fig. 5.8 (**a**) Comparison of structure based on combining the amorphous overlayer on crystalline TiO_2 with that of typical disordered-black composition obtained via hydrogenation. The value of stoichiometry for amorphous TiO_2 is obtained from original study. (**b**) Current-voltage curves of TiO_2 thin film (anatase) covered with amorphous TiO_2 with various thicknesses. For simplicity of interpretation, designation of TiO_2 thicknesses is presented in nanometer scale, while in the original study, they are designated in number of ALD cycles. (Adapted from Ref. [93] with permission from *The Royal Chemical Society*. Copyright 2016)

goal due to the following reasons: *Firstly*, it can be deposited on any morphology and composition, whether it is 0-D or 3-D structure; *secondly*, its thickness can be controlled at atomic scale, thus, reaching very low thickness that can protect these semiconductors and, also, has very little influence on their photocatalytic performance; and *thirdly*, most importantly, due to hole diffusion, it has electronic deficiency which leads to high conductivity and thus can also contribute to the photocatalytic reactions exceeding its original role as stabilizer. Based on this, amorphous TiO_2 layer can act as a highly effective corrosion barrier while facilitating interfacial charge transport with minimal resistive loss [96].

5.3 Final Remarks About Defective TiO_2

Titanium dioxide filled with various defects has attracted extensive interest in recent years, and various synthesis strategies were suggested to realize it. Introduction of defects was determined not only to cause specific structural and chemical modifications within this material but also significantly influence its electronic configuration, transport characteristics of charge carriers, optical absorbance, appearance of ferromagnetic response, etc. Thus, defective TiO_2 have been extensively adopted for photocatalytic and photoelectrochemical applications. Yet, despite many in-depth studies dedicated to the investigation of this compound, clear understanding regarding the processes which happened due to introduction of defects, the reasons laid beyond such dramatic changes in the features of TiO_2, and also how to achieve precise control over them via fabrication or post-fabrication treatment is still far from satisfactory. Furthermore, the correlation between results of theoretical and experimental studies regarding the influence of defects on electrical properties and electronic structure of defective TiO_2 also should be improved as there are certain contradictions still available in literature between them.

It is also necessary to notice that investigation of amorphous TiO_2 is highly required to be extended since this compound possesses great potential to serve as important and valuable addition to its crystalline counterpart in improving photoactivity. Moreover, serving the role of passivation layer, it has a crucial effect on preserving the stability of various nanoscaled semiconductors. Overall, defect engineering opens a new chapter in investigating TiO_2 as it provides access to its previously unknown yet highly desirable characteristics.

References

1. Y. Djaoued, J. Robichaud, S. Priya, B. Subramanian, E. Gondek, M. Pokladko-Kowar, P. Karasinski, I.V. Kityk, Implication of porous TiO_2 nanoparticles in PEDOT:PSS photovoltaic devices, in *High-Efficiency Solar Cells: Physics, Materials, and Devices*, ed. by X. Wang, Z. M. Wang, (Springer International Publishing, Cham, 2014), pp. 389–447. https://doi.org/10.1007/978-3-319-01988-8_13

2. A. Bartolotta, G. Calogero, Chapter Four - Dye-sensitized solar cells: from synthetic dyes to natural pigments, in *Solar Cells and Light Management*, ed. by F. Enrichi, G. C. Righini, (Elsevier, 2020), pp. 107–161. https://doi.org/10.1016/B978-0-08-102762-2.00004-5
3. S. Na-Phattalung, M.F. Smith, K. Kim, M.-H. Du, S.-H. Wei, S.B. Zhang, S. Limpijumnong, First-principles study of native defects in anatase TiO_2. Phys. Rev. B **73**, 125205 (2006). https://doi.org/10.1103/PhysRevB.73.125205
4. H. Li, Y. Guo, J. Robertson, Calculation of TiO_2 surface and subsurface oxygen vacancy by the screened exchange functional. J. Phys. Chem. C **119**, 18160–18166 (2015). https://doi.org/10.1021/acs.jpcc.5b02430
5. A. Malashevich, M. Jain, S.G. Louie, First-principles DFT+GW study of oxygen vacancies in rutile TiO_2. Phys. Rev. B **89**, 075205 (2014). https://doi.org/10.1103/PhysRevB.89.075205
6. J. Chen, L.-B. Lin, F.-Q. Jing, Theoretical study of F-type color center in rutile TiO_2. J. Phys. Chem. Solids **62**, 1257–1262 (2001). https://doi.org/10.1016/S0022-3697(01)00018-X
7. M. Arrigoni, G.K.H. Madsen, A comparative first-principles investigation on the defect chemistry of TiO_2 anatase. J. Chem. Phys. **152**, 044110 (2020). https://doi.org/10.1063/1.5138902
8. A. Boonchun, P. Reunchan, N. Umezawa, Energetics of native defects in anatase TiO_2: A hybrid density functional study. Phys. Chem. Chem. Phys. **18**, 30040–30046 (2016). https://doi.org/10.1039/C6CP05798E
9. B.A.D. Williamson, J. Buckeridge, N.P. Chadwick, S. Sathasivam, C.J. Carmalt, I.P. Parkin, D.O. Scanlon, Dispelling the myth of passivated codoping in TiO_2. Chem. Mater. **31**, 2577–2589 (2019). https://doi.org/10.1021/acs.chemmater.9b00257
10. S. Wang, L. Pan, J.-J. Song, W. Mi, J.-J. Zou, L. Wang, X. Zhang, Titanium-defected undoped anatase TiO_2 with p-type conductivity, room-temperature ferromagnetism, and remarkable photocatalytic performance. J. Am. Chem. Soc. **137**, 2975–2983 (2015). https://doi.org/10.1021/ja512047k
11. B.J. Morgan, G.W. Watson, Intrinsic n-type defect formation in TiO_2: A comparison of rutile and anatase from GGA+U calculations. J. Phys. Chem. C **114**, 2321–2328 (2010). https://doi.org/10.1021/jp9088047
12. H.-Y. Lee, S.J. Clark, J. Robertson, Calculation of point defects in rutile TiO_2 by the screened-exchange hybrid functional. Phys. Rev. B **86**, 075209 (2012). https://doi.org/10.1103/PhysRevB.86.075209
13. H. Liu, H.T. Ma, X.Z. Li, W.Z. Li, M. Wu, X.H. Bao, The enhancement of TiO_2 photocatalytic activity by hydrogen thermal treatment. Chemosphere **50**, 39–46 (2003). https://doi.org/10.1016/S0045-6535(02)00486-1
14. X. Pan, M.-Q. Yang, X. Fu, N. Zhang, Y.-J. Xu, Defective TiO_2 with oxygen vacancies: Synthesis, properties and photocatalytic applications. Nanoscale **5**, 3601–3614 (2013). https://doi.org/10.1039/C3NR00476G
15. M.L. Knotek, P.J. Feibelman, Ion desorption by core-hole Auger decay. Phys. Rev. Lett. **40**, 964–967 (1978). https://doi.org/10.1103/PhysRevLett.40.964
16. O. Dulub, M. Batzilln, S. Solovev, E. Loginova, A. Alchagirov, T.E. Madey, U. Diebold, Electron-induced oxygen desorption from the TiO_2(011)-2×1 surface leads to self-organized vacancies. Science **317**, 1052–1056 (2007). https://doi.org/10.1126/science.1144787
17. S. Majumder, D. Paramanik, V. Solanki, I. Mishra, D.K. Avasthi, D. Kanjilal, S. Varma, Ion irradiation induced nano pattern formation on TiO_2 single crystal. Appl. Surf. Sci. **258**, 4122–4124 (2012). https://doi.org/10.1016/j.apsusc.2011.11.067
18. K. Onda, B. Li, H. Petek, Two-photon photoemission spectroscopy of TiO_2 (110) surfaces modified by defects and O_2 or H_2O adsorbates. Phys. Rev. B **70**, 045415 (2004). https://doi.org/10.1103/PhysRevB.70.045415
19. B.S. Thomas, N.A. Marks, L.R. Corrales, R. Devanathan, Threshold displacement energies in rutile TiO_2: A molecular dynamics simulation study. Nucl. Instrum. Methods Phys. Res. B **239**, 191–201 (2005). https://doi.org/10.1016/j.nimb.2005.04.065
20. B. Li, Z. Zhao, Q. Zhou, B. Meng, X. Meng, J. Qiu, Highly efficient low-temperature plasma-assisted modification of TiO_2 nanosheets with exposed 001 facets for enhanced visible-light

photocatalytic activity. Chem. Eur. J. **20**, 14763–14770 (2014). https://doi.org/10.1002/chem.201402664
21. S. Ghosh, P.M.G. Nambissan, Evidence of oxygen and Ti vacancy induced ferromagnetism in post-annealed undoped anatase TiO_2 nanocrystals: A spectroscopic analysis. J. Solid State Chem. **275**, 174–180 (2019). https://doi.org/10.1016/j.jssc.2019.04.010
22. L. Hou, M. Zhang, Z. Guan, Q. Li, J. Yang, Effect of annealing ambience on the formation of surface/bulk oxygen vacancies in TiO_2 for photocatalytic hydrogen evolution. Appl. Surf. Sci. **428**, 640–647 (2018). https://doi.org/10.1016/j.apsusc.2017.09.144
23. H. Tomaszewski, H. Poelman, D. Depla, D. Poelman, R. De Gryse, L. Fiermans, M.-F. Reyniers, G. Heynderickx, G.B. Marin, TiO_2 films prepared by DC magnetron sputtering from ceramic targets. Vacuum **68**, 31–38 (2002). https://doi.org/10.1016/S0042-207X(02)00279-8
24. S.A. Abdullah, M.Z. Sahdan, N. Nafarizal, H. Saim, A.S. Bakri, C.H.C. Rohaida, F. Adriyanto, Y. Sari, Photoluminescence study of trap-state defect on TiO_2 thin films at different substrate temperature *via* RF magnetron sputtering. J. Phys.: Conf. Ser. **995**, 012067 (2018). https://doi.org/10.1088/1742-6596/995/1/012067
25. Q. Zhang, C. Li, Pure anatase phase titanium dioxide films prepared by nist chemical vapor deposition. Nanomaterials (Basel) **8**, 827 (2018). https://doi.org/10.3390/nano8100827
26. F. Teng, M. Li, C. Gao, G. Zhang, P. Zhang, Y. Wang, L. Chen, E. Xie, Preparation of black TiO_2 by hydrogen plasma assisted chemical vapor deposition and its photocatalytic activity. Appl Catal B **148–149**, 339–343 (2014). https://doi.org/10.1016/j.apcatb.2013.11.015
27. P. Arifin, M.A. Mustajab, S. Haryono, D.R. Adhika, A.A. Nugraha, MOCVD growth and characterization of TiO_2 thin films for hydrogen gas sensor application. Mater. Res. Express **6**, 076313 (2019). https://doi.org/10.1088/2053-1591/ab192b
28. Y.-H. Chang, C.-M. Liu, C. Chen, H.-E. Cheng, The effect of geometric structure on photoluminescence characteristics of 1-D TiO_2 nanotubes and 2-D TiO_2 films fabricated by atomic layer deposition. J. Electrochem. Soc. **159**, D401 (2012). https://doi.org/10.1149/2.004207jes
29. D. Wei, T. Hossain, N.Y. Garces, N. Nepal, H.M. Meyer, M.J. Kirkham, C.R. Eddy, J.H. Edgar, Influence of atomic layer deposition temperatures on TiO_2/n-Si MOS capacitor. ECS J. Solid State Sci. Technol. **2**, N110 (2013). https://doi.org/10.1149/2.010305jss
30. X. Liu, S. Gao, H. Xu, Z. Lou, W. Wang, B. Huang, Y. Dai, Green synthetic approach for Ti^{3+} self-doped TiO_{2-x} nanoparticles with efficient visible light photocatalytic activity. Nanoscale **5**, 1870–1875 (2013). https://doi.org/10.1039/C2NR33563H
31. Q. Kang, J. Cao, Y. Zhang, L. Liu, H. Xu, J. Ye, Reduced TiO_2 nanotube arrays for photoelectrochemical water splitting. J. Mater. Chem. A **1**, 5766–5774 (2013). https://doi.org/10.1039/C3TA10689F
32. C.B.D. Marien, C. Marchal, A. Koch, D. Robert, P. Drogui, Sol-gel synthesis of TiO_2 nanoparticles: Effect of Pluronic P123 on particle's morphology and photocatalytic degradation of paraquat. Environ. Sci. Pollut. Res. **24**, 12582–12588 (2017). https://doi.org/10.1007/s11356-016-7681-2
33. I.E. Grey, N.C. Wilson, Titanium vacancy defects in sol-gel prepared anatase. J. Solid State Chem. **180**, 670–678 (2007). https://doi.org/10.1016/j.jssc.2006.11.028
34. S.-P. Hong, J. Park, S.S.M. Bhat, T.H. Lee, S.A. Lee, K. Hong, M.-J. Choi, M. Shokouhimehr, H.W. Jang, Comprehensive study on the morphology control of TiO_2 nanorods on foreign substrates by the hydrothermal method. Cryst. Growth Des. **18**, 6504–6512 (2018). https://doi.org/10.1021/acs.cgd.8b00609
35. J. Yu, G. Wang, B. Cheng, M. Zhou, Effects of hydrothermal temperature and time on the photocatalytic activity and microstructures of bimodal mesoporous TiO_2 powders. Appl Catal B **69**, 171–180 (2007). https://doi.org/10.1016/j.apcatb.2006.06.022
36. Y. Song, B. Li, Y. Shi, Q. Wang, R. Jin, B. Huang, Y. Dai, S. Gao, Preparation of fusiform Ti^{3+} self-doped TiO_2 nanoparticles by mixed solvothermal method and its photoelectrochemical properties. Mater. Lett. **252**, 134–137 (2019). https://doi.org/10.1016/j.matlet.2019.05.134
37. C. Dwivedi, T. Mohammad, V. Kumar, V. Dutta, Ti^{3+} and oxygen defects controlled colored TiO_2 nanoparticles by continuous spray pyrolysis. Vacuum **182**, 109612 (2020). https://doi.org/10.1016/j.vacuum.2020.109612

38. C. Xu, Y. Song, L. Lu, C. Cheng, D. Liu, X. Fang, X. Chen, X. Zhu, D. Li, Electrochemically hydrogenated TiO_2 nanotubes with improved photoelectrochemical water splitting performance. Nanoscale Res. Lett. **8**, 391 (2013). https://doi.org/10.1186/1556-276X-8-391
39. H. Zhou, Y. Zhang, Electrochemically self-doped TiO_2 nanotube arrays for supercapacitors. J. Phys. Chem. C **118**, 5626–5636 (2014). https://doi.org/10.1021/jp4082883
40. A. Hazra, K. Dutta, B. Bhowmik, P.P. Chattopadhyay, P. Bhattacharyya, Room temperature alcohol sensing by oxygen vacancy controlled TiO_2 nanotube array. Appl. Phys. Lett. **105**, 081604 (2014). https://doi.org/10.1063/1.4894008
41. L. Tsui, T. Homma, G. Zangari, Photocurrent conversion in anodized TiO_2 nanotube arrays: Effect of the water content in anodizing solutions. J. Phys. Chem. C **117**, 6979–6989 (2013). https://doi.org/10.1021/jp400318n
42. K. Wessels, M. Maekawa, J. Rathousky, T. Yoshida, M. Wark, T. Oekermann, Highly porous TiO_2 films from anodically deposited titanate hybrids and their photoelectrochemical and photocatalytic activity. Micropor. Mesopor. Mater. **111**, 55–61 (2008). https://doi.org/10.1016/j.micromeso.2007.07.004
43. Z. Ertekin, N.Ö. Pekmez, K. Pekmez, One-step electrochemical deposition of thin film titanium suboxide in basic titanyl sulfate solution at room temperature. J. Solid State Electrochem. **24**, 975–986 (2020). https://doi.org/10.1007/s10008-020-04555-9
44. K. Ralphs, C. Hardacre, S.L. James, Application of heterogeneous catalysts prepared by mechanochemical synthesis. Chem. Soc. Rev. **42**, 7701–7718 (2013). https://doi.org/10.1039/C3CS60066A
45. G. Rajender, P.K. Giri, Strain induced phase formation, microstructural evolution and bandgap narrowing in strained TiO_2 nanocrystals grown by ball milling. J. Alloy Compd. **676**, 591–600 (2016). https://doi.org/10.1016/j.jallcom.2016.03.154
46. T. Prozorov, R. Prozorov, K.S. Suslick, High velocity interparticle collisions driven by ultrasound. J. Am. Chem. Soc. **126**, 13890–13891 (2004). https://doi.org/10.1021/ja049493o
47. P.A. Osorio-Vargas, C. Pulgarin, A. Sienkiewicz, L.R. Pizzio, M.N. Blanco, R.A. Torres-Palma, C. Pétrier, J.A. Rengifo-Herrera, Low-frequency ultrasound induces oxygen vacancies formation and visible light absorption in TiO_2 P-25 nanoparticles. Ultrason. Sonochem. **19**, 383–386 (2012). https://doi.org/10.1016/j.ultsonch.2011.11.013
48. A. Jena, R. Vinu, S.A. Shivashankar, G. Madras, Microwave assisted synthesis of nanostructured titanium dioxide with high photocatalytic activity. Ind. Eng. Chem. Res. **49**, 9636–9643 (2010). https://doi.org/10.1021/ie101226b
49. S. Horikoshi, F. Sakai, M. Kajitani, M. Abe, A.V. Emeline, N. Serpone, Microwave-specific effects in various TiO_2 specimens. Dielectric properties and degradation of 4-chlorophenol. J. Phys. Chem. C. **113**, 5649–5657 (2009). https://doi.org/10.1021/jp810002z
50. R.E. Morris, Ionothermal synthesis-ionic liquids as functional solvents in the preparation of crystalline materials. Chem. Commun., 2990–2998 (2009). https://doi.org/10.1039/B902611H
51. G. Li, Z. Lian, X. Li, Y. Xu, W. Wang, D. Zhang, F. Tian, H. Li, Ionothermal synthesis of black Ti^{3+}-doped single-crystal TiO_2 as an active photocatalyst for pollutant degradation and H_2 generation. J. Mater. Chem. A **3**, 3748–3756 (2015). https://doi.org/10.1039/C4TA02873B
52. F.A. Deorsola, D. Vallauri, Synthesis of TiO_2 nanoparticles through the gel combustion process. J. Mater. Sci. **43**, 3274–3278 (2008). https://doi.org/10.1007/s10853-008-2530-4
53. Q. Xiao, Z. Si, Z. Yu, G. Qiu, Sol-gel auto-combustion synthesis of samarium-doped TiO_2 nanoparticles and their photocatalytic activity under visible light irradiation. Mater. Sci. Eng. B **137**, 189–194 (2007). https://doi.org/10.1016/j.mseb.2006.11.011
54. B. Liu, K. Cheng, S. Nie, X. Zhao, H. Yu, J. Yu, A. Fujishima, K. Nakata, Ice-water quenching induced Ti^{3+} self-doped TiO_2 with surface lattice distortion and the increased photocatalytic activity. J. Phys. Chem. C **121**, 19836–19848 (2017). https://doi.org/10.1021/acs.jpcc.7b06274
55. Y. Yang, Y. Ling, G. Wang, Y. Li, The effect of the hydrogenation temperature on TiO_2 nanostructures for photoelectrochemical water oxidation. Eur. J. Inorg. Chem. **2014**, 760–766 (2014). https://doi.org/10.1002/ejic.201300760

56. B. Choudhury, A. Choudhury, Oxygen defect dependent variation of band gap, Urbach energy and luminescence property of anatase, anatase-rutile mixed phase and of rutile phases of TiO_2 nanoparticles. Physica E: Low Dimens. Syst. Nanostruct. **56**, 364–371 (2014). https://doi.org/10.1016/j.physe.2013.10.014
57. M. Elahifard, M.R. Sadrian, A. Mirzanejad, R. Behjatmanesh-Ardakani, S. Ahmadvand, Dispersion of defects in TiO_2 semiconductor: Oxygen vacancies in the bulk and surface of rutile and anatase. Catalysts **10**, 397 (2020). https://doi.org/10.3390/catal10040397
58. X. Zhou, E. Wierzbicka, N. Liu, P. Schmuki, Black and white anatase, rutile and mixed forms: Band-edges and photocatalytic activity. Chem. Commun. **55**, 533–536 (2019). https://doi.org/10.1039/C8CC07665K
59. J. Lei, H. Li, J. Zhang, M. Anpo, Mixed-phase TiO_2 nanomaterials as efficient photocatalysts, in *Low-Dimensional and Nanostructured Materials and Devices: Properties, Synthesis, Characterization, Modelling and Applications*, ed. by H. Ünlü, N. J. M. Horing, J. Dabrowski, (Springer International Publishing, Cham, 2016), pp. 423–460. https://doi.org/10.1007/978-3-319-25340-4_17
60. Y. Wei, M.V. Tokina, A.V. Benderskii, Z. Zhou, R. Long, O.V. Prezhdo, Quantum dynamics origin of high photocatalytic activity of mixed-phase anatase/rutile TiO_2. J. Chem. Phys. **153**, 044706 (2020). https://doi.org/10.1063/5.0014179
61. V. Vrakatseli, E. Farsari, D. Mataras, Wetting properties of transparent anatase/rutile mixed phase glancing angle magnetron sputtered nano-TiO_2 films. Micromachines **11**, 616 (2020). https://doi.org/10.3390/mi11060616
62. E.M. Samsudin, S.B.A. Hamid, J.C. Juan, W.J. Basirun, A.E. Kandjani, Surface modification of mixed-phase hydrogenated TiO_2 and corresponding photocatalytic response. Appl. Surf. Sci. **359**, 883–896 (2015). https://doi.org/10.1016/j.apsusc.2015.10.194
63. H.H. Pham, L.-W. Wang, Oxygen vacancy and hole conduction in amorphous TiO_2. Phys. Chem. Chem. Phys. **17**, 541–550 (2014). https://doi.org/10.1039/C4CP04209C
64. V. Gurylev, C.-Y. Su, T.-P. Perng, Surface reconstruction, oxygen vacancy distribution and photocatalytic activity of hydrogenated titanium oxide thin film. J. Catal. **330**, 177–186 (2015). https://doi.org/10.1016/j.jcat.2015.07.016
65. C. Di Valentin, G. Pacchioni, A. Selloni, Reduced and n-type doped TiO_2: Nature of Ti^{3+} species. J. Phys. Chem. C **113**, 20543–20552 (2009). https://doi.org/10.1021/jp9061797
66. X. Chen, L. Liu, P.Y. Yu, S.S. Mao, Increasing solar absorption for photocatalysis with black hydrogenated titanium dioxide nanocrystals. Science **331**, 746–750 (2011). https://doi.org/10.1126/science.1200448
67. P.G. Moses, A. Janotti, C. Franchini, G. Kresse, C.G. Van de Walle, Donor defects and small polarons on the TiO_2(110) surface. J. Appl. Phys. **119**, 181503 (2016). https://doi.org/10.1063/1.4948239
68. C. Lin, D. Shin, A.A. Demkov, Localized states induced by an oxygen vacancy in rutile TiO_2. J. Appl. Phys. **117**, 225703 (2015). https://doi.org/10.1063/1.4922184
69. A. Janotti, C.G. Van de Walle, Native point defects in ZnO. Phys. Rev. B **76**, 165202 (2007). https://doi.org/10.1103/PhysRevB.76.165202
70. S.A. Campbell, H. Kim, D.C. Gilmer, B. He, T. Ma, W.L. Gladfelter, Titanium dioxide (TiO_2)-based gate insulators. IBM J. Res. Dev. **43**, 383–392 (1999). https://doi.org/10.1147/rd.433.0383
71. T.S. Rajaraman, S.P. Parikh, V.G. Gandhi, Black TiO_2: A review of its properties and conflicting trends. Chem. Eng. J. **389**, 123918 (2020). https://doi.org/10.1016/j.cej.2019.123918
72. J.R. Smith, F.C. Walsh, R.L. Clarke, Electrodes based on Magnéli phase titanium oxides: The properties and applications of Ebonex® materials. J. Appl. Electrochem. **28**, 1021–1033 (1998). https://doi.org/10.1023/A:1003469427858
73. D.X. Li, R.Q. Li, Y. Chen, J. Yang, X.T. Guo, Electronic structures and magnetism of rutile TiO_2 with vacancy defects from first principles: GGA + U calculations. J. Supercond. Nov. Magn. **30**, 243–249 (2017). https://doi.org/10.1007/s10948-016-3700-2

74. D. Kim, J. Hong, Y.R. Park, K.J. Kim, The origin of oxygen vacancy induced ferromagnetism in undoped TiO_2. J. Phys. Condens. Matter. **21**, 195405 (2009). https://doi.org/10.1088/0953-8984/21/19/195405
75. A.K. Rumaiz, B. Ali, A. Ceylan, M. Boggs, T. Beebe, S. Ismat Shah, Experimental studies on vacancy induced ferromagnetism in undoped TiO_2. Solid State Commun. **144**, 334–338 (2007). https://doi.org/10.1016/j.ssc.2007.08.034
76. K.M. Ok, Y. Ohishi, H. Muta, K. Kurosaki, S. Yamanaka, Effect of point and planar defects on thermal conductivity of TiO_{2-x}. J. Am. Ceram. Soc. **101**, 334–346 (2018). https://doi.org/10.1111/jace.15171
77. J.A. Quirk, V.K. Lazarov, K.P. McKenna, First-principles modeling of oxygen-deficient anatase TiO_2 nanoparticles. J. Phys. Chem. C **124**, 23637–23647 (2020). https://doi.org/10.1021/acs.jpcc.0c06052
78. B.J. Morgan, G.W. Watson, A DFT+U description of oxygen vacancies at the TiO_2 rutile (110) surface. Surf. Sci. **601**, 5034–5041 (2007). https://doi.org/10.1016/j.susc.2007.08.025
79. L. Mohrhusen, J. Kräuter, M. Willms, K. Al-Shamery, Argon embedded by ion bombardment: Relevance of hidden dopants in rutile TiO_2. J. Phys. Chem. C **123**, 20434–20442 (2019). https://doi.org/10.1021/acs.jpcc.9b05975
80. H. Zhao, F. Pan, Y. Li, A review on the effects of TiO_2 surface point defects on CO_2 photoreduction with H_2O. J. Mater. **3**, 17–32 (2017). https://doi.org/10.1016/j.jmat.2016.12.001
81. L. Liu, H. Zhao, J.M. Andino, Y. Li, Photocatalytic CO_2 reduction with H_2O on TiO_2 nanocrystals: Comparison of anatase, rutile, and brookite polymorphs and exploration of surface chemistry. ACS Catal. **2**, 1817–1828 (2012). https://doi.org/10.1021/cs300273q
82. G. Zhang, X. Yang, C. He, P. Zhang, H. Mi, Constructing a tunable defect structure in TiO_2 for photocatalytic nitrogen fixation. J. Mater. Chem. A **8**, 334–341 (2019). https://doi.org/10.1039/C9TA10471B
83. Q. Wu, R. van de Krol, Selective Photoreduction of nitric oxide to nitrogen by nanostructured TiO_2 photocatalysts: Role of oxygen vacancies and iron dopant. J. Am. Chem. Soc. **134**, 9369–9375 (2012). https://doi.org/10.1021/ja302246b
84. S. Sun, P. Song, J. Cui, S. Liang, Amorphous TiO_2 nanostructures: Synthesis, fundamental properties and photocatalytic applications. Cat. Sci. Technol. **9**, 4198–4215 (2019). https://doi.org/10.1039/C9CY01020C
85. M.A. Vargas, J.E. Rodríguez-Páez, Amorphous TiO_2 nanoparticles: Synthesis and antibacterial capacity. J. Non-Cryst. Solids **459**, 192–205 (2017). https://doi.org/10.1016/j.jnoncrysol.2017.01.018
86. H. Bao, H. Zhang, G. Liu, Y. Li, W. Cai, Nanoscaled amorphous TiO_2 hollow spheres: $TiCl_4$ liquid droplet-based hydrolysis fabrication and strong hollow structure-enhanced surface-enhanced Raman scattering effects. Langmuir **33**, 5430–5438 (2017). https://doi.org/10.1021/acs.langmuir.7b00298
87. W.-T. Chang, Y.-C. Hsueh, S.-H. Huang, K.-I. Liu, C.-C. Kei, T.-P. Perng, Fabrication of Ag-loaded multi-walled TiO_2 nanotube arrays and their photocatalytic activity. J. Mater. Chem. A **1**, 1987–1991 (2013). https://doi.org/10.1039/C2TA00806H
88. A.K. Bishal, C. Sukotjo, C.G. Takoudis, Room temperature TiO_2 atomic layer deposition on collagen membrane from a titanium alkylamide precursor. J. Vac. Sci. Technol. A **35**, 01B134 (2016). https://doi.org/10.1116/1.4972245
89. H. Jiang, T. Wang, L. Wang, C. Sun, T. Jiang, G. Cheng, S. Wang, Development of an amorphous mesoporous TiO_2 nanosphere as a novel carrier for poorly water-soluble drugs: Effect of different crystal forms of TiO_2 carriers on drug loading and release behaviors. Micropor. Mesopor. Mater. **153**, 124–130 (2012). https://doi.org/10.1016/j.micromeso.2011.12.013
90. K.-I. Liu, C.-Y. Su, T.-P. Perng, Highly porous N-doped TiO_2 hollow fibers with internal three-dimensional interconnected nanotubes for photocatalytic hydrogen production. RSC Adv. **5**, 88367–88374 (2015). https://doi.org/10.1039/C5RA16492C

91. K. Yang, A. Kachmar, B. Wang, N.M.A. Krishnan, M. Balonis, G. Sant, M. Bauchy, New insights into the atomic structure of amorphous TiO_2 using tight-binding molecular dynamics. J. Chem. Phys. **149**, 094501 (2018). https://doi.org/10.1063/1.5042783
92. L. Zhu, Q. Lu, L. Lv, Y. Wang, Y. Hu, Z. Deng, Z. Lou, Y. Hou, F. Teng, Ligand-free rutile and anatase TiO_2 nanocrystals as electron extraction layers for high performance inverted polymer solar cells. RSC Adv. **7**, 20084–20092 (2017). https://doi.org/10.1039/C7RA00134G
93. V. Gurylev, M. Mishra, C.-Y. Su, T.-P. Perng, Enabling higher photoelectrochemical efficiency of TiO_2 *via* controlled formation of a disordered shell: An alternative to the hydrogenation process. Chem. Commun. **52**, 7604–7607 (2016). https://doi.org/10.1039/C5CC10610A
94. S. Pan, X. Liu, M. Guo, S. fung Yu, H. Huang, H. Fan, G. Li, Engineering the intermediate band states in amorphous Ti^{3+}-doped TiO_2 for hybrid dye-sensitized solar cell applications. J. Mater. Chem. A **3**, 11437–11443 (2015) https://doi.org/10.1039/C5TA00956A
95. K. Kaur, C.V. Singh, Amorphous TiO_2 as a photocatalyst for hydrogen production: A DFT study of structural and electronic properties. Energy Procedia **29**, 291–299 (2012). https://doi.org/10.1016/j.egypro.2012.09.035
96. S. Hu, M.R. Shaner, J.A. Beardslee, M. Lichterman, B.S. Brunschwig, N.S. Lewis, Amorphous TiO_2 coatings stabilize Si, GaAs, and GaP photoanodes for efficient water oxidation. Science **344**, 1005–1009 (2014). https://doi.org/10.1126/science.1251428
97. Z. Guo, F. Ambrosio, A. Pasquarello, Hole diffusion across leaky amorphous TiO_2 coating layers for catalytic water splitting at photoanodes. J. Mater. Chem. A **6**, 11804–11810 (2018). https://doi.org/10.1039/C8TA02179A
98. J. Huang, Y. Liu, L. Lu, L. Li, The photocatalytic properties of amorphous TiO_2 composite films deposited by magnetron sputtering. Res. Chem. Intermed. **38**, 487–498 (2012). https://doi.org/10.1007/s11164-011-0365-0
99. R. Beranek, H. Tsuchiya, T. Sugishima, J.M. Macak, L. Taveira, S. Fujimoto, H. Kisch, P. Schmuki, Enhancement and limits of the photoelectrochemical response from anodic TiO_2 nanotubes. Appl. Phys. Lett. **87**, 243114 (2005). https://doi.org/10.1063/1.2140085

Chapter 6
Case Study II: Defect Engineering of ZnO

6.1 ZnO: Fundamentals

ZnO is an industrially important, environmentally friendly, abundant, resistant to corrosion, and biocompatible n-type semiconductor material with a direct band gap of 3.37 eV, large exciton binding energy (60 meV), strong luminescence, and excellent piezoelectric response. Due to very similar characteristics to TiO_2, it is considered as its alternative for using in various photocatalytic systems. Yet, given relatively lower price, ability to absorb more portion of light and higher mobility of electrons is, in fact, often determined to be more attractive choice. ZnO is usually available in three crystal structures, namely, zincblende, rock salt, and würtzite out of which only the latter one is considered to be thermodynamically stable as it can exist at ambient pressure and temperature and thus is relatively easy to be synthesized and stored. In turn, zincblende structure can be grown only on cubic substrates, while the rock salt or Rochelle salt (NaCl) structure requires application of high pressures. Thus, in this chapter the würtzite structure is the only one to be considered. It is belonging to group of C64v in the Schoenflies notation and P63mc in the Hermann-Mauguin notation and has a hexagonal unit cell defined by only two lattice parameters of c and a which has a ratio of $c/a = \sqrt{\frac{8}{3}} = 1.633$ in the ideal structure. This stricture is composed of two interpenetrating sublattices, and they are displaced with certain respect to each other to form a ZnO_4^{6-} tetrahedron, i.e., Zn atom is surrounded by four O atoms and vice versa. These faces are defined as O-polarity or Zn-polarity, respectively, and their appearances usually occurred along vertically oriented c-axis which in turn is regarded as the lowest surface energy direction. Thus, due to its often appearance in ZnO, polar symmetry plays a crucial role in identifying its physical and chemical characteristics. Definitely, nonpolar faces which represent equivalent number of Zn and O atoms are also existing, yet their realization can only occur through formation of crystals with planes oriented toward less energy favorable orientations such as, for example, *a*-axis.

V. Gurylev, *Nanostructured Photocatalyst via Defect Engineering*,
https://doi.org/10.1007/978-3-030-81911-8_6

6.2 Intrinsic Defects in ZnO

6.2.1 Introduction

Knowledge about the behavior of intrinsic defects regardless their identification as deliberately introduced species or already naturally existed ones are highly important and essential as it provides clear understanding regarding various electronic, electrical, optical, and structural particularities of defined material. To be more correct, it allows to achieve precise and very accurate control over synthesis and consequent manipulation of morphological and structural features as well as surface composition and also can be used to realize accurate tuning of charge carriers in terms of adjusting and extending their concentration, distribution, mobility and duration of lifetimes. Intrinsic defects also play a crucial role in tuning of doping mechanism since they might serve as compensation centers. Thus, their existence determines accessible presence of foreign atoms and also identifies exactly how many of them actually can contribute to the strengthening of already existed conductivity or is necessary to create its transition. For example, the more donor-related defects are available, the more acceptor-like dopants should be introduced as to make the change of n-type to p-type conductivity become possible. In case of zinc oxide, it is especially an important concept as the role of each defect and its basic characteristics including positioning of transition levels or accessing its role as shallow or deep contributor is still far from full understanding. In fact, as there are a lot of controversy, it is often the case that absolutely oppose opinions exist in literature regarding the same phenomenon, even comparing relatively close studies. Particularly, it is still unclear not only how many acceptor-like zinc vacancies are required to transform ZnO into p-type conductive material, but also whether it is thermodynamically feasible process.

Yet, regardless these disputes, it is generally accepted that application of defect engineering toward modifying ZnO is a very attractive methodology as it allows to achieve sufficient advancement of its various characteristics, for example, making it become sensitive for visible light despite naturally existed band gap of ~3.4 eV, or highly enhancing the transportation of electrons resulting in their effective delivery toward surface by avoiding the recombination within the bulk. The question is, however, how far these improvements can be extended. To answer it, one might assume that the presence of defects in ZnO should be deeply addressed from various positions.

6.2.2 Defect Chemistry of ZnO

6.2.2.1 Brief Overview

According to numerous reports available in literature in recent years regarding non-stoichiometric or defective ZnO, there is a clear evidence that it has a rich family of various structural imperfections including vacancies that represent empty O or Zn

atomic sites (V_O and V_{Zn}, respectively), interstitials that are determined as extra atoms occupying interstices in the lattice (O_i and Zn_i), and antisites ascribed as Zn atom occupying an O lattice site (Zn_O) or vice versa (O_{Zn}). Among them, oxygen and zinc vacancies deserve the most attention due to the following reasons. *Firstly*, they are considered to be the defects of the lowest formation energy, and thus their presence in nominally undoped ZnO is the most probable and recognizable [1]. *Secondly*, it is of general consensus, via both experimental studies and theoretical approaches, that these defects among others have the most prominent and recognizable effects on modification of ZnO. *Thirdly*, control over their generation requires application of much less efforts as it can be easily realized via treatment in oxygen- or zinc-deficient atmosphere, and their concentration and distribution are precisely controlled by changing its associated parameters such as depth of ambient or duration and temperature of treatment.

Yet, it would be absolutely incorrect to say that apart from vacancies, other defects should be ignored. In fact, their presence even in very low concentration in perspective might have highly profound impact on geometrical and electronic configurations of ZnO. As can be seen from Fig. 6.1a, zinc interstitials and zinc antisites have clearly visible donor-like characteristics (similar to oxygen vacancies), and thus their formation enables to shift Fermi level toward conduction band which leads to strengthening of n-type conductivity of ZnO as they provide additional electrons and/or serve as compensating centers. In contrast, oxygen interstitials and oxygen antisites are identified to have acceptor-like characteristics (similar to zinc vacancies), and therefore, their introduction serves absolutely opposite role reducing the number of available electrons. In fact, their defined existence might in perspective cause even the appearance of n → p transition within ZnO, yet it is still debatable. Furthermore, one might consider that under the synthesis or treatment conditions similar to that used to generate V_{Zn} or V_O, interstitial and antisite defects also can be produced as accompanies, and they can exist in parallel as separated defects or in the form of specific defective complexes. Consequently, they have a great possibility to serve two absolutely different roles: whether as balance species for recovering the original stoichiometry and restoring the overall electrical neutrality or oppositely deepening the deficiency level of ZnO and increasing the domination of certain type of charge carriers.

However, despite these bright prospects, several moments need to be considered regarding these defects. *Firstly*, as it was determined by Janotti and van de Walle [2], appearances of interstitials and antisites can mostly be proceeded under extremely non-equilibrium conditions due to their very high formation energies. Thus, they only are available in very insufficient concentration as their presence is limited. *Secondly,* each type of these defects has its own additional complication which might seriously restrict their influence on the geometrical and electronic structures of ZnO even though it was possible to create them somehow in significant concertation. For example, Zn interstitial poses extremely low migration barrier compared with other defect which implies that they have a high tendency to either diffuse out of ZnO or to bind with other defects or impurities at temperature even lower than room temperature [1]. In turn, the most stable split-based configuration

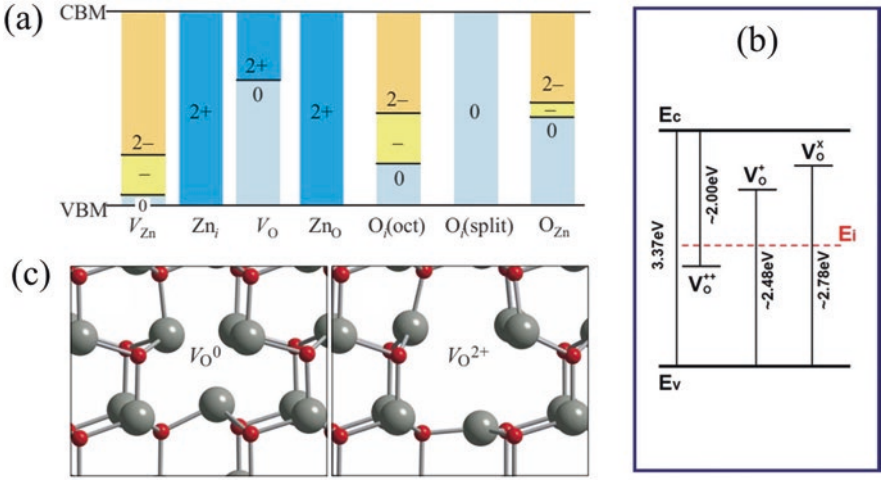

Fig. 6.1 (**a**) Thermodynamic transition levels for defects in ZnO. (Reprinted from Ref. [1] with permission from *American Physical Society*. Copyright 2007) (**b**) Energy levels of oxygen vacancies with different charge states. (Adapted from Ref. [4] with permission from *The Royal Chemical Society*. Copyright 2014) (**c**) Local atomic relaxations around the oxygen vacancy in the neutral and +2 charge states. In the neutral charge state, the four Zn nearest neighbors are displaced inward by 12% of the equilibrium Zn-O bond length, whereas for the +2 charge states, the displacements are outward by 23%. (Reprinted from Ref. [1] with permission from *American Physical Society*. Copyright 2007)

of oxygen interstitials where two oxygen atoms "share" a substitutional site appeared to be electrically neutral [3]. Definitely, it is possible to make oxygen interstitials become active, yet, it occurred only when they occupy octahedral site with accompanied positioning of Fermi level localized over ~2.8 eV, i.e., strong n-type conditions (6.1). Furthermore, even in this case it is deep rather than shallow acceptor and cannot contribute to p-type conductivity, thus serving only as compensation centers. *Thirdly*, it is not easy to correctly estimate and identify interstitials and antisites in ZnO. Simply to say, apart from well-known yet debatable PL spectra, most of other commonly used techniques such as X-ray, Raman, or electron paramagnetic spectroscopies can provide certain difficulties for straightforward recognition of their existence and relative characteristics. Alternatively, detecting of V_O and V_{Zn} has an established analyzing protocol which can be easily realized via various approaches and instruments.

Thus, following the above, this current chapter is fully dedicated and also limited to discussion and investigation of oxygen and zinc vacancies in ZnO. To be clear, it describes methods to form them, the influence on characteristics of host material, and consequent employment in photocatalytic-based applications. In this regard, other defects are considered in much less if any extent. Thus, readers interested in their deep investigation are suggested to search for special literature such as Refs. [1] and [2].

6.2.2.2 Oxygen vs Zinc Vacancies: Particularities in Electronic and Geometrical Configurations

Oxygen Vacancies *Electronic Configuration*. Among various defects that behave as donors, oxygen vacancies have the lowest formation energy [1]. Similar to TiO_2 discussed in Chap. 5, their presence in ZnO is defined by three charge states [4]: the doubly ionized oxygen vacancy V_o^{2+} which cannot capture any electrons, the singly ionized oxygen vacancy V_o^{1+} which captures only one electron, and, finally, the neutral oxygen vacancy V_o^x which can capture two electrons. The following defect levels within the band gap of ZnO are experimentally identified for these three charge states: the recombination of V_o^{2+} with delocalized electrons close to the conduction band edge that correlates with the PL band at ~2.00 eV and the electron transitions from V_o^{1+} and V_o^x centers to the valence band edge equaled to the PL bands at ~2.48 eV and 2.79 eV, respectively [4] (Fig. 6.1b). Theoretical estimation revealed that V_O is a negative U center as it is only stable in +2 or neutral charge states, while V_o^{1+} is determined to be a thermodynamically unfavorable specie which lifetime is very limited [1, 2]. Thus, to create V_o^{1+}, it is necessary to apply highly metastable conditions. Nevertheless, transition level associated with $V_o^x \rightarrow V_o^{1+}$ (losing an electron) was determined to exist at ~2.0 eV [5]. As for oxygen vacancies with other charge states, it was theoretically calculated that the level of Fermi energy (E_F) in the band gap dictates its type. Once E_F approaches the bottom of the conduction band (oxygen-deficient condition), V_O are available in neutral charge state, while positioning of E_F near the top of the valence band (oxygen-rich condition) causes their stabilization in the charge state of +2. Following it, the (+2/0) transition usually occurs at ~1 eV from the conduction band [2] which means that below or above it, the total energies of V_o^{2+} or V_o^x, respectively, are dominated in ZnO, and it clearly determines their monopolized presence. As ZnO is an n-type semiconductor, the position of Fermi energy is eventually ascribed as been located in the upper part of band gap. Following it, oxygen vacancies are expected to be accessible mostly in the form of V_o^x. Thus, they cannot provide electrons to the conduction band given their dominated residence in the lower part of band gap and, consequently, are considered as deep donors. In this case, they unable to contribute into natural n-type conductivity [2]. It is of interest to notice that experimental evidence strongly opposes it and has stated that the most stable appearance of V_O in ZnO is in the form of +2 charge state [6].

Geometrical Configuration. As for the rearrangement of chemical bonding within ZnO after formation of oxygen vacancies, it is highly depended on their charge states [5]. Particularly, appearance of V_o^x leads to an inward displacement of the four nearest Zn atoms by 12% with respect to the equilibrium Zn-O bond length. In turn, the presence of V_O with charge states of +1 and +2 causes an opposite process, i.e., lattice expansion as to compensate their formation. In this case, nearest-neighboring atoms are required to make outward displacements by 2% and 23%, respectively (Fig. 6.1c).

Zinc Vacancies *Electronic Configuration.* Zn vacancy is determined to have the lowest formation energy among all other types of intrinsic acceptors existed in ZnO [1], and it is stable in the charge states of 0, −1, and −2. Calculation via local density approximation determined that (−1/−2) and (0/−) acceptor levels are located at ~0.87 and ~0.18 eV above the valence band maximum (VBM), respectively, and thus V_{Zn} was stated as double and rather deep acceptor [1]. Later, Wang et al. [7] confirmed via experimental investigation that (−/2-) definitely occurs at ~1 eV above the VBM. It was proposed that charge state of −2 is the most favorable state of V_{Zn} in n-type ZnO, and position of Fermi level in this case is the nearest to the conduction band [8]. However, once the Fermi level shifts down toward valence band, gradually increased appearance of V_{Zn} with −1 and neutral states becomes realized [1]. Several words need to say about contribution of zinc vacancies to famous green luminescence at around 2.4–2.5 eV observed during PL measure. Based on analysis by Gurylev and Perng [9], it was suggested that it is composed of several origins which are attributed to existence of both oxygen- and zinc-deficient regions in ZnO whether in the form of defect complexes or as separated yet locally linked components described by donor-acceptor transition. Changes in concentration of one of these defects or even both inevitably lead to increasing or reducing the overall intensity of green luminescence and appearance of accompanied shift. Thus, it cannot be assigned to only one defined type of defect. Finally, it is necessary to mention that transition levels of Zn vacancies in ZnO are not limited by those mentioned above as there are exist two additional charge states, namely, +1 and +2 which are determined as neutral V_{Zn} with trapped holes. Theoretical estimations revealed that they are located at ~0.2 from maximum of valence band and ~4.89 eV from the bottom of conduction bands, respectively [10]. One can notice that while the former level is referred to position of shallow acceptor, the latter one is resided deeply inside the valence band as its value is far beyond width of ZnO band gap.

Geometrical Configuration. In contrast to oxygen vacancy, the geometrical structure of zinc vacancy is practically having no correlation to its charge states. Theoretical modeling revealed that symmetric outward relaxation of the first nearest-neighbor shell is realized by 10% and 14% taking equilibrium and bulk Zn-O bond lengths as a standard, respectively [2, 11]. Such a slight discrepancy is probably related to the specifications of each applied calculation approach and chosen standard to compare. Nevertheless, it leads to lowering the overall symmetry within crystal lattice and reducing the total available energy. It is also necessary to notice that holes can be localized on each of four nearest-neighbor oxygen atoms [11].

6.2.3 How to Create Defects

6.2.3.1 Hydrogenation

Thermally activated hydrogenation is an efficient method to alter surface and related properties of ZnO as it results in formation of oxygen and zinc vacancies along with introduction of interstitial and substitutional hydrogen. This process is usually

described via following steps [12] (Fig. 6.2a). *Firstly*, hydrogen atoms become adsorbed on already existed V_O and V_{Zn} sites leading to their ionization and passivation. The realization of this step can be evidenced by disappearance of defect-related band in PL spectra. Theoretical calculation performed by Bruno et al. [13] suggested that energetically stable configuration could be achieved by adsorbing on both O and Zn sites or on O sites only, while adsorption on Zn sites is less favorable. *Secondly*, with extending further thermal treatment process, newly arrived hydrogen atoms due to absence of unoccupied vacancy sites begin to interact with surface species leading to breakage of Zn-O bonds and formation of adsorbed H_2O molecules and reduced Zn atoms. *Thirdly*, owing to relatively high temperature at which the hydrogenation usually occurs (over at least ~300 °C), it eventually leads to release of H_2O that causes generation of additional oxygen vacancies and appearance of metallic Zn. In turn, owing to its low melting point, desorption of zinc atoms also is realized in the following step. This process could be clearly identified by the increased intensity of visible band in PL spectra. Kim et al. [14] suggested that desorption of water molecules from the surface of ZnO is proceeded at temperatures as low as 250–300 K, while the loosening of metallic zinc atoms was identified to occur at ~440 K. It has to be noticed that the more hydrogen atoms attack the surface of ZnO, the more vacancies can be produced. The following model suggested by Gurylev et al. [12] was used to describe the interaction of hydrogen and ZnO under conditions of thermal treatment:

$$Zn_{1-\varphi}O_{1-\delta} \xrightarrow{H_2(g)} Zn_{1-\varphi}O_{1-\delta}\left(\left(V_{Zn}-H\right)+H_0^+\right) \xrightarrow{H_2(g)} Zn_{1-\varphi-x}O_{1-\delta-y}+xZn\left(g\right)+yH_2O\left(g\right) \quad (6.1)$$

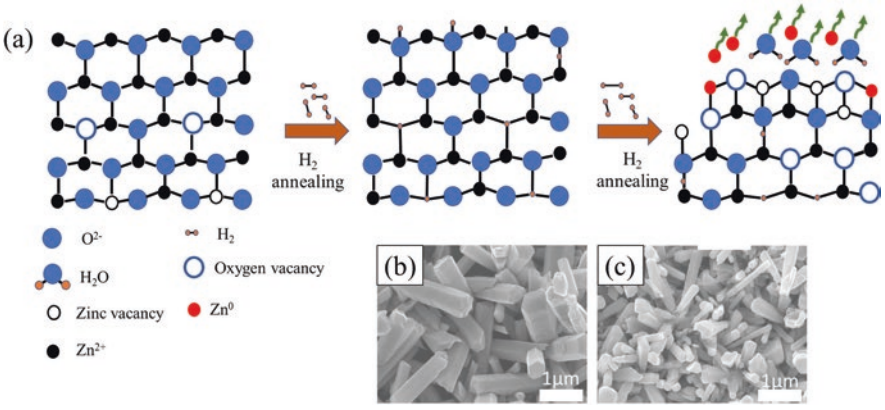

Fig. 6.2 (**a**) Schematic representation of interaction between ZnO and H atoms during thermally activated hydrogenation (Reprinted from Ref. [9] with permission from *Elsevier*. Copyright 2021). SEM images of ZnO nanorods grown on ITO substrate (**b**) before and (**c**) after hydrogenation at 350 °C. (Reprinted from Ref. [12] with permission from *Elsevier*. Copyright 2017)

It is evident that formation of oxygen vacancies in hydrogenated ZnO is assuming to be accompanied by co-generation of zinc vacancies and might not be considered as a fully independent and isolated process. Yet, it is of general acceptance that thermal hydrogenation mostly leads to formation of ZnO filled with only V_O, while appearance of V_{Zn} has been seldom reported [15, 16]. Despite this controversy, these results, in fact, are highly justified since the temperature of H_2O desorption is much lower than that of releasing metallic Zn. It is of interest to notice that hydrogenation results in increasing the roughness of ZnO, or its very serious etching (Fig. 6.2b, c) which in certain cases might lead to appearance of gas produced that in turn can be redeposited back thus creating new complex structures [4]. Thus, conditions of this treatment should be determined with care.

6.2.3.2 High-Energy Particles Bombardment

Electron Bombardment In order to avoid impact of high temperature treatment and thus to reach precise control over desorption of oxygen and zinc atoms, alternative approaches are required to be applied for the formation of defective ZnO. Among various methods available in literature, electron irradiation was determined to be an effective tool which enables the modification of ZnO surface and consequent appearance of both vacancies and complexes based on them. It is necessary to keep in mind that this material is considered to be one of the hardest among II–VI families of semiconductors and have great resistance to structural degradation [9]; thus, the applied energies of irradiation should be comparatively high. Another particularity of ZnO is that displacement energy of zinc atoms equaled to 18.5 eV is more than two time lower than that of oxygen atoms determined as 41.4 eV [17]. Thus, using electron bombardments at energies within the range of 1–3 meV usually results in dominated appearance of V_{Zn}, while to realize accompanied generation of V_O, it should be increased at least up to ~15 meV or over [9]. Yet, such an intensive irradiation greatly affects the morphology of ZnO since causing sufficient change of its features and dimensions. Following it, fabrication of oxygen-deficient ZnO via this strategy is hardly considered to be an attractive approach. In turn, electron bombardment at moderate energy as a method to create zinc vacancies is more accessible and applicable. It introduces very negligible damage to the surface, and thus various nanoscale compounds with sensitive compositions can be treated. Finally, for restoring the original stoichiometry, it is enough to subject irradiated ZnO to the treatment at temperatures as low as ~200 °C under nitrogen flow [18].

Ion Implantation As alternative to electron bombardment, ion sputtering enables to desorb oxygen atoms from the surface of ZnO even at energies as low as several keV. Yet, in this case, the changes in stoichiometry and overall compositions could be accessed only by highly specialized analysis as their range is limited within topmost layers. As an example, Sulyok et al. [19] demonstrated that employment of Ar^+

treatment at 1 and 2 keV decreases the number of O atoms by up to ~27% in the very first atomic layer in comparison to that of a bulk double layer, while the positioning and existence of Zn atoms was not influenced. This information was obtained by Auger electron spectroscopy (AES) analysis and electron energy loss spectroscopy (EELS), while other instrumentation techniques such as Raman and photoluminescence spectroscopies were unable to detect formation of any vacancies [17]. Thus, to extend deeper the changes in atomic arrangement so that they become easily detectable, the increase in intensity of ion treatment up to several hundreds of keV is necessary. For instance, Lv et al. [20] used H^+ ions with energies ~90 keV to modify ZnO whiskers, which resulted in effective formation of non-radioactive oxygen and zinc vacancies that presences were easily identified by common analysis. It represented that range of their existence was extended beyond several surface atomic layers. With increasing the dose of irradiation, the concentrations of both V_O and V_{Zn} became higher. The defects introduced via this strategy have better stability than those caused by electron bombardment, and higher temperatures of treatment are required to remove them. For instance, Chen et al. [21] reported that defective ZnO created by implantation with N^+, O^+, and Al^+ and co-implantation with O^+/N^+ and Al^+/N^+ ions should be subjected to thermal treatment above 800 °C to restore its original stoichiometry.

Plasma Treatment Exposure to plasma created by various reducing gaseous compounds is also a highly popular method to realize the formation of oxygen- and zinc-deficient ZnO. The conditions of this treatment including duration time, strength of electric field, pressure, and temperature inside the chamber can define the degree of desired non-stoichiometry as well as the level of introduced changes in chemical composition and also can be used to tune the depth of their distribution. As an example, Ra et al. [22] demonstrated that utilization of Ar plasma for 1 min expectedly resulted in desorption of oxygen atoms from the surface of ZnO and consequent development of V_O. In turn, Gurylev et al. [23] reported utilization of hydrogen plasma treatment for 5–20 min at room temperature to fabricate zinc-deficient ZnO. It was stated that formation of this compound could be attributed to reactive nature of hydrogen atoms as they actively break Zn-O bonds. Due to absence of any influence from temperature rise, and considering that pressure inside the reaction chamber was constantly maintained at ~5 Torr, the release of H_2O molecules was greatly restrained. In turn, it triggered the departure of metallic Zn especially given that V_{Zn} has the lowest formation energy in n-type ZnO [1]. The longer the treatment time, the deeper the deficiency of zinc in ZnO. It has to be noticed that plasma treatment using H_2 can also serve the opposed role, and instead of creating new defects, it can passivate the already existing ones, thus advancing the crystallinity and stoichiometry [24]. This phenomenon is explained by the insufficient concentration of arrived reactive ions as they only enable to fill into the naturally existing vacancy sites and simply cannot contribute much to the breakage of Zn-O bond not mentioning the formation of H_2O molecule or Zn atoms. Yet, once the

intensity or duration of plasma treatment is increased, the formation of oxygen and/or zinc-defective ZnO can be effectively realized.

6.2.3.3 Treatment in Reduced Atmosphere

Introduction of oxygen and zinc vacancies into ZnO also can be proceeded via thermal treatment at specified temperatures in oxygen-poor or oxygen-rich environments, respectively. To create ambient with low pressure of oxygen, it is common to use specific neutral gases such as Ar, N_2, and He or simply apply vacuum conditions. At the same time, to achieve the appearance of zinc vacancies, annealing of ZnO in a flow of pure O_2 gas might be enough. Various parameters of this processing including the presence of oxygen in the surrounding environment, specific temperature, and duration of treatment regulate the formation of both types of vacancies and also influence the range of their concentration and distribution. It is also possible to adjust their allocation, for example, whether they accumulate in bulk or surface layer. In turn, incorrect conditions of utilized treatment can lead to opposite effect as instead of creating new defects, it would lead to strengthened crystallinity and improved stoichiometry. This concept can be perfectly illustrated following the study of Børtseth et al. [25] where ZnO was annealed in Zn-rich and O-rich atmospheres. It was determined that out-diffusion of V_O and V_{Zn} occurs during low-temperature treatment up to 700 °C. Once the higher temperature was introduced, the generation of new vacancies was detected as this process begins to dominate over that of their out-diffusion. In turn, Chen et al. [26] revealed similar trend during exposure of ZnO to the flow of N_2 at 400–800 °C. It was determined that newly generated V_O was detected only at temperature above 700 °C. However, it is important to notice that this mechanism is mostly applicable to the formation of only bulk defects. In turn, to realize their presence within surface layer, the employment of much lower temperatures down to ~400–300 °C is enough as much less energy is necessary to activate the desorption of atoms resided in it [9]. Yet, the detection and analysis of these vacancies is more challengeable and problematic as more advanced instrumentations are required to be used for confirmation of their existence.

One should be aware that high-temperature treatment in oxygen-deficient conditions can also result in co-generation of zinc vacancies. Simply to say, the evacuation of oxygen atoms from their sites leaves behind isolated Zn atoms. As it has low melting point of 227 °C [14], its release can be hardly avoidable. In particular, Ke et al. [27] studied ZnO thermally treated in Ar atmosphere at 400–700 °C via PL spectroscopy and discovered that changes in the intensity of green-yellow emission (~560 nm) associated with oxygen vacancies were always traced by that of green emission (~535 nm) which had relation to zinc vacancies. Thus, it was determined that treatment in Ar atmosphere also induces the accompanied formation of V_{Zn}. As appearance of both types of vacancies follows each other, it might be suggested that these defects have locally connected to each other in a way similar to that detected during hydrogenation process [28].

6.2.3.4 Vapor Phase Synthesis

Physical Vapor Deposition Physical vapor deposition (PVD) in the form of sputtering and evaporation has been intensively utilized to produce defective ZnO nanostructures. Due to the nature of this fabrication approach, the realization of non-stoichiometric composition is mostly proceeded as appearance of oxygen vacancies. Both techniques provide high flexibility in precise adaptation of their parameters thus allowing to reach high accuracy in governing and adjusting concentration and distribution of introduced defects. It is important to notice that even though sputtering and evaporation have certain differences, control over the formation of defective ZnO structures via both of them is proceeded following relatively similar scenarios. As for more detailed description, during evaporation, Zn metal is usually used as a source material to be heated. The level of its consequent oxidation determined by the presence of O_2 in flowing ambient, temperature during deposition, or distance at which the diffusion of zinc atoms should be proceeded is used to control the deficiency level of ZnO. For instance, Zou et al. [29] prepared ZnO nanotubes by heating Zn powder at 600–700 °C in gas mixture of Ar and O_2 and discovered that the lower the temperature, the more the oxygen vacancies produced. In turn, sputtering undoubtedly provides more parameters to be adjusted since it uses assistance of plasma source as addition to thermally activated conditions for deposition of ZnO. Formation of oxygen vacancies during it follows well-known trends. As an example, Camacho-Berrios et al. [30] investigated zinc oxide thin films deposited by reactive sputtering deposition at room temperature under oxygen-deficient and oxygen-rich conditions that switch was realized via changing the oxygen to argon ratio (O_2/Ar) of applied plasma source from 20% to 70%. Assuredly, it was determined that concentration of oxygen vacancies increases with decreasing this ratio.

Chemical Vapor Deposition Chemical vapor deposition is considered to be an effective technique to realize highly manageable fabrication of defective ZnO with specific stoichiometries and morphologies. It is available in several types and specifications including metalorganic chemical vapor deposition, molecular beam epitaxy (MBE), metal-organic vapor phase epitaxy (MOVPE), etc. which enable to provide great flexibility in reaching precise control over introducing desirable changes in Zn/O ratio within fabricated films by adjusting defined parameters and conditions. For example, manipulation over presence of oxygen and zinc in the carrier gases allows to achieve the formation of certain types of defects. Simply to say, at constant O pressure, the increase in Zn pressure usually results in a higher amount of V_O. Oppositely, the decrease in Zn pressure can be used to increase the concentration of V_{Zn} [31]. In turn, the temperature of deposition also influences the ratio of Zn/O vapors delivered to the substrate. This principle was utilized in the study of Venkatachalapathy et al. [32] who prepared defective ZnO films via MOVPE. It was revealed that respective concentration of each Zn and O gases supplied to the reaction zone is controlled by changing the temperature inside the chamber. Particularly, appearance of Zn-lean condition was identified for the temperature of 325 °C which

resulted in favorable formation V_{Zn}, while utilization of higher temperatures was associated with proceeded fabrication of oxygen-deficient ZnO. Alternatively, a very interesting method to tune the concentration and distribution of defects was proposed by Zubiaga et al. [33] who determined that orientation of sapphire substrate has a clear correlation with development of zinc vacancies in ZnO films prepared by MOCVD. It was revealed that *a*- and *c*-oriented sapphires led to sufficient accumulation of V_{Zn}, while employment of *m*-plane-oriented sapphire substrate initiated opposite trend, i.e., restored stoichiometry in deposited film. As expected, with increasing the thickness of fabricated ZnO, its dependency on the substrate orientation gradually decreases.

Atomic Layer Deposition Atomic layer deposition method is considered to be a specially designed modification of chemical vapor deposition which has characteristics of sequential, self-terminated surface reactions that allow to reach pin hole-free and uniform composition within a thickness of only several nanometers. It is able to precisely adjust the composition of deposited film thus allowing to reach accurate control over introduction and presence of specific defects with accuracy that is much higher than that of previously described PVD and CVD. For example, changing the cycle number of ALD enables to activate its correlation with nature and concentration of vacancies generated in ZnO as it was shown by Chaaya et al. [34] who investigated ZnO with thicknesses ranging from 100 cycles (~25 nm) to 1000 cycles (~250 nm) deposited on Si substrate and discovered that the higher the cycle number, the lower the O:Zn ratio. In turn, changes in stoichiometry of deposited ZnO lead to increased surface roughness which could be attributed to the minimization of free energy and rearrangements of atomic positions due to formation of vacancies (Fig. 6.3a, b). Another parameter of ALD process which has influence on the presence of V_O in ZnO is the temperature of substrate during deposition, i.e., the higher the temperature, the lower the ratio of O/Zn [35] (Fig. 6.3c). Overall, one should notice that ALD is more preferable for fabrication of oxygen-deficient rather than zinc-deficient ZnO. Even though V_{Zn} has the lowest formation energy in n-type ZnO among other defects [1] and displacement Zn atoms can be realized as much less efforts compared with that of creating V_O [17], it is much easier to initiate conditions during deposition that favor the release of oxygen species or incomplete filling of oxygen sites inside ZnO crystal lattice. However, formation of zinc-deficient ZnO still can be reached by ALD. As it was demonstrated by Jin et al. [36], it becomes possible by applying its plasma-enhanced version where oxygen source is used as one of precursors to proceed chemical reaction. It was determined that increasing the time plasma exposure resulted in appearance of Zn vacancies.

6.2.3.5 Chemical-Based Approaches

Sol-Gel Method According to Znaidi [37], the sol-gel process allows elaborating a solid material from a solution by using a sol or a gel as an intermediate step and at much lower temperatures than it is accessible by traditional methods of preparation.

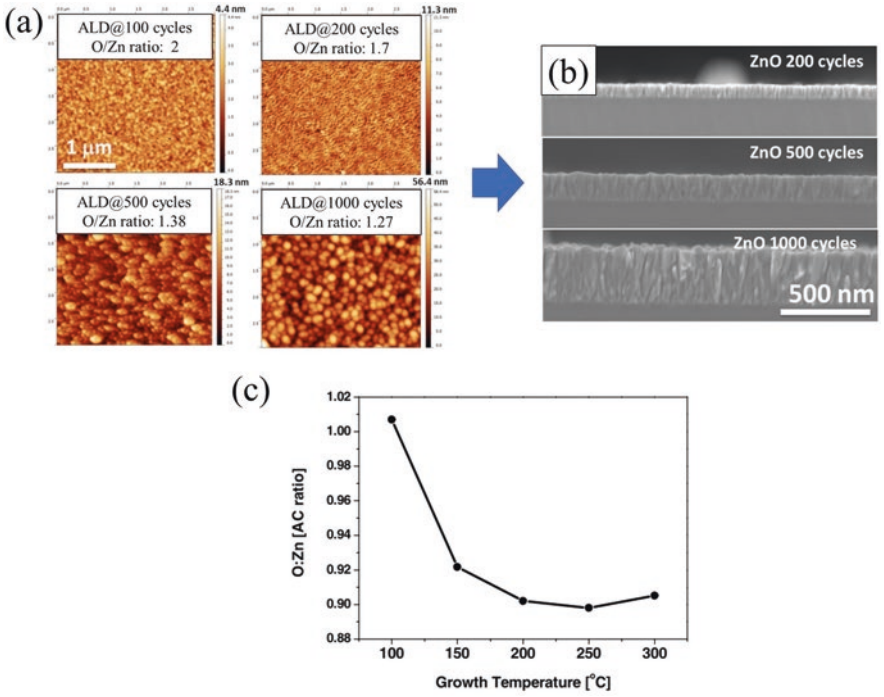

Fig. 6.3 (**a**) AFM and (**b**) SEM cross-sectional images ZnO with different cycle number. (Adapted from Ref. [34]. Copyright 2013, *Beilstein-Institute*. Available under the Creative Commons Attribution 2.0 Generic License, http://creativecommons.org/licenses/by/2.0/) (**c**) Normalized O/Zn atomic concentration ratio in ZnO-ALD films grown at different temperatures. For comparison, commercial ZnO crystal (MaTecKTM) with O/Zn value of 0.716 was used. (Reprinted from Ref. [35] with permission from *Institute of Physics Publishing*. Copyright 2013)

The resulting materials are usually available in the form of nanoparticle-based powder or thin film deposited either via spin or dip coatings. Due to wide range of available chemicals and consequently different routes of proceeded reaction, various types of defects can be introduced into ZnO. Furthermore, adjusting the parameters of synthesis, such as molar ratios of reaction components, aging time, and necessity of water can be used to adjust their concentration, distribution, and diffusion pathway. It has to be noticed that as sol-gel synthesis of ZnO is often realized in oxygen-rich growth environment, thus the formation of V_{Zn} can be achieved much easier than that of V_O [38]. Yet, it is still possible to obtain oxygen-deficient ZnO by applying post-synthesis thermal treatment in desired atmosphere which, in fact, also serves as necessary step to remove the residual chemicals and strengthen the obtained structure by making it crystallized since sol-gel process is frequently enable only to produce amorphous or partially amorphous structures. For example, Dejene et al. [39] investigated how the characteristics of obtained ZnO quantum dots can be modified by changing the OH^-/Zn^{2+} molar ratio of the precursor via varying the amount of added NaOH to $Zn(CH_3COO)$. Prior to analysis, the samples

were subjected to annealing at 600 °C. It was demonstrated that with increasing OH^-/Zn^{2+}molar ratio to about 5.5, the intensity of green luminescence which was identified to be related to oxygen vacancies reaches the maximum value and then reduces thereafter. For its part, the morphology of fabricated ZnO quantum dots did not show any correlation to changes in concentration of utilized chemicals.

Hydrothermal Method Hydrothermal method allows to obtain ZnO with various morphologies including nanowires, nanorods, nanoparticles, nanoforests, etc. that demonstrate highly defined structural characteristics and precisely tuned chemical compositions. This process is usually realized via creating aqueous solution from specified chemicals which in the following step becomes subjected to certain temperature and pressure thus to initiate reactions. Compared with TiO_2 discussed in Chap. 5, the conditions of this process with regard to growth of ZnO are much softer as hydrothermal synthesis of this material can occur at temperatures as low as 70 °C [40]. The choice of chemicals, their molar ratios, and particularities of preparation route to make the solution as well as parameters of thermal treatment process such as its temperature and duration can be used not only to identify the stoichiometry of obtained structures but also to predict the positions of defects, whether their preferable location is in the surface or deeply inside the bulk. Yet, most of ZnO obtained via this method has clearly defined oxygen deficiency due to excess of zinc atoms from the precursors. For example, Alshehri et al. [41] investigated the growth of ZnO nanorods by placing solution containing $ZnCl_2$ and Na_2CO_3 into Teflon autoclave which was then heated for 140 °C and kept at time range from 3 to 12 h. Analysis of PL spectra revealed that the longer the duration of treatment, the more the oxygen vacancies produced. It is important to notice that the difference in morphological and topological features of synthesized ZnO obtained by altering certain specific parameter might not always guarantee that any changes occurred in their stoichiometries. As an illustration, Akhavan et al. [40] determined that changes in molar concentration of NaOH used as addition to $Zn(NO_3)_2$ for synthesis at 70 °C and 1.5 h "did not substantially affect the chemical composition of the grown ZnO nanostructures" even though their diameters, height, hydrophilic property, and optical absorption were influenced significantly.

Solvothermal Method In perspective, solvothermal method has a huge resemblance to that of hydrothermal since almost identical chemicals are utilized there as precursors and conditions of applied thermal treatment are quite similar. The only difference is that instead of adding water, the former approach uses various organic solvents which have non-aqueous nature, and thus there is no need to consider their boiling point. In this regard, it is possible to apply higher temperature of synthesis which allows to achieve more complete and fast reactions between solid species. Furthermore, these organic solvents are available in wide range, and thus it is possible to use them not only as a single compound but also via mixing several of them. It provides better flexibility in controlling the morphological features and stoichiometry of obtained ZnO as more particulate and specific generation of structural defects accompanied by wider changes in chemical compositions can be reached

compared with that of hydrothermal method. As an illustration, Ghoshal et al. [42] investigated the formation of ZnO via applying mixed system of ethylene glycol (EG) and ethanol as a solvent under the temperature range of 135–200 °C. It was discovered that the higher the temperature of treatment, the more the V_O produced. In turn, formation of zinc-deficient ZnO structure also could be effectively realized by choosing correct mixture of organic solvents. Pan et al. [43] perfectly demonstrated reliability of this concept. In their study, the solvothermal treatment was proceeded via combining zinc acetate with both propanetriol and ethanol and consequent treatment of obtained solution under the temperatures of 180 °C for 24 h followed by thermally activated calcination at 400 °C for 1 h in air. It was discovered that addition of propanetriol results in appearance of zinc deficiency, while its absence led to formation of fully stoichiometric ZnO.

Chemical Bath Deposition Method Chemical bath deposition method to produce ZnO becomes very popular recently as it allows to reach the formation of this material with highly defined morphology, structure, and stoichiometry without using Teflon-based autoclave. Simply to say, there is no need to apply additional pressure as all reactions are proceeded with assistance of thermal activation at temperatures of only 90 °C or lower which means that the employment of specific equipment can be omitted. Thus, successful realization of this synthesis is easily achievable, for example, in commonly used borosilicate glass bottle. The growth of ZnO nanostructures usually proceeded on certain substrate covered with seed layer; yet it is not a necessary and mandatory requirement. In this regard, more parameters can be controlled and adapted during synthesis compared with mentioned above hydrothermal method as apart from the standard one such as the temperature of treatment, its duration, choice of chemicals, and their concentrations and molar ratios, the composition of finalized product also can be adjusted by the tuning the dimension, size, and structure of seed layer as well as its compositional features. For example, Barbagiovanni et al. [44] demonstrated that by changing the molar ratio of hexamethylenetetramine and zinc acetate used to prepare reaction solution, it is possible to modify the ratio of V_O/V_{Zn}. In turn, Gu et al. [45] investigated the influence of precursor concentration of sols on the properties of seed layer and its impact to modify the chemical composition of grown ZnO nanorods. It was discovered that the more excessive the presence of zinc in seed layer, the higher the crystallinity of produced 1-D structures, and the more defined their orientations along c-axis, the more the V_O generated. Yet, this relation is only reliable till reaching only specific precursor concentration.

Chemical Reduction Method Chemical reduction is considered to be one of the most commonly applied methods to create oxygen deficiency in ZnO. In general terms, the proceeded reactions have very similar character to that occurred during thermal reduction with only difference is that instead of activation via high temperature, it can be processed at mid-range conditions as imbalance of chemical potentials appeared to be the main driving force. Changes in the parameters at which this processing occurs such as the duration of reaction or the temperature of its environ-

ment as well as specific type of chosen chemicals to serve as reducing agent and their molar ratio have great affection on the formation of V_O and also can be used to adjust its concentration and precise allocation As an example, Wang et al. [46] investigated chemical reduction of hydrothermally grown ZnO nanorod arrays via their immersion into 0.1 M $NaBH_4$ solution at room temperature for different durations. It was discovered that shorter treatment time up to 30 min resulted in appearance of V_O on the surface of nanorods, while it increases to 45 min led to generation of their bulk-resided analogies. The temperature of chemical reduction also might play a crucial role in creating defective ZnO as its increase within reasonable range can lead to speeding up the reaction and intensifying the release rate of surface oxygen atoms [47].

6.2.3.6 Electrochemical Methods

Electrochemical synthesis is highly a applicable method to prepare nanosized ZnO with specific morphologies and stoichiometries as it can suggest various advantages compared with other fabrication methodologies described above including simplicity, operation at low temperature, high energy-efficiency, and greater purity of the obtained composition. In a typical experiment, zinc plate or conductive substrate is used as anode or cathode (it is depended on the experimental setup), and deposition of desired compounds is realized on its surface via dissolution of Zn atoms, and their consequent assemblance with (OH) radicals existed in electrolyte. The resulting zinc hydroxide then is transformed into ZnO following dehydration [48] or water oxidation reaction [49]. Various parameters during this synthesis can be adjusted to control the morphology and stoichiometry of fabricated nanostructures such as applied voltage (potential), duration of its application, type and concentration of electrolyte solution and its PH value, characteristics of substrate, whether it has a presence of additional compounds, etc. For example, Dai et al. [50] investigated stoichiometric compositions of ZnO thin film produced via its deposition on PHEMA hydrogel-coated ITO using zinc nitrate aqueous solutions as electrolyte and discovered that while at surface it has very standard Zn/O ratio, the bulk shows very clear appearance of oxygen vacancies which concentration and spread increase following the time of treatment. In turn, Mika et al. [51] revealed that formation of V_O in electrodeposited ZnO could be adjusted by varying the potentials as its rise leads to gradual strengthening of surface-based oxygen deficiency.

6.2.3.7 Mechanical Methods

High-energy ball milling (BM) has been considered to be an effective, simple, and accessible technique which can be used to realize the fabrication of nanoparticle-based powders with desired stoichiometries. During this process, the friction and collision created by interactions with balls could result in appearance of relatively high temperatures over 1000 °C at very localized area for the duration of 10^{-3} to

10^{-4} s [52]. Such conditions can lead to disturbance of periodic array in crystal lattice and often cause the release of atoms which are eventually associated with formation of vacancies. Their concentrations could be easily controlled by adjusting various parameters during this processing including rotating speed, time of milling, or using specific starting compounds. Yet, it is generally accepted that to manage the exact type and spatial distribution of structural changes in ZnO nanostructures as to make it become more oxygen- or zinc-deficient is a very challengeable task as apart from mentioned above, other defect including zinc interstitials, oxygen interstitials, and oxygen antisites also can be generated [53]. Another disadvantage of BM processing is that it usually results in introduction of defects resided in bulk which are considered to have a negative impact on the photocatalytic activity of ZnO, while their accumulated appearance in surface is hardly reachable.

In response to the above, Kaftelen et al. [54] demonstrated that application of low temperature condition to the BM treatment can lead to advancement of this process. In their study, ZnO filled with V_{Zn} was considered as a starting material. Using electron paramagnetic resonance and PL spectroscopy, it was discovered that the longer the time of milling results, the higher the presence of V_O in the surface, while bulk was kept its original composition. Thus, core-shell structure was fabricated, where the shell showed oxygen deficiency, while core demonstrated dominated presence of zinc vacancies (Fig. 6.4).

6.2.3.8 Crystallinity, Size, and Dimension of ZnO vs Formation of Defects

As ZnO nanomaterials can be designed with different crystallinity, sizes, dimensions, etc., formation of defects in them cannot be considered as to follow one defined tendency since their appearance has certain and clear correlation with changes in these features. Simply to say, proceeding correct designation and adjustment of characteristics in fabricated ZnO allows to estimate with certain degree of accuracy what kind of defects it might have and how to control them. Thus, it can serve as a powerful tool to define their appearances in advance. However, it should be noticed that for each particulate structures and synthesis or post-synthesis methods, these changes follow its own trend, and thus they cannot be equalized. As an illustration, by varying the thickness of ZnO thin film deposited by ALD, it is possible to adjust the oxygen deficiency with very precise accuracy. The higher the cycle number, the lower the O/Zn stoichiometry [34]. In turn, opposite trend was observed in case of 0-D structures. Xu et al. [55] reported that with decreasing the size of ZnO nanoparticles, the concentration of oxygen vacancies becomes higher. Similar observation is also can be referred to influence of crystallinity. For example, it was shown that increasing the temperature inside the reaction chamber during ALD depositions leads to minimizing the fraction of amorphous regions in deposited ZnO results in dominated appearance of oxygen vacancies [35]. In alternative, Mohammad et al. [56] showed that during chemical bath deposition of ZnO nanorods, the highest intensity of XRD peaks might not correlate with largest concentration of surface and sub-surface oxygen vacancies. In turn, it was often reported

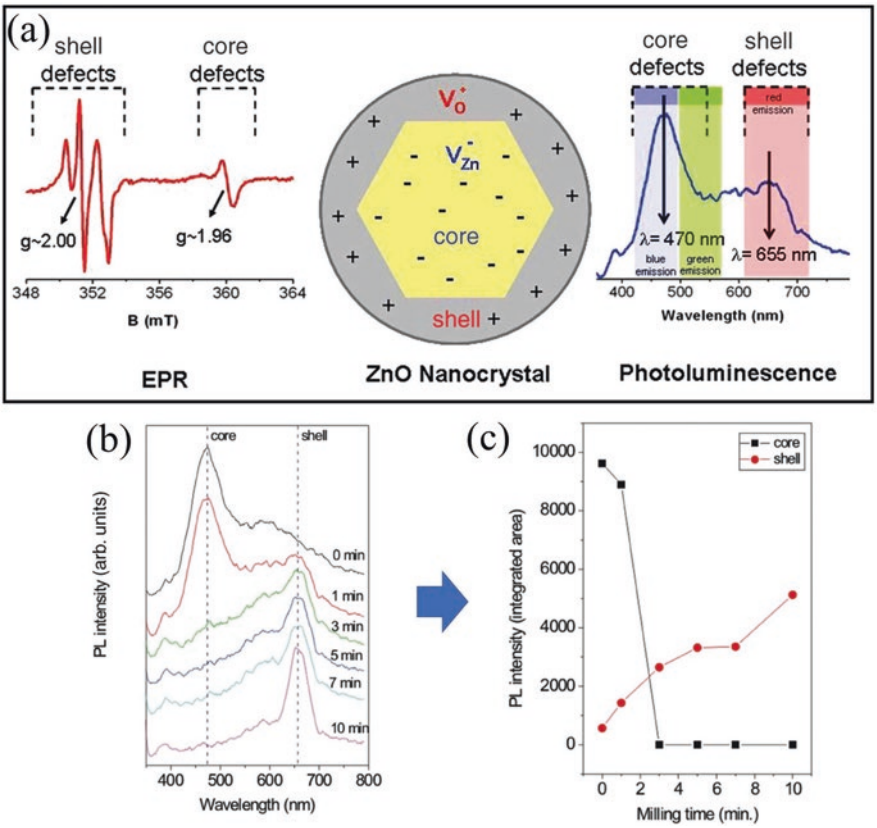

Fig. 6.4 (**a**) Schematic illustration of a ZnO nanocrystal, obtained from freezer milling. It consists of a negatively charged interior core and a positively charged outer shell. The EPR and PL spectra are given for the 1 min milled sample where core and shell defects can be clearly observed in simultaneous manner. (**b**) PL spectra recorded at room temperature and (**c**) integrated area of core and shell signals from PL spectra show the evolution of defect concentrations in samples milled at different times. (Reprinted from Ref. [54] with permission from *American Physical Society*. Copyright 2012)

that changes in the dimensionality of ZnO nanostructures also can be used to adjust the concentration of defects within them, particularly V_O. It is usually defined by the qualitative and quantitative presence of polar plane [0001] that is highly favorable for the formation of oxygen-deficient regions. Yet, it would be incorrect to say that the higher the surface area, the higher the fraction of this plane available in the ZnO [57], as this correlation is influenced by additional factors including fabrication method, method of analysis or mentioned above crystallinity and changes in size, etc. Thus, it is evident that it is possible to control the existence of defect in ZnO through playing with particularities of its structure and other related factors; yet application of this strategy should be taken with extreme caution as a lot of factors affect its correct procedure.

6.2.4 Properties of Defective ZnO

6.2.4.1 Structural Properties

Oxygen Vacancies Theoretical calculation performed by Janotti and Van de Walle [1] determined that formation of oxygen vacancies in neutral charge state results in inward displacement of the four nearest Zn atoms, while for V_O in charge states of +1 and +2, the outward relaxation was identified. Partial reliability of this model was experimentally demonstrated by Lorenz et al. [58]. It was determined that changes in the lattice parameters of ZnO prepared by pulsed laser deposition had a defined dependency from the presence of neutral oxygen vacancies. Applying Mn atoms as a local probe revealed that with decreasing the oxygen partial pressure during deposition, i.e., increased concentration of V_O, *c*-axis experienced expansion, while a-axis was compressed. Overall, the reduction of unit cell in the direction perpendicular to the crystallographic *c*-axis was observed, and it was accompanied by the decreased bond length between zinc and oxygen atoms in the ZnO_4 tetrahedron. Oxygen vacancies also influence the orientation of crystal lattice as their introduction results in breakage of thermodynamic balance within it which leads to reorientation of some crystallites toward less energy-favorable axis in order to restore equilibrium. Following it, the increasing of polycrystallinity in V_O-ZnO could be observed [59]. The presence of oxygen deficiency that defines lattice ordering can be visualized by direct high-resolution transmission electron microscopy (HRTEM) observation. Asok et al. [60] demonstrated that its introduction into ZnO resulted in appearance of lines of dark spots in the lattice which were eventually determined as missing oxygen atoms. Finally, it was revealed that realization of ZnO with surface-based oxygen deficiency leads to formation of amorphous shell with a thickness of ~1–2 nm around the crystallite core [61], similar to that observed in case of hydrogenated TiO_2.

Zinc Vacancies As it was calculated via DFT simulation [1], the presence of these defects is followed by the expansion of crystal lattice. For example, Pan et al. [43] investigated ZnO fabricated via solvothermal treatment and demonstrated that characteristic X-ray diffraction peaks of zinc-deficient sample were shifted toward lower angle compared with that of fully stoichiometric sample due to enlargement of *c*-axis. Analysis via HRTEM visualization also can be used to determine the existence of V_{Zn} in ZnO; yet direct assessment of its outcome might suffer from correct interpretation due to certain resemblance of their appearance with that of oxygen vacancies. Ding et al. [62] analyzed ZnO nanobelts prepared by solid-vapor deposition process and observed the existence of black spots within the crystal lattice which identification however was hardly possible without additional evaluation. Thus, to clarify whether it belongs to V_{Zn} or V_O, it was required to combine simulated image created via atomic model of superstructure with real HRTEM image. Based on this, it was discovered that changes in contrast could only be sensitive to vacant Zn spot.

6.2.4.2 Optical Properties

The presence of oxygen or zinc vacancies in ZnO causes the formation of local defective states within the band gap that not only enable increasing the overall absorption in parallel but also allow to make this material become sensitive to visible light. Following this mode, electron firstly is excited from the valence band to the oxygen or zinc vacancy state which serves as an intermediate transition level, and later with absorption of another photon, it traverses further toward the conduction band. The positioning of these V_O- and V_{Zn}-supported defective states are supposed to be near the conduction and valence bands given their donor- and acceptor-like characteristics, respectively, or deeply inside the band gap depending on many factors such as presence of impurities, condition of synthesis or post-synthesis treatment, etc. Formation of defects in ZnO and their ability to make it become sensitive to the visible light can result in changing of its color as it follows their nature and concentration. As for individual influences of oxygen and zinc vacancies, the introduction of V_O usually results in more profound and resonant effect as the changes in the narrowing of band gap and parallelly increasing absorptions in both UV and visible spectra are highly evident. In turn, the presence of V_{Zn} leads to less obvious changes in the red shift of absorption edge. In fact, under certain conditions, it even enables to degrade original optical characteristics of ZnO via, for example, lowering sensitivity toward UV light [9].

6.2.4.3 Electronic Properties

Oxygen-Deficient ZnO Theoretical simulation revealed that V_O in ZnO exists in the form of negative U-center which means that it is stable only in neutral or +2 charge states [1]. The position of Fermi level determines which one out of these two types is more dominant in ZnO. Under n-type conditions, when Fermi level is close to conduction band, the neutral charge state of V_O is more favorable, while under steadily increasing p-type conditions, when Fermi level gradually moves to valence band, the charge state of +2 becomes dominated. The transition level between two types of oxygen vacancies was generally accepted as ~2.2 eV from valence band (~1 eV from conduction band) [2] even though some author argues it. For example, Clark et al. [63] reported the values of ~1.67 and even ~2.02 eV above valence band depending on the applied theoretical approach. Since ZnO has characteristics of n-type semiconductor, the position of Fermi level is expected to be in upper part of band gap, and it means that V_O has neutral charge state and is considered to be deep rather than shallow donors. In this case, these defects are located in the lower part of conduction band which make them unsuitable for providing electrons to the conduction band. Thus, they serve as compensation centers. In this regard, they result in narrowing the width of band gap by making the appearance of a tail that leads to broadening of valence band [61]. In turn, experimental evidence demonstrated that the latter scenario might not always work due to the following reasons: firstly, as

bulk V_O is introduced and, secondly, when that V_o^{2+} becomes dominated, and in this case, the mid-gap energy levels are located close to conduction band [64].

Zinc-Deficient ZnO Zinc vacancies in ZnO have five charge states, named +2, +1, 0, −1, and −2; yet most reports available in literature do not recognize the first two. It can be justified as follows. In order to create them, V_{Zn}^{2+} and V_{Zn}^{1+} from the most stable configuration of zinc vacancies, i.e., V_{Zn}^{2-}, it is necessary to catch four and three holes, respectively. According to Frodason et al. [11], it is a very unlikely scenario if only the concentration of photogenerated holes is extremely high. Thus, formation of these defects cannot occur in naturally existed n-type ZnO. Simulation based on density functional theory (DFT) predicted that (−/−2) and (0/−1) transition levels of zinc vacancies are located at ~0.87 and 0.18 eV, respectively, above valence band maximum which makes it double and deep acceptor [1]. The former transition which existence is confirmed, for example, via analysis by electron paramagnetic and optically detected magnetic resonances [7], is often considered to be responsible for the appearance of emission in PL spectra at ~2.35 eV measured at ambient conditions [28]. In turn, the transition at ~0.18 eV could be easily detected by temperature-dependent PL analysis [65]. Yet, it has to be noticed that apart from the above, alternative positions of these transition levels are also available in the literature. In particular, Oba et al. [66] used hybrid Hatree-Fock DFT calculation to estimate these donor levels at ~0.8 eV and ~2.5 eV above the VBM, respectively, while Frodason et al. [11] via HSE hybrid functional determined them to occur at ~0.71 and ~1.26 eV. In turn, experimental results often stated that V_{Zn}^{-} centers give rise to PL emission in the range of 1.6–2.1 eV [67]. Wang et al. [7] attributed its appearance to the presence of large lattice displacement occurred as a result of Jahn-Teller (JT) distortion that can shift localization of (−/-2) transition level toward conduction band for ~0.8 eV. Furthermore, it was also discovered that positioning of this PL emission has clear dependency on the assemblance of V_{Zn}^{-} centers, as at their higher clusterization and lower presence of isolated defects, it is shifted to higher energy for 0.3 eV, i.e., closer to valence band [67].

6.2.4.4 Electrical Properties

Introduction of oxygen or zinc vacancies has great influence on the electrical properties of ZnO. As V_O has defined donor-related characteristics [1], their appearances usually lead to increased conductivity via rising the concentration of electrons and their mobility whether in relative or absolute units. Simply to say, if they presented in the state of neutral charge which is equal to position of Fermi level close to conduction band, they can serve as compensation center for acceptor-related defects, thus lowering the probability for recombination of electrons. Alternatively, if they become available in the charge state of +2 that appeared once the Fermi level is shifted to valence band, they have direct contribution to the strengthening of the n-type electrical conductivity as they can supply electrons to conduction band. It is

interesting to notice that theoretical models strongly support the former scenario (Fig. 6.5), while experimental studies revealed that the latter one, in fact, is the most probable. Gurylev and Perng [9] suggested that this contradiction is likely referred to the fact that the Fermi level of n-type ZnO might not always be located near the conduction band due to the presence of numerous unavoidable impurities such as H and Cu or co-existence of acceptor-type V_{Zn} whose formation is the most favorable in n-type ZnO. Following it, E_F is likely to shift toward the valence band, and thus the appearance of V_o^{2+} is highly favorable. As a final word, it is necessary to notice that certain caution should be taken while playing with concentration of these defects as its continuous advancement cannot always lead to increase of conductivity. To be clear, excess of oxygen deficiency usually causes an opposite outcome and results in increasing the resistivity of ZnO, i.e., overloading with electrons would induce the shortening of mean free path and higher chance to be recombined.

In turn, zinc vacancies are determined to be an acceptor-type defect, and thus their generation might result in formation of p-type conductivity in ZnO or its enhancement if other acceptor-type impurities are introduced. In fact, the situation with this type of defects, very similar to that of V_O as while numerous experimental evidence confirmed its direct contribution to the increasing concentration of holes and thus appearance of $n \rightarrow p$ transition, theoretical simulations in turn strongly oppose it as they define V_{Zn} to be deep acceptors that can only enable compensation of donor-related impurities and "unlikely play any role in p-type conductivity" [1]. As it was stated by Gurylev and Perng [9], this discrepancy in describing the defect-induced appearance of p-type conductivity via both approaches might originate from the partial inability of simulated approximations to fully access the processes occurring in the crystal lattice of ZnO during the experiments. For instance, it is often the case that its band gap estimated via theoretical calculations has width much different from that of real one, and in this matter, the positions of V_{Zn} acceptor levels shown in these models might need additional verification via real-time measurements as it is located beyond it. Even if a correct band gap could be achieved [66], other processes which happened during experimental procedure or analysis routine are hardly to be included into simulation and described properly as it increases it complexness and resource cost. Yet, it also cannot be said that formation of intrinsic p-type conductive ZnO can be always realized as introduction of zinc deficiency alone very often unable to initiate the appearance of required transitions. Thus, it was suggested that certain phenomenon connected with the generation of V_{Zn} that cannot be detected either by currently existed analysis equipment or identified via theoretical methodology might occur within the electronic structure of ZnO [9]. Access to them might be the key to resolve the existed controversy regarding capability of this type of defect to serve as a source of positively charge carriers.

6.2.4.5 Other Properties

Apart from the above-mentioned characteristics, formation of defects in ZnO can influence other properties which are briefly discussed here.

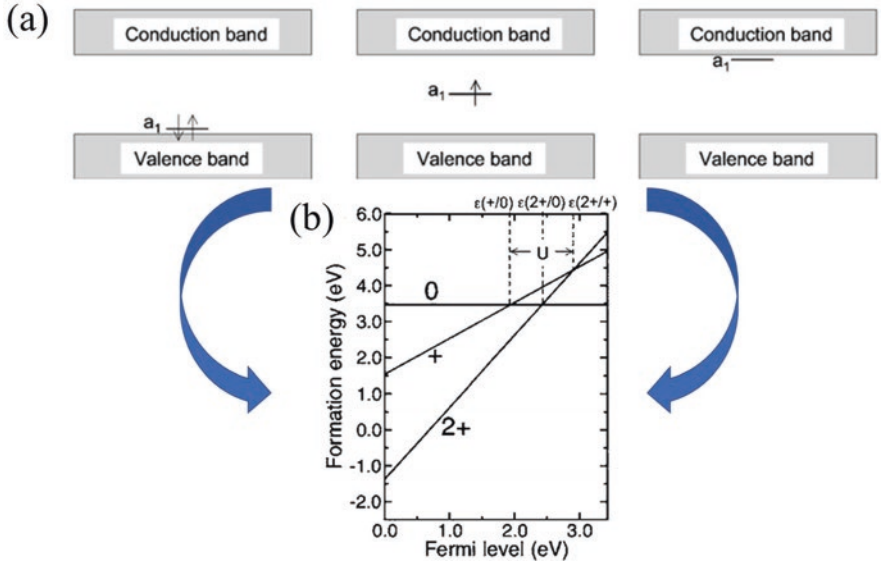

Fig. 6.5 (**a**) The position of the created a_1 state for the equilibrium configuration of each charge state that oxygen vacancy has in ZnO. Arrows show the presence of electrons. (**b**) Formation energies vs Fermi level for oxygen vacancies in ZnO in each charge states, under Zn-rich conditions. (Adapted from Ref. [5] with permission from *AIP Publishing*. Copyright 2007)

(a) *Ferromagnetism.* Recently, it was discovered that introduction of zinc vacancies might cause the appearance of room-temperature ferromagnetism in nominally undoped ZnO, and its value can even be comparable with that of conventional ferromagnetic materials such as Fe_3O_4 [68]. Furthermore, it was determined that introduction of zinc deficiency into the bulk cannot contribute to the magnetism, while its presence in the surface can sufficiently increase its response [38]. In turn, oxygen deficiency also can cause the appearance of ferromagnetism; yet its magnitude is much lower compared with that of zinc-deficient ZnO [9].

(b) *Thermal Conductivity.* Introductions of point defects such as oxygen and zinc vacancies are an effective approach to reduce thermal conductivity of ZnO. Their extensive appearances also might lead to formation of additional dislocations accompanied by micro- or nanosized distortions that can enhance the phonon scattering and generation of localized heating spot. Thus, the more the defects produced, the lower the thermal conductivity.

(c) *Mechanical Properties*. As it was demonstrated by Gurylev et al. [28], formation of vacancies on the surface of ZnO can effectively decrease stiffness coefficient making it "softer". It might be explained due to reduced strength of crystal lattice as removal of atoms from it results in decreasing of overall energy and lowering the barriers which is necessary to overpass in order to deform it. Thus, the more the vacancies introduced, the more influenced the stuffiness coefficient.

6.2.5 *Application of Defective ZnO as Photocatalyst*

6.2.5.1 Brief Overview

Given its exceptional features, such as low cost, non-toxicity, favorable band edge position, and chemical stability, zinc oxide has been widely considered as an effective photocatalytic material for various important and emerging applications such as removal of harmful dyes, generation of ammonia via nitrogen fixation, water splitting and production of hydrogen, degradation of CO_2, etc. Yet, successful realization of these processes at level that is required for their full industrialization cannot be proceeded due to certain limitations of ZnO as a material. Despite the advantages mentioned above, it has wide band gap which makes the absorption of visible light hardly possible and also possesses extremely high recombination rate of photogenerated electron/hole pairs that lead to their low presence on the surface. Various methodologies were applied to overcome these problems such as decoration with noble metal, utilizing immobilization with cocatalyst, combining with other semiconductors, etc. Employment of intrinsic defect engineering can be considered as a fascinating alternative to them as it enables to advance properties and characteristics of ZnO through altering of its own composition and structure without application of any external materials or chemical as only to initiate these changes. Thus, projecting this approach on the above-mentioned disadvantages of ZnO, it can be, for example, used to extend its absorption profile thus promoting utilization of full solar spectra. In addition, given that Vo and V_{Zn} are donor- and acceptor-like defects, respectively, they also effectively increase the presence of charge carriers as well as improve their mobility and lifetimes which also sufficiently enhance the light-induced activity. More detailed discussion of application of defective ZnO to each photocatalytic process is provided below.

6.2.5.2 Photocatalytic and Photoelectrochemical Water Splitting

Solar light-assisted production of hydrogen using water splitting process is determined to be the most sustainable and potential method for meeting the current need in energy. As the conduction band minimum and valence band maximum of ZnO are thermodynamically and kinetically favorable for water reduction and oxidation, introduction of controlled deficiency into it allows to extend further its current effectiveness and steadiness transforming this material into highly attractive photocatalyst. For example, Lu et al. [15] demonstrated that formation of oxygen vacancies via hydrogenation treatment at 350 °C in ZnO nanorods array grown on FTO led to detection of fivefold increase in hydrogen evolution under solar light compared with that of fully stoichiometric sample (Fig. 6.6a, b). In turn, Yao et al. [69] showed that as ZnO can be employed in the role of photoanode during photoelectrochemical water splitting, the existence of V_O enhances the value of its light-induced current density. Yet, it has to be noticed that even though these promising results are

widely available in the literature, there still exists some inconsistency between the value of extended absorption edge and/or consequently narrowed band gap and related photocatalytic performance [9], very similar to that observed in previous chapter in case of TiO_2. Simply to say, visible light-driven reaction activity often cannot be detected, and the overall enhancement of water splitting efficiency is mainly referred to the enhanced utilization of UV light accompanied by higher concentration of charge carriers and their consequently reduced recombination rate. It perfectly can be demonstrated using studies of Lu et al. [15] and Yao et al. [69] mentioned above. Once the light wavelength was limited to the visible spectra, the hydrogen evolution rate and photocurrent density, respectively, approached to zero even though both studies stated that V_O-ZnO demonstrated capability to absorb visible light (Fig. 6.6c). Gurylev and Perng [9] suggested that it might be referred to the positioning of energy levels created by oxygen vacancies in the band gap, as their localization occurs below the reduction potentials of H_2O, and thus, they are unable to contribute electrons resided there for participating in hydrogen evolution reaction. Thus, to initiate visible light activity of defective ZnO that can contribute to the photocatalytic water splitting, it could be suggested to create more transition levels within the band gap via, for example, co-introduction of both V_O and V_{Zn} [12]. Finally, it is necessary to become aware that there exists an optimized concentration of defects, which results in most efficient photocatalytic/photoelectrochemical performance. Simply increasing their presence till reaching maximum might not be the best approach, and instead accurate turning is required.

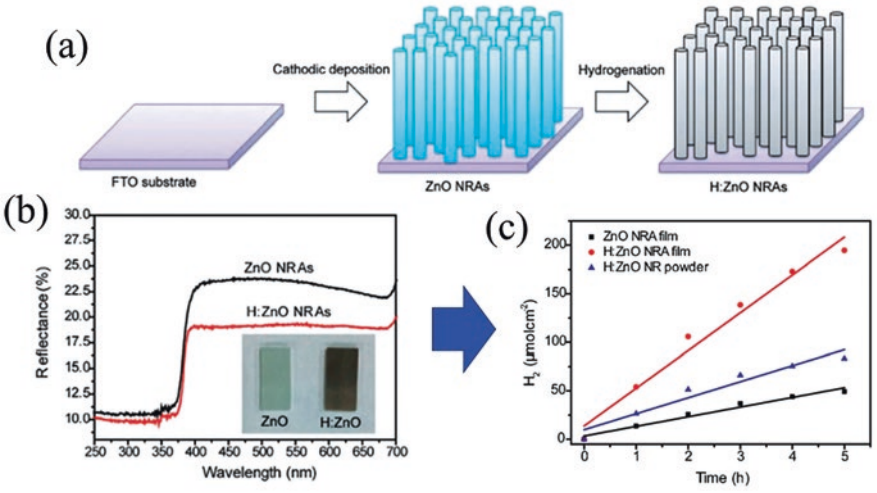

Fig. 6.6 (**a**) A schematic diagram showing the fabrication of hydrogenated ZnO nanorods array (H:ZnO NRA). (**b**) Photocatalytic hydrogen production rate collected for ZnO NRA film, H:ZnO NRA film, and H:ZnO NRs (powder) in a solution containing 0.1 M Na_2SO_3 and 0.1 M Na_2S under white light irradiation. (**c**) Diffuse reflectance UV-visible spectra of ZnO and H:ZnO NRAs. *Inset:* their optical images. (Reprinted from Ref. [15] with permission from *The Royal Chemical Society*. Copyright 2012)

6.2.5.3 Light-Induced Water Purification

Photocatalytic degradation of dyes using solar light is applied to remove highly toxic molecules from aqueous media via their transformation into various non-hazardous compounds such as carbon dioxide and water. It is considered to be a highly promising approach to resolve the problem of clean water around the globe. Defective ZnO due to its unique characteristics and features can become a promising solution for the enhancement of its efficiency. Furthermore, compared with hydrogen production, this processing has much higher chances to be effectively realized under visible light as positions of mid-gap levels with respect to potentials of redox reactions should satisfy less criterions. For example, Lv et al. [61] demonstrated that removal percentage of total organic carbon (TOC) for decomposition of methylene blue by reduced and stoichiometric ZnO was determined to be 83% and 6% after 6 h of visible-light irradiation, respectively. The more vacancies were produced, the better efficiency of photocatalytic degradation was detected; yet, it only works till their concentration reaches saturation, which is very similar to that ascribed for water splitting. In turn, Gurylev et al. [12] showed that V_{Zn} also can contribute to the enhancement of photocatalytically activated removal of dye via defective ZnO as their simultaneous introduction with V_O and consequent synergy resulted in threefold higher rate of MB degradation under visible light compared with standard sample. It has to be noticed that in both mentioned cases, the absorption capability of ZnO was extended due to the presence of defects. Thus, it perfectly matched demonstrated performances.

6.2.5.4 Photoconversion of CO_2

Photocatalytic conversion of CO_2 via reaction with water to produce solar fuels is a highly promising approach to significantly decrease the negative impact of its emission and to make it serve as a source of various valuable carbon-neutral fuels. Band gap positions of ZnO perfectly match the reduction potential of CO_2 as well as water oxidation; thus it is considered to be a potential candidate to serve as an efficient photocatalyst. In turn, its filling with various defect including oxygen or zinc vacancies can sufficiently contribute to the continuous advancement of this processing. It is attributed to the appearance of the following particularities which in some terms are very similar to that mentioned in previous chapter with regard to TiO_2. *Firstly*, oxygen-deficient surface of ZnO is thermodynamically more favorable to trap CO_2 than a defect-free surface. *Secondly*, defect sites can be used for selective reduction of CO_2, as, for example, its transformation into CO_2 rather than CH_4 [70]. *Thirdly*, oxygen vacancies facilitate the electron transfer to the adsorbed HCO_3^- and CO_3^{2-} intermediates on ZnO surface initiating its reduction process [71]. For example, Liu et al. [70] investigated the photoreduction of CO_2 by ZnO microspheres, microflowers, and nanorods. As they possessed different ratios of [0001] facet that was determined to be highly favorable for the formation of oxygen vacancies, it was revealed that the higher its presence in ZnO, the more efficient is the photocatalytic reaction

and the higher its selectivity. In turn, continuously increased presence of V_O cannot always guarantee enhanced performance in parallel as these defects have certain optimized concentration beyond which they begin to act as recombination centers, and thus the efficiency of CO_2 photoreduction would show sharp drop.

6.2.5.5 Antibacterial and Antimicrobial Applications

Among various inorganic antimicrobial materials, ZnO attracted greatest attention as it provides good thermal stability, marked antimicrobial activity, environmentally friendliness, and low cost. A general view point about ZnO is that it becomes easily internalized with the cells via electrostatic interaction and promotes the appearance of sufficient amount of various reactive oxygen species (ROS) which formation mechanism, in fact, has a lot of resemblance to that realized during degradation of dye, and thus interest readers are suggested to address Chap. 1 of this book for more details. Nevertheless, continuing this discussion, it was of general acceptance that surface defects such as oxygen vacancies play a vital role in their generation, in the presence as well as in the absence of light. The more the oxygen vacancies, the more the ROS species generated and the better the antibacterial activity of ZnO.

It was also sometimes reported that antibacterial and anticancer activities of ZnO nanoparticles might be explained by the release of Zn^{2+} ions due to dissolution that might in relative terms be associated with formation of zinc vacancies. This mechanism deserved much less attention in literature compared with that where V_O is used. As for more details, Zn^{2+} ions usually penetrate into the cells and break cellular components such as DNA and proteins and hence cause cell death. Various parameters including pH of aqueous solution, its temperature, chemical composition of catalyst, and concentration/biological nature of target organic matter critical can influence the rate of Zn^{2+} released.

6.2.5.6 Other Applications

Apart from the above-mentioned well-known photocatalytic reactions where defective ZnO can be applied, it also can be used successfully in other less-studied but nevertheless also highly important light-induced processes.

(a) *Photocatalytic Depolymerization of Sodium Lignosulfonate*. Xu et al. [72] (Fig. 6.7) investigated Ni-doped ZnO filled with oxygen vacancies and determined that their presence improves separation efficiency of photogenerated charge carriers to some extent and also enhances the absorption characteristics. Following it, they greatly assisted in enhancing the decomposing rate of sodium lignosulfonate into CO_2 and H_2O under simulated solar light.

(b) *Photocatalytic Reduction of Cr (VI)*. According to Pan et al. [73], introduction of oxygen vacancies into ZnO via its coupling with reduced graphene oxide resulted in activation of capability to reduce Cr (VI) under visible light. In turn, fully stoichiometric ZnO could realize this process using only UV light irradia-

tion. It was proposed that the presence of V_O led to appearance of additional defect states located close to valence band thus causing narrowing band gap, increase in overall absorption in parallel, and appearance of higher number of available electron-hole pairs that can participate in reaction with absorb metal molecules.

6.2.5.7 Current Challenges and Future Perspectives

Application of defective ZnO filled with oxygen or zinc vacancies in photocatalytic processing has achieved great advancement in recent years as demonstrated efficiency becomes one of the highest reported in literature in comparison with other related compositions. It was determined that the presence of these defects resulted in great advancement of various characteristics and features including optical, structural, electrical, and electronic properties. Yet, current achievements are still far from expected, and very long and hard pathway is still laid ahead that is necessary to overcome for making ZnO-based photocatalyst a widely available technology that is presented in each household. Summarizing the above, the following problems need to be solved. *Firstly*, it is still hard to control the introduction of defects into ZnO in very precise and accurate terms. For example, there are a lot of reports mentioning that concentration of oxygen vacancies could increase or decrease following the conditions of treatment or synthesis; yet the exact quantity of these changes in absolute values or units often cannot be accessed, and it is only demonstrated in qualitative manner as comparison to some dedicated standard sample which, in fact, is different in each study. Thus, it might be not easy to apply these results to ZnO materials prepared via other than reported approaches as they might have slightly different compositions and structure. *Secondly*, visible light photoactivity still appeared to be a challenge as the presence of defects cannot guarantee its appearance for certain. *Thirdly*, in analogy to TiO_2, it is important that more efficient fabrication processing or treatment protocol to create defective compositions would be developed. Currently, available approaches have a lot of limitations which prevent their wide application. For example, thermal treatment in vacuum apart from creating V_O also can strengthen the crystallinity of ZnO structure which can lower the impact of these defects and lead to reduced performance. Furthermore, utilization of high temperature also might influence other characteristics of this material. *Fourthly*, and the most importantly, efficiency of photocatalytic processing is still appearing to be the main problem, and additional efforts are necessary to extend it further.

6.3 Final Remarks About Defective ZnO

ZnO filled with oxygen and zinc vacancies has attracted extensive interest in recent years, and various approaches were applied to deeply understand its characteristics and related features as introduction of these defects is determined to cause specific

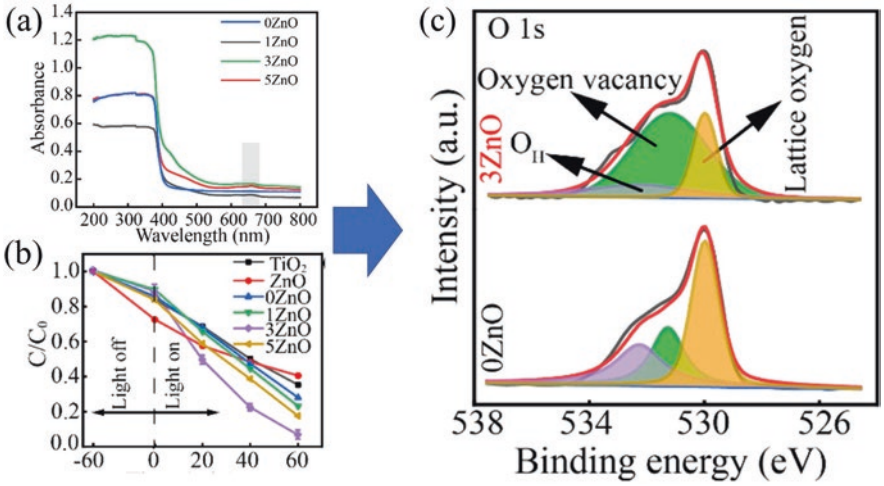

Fig. 6.7 (**a**) UV-vis diffuse reflection spectra of ZnO doped with different amount of N^{2+} and (**b**) photocatalytic depolymerization of sodium lignosulfonate under simulated solar light. The number in front of ZnO represents mass fraction of Ni^{2+} doping. As can be seen, 3ZnO shows the best optical characteristics and best performance. (**c**) XPS O1s spectra of 3ZnO and 0ZnO. As can be seen, doping with Ni^{2+} results in highly increased presence of V_O. (Reprinted from Ref. [72]. With permission from *Elsevier*. Copyright 2020)

structural and chemical modifications leading to crucial changes in its electronic configuration, transport characteristics of charge carriers, optical absorbance, appearance of ferromagnetic response, etc. Yet, despite appearance of many in-depth reports dedicated to the investigation of defective ZnO, some controversies still exist which provide certain difficulties for full and unconditional realization of accumulated knowledge. *Firstly*, it is highly challengeable to compare the results of theoretical and experimental studies as each of them demonstrates absolutely opposite outcome regarding the influence of oxygen and zinc vacancies on electrical properties and electronic structure of defective ZnO. DFT simulations determine that these defects cannot by any chance be a source of either n- or p-type conductivity, respectively. In turn, real-time observations via application of most advanced analyzing protocols strongly disagree with it as they discovered that oxygen and zinc deficiencies indeed contribute to them significantly. *Secondly*, it is noted that ZnO has two major defects, namely, V_O and V_{Zn}, and their existence is highly unavoidable as they have the lowest formation energies among other related defects. Yet, it is unclear which one has more prominent influence on the properties and characteristics of ZnO in terms of its application as photocatalysis since the majority of reports available in the literature are dedicated to oxygen-deficiency, and investigation of ZnO filled with zinc vacancies with regard to its synthesis, properties, and consequent application has been presented in much less extent [9]. For example, ZnO filled with various concentration and types of zinc vacancies can be tested for CO_2 conversion as these defects might play the role of active sites, similar to that of V_O, to adsorb and optimize its molecules.

Overall, there is a strongly belief that defective ZnO due to its unique electrical, optical, magnetic, etc. properties is highly promising materials that might be considered as a future candidate for wide application in various photocatalytic based devices. Yet, more efforts expressed in further deepening of the existed theoretical and experiment directions are necessary to broaden the current knowledge of the nature and behavior of O- and Zn-based defects in ZnO and to extend present understanding toward more efficient realization of accessible light-activated devices.

References

1. A. Janotti, C.G. Van de Walle, Native point defects in ZnO. Phys. Rev. B **76**, 165202 (2007). https://doi.org/10.1103/PhysRevB.76.165202
2. A. Janotti, C.G.V. de Walle, Fundamentals of zinc oxide as a semiconductor. Rep. Prog. Phys. **72**, 126501 (2009). https://doi.org/10.1088/0034-4885/72/12/126501
3. M.D. McCluskey, 1 – Defects in ZnO, in *Defects in Advanced Electronic Materials and Novel Low Dimensional Structures*, ed. by J. Stehr, I. Buyanova, W. Chen, (Woodhead Publishing, 2018), pp. 1–25. https://doi.org/10.1016/B978-0-08-102053-1.00001-6
4. Q. Zhu, C. Xie, H. Li, C. Yang, S. Zhang, D. Zeng, Selectively enhanced UV and NIR photoluminescence from a degenerate ZnO nanorod array film. J. Mater. Chem. C **2**, 4566–4580 (2014). https://doi.org/10.1039/C4TC00011K
5. A. Janotti, C.G. Van de Walle, Oxygen vacancies in ZnO. Appl. Phys. Lett. **87**, 122102 (2005). https://doi.org/10.1063/1.2053360
6. L. Liu, Z. Mei, A. Tang, A. Azarov, A. Kuznetsov, Q.-K. Xue, X. Du, Oxygen vacancies: The origin of n-type conductivity in ZnO. Phys. Rev. B **93**, 235305 (2016). https://doi.org/10.1103/PhysRevB.93.235305
7. X.J. Wang, L.S. Vlasenko, S.J. Pearton, W.M. Chen, I.A. Buyanova, Oxygen and zinc vacancies in as-grown ZnO single crystals. J. Phys. D. Appl. Phys. **42**, 175411 (2009). https://doi.org/10.1088/0022-3727/42/17/175411
8. M. Hadis, Ö. Ümit, *Zinc Oxide: Fundamentals, Materials and Device Technology* (Wiley-VCH, Weinheim, 2009), p. 188
9. V. Gurylev, T.P. Perng, Defect engineering of ZnO: Review on oxygen and zinc vacancies. Eur. J. Ceram. Soc. **41**, 4977–4996 (2021). https://doi.org/10.1016/j.jeurceramsoc.2021.03.031
10. A.A. Sokol, S.A. French, S.T. Bromley, C.R.A. Catlow, H.J.J. van Dam, P. Sherwood, Point defects in ZnO. Faraday Discuss. **134**, 267–282 (2006). https://doi.org/10.1039/B607406E
11. Y.K. Frodason, K.M. Johansen, T.S. Bjørheim, B.G. Svensson, A. Alkauskas, Zn vacancy as a polaronic hole trap in ZnO. Phys. Rev. B **95**, 094105 (2017). https://doi.org/10.1103/PhysRevB.95.094105
12. V. Gurylev, C.-Y. Su, T.-P. Perng, Hydrogenated ZnO nanorods with defect-induced visible light-responsive photoelectrochemical performance. Appl. Surf. Sci. **411**, 279–284 (2017). https://doi.org/10.1016/j.apsusc.2017.03.146
13. G. Bruno, M.M. Giangregorio, G. Malandrino, P. Capezzuto, I.L. Fragalà, M. Losurdo, Is there a ZnO face stable to atomic hydrogen? Adv. Mater. **21**, 1700–1706 (2009). https://doi.org/10.1002/adma.200802579
14. W. Kim, G. Kwak, M. Jung, S.K. Jo, J.B. Miller, A.J. Gellman, K. Yong, Surface and internal reactions of ZnO nanowires: Etching and bulk defect passivation by H atoms. J. Phys. Chem. C **116**, 16093–16097 (2012). https://doi.org/10.1021/jp304191m
15. X. Lu, G. Wang, S. Xie, J. Shi, W. Li, Y. Tong, Y. Li, Efficient photocatalytic hydrogen evolution over hydrogenated ZnO nanorod arrays. Chem. Commun. **48**, 7717–7719 (2012). https://doi.org/10.1039/C2CC31773G

16. T. Xia, P. Wallenmeyer, A. Anderson, J. Murowchick, L. Liu, X. Chen, Hydrogenated black ZnO nanoparticles with enhanced photocatalytic performance. RSC Adv. **4**, 41654–41658 (2014). https://doi.org/10.1039/C4RA04826A
17. R.F. Allah, T. Ben, D. González, V. Hortelano, O. Martínez, J.L. Plaza, Modification of the optical and structural properties of ZnO nanowires by low-energy Ar^+ ion sputtering. Nanoscale Res. Lett. **8**, 162 (2013). https://doi.org/10.1186/1556-276X-8-162
18. Z.Q. Chen, K. Betsuyaku, A. Kawasuso, Vacancy defects in electron-irradiated ZnO studied by Doppler broadening of annihilation radiation. Phys. Rev. B **77**, 113204 (2008). https://doi.org/10.1103/PhysRevB.77.113204
19. A. Sulyok, M. Menyhard, J.B. Malherbe, Stability of ZnO{0001} against low energy ion bombardment. Surf. Sci. **601**, 1857–1861 (2007). https://doi.org/10.1016/j.susc.2007.02.011
20. J. Lv, C. Li, J.J. BelBruno, Defect evolution on the optical properties of H^+-implanted ZnO whiskers. CrystEngComm **15**, 5620–5625 (2013). https://doi.org/10.1039/C3CE40655E
21. Z.Q. Chen, T. Sekiguchi, X.L. Yuan, M. Maekawa, A. Kawasuso, N^+ ion-implantation-induced defects in ZnO studied with a slow positron beam. J. Phys. Condens. Matter **16**, S293–S299 (2003). https://doi.org/10.1088/0953-8984/16/2/035
22. H.-W. Ra, K.S. Choi, C.W. Ok, S.Y. Jo, K.H. Bai, Y.H. Im, Ion bombardment effects on ZnO nanowires during plasma treatment. Appl. Phys. Lett. **93**, 033112 (2008). https://doi.org/10.1063/1.2965109
23. V. Gurylev, A. Useinov, P.Y. Hsieh, C.Y. Su, T.P. Perng, Hydrogenated ZnO thin film with p-type surface conductivity from plasma treatment. J. Phys. D. Appl. Phys. **50**, 24LT02 (2017). https://doi.org/10.1088/1361-6463/aa6e91
24. C. Chen, H. He, Y. Lu, K. Wu, Z. Ye, Surface passivation effect on the photoluminescence of ZnO nanorods. ACS Appl. Mater. Interfaces **5**, 6354–6359 (2013). https://doi.org/10.1021/am401418b
25. T.M. Børseth, B.G. Svensson, A.Y. Kuznetsov, P. Klason, Q.X. Zhao, M. Willander, Identification of oxygen and zinc vacancy optical signals in ZnO. Appl. Phys. Lett. **89**, 262112 (2006). https://doi.org/10.1063/1.2424641
26. Y. Chen, Y. Pu, L. Wang, C. Mo, W. Fang, B. Xiong, F. Jiang, Influence of nitrogen annealing on structural and photoluminescent properties of ZnO thin film grown on c-Al_2O_3 by atmospheric pressure MOCVD. Mater. Sci. Semicond. Proc. **8**, 491–496 (2005). https://doi.org/10.1016/j.mssp.2004.07.006
27. L. Ke, S.C. Lai, J.D. Ye, V.L. Kaixin, S.J. Chua, Point defects analysis of zinc oxide thin films annealed at different temperatures with photoluminescence, Hall mobility, and low frequency noise. J. Appl. Phys. **108**, 084502 (2010). https://doi.org/10.1063/1.3494046
28. V. Gurylev, C.-Y. Su, T.-P. Perng, Distribution pattern and allocation of defects in hydrogenated ZnO thin films. Phys. Chem. Chem. Phys. **18**, 16033–16038 (2016). https://doi.org/10.1039/C6CP01768A
29. C. Zou, F. Liang, S. Xue, Synthesis and oxygen vacancy-related photocatalytic properties of ZnO nanotubes grown by thermal evaporation. Res. Chem. Intermed. **41**, 5167–5176 (2015). https://doi.org/10.1007/s11164-014-1620-y
30. A.A. Camacho-Berríos, V.M. Pantojas, W. Otaño, Reactive sputtered ZnO thin films: Influence of the O_2/Ar flow ratio on the oxygen vacancies and paramagnetic active sites. Thin Solid Films **692**, 137641 (2019). https://doi.org/10.1016/j.tsf.2019.137641
31. Y.W. Heo, D.P. Norton, S.J. Pearton, Origin of green luminescence in ZnO thin film grown by molecular-beam epitaxy. J. Appl. Phys. **98**, 073502 (2005). https://doi.org/10.1063/1.2064308
32. V. Venkatachalapathy, A. Galeckas, A. Zubiaga, F. Tuomisto, A.Y. Kuznetsov, Changing vacancy balance in ZnO by tuning synthesis between zinc/oxygen lean conditions. J. Appl. Phys. **108**, 046101 (2010). https://doi.org/10.1063/1.3462394
33. A. Zubiaga, F. Tuomisto, F. Plazaola, K. Saarinen, J.A. Garcia, J.F. Rommeluere, J. Zuñiga-Pérez, V. Muñoz-Sanjosé, Zinc vacancies in the heteroepitaxy of ZnO on sapphire: Influence of the substrate orientation and layer thickness. Appl. Phys. Lett. **86**, 042103 (2005). https://doi.org/10.1063/1.1855412

34. A.A. Chaaya, R. Viter, M. Bechelany, Z. Alute, D. Erts, A. Zalesskaya, K. Kovalevskis, V. Rouessac, V. Smyntyna, P. Miele, Evolution of microstructure and related optical properties of ZnO grown by atomic layer deposition. Beilstein J. Nanotechnol. **4**, 690–698 (2013). https://doi.org/10.3762/bjnano.4.78
35. E. Guziewicz, M. Godlewski, L. Wachnicki, T.A. Krajewski, G. Luka, S. Gieraltowska, R. Jakiela, A. Stonert, W. Lisowski, M. Krawczyk, J.W. Sobczak, A. Jablonski, ALD grown zinc oxide with controllable electrical properties. Semicond. Sci. Technol. **27**, 074011 (2012). https://doi.org/10.1088/0268-1242/27/7/074011
36. M. Jin, J. Jo, G.P. Neupane, J. Kim, K.-S. An, J.-W. Yoo, Tuning of undoped ZnO thin film via plasma enhanced atomic layer deposition and its application for an inverted polymer solar cell. AIP Adv. **3**, 102114 (2013). https://doi.org/10.1063/1.4825230
37. L. Znaidi, Sol-gel-deposited ZnO thin films: A review. Mater. Sci. Eng. B **174**, 18–30 (2010). https://doi.org/10.1016/j.mseb.2010.07.001
38. G.Z. Xing, Y.H. Lu, Y.F. Tian, J.B. Yi, C.C. Lim, Y.F. Li, G.P. Li, D.D. Wang, B. Yao, J. Ding, Y.P. Feng, T. Wu, Defect-induced magnetism in undoped wide band gap oxides: Zinc vacancies in ZnO as an example. AIP Adv. **1**, 022152 (2011). https://doi.org/10.1063/1.3609964
39. F. Dejene, A. Ali, H. Swart, R. Botha, K. Roro, L. Coetsee, M. Biggs, Optical properties of ZnO nanoparticles synthesized by varying the sodium hydroxide to zinc acetate molar ratios using a Sol-Gel process. Open Phys. **9**, 1321–1326 (2011). https://doi.org/10.2478/s11534-011-0050-3
40. O. Akhavan, M. Mehrabian, K. Mirabbaszadeh, R. Azimirad, Hydrothermal synthesis of ZnO nanorod arrays for photocatalytic inactivation of bacteria. J. Phys. D. Appl. Phys. **42**, 225305 (2009). https://doi.org/10.1088/0022-3727/42/22/225305
41. N.A. Alshehri, A.R. Lewis, C. Pleydell-Pearce, T.G.G. Maffeis, Investigation of the growth parameters of hydrothermal ZnO nanowires for scale up applications. J. Saudi Chem. Soc. **22**, 538–545 (2018). https://doi.org/10.1016/j.jscs.2017.09.004
42. T. Ghoshal, S. Biswas, M. Paul, S.K. De, Synthesis of ZnO nanoparticles by solvothermal method and their ammonia sensing properties. J. Nanosci. Nanotechnol. **9**, 5973–5980 (2009). https://doi.org/10.1166/jnn.2009.1290
43. L. Pan, S. Wang, W. Mi, J. Song, J.-J. Zou, L. Wang, X. Zhang, Undoped ZnO abundant with metal vacancies. Nano Energy **9**, 71–79 (2014). https://doi.org/10.1016/j.nanoen.2014.06.029
44. E.G. Barbagiovanni, V. Strano, G. Franzò, S. Mirabella, The role of Zn vacancies in UV sensing with ZnO nanorods. Appl. Phys. Lett. **109**, 143104 (2016). https://doi.org/10.1063/1.4963890
45. P. Gu, X. Zhu, D. Yang, Vertically aligned ZnO nanorods arrays grown by chemical bath deposition for ultraviolet photodetectors with high response performance. J. Alloys Compd. **815**, 152346 (2020). https://doi.org/10.1016/j.jallcom.2019.152346
46. C. Wang, D. Wu, P. Wang, Y. Ao, J. Hou, J. Qian, Effect of oxygen vacancy on enhanced photocatalytic activity of reduced ZnO nanorod arrays. Appl. Surf. Sci. **325**, 112–116 (2015). https://doi.org/10.1016/j.apsusc.2014.11.003
47. X.-F. Su, J.-B. Chen, R.-M. He, Y. Li, J. Wang, C.-W. Wang, The preparation of oxygen-deficient ZnO nanorod arrays and their enhanced field emission. Mater. Sci. Semicond. Process. **67**, 55–61 (2017). https://doi.org/10.1016/j.mssp.2017.05.012
48. T. Yoshida, D. Komatsu, N. Shimokawa, H. Minoura, Mechanism of cathodic electrodeposition of zinc oxide thin films from aqueous zinc nitrate baths. Thin Solid Films **451-452**, 166–169 (2004). https://doi.org/10.1016/j.tsf.2003.10.097
49. V. Anand, V.C. Srivastava, Zinc oxide nanoparticles synthesis by electrochemical method: Optimization of parameters for maximization of productivity and characterization. J. Alloys Compd. **636**, 288–292 (2015). https://doi.org/10.1016/j.jallcom.2015.02.189
50. S. Dai, Y. Li, Z. Du, K.R. Carter, Electrochemical deposition of ZnO hierarchical nanostructures from hydrogel coated electrodes. J. Electrochem. Soc. **160**, D156 (2013). https://doi.org/10.1149/2.064304jes
51. K. Mika, R.P. Socha, P. Nyga, E. Wiercigroch, K. Małek, M. Jarosz, T. Uchacz, G.D. Sulka, L. Zaraska, Electrochemical synthesis and characterization of dark nanoporous zinc oxide films. Electrochim. Acta **305**, 349–359 (2019). https://doi.org/10.1016/j.electacta.2019.03.052

52. K. Ralphs, C. Hardacre, S.L. James, Application of heterogeneous catalysts prepared by mechanochemical synthesis. Chem. Soc. Rev. **42**, 7701–7718 (2013). https://doi.org/10.1039/C3CS60066A
53. D. Chen, Z. Wang, T. Ren, H. Ding, W. Yao, R. Zong, Y. Zhu, Influence of defects on the photocatalytic activity of ZnO. J. Phys. Chem. C **118**, 15300–15307 (2014). https://doi.org/10.1021/jp5033349
54. H. Kaftelen, K. Ocakoglu, R. Thomann, S. Tu, S. Weber, E. Erdem, EPR and photoluminescence spectroscopy studies on the defect structure of ZnO nanocrystals. Phys. Rev. B **86**, 014113 (2012). https://doi.org/10.1103/PhysRevB.86.014113
55. X. Xu, C. Xu, J. Dai, J. Hu, F. Li, S. Zhang, Size dependence of defect-induced room temperature ferromagnetism in undoped ZnO nanoparticles. J. Phys. Chem. C **116**, 8813–8818 (2012). https://doi.org/10.1021/jp3014749
56. S.M. Mohammad, N.M. Abd-Alghafour, R.A. Talib, Z. Hassan, N.M. Ahmed, A.A. Abuelsamen, N. Afzal, Influence of growth temperature and duration on different properties of ultra-long ZnO nanorods grown by modified chemical bath deposition method. Mater. Res. Express **5**, 095020 (2018). https://doi.org/10.1088/2053-1591/aad76b
57. G.R. Li, T. Hu, G.L. Pan, T.Y. Yan, X.P. Gao, H.Y. Zhu, Morphology-function relationship of ZnO: Polar planes, oxygen vacancies, and activity. J. Phys. Chem. C **112**, 11859–11864 (2008). https://doi.org/10.1021/jp8038626
58. M. Lorenz, R. Böttcher, S. Friedländer, A. Pöppl, D. Spemann, M. Grundmann, Local lattice distortions in oxygen deficient Mn-doped ZnO thin films, probed by electron paramagnetic resonance. J. Mater. Chem. C **2**, 4947–4956 (2014). https://doi.org/10.1039/C4TC00407H
59. Y. Wang, K.-M. Kang, M. Kim, H.-H. Park, Oxygen vacancy-passivated ZnO thin film formed by atomic layer deposition using H_2O_2. J. Vac. Sci. Technol. A **36**, 031504 (2018). https://doi.org/10.1116/1.5012022
60. A. Asok, M.N. Gandhi, A.R. Kulkarni, Enhanced visible photoluminescence in ZnO quantum dots by promotion of oxygen vacancy formation. Nanoscale **4**, 4943–4946 (2012). https://doi.org/10.1039/C2NR31044A
61. Y. Lv, W. Yao, X. Ma, C. Pan, R. Zong, Y. Zhu, The surface oxygen vacancy induced visible activity and enhanced UV activity of a ZnO_{1-x} photocatalyst. Cat. Sci. Technol. **3**, 3136–3146 (2013). https://doi.org/10.1039/C3CY00369H
62. Y. Ding, R. Yang, Z.L. Wang, Ordered zinc-vacancy induced $Zn_{0.75}O_x$ nanophase structure. Solid State Commun. **138**, 390–394 (2006). https://doi.org/10.1016/j.ssc.2006.03.032
63. S.J. Clark, J. Robertson, S. Lany, A. Zunger, Intrinsic defects in ZnO calculated by screened exchange and hybrid density functionals. Phys. Rev. B **81**, 115311 (2010). https://doi.org/10.1103/PhysRevB.81.115311
64. Q. Zhang, X. Zhao, L. Duan, H. Shen, R. Liu, Controlling oxygen vacancies and enhanced visible light photocatalysis of CeO_2/ZnO nanocomposites. J. Photochem. Photobiol. A **392**, 112156 (2020). https://doi.org/10.1016/j.jphotochem.2019.112156
65. Y.J. Zeng, Z.Z. Ye, W.Z. Xu, J.G. Lu, H.P. He, L.P. Zhu, B.H. Zhao, Y. Che, S.B. Zhang, p-Type behavior in nominally undoped ZnO thin films by oxygen plasma growth. Appl. Phys. Lett. **88**, 262103 (2006). https://doi.org/10.1063/1.2217165
66. F. Oba, M. Choi, A. Togo, A. Seko, I. Tanaka, Native defects in oxide semiconductors: A density functional approach. J. Phys. Condens. Matter **22**, 384211 (2010). https://doi.org/10.1088/0953-8984/22/38/384211
67. Y. Dong, F. Tuomisto, B.G. Svensson, A.Y. Kuznetsov, L.J. Brillson, Vacancy defect and defect cluster energetics in ion-implanted ZnO. Phys. Rev. B **81**, 081201 (2010). https://doi.org/10.1103/PhysRevB.81.081201
68. X. Yin, Y. Wang, R. Jacobs, Y. Shi, I. Szlufarska, D. Morgan, X. Wang, Massive vacancy concentration yields strong room-temperature ferromagnetism in two-dimensional ZnO. Nano Lett. **19**, 7085–7092 (2019). https://doi.org/10.1021/acs.nanolett.9b02581
69. C. Yao, B. Wei, H. Ma, H. Li, L. Meng, X. Zhang, Q. Gong, Enhanced photoelectrochemical performance of hydrogenated ZnO hierarchical nanorod arrays. J. Power Sources **237**, 295–299 (2013). https://doi.org/10.1016/j.jpowsour.2013.02.062

70. X. Liu, L. Ye, S. Liu, Y. Li, X. Ji, Photocatalytic reduction of CO_2 by ZnO micro/nanomaterials with different morphologies and ratios of {0001} facets. Sci. Rep. **6**, 38474 (2016). https://doi.org/10.1038/srep38474
71. I.M. Hegazy, R.A. Geioushy, S.M. El-Sheikh, A. Shawky, S. El-Sherbiny, A.-H.T. Kandil, Influence of oxygen vacancies on the performance of ZnO nanoparticles towards CO_2 photoreduction in different aqueous solutions. J. Environ. Chem. Eng. **8**, 103887 (2020). https://doi.org/10.1016/j.jece.2020.103887
72. J. Xu, M. Li, L. Yang, J. Qiu, Q. Chen, X. Zhang, Y. Feng, J. Yao, Synergy of Ni dopant and oxygen vacancies in ZnO for efficient photocatalytic depolymerization of sodium lignosulfonate. Chem. Eng. J. **394**, 125050 (2020). https://doi.org/10.1016/j.cej.2020.125050
73. X. Pan, M.-Q. Yang, Y.-J. Xu, Morphology control, defect engineering and photoactivity tuning of ZnO crystals by graphene oxide – a unique 2D macromolecular surfactant. Phys. Chem. Chem. Phys. **16**, 5589–5599 (2014). https://doi.org/10.1039/C3CP55038A

Chapter 7
Case Study III: Defect Engineering of Ta_2O_5, Ta_3N_5, and TaON

7.1 Ta_2O_5, Ta_3N_5, and TaON: Fundamentals

Ta_2O_5 (Tantalum Pentoxide) It is generally accepted that Ta_2O_5 has two main polymorphs which are determined as high-temperature (HT) and low-temperature (LT) configuration. Transitions between them usually occurred at ~1360 °C. Thus, for the technological purposes, the LT configuration is more practically applicable as it can be available at ambient environment and conditions. It existed mainly as orthorhombic crystal structure which is considered to be the most stable constitution even though other phases such as tetragonal, monoclinic, triclinic, and hexagonal along with several high-pressures formations are also identified. Overall, the composition of Ta_2O_5 is ascribed as a network of octahedral (TaO_6), pentagonal bipyramidal (TaO_7), and hexagonal pyramid (TaO_8) polyhedra which rearrangement and adaptation such as introduction of certain distortion, appearance of edge- and corner-sharing, joined existence, etc. defines the exact type of Ta_2O_5 structure [1]. In turn, fabrication of Ta_2O_5 in the form of single crystal is technically difficult, and thereby, it mostly exists as polycrystalline or amorphous compound. The length of orthorhombic Ta-O bond was experimentally measured to be ~0.15 nm [2], while theoretical simulation predicated that this value is equaled to ~0.2 nm [1]. As for the optical properties, Ta_2O_5 cannot absorb visible light due to wide band gap ranging from ~3.8 to ~5.3 eV [3], and thus, it is often represented as white powder similar to that of TiO_2. Nevertheless, Ta_2O_5 has good chemical stability, n-type conductivity, and very high dielectric constant and enables to demonstrate efficient photocatalytic activity under UV light especially for water splitting given its suitable positions of its valence and conduction bands with respect to both hydrogen and oxygen evolution potentials.

Tantalum Nitride (Ta_3N_5) Tantalum nitride is an n-type semiconductor and has an orthorhombic structure with space group *Cmcm*. It is composed of edge-sharing

V. Gurylev, *Nanostructured Photocatalyst via Defect Engineering*,
https://doi.org/10.1007/978-3-030-81911-8_7

irregular TaN_6 octahedra where each Ta atom is coordinated by two N (which is threefold coordinated) and four N (which is fourfold coordinated) atoms with Ta-N bond lengths ranging from 2.00 to 2.23 Å [4] (Fig. 7.1a). Due to absorption edge located at ~600 nm, Ta_3N_5 is sensitive to the visible light, and it is attributed to electron transitions from the N 2p orbitals that is located higher compared with O 2p orbital in Ta_2O_5 with regard to its distance from empty Ta 5d orbitals. Thus, direct band gap and indirect band gap are determined to be ~2.0 and ~2.1 eV, respectively, and as a result, Ta_3N_5 usually appears as red-colored compound. It is technically impossible to obtain this material as absolutely pure and in full stoichiometry since oxygen often is presented in its structure in the form of impurity that substitutes nitrogen often resulting in formation of reducing metallic states in its surface or in the bulk. It is generally disputing whether it has a positive or negative impact on its characteristics as controversial reports are available in literature [5, 6]. Apart from it, formation of Ta_3N_5 also can be accompanied by co-existence of other related nitride phases presented in the form of Ta_xN_y such as Ta_5N_6 or Ta_2N [7]. Thus, precise chemical composition of Ta_3N_5 and accompanied geometrical and electronic structures might be not easy to generalize as it is fully depended on the fabrication method and conditions of consequent post-treatment or storage. Nevertheless, Ta_3N_5 is considered to be a very attractive candidate for photocatalysis as it is a non-toxic compound and has high dialectic constant and suitable position of band gap edges that perfectly match, for example, the potential of photocatalytic water splitting.

Tantalum Oxynitride (TaON) Tantalum oxynitride is available in several polymorphs among which the most thermodynamically stable is identified to be β-phase. It is existing in the form of well-known monoclinic baddeleyite-type structure which is composed of edge-sharing irregular TaO_3N_4 polyhedra where each Ta atom is coordinated to three O (which threefold coordinated) and four N (which is fourfold coordinated) atoms. Consequently, Ta-O and Ta-N bond lengths were identified to be ranging from 2.03 to 2.15 Å and from 2.06 to 2.13 Å, respectively [4]

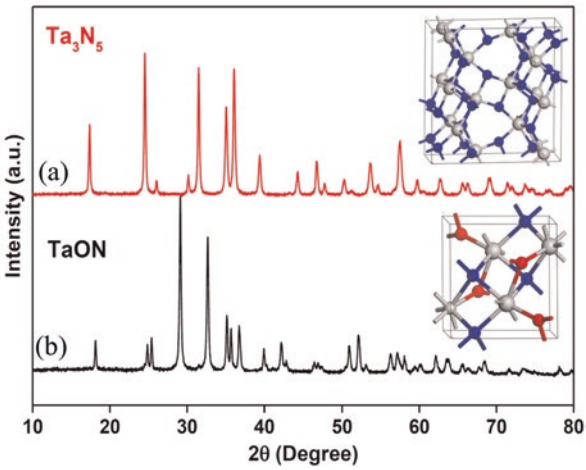

Fig. 7.1 XRD patterns and crystal structures of (**a**) Ta_3N_5 and (**b**) TaON. Color legend: Ta in gray, O in red, and N in blue. (Reprinted from Ref. [4] with permission from *Elsevier*. Copyright 2015)

(Fig. 7.1b). TaON has bright yellow color due to optical band gap of ~2.6 eV that allows to absorb certain portion of visible light [8]. Furthermore, compared with Ta_3N_5, this material has optical anisotropy which means that positioning of absorption edge follows the polarization of light along defined crystal axes [4]. Another two polymorphs of TaON are determined to be metastable, and their synthesis is less reported as it requires complex procedure, and the obtained compound often might not represent required purity. One of them is considered to be γ-TaON that was firstly discovered by Schilling et al. in 2007 [9]. It has light brown color (optical band gap of ~2.15 eV), and its composition is similar to VO_2(B) in the monoclinic crystal system due to structure composed of $Ta(ON)_6$. It also has an ordered distribution of oxygen and nitrogen similar to that found in β-TaON. Another metastable polymorph is referred as δ-phase which structure was identified to have anatase-type form (due to high resemblance to TiO_2), and it is crystallized in the tetragonal crystal system. Theoretical simulation is determined that its thermodynamic stability is very similar to that of γ-type with difference equaled only to 0.07 eV [8]. The band gap of δ-TaON was measured to be ~2.37 eV [10]. Apart from existence of different phases, compositions of TaON also are highly sensitive to the proportion of nitrogen to oxygen content. Simply to say, as electronegativity and polarizability of former element is lower than that of the latter one, thus, dominated and increased presence of Ta-N bonds over that of Ta-O increases the overall charge of TaON resulting in narrower band gap, increased refractive index, and better optical transparency [11]. Yet too much nitrogen might lead to its transformation into Ta_3N_5. It is necessary to notice that this phenomenon should not be confused with situation when absence of Ta-N bond in TaON is defined as presence of nitrogen vacancies since in this case oxygen atoms take another role and absolutely different processes and perturbations within geometrical and electronic structures should be considered. It is discussed below in detail. In the end, one should mention that TaON is an n-type semiconductor and has great chemical stability in various aggressive environments including reactive aqueous media, and due to the fact that edges of its band gap greatly match with potentials of reduction and oxidation potentials of some specific photocatalytic reactions, such as water splitting, this material recently deserved an increased attention.

7.2 Intrinsic Defects in Ta_2O_5, Ta_3N_5, and TaON

7.2.1 Introduction

Despite great perspectives of Ta-based materials as photocatalysts for certain reactions since they possess various attractive features and particularities, there still remain questions about their efficiencies since certain limitations are existed regarding them. For example, Ta_3N_5 suffers from high recombination rate of charge careers which restrict their transportation to surface thus greatly reducing the productivity

of both oxidation and reduction reactions. Another problem of this material is referred to its extreme overpotential which means that much higher voltage is required to initiate redox potentials than it is determined thermodynamically. As a result, even though theoretically it was predicted that this material enables to reach the efficiency of 15.9% for photoelectrochemical water splitting, practically, the value of around 2.72% has been achieved so far [12]. In turn, absorption edges of TaON and especially Ta_2O_5 still cannot satisfy the most optimal requirement toward reaching the best quantum efficiency, and it is necessary to be extended further as to fully realize solar spectrum. Apart from other techniques applied widely to solve these problems such as combining with other semiconductors or depositing noble metals, self-doping with various intrinsic defects can be considered as one of the most attractive alternatives to them. To be clear, manageable introduction of certain imperfections within crystal lattice of Ta-based materials followed by precise and defined control over their existences through accurate adjustment of type, concentration, and distribution can be used to regulate various important features including width of the band gap, introduction of additional energy levels, etc. which can lead to not only increase mobility, lifetimes, and transportation characteristics of charge carriers but also to advance other related properties.

Following it, one can say that non-stoichiometric Ta-based materials have a great potential to be used in solar light-based devices. Yet, as their photocatalytic applicability was discovered recently, deep and profound understanding of their defect engineering is still very far from full and complete awareness and definitely cannot be compared with that of other well-known materials such as, for example, TiO_2 and ZnO discussed in previous chapters. Thus, the source of defined and solid knowledge is required to push further the progress in this direction.

7.2.2 Defects in Oxide, Nitrides, and Oxynitrides: What Is Difference

7.2.2.1 Brief Overview

Tantalum Pentoxide (Ta_2O_5) and Tantalum Nitride (Ta_3N_5) Large percentage of experimental studies presented in literature regarding the introduction of various defects into binary compounds such as Ta_2O_5 and Ta_3N_5 are almost fully dedicated to discussion and identification of their non-metallic vacancies as their formation and proper adjustment of related characteristics as well as consequent detection and analysis of their existences can be easily realized using commonly applied processing, protocols, and instrumentations. To be clear, it is often the case that vacancies among other defects have the lowest formation energy and their appearances are the most probable and recognizable. Furthermore, realization of O- or N-deficient compounds can be achieved much easier and readily through playing with conditions of synthesis

or post-synthesis treatment, for example, simply by changing the ratios of used precursors or via reducing the presence of nitrogen or oxygen in the surrounding environment, respectively. At the same time, it would be incorrect to say that availability of other defects such as interstitials or antisites can be fully ignored in Ta_2O_5 and Ta_3N_5 as, in fact, their formation often is considered as accompanies to that of vacancies or even regarded as to be the dominated type of defects in some cases. Thus, they enable to make very evident contribution or to be the only and sole initiators of observed and detected changes in the electronic, electrical, and optical characteristics of these materials. For instance, they also can cause the development of relevant energy levels within the band gap or initiate structural modifications and adjustment of crystal lattice. Thus, they deserve to be discussed as well. In turn, one should notice that O- or N-rich compositions in Ta_2O_5 and Ta_3N_5, respectively, also can be formed as well due to escape of Ta atoms and appearance of relevant vacancies; yet their presence is energetically unfavorable and, also practically to be less attractive as they reduce the level of metallization leading to increase of resistivity, poorer charge transport that correlates with worsening photocatalytic characteristics.

Tantalum Oxynitride (TaON) As for TaON, its ternary system and appearance of defects are different for that of binary Ta_2O_5 and Ta_3N_5 mentioned above. Surely, it could be attributed to the simultaneous presence of N and O, as their interaction cannot be limited only by the formation of vacancies alone and results in development of other forms of defects. For example, it is possible with certain level of easiness to make substitution of nitrogen atoms with that of oxygen atom and vice versa especially given their only slight differences in atomic radii. In addition, instead of comparing the content of each N or O with respect to Ta, direct adjustment of N/O ratio can be proceeded thus making visualization of their localized distribution to be more feasible. Yet, despite such a bright perspective, processing of defects in TaON given its chemical composition is a complex phenomenon, and it requires detailed access and proper understanding. For example, its non-stoichiometry is supposed to be always identified as N-deficient since the opposite trend, namely, lowering the existence of oxygen and increasing the presence of nitrogen in it might lead to appearance of localized Ta_3N_5 phases.

Overall, detailed description regarding proper application of defect engineering principles to Ta-based materials is provided below. It has to be noticed that discussion and consideration of N substitution to that of O atoms occurred during nitridization process when oxide is transformed into nitride or oxynitride following thermally activated reaction is avoided here as this process is referred rather to the synthesis procedure and cannot be specified as intentional introduction of substitutional (antisites) defects. In addition, existence of oxygen in Ta_3N_5 which cannot be avoided and thus is determined to be an unintentional impurity (for analogy, reader can consider presence of hidden hydrogen in ZnO) would be discussed below only at the minimum level when necessary as only to provide brief overview since its presence is classified not as a part of intrinsic but rather extrinsic deficiency discussed in later chapters.

7.2.2.2 Defects in Ta_2O_5

Defect chemistry of crystalline Ta_2O_5 is usually limited by the discussion of V_O as oxygen in this compound has a high degree of volatility, and thus formation of this type of defects is considered to be the most favorable among others. Yet, its complex geometrical and electronic structures might not be easy to access as there exist certain difficulties toward its correct description and identification via both experimental and theoretical approaches. Overall, the following particularities are determined regarding them. *Firstly*, classification of V_O is proceeded in terms of their positioning in the crystal lattice, whether they occupy basal planes, which might represent either TaO_5 and TaO_6 depending on the original configuration or sitting between them. In the former configuration, the defects are called to be "in-plane," while in the latter they are determined as "cap" formations [13] (Fig. 7.2a). For simplicity, these identifications are used latter in text. It has to be noticed that within both residences, V_O also can take different positioning depending on the type and number of basal planes, type of coordination and other related parameters. *Secondly*, as the O atom at cap and in-plane sites share two and three polyhedra, consequently, lattice relaxation due to formation of vacancy is strikingly long ranged for the former one, and it is consequently shorter for the latter one [14]. *Thirdly*, considering the bulk model, formation energy of in-plane V_O is lower than that of the cap V_O which represents that they have higher stability [15]. In turn, for the surface-based defects, it

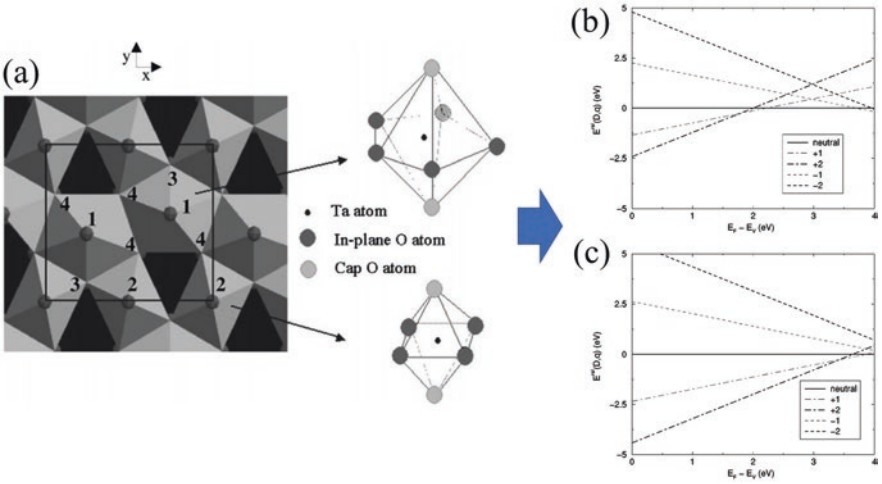

Fig. 7.2 (**a**) Schematic of the Ta_2O_5 structure used in the present calculation, with the rectangle highlighting the unit cell. Also shown are perspective views of the TaO_7 (top, right) and TaO_6 (bottom, right) building blocks, with the in-plane and cap site O locations explicitly identified. The four symmetry-inequivalent atoms are labeled within the unit cell, with labels 1 and 2 denoting cap sites and labels 3 and 4 denoting in-plane sites. Relative total energy E^{rel} (D, q) of (**b**) the in-plane vacancy with site label 4 and (**c**) the cap type vacancy with site label 1, as a function of the local Fermi energy, where q denotes the charge state of the vacancy (q is +2; +1; 0; −1; −2). (Reprinted from Ref. [13] with permission from *AIP Publishing*. Copyright 2003)

is *vice versa* [16]. *Fourthly*, for a wide range of Fermi levels or chemical potentials, the neutral and +2 charged states of the in-plane type vacancy and the +2 charged state of the cap type vacancy are found to be most stable, while +1 charge state is identified to be metastable formation for both types [13]. Thus, oxygen vacancies in Ta_2O_5 are determined as negative U center, similar to TiO_2 and ZnO. *Fifthly*, following it, the oxygen vacancies resided within in-plane positions are generally considered to enable the appearance of deep mid-gap occupied and shallow unoccupied states depending on their geometrical particularities and positioning of Fermi level with respect to both bands, while cap V_O is identified to be the source of only shallow occupied levels [13, 15, 17]. *Sixthly*, the localization of (+2/0) transition level is clearly influenced by the type of V_O. For the in-plane and cap configurations, it was discovered to be located ~1.9 and ~3.5 eV from valence band, respectively, taking the band gap of Ta_2O_5 as ~4 eV [13] (Fig. 7.2b, c). This transition level means that below or above it, the total energies of vacancies with +2 or neutral charge states are dominated in Ta_2O_5 which clearly can be defined as their monopolized presence. Definitely, other positions of a (+2/0) transition level were also identified in literatures, which, however, have the same tendency with respect to the type of oxygen vacancy and are also mostly laid in the upper part of band gap or close to the conduction band [15, 18]. *Seventhly*, each oxygen vacancy results in formation of dangling bonds that in turn leads to appearance of additional multilevel electronic states in the band gap.

It has to be noticed that apart from presence of oxygen vacancies, existence of other defects in Ta_2O_5 was also verified; yet the available information regarding them is very limited. For example, Perevalov et al. [19] applied density functional theory (DFT) to investigate atomic and electronic structures of interstitial Ta and O as well as Ta atoms substituting O. It was revealed that these defects enable to trap both electrons and holes thus contributing to increase of overall conductivity. Furthermore, comparing their formation energies with that of V_O, it was also discovered that the latter type of defect under specifically determined O-rich or O-poor conditions cannot be considered as the most favorable formation in Ta_2O_5, and this role can be transferred to interstitial oxygen or tantalum, respectively [19, 20].

7.2.2.3 Defects in Ta_3N_5

Making the parallel with mentioned above Ta_2O_5, nitrogen vacancy is considered to be the most recognized, accessible, and investigated type of defect in Ta_3N_5 given simplicity of their introduction, consequent manipulation, precise and accurate detections, and analysis. It is existed in the form of threefold and fourfold geometry among which the latter one has lower formation energy with the positioning of Fermi level located in the upper part of band gap (n-type conditions) [21]. Overall, nitrogen vacancies can exist in several charge states among which +2 is considered to be thermodynamically unstable, while that of neutral, +1 and +3 with certain restrictions enable to preserve their existence in Ta_3N_5. Their

appearances and dominance with regard to each other are determined by exact and concrete localization of Fermi level [22]. Based on this, the following observation can be made: (0/+1) transition level locates closest to the conduction band which determines its shallow nature, while presence of other transitions can be identified to be deeper into band gap, i.e., (+1/+2) and (+2/+3), or even out of it, i.e., within the conduction band, i.e., (+1/+3) [23]. Geometrical composition of nitrogen vacancies is defined by their structural particularities, i.e., threefold configuration causes the relaxation of surrounded Ta by about ~1.7% which is sufficiently larger compared to fourfold configuration where this motion is equaled to only ~0.22% [22]. Stampfl and Freeman [24] revealed that appearance of V_N in low concentration is considered to be a thermodynamically unstable configuration, while their larger presence is more favorable for whole range of nitrogen chemical potential. Finally, it has to be noticed that formation of V_N is supposed to be accompanied by the development of reduced Ta species (Ta^{3+} or Ta^{4+}) that might serve as compensation centers to maintain the charge balance. These defects are considered to be deep rather than shallow donors as they create energy states located at sufficient distance from the conduction band.

Apart from nitrogen vacancies, other defects such as Ta vacancy (V_{Ta}), interstitial N (N_i), interstitial Ta (Ta_i), and antisites ascribed as Ta atom occupying an N lattice site (Ta_n) or *vice versa* (N_{Ta}) are also detected to exist in Ta_3N_5 even though they deserve much less attention, and thus knowledge about them is very limited as it is mostly provided by theoretical studies, while experimental evidence of their presence is still a rare phenomenon. For example, Jing et al. [22] used spin-polarized DFT calculations to access various defects in Ta_3N_5 in terms of their geometrical and electronic compositions. Particularly, it was determined that N_i can only show stability if only it is presented in the form of +1 and −1 charge states which transition level was identified to locate at 0.58 eV above the valence band maximum (VBM). It indicates that this defect can demonstrate both donor- and acceptor-like characteristics, i.e., enable to donate electrons to conduction band and also undertake them from valence band, respectively. In turn, thermodynamically accessible formation of interstitial Ta in terms of its charge state was revealed to be fully dependent on the position of Fermi level, and in fact it is very similar to V_N. The existence of the following transition levels along with their distances from conduction band minimum (CBM) was calculated: (1/+2) at 0.05 eV, (+2/+3) at 0.55 eV, (+3/+4) at 0.67 eV, and (+4/+5) at 1.11 eV [22]. As for the appearance of Ta vacancies, their presence results in reduce number of available density of states around Fermi level and consequent increase in the universal resistivity as these defects release holes that might recombine with electrons [24]. Overall, it has to be noticed that the presence of these defects (except V_N and reduced Ta species) was calculated to be a very rare phenomenon in n-type Ta_3N_5 given their exceptionally high formation energy which makes them thermodynamically unfavorable species [22]. Thus, they are very seldom used to improve and extend certain characteristics and features of this material.

7.2.2.4 Defects in TaON

Even though there is a clear resemblance of TaON to the mentioned above Ta_2O_5 and Ta_3N_5 and one may expect that similar to them anion-like defects such as O and N vacancies plays crucial role in determining its non-stoichiometric compositions, in reality, it is only half-true as other defects are considered to be dominated over them. Particularly, Chen et al. [25] determined that appearance of O_N antisites determined as oxygen resided in nitrogen positions is highly favorable in Ta_3N_5 due to its extremely low formation energy, and its presence determines the intrinsic n-type conductivity of TaON since it leads to development of shallow donor level located close to conduction band. Calculation *via* hybrid functional revealed that due to relatively similar atomic radii of both elements, thus substitution of an N atom by an O atom results in smaller chemical bonding and size change compared with substitution of N or O atoms by an empty spot [25] which is energetically more favorable. In addition, it was also determined that energy of barrier exchange which makes the diffusion of atoms possible is lower for O_N compared with that of N_O antisites that are ascribed as nitrogen resided in oxygen position [21]. Finally, it is also necessary to consider the strength of Ta-N bond which is weaker compared with that of Ta-O [25]. Thus, TaON has higher preferability and tendency toward nitrogen deficiency in contrast with that of its oxygen analogy. Yet, N_O cannot be fully ignored as under specific chemical potential, with Fermi level approaching CBM, the formation of N_O becomes spontaneous, and it is thermodynamically more accessible than that of O_N. Given the acceptor-like characteristics of this defect, its presence would lead to lowering the concentration of available active charge carriers thus limiting the original n-type conductivity [21].

Furthermore, occurrence of anion vacancies in TaON also should not be overlooked, as, in fact, they serve a crucial role in initiating, stabilizing, and extending the existence and lifetimes of both types of antisite defects. To be clear, formation of O_N or N_O is only possible when atoms of one element reside in an empty site of another element which represents that vacancy of the latter one for the best should be formed ahead. In turn, when this exchange happened, there also appeared an unoccupied site as atoms in order to reside somewhere else are supposed to abandon its original position leaving it empty. Thus, it would be accurate to say that, during formation of these defects, the following phenomena occurred: *firstly,* there is a switch between type of vacancies and, *secondly*, the presence of antisites cannot be considered as independent event, and instead the appearance of N_O/V_N and O_N/V_O pairs should be identified in TaON. Yet, one should be aware that concentration of V_O would always be lower than that of V_N as TaON tends to become more a nitrogen-deficient rather than oxygen-deficient compound (unless the structure is directed toward conversion into Ta_3N_5 and in this case stoichiometry of N should be over 1 and definitely higher than that of O), and thus identification of V_O due to oxygen atom escaped to V_N is very challenging as it is shadowed by the formation of O_N. Furthermore, it is also necessary to consider the variations in the charge states of vacancies as it has a certain influence on the concrete appearance and detection of O_N or N_O. For example, Bown and Page [21] revealed that V_N with neutral and +1

charge states is endothermic, while V_N with +2 and +3 charge states is determined to be spontaneous species which make them to have higher suitability toward serving as a source of respective antisites. As for the development of N_O, it was observed that increasing V_O charge state leads to the rise of their formation energies which, in turn, negatively influence the diffusion of N atoms into them.

7.2.3 How to Create Defects

7.2.3.1 Ta_2O_5

Synthesis Protocol Given volatility of oxygen, fabrication of Ta_2O_5 filled with V_O can be easily realized *via* various fabrication procedure simply by applying defined non-equilibrium conditions that favor the release of O atoms. *Firstly*, it is mostly proceeded in the form of chemical-based methods given their simplicity, cost-effectiveness, and other related advantages allowing to play with natures of certain precursors as well as their particularities such as concentrations, ratios, etc. Furthermore, along with formation of deficient structure, it is also possible to specify its morphology thus providing higher flexibility in reaching the required composition. For example, Fu et al. [26] reported that implementation of solvothermal process under 220 °C for 24 h using tantalum ethoxide ($Ta(C_2H_5O)_2$) as starting materials enables to fabricate Ta_2O_5 filled with oxygen vacancies. In turn, Zhang et al. [27] demonstrated that mesoporous ultrafine V_O-Ta_2O_5 nanoparticles with diameter of ~8 nm could be also realized by similar approach and using the same chemical as in Ref. [26] for serving the role of main precursor; yet treatment temperature should be set at 250 °C. *Secondly*, another method which is widely used to reach the goal of producing defective Ta_2O_5 is vapor synthesis approach. It provides high flexibility and precise accuracy in adjusting the parameters of depositions by changing, for example, temperature inside reaction chamber, pressure of utilized compounds, or other related parameters. Thus, defined chemical composition can be achieved. As an illustration, Skaja et al. [28] applied sputtering deposition to prepare Ta_2O_{5-x} thin film and discovered that increasing power density along with decreasing the oxygen partial pressure resulted in higher presence of V_O. It has to be noticed that similar to chemical-based synthesis, vapor-related methods also enable to create defective structures with various dimensions and morphologies. Particularly, Devan et al. [29] used filament metal-oxide vapor deposition technique to prepare one-dimensional Ta_2O_5 nanorods array filled with certain types of defects including oxygen vacancies.

Post-synthesis Protocol There exist several methods to introduce defects into already synthesized Ta_2O_5 *via* additional post-synthesis treatment procedure. *Firstly, g*iven the chemical compositions of Ta_2O_5, it is obvious that thermal annealing in oxygen-deficient environment or using various reducing agents would greatly assist in proper and controlled introduction of V_O. Notably, the former strategy was successfully realized by Liu et al. [16] who used annealing in vacuum at 850 °C to

transform Ta_2O_5 prepared *via* sol-gel method using $TaCl_5$ into oxygen-deficient and highly disordered compound compared with that treated in air at the same conditions. The applicability of the latter strategy in slightly modified form was also demonstrated by Zhu et al. [30] where Al was used as reducing agents to reach designated non-stoichiometry. Much like any other binary oxide materials, the higher the temperature of reduction, the more the V_O produced. Yet, one should become aware that resulted changes in the chemical composition are usually limited only by the surface layer up to the depth of only several nanometers and thus might not be suitable for the bulk modifications. In addition, prolonged and extended release of oxygen can result in appearance of Ta-based suboxides such as TaO_3, Ta_2O_3, or TaO; thus parameters of reduction processing are required to be accessed with extreme caution. *Secondly*, plasma treatment also has been reported in literature as an efficient approach to achieve required changes in the presence of defects with very certain degree of accuracy. For instance, Chen et al. [31] revealed that application of Nd:YAG-supported laser plasma enables to induce formation of oxygen vacancies within Ta_2O_5 surface which degree was correlated through the appearance of shock waves.

7.2.3.2 TaN_5

Synthesis Protocol Following the mentioned above Ta_2O_5, it is much easier to prepare Ta_3N_5 filled with N vacancies rather than any other defects (O impurities are excluded from consideration) which is explained by lower energies required to release the nitrogen atoms from the surface and simplicity of introducing required conditions and methodologies to realize this step. The following approaches are commonly applied. *Firstly*, thermally activated nitridation of Ta_2O_5 or other Ta-oxide-based compound in dry or wet ammonia is a popular method to produce Ta_3N_5 with nitrogen deficiency. Its level can be easily tuned by conditions of this processing such as the temperature and duration, pressure of gaseous ambient, its quality or particularities of Ta-based compounds used as precursors through adjusting its morphological features, chemical composition, etc. For instance, Wang et al. [7] demonstrated that preliminary applied thermal treatment of Ta_2O_5 tube layers under reducing atmosphere (Ar/H_2) led to development of suboxide domain close to the substrate. Further annealing in ammonia for 950 °C resulted in converting this structure into subnitride (Ta_2N/Ta_5N_6)-containing Ta_3N_5 tubes which possessed relatively similar morphology compared with non-treated sample (Fig. 7.3). In turn, Pinaud et al. [32] investigated how the type of starting materials influences the quality of Ta_3N_5 *via* oxidation and consequent nitridation process at 850–1000 °C and revealed that application of Ta foil instead of Ta film deposited on fused silica caused the appearance of Ta-rich structure. *Secondly*, analogous to Ta_2O_5, deficient Ta_3N_5 also can be obtained *via* vapor phase synthesis approaches that enables very precise control not only over its chemical composition but also allow to manage various structural and morphological features such as film thickness and its quality including roughness, appearance of pin holes, etc. Particularly, Hajibabaei et al.

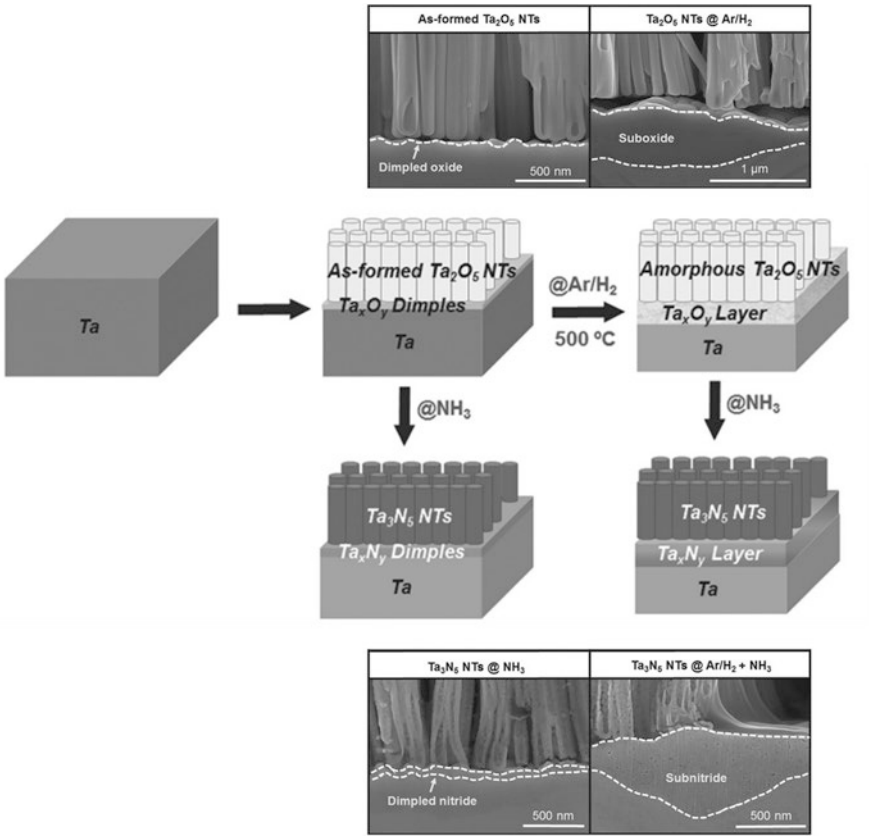

Fig. 7.3 Schematic illustration of the synthesis process for Ta_2O_5 NTs and Ta_3N_5 nanotubes (NTs) and accompanied SEM cross-sectional images of as-formed Ta_2O_5 NTs, Ta_2O_5 NTs in Ar/H_2, Ta_3N_5 NTs, and Ta_3N_5 NTs in Ar/H_2. (Adapted from Ref. [7] with permission from *John Wiley and Sons*. Copyright 2016)

[33] demonstrated fabrication of Ta_3N_5 film filled with nitrogen vacancies and reduced Ta sites *via* atomic layer deposition using $TaCl_5$ and ammonia as precursors. One should notice that the temperature inside reaction chamber was set to be 550 °C which is relatively high for the ALD processing and might not be suitable for some specific substrates, and this appeared to be a serious drawback. Even though the lower deposition temperature can be applied using different precursor, it is not clear whether it facilitates the formation of structural defects in desirable range or in a form of uncontrollable internal species. *Thirdly*, thermal nitridation process using NH_4Cl and Ta metal can be considered as an attractive alternative to the ammonia-supported approach as it requires much softer conditions of treatment and application of more accessible chemicals. As it was evidenced by Xiang et al. [34], its utilization leads to appearance of nitrogen-deficient interlayers randomly distributed within the stoichiometric Ta_3N_5.

Post-synthesis Protocol Compared with various binary oxide materials including Ta_2O_5 or TiO_2, where introduction of anion defects such as V_O can be reached *via* annealing in reducing atmosphere, for the nitrogen-based compounds it is more challenging to create conditions that favor the release of atoms from its surface. In fact, to the best of my knowledge, there is no available reports up to date where formation for N-deficient Ta_3N_5 was achieved during its consequent post-synthesis treatment. Following it, one might consider that the most practical method to obtain the desired non-stoichiometric composition of this material is to regulate the conditions and parameters of its synthesis as currently it is the only available and practically realizable option.

7.2.3.3 TaON

Synthesis Protocol Formation of deficient TaON filled with O atoms resided in empty sites of N atoms despite its ternary composition has a lot of similarity to that of Ta_3N_5 as almost identical processing and methods are applied to implement the desired changes in their both stoichiometries. *Firstly*, thermally activated nitridation of Ta_2O_5 or Ta-base materials in ammonia is widely utilized. To be clear, for obtaining TaON, but not Ta_3N_5, the conditions of this treatment should satisfy the following requirements: lower temperature (<850 °C), shorter treatment (<10 h), and reduced NH_3 gas flow (<20 mL min^{-1}) [35]. Surely, precise parameters are fully dependent on specific and individual criterion of defined processing. For example, one should be aware that obtained structure is required to show absence of Ta-oxide traces (conditions of treatment cannot be too soft) and at the same time to be free from any traces of Ta_3N_5 nucleation (conditions of treatment cannot be too harsh). Thus, it is clear that formation of TaON and adjusting its stoichiometry could only be achieved in a very narrow range of nitridation parameters. In fact, it is often the case that changes in the specifications of precursor compound might provide more reliable and efficient tool to correct the range of obtained chemical compositions. For instance, Feng et al. [36] demonstrated perfect application of this strategy as by varying only the amount of Ta_2O_5 starting materials it was possible to adjust the N:O ratio in synthesized TaON with impressive accuracy. It is interesting that conditions of thermally activated nitridation were constantly kept at 850 °C, 15 h, and 20 mL min^{-1}. *Secondly*, non-stoichiometric TaON also can be achieved *via* vapor synthesis approach. As various parameters of this processing such as temperature inside reaction chamber, pressure, and flow rate of utilized precursors or other related parameters can be adjusted, it is possible to obtain defined chemical composition without applying extreme conditions that can damage its morphology and structure and also influence the choice of substrate as it was in case of Ta_3N_5. Particularly, Cho et al. [37] used metalorganic low pressure chemical vapor deposition to prepare TaON film by employing pentaethoxytantalum ($Ta(OC_2H_5)_5$) and NH_3 as precursors at temperatures from 375 to 500 °C. It was revealed that with the higher flow of NH_3, the concentration of O decreases consequently, and it might be interpreted as to lowering the potential number of newly generated O_N defects. In

turn, formation of TaO_xN_y structures is also possible *via* PVD techniques such as reactive magnetron sputtering which provides great flexibility in adjusting the stoichiometry ranging from Ta_2O_5 to Ta_3N_5 [38]. *Thirdly*, it is possible to anneal Ta_3N_5 in oxidizing atmosphere in order to make it become transformed into TaON as it was demonstrated by Dabirian et al. [39] who utilized Ar/O_2 flowing ambient at temperature of 800 °C to realize this step. In this case, similar to nitridation, various conditions of this treatment can be used to adjust precisely the ratio of N:O. Yet, it is considered as future perspective since up to date there is the absence of any available report that shows the success of this approach.

Post-synthesis Protocol Given that fabrication and structure of TaOH has high resemblance to that of Ta_3N_5, the similar commentary used for the latter compound regarding the development and application of consequent post-synthesis treatment protocol to create defective compositions can be as well applied to the former structure given that for today this topic is rarely demonstrated and discussed in literature. It means that as there is no current standard or milestone which can take the role of guidance where the efforts should be applied, various approaches can be suggested for the initiating and development of this direction as to push forward the required changes in chemical composition of TaON since in absence of any results, negative or positive, the only restriction would be how applicable they are. For example, thermal treatment of fabricated and fully stoichiometric compounds in nitrogen-poor (oxygen-rich) or nitrogen-rich (oxygen-poor) atmosphere might be proceeded. In turn, reduction using various chemicals also is considered as a great alternative and possible course of expected action.

7.2.4 Properties of Defective Ta_2O_5, Ta_3N_5, and TaON

7.2.4.1 Structural Properties

Tantalum Pentoxide (Ta_2O_5) Formation of defects in Ta_2O_5, particularly V_O, results in certain adjustment of its structural characteristics which are described as follows: *Firstly*, even though changes in the rearrangement/relaxation of near-neighbor atoms due to appearance of vacancy were clearly identified theoretically *via* various simulation approaches [13, 14], experimental evidences revealed that generally the main parameters of crystal lattice remained relatively similar in both stoichiometric and non-stoichiometric Ta_2O_5 as no related shift in position of peaks after analysis with X-ray diffraction [16] or increasing/decreasing of interplanar distances during high-resolution transmission electron microscopy analysis [30] was observed. *Secondly*, it was determined that introduction of V_O *via* thermal treatment in vacuum resulted in appearance of disorder layer with thickness of 1–2 nm similar to that observed in hydrogenated TiO_2 or ZnO [16]. *Thirdly*, existence of deliberately introduced defects in Ta_2O_5 leads to significant changes in morphology as its dimension and size distribution increase [16].

Tantalum Nitride (Ta_3N_5) Formation of defects in Ta_3N_5, particularly V_N and reduced Ta species, causes the appearance of specific changes in its structural characteristics which is summarized as follows: *Firstly*, in analogy with Ta_2O_5, insufficient presence of nitrogen might result in the appearance of 1–2 nm thick subnitride-based structures resided on the surface of Ta_3N_5. Their uniformity, continuity, stoichiometry, and level of disordering are fully dependent on the chemical composition of Ta-oxide precursor and its own deficiency [40]. *Secondly*, due to low displacement of Ta atoms as a result of V_N appearance, which was calculated to be only within ~1.7% [22], the experimental observation of any changes in Ta_3N_5 crystal lattice is hardly possible *via* conventionally used techniques such as X-ray diffraction or even HRTEM. For comparison, introduction of oxygen efficiency into ZnO causes outward relaxation up to ~23% [41] which can be easily detected.

Tantalum Oxynitride (TaON) Introduction of defects in TaON, particularly oxygen atoms substituting nitrogen, leads to development of specific changes in its structural characteristics which can be outlined as follows: *Firstly,* given that oxygen atomic radii are smaller than that of nitrogen, formation of O_N antisites results in development of positive shift in position of XRD peaks which is defined as shrinkage of crystal lattice. Thus, the lower the stoichiometry of nitrogen, the more evident the shift [36]. *Secondly*, it was discovered that increasing of oxygen content in TaON, which also can be interpreted as higher deficiency of nitrogen, leads to lowering the level of overall surface roughness [38].

7.2.4.2 Optical Properties

Tantalum Pentoxide (Ta_2O_5) Introduction of oxygen vacancies into Ta_2O_5 results in significant improvement of its optical characteristics as absorption in visible spectra is increased in parallels along with reduced the band gap. It determines that more photons with wider range of energies could be consumed. Specifically, Zhu et al. [30] revealed that while pristine Ta_2O_5 enables to utilize only 10.6% of solar spectra, after release of oxygen atoms due to Al-assisted reduction this value increased to over 40%, and its continuous advancement follows the treatment temperature. Another particularity of oxygen-deficient Ta_2O_5 is that it changes color from white to gray in the manner very similar to that observed for TiO_2 and ZnO in the previous chapters.

Tantalum Nitride (Ta_3N_5) As it was shown by Wang et al. [7], combination of Ta_3N_5 with subnitrides results in highly improved absorption of visible light, while band gap remains relatively the same. Furthermore, it was also reported that changing the ratio of these subnitrides with respect to main Ta_3N_5 phases and playing with their geometrical configuration also can be used to increase the overall sensitivity toward irradiation with visible and UV spectra [40]. Yet, the significance and level of this improvement depend on many factors, and precise tuning of various morphological features is required to achieve the best outcome. In turn, theoretical calculation

of self-defective Ta_3N_5 filled with Ta and N vacancies demonstrated that its band gap decreases from ~2.2 to 2.0 eV compared with its fully stochiometric counterpart [42]. It is interesting to notice that well-known optical absorption at around 720 nm that is often observed for Ta_3N_5 regardless of its structural and composition particularities and which is beyond its band gap, apart from its attribution to O impurities, also was determined to have certain relation with existence of V_N [23].

Tantalum Oxynitride (TaON) Playing with O/N ratio in TaON not only results in increase in overall absorption in parallels [36] (Fig. 7.4a) but also changes the width of band gap as dominated presence of oxygen or nitrogen leads to its increase or decrease, respectively [38]. Defined and specific adjustment of optical characteristics is dependent on the concrete experimental setup and also is influenced by the nature and chemical composition of original compound. Another particularity of defective TaON is that its color is very sensitive to variation of O/N ratio and can vary from green yellow to bright or orange yellow [36] (Fig. 7.4b, c).

7.2.4.3 Electronic Properties

Tantalum Pentoxide (Ta_2O_5) Formation of oxygen vacancies, in Ta_2O_5, has a crucial effect on electronic structure of its band gap since their presence leads to development of additional mid-energy levels and their concrete presence and location

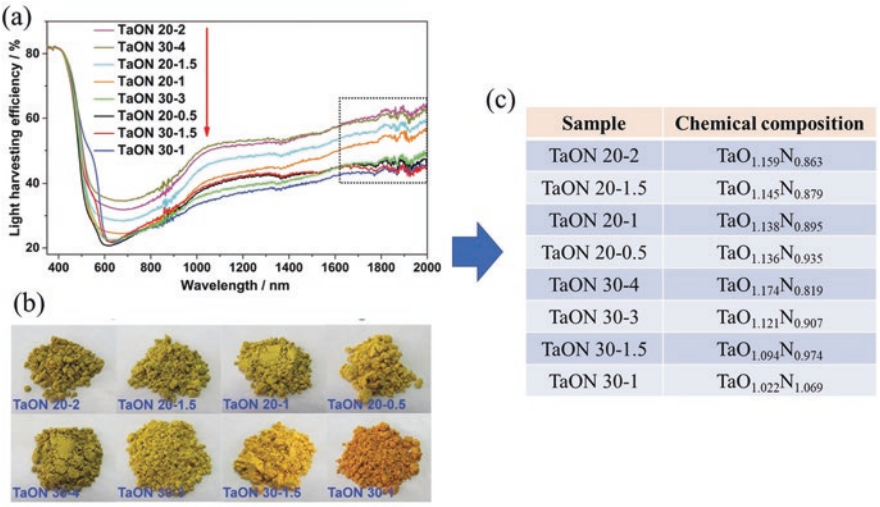

Sample	Chemical composition
TaON 20-2	$TaO_{1.159}N_{0.863}$
TaON 20-1.5	$TaO_{1.145}N_{0.879}$
TaON 20-1	$TaO_{1.138}N_{0.895}$
TaON 20-0.5	$TaO_{1.136}N_{0.935}$
TaON 30-4	$TaO_{1.174}N_{0.819}$
TaON 30-3	$TaO_{1.121}N_{0.907}$
TaON 30-1.5	$TaO_{1.094}N_{0.974}$
TaON 30-1	$TaO_{1.022}N_{1.069}$

Fig. 7.4 (**a**) Light harvesting efficiency spectra, (**b**) optical images, and (**c**) chemical composition of TaON samples prepared via nitridation of Ta_2O_5 with different parameters. For example, naming of sample as TaON 20-2 is designated that 2 g of Ta_2O_5 were thermally treated in a NH_3 which flow rate was kept at 20 mL min^{-1}. (Adapted from Ref. [36] with permission from *John Wiley and Sons*. Copyright 2019)

within the band gap are determined by geometrical configurations of V_O. As this defect is available in "in-plane" and "cap" arrangements, they result in appearance of (+2/0) transition level located at ~1.9 eV and ~3.5 eV, respectively, from VBM [13], and the later value is generally more recognizable in literature. As additional remark, it has to be noticed that appearance of this type of defect results in accompanied development of dangling bonds that enable the existence of multiscale additional energy states within the band gap which can be easily detected by various analysis such as PL spectroscopy [29]. In turn, the presence of other transition levels is also recognizable in the band gap of this materials; yet due to their unfavorable positions with respect to Fermi level and also with regard to formation energies of vacancies that create them, they deserve much less attention in literature. For example, "in-plane" vacancies can also exist in the form of −1 and +1 states; yet it only happened within very small region of Fermi level [13] and thus is seldom observable as it is not easy to obtain them.

Tantalum Nitride (Ta_3N_5) Introduction of nitrogen vacancies leads to generation of several energy levels located in the upper part of band gap depending on the localization of Fermi level and specific charge state of these defects. Particularly, it was identified that (+1/+2) and (+2/+3) transitions have deep donor characteristics, and they position almost in the middle of the band gap, while that of (0/+1) is located only ~0.16 eV from conduction band or even within it [22, 23]. In turn, the reduced Ta metal states in the form of Ta^{4+} and Ta^{3+} often tend to appear along with V_N as to compensate changes in geometrical and electronic configurations. They have their own defect states which are supposed to locate very deep inside band gap and thus only can act as recombination centers even though some authors debate it [43]. Apart from intrinsic defects, several words also need to be said about the presence of oxygen atoms in Ta_3N_5 as they have certain influence on the transitions of electrons in the band gap. It is generally accepted that they are considered to be unavoidable impurity in this material and their positioning is defined by substituting nitrogen atoms creating O_N antisites. Thus, they enable to create transition level (0/+1) which is located within only ~0.06 V from conduction band [22], and following it are considered to have shallow characteristics [44].

Tantalum Oxynitride (TaON) Theoretical simulation demonstrated that substitution of nitrogen with oxygen atoms which resulted in appearance of O_N antisites is determined to be the dominated defective formation in the TaON. Their presence leads to development of (0/+1) transition level located at 0.29 eV below the conduction band [25]. It allows to identify O_N as shallow donors that contribute significantly to the origin of n-type conductivity. Thus, increased O/N ratio gradually pushes up the Fermi level [36]. It is suggested that narrowing of TaON band gap due to increased presence of O_N defect often observed in literature might be attributed to lowering of conduction band as a result of increasing its width *via* formation of transition level-supported band tail. Yet, additional experimental verification is necessary to confirm it. As for the other defects and influence of their appearance on the structure of band gap, it was revealed that V_O and V_N initiate the presence of (0/+2)

and (+1/+3) transitions at 0.50 eV and 0.65 eV below the CBM, respectively [25], which make them to be referred as deep donors that are unable to provide electrons and only serve as compensation centers for acceptor-like defects.

7.2.4.4 Electrical Properties

Tantalum Pentoxide (Ta_2O_5) As oxygen vacancies have clearly defined donor-like characteristics and given that transition levels associated with them are located relatively close to conduction band, it is expected that their presence in Ta_2O_5 might result in increased density of free charge carriers and improved electrical characteristics. This supposition was perfectly proved by Perevalov et al. [45] who accessed current-voltage characteristic of non-stochiometric Ta_2O_5 *via* both theoretical and experimental approaches. It was revealed that lowering the oxygen content leads to almost proportional increase in the strength of electrical current at fixed field. Definitely, positions of these defects and their concentration also play a crucial role as under certain conditions they might become annihilation centers for charge carriers thus greatly reducing their presence and transportation characteristics which inevitably cause an overall declining of conductivity.

Tantalum Nitride (Ta_3N_5) Introduction of nitrogen vacancies with defined charge state or oxygen substitutional plays a highly positive role in increasing the electrical properties of Ta_3N_5 *via* strengthening of its n-type conductivity as they enable to create transition level close to conduction band and thus assisting in increased supply of electrons toward it. In turn, Ta-reduced species such as Ta^{3+} and Ta^{4+} also are considered to have donor-like nature; yet, as their transition levels are located almost in the middle of band gap, they are identified to be deep defect [44]. Thus, their contribution to the increase conductivity is only limited by serving as compensation centers. In turn, they also can play a negative role by causing the trapping and consequent recombinations of available charge carriers thus affecting their concentration and accessibility. As additional remark, it is also necessary to notice that introduction of Ta vacancies results in lowering the density of states around Fermi level which leads to reducing overall conductivity and appearance of insulating characteristics [24].

Tantalum Oxynitride (TaON) Similar to Ta_3N_5, in TaON transition level created by O_N antisites are located closest to conduction band compared with that of other related defect such as nitrogen or oxygen vacancies. Thus, they enable to make significant contribution to the strengthening of natural n-type conductivity by increasing the concentration and presence of free charge carriers. Following it, one could assume that the more the O_N formed and the higher the deficiency of nitrogen that initiates them, the more evident the advancement of TaON electrical characteristics [36]. It is interesting that theoretical estimation demonstrated by Chen et al. [25] predicted difficulty in p-type doping of this material as with shifting the Fermi

level toward valence band, the formation energy of O_N becomes negative which represents their spontaneous and uncontrollable generation. Given its donor-like characteristics, newly introduced positively charge carriers would be easily neutralized.

7.2.5 Application of Defective Ta_2O_5, Ta_3N_5, and TaON as Photocatalyst

7.2.5.1 Brief Overview

Due to their exceptional properties and relative availability, Ta_2O_5, Ta_3N_5, and TaON are considered to be an attractive alternative to well-known and widely utilized materials such as TiO_2, ZnO, etc. in terms of their efficient application in various photocatalytic processing including decomposition of dangerous pollutant in water, hydrogen production, CO_2 reduction, etc. For example, Ta_3N_5 and TaON enable the absorption of visible light, while Ta_2O_5 has high chemical and mechanical sustainability. In addition, position of band gaps with respect to vacuum level suits perfectly the reduction and oxidation potentials associated with most of chemical reactions. Yet, full and successful implementation of these materials might be restricted by certain particularities of their compositions and related characteristics that need to be addressed properly in order to make them become widely accessible. As an illustration, despite its readily accepted optical properties, Ta_3N_5 and TaON can be subjected to photocorrosion that leads to decline of their performance with prolonged time. Meanwhile, their practically measured performance is far beyond that predicted *via* theoretical simulation. It might be suggested that extremely high recombination rate of photoinduced charge carriers is one of the reasons to this unexpected outcome as it results in lower supply of surface with them and thus limits the activation of adsorbed molecules. In turn, Ta_2O_5 can only absorb UV light, and this unable to fully use solar spectra.

Numerous attempts have been applied to overcome these problems including decoration with noble metal, co-catalyst immobilization, and controlled faceting. In this regard, intrinsic defect engineering is determined to be a highly attractive alternative to them as it enables to alter properties and characteristics of Ta-based materials through modification of their own compositional structure without use of any external materials or chemicals. As it was shown above, these changes can address their most basic problems such as increasing the concentration of available charge carriers, enhancing their separation existences, lowering the band gap, and/or extending the absorption profile thus making the utilization of more light to be possible, increasing the stability and reliability, etc. Overall, it leads to higher rate of redox reactions and improved efficiency of photocatalytic processing. More detailed discussion related to application of defective Ta-based materials is provided below.

7.2.5.2 Photocatalytic and Photoelectrochemical Water Splitting

Production of hydrogen using light-supported water splitting process is identified to be the most attractive and desired method to address current requirements in consumption of energy due to its substantiality and environmental friendliness. It was generally accepted that band gap positions of Ta-based materials well suit both reduction and oxidation potentials of this processing even though Ta_3N_5 and TaON might not always be able to initiate both of them in a simultaneous manner given that additional impurities or unregistered species and states might exist within their structures which shift the conduction or valence bands toward undesirable directions making them become allocated beyond the required energies. The development of controlled deficiency can greatly address these problems. *Firstly*, it results in sufficiently increased efficiency of water splitting reaction leading to enhanced outcome of hydrogen yield compared with that of fully stoichiometric sample. For instance, Liu et al. [16] demonstrated that Ta_2O_5 filled with V_O formed *via* vacuum-supported thermal treatment exhibited 48% higher H_2 generation rate than that of original Ta_2O_5 (22.2 μmol/g vs. 15.0 μmol/g per hour) under illumination with Xe lamp (Fig. 7.5a). Furthermore, the stability of defective Ta_2O_5 was also tested by cycling test, and very good repetition of hydrogen production within 12 h was observed (Fig. 7.5b). In turn, playing with ratio of O/N in TaON could increase the

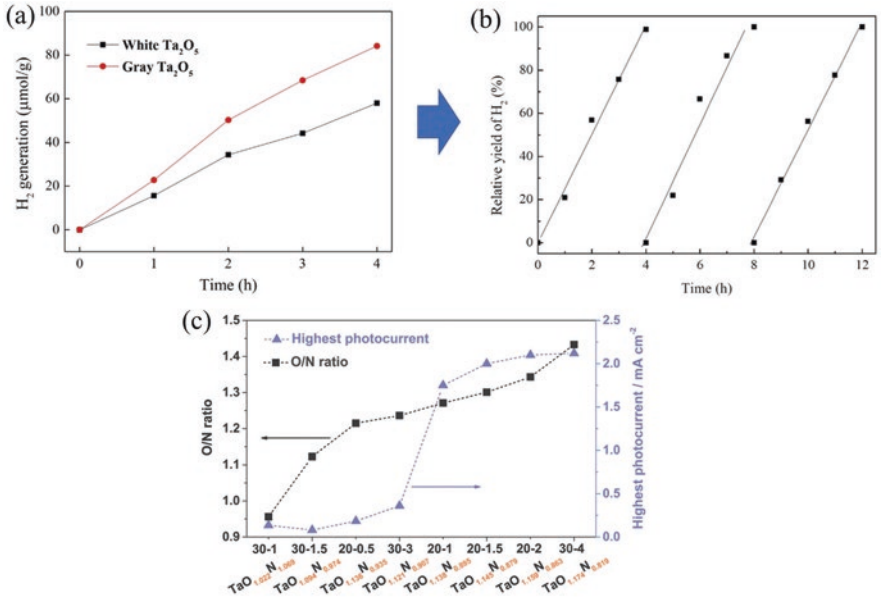

Fig. 7.5 (**a**) Hydrogen generation rates under 300 W Xe lamp irradiation in the presence of white- and oxygen-deficient (gray) Ta_2O_5. (**b**) Cycling test of oxygen-deficient (gray) Ta_2O_5 under 300 W Xe lamp irradiation for 12 h. (Reprinted from Ref. [16] with permission from *Elsevier*. Copyright 2020) (**c**) O/N ratios and highest photocurrents for TaON photoanodes. The elemental analysis results are given below the corresponding TaON samples. (Reprinted from Ref. [36] with permission from *John Wiley and Sons*. Copyright 2019)

photocurrent more than in 1.5 times [36] (Fig. 7.5c). *Secondly*, introduction of controlled deficiency enables to make the realization of overall water splitting process possible regardless of initial composition. This concept can be readily illustrated using work of Nurlaela et al. [40] as an example. It was revealed that the presence of amorphized TaN layer with thickness of 1–2 nm on surface of Ta_3N_5 prepared through nitridation of Ta_2O_5 precursor determines the reliability of photocatalytic hydrogen evolution. Simply to say, once this layer is absent or positioned as randomly distributed island configuration, splitting of water is limited only by the production of oxygen, while the reduction reaction was revealed to be utterly unavailable. In turn, their continuous and uniform arrangement results in clearly detectable appearance of hydrogen as a final product. As a final word, it is necessary to say that not absolutely all intrinsic defects formed in target materials could contribute to the enhanced performance, as some of them might play an opposite role, i.e., significantly lowering it. This recognition is mostly determined by the position of transition or energy levels in band gap which accompany the formation of each particulate type of defects. For example, according to Fu et al. [44], reduced Ta metallic states in Ta_3N_5 form deep states centered at ~0.64 eV from conduction band that lay below the water reduction potential, and thus electron trapped there is unable to be part of this reaction. Thus, it becomes recombined which negatively influence the outcome of hydrogen production.

7.2.5.3 Light-Induced Water Purification

Light-induced water purification usually is reached *via* degradation of dyes using proper photocatalysis that causes their transformation into various non-hazardous compounds such as carbon dioxide. It is a highly promising approach to resolve the problem of clean water worldwide. Defective Ta-based materials due to their unique characteristics and features can become a promising solution for the improvement and stabilization of this proceeding and its outcome. Furthermore, compared with hydrogen production, photocatalytic reaction associated with dye degradation has much higher chances to be properly addressed as it can be easily performed under visible light and with higher effectiveness since the alignment of energies and positioning of conduction of valence bands including the formation of defect-induced transition levels within them require much less restrictions and requirements with regard to relevant redox potentials. For example, Zhu et al. [30] demonstrated that Al-reduced oxygen-deficient Ta_2O_5 nanowires enable to greatly enhance the degradation of methylene blue under illumination of Xe lamp with cut-off filter ($\lambda > 420$ nm). The removal efficiency was estimated after 2 h of testing and equaled to ~35% and 5% for non-stoichiometric and stochiometric Ta_2O_5, respectively, which equaled to nearly sevenfold improvement (Fig. 7.6a). It is interesting to notice that increased temperature of reduction, i.e., higher oxygen deficiency in Ta_2O_5, resulted in gradual improvement of dye degradation rate. In turn, when full solar spectra were used and the dye was changed to methylene orange (MO), the difference in efficiency to remove it by both defective and defectless structures

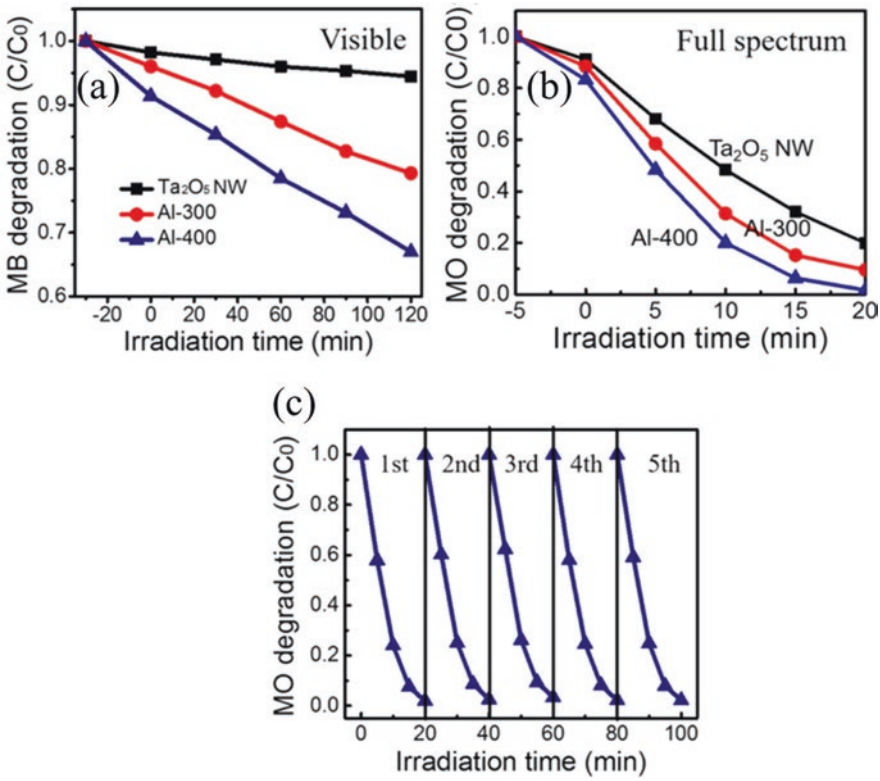

Fig. 7.6 (**a**) Visible-light-driven photodegradation of methyl blue (MB) and (**b**) full-spectrum solar-driven photodegradation of aqueous methylene orange (MO) in the presence of the original and Al-reduced Ta_2O_5. (**c**) Cycling tests of solar-driven MO photodegradation over the Al-400 sample. The number after word "Al" means the temperature of reduction. (Reprinted from Ref. [30] with permission from *American Chemical Society*. Copyright 2016)

lowered down and reached the maximum value of only ~2.5 times (Fig. 7.6b). The MO degradation cycling tests demonstrate that the V_O-Ta_2O_5 has very stable activity in five photodegradation cycles (Fig. 7.6c).

7.2.5.4 Photoconversion of CO_2

Photocatalytic conversion of CO_2 *via* reaction with water is a highly attractive approach not only to significantly reduce its concentration in the atmosphere but also to make it serve as a source of various valuable carbon-neutral raw materials for chemical industry. Band gap positions of Ta_2O_5, Ta_3N_5, and TaON perfectly match both potentials of CO_2 reduction (into various compounds) and water oxidation making them very promising candidates to utilize an efficient photocatalyst. Yet, currently, most of studies regarding them in terms of applications in these reactions

are concentrated on investigation of their fully stoichiometric composition. To be clear, it is generally believing that the presence of defects might play a negative role in efficiency of Ta materials serving the role of recombination centers for charge carriers. Thus, it is often the case that their deliberate removal is identified to be the main reason of improved outcome in light-induced CO_2 reduction [46]. Yet, this strategy is hardly to be considered as perfect since ideal structure is unavailable in any way and defects are always present there, i.e., their existence cannot be fully eliminated and, moreover, ignored. Thus, in a manner similar to that applied for water splitting and dye degradation ascribed above, it is believed that proper managements and adjustment of their concentration, distribution, and, most importantly, nature might become an attractive approach that can boost further the current limits of CO_2 photoconversion. The following reasons are used to justify this conclusion. *Firstly*, defects play a significant role in governing the transport of charge carriers toward surface by increasing their separation rate, providing additional electrons, etc. S*econdly*, in analogy to TiO_2 and ZnO, defects enable to act as adsorption and activation spots for CO_2 molecules thus enhancing the rate of overall photoconversion reaction. For example, Muraoka et al. [47] investigated Ta_3N_5 prepared via nitridation of Ta_2O_5 with various temperatures. It was discovered that the best photocatalyst for CO_2 reaction was received as very moderate conditions as they lead to incomplete fulfillment of Ta_3N_5 with N atoms and also causes the presence of residual oxygen. Needless to say, both of them create donor-like energy levels within band gap that position is considered to be shallow and thus leads to sufficient contribution into enhanced conductivity.

7.2.5.5 Current Challenges and Future Perspectives

Application of defect engineering to modify Ta-based materials including Ta_2O_5, Ta_3N_5, and TaON for application in various photocatalytic processing only recently begins to deserve specific and increased attention of scientific community as it was recognized that their controlled introduction under strictly defined conditions might initiate the appearance of additional, unexpected yet highly desirable features or strengthening of already existed ones which might seriously influence their effectiveness. For instance, Ta_2O_5 suffers from inability to be sensitive toward visible light; yet with presence of oxygen vacancies, the width of band gap becomes greatly reduced making the absorption edge to be shifted toward higher wavelength accompanied by overall increase in sensitivity. However, there are several challenges which need to be overcome as to make these materials available, recognizable, and most importantly accessible at last in a level equaled to that of ZnO and TiO_2 discussed above. *Firstly*, it is necessary to acquire the proper knowledge and information regarding them in terms of their defective structure and composition that can be used to determine the direction in which their specific characteristics and properties can be developed following the most basic and fundamental principles of defect engineering. To be clear, currently available data generally speaking is insufficient and partially incomplete. Furthermore, it suffers from certain contradiction and thus

often provides additional difficulties to analyze it and predict the expected photocatalytic response. Taking Ta-reduced states as illustration, one can notice that according to reports in literature, its presence can influence positively on photocatalytic activity of Ta-based materials [43], or oppositely, they serve as deep donors [44] which lower the efficiency. *Secondly*, in terms of reported and investigated applications toward using defective Ta-based materials in certain photocatalytic reactions, there is also a huge gap. As it was mentioned above, water splitting and dye degradation have deserved very considerable attention as they are covered at certain extent, while, for example, CO_2 production was discussed in much less if any range. As for other processing such as nitrogen fixation or oxidation/reduction of certain compounds, to find information about them might become a very challenging task as their proper investigation is only expected. It can be explained by the fact that utilization of defective Ta-materials as a photocatalytic material is a very novel and recently discovered topic which proper development is only considered. It has a great potentiality, and thus more investigations are expected to appear.

7.3 Final Remarks About Defective Ta_2O_5, Ta_3N_5, and TaON

The future of photocatalytic processing can be easily and even eagerly connected with Ta-based materials as they offer a variety of properties that other related semiconductors cannot provide. It includes positioning of their band gaps which allows to easily perform redox reactions of the most demanding and challenging processing including water splitting and CO_2 conversion. Furthermore, Ta_3N_5 and TaON are sensitive to the visible light which enables to utilize sufficient part of solar spectra, while Ta_2O_5 demonstrates great chemical and mechanical stabilities which make it functional for a long period of time. Yet, as any other materials, they have a very defined disadvantages and drawbacks which decrease the efficiency of their applications making it become much lower than that predicted by theoretically developed simulation models. Defect engineering can address these problems effectively as it provides great opportunity to modify their chemical composition and structural/morphological characteristics via simple rearrangement of atomic positioning in periodical lattice and proper adjustment of consequent relaxation which inevitably lead to dramatic changes in their geometrical and electronic configurations. Despite apparent easiness of this approach as, for example, to create vacancy, it is only enough to remove atoms of designated elements, with regard to Ta_2O_5, Ta_3N_5, and TaON, it is a very difficult and even challenging task given that knowledge about formation of defects in these materials is only in the beginning of acquiring process, and many aspects regarding their specific particularities and influences remained unknown as they are covered within partial accessibility or only are available via theoretical approach. Thus, for complete and more thorough clarification, additional experimental confirmation is strongly required. In this regard, it is suggested that the future of defected Ta-based materials seems very bright given that already in the beginning of their development and consequent progression they enable to show

very impressive outcome in terms of their applications in various photocatalytic reactions as well as in demonstrating more advanced characteristics. Yet, there is still very long way ahead to make the expected modification follow certain pathways and designated roadmap in order to be sure that the achieved outcome would reach defined expectations and thus become readily and easily accessible.

References

1. Y. Yang, Y. Kawazoe, Prediction of new ground-state crystal structure of Ta_2O_5. Phys. Rev. Mater. **2**, 034602 (2018). https://doi.org/10.1103/PhysRevMaterials.2.034602
2. W.-S. Liu, S.-H. Huang, C.-F. Liu, C.-W. Hu, T.-Y. Chen, T.-P. Perng, Nitrogen doping in Ta_2O_5 and its implication for photocatalytic H_2 production. Appl. Surf. Sci. **459**, 477–482 (2018). https://doi.org/10.1016/j.apsusc.2018.07.185
3. J. Ni, M. Sun, Chapter nine – Anodic tantalum oxide: Synthesis and energy-related applications, in *Nanostructured Anodic Metal Oxides*, ed. by G. D. Sulka, (Elsevier, 2020), pp. 305–319. https://doi.org/10.1016/B978-0-12-816706-9.00009-1
4. E. Nurlaela, M. Harb, S. del Gobbo, M. Vashishta, K. Takanabe, Combined experimental and theoretical assessments of the lattice dynamics and optoelectronics of TaON and Ta_3N_5. J. Solid State Chem. **229**, 219–227 (2015). https://doi.org/10.1016/j.jssc.2015.06.029
5. M. Rudolph, D. Stanescu, J. Alvarez, E. Foy, J.-P. Kleider, H. Magnan, T. Minea, N. Herlin-Boime, B. Bouchet-Fabre, M.-C. Hugon, The role of oxygen in magnetron-sputtered Ta_3N_5 thin films for the photoelectrolysis of water. Surf. Coat. Technol. **324**, 620–625 (2017). https://doi.org/10.1016/j.surfcoat.2016.09.007
6. E. Nurlaela, A. Ziani, K. Takanabe, Tantalum nitride for photocatalytic water splitting: Concept and applications. Mater. Renew. Sustain. Energy **5**, 18 (2016). https://doi.org/10.1007/s40243-016-0083-z
7. L. Wang, X. Zhou, N.T. Nguyen, I. Hwang, P. Schmuki, Strongly enhanced water splitting performance of Ta_3N_5 nanotube photoanodes with subnitrides. Adv. Mater. **28**, 2432–2438 (2016). https://doi.org/10.1002/adma.201505312
8. T. Lüdtke, A. Schmidt, C. Göbel, A. Fischer, N. Becker, C. Reimann, T. Bredow, R. Dronskowski, M. Lerch, Synthesis and crystal structure of δ-TaON, a metastable polymorph of tantalum oxide nitride. Inorg. Chem. **53**, 11691–11698 (2014). https://doi.org/10.1021/ic501726m
9. H. Schilling, A. Stork, E. Irran, H. Wolff, T. Bredow, R. Dronskowski, M. Lerch, γ-TaON: A metastable polymorph of tantalum oxynitride. Angew. Chem. Int. Ed. **46**, 2931–2934 (2007). https://doi.org/10.1002/anie.200604351
10. W. Dang, H. Chen, N. Umezawa, J. Zhang, Electronic structures of anatase $(TiO_2)_1-x(TaON)x$ solid solutions: A first-principles study. Phys. Chem. Chem. Phys. **17**, 17980–17988 (2015). https://doi.org/10.1039/C5CP02110C
11. A. Fuertes, Nitride tuning of transition metal perovskites. APL Mater. **8**, 020903 (2020). https://doi.org/10.1063/1.5140056
12. Y. Xiao, C. Feng, J. Fu, F. Wang, C. Li, V.F. Kunzelmann, C.-M. Jiang, M. Nakabayashi, N. Shibata, I.D. Sharp, K. Domen, Y. Li, Band structure engineering and defect control of Ta_3N_5 for efficient photoelectrochemical water oxidation. Nat. Catal. **3**, 932–940 (2020). https://doi.org/10.1038/s41929-020-00522-9
13. R. Ramprasad, First principles study of oxygen vacancy defects in tantalum pentoxide. J. Appl. Phys. **94**, 5609–5612 (2003). https://doi.org/10.1063/1.1615700
14. Y. Yang, O. Sugino, Y. Kawazoe, Exceptionally long-ranged lattice relaxation in oxygen-deficient Ta_2O_5. Solid State Commun. **195**, 16–20 (2014). https://doi.org/10.1016/j.ssc.2014.06.021

15. Y. Yang, H.-H. Nahm, O. Sugino, T. Ohno, Electronic structures of oxygen-deficient Ta_2O_5. AIP Adv. **3**, 042101 (2013). https://doi.org/10.1063/1.4800899
16. W.-S. Liu, M.-W. Liao, S.-H. Huang, Y.I.A. Reyes, H.-Y. Tiffany Chen, T.-P. Perng, Formation and characterization of gray Ta_2O_5 and its enhanced photocatalytic hydrogen generation activity. Int. J. Hydrog. Energy **45**, 16560–16568 (2020). https://doi.org/10.1016/j.ijhydene.2020.04.154
17. R. Ramprasad, M. Sadd, D. Roberts, T. Remmel, M. Raymond, E. Luckowski, S. Kalpat, C. Barron, M. Miller, Oxygen vacancy defects in tantalum pentoxide: A density functional study. Microelectron. Eng. **69**, 190–194 (2003). https://doi.org/10.1016/S0167-9317(03)00296-X
18. Y. Guo, J. Robertson, Oxygen vacancy defects in Ta_2O_5 showing long-range atomic rearrangements. Appl. Phys. Lett. **104**, 112906 (2014). https://doi.org/10.1063/1.4869553
19. T.V. Perevalov, D.R. Islamov, I.G. Chernykh, Atomic and electronic structures of intrinsic defects in Ta_2O_5: Ab initio simulation. JETP Lett. **107**, 761–765 (2018). https://doi.org/10.1134/S0021364018120111
20. L. Zhu, J. Zhou, Z. Guo, Z. Sun, Synergistic resistive switching mechanism of oxygen vacancies and metal interstitials in Ta_2O_5. J. Phys. Chem. C **120**, 2456–2463 (2016). https://doi.org/10.1021/acs.jpcc.5b11080
21. J.J. Bown, A.J. Page, Vacancy diffusion barriers in TaON and Ta_3N_5 water-splitting photocatalysts. J. Mater. Chem. A **7**, 13029–13035 (2019). https://doi.org/10.1039/C9TA02280E
22. T. Jing, Y. Dai, X. Ma, W. Wei, B. Huang, Effects of intrinsic defects and extrinsic doping on the electronic and photocatalytic properties of Ta_3N_5. RSC Adv. **5**, 59390–59397 (2015). https://doi.org/10.1039/C5RA08563B
23. J. Wang, A. Ma, Z. Li, J. Jiang, J. Feng, Z. Zou, Unraveling the mechanism of 720 nm sub-band-gap optical absorption of a Ta_3N_5 semiconductor photocatalyst: A hybrid-DFT calculation. Phys. Chem. Chem. Phys. **17**, 8166–8171 (2015). https://doi.org/10.1039/C4CP04931D
24. C. Stampfl, A.J. Freeman, Metallic to insulating nature of TaN: Role of Ta and N vacancies. Phys. Rev. B **67**, 064108 (2003). https://doi.org/10.1103/PhysRevB.67.064108
25. S. Chen, L.-W. Wang, Intrinsic defects and electronic conductivity of TaON: First-principles insights. Appl. Phys. Lett. **99**, 222103 (2011). https://doi.org/10.1063/1.3664346
26. W. Fu, P. Zhuang, M. OliverLam Chee, P. Dong, M. Ye, J. Shen, Oxygen vacancies in Ta_2O_5 nanorods for highly efficient electrocatalytic N_2 reduction to NH_3 under ambient conditions. ACS Sustain. Chem. Eng. **7**, 9622–9628 (2019). https://doi.org/10.1021/acssuschemeng.9b01178
27. R.H. Zhang, T.S. Zhao, M.C. Wu, H.R. Jiang, L. Zeng, Mesoporous ultrafine Ta_2O_5 nanoparticle with abundant oxygen vacancies as a novel and efficient catalyst for non-aqueous Li-O_2 batteries. Electrochim. Acta **271**, 232–241 (2018). https://doi.org/10.1016/j.electacta.2018.03.164
28. K. Skaja, M. Andrä, V. Rana, R. Waser, R. Dittmann, C. Baeumer, Reduction of the forming voltage through tailored oxygen non-stoichiometry in tantalum oxide ReRAM devices. Sci. Rep. **8**, 10861 (2018). https://doi.org/10.1038/s41598-018-28992-9
29. R.S. Devan, W.-D. Ho, C.-H. Chen, H.-W. Shiu, C.-H. Ho, C.-L. Cheng, S.Y. Wu, Y. Liou, Y.-R. Ma, High room-temperature photoluminescence of one-dimensional Ta_2O_5 nanorod arrays. Nanotechnology **20**, 445708 (2009). https://doi.org/10.1088/0957-4484/20/44/445708
30. G. Zhu, T. Lin, H. Cui, W. Zhao, H. Zhang, F. Huang, Gray Ta_2O_5 nanowires with greatly enhanced photocatalytic performance. ACS Appl. Mater. Interfaces **8**, 122–127 (2016). https://doi.org/10.1021/acsami.5b07685
31. H. Chen, G. Feng, W. Fan, J. Han, Y. Li, Q. Lai, Laser plasma-induced damage characteristics of Ta_2O_5 films. Opt. Mater. Express **9**, 3132–3145 (2019). https://doi.org/10.1364/OME.9.003132
32. B.A. Pinaud, A. Vailionis, T.F. Jaramillo, Controlling the structural and optical properties of Ta_3N_5 films through nitridation temperature and the nature of the Ta metal. Chem. Mater. **26**, 1576–1582 (2014). https://doi.org/10.1021/cm403482s
33. H. Hajibabaei, D.J. Little, A. Pandey, D. Wang, Z. Mi, T.W. Hamann, Direct deposition of crystalline Ta_3N_5 thin films on FTO for PEC water splitting. ACS Appl. Mater. Interfaces **11**, 15457–15466 (2019). https://doi.org/10.1021/acsami.8b21194

34. Y. Xiang, B. Zhang, J. Liu, S. Chen, T. Hisatomi, K. Domen, G. Ma, A one-step synthesis of a Ta_3N_5 nanorod photoanode from Ta plates and NH_4Cl powder for photoelectrochemical water oxidation. Chem. Commun. **56**, 11843–11846 (2020). https://doi.org/10.1039/D0CC05044J
35. M. Xiao, S. Wang, S. Thaweesak, B. Luo, L. Wang, Tantalum (oxy)nitride: Narrow band-gap photocatalysts for solar hydrogen generation. Engineering **3**, 365–378 (2017). https://doi.org/10.1016/J.ENG.2017.03.019
36. J. Feng, H. Huang, T. Fang, X. Wang, S. Yan, W. Luo, T. Yu, Y. Zhao, Z. Li, Z. Zou, Defect engineering in semiconductors: Manipulating non-stoichiometric defects and understanding their impact in oxynitrides for solar energy conversion. Adv. Funct. Mater. **29**, 1808389 (2019). https://doi.org/10.1002/adfm.201808389
37. S.-L. Cho, B.-S. Kim, H.-M. Kim, I.K. Chun, K.-B. Kim, Metallorganic chemical vapor deposition of TaO_xN_y as a high-dielectric-constant material for next-generation devices. J. Electrochem. Soc. **149**, C529 (2002). https://doi.org/10.1149/1.1507786
38. S.T. Bah, C.O.F. Ba, M. D'Auteuil, P.V. Ashrit, L. Sorelli, R. Vallée, Fabrication of TaO_xN_y thin films by reactive ion beam-assisted ac double magnetron sputtering for optical applications. Thin Solid Films **615**, 351–357 (2016). https://doi.org/10.1016/j.tsf.2016.07.055
39. A. Dabirian, H. van't Spijker, R. van de Krol, Wet ammonia synthesis of semiconducting N:Ta_2O_5, Ta_3N_5 and β-TaON films for photoanode applications. Energy Procedia **22**, 15–22 (2012). https://doi.org/10.1016/j.egypro.2012.05.222
40. E. Nurlaela, S. Ould-Chikh, M. Harb, S. del Gobbo, M. Aouine, E. Puzenat, P. Sautet, K. Domen, J.-M. Basset, K. Takanabe, Critical role of the semiconductor–electrolyte interface in photocatalytic performance for water-splitting reactions using Ta_3N_5 particles. Chem. Mater. **26**, 4812–4825 (2014). https://doi.org/10.1021/cm502015q
41. A. Janotti, C.G. Van de Walle, Oxygen vacancies in ZnO. Appl. Phys. Lett. **87**, 122102 (2005). https://doi.org/10.1063/1.2053360
42. M. Harb, L. Cavallo, J.-M. Basset, Major difference in visible-light photocatalytic features between perfect and self-defective Ta_3N_5 materials: A screened Coulomb hybrid DFT investigation. J. Phys. Chem. C **118**, 20784–20790 (2014). https://doi.org/10.1021/jp506066p
43. M. Zhang, P. Hou, Z. Wang, P. Kang, Nitrogen-doped Ta_2O_5 nanocomposites for the electrocatalytic reduction of carbon dioxide to CO with photoassistance. ChemElectroChem **5**, 799–804 (2018). https://doi.org/10.1002/celc.201701353
44. J. Fu, F. Wang, Y. Xiao, Y. Yao, C. Feng, L. Chang, C.-M. Jiang, V.F. Kunzelmann, Z.M. Wang, A.O. Govorov, I.D. Sharp, Y. Li, Identifying performance-limiting deep traps in Ta_3N_5 for solar water splitting. ACS Catal. **10**, 10316–10324 (2020). https://doi.org/10.1021/acscatal.0c02648
45. T.V. Perevalov, V.A. Gritsenko, A.A. Gismatulin, V.A. Voronkovskii, A.K. Gerasimova, V.S. Aliev, I.A. Prosvirin, Electronic structure and charge transport in nonstoichiometric tantalum oxide. Nanotechnology **29**, 264001 (2018). https://doi.org/10.1088/1361-6528/aaba4c
46. C. Zhou, J. Zhou, L. Lu, J. Wang, Z. Shi, B. Wang, L. Pei, S. Yan, Y. Zhentao, Z. Zou, Surface electric field driven directional charge separation on Ta_3N_5 cuboids enhancing photocatalytic solar energy conversion. Appl. Catal. B **237**, 742–752 (2018). https://doi.org/10.1016/j.apcatb.2018.06.036
47. K. Muraoka, J.J.M. Vequizo, R. Kuriki, A. Yamakata, T. Uchiyama, D. Lu, Y. Uchimoto, O. Ishitani, K. Maeda, Oxygen-doped Ta_3N_5 nanoparticles for enhanced Z-scheme carbon dioxide reduction with a binuclear ruthenium(II) complex under visible light. ChemPhotoChem **3**, 1027–1033 (2019). https://doi.org/10.1002/cptc.201900120

Chapter 8
Case Study IV: Defect Engineering of MoS_2 and WS_2

8.1 MoS_2 and WS_2: Fundamentals

Molybdenum Disulfide (MoS_2) Bulk MoS_2 is considered to be layered material where each layer is identified to have sandwich-like composition with thickness of only three atomic layers. They are composed of S-Mo-S sequences which existence and consequent assembly are associated with the presence of relatively weak Van der Waals forces. It enables the atomic planes to be properly arranged with respect to each other. As for more detailed description, in every such a layer, Mo atoms are connected to six S atoms, and the exact geometry of this configuration is determined by the type of crystal lattice. Following various experimental evidence available in literature [1], it was revealed that MoS_2 is defined by polytypism that regulates the appearance of three different forms of phases such as 1T, 2H, and 3R in which the digit stands for number of monolayers in the unit cell and the letters T, H, and R ascribe the structural symmetry which has trigonal, hexagonal, and rhombohedral compositions, respectively. In this regard, one has to notice that 1T phase ascribes the presence of Mo-S coordination as octahedral formation, while in 2H and 3R phases, it is represented in the form of trigonal prismatic [2]. The most thermodynamically stable arrangement out of these three are considered to be 2H and 3R phases which also existed naturally. They demonstrate evident semiconducting properties characterized by n-type conductivity. As for 1T phase, it is determined to be metastable compound that at relatively low temperature up to only 95 °C can be decomposed into 2H structure [3]. 1T phase shows clearly defined metallic behavior which is justified by the presence of crystal distortion. It has several polymorphs that are ascribed as 1T′, 1T″, and 1T‴ superstructures. Their dissimilarities are associated with the difference in specification of unit cells, i.e., whether Mo atoms are dimerized or trimerized [2]. It is highly debatable to ascertain which one of them is more thermodynamically favorable. As for the optical properties, bulk MoS_2 has indirect band gap equaled to ~1.2 eV that makes it unsuitable for performing any

V. Gurylev, *Nanostructured Photocatalyst via Defect Engineering*,
https://doi.org/10.1007/978-3-030-81911-8_8

photocatalytic processing. In turn, once its dimension is lowered down to mono- or several-layered structure that represents 2-D constitution, there appeared clearly defined confinement and long-range Coulomb effects which result in increasing the width of band gap up to ~1.8–1.9 eV and transforming it into direct type. In turn, these modifications are also followed by changing of color from absolutely black to yellow, green, or their various combinations and shades including bright yellow, green-yellow, etc. as it depends on the internal structure and chemical compositions. Accordingly, it was determined that positions of conduction and valence bands in 2-D MoS_2 can match redox potentials of certain photocatalytic processing such as water splitting or CO_2 conversion thus at certain conditions enabling their activation without using additional co-catalyst or combining with other semiconductors. Finally, this compound has great chemical stability, abundance, high carrier mobility, environmental friendliness, and relatively simple synthesis protocol. Thus, its attractiveness to initiate various reactions under solar light is evident.

Tungsten Disulfide (WS_2) Almost similar description of crystal structure also can be applied to WS_2 as this material is very comparable to that of MoS_2. *Firstly,* it is also available as of layered composition where each layer has thickness of three atomic planes, and it is presented in the sandwich-like architecture that has form of S-W-S. *Secondly*, this arrangement is associated with van der Waals forces that enable the distance between each layer to be ~0.65 nm [4]. *Thirdly,* the most stable appearance of W is trigonal prismatic which contributes to the formation of semiconducting 2H (1H) and 3R phases. In turn, WS_2 also has the octahedral coordination that is presented as metastable 1T phase. As for the optical properties, bulk WS_2 shows the value of band gap equaled to ~1.3 eV, and it appeared to have indirect type. Lowering the dimension of this materials results not only in gradually increasing its width which reaches ~2.0 eV for single monolayer but also transformating it into direct type [5]. Its typical composition as 2H phase has brown-yellow color, while realization of 1T phase makes it appear as gray-shaded formation [6]. The band gap position of WS_2 also greatly matches redox potentials of variolous photocatalytic reactions, thus making this material to be greatly an attractive alternative to well-known wide-band gap semiconductors.

Finally, several words need to be said about comparisons of both nanoscaled MoS_2 and WS_2 in terms of their chemical, electrical, electronic, and other characteristics. As tungsten is heavier than that of molybdenum, MoS_2 consequently has lower thermal, mechanical, and chemical stabilities. Theoretical estimation determined that 2-D WS_2 and specifically its monolayered structure are supposed to have greater charge transport characteristics than that of MoS_2 [7]. In fact, it has one of the highest electrons and hole mobilities among currently reported transition metal dichalcogenides [4]. By turn, several layered compositions have an opposite trend. Particularly, Kaushik et al. [8] demonstrated that position of Fermi level in WS_2 single-crystalline flakes is located deeper inside band gap than that of MoS_2 which means that lower concentration of negatively charge carriers is available and can be delivered to conduction band. Thus, while as-prepared MoS_2 was clearly defined as

strong n-type semiconductor, WS_2 for its part appeared to have its much weaker characteristics. In conclusion, one might notice that even though natural abundance of tungsten and molybdenum is relatively similar, the industrial adoption and usage of the latter currently is higher due to its applicability in various fields while having a lower availability of mineral resources. As a result, commercial attractiveness of WS_2 for future processing is more evident.

8.2 Intrinsic Defects in MoS_2 and WS_2

8.2.1 Introduction

Molybdenum and tungsten disulfides in the form of mono- or several-layered structure are considered to be greatly attractive materials that are successfully applied as photocatalysts given their sensitivity toward irradiation with visible light, perfect alignment of band gaps with respect to redox potentials of various reactions, and also highly adjustable properties and characteristics that accurately follow the changes in their dimensions, phases, etc. Yet, despite great perspectives, to completely realize the potentials of these materials and overcome any limit in acquiring the expected efficiencies and thus fully satisfy theoretically predicted expectations and outcome, certain drawbacks regarding them should be addressed properly. Particularly, it was reported that WS_2 and MoS_2 have extremely high excitation recombination ratio and also possess weak absorption capability toward irradiation with incident light [9]. It means that sufficient part of photons with required energies might simply avoid being captured. Furthermore, low dimensionality evidently leads to extremely high sensitivity toward alternation of internal structures as any even minor changes in surrounding environment such as non-ideality of synthesis or storage conditions, presence, and consequent unintended incorporation of various impurities whether in the form of metal or non-metallic compounds might lead to introduction of highly undesirable formations within these materials. It enables to break periodical atomic arrangement thus causing the appearance of localized regions filled with certain composition which existence could lead to the development of unpredicted phenomenon and appearance of very surprising findings. It is very not easy to achieve control over them as there might be a positive and negative outcome in terms of expected photocatalytic performance.

Following it, defect engineering can be considered as an attractive approach which provides collateral solution for mentioned above problems. To be clear, it enables to address most of drawbacks that have MoS_2 and WS_2 as processing and realization of defined chemical composition and certain crystal structure can be achieved via limited access and introduction of only desirable type of defects. In this regard, their particularities such as concentration, distribution, and localization are precisely adjustable as to make them serve only specific and desired role. In this regard, it would allow to reduce dependency on the unexpected changes of

surrounding conditions as it is believed that modified structure of MoS_2 and WS_2 could adapt them with less impact. Yet, as this topic is very new and began to deserve attention only were recently, thus its deep and profound understanding is still very far even from partial awareness, and additional efforts are required to fulfill the gap. It would allow to push further the progress in this direction.

8.2.2 *Defects in MoS_2*

Discussion of defects in this material is limited by only assessment of its 2H or 3R phases which have semiconductor-like compositions with clearly defined band gap. The most recognized type of defect in MoS_2 is considered to be sulfur vacancy (V_S) which has one of the lowest formation energies, and thus its appearance often cannot be avoided. In fact, it can even be detected in naturally existed samples. Theoretical calculation predicted that V_S is a deep acceptor and its most accessible form represents neutral monovacancy [10]. Its existence correlates well with the position of Fermi level expanding though significant part of band gap except regions close to conduction band. Generation of these defects in MoS_2 results in development of new mid-gap energy levels, designated as occupied and unoccupied states that lay very near valence band maximum and in upper part of the band gap, respectively [11]. It was determined that the former one enables to donate electrons, while the latter one can accept one or several of them. This processing leads to appearance of V_S with charge states of −1 which presence satisfies the position of Fermi level approaching the conduction band [12]. The transition level associated with 0/−1 change was determined to be within ~1.2 to ~1.7 eV above valence band, depending on the model of applied calculation [10, 13] (Fig. 8.1a). In turn, it is also possible at

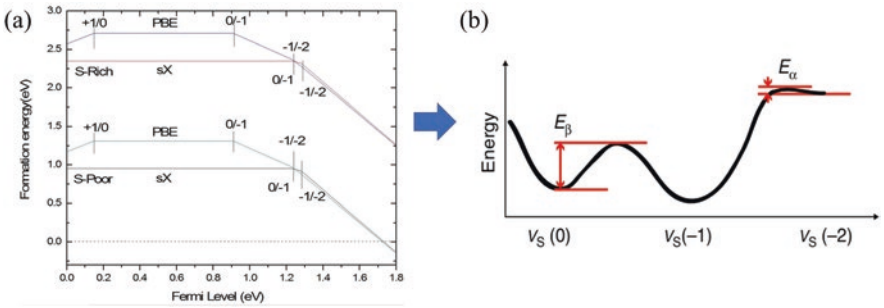

Fig. 8.1 (**a**) Charge transition states for the S vacancy in calculated via density functional theory using Perdew-Burke-Ernzerh (PBE) and screened exchange hybrid (sX) functional. (Reprinted from Ref. [13] with permission from *AIP Publishing*. Copyright, 2013) (**b**) Schematic energy diagram of V_S in the charge states 0, −1, and −2 The energy barriers E_β and E_α determine the degree of meta-stability of V_S (0) and V_S (−2), respectively. (Reprinted from Ref. [12]. Copyright 2017, *Springer Nature*. Available under the Creative Commons Attribution 4.0 Generic License, http://creativecommons.org/licenses/by/4.0/)

certain circumstances to realize the presence of V_S with charge states of −2. Its transition level is supposed to locate very close to conduction band or even within it. This defect is often considered as metastable specie since formation energy associated with its appearance is much higher than that of V_S (0) and V_S (−1) [12] (Fig. 8.1b). Thus, additional experimental evidence is necessary to confirm its continuous and detectable existence in MoS_2 that enables to make any evident and lasting contribution to the changes in surrounding electronic structures. It is of interest that another view existed in literature on the identifying of these defect levels, as it was revealed that, *firstly*, they are positive which means they donate electrons and thus are attributed to donor-like states and, *secondly*, their positioning follows opposite trend; the higher the charge state, the deeper within the band gap their dominated presence is detected [14]. Given that MoS_2 represents binary compound and by its chemical composition is close to, for example, ZnO or TiO_2 described in previous chapters, where oxygen vacancies have donor-like characteristics, the identification of V_S might lead to additional difficulties given that its transition levels locate in the upper part of band gap within very close distance from conduction band and considering their role in strengthening of n-type conductivity [12], as it will be shown below. Yet, the detailed assessment regarding this topic is left aside as it is beyond the scope of this work. Following the recognizable and generally accepted trend in literature, the discussion below is fully based on assumption and consequent recognition that V_S is as acceptor.

As for the geometrical structure and its changes, it was discovered that in order to maintain thermodynamic balance of internal energy, atoms surrounding vacancy become subjected to certain relaxation toward inward direction which degree follows its charge state. Particularly, for the neutral V_S, the first and the second near-neighboring Mo and S ions are adjusted for about 0.4% and 1.5%, respectively, while for the V_S in charge state of −2 these values were identified to be 1.2% and 2.2%, respectively [14]. This relaxation is considered to be very insufficient compared, for example, for other binary materials, such as ZnO where it reaches over 20% after introduction of oxygen vacancies [15]. Thus, it can be said that threefold symmetry in monolayered MoS_2 is maintained and there is the absence of any electron localization due to symmetry breaking or polaronic distortion [13]. Finally, it has to be noticed that apart from those mentioned above, definitely, there exist other charge states of S vacancies; yet they are considered to be thermodynamically less favorable species as transition levels related to their positioning are laid beyond band gap, i.e., within the conduction or valence bands. In addition, it is also important to state that sulfur vacancy also can exist in the form of divacancy (V_{S2}) [16] which results in appearance of additional occupied states within the conduction band. The formation energy of this type of defects was determined to be relatively high which means that their concentration is low compared with that of V_S.

Another important defect of MoS_2 is considered to be Mo vacancy. Theoretical estimation demonstrated that its formation is followed by breaking of six Mo-S bonds where Mo atom is eliminated. As a result, six S dangling bonds remain in the structure [17]. The relaxation of the surrounding near-neighbor atoms is proceeded

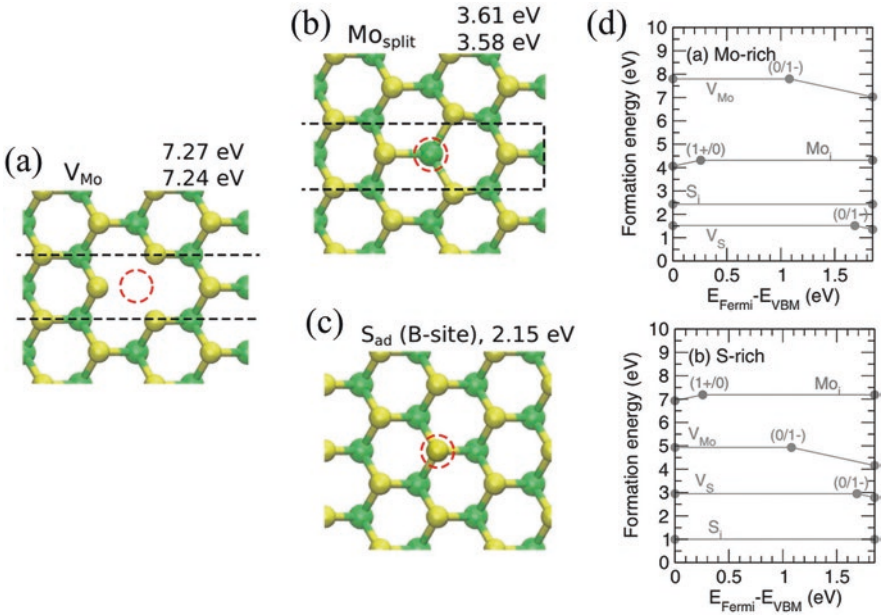

Fig. 8.2 Final optimized geometries of the defects within a MoS_2 layer. (**a**) Mo vacancy, (**b**) Mo interstitial, (**c**) S interstitial. Dashed circles (red) denote the position of the defect. The monolayer (up) and bulk (down) formation energies in the neutral state are provided above each atomic configuration. All configurations demonstrate top view. (Adapted from Ref. [11] with permission from *American Physical Society*. Copyright 2015) (**d**) Difference in calculated formation energies of the isolated native defects of V_S, S_i, V_{Mo}, and Mo_i in a single-layer MoS_2 as a function of the Fermi level in the Mo-rich (up) and S-rich (down) limit conditions. (Reprinted from Ref. [17] with permission from *American Physical Society*. Copyright 2014)

in outward direction (Fig. 8.2a). This defect is available in the neutral or negative charge states (−1 and −2) [11], which are considered to be the most stable configurations. They create transition levels relatively far from the valence band, thus allowing to classify V_{Mo} as acceptor with deep rather than shallow characteristics. In this regard, it is unable to serve as a source of intrinsic p-type conductivity and only takes the role of compensating centers, in a part similar to that of zinc vacancies in ZnO as it was shown in Chap. 6. In turn, V_{Mo} (−3) and V_{Mo} (−4) also existed; yet, they are seldom considered given that, *firstly*, they are unstable formations and, *secondly*, defect states associated with them are localized farther away in band gap [14]. Thus, certain difficulties might appear in their successful realization and consequent preservation in MoS_2. In addition, one may notice that V_{Mo} can appear in +1 charge state; yet it is only possible once the Fermi level is located in the lower part of band gap [11] which is associated with dominated presence of positively charge carriers and appearance of strong p-type conductivity. As for practical realization of metal-deficient MoS_2, it might be considered as a challengeable task since introduction of isolated molybdenum vacancy is accompanied by its extremely high formation energy even in S-rich conditions [10]. Furthermore, its presence often is

supposed to be accompanied by the release of near-neighbor sulfur atoms due to loss of strong chemical bonding that support them, thus resulting in development of defect complexes which have structure of V_{MoS3} or V_{MoS6} depending on the type of V_S [16]. Even though its formation energy for almost all range of chemical potentials is higher than that of isolated V_{Mo}, they have dominated appearance creating conditions at which near-located S atoms can easily loss their positions.

The most stable geometry of Mo interstitial (Mo_i) is determined to be split configuration directed toward *c*-axis [11] (Fig. 8.2b). As for its electronic structure, regardless of the surrounding environment, it is usually ascribed in terms of (+1) or neutral charge states which satisfy the positions of Fermi level inside the band gap. This defect is considered to be deep single donor, as (+/0) transition level is found at 0.3 eV above the valence band maximum. In this regard, it can serve only as hole trap center [17]. It has relatively high formation energy regardless of the conditions of outside environment, and thus the presence of this defect is often ignored in MoS_2 due to low concentration. In turn, the most stable atomic geometry of sulfur interstitial (S_i) in atomic scale MoS_2 is found to be S adatom structure on top of S atom [11] (Fig. 8.2c), while its electronic structure is limited by existence of only neutral charge states as with Fermi level presented inside the band gap, it is the only available configuration [17]. Therefore, this defect is neither donor nor acceptor and has no influence on the concentration of electrons or holes or changes within the band gap configuration. As a final remark, one need to notice that its formation energy is second low after V_S [11] in Mo-rich conditions and the lowest in S-rich conditions (Fig. 8.2d) which determine its significant existence and concentration in MoS_2.

Antisites are formed when atom of one element is evacuated from its original position, and it became occupied by atoms of other element which is intrinsically available in crystal structure. Thus, the more thermodynamically favorable is the formation of vacancy, the more chances that antisites could appear. It is suggested [18] that Mo-rich conditions enable to stabilize both S vacancies and Mo adatoms and therefore highly favor the formation of Mo_S antisites, while S-rich conditions are more conductive to the development of Mo vacancies and S adatoms, hence leading to appearance of S_{Mo} antisites. Yet, following the above discussion, it is obvious that it might not work to 2-D MoS_2 as to realize the presence of Mo_S much less efforts are required compared with that of S_{Mo} which means that their concentration would be more dominated. This defect is determined to have donor-like characteristics as it is stable in charge state of +1, and transition level is located in the conduction band [11]. As for geometry, substitution of an S atom for Mo atom leads to a distortion in the lattice due to the larger atomic radius of Mo atom compared to the S atom [18]. In turn, S_{Mo} demonstrates the existence of two transition levels of (+2/+1) and (+1/0) located at 1.16 eV and 0.95 eV, respectively, below the conduction band, which make this defect to serve the role of deep donor [19]. Overall, it has to be said that due to high formation energies, S and Mo antisites might be presented only in very limited concentrations,

8.2.3 *Defects in WS_2*

Defect chemistry of WS_2 has a lot of similarity to that of MoS_2 given that their crystal and chemical compositions as well as configuration of band gaps demonstrate very high resemblance. Simply to say, sulfur vacancies in WS_2 also are the most thermodynamically favorable type of defects as it has the lowest formation energy. Their electronic structures are ascribed by existence of stable 0 and −1 charge states that correspond to Fermi level located close to the conduction band. Accordingly, the 0/−1 transition state is determined to reside in the upper gap within distance of ~0.33 eV [20] from conduction band which in general terms is determined to be higher than that of MoS_2. Nevertheless, in analogy, this defect is identified as deep acceptors. Definitely, the existence of V_S with charge state of −2 was also determined via theoretical simulation. Its transition level is supposed to locate at a distance of only ~0.02 eV from that of (0/−1) [21]; yet its existence might be considered as metastable and thus could only be proceeded under extreme non-equilibrium conditions. Calculation performed via density functional theory (DFT) by Chu et al. [22] confirmed the availability of two in-gap states associated with V_S that are located close to conduction band. They are considered to serve as electron-trap centers and thus contributing to the above-mentioned changes in charge state. Nevertheless, formation energy of sulfur vacancies in WS_2 is much higher than that of MoS_2 regardless which environment, S-rich or Mo-rich, is applied; thus it makes their presence in the former material less evident and detectable and also restricts spontaneous appearances [21]. This conclusion is mostly referred to basal-based V_S as they are determined to have higher stability than those one located at edges [23]. It has to be noticed that WS_2 also can demonstrate the presence of double V_S which enables to create four states in band gap thus realizing potentially high influence on changes in charge distribution [22]. To be more precise, two of these states are located in the upper part of band gap serving as electron traps, while the third one resides very close to valence band, and it is considered to be hole trap. In turn, the existence of fourth level occurs almost in equivalent distance from both bands, and with certain level of speculation, it has high probability to annihilate both types of charge carriers [22]. However, due to the fact that disulfur vacancies in WS_2 have high formation energy that is roughly twice of that compared with their monosulfur counterpart [24], appearance of these defects is hardly possible, and thus their influence on the availability of charge carriers can be neglected.

As for the W vacancy, it is also considered to have acceptor-like characteristics *aka* Mo vacancy which create defect states located in the lower part of band gap serving only as compensation centers. Yet, their positions are closer to valence band than that of MoS_2, indicating that the transformation of metal-deficient WS_2 into strong p-type material is a more realistic scenario [24]. Tungsten vacancies can create defect complexes as nearest-neighbors three or six sulfur atoms are tending to be released due to weak chemical bonding [25]. In turn, WS_2 also enables to demonstrate the presence of interstitial defects; yet their concentrations are considered to be relatively negligible as this material has small interatomic spacing which might not

provide thermodynamically favorable site for residing an additional atom [26]. Moreover, it might be noticed that in analogy to MoS_2, S_i interstitial in WS_2 is a neutral defect and thus is unable to create any transition levels within the band gap and thus its presence. Hence, even though it has low formation energy and can be readily available, electronic and electrical characteristics of WS_2 proceed very negligible if any changes. In turn, appearance of W_i interstitial is determined to be an unfavorable feature in WS_2 due to requirement of high formation energy which seriously limits its accessible concentration. In fact, the same also could be said about S and W antisites, and thus they are also regarded as unexpected features in WS_2 [27]. Yet, it should be noticed that the latter conclusion was obtained via theoretical frameworks and experimental evidence contradicts it. For example, Wang et al. [25] revealed that monolayered WS_2 demonstrates the presence of double sulfur column substituted for a single tungsten vacancy which was discovered to take the role of single dominant defect. Thus, more studies on the defects in this compound are required.

As a final remark, it has to be noticed that sulfur vacancies in both MoS_2 and WS_2 often act as electron donors, and their introduction might result in increasing the strength of n-type conductivity despite the fact that these defects are serving as deep acceptor due to positive charge states. The origin of this contradictive behavior is still debatable as it can be attributed to various processes correlated with changes in chemical, structural, and electronic configurations. The more detailed discussion is provided below, specifically, in chapter dedicated to investigation of electrical properties.

8.2.4 How to Create Defects

8.2.4.1 Exfoliation

Mechanical Exfoliation Mechanical exfoliation is one of the simplest and accessible methods to synthesize atomic scaled MoS_2 and WS_2 from their bulk crystals using only mechanical forces. It is described as follow: *Firstly,* adhesive Scotch tape is used to peel off appropriate layer from the surface of starting material creating a freshly cleaved thin component. *Secondly*, target substrate is brought into contact with this Scotch type, and the transfer of required composition is realized once they are combined. It is often the case that additional efforts such as, for example, rubbing with specific tools, are required to make this process smoother and less distractive. After the Scotch tape is removed, MoS_2 and WS_2 mono- or several layered nanosheets or flakes are remained on the substrate due to van der Waals forces. Playing with number of times how often Scotch tape is used or starting material and substrate are in contact usually results in synthesis of flakes or nanosheets with different sizes, dimensions, and distribution. It is also possible that this process can be effectively realized in solution using shearing, grinding, etc. In this case, bubbles take the role of Scotch tape pushing forward the cleavage, and this fabrication route is called as exfoliation in liquid phase.

Overall, this method enables the formation of various defects in MoS_2 and WS_2 as it requires the employment of certain mechanical strength to create the desired nanoscaled structure via breakage of its original composition in bulk and consequent cleavage. Thus, due to nonideality of applied conditions, it is often resulted in disruption of localized symmetry and introduction of certain disorganization and disorders within the periodic arrangement of atoms. Mechanically, exfoliate MoS_2 and WS_2 are mostly considered as sulfur-deficient compounds given that this type of defect has the lowest formation energy and that this synthesis is usually realized at ambient conditions. In turn, the presence of metallic vacancies, interstitials, or antisites is less evident in these materials [28].

Chemical Exfoliation Chemical exfoliation is ascribed as transformation of bulk crystals into mono- or several-layered compositions via realization of an appropriate chemical reaction that is based on application of various intercalants such as acids/bases, inorganic salts, oxidizing agents, and reactive functional molecules. Typically, disruption of chemical bonding in the basal plane of starting materials is proceeded by involvement of heteroatoms or functional groups that facilitate the cleavage of surface and appearance of flakes and nanosheets. As they are presented in separated forms, it enables the appearance of resistance to prevent aggregation [29]. Thus, they can be easily collected in the form of dispersion and transferred into target substrate via, for example, spin coating process. To facilitate the reaction, sonication or stirring can be usually applied; furthermore, it is possible to change the temperature or time at which the chemical reaction is processed thus reaching optimal and very precise control over distribution, shape, and other features of obtained 2-D nanostructures. The only disadvantage of this process apart from low yield which is very common for exfoliation regardless its type is that the chemical reaction is required to be proceeded for several days which is very time consuming. In terms of its employment to the MoS_2 and WS_2, the appeared defects are also ascribed mostly in the form of S vacancies.

8.2.4.2 Vapor Phase Synthesis

As exfoliation is not suitable for the large-scale production of 2-D materials and given that it is unable to manage the number of obtained layers and their sizes, distribution, and phase, there is a need in developing of other methods which can successfully address all of these problems. In this regard, vapor phase synthesis is considered to be a very attractive alternative as it shows several advantages that are highly praised. *Firstly*, it enables to grow uniform MoS_2 and WS_2 in a large scale directly on the surface of desired substrate through chemical reaction or physical assemblance using various gaseous precursors and, *secondly*, their structure and chemical composition can be easily adjusted with precise accuracy given that various parameters of deposition such as temperature and pressure inside chamber, flow rate of carrier gases, type of used chemicals and their particularities, etc. could be monitored and controlled. Thus, not only introduction of various defect in MoS_2 and

WS_2 can be easily realized, but also managing of their specific characteristics also is possible as well. Yet, due to difference in utilized protocol between physical and chemical deposition, this processing has their own particulates and specifications regarding the introduction of defined non-stoichiometry into fabricated compound which determines their proper application toward reaching the desired composition.

Specifically, Hong et al. [30] revealed that employment of physical vapor depositions ascribed as sublimation of precursors into the gas phase followed by its transformation into a desired solid-based layered composition to fabricate monolayered MoS_2 might result in dominated appearance of antisites defects within it. This phenomenon was explained by extensive development of sulfur vacancies which became filled with nearby Mo atoms given high mobilities of latter. It was revealed that resulted antisites have higher stability with respect to V_S which makes them to be considered as thermodynamically more favorable species in MoS_2 thus leading to their dominance. It has to be noticed that realization of this scenario is only applicable to specific conditions of PVD processing and might be different once certain changes within its specification or course of actions are implemented. In turn, employment of chemical vapor deposition usually leads to development of MoS_2 filled with large number of V_S. Their occurrence is ascribed as replacement of oxygen in the utilized precursor that mostly presented in the form of MoO_3 by sulfur under controlled S-rich condition. Thus, V_S is formed once incomplete filling of these O empty sites is realized. Furthermore, CVD-prepared samples, in addition to development of sulfur-deficient composition, also enable to demonstrate the presence of Mo interstitials [31] and Mo vacancies [16] even though their concentrations are lower than that of V_S. One might notice that the latter type of defect is seldom available as individual specie since their development usually is accompanied by the release of near-neighbor sulfur atoms, and thus formation of defect complexes such as Mo_{S3} and Mo_{S6} often can be observed instead. It is also possible to create antisite defects via CVD fabrication, yet is mostly achieved by playing with stoichiometry of the precursor compounds, i.e., lowering or increasing the number of anion defects in it as it happened, for example, by using WO_3 contained sub-oxides to prepare WS_2 [32] (Fig. 8.3). Finally, atomic layer deposition also can be used to proceed controlled deficiency in MoS_2 and WS_2. Apart from well-known and already mentioned sulfur vacancies, the resulted compositions in addition can demonstrate appearance of other type of defects such as S interstitials which development and adjustment follow the changes in the parameters of this processing [33].

8.2.4.3 Hydrothermal Method

Hydrothermal method is a very simple, efficient, easily accessible, and thus extremely attractive route for the fabrication of defective MoS_2 and WS_2 as it allows to achieve their formation with desirable and adjustable stoichiometry, chemical composition, and the level of overall crystallinity via simple route. To be clear, playing with various parameters of this synthesis such as ratio and choice of utilized chemicals, temperature and time of reaction, etc. can be used to precisely tune the

Fig. 8.3 Effects of precursor pre-treatment on the vapor deposition of WS_2 monolayers. (Reprinted from Ref. [32]. Copyright 2019, *The Royal Society of Chemistry*. Available under Creative Commons Attribution-Non Commercial 3.0 Unported License, https://creativecommons.org/licenses/by-nc/3.0/)

relative amount of introduced defects and also enable to specify their types, distribution, concentration, and expected behavior. For example, Liu et al. [34] investigated how the application of $(NH_4)_2MoS_4$ and $Na_2MoO_4{\cdot}2H_2O$ served as precursors can influence the introduction of defects in nanolayered MoS_2 which was fabricated via hydrothermal treatment at 200 °C for 24 h. It was discovered that apart from forming flower-shaped aggregates and mesoporous structure, respectively, the former compound demonstrated relatively higher presence of sulfur vacancies compared with that of the latter one. It is also possible to apply this method for introduction of Mo vacancies as addition to V_S [35]. As for deficient WS_2, its synthesis follows similar scenario with only difference that other chemicals are applied as precursors. The resulted structure usually demonstrates the presence of large number of both W and S vacancies [36].

Hydrothermal synthesis also allows to achieve realization of particulate architecture since it can easily overpass limitation to form only 2-D structures. In this regard, nanoparticles, nanorods [37], nanoflowers [38], etc. can be fabricated. Thus, compared with other methods described above, it provides higher flexibility in achieving the desired composition as its adjustment can be correlated with surface morphology. For example, it was discovered that "thin folding leaves" of nanoflowers are highly attractive to accommodate various defects [38].

8.2.4.4 Other Methods

Definitely, fabrication of defective MoS_2 and WS_2 can be achieved via more strategies than described above. However, they cannot be discussed fully here due to the limitation of pages. Nevertheless, several most distinguish approaches are necessary to be mentioned briefly as to provide general overview regarding current progress in synthesis of defective MoS_2 and WS_2. For a more detailed discussion, readers are suggested to search for appropriate and relevant literature.

(a) *Ball Milling*. Ball milling is considered as post-synthesis treatment that can be applied to fully stoichiometric and relatively ideal nanostructures for introduction of specific defects within their structure accompanied by certain level of disorder. Simply to say, this processing is considered to be very violent due to mechanical interactions with stainless steel balls under large rotational speed. In addition, it is accompanied by rising of temperature up to 1000 K within very localized domains thus easily breaking the periodic arrangement of atoms causing some of them to be rapidly evacuated. It degrades the overall quality of crystal lattice. For example, Li et al. [39] demonstrated that applying milling at 400 rpm for 24 h in an atmosphere of argon resulted in transformation of MoS_2 nanosheets into highly defective compounds filled with large number of S vacancies.

(b) *Thermal Decomposition*. Chemical decomposition of certain chemicals catalyzed by increased temperatures of surrounded environment is considered to be a simple and very attractive approach to prepare nanoscaled MoS_2 or WS_2 with desired stoichiometries and 2-D architecture. The obtained structures usually represent powder-shape composition that can be easily collected or film-like arrangement supported on specific substrate. The introduction of defects and specifically their classifications and consequent concentrations are fully depended on the conditions of this processing such as changes in type of atmosphere and which temperature is used during it. Also, correct choice of chemicals employed as precursors play an important if not the main role [40]. This method is perfectly applicable to realize deficiency or excess of sulfur within the fabricated materials.

(c) *Electrochemical Desulfurization*. Electrochemical desulfurization can be ascribed as facilitating the formation of sulfur vacancies within layered MoS_2 [41] and possibly WS_2 by using them as working electrode during linear sweep voltammetry process. The choice of applied potentials and sweeping speed determines how many and how fast sulfur atoms are going to leave the surface of these materials and also the stability of remaining empty sites.

8.2.5 Properties of Defective MoS_2 and WS_2

8.2.5.1 Structural Properties

Formation of intrinsic defects in MoS_2 and WS_2 depending on their nature, concentration, and distribution results in certain adjustment of its structural characteristics, their evolution, and possible extension. Particularly, taking MoS_2 as an example, it was determined via theoretical simulation that the presence of V_{Mo} and V_S induces an outward and inward relaxation of its near neighbor atoms, respectively [14]. As the latter defect can be introduced much easier and its existence as individual specie is more thermodynamically favorable, the discussion below is mostly referred to it. *Firstly*, the presence of V_S is supposed to result in decrease of S-Mo-S angle that, in

turn, results in contraction of the lattice constant which was confirmed via positive shift of (002) characteristics peak in XRD pattern [42]. *Secondly*, this defect, in turn, causes the increase of interlayer distance, as it was, for instance, revealed by Geng et al. [43] who demonstrated that this value was changed from 0.61 nm to that ranging from 0.63 to 0.66 nm. It is suggested that observed irregularity of this value could be attributed to the different level of S-deficiency within adjusted layers. *Thirdly*, deviation in stoichiometry within the surface of MoS_2 might cause the breakage of its thermodynamic equilibrium. It results in perturbation of mass that eventually results in developing the increased roughness or appearance of additional edge sites, dislocations, distortions, and even segments with disordered structure on the outside layer [44, 45]. It has to be noticed that very similar observation regarding the evolution of structure due to presence of sulfur vacancies can be attributed to WS_2. Specifically, it was also observed that introduction of these defects leads to increased interlayer distance as well as development of surface composition with higher roughness accompanied by presence of clearly visible discontinuous nature [46].

8.2.5.2 Optical Properties

Optical characteristics as well as band gap of MoS_2 and WS_2 have clear dependence on the presence of defects as their types and concentrations determine the range of observed changes. Overall, the following particulates are determined for these correlations. For simplifying this discussion, mono- and several-layered MoS_2 are taken as typical structure. *Firstly*, theoretical simulation revealed that with the presence of V_S, the band gap becomes slightly narrowed and relatively similar for all accessible charge states [14] (Fig. 8.4a, red curve). In turn, experimental evidence confirmed that this is indeed the case as the absorbance edge was extended toward near-infrared region within wavelength range of 750–1100 nm [44] (Fig. 8.4b). Furthermore, there is also high possibility that more photons become trapped within the defective MoS_2 given that its surface has higher roughness accompanied by the presence of dislocation and distortion thus increasing the absorbance strength. *Secondly*, it was discovered that introduction of sulfur deficiency might lead to the transformation of direct band gap in monolayered MoS_2 back into indirect one similar to that of its bulk counterpart [47]. The origin of this transition was referred to the contraction of the neighboring atoms around the empty S site and appearance of local state within the band gap. *Thirdly*, evacuation of molybdenum atoms and consequent formation of V_{Mo} also can reduce the width of band gap. Yet, compared with that of V_S, the observed decrement is more dramatic since the resulted distance between valence and conduction bands might become even lower than that of its bulk counterpart and reaches the minimum value of ~0.95 eV [14] (Fig. 8.4a, blue curve). In addition, this value has linear dependency with the change of V_{Mo} charge state. Finally, as an explanation of reduced band gap in S- and Mo-deficient MoS_2, Feng et al. [47] proposed model via density of state that introduction of both types of defects might activate the expansion of conduction and valence bands, respectively, toward lower energies given the position of their transition levels.

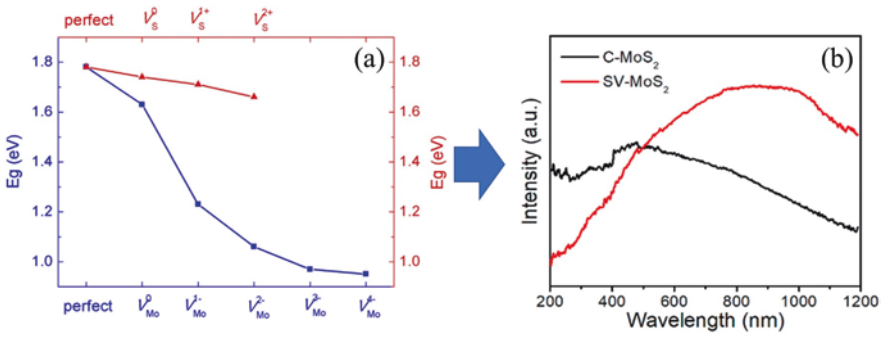

Fig. 8.4 (**a**) The calculated band gaps for perfect monolayer MoS_2 and defective monolayer MoS_2 with charged vacancies. (Reprinted from Ref. [14] with permission from *Elsevier.* Copyright, 2014) (**b**) UV-vis-NIR absorbance spectra of C-MoS_2 (conventional) and SV-MoS_2 (filled with V_S) samples. (Reprinted from Ref. [44] with permission from *American Chemical Society*. Copyright 2020)

8.2.5.3 Electronic Properties

Formation of various types of defects, specifically sulfur vacancies, in MoS_2 and WS_2 leads to development of additional mid-energy states within band gap which concrete positioning with respect to conduction and valence bands and the role they take in governing the presence and consequent transportation of electrons and holes are determined by their certain and defined particularities such as charge state, geometrical configurations, etc. Specifically, taking MoS_2 as an example, it was discovered that introduction of neutral sulfur vacancies results in appearance of two defect states located within the valence band and in the upper part of band gap. The first one is considered to be fully occupied, while the latter one enables to accept electrons thus transforming the V_S into – or −2 charge states. Needleless to say that transition levels associated with them are located close to conduction band which sometimes lead to mispresenting V_S as donor-like defects while, in fact, it is considered to be deep acceptors given how far the corresponding Fermi level is located with respect to the valence band. The higher the charge state of this defect, the higher the position of the corresponding transition level in the band gap [11] as it is gradually approaching conduction band following the increment of Fermi level even though some authors provide opposite opinion [14].

In turn, V_{Mo} is also generally determined to be an acceptor which existences in neutral form is considered to be the most stable as it satisfies the position of Fermi energy located within the middle of band gap (~0.9 eV). The appearance of this defect is accompanied with the development of five energy states within the band gap. Out of them, only three states, namely, one double and one singlet, are considered to be unoccupied and thus enable to accept an electron and contribute to its transfer [11]. Following it, V_{Mo} might be presented in the form of other charges which correspond to the various shift of Fermi energy toward conduction band and consequent strengthening of n-type conductivity. For example, (0/−1) and (−1/−2) transition levels were reported to be located at ~1.1 eV and ~1.5 eV, respectively,

from maximum of valence band regardless of which conditions, S-rich or Mo-rich, were applied [17]. In this regard, V_{Mo} is considered to be deep acceptor similar to that of V_S and serves as compensation centers. As for V_{Mo} with −3 and especially −4 charge states, their appearance is only possible when Fermi level is moved inside the conduction band, and thus these defects are very rare phenomena as it is satisfying highly degenerated structure.

It has to be noticed that alternative view exists on the positioning of V_{Mo} in the band gap of MoS_2. Feng et al. [14, 47] revealed via theoretical framework that corresponding defect levels associated with this vacancy are fully localized in the lower part of band gap relatively close to the valence band. In this regard, it was proposed that as the Fermi level increases ranging from 0.11 to 0.69 eV, the formation energies of Mo vacancies decrease following the consequent changes in the negative charge states. Accordingly, V_{Mo} (0), V_{Mo} (−1), and V_{Mo} (−2) were identified to have low stability which means they are less available, while V_{Mo} (−4) was regarded as the most thermodynamically favorable specie in MoS_2. It is noted that this scenario is applicable to oxidizing conditions. Thus, it is evident that additional experimental evidence is highly necessary to identify which scenario is more plausible.

Mo interstitials usually exist in the neutral form that is considered to be the most stable configuration over wide range of Fermi level [11]. Its appearance in MoS_2 is accompanied by development of three states in the band gap out of which the one that is located close to the conduction band and identified as doublet was calculated as the only one that is unoccupied [17]. Thus, given donor-like characteristics of Mo_i, it enables to accept hole. This process leads to ionization of this defect into (+1) charge state accompanied by appearance of corresponding transition level in band gap which is laid relatively close to valence band. In turn, formation of S interstitials results only in development of occupied deep levels that determine the existence of this defect only in the neutral form. Thus, its presence has almost no influence on the structure or changes of band gap.

The important remark that the above discussion regarding the changes in electronic structure of MoS_2 can be attributed to WS_2 yet with certain reservation as positioning and numbering of newly created mid-gap states which are accompanied by the presence of specific defect has slight difference among these materials. For example, V_S in WS_2 results in appearance of two defect states [22] that in turn might be classified as consisting of certain number of closely located sub-bands as they are distributed within the range of ~0.02 eV [48]. In turn, energy levels associated with the presence of W vacancy in WS_2 are laid slightly closer to valence band than that of M vacancy that existed in MoS_2, which makes the former defect to have higher p-type orientation [24].

8.2.5.4 Electrical Properties

Introduction of various defects has great correlation with the electrical properties of MoS_2 and WS_2 as it can be used to adjust concentration and mobility of charge carriers thus influencing their transportation characteristics and lifetimes. Several

important particularities should be emphasized regarding this process. *Firstly*, as theoretical assessments of sulfur vacancies available in literature determine them as deep acceptors [17], their introduction might contribute to the appearance and strengthening of p-type conductivity given their role as compensation centers. *Secondly*, it would be also correct to say that the presence of these defects in the form of negatively charge states causes the localized increase of chemical potentials around them that inevitably lead to stabilizing the position of Fermi level close to conduction band. These conditions are considered to be the evidence for existence of persistent and strong n-type behavior [12]. Experimental results obtained via investigation of MoS_2 fabricated by CVD with controlled level of sulfurization fully confirmed that introduction of V_S can assist in the donation of electrons [49]. Thus, their overall concentration and mobility within defined volume became higher which resulted in net positive contribution to the conductivity. As additional remark, it has to be noticed that as $(-1/-2)$ transition level is located higher than that of $(0/-1)$, it is suggested that dominated presence of uniformly distributed yet metastable V_S (-2) would result in more apparently intensifying the role of electrons as main charge carriers. Thus, it is evident that there is a clear discrepancy toward understanding the role of V_S in governing the charge carrier-related processes in MoS_2 as in literature it is considered to have both donor- and acceptor-like characteristics thus degrading or improving naturally available n-type conductivity. In fact, it also can be addressed to WS_2 which has very similar controversy. Thus, there must exist certain boundary conditions which determine and distinguish the function of V_S as annihilation or contributing centers for negatively charged carriers. To partially resolve this issue, the following explanation of this phenomenon can be proposed [50]. Simply to say, at low or medium concentration, V_S plays the role of acceptors and thus stimulates the appearance of p-type behavior as electrons are accumulated around these defects; thus, their movement within crystal lattice becomes limited. It reduces their participation in overall conductivity. Yet, as more sulfur atoms continue to release, the gradual metallization begin to appear in MoS_2 and WS_2 which means that the role of M and W atoms, respectively, as charge centers is enhanced, and it follows steadily increased number of saturated electrons around them. The same process occurs, for example, in ZnO when significant part of oxygen is removed, and it gradually reduces into metallic Zn [51]. Theoretical simulation [50] predicted that concentration of V_S equaled to 6.3% and 1.8% for MoS_2 and WS_2, accordingly, was designated as enough for enabling these defects to show evidence of donor-like characteristics as enhanced presence led to reducing their contribution into p-type behavior by initiating its progressive transition (Fig. 8.5). It is of interest that the more the V_S introduced, the more evident the split of unoccupied related defect level in MoS_2 and WS_2 and the closer their Fermi level is located to conduction band. *Thirdly*, the co-existence of V_S with neutral and negative charge states might result in locally inhomogeneous surface potential which causes charge scattering and degradation of carrier mobilities [12], hence downgrading their transportation characteristics due to increased recombination rate.

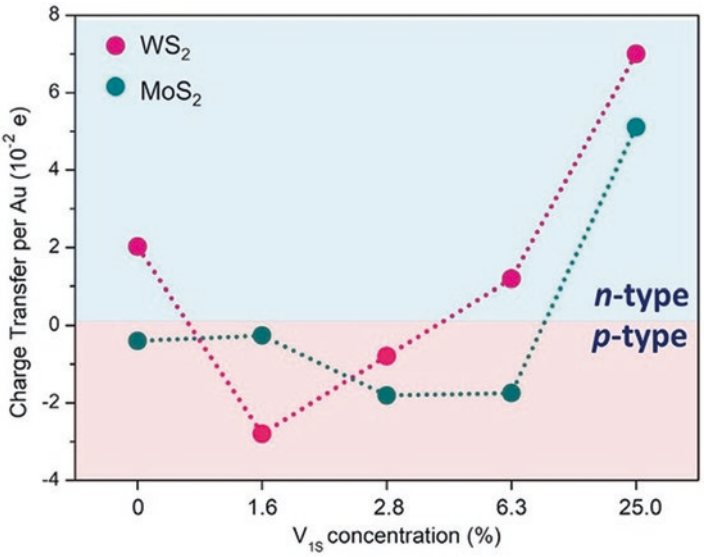

Fig. 8.5 The effect of V_{1S} (single sulfur vacancies) density in MoS_2 and WS_2 on interface charge transfer. The charge transfer amount is represented as per surface Au atom to allow comparison between different defect densities. Green and pink dots correspond to Au-MoS_2 and Au-WS_2 interfaces, respectively. For more detailed explanation of this figure readers are suggested to address the relevant publication. (Reprinted from Ref. [50] with permission from *John Wiley and Sons*. Copyright 2020)

Fourthly, Mo and W vacancies are considered to be deep acceptors; thus their presence would also influence but not directly on establishing and preserving strong and evident p-type conductivity [24]. Yet, it is a very controversial issue as opposite opinion exists in literature. For example, Zheng et al. [52] investigated Mo deficiency in MoS_2 via DFT calculation and revealed that its introduction results in appearance of states above valence band that are fully filled. Based on this, it was concluded that in this case "holes can hardly be generated." *Fifthly*, other defects also can play a certain yet very limited role in governing the electrical properties of host materials. Taking MoS_2 as example, it is determined that Mo interstitials and S antisites are evaluated as deep donors, while Mo antisites take the role of deep acceptors. Thus, they only serve as compensation centers. Furthermore, given their high formation energies regardless the applied environment [11], their existence in MoS_2 is very limited, and thus the overall contribution to establishing and strengthening of the relative type of conductivity is very minor. It has to be noticed that the presence of S interstitials is ignored despite its low formation energy as the only stable charge state in which it can exist is neutral. Thus, none of intrinsic defects have shallow-like characteristics, and this role could be assigned to various impurities existing in MoS_2 and WS_2.

8.2.6 Application of Defective MoS_2 and WS_2 as Photocatalyst

8.2.6.1 Brief Overview

MoS_2 and WS_2 are considered to be non-toxic, inexpensive, environmentally friendly, and earth-abundant semiconductors which presence as nanoscale compounds with atomically resolved composition enables to fill them with various important and highly desirable properties and features that could not be discovered in their bulk counterparts. For example, monolayered compositions of MoS_2 and WS_2 demonstrate the width of band gap equaled to ~1.8 eV and 2.0 eV, respectively, which make them to show sensitivity toward sufficient part of solar irradiation allowing to absorb light with higher wavelengths than that of other very similar semiconductor-based catalysis such as, for example, TaON (2.7 eV) or Ta_3N_5 (2.1 eV) described in previous chapter. However, the most important positioning of conduction and valence bands of MoS_2 and WS_2 shows high suitability toward matching the reduction potentials of specific photocatalytic reactions such as water splitting or dye degradation. Thus, theoretically both materials can serve as the main and only utilized compound that enables to initiate and realize their proceeding. Yet, the experimentally observed performances are far from expected given several reasons. *Firstly*, most of active sites that have accessibility toward absorbing required molecules are located at edge planes rather than basal planes. Given that these MoS_2 and WS_2 are usually fabricated in the form of nanosheets or flakes, it is often the case that internal structure is hidden or its exposure is very limited. *Secondly*, it is also necessary to scrutinize extremely high excitation recombination ratio that is accompanied by weak absorption capability of the incident light [9] as substantial part of photons with required energies simply is avoided to be captured. Thus, the photocatalytic performance becomes affected since lower amount of photo-induced charge carriers becomes only available, and it also contributes to reducing the performance making its outcome to be far from expected. *Thirdly*, even though electrical properties of MoS_2 and WS_2 are superior, they are still suffering from high recombination rate of charge carriers as sufficient part of them is annihilated without reaching the surface and participating in reaction. Thus, more efficient transportation characteristics of photo-induced electrons and holes are required to be provided. *Fourthly*, the stability issue is also a hot topic for these materials as existence within 2-D geometries that is the mostly studied and applied forms of them in literature is associated with atomically scaled structure which is very sensitive to any changes in surrounding environment or deviation of other related factors. Thus, it becomes highly conducive to appearance and developing of various unnecessary and unavoidable defects that can lead to certain self-alteration. Ignoring to take them under control or properly adjusting their features might not be considered as correct strategy since it likely would result in extremely negative outcome. In addition, it also might worsen some of those problems mentioned above, thus transforming MoS_2 and WS_2 into non-effective photocatalysis.

In this regard, application of defect engineering is considered to be highly attractive and promising solution since it enables to deal with any unexpected changes in the chemical composition, stoichiometry, crystal lattice, and morphology making them to serve the required goal. Furthermore, this approach also can be used to design and implement conditions that trigger intentional changes in the internal structure in such a way that already existed properties and characteristics become enhanced, thus making them approach the designated and most importantly desired level. In turn, it also might lead to introduction of new and unexpected particularities that existence could hardly be detected within fully stoichiometric compound. Thus, the resulted MoS_2 and WS_2 could show much improved performance toward full realization of photocatalytic processing serving. More detailed discussion regarding each specific reaction is provided below.

8.2.6.2 Photocatalytic and Photoelectrochemical Water Splitting

Photocatalytic water splitting consisted of two half-reactions, namely, the hydrogen evolution reaction (HER) and oxygen evolution reaction (OER) which successful and concurrent accomplishment governs the production of hydrogen. It is a complex process that involves generation of electrons and holes under light irradiation and their consequent transfer to the surface of catalyst for interaction with adsorbed molecules. As for more detailed descriptions, given the position of band gap which perfectly matches the redox potentials of both reactions, nanoscaled MoS_2 is supposed to be capable for relatively easy realization of the overall water splitting process. Yet, to great surprise, the literature is mostly filled with reports where it is strictly utilized as catalyst to advance only HER reaction. The reason for such strategy is very trivial. Recent theoretical study revealed that due to weak binding of the HO^* and HOO^* intermediates to surface of MoS_2 and consequent appearance of high overpotential, accomplishment of OER via photoelectrochemical cell setup by using this compound results in very low catalytic activity [53]. In turn, 2-D structured WS_2 was recorded to have better adaptivity toward performing this reaction which resulted in its higher efficiency under similar conditions (Fig. 8.6). Apart from other possible reasons, this outcome was referred to longer lifetime of charge carriers in it compared with that of MoS_2 (100 vs 50 ns) [54]. In fact, mono- and several-layered WS_2 enables to accomplish both steps and reach certain level of photocatalytic performance toward hydrogen production. However, it is still far from expected. Thus, this compound is also often used as only capable to realizing HER reaction since serving this role and in combination with other semiconductors, the obtained outcome is considered to be more attractive. It is interesting that heterojunction of MoS_2 and WS_2 demonstrated to have relatively high outcome [54].

Accordingly, application of defect engineering to modify both materials can successfully improve their performance in this half-reaction and thus in perspective might push further the limitation in the efficiency that is currently set for overall photocatalytic water splitting. Specific particularities regarding this process are ascribed as follows: *Firstly*, evacuation of sulfur atoms from surface results in

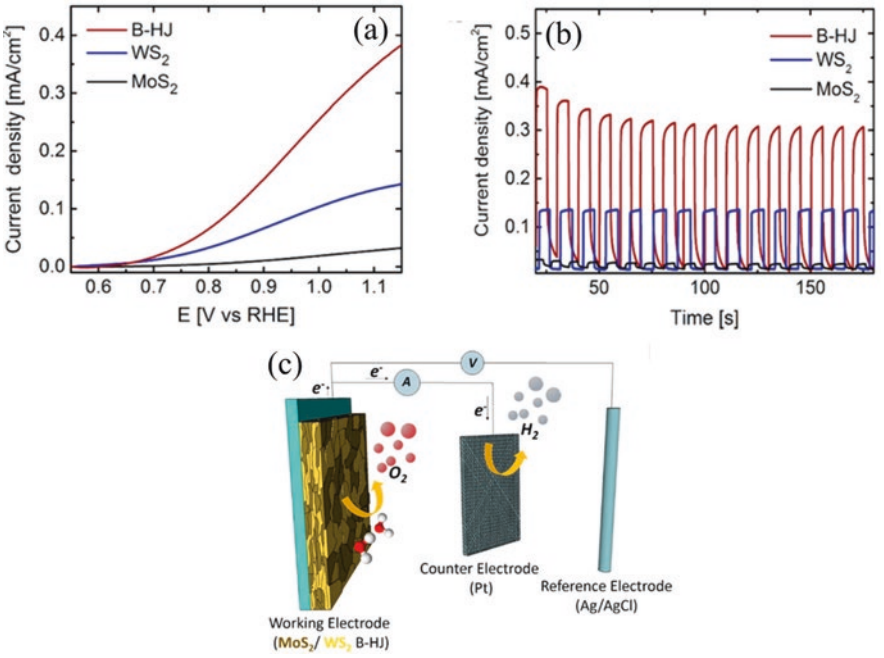

Fig. 8.6 Photoelectrochemical activity for water oxidation of MoS_2, WS_2, and MoS_2/WS_2 B-HJ photoanodes: (**a**) linear sweep voltammetry curves and (**b**) chronoamperometry (+1 V vs RHE, under intermitted illumination) scans recorded for WS_2 (blue line), MoS_2 (black line), and MoS_2/WS_2 bulk heterojunctions (red line) photoanodes ~60 nm thick. (**c**) Illustration of photoelectrochemical cell components using B-NJ as example. (Reprinted from Ref. [54] with permission from *American Chemical Society*. Copyright 2017)

changes of its thermodynamic equilibrium that causes consequent breakage of morphology. It allows to appear large number of metal-based edge-like features that can enhance the strength of HER reaction. *Secondly*, as V_S causes the development of various defect states within the band gap, their presence leads to activation and optimization of basal planes thus making them highly attractive for adsorbing of H atoms in manner that is applied to mentioned metal edges [55]. In turn, the same study also revealed that accompanied employment of tensile stress to S-deficient MoS_2 can change the positions of these states by shifting them, for example, closer to conduction band thus leading even to higher HER activity. One should notice that among molybdenum sulfide-based catalysts, this outcome has been considered to be one of the best up to date. *Thirdly*, defects can significantly increase the stability of defective compounds toward water splitting process. Particularly, Geng et al. [43] revealed that HER measurements of MoS_2 filled with V_S demonstrated constant overpotential for up to 15 h, and the current density also showing minimal changes. *Fourthly*, introduction of sulfur vacancies with certain concentration can create dominated presence of reduced metal states that enable to increase the availability and mobility of electrons, thus not only enhancing their transport characteristics but

also reducing the overall recombination rate. As a result, the kinetic of HER reaction becomes highly improved [34].

Definitely, introduction of defects into MoS_2 and WS_2 can also lead to absolutely opposite outcome, i.e., inability to realize light-induced hydrogen production. For instance, Piskunov et al. [56] stated that "induced localized states [by S and W vacancies] would prohibit water splitting in the proximity of defective WS_2 (0001) … only pristine or almost defectless tungsten disulfide nanosheets can be suitable for photocatalytic applications." It is not surprising as, in fact, similar observation also might be referred to other binary compounds such as TiO_2 or ZnO where the presence of oxygen vacancies cannot always guarantee improvement of their photocatalytic performance. Thus, to avoid it, the application of defect engineering toward 2-D MoS_2 and WS_2 should be proceeded with extreme care and proper management to make these compounds to show extended photoactivity toward water splitting.

8.2.6.3 Light-Induce Water Purification

Photocatalytic degradation of dyes via light irradiation is applied to remove highly toxic molecules from aqueous media by transforming them into various non-hazardous compounds such as carbon dioxide and water. Defective MoS_2 and WS_2 due to their unique characteristics and features can become a promising solution for the enhancement of its outcome. Moreover, this processing has much higher chances to be effectively realized since the positions of mid-gap levels created by defects should satisfy less requirements to have perfect matching with redox potentials of respective reactions. In addition, the environment at which dye degradation occurs does not obligate to use specific acidic or other chemical-based chemicals that are often necessary during water spitting in order to initiate and maintain charge transfer thus providing higher stability for this processing. The mechanism of improvement usually has the same origin as those described above in case of photocatalytic hydrogen production. For example, Lin et al. [57] investigated how the presence of sulfur vacancies influences the capability of MoS_2 nanosheets to remove various dyes from water under solar irradiation. Particularly, it was revealed that complete degradation of methylene blue (MB) by fully stoichiometric compound was achieved after 180 m of continuous stirring, while for MoS_2 filled with V_S, it required only 7 min to reach similar outcome. It represents nearly 25-fold improvement. In turn, when MB was replaced by more stable methylene orange with the same concentration and volume, its almost full degradation (~98%) by V_S-MoS_2 was realized only within 3 min which was determined to be much faster than almost any currently available and reported photocatalysts. In turn, it was also discovered that sulfur-deficient WS_2 in conjunction with other materials can effectively assist in antibacterial protection by removing them from water even under visible light [58]. This process occurs via generation of radicals and the extraction of membrane phospholipids that lead to the bacterial inactivation.

8.2.6.4 Photoconversion of CO_2

Conversion of CO_2 via presence of catalyst that is activated by light irradiation is an extremely attractive approach that can greatly lower concentration of this harmful gaseous compound in the atmosphere and also make it become remodeled as a source of various highly valuable carbon-neutral raw materials that can be used for chemical industry. Band gap positions of MoS_2 and WS_2 perfectly match the redox potentials of most of reactions that are involved in this photocatalytic processing, and thus given their ability to absorb visible light and other important characteristics, they might be considered as promising candidates. Yet, as this reaction involved OER-based step, the resulted outcome might not be considered as satisfactory. Following it, introduction of various defects, such as sulfur and metal vacancies, can contribute significantly to the overall efficiency of CO_2 conversion pushing it further as these defects can provide more active sites for the adsorbed molecules, decrease overall recombination rate of charge carries, improve the ratio of absorbed photons, lower the band gap, etc. In this regard, the control over defect presence is highly important as to reach their most optimal concentration and availability. For example, Meier et al. [59] fabricated MoS_x nanoflowers with various stoichiometries via CVD using different ramp rates and discovered that only at x equaled to ~1.8, the highest performance for CO_2 photoreduction and its consequent transformation into CO was obtained under irradiation with visible light compared with that of samples where x was identified to be ~2 and ~1.6. It has to be noticed that these stoichiometries are referred to bulk compositions as it was obtained by energy dispersive X-ray. In turn, post-synthesis thermal treatment in hydrogen at 480 °C for 30 min was applied to $MoS_{1.8}$ to further improve its performance by increasing the overall crystal distortion within it as more S atoms become removed from the surface. It resulted in exposure of additional active edges. Thus, the obtained structure demonstrated two times higher CO yield compared with that of untreated sample [59].

8.2.6.5 Other Applications

Apart from the above-mentioned well-known and recognizable photocatalytic reactions where defective MoS_2 and WS_2 can be applied, it also can be used successfully in other less studied but nevertheless also highly important light-induced processing.

(a) *Photocatalytic Nitrogen Fixation*. Following recent report of Sun et al. [60], it was revealed that O-doped MoS_2 nanosheets can demonstrate higher activity as co-catalysts than that of Pt to assist in the photocatalytic nitrogen fixation of CdS nanorods. The origin of this improvement was attributed to the presence of S vacancies which resulted in higher electronic conductivity, consequent appearance of more active edge sites, improved specific surface area, enhanced visible light absorption, and reduced charge separation rate compared with that

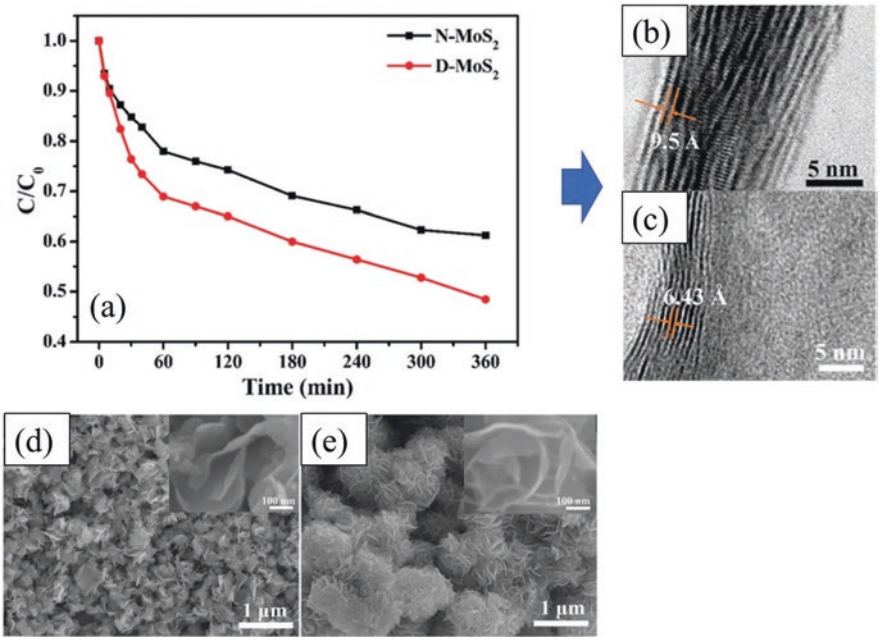

Fig. 8.7 (**a**) Comparison of the removal of Cr (VI) using D-MoS_2 and N-MoS_2. Cross-sectional HRTEM image of (**b**) D-MoS_2 and (**c**) N-MoS_2. FESEM images of (**d**) D-MoS_2 and (**e**) N-MoS_2. D-MoS_2 and N-MoS_2 represents defective and fully stoichiometric compounds, respectively. (Adapted from Ref. [61] with permission of *The Royal Society of Chemistry (RSC)* on behalf of the *Centre National de la Recherche Scientifique (CNRS) and the RSC*. Copyright 2018)

of fully stoichiometric MoS_2. Consequently, the resulted composite exhibited an outstanding production rate of ammonia equaled to 8220.83 μmol L^{-1} h^{-1} g^{-1} and long-term stability under simulated solar light irradiation, in fact, significantly higher than that of pure CdS nanorods, CdS-Pt of defect-free MoS_2-CdS.

(b) *Photocatalytic Reduction of Cr (IV).* Sun et al. [61] revealed that MoS_2 filled with defects demonstrated nearly 1.5-fold higher activity toward photocatalytic reduction of Cr (IV) compared with that of fully stoichiometric sample (Fig. 8.7a). The origin of this improvement was referred to the introduction of disorder composition that led to enlargement of interlayer spacing (Fig. 8.7b, c). It allowed to significantly improve the insertion of the chromium ions, to enhance the exposure of the active sites, and also to advance the ion diffusion. In addition, the formation of mesoporous structure in defective MoS_2 nanosheets (Fig. 8.7d, e) resulted in almost twofold enlargement of surface area taking fully stoichiometric sample as standard, and thus more reactive sites can be accommodated.

8.2.6.6 Current Challenges and Future Perspectives

As a visible light-sensitive photocatalyst, MoS_2- and WS_2-based nanostructured materials have been extensively applied in various photocatalytic processing, such as hydrogen production, dye degradation, CO_2 conversion, etc. However, despite their very attractive and great characteristics, it was revealed that rapid recombination of light-induced charge carriers, limited presence of active edge sites, and low mechanical and chemical stabilities due to atomic-scale compositions are the main obstacles that prevent the high performance of these materials. To address these problems, it was suggested to use defect engineering which correct and successful adaption not only might lead to advancement of basic properties of these materials but also results in appearance of new and unexpected yet highly desirable features that presence can only be extended further the existed boundaries and limitations in photocatalytic application.

For example, MoS_2 filled with sulfur vacancies and supported by applied tensile stress that is used to adjust newly created mid-gap states demonstrated one of the highest efficiencies for HER reactions achieved so far [55]. In turn, performance of oxidation-based reactions, namely, OER, is still extremely low, and it is very far from any expectations as there is high overpotentials associated with this reaction. Thus, if MoS_2 or WS_2 are used to proceed the overall photocatalytic process including all intermediate steps, its outcome is insufficient and often cannot be compared with that associated with other recognizable materials such as Ta_3N_5 or TaON. Definitely, they still can be used as co-catalyst or in combination with other structures thus creating complex compositions. Yet, this pathway might not be considered as optimal. *Firstly*, as overall reaction rate, for example, for water splitting is determined by both half reaction, thus improving only HER outcome would not ultimately mean that production of hydrogen in this case becomes significantly higher. To achieve it, the catalyst which is responsible for proceeding of OER reaction also is supposed to show high and prolong activity. *Secondly*, this geometry requires additional efforts such as searching, adoption, development, and application of proper synthesis procedure, etc. which brings more complication and time/resource consumption thus making the attractiveness of these complex compositions very questionable.

In this regard, it is suggested that defect engineering can greatly assist in overcoming problems associated with OER as it was shown that using the changes in intrinsic structure enable to effectively increase the performance of MoS_2 and WS_2 toward progressing this reaction without using external materials or chemicals. As an illustration, sulfur vacancies improve into several times the productivity of overall CO_2 photoconversion process [59] that includes both reduction and oxidation steps. Even though it is a local success, however, it shows the direction where the current progress can move. Thus, as application of defect engineering toward these materials is a very novel and only recently discovered topic, there is more unknown laid ahead compared with already obtained knowledge. Following it, deeper and more extended investigation is in a great need as to understand how far the photocatalytic activities of MoS_2 and WS_2 toward performing overall reaction can be advanced.

8.3 Final Remarks About Defective MoS_2 and WS_2

Investigation of nanoscaled MoS_2 and WS_2 has very short history as their unique properties and characteristics were discovered only very recently. Initially, it was generally accepted that production of completely crystallized and fully stoichiometric compounds is the most effective method to reach their best characteristics and features. Thus, it can be effectively utilized in boosting further the productivity of photocatalytic processing. In turn, later discoveries revealed that defects introduced in proper way and adjusted accordingly to accurately determined strategy and pattern can provide more benefits as the accompanied evolution of structural and chemical properties enables to control other important characteristics such as charge transportation, activation, and optimization of adsorbed molecules, etc. Yet, defect engineering approach still suffers from specific uncertainties which prevent its full and accurate implementation toward both MoS_2 and WS_2. *Firstly,* it is still debatable how the presence of V_S might influence the strengthening and increase of n-type conductivity given that these defects have acceptor-like characteristics and are supposed to cause an opposite effect. Even though some mechanism was proposed via theoretical simulations [50], experimental verification is highly necessary as to fully support them. *Secondly*, most efforts in literature are designated to investigation of defective MoS_2, while WS_2 which has better electron mobility and higher chemical and mechanical stabilities is studied in much less extent. *Thirdly*, the application of both materials filled with intrinsic defects other than sulfur vacancies is seldom reported in literature with regard to its application in photocatalytic reactions. For instance, ZnO has interstitials which play a crucial role in this processing. It would be great to obtain the same knowledge regarding nanoscaled MoS_2 and WS_2. *Fourthly*, given that synthesis of both materials can allow to fabricate structures that extend single monolayer and even reach formation of 1-D and 3-D compositions, it would be of interest to understand the specific characteristics and features of surface and bulk defects and how their localized appearance can be used to adjust their features and influence on performance as this topic is very seldom discussed in literature. *Fifthly*, as sulfur and metallic vacancies are one of the most dominant defects and given their acceptor-like characteristics, it will be of interest to see the synthesis of WS_2 and MoS_2 with intrinsically supported p-type conductivities accompanied by detailed investigation of their relevant properties and photocatalytic activities. Definitely, given that these acceptors are deep, additional negatively charged centers might be necessary in order to assist in realization of this transition.

Thus, given the above-mentioned, it is evident that the already existed accumulation of knowledge about defective MoS_2 and WS_2 cannot be considered as defined and finalized since there still exist a lot of questions which need to be answered. Thus, continuous efforts are required, and it is expected that many new and exciting findings are still awaiting ahead to be discovered.

References

1. D. Gupta, V. Chauhan, R. Kumar, A comprehensive review on synthesis and applications of molybdenum disulfide (MoS_2) material: Past and recent developments. Inorg. Chem. Commun. **121**, 108200 (2020). https://doi.org/10.1016/j.inoche.2020.108200
2. W. Zhao, J. Pan, Y. Fang, X. Che, D. Wang, K. Bu, F. Huang, Metastable MoS_2: Crystal structure, electronic band structure, synthetic approach and intriguing physical properties. Chem. Eur. J. **24**, 15942–15954 (2018). https://doi.org/10.1002/chem.201801018
3. I. Song, C. Park, H.C. Choi, Synthesis and properties of molybdenum disulphide: From bulk to atomic layers. RSC Adv. **5**, 7495–7514 (2014). https://doi.org/10.1039/C4RA11852A
4. C. Lan, C. Li, J.C. Ho, Y. Liu, 2D WS_2: From vapor phase synthesis to device applications. Adv. Electron. Mater. **7**, 2000688 (2021). https://doi.org/10.1002/aelm.202000688
5. J. Gusakova, X. Wang, L.L. Shiau, A. Krivosheeva, V. Shaposhnikov, V. Borisenko, V. Gusakov, B.K. Tay, Electronic properties of bulk and monolayer TMDs: Theoretical study within DFT framework (GVJ-2e method). Phys. Status Solidi (a) **214**, 1700218 (2017). https://doi.org/10.1002/pssa.201700218
6. B. Mahler, V. Hoepfner, K. Liao, G.A. Ozin, Colloidal synthesis of 1T-WS_2 and 2H-WS_2 nanosheets: Applications for photocatalytic hydrogen evolution. J. Am. Chem. Soc. **136**, 14121–14127 (2014). https://doi.org/10.1021/ja506261t
7. L. Liu, S.B. Kumar, Y. Ouyang, J. Guo, Performance limits of monolayer transition metal dichalcogenide transistors. IEEE Trans. Electron Devices **58**, 3042–3047 (2011). https://doi.org/10.1109/TED.2011.2159221
8. V. Kaushik, M. Ahmad, K. Agarwal, D. Varandani, B.D. Belle, P. Das, B.R. Mehta, Charge transport in 2D MoS_2, WS_2, and MoS_2-WS_2 heterojunction-based field-effect transistors: Role of ambipolarity. J. Phys. Chem. C **124**, 23368–23379 (2020). https://doi.org/10.1021/acs.jpcc.0c05651
9. C. Wu, J. Zhang, X. Tong, P. Yu, J.-Y. Xu, J. Wu, Z.M. Wang, J. Lou, Y.-L. Chueh, A critical review on enhancement of photocatalytic hydrogen production by molybdenum disulfide: From growth to interfacial activities. Small **15**, 1900578 (2019). https://doi.org/10.1002/smll.201900578
10. A.M.Z. Tan, C. Freysoldt, R.G. Hennig, Stability of charged sulfur vacancies in 2D and bulk MoS_2 from plane-wave density functional theory with electrostatic corrections. Phys. Rev. Mater. **4**, 064004 (2020). https://doi.org/10.1103/PhysRevMaterials.4.064004
11. H.-P. Komsa, A.V. Krasheninnikov, Native defects in bulk and monolayer MoS_2 from first principles. Phys. Rev. B **91**, 125304 (2015). https://doi.org/10.1103/PhysRevB.91.125304
12. S.H. Song, M.-K. Joo, M. Neumann, H. Kim, Y.H. Lee, Probing defect dynamics in monolayer MoS_2 via noise nanospectroscopy. Nat. Commun. **8**, 2121 (2017). https://doi.org/10.1038/s41467-017-02297-3
13. D. Liu, Y. Guo, L. Fang, J. Robertson, Sulfur vacancies in monolayer MoS_2 and its electrical contacts. Appl. Phys. Lett. **103**, 183113 (2013). https://doi.org/10.1063/1.4824893
14. L. Feng, J. Su, Z. Liu, Effect of vacancies on structural, electronic and optical properties of monolayer MoS_2: A first-principles study. J. Alloys Compd. **613**, 122–127 (2014). https://doi.org/10.1016/j.jallcom.2014.06.018
15. A. Janotti, C.G. Van de Walle, Oxygen vacancies in ZnO. Appl. Phys. Lett. **87**, 122102 (2005). https://doi.org/10.1063/1.2053360
16. W. Zhou, X. Zou, S. Najmaei, Z. Liu, Y. Shi, J. Kong, J. Lou, P.M. Ajayan, B.I. Yakobson, J.-C. Idrobo, Intrinsic structural defects in monolayer molybdenum disulfide. Nano Lett. **13**, 2615–2622 (2013). https://doi.org/10.1021/nl4007479
17. J.-Y. Noh, H. Kim, Y.-S. Kim, Stability and electronic structures of native defects in single-layer MoS_2. Phys. Rev. B **89**, 205417 (2014). https://doi.org/10.1103/PhysRevB.89.205417
18. M. Pizzochero, O.V. Yazyev, Point defects in the 1T' and 2H phases of single-layer MoS_2: A comparative first-principles study. Phys. Rev. B **96**, 245402 (2017). https://doi.org/10.1103/PhysRevB.96.245402

19. A. Singh, A.K. Singh, Origin of n-type conductivity of monolayer MoS_2. Phys. Rev. B **99**, 121201 (2019). https://doi.org/10.1103/PhysRevB.99.121201
20. V. Carozo, Y. Wang, K. Fujisawa, B.R. Carvalho, A. McCreary, S. Feng, Z. Lin, C. Zhou, N. Perea-López, A.L. Elías, B. Kabius, V.H. Crespi, M. Terrones, Optical identification of sulfur vacancies: Bound excitons at the edges of monolayer tungsten disulfide. Sci. Adv. **3**, e1602813 (2017). https://doi.org/10.1126/sciadv.1602813
21. Y. Guo, D. Liu, J. Robertson, Chalcogen vacancies in monolayer transition metal dichalcogenides and Fermi level pinning at contacts. Appl. Phys. Lett. **106**, 173106 (2015). https://doi.org/10.1063/1.4919524
22. Z. Chu, C.-Y. Wang, J. Quan, C. Zhang, C. Lei, A. Han, X. Ma, H.-L. Tang, D. Abeysinghe, M. Staab, X. Zhang, A.H. MacDonald, V. Tung, X. Li, C.-K. Shih, K. Lai, Unveiling defect-mediated carrier dynamics in monolayer semiconductors by spatiotemporal microwave imaging. PNAS **117**, 13908–13913 (2020). https://doi.org/10.1073/pnas.2004106117
23. F. Fabbri, F. Dinelli, S. Forti, L. Sementa, S. Pace, G. Piccinini, A. Fortunelli, C. Coletti, P. Pingue, Edge defects promoted oxidation of monolayer WS_2 synthesized on epitaxial graphene. J. Phys. Chem. C **124**, 9035–9044 (2020). https://doi.org/10.1021/acs.jpcc.0c00350
24. S. Salehi, A. Saffarzadeh, Atomic defect states in monolayers of MoS_2 and WS_2. Surf. Sci. **651**, 215–221 (2016). https://doi.org/10.1016/j.susc.2016.05.003
25. X. Wang, J. Dan, Z. Hu, J.F. Leong, Q. Zhang, Z. Qin, S. Li, J. Lu, S.J. Pennycook, W. Sun, C.H. Sow, Defect heterogeneity in monolayer WS_2 unveiled by work function variance. Chem. Mater. **31**, 7970–7978 (2019). https://doi.org/10.1021/acs.chemmater.9b02157
26. B. Schuler, J.-H. Lee, C. Kastl, K.A. Cochrane, C.T. Chen, S. Refaely-Abramson, S. Yuan, E. van Veen, R. Roldán, N.J. Borys, R.J. Koch, S. Aloni, A.M. Schwartzberg, D.F. Ogletree, J.B. Neaton, A. Weber-Bargioni, How substitutional point defects in two-dimensional WS_2 induce charge localization, spin-orbit splitting, and strain. ACS Nano **13**, 10520–10534 (2019). https://doi.org/10.1021/acsnano.9b04611
27. W.-F. Li, C. Fang, M.A. van Huis, Strong spin-orbit splitting and magnetism of point defect states in monolayer WS_2. Phys. Rev. B **94**, 195425 (2016). https://doi.org/10.1103/PhysRevB.94.195425
28. P. Vancsó, G.Z. Magda, J. Pető, J.-Y. Noh, Y.-S. Kim, C. Hwang, L.P. Biró, L. Tapasztó, The intrinsic defect structure of exfoliated MoS_2 single layers revealed by scanning tunneling microscopy. Sci. Rep. **6**, 29726 (2016). https://doi.org/10.1038/srep29726
29. T.-H. Le, Y. Oh, H. Kim, H. Yoon, Exfoliation of 2D materials for energy and environmental applications. Chem. Eur. J. **26**, 6360–6401 (2020). https://doi.org/10.1002/chem.202000223
30. J. Hong, Z. Hu, M. Probert, K. Li, D. Lv, X. Yang, L. Gu, N. Mao, Q. Feng, L. Xie, J. Zhang, D. Wu, Z. Zhang, C. Jin, W. Ji, X. Zhang, J. Yuan, Z. Zhang, Exploring atomic defects in molybdenum disulphide monolayers. Nat. Commun. **6**, 6293 (2015). https://doi.org/10.1038/ncomms7293
31. M. Precner, T. Polaković, Q. Qiao, D.J. Trainer, A.V. Putilov, C. Di Giorgio, I. Cone, Y. Zhu, X.X. Xi, M. Iavarone, G. Karapetrov, Evolution of metastable defects and its effect on the electronic properties of MoS_2 films. Sci. Rep. **8**, 6724 (2018). https://doi.org/10.1038/s41598-018-24913-y
32. M.E. Pam, Y. Shi, J. Hu, X. Zhao, J. Dan, X. Gong, S. Huang, D. Geng, S. Pennycook, L.K. Ang, H.Y. Yang, Effects of precursor pre-treatment on the vapor deposition of WS_2 monolayers. Nanoscale Adv. **1**, 953–960 (2019). https://doi.org/10.1039/C8NA00212F
33. B. Groven, M. Heyne, A. Nalin Mehta, H. Bender, T. Nuytten, J. Meersschaut, T. Conard, P. Verdonck, S. Van Elshocht, W. Vandervorst, S. De Gendt, M. Heyns, I. Radu, M. Caymax, A. Delabie, Plasma-enhanced atomic layer deposition of two-dimensional WS_2 from WF_6, H_2 plasma, and H_2S. Chem. Mater. **29**, 2927–2938 (2017). https://doi.org/10.1021/acs.chemmater.6b05214
34. Y. Liu, Y. Xie, L. Liu, J. Jiao, Sulfur vacancy induced high performance for photocatalytic H_2 production over 1T@2H phase MoS_2 nanolayers. Catal. Sci. Technol. **7**, 5635–5643 (2017). https://doi.org/10.1039/C7CY01488K

35. Z. Zhang, Y. Dong, H. Sun, G. Liu, S. Liu, X. Yang, Defect-rich 2D reticulated MoS_2 monolayers: Facile hydrothermal preparation and marvellous photoelectric properties. J. Taiwan Inst. Chem. Eng. **101**, 221–230 (2019). https://doi.org/10.1016/j.jtice.2019.04.035
36. D. Zhang, T. Liu, J. Cheng, Q. Cao, G. Zheng, S. Liang, H. Wang, M.-S. Cao, Lightweight and high-performance microwave absorber based on 2D WS_2-RGO heterostructures. Nano-Micro Lett. **11**, 38 (2019). https://doi.org/10.1007/s40820-019-0270-4
37. S. Cao, T. Liu, S. Hussain, W. Zeng, X. Peng, F. Pan, Hydrothermal synthesis of variety low dimensional WS_2 nanostructures. Mater. Lett. **129**, 205–208 (2014). https://doi.org/10.1016/j.matlet.2014.05.013
38. X. Lu, Y. Lin, H. Dong, W. Dai, X. Chen, X. Qu, X. Zhang, One-step hydrothermal fabrication of three-dimensional MoS_2 nanoflower using polypyrrole as template for efficient hydrogen evolution reaction. Sci. Rep. **7**, 42309 (2017). https://doi.org/10.1038/srep42309
39. Y. Li, K. Yin, L. Wang, X. Lu, Y. Zhang, Y. Liu, D. Yan, Y. Song, S. Luo, Engineering MoS_2 nanomesh with holes and lattice defects for highly active hydrogen evolution reaction. Appl. Catal. B **239**, 537–544 (2018). https://doi.org/10.1016/j.apcatb.2018.05.080
40. G. Alonso, V. Petranovskii, M. Del Valle, J. Cruz-Reyes, A. Licea-Claverie, S. Fuentes, Preparation of WS_2 catalysts by in situ decomposition of tetraalkylammonium thiotungstates. Appl. Catal. A **197**, 87–97 (2000). https://doi.org/10.1016/S0926-860X(99)00536-0
41. C. Tsai, H. Li, S. Park, J. Park, H.S. Han, J.K. Nørskov, X. Zheng, F. Abild-Pedersen, Electrochemical generation of sulfur vacancies in the basal plane of MoS_2 for hydrogen evolution. Nat. Commun. **8**, 15113 (2017). https://doi.org/10.1038/ncomms15113
42. R. Chaabani, A. Lamouchi, B. Mari, R. Chtourou, Effect of sulfurization on physical and electrical properties of MoS_2 films synthesized by electrodeposition route. Mater. Res. Express **6**, 115902 (2019). https://doi.org/10.1088/2053-1591/ab438c
43. S. Geng, W. Yang, Y. Liu, Y. Yu, Engineering sulfur vacancies in basal plane of MoS_2 for enhanced hydrogen evolution reaction. J. Catal. **391**, 91–97 (2020). https://doi.org/10.1016/j.jcat.2020.05.042
44. Y. Xia, C. Hu, S. Guo, L. Zhang, M. Wang, J. Peng, L. Xu, J. Wang, Sulfur-vacancy-enriched MoS_2 nanosheets based heterostructures for near-infrared optoelectronic NO_2 sensing. ACS Appl. Nano Mater. **3**, 665–673 (2020). https://doi.org/10.1021/acsanm.9b02180
45. L. Li, Z. Qin, L. Ries, S. Hong, T. Michel, J. Yang, C. Salameh, M. Bechelany, P. Miele, D. Kaplan, M. Chhowalla, D. Voiry, Role of sulfur vacancies and undercoordinated Mo regions in MoS_2 nanosheets toward the evolution of hydrogen. ACS Nano **13**, 6824–6834 (2019). https://doi.org/10.1021/acsnano.9b01583
46. Q. Zhu, W. Chen, H. Cheng, Z. Lu, H. Pan, WS2 Nanosheets with highly-enhanced electrochemical activity by facile control of sulfur cacancies. ChemCatChem **11**, 2667–2675 (2019). https://doi.org/10.1002/cctc.201900341
47. L. Feng, J. Su, S. Chen, Z. Liu, First-principles investigations on vacancy formation and electronic structures of monolayer MoS_2. Mater. Chem. Phys. **148**, 5–9 (2014). https://doi.org/10.1016/j.matchemphys.2014.07.026
48. J. Wei, Z. Ma, H. Zeng, Z. Wang, Q. Wei, P. Peng, Electronic and optical properties of vacancy-doped WS_2 monolayers. AIP Adv. **2**, 042141 (2012). https://doi.org/10.1063/1.4768261
49. I.S. Kim, V.K. Sangwan, D. Jariwala, J.D. Wood, S. Park, K.-S. Chen, F. Shi, F. Ruiz-Zepeda, A. Ponce, M. Jose-Yacaman, V.P. Dravid, T.J. Marks, M.C. Hersam, L.J. Lauhon, Influence of stoichiometry on the optical and electrical properties of chemical vapor deposition derived MoS_2. ACS Nano **8**, 10551–10558 (2014). https://doi.org/10.1021/nn503988x
50. J. Yang, F. Bussolotti, H. Kawai, K.E.J. Goh, Tuning the conductivity type in monolayer WS_2 and MoS_2 by sulfur vacancies. Phys. Status Solidi RRL **14**, 2000248 (2020). https://doi.org/10.1002/pssr.202000248
51. W. Kim, G. Kwak, M. Jung, S.K. Jo, J.B. Miller, A.J. Gellman, K. Yong, Surface and internal reactions of ZnO nanowires: Etching and bulk defect passivation by H atoms. J. Phys. Chem. C **116**, 16093–16097 (2012). https://doi.org/10.1021/jp304191m

52. X. Zheng, A. Calò, T. Cao, X. Liu, Z. Huang, P.M. Das, M. Drndic, E. Albisetti, F. Lavini, T.-D. Li, V. Narang, W.P. King, J.W. Harrold, M. Vittadello, C. Aruta, D. Shahrjerdi, E. Riedo, Spatial defects nanoengineering for bipolar conductivity in MoS_2. Nat. Commun. **11**, 3463 (2020). https://doi.org/10.1038/s41467-020-17241-1
53. E. German, R. Gebauer, Why are MoS_2 monolayers not a good catalyst for the oxygen evolution reaction? Appl. Surf. Sci. **528**, 146591 (2020). https://doi.org/10.1016/j.apsusc.2020.146591
54. F.M. Pesci, M.S. Sokolikova, C. Grotta, P.C. Sherrell, F. Reale, K. Sharda, N. Ni, P. Palczynski, C. Mattevi, MoS_2/WS_2 heterojunction for photoelectrochemical water oxidation. ACS Catal. **7**, 4990–4998 (2017). https://doi.org/10.1021/acscatal.7b01517
55. H. Li, C. Tsai, A.L. Koh, L. Cai, A.W. Contryman, A.H. Fragapane, J. Zhao, H.S. Han, H.C. Manoharan, F. Abild-Pedersen, J.K. Nørskov, X. Zheng, Activating and optimizing MoS_2 basal planes for hydrogen evolution through the formation of strained sulphur vacancies. Nat. Mater. **15**, 48–53 (2016). https://doi.org/10.1038/nmat4465
56. S. Piskunov, O. Lisovski, Y.F. Zhukovskii, P.N. D'yachkov, R.A. Evarestov, S. Kenmoe, E. Spohr, First-principles evaluation of the morphology of WS_2 nanotubes for application as visible-light-driven water-splitting photocatalysts. ACS Omega **4**, 1434–1442 (2019). https://doi.org/10.1021/acsomega.8b03121
57. L. Lin, N. Miao, J. Huang, S. Zhang, Y. Zhu, D.D. Horsell, P. Ghosez, Z. Sun, D.A. Allwood, A photocatalyst of sulphur depleted monolayered molybdenum sulfide nanocrystals for dye degradation and hydrogen evolution reaction. Nano Energy **38**, 544–552 (2017). https://doi.org/10.1016/j.nanoen.2017.06.008
58. X. Hou, T. Shi, C. Wei, H. Zeng, X. Hu, B. Yan, A 2D-2D heterojunction Bi_2WO_6/WS_{2-x} as a broad-spectrum bactericide: Sulfur vacancies mediate the interface interactions between biology and nanomaterials. Biomaterials **243**, 119937 (2020). https://doi.org/10.1016/j.biomaterials.2020.119937
59. A.J. Meier, A. Garg, B. Sutter, J.N. Kuhn, V.R. Bhethanabotla, MoS_2 nanoflowers as a gateway for solar-driven CO_2 photoreduction. ACS Sustain. Chem. Eng. **7**, 265–275 (2019). https://doi.org/10.1021/acssuschemeng.8b03168
60. B. Sun, Z. Liang, Y. Qian, X. Xu, Y. Han, J. Tian, Sulfur vacancy-rich O-doped 1T-MoS_2 nanosheets for exceptional photocatalytic nitrogen fixation over CdS. ACS Appl. Mater. Interfaces **12**, 7257–7269 (2020). https://doi.org/10.1021/acsami.9b20767
61. H. Sun, T. Wu, Y. Zhang, D.H.L. Ng, G. Wang, Structure-enhanced removal of Cr (VI) in aqueous solutions using MoS_2 ultrathin nanosheets. New J. Chem. **42**, 9006–9015 (2018). https://doi.org/10.1039/C8NJ01062E

Chapter 9
Defect Engineering of Other Nanostructured Semiconductors

9.1 Introduction

As photocatalytic reaction is considered to be complex, multistep processing, the material which is going to be applied for its activation and consequent optimization should demonstrate the accumulation of various features such as capability to absorb visible light, suitable positions of conduction and valence bands with respect to redox potentials, low recombination rate of charge carriers, their perfect transportation characteristics and kinetics, chemical and mechanical stabilities, etc. In addition, it should have high affordance and abundance, relative simplicity in fabrication or synthesis processes, non-toxicity, and environmental friendliness. Overall, there is a strong believe that complete and ultimate fulfillment of these requirements would enable the appearance of an efficient and readily accessible photocatalyst which proper utilization might pave the way into the future where consumption industries play less role. However, despite numerous efforts, currently, it is considered as ultimate and hardly achievable goal given the difficulties and challenges that need to be overpassed for reaching it. Simply to say, most of the presently available materials that are used to proceed light-induced reactions have too many restrictions which prevent them from showing their best characteristics including high efficiency and prolong stability. For example, widely reported ZnO and TiO_2 have gap of ~3.2–3.4 eV; thus they show sensitivity only for irradiation with UV light. It limits the concentration of available photoinduced electrons and holes that can be used to react with adsorbed molecules. In turn, Ta_3N_5, despite capability to absorb significant part of solar spectra, suffers from chemical instability and high overpotential.

In this regard, it is evident that certain modifications of materials are required to be implemented in order to advance their performance. Out of all available techniques and methods that can be employed to make it, defect engineering has been considered as one of the most attractive approaches to serve this goal given its

V. Gurylev, *Nanostructured Photocatalyst via Defect Engineering*,
https://doi.org/10.1007/978-3-030-81911-8_9

simplicity and accessibility. To be clear, reorganizing the periodical atomic arrangement within crystal lattice, playing with stoichiometry, or adjusting chemical composition within specific range is enough to strengthen the most significant and useful characteristics of target material. Following it, the overall performance can increase greatly hence allowing to approach one step closer toward satisfying the most demanding requirements for achieving the desire efficiency. However, it is necessary to consider one important issue. Given that for years the concept of "ideal structure" has been dominated in literature, this approach becomes applied only recently. Thus, it is unsurprising that the most intensive development of defect engineering for the present is generally associated with its employment toward modifying already established and widely recognizable photocatalysis. To put it simply, numerous studies and review are available in literature that are fully or partially dedicated to understanding, investigating, and utilizing of defective TiO_2, ZnO, MoS_2, and other related well-known compounds and structures.

Accordingly, it would be also very interesting to determine how intentional introduction of intrinsic defects can be implemented to advance other less accessible and studied but nevertheless also very attractive materials that also have great potentials to be used as photocatalysis. In fact, some of them possess very unique and highly desirable characteristics that existence and consequent enhancement are directly associated with geometrical and electronic structures. However, their full and non-limited contribution to overall performance often is limited as it been shadowed by the presence of certain and defined shortcomings or handicaps. Hence, these materials are regarded as low-active, non-stable, or having important specifications beyond certain acceptable standards which make them to be unable for showing the required performance. It leads to reduced interest toward them which is expressed in consequently slower and less sophisticated development of their features. In this regard, it is believed that defect engineering can be employed to effectively increase their applicability and attractiveness.

9.2 Methods to Introduce Intrinsic Defects: Recent Trends and Future Perspectives

Current achievements in introducing various intrinsic defects can provide very wide spectrum of different approaches and techniques that can be utilized to obtain the required composition within almost any type of materials regardless its attribution to binary or ternary compounds; presence of oxide, sulfide, or other chemicals within its composition; or existence of defined particularities in chemical composition. Consequently, more precise adjustment of relevant parameters and tuning of certain settings can be used to reach even higher level of precisions with respect to the scope of produced changes and their association with the appearance of desired

characteristics and features. It is commonly accepted that synthesis or post-synthesis treatment is the most utilized approaches to realize these protocols, and there is not so much difference in quality and outcome with respect to applicability of both of them as their specified and designated influences are determined mostly by the essence of materials as well as the scope and nature of resulted transformations. For example, formation of non-metallic vacancies in MoS_2 and TiO_2 via evacuation of relevant atoms would follow very different mechanisms given dissimilarities in chemical composition of both materials even though the same approaches can be used to create them.

Recent trends toward continuous production of nanostructured materials leads to gradual appearance of certain very critical and extremely strict requirements for introducing defects. Simply to say, this process should be considered in terms of its straightforward and prosperous adaptation along with suitability toward expected industrial implementation, and it is often the case that methodologies which currently are developed and successfully utilized within the laboratories might show less practicability outside of them. It might refer to various factors such as utilization of complex multistep agenda, application of very dangerous and thus difficult to handle chemicals, inability to form strictly defined and highly specific composition within limited number of experimental attempts, etc. In this regard, it is believed that the future of creating defect structures is laid in their direct synthesis via only single fabrication step by using the approaches that allow to achieve precise control over morphology, crystal structures, and stoichiometry at the level when these changes take the form of very accurate quantitative adjustments within defined range and dimension. Following it, one might consider that chemical and atomic vapor deposition (CVD and ALD, respectively) has a very high compliance with these requirements. In fact, their proper employment makes the formation of defective composition being presented in analogy of cooking a cake where the parameters of fabrication process such as choice of proper precursor, its concentration, and pressures take the role of various ingredients utilized for preparing drought, while the adjustments of conditions within the reaction chamber can have parallel to tuning the regime of baking oven. Furthermore, full automatization can effectively address the question of repeatability and reproducibility granting possibility to minimize human error and influence of other related factors.

However, one has to admit that it is a far-reaching dream as currently CVD- and ALD-based processes are regarded to be highly demanding, expensive, and thus often unaffordable technologies. Accordingly, chemical-based fabrication or other related approaches along with post-synthesis treatment are still very popular routines to be used given their accessibility and evident simplicity of each step which accounts for their widespread. Thus, main information regarding defect compositions up to the present is mostly obtained by them. Yet, it is believed that proper optimization and adaptation of CVD or ALD processes might very soon change this trend.

9.3 Defect-Controlled Properties: Tuning and Adjustment

Formation of defective compositions or deviations in stoichiometry within the target material often results in certain modifications of its characteristics and features leading to their advancement or oppositely causing them to be degraded. The following trends are generally defined.

Changes in Structural Properties The presence of intrinsic defect especially in the form of vacancies can cause the shrinkage or expansion of crystal lattice, depending on whether the anion or cation-like atoms were evacuated. It also leads to appearance of disordered or distorted highly localized compositions. In turn, the overall roughness of surface can increase significantly accompanied by development of mesoporous composition or exposure of internal and previously hidden structural features. To realize these modifications, it is suggested that formation of defects is supposed to be proceeded within the surface or sub-surface layers as shifting their residence deeper to the bulk might result in opposite trend, i.e., reducing the specific surface area.

Changes in Optical Properties It is generally accepted that materials filled with defects enable to show extended optical characteristics. This improvement can be attributed to several origins. *Firstly*, there are appearance of additional energy states within the band gap that localized close to valence or conduction bands resulting in their expansion. Hence, the shift of absorption edge toward visible or infrared wavelength can be observed. *Secondly*, it is also suggested that these additional mid-gap states can serve as step for electrons to travel between valence and conducted band thus allowing to utilize photons with lower energies. *Thirdly*, higher porosity of surface morphology mentioned above can contribute greatly to increasing the trap of light.

Changes in Electronic Properties The type of defects and its charge states and also the nature of material determine the exact positions of corresponding energy states in band gap with respect to valence or conduction bands as well as their defined influences on transportation characteristics of charge carriers. In this regard, it might be difficult to establish general description and classification that could be commonly accepted and recognized as there are a lot of exceptions and abnormalities regarding each investigated system thus making their comparisons and systematizing to be challenging. For instance, it is widely accepted that in binary materials, especially the ones that have oxygen as its part, anion and cation vacancies are identified to represent donor- and acceptor-like characteristics which are ascribed by the appearance of corresponding localized energy states close to conduction and valence band, respectively. This classification is perfectly applied to ZnO or TiO_2 where transition levels associated with oxygen deficiencies were determined to be located in the upper part of band gap. In turn, MoS_2 is drastically different since

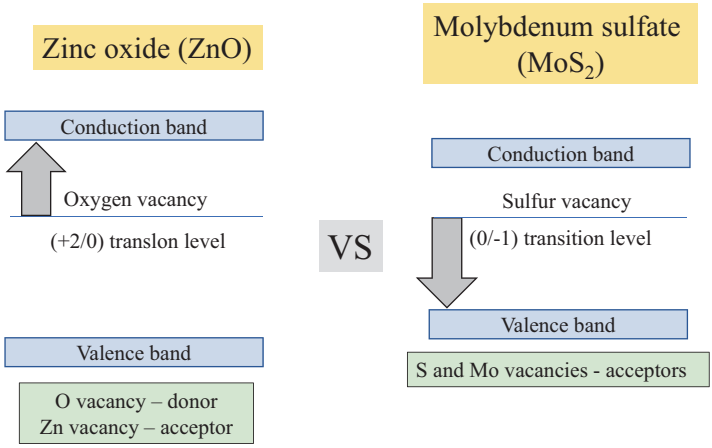

Fig. 9.1 Schematic representation of transition level associated with oxygen and sulfur vacancies in ZnO and MoS_2, respectively

even though S vacancy has very similar positioning of its transition within band gap, yet this defect is recognized as deep acceptor that has association with appearance of holes (Fig. 9.1). Yet, it would be incorrect to say that ZnO and MoS_2 are totally different as both Zn and Mo vacancies, respectively, are acceptors. Thus, it is evident that the only common ground regarding the influence of defects in the electronic structure of band gap is the formation of corresponding energy states while their exact specification and consequent particulates of tuning should be accessed very carefully and with regard to each defined material.

Changes in Electrical Properties It is evident that correctly chosen defects can serve a highly positive role in making a beneficial and crucial contribution toward increasing the conductivity of material as their introduction and proper managements can be used to enhance concentration and mobility of desirable type of charge carriers. As an illustration, oxygen vacancies in most of binary oxides show shallow donor-like characteristics; thus their presence usually leads to the strengthening of n-type behavior. In turn, introduction of acceptor-like defects and their dominance might cause the appearance of n → p transition which can be realized in the form of localized domain or include whole body of material. Yet, it would be incorrect to assume that the more defects, the more enhanced the corresponding conductivity becomes. In fact, under improper management, they can be transformed into trapping center that increases the recombination of charge carriers or makes other negative impacts. As a result, the material might lose its semiconductor nature and become an insulator.

9.4 Defective Nanostructures: Examples

9.4.1 Brief Overview

Introduction of defect within various nanostructured materials usually follows very similar trends as the only parameter which defines the applicability and uniqueness of certain and defined strategy toward realization of changes within their internal compositions, and subsequent influence on photoactivity is usually associated with specific features of geometrical and electronic structures. Thus, employment of this approach toward each particulate chemical system is very delicate and even in some way an intimate process and cannot be considered to follow once established and approved course if only within very general and broad terms leaving aside specifications toward certain details. Its means that in the absence of deep and thorough awareness to properly access and understand the presence of defects, it might lead to absolutely opposite results, and instead of creating highly effective photocatalyst with desirable characteristics, the development of compound that has partially or even fully degraded features causing the reduced performance can be proceeded instead. The borderline which separates both consequences and thus is used to identify the plausibility and relevance of changes within structure and compositions is defined by nature and characteristics of intrinsic defects such as their position in the band gap with regard to conduction and valence bands, which charge states has higher dominance, type of interaction with already existed charge carriers, etc. For example, it is evident that deep donors and acceptors mostly have very little contribution to the improving and strengthening of overall conductivity if only to serve as compensation centers. Furthermore, their extreme presence might lead to their transformation into centers that trap and consequently recombine charge carriers. Thus, their existence can lead to more harm than profits, and for the rare exemptions, they should be avoided.

The above-mentioned is especially important given that only limited information is accessible regarding the achieved progress toward applicability of defect engineering to advance less-studied materials such as C_3N_4, WO_3, Fe_2O_3, etc. that are often considered to be attractive alternatives and very promising substitution to already well-known and widely available photocatalysts. Hence, it might be difficult to identify how the proper management of their internal structure can be realized effectively so that the correlated changes in characteristics and properties would surely lead to positive impact and consequently increased performance, thus avoiding the possibility toward occurrence of any negative effect. In this regard, it is necessary to fully address each of these materials as to demonstrate particularities that are associated with introduction and further control of intrinsic defects within them.

9.4.2 Case Example I: g-C_3N_4

9.4.2.1 g-C_3N_4: Fundamentals

The graphite-like carbon nitride (g-C_3N_4), a metal-free n-type polymer-like semiconductor, is considered a very promising candidate to serve the role of an efficient photocatalysts given its various attractive properties and characteristics. This material is determined to have stacked two-dimensional layered planar structure regarded as N-substitute graphite framework which contains p-conjugated systems formed by sp^2 hybridization of carbon and nitrogen atoms [1]. Similar to other 2-D material, van der Waals force holds the stacking layers together, and each layer is composed of tri-s-triazine units connected with planar amino groups [2]. The distance of two layers in g-C_3N_4 is 3.26 Å, and it is slightly denser than the packing in crystalline graphite (d = 3.35 Å) which is explained by altering the localization of electrons and strengthening the binding between layers due to nitrogen atom substitution [3]. The following particularities are associated with this material. *Firstly*, g-C_3N_4 is considered to have high accessibility and affordance as it is composed of earth-abundant elements. It also has high biocompatibility and non-toxicity. *Secondly*, strong covalent bonding between carbon and nitrogen atoms allows g-C_3N_4 to demonstrate eminent chemical and thermal stability. To be clear, despite its polymeric nature, the decomposition process only can be activated after the temperature of the surrounding reaches over 600 °C [2]. *Thirdly*, this material can be fabricated by using extremely cheap and easily available precursors *via* very simple synthesis route and procedures. *Fourthly*, g-C_3N_4 has moderate width of band gap equaled to ~2.7–2.8 eV that allows to absorb light with wavelength up to 450–460 nm. In this regard, it is especially attractive that the positioning of both conduction and valence bands suits well the redox potentials of various photocatalytic processing such as water spiting, CO_2 reduction, etc. allowing to realize them without presence of additional co-catalyst. *Fifthly*, electronic and optical characteristics can be easily modified and adjusted by changing the number of layers that contribute to its structure [4].

Yet, along with these advantages, g-C_3N_4 also possesses several crucial drawbacks that significantly influence the efficiency of its utilization as photocatalysis such as high electron-hole recombination rate, still insufficient visible absorption (above 460 nm), low surface area (~10 m^2/g), small number of active sites for interfacial photoreactions, slow surface reaction kinetics, moderate strength for oxidation, and low charge mobility [5]. Additionally, given the position of valence band, it is evident that photo-generated holes of C_3N_4 can only be used for oxygen evolution from water oxidation but not for assistance in oxidation of -OH into hydroxyl radicals [6]. In this regard, proper and correct changes of internal structure and composition enable to address some of these problems. Out of all defects which can exist in this material, the main attention is given to nitrogen and carbon vacancies given how easy they can be produced, the capability to control their various particularities, and their consequent influence on the properties and characteristics of g-C_3N_4 with perspective to consequent usage of this material in photocatalytic processing.

9.4.2.2 How to Create Defects

There are numerous methods demonstrated in literature that can be used to achieve the formation of defects in g-C_3N_4. Compared with synthesis approach, post-synthesis treatment has higher attractiveness as it provides better flexibility towards choosing appropriate strategy and also by realizing more precise control over the changes in stoichiometric ratio even though there is additional complexity of the process. Overall, several most notable routes are briefly introduced below as to provide general overview of recent trends in this filed. For more detailed description, readers are suggested to address specialized literature.

Synthesis Approaches

(a) *Thermal Condensation of Nitrogen-Rich Materials*. Certain materials could be easily transformed into g-C_3N_4 after they become subjected to thermal treatment. In this case, temperature and duration of this processing; the choice of precursors, whether it is mixed with other chemicals; etc. influence crucially on the presence of vacancies in resulted composition. For example, Chen et al. [7] demonstrated that annealing of trithiocyanuric acid instead of melamine at 550 °C resulted in formation of sulfur-doped and nitrogen-deficient g-C_3N_4. In turn, Ding et al. [8] revealed that relatively similar composition could be achieved by adding nitric acid to the starting solution.

(b) *Hydrothermal/Solvothermal Methods*. Generally, application of this approach usually results in appearance of g-C_3N_4 with very low concentration of defects. In order to facilitate their formation and also to obtain precise control over their characteristics, it is suggested to use the inclusion of specific chemicals during preparation of solution as to facilitate the release of atoms from surface. For instance, it was demonstrated that addition of nitric acid to reaction solution during solvothermal synthesis can result in appearance of N vacancies in g-C_3N_4 [9]. It is of interest that this strategy also can be applied toward already prepared samples serving as extra treatment protocol. Particularly, Lin et al. [10] revealed that fluorine-modified g-C_3N_4 obtained via placing it into Teflon autoclave filled with designated chemicals at 140 °C demonstrated the presence of nitrogen deficiency.

Post-synthesis Approaches

(a) *Thermal Treatment in Various Atmospheres*. Annealing in various atmospheres including vacuum under relatively high temperatures over 200–300 °C can be used to introduce carbon or nitrogen vacancies into g-C_3N_4. In addition, it also has applicability of creating controlled disorder within its structure or even enable to greatly weaken van der Waals forces between layers and thus can advance even complete amorphization of fully crystalline compound that is accompanied by formation of short-range order atomic arrangement [11]. Particulate conditions of this process such as its duration as well as choice of the utilized gaseous ambient, flow rate, and purity play significant role in identifying not only which type of defects is introduced but also can be used to control its features such as concentration and distribution. For example,

Yang et al. [12] revealed that the longer the time and the higher the temperature of treatment under HN_3 atmosphere, the more the carbon vacancies produced.

(b) *Acid Treatment*. Soaking of already synthesized g-C_3N_4 in various acids for a defined period of time and at designated conditions can influence significantly on the overall chemical composition. For instance, Pawar et al. [13] investigated how treatment in concentrated HCl, HNO_3, and H_2SO_4 influences the transformation of as-fabricated g-C_3N_4 into nitrogen-deficient compound. It was discovered that after using these acids, the C/N ratio at the surface proceeded changes from original value of 0.93 to 0.99, 1.01, and 1.97, respectively.

(c) *Plasma Treatment*. Plasma treatment is also an effective method to create various defects in g-C_3N_4. Particularly, Qu et al. [14] demonstrated that realization of nitrogen deficiency can be proceeded *via* using dielectric barrier discharge plasma in H_2 atmosphere. It was determined that compared with traditional annealing processing using similar ambient, the utilization of this treatment resulted in higher concentration of nitrogen vacancies. In turn, Li et al. [15] by using very similar methodology and experimental setup determined that the longer the time of plasma exposure, the higher the C/N ratio.

9.4.2.3 Properties of Defective g-C_3N_4

Structural Properties Introduction of vacancies into this material usually results in significant enhancement of the roughness, development of integrated bubbly surface [16], and appearance of mesoporous compositions which greatly increase the availability of active sites for adsorption and consequent activation of molecules. For example, Kong et al. [9] demonstrated that stoichiometric and non-stoichiometric C_3N_4 had specific surface area of ~5 m^2/g and 52 m^2/g, respectively. In addition, the presence of nitrogen vacancies results in changes of the lattice constant as it was confirmed *via* positive shift of (002) characteristics peak in XRD pattern [10, 16]. In turn, it also could be interpreted as denser stacking and decreasing of the interlayer distance [9]. The more vacancies are introduced, the higher is the shift. This process is accompanied by degradation of the crystallinity, appearance of disorder localized sites, and consequent vanishment of long-range order. It is interesting that formation of carbon-deficient C_3N_4 demonstrates the absence of any shifts in characteristics peaks in X-ray diffraction pattern, and it only correlates with their reduced intensities regarded as decrease of periodical order [17, 18].

Optical Properties It is generally accepted that the presence of defects in g-C_3N_4 greatly influences its optical properties. Yet, whether it has positive or negative character is determined by which type of them is introduced. For example, formation of nitrogen vacancies often results in narrowing band gap, thus leading to increased sensitivity toward irradiation with visible light [8]. The more drastic the changes in stoichiometry, the more apparent the shift of absorption edge toward longer wavelength. In turn, carbon vacancies might lead to opposite phenomenon as their presence enables to increase the width of band gap [17, 18]. It is also necessary to

mention that accompanied appearance of defect-induce mesoporous composition also contributes greatly to the optical sensitivity of g-C_3N_4 as although some of the photons cannot be directly consumed by this material, they might become trapped within the bubbly surface composition which causes their repeated reflection until being totally consumed. Thus, the absorption of visible light with wavelength that is laid beyond band gap is increased greatly in parallel for both nitrogen- and carbon-deficient g-C_3N_4 (Fig. 9.2a). Finally, the presence of disorder structure or even complete amorphization also significantly enhances optical characteristics of this material. For example, Kang et al. [11] reveled that g-C_3N_4 after this transformation showed the change of band gap value from 2.82 to 1.90 eV.

Electronic Properties As the investigation of g-C_3N_4 only has begun very recently, the information about its defective composition is very limited. Overall, formation of nitrogen vacancies leads to appearance of energy states located close to conduction band within the distance of 0.18–1.1 eV from conduction band depending on their concentration or other related factors [16, 19]. Following it, these defects can be identified to have shallow or deep characteristics. They also have possibility to bring several additional changes into electronic configuration of band gap which however cannot be considered as mandatory since their occurrence follow the original experimental setup. *Firstly*, positions of both bands with respect to vacuum level can be slightly shifted up [10, 16] (Fig. 9.2b). This phenomenon can be correlated with altering the degree of π-electron delocalization in the conjugated system. *Secondly*, their presence potentially might result in appearance of overlapping with conduction band minimum causing development of band tail or shifting down its minimum thus, leading to reduced width of band gap. In turn, the presence of carbon vacancies causes the development of energy states at ~0.26 eV from conduction band [20]. Their existence leads to very significant edge-shifting of both valence and conduction bands compared with that of fully stoichiometric g-C_3N_4 which eliminates any possibility to appear the overlapping phenomena. Following it, these

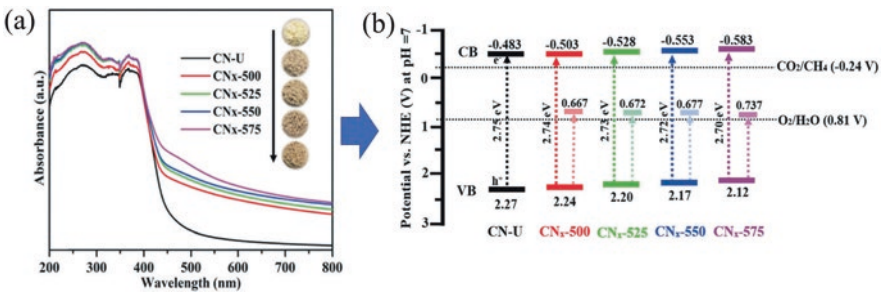

Fig. 9.2 (**a**) UV-vis DRS spectra of the g-C_3N_4 thermally treated under different temperatures in 3% hydrogen-argon gas (inset shows the color of each sample). These samples are identified to have nitrogen deficiency. (**b**) Schematic illustration of the electronic band configuration for each sample, with a lighter shade of colors representing the midgap state for the corresponding photocatalyst. (Reprinted from Ref. [16] with permission from *The Royal Chemical Society*. Copyright 2019)

defects are considered as deep donors which are unable to contribute into establishing of n-type conductivity; yet they can serve as compensation centers assisting in its strengthening.

Electrical Properties It is evident that the presence of nitrogen and carbon vacancies in g-C_3N_4 given their donor-like characteristics results in significant increase of charge transportation characteristics *via* enhancing their concentration and mobility and also by reducing the recombination rate thus resulting in strengthening of overall conductivity. In addition, it was suggested that mesoporous structures diminished interior resistance of C_3N_4 and contribute to the transfer of photogenerated carriers from bulk to surface [21] where they can participate in activation of redox reactions.

9.4.2.4 Photocatalytic Application of Defective g-C_3N_4

Defective g-C_3N_4 filled with nitrogen or carbon vacancies was identified to have greatly enhanced performance with regard to various photocatalytic reactions. In fact, many drawbacks which are associated with this material such as low specific surface area, very slow transport of charge carriers, and insufficient absorption of visible light could be easily addressed by properly adjusting the internal composition and stoichiometry thus extending them. Given very suitable positions of conduction and valence bands, modified g-C_3N_4 could be applied the following applications.

Photocatalytic and Photoelectrochemical Water Splitting It was revealed that introduction of carbon and nitrogen vacancies into g-C_3N_4 has positive influence on realizing this processing with higher efficiency. Yet, there is certain differences in the range of this improvement as it is not the same for both of these defects. Particularly, Li et al. [17] demonstrated that the presence of carbon deficiency led to twofold higher hydrogen production rate under irradiation with visible light in comparison with its fully stoichiometric counterpart. In turn, Tu et al. [19] utilized g-C_3N_4 filled with nitrogen vacancies under relatively the same conditions and revealed that efficiency of photocatalytic reaction enhanced for ~18-fold. Such an impressive performance could be explained by several origins including narrower band gap and presence of mid-gap states closer to conduction band that enables greatly assistance in transportation of charge carriers.

Light-Induced Water Purifications Defective g-C_3N_4 is excellent photocatalysts for this processing as it shows very high efficiency and stability. For instance, Lin et al. [10] reported that degradation rate of rhodamine B (RhB) under visible light by g-C_3N_4 filled with nitrogen vacancies was up to ~3.4 times faster compared with that of samples with higher stoichiometry. In turn, this enhancement for carbon-deficient g-C_3N_4 is less evident. Liang et al. [22] investigated the degradation of bisphenol A under relatively similar conditions and revealed that the presence of these defects only led to nearly ~1.6 times higher efficiency.

Photoconversion of CO_2 The presence of nitrogen vacancies in g-C_3N_4 results in increasing the yield of CO and CH_4 as a result of CO_2 photoconversion under visible light up to ~4.2 and ~3.16 times, respectively, versus non-modified samples [16, 19]. Considering absolute values, these demonstrated efficiencies could be comparable with outcome of some currently available most active catalysts [23]. For its part, carbon-deficient g-C_3N_4 showed lesser enhancement as the yield of CO evolution increased only for ~2.3 times using relatively similar conditions *via* irradiation by light with wavelength over 420 nm and taking stoichiometric counterpart as a standard [18]. In real terms, this composition also showed lower performance.

9.4.3 Case Example II: WO_3

9.4.3.1 WO_3: Fundamentals

Tungsten oxide (WO_3) has several thermodynamic phases out of which the most stable formation at room temperature is the monoclinic (γ-WO_3). When heated above 330 °C, it transforms to other phases, which, however, are considered as metastable since once cooled down, they all become converted back into γ-WO_3 [24]. There also exist a number of other metastable phases such as hexagonal of cubic ones which can be obtained at ambient conditions; yet, their preservation might be challengeable, and thus they are not discussed here. As for more detailed description, WO_3 crystal is composed of corner and edge-sharing WO_6 octahedral units, and they have a rhenium oxide (ReO_3) cubic structure [25]. It is determined to be d^0-transition metal oxide which has n-type conductivity. The width of band gap usually is estimated to be within the range of 2.6–2.8 eV where the valence band is formed by filled O2p orbitals, and the conduction band represents empty W5d orbitals. It is evident that WO_3 cannot absorb much of solar spectra given the limited sensitivity toward visible light. Following it, the color of this materials is yellow, similar to C_3N_4 as their abortion edges are almost identical. The lower boundary of conduction band locates below the redox potentials of photocatalytic hydrogen evolution; thus it is unable to be used for overall hydrogen generation and also provides limited choice of reaction pathways to proceed CO_2 conversion. On its part, the positioning of valence band (VB) potential allows to promote oxygen evolution reaction and also successfully realize the reduction of various organic pollutants *via* generation of hydroxyl radicals. Among the main advantages of WO_3, also need to mention are low price, accessibility, non-toxicity, and biocompatibility.

In turn, it also possesses very serious drawbacks that reduce its expected performance such as rapid recombination of electron-hole pairs, low stability due to the formation of peroxo species, and slow transportation characteristics of charge carriers which make their transfer toward surface for activation of adsorbed molecules highly ineffective. In this regard, it was demonstrated that proper and accurate employment of defect engineering can greatly address some of these problems, thus increasing the applicability and attractiveness of WO_3. Aside from all defects that

are available in this material, the main attention usually is given to oxygen vacancies given simplicity toward their introduction and consequent easiness of manipulation over their specific particularities and defined features. As for the W vacancies, they are described by very high formation energy, and employment of only very specialized conditions can induce their appearance.

9.4.3.2 How to Create Defects

As numerous methods are demonstrated in literature to realize the formation of defects in WO_3 including both synthesis approaches and post-synthesis treatment, several of their most notable examples are demonstrated below in order to provide general overview regarding recent trends in this filed. More detailed description can be found in specialized literature.

Synthesis Approaches

(a) *Sol-Gel Method*. It is a very applicable and effective route to create oxygen-deficient WO_3 as it does not require utilization of heavy and expensive equipment or presence of extreme and critical conditions during fabrication process. The proper choice of applied chemicals and adjusting their specifications such as concentration or molar ratio as well as playing with other related parameters of synthesis allows to achieve precise control over the changes in stoichiometric ratio and chemical compositions in finalized compound. Furthermore, it also can be used to acquire the formation of nanostructures with desired geometries. For example, Koo and Ahn [26] reported the synthesis of mesoporous WO_3 films filled with oxygen vacancies fabricated on commercial FTO glass using the camphene-assisted sol-gel method and consequently annealed at 300 °C in air. It was revealed that the higher the percentages of added camphene, the more evident the changes in stoichiometry (Fig. 9.3).

(b) *Hydrothermal/Solvothermal Method*. These methods can provide very accessible synthesis route to create the target material with desired chemical composition thus allowing to reach the formation of structures with various dimensions that can hardly be produced, for example, by mentioned above sol-gel method. Changing the temperature of treatment, its duration and which chemicals are going to be used for preparation of reaction solution allow to adjust the level and also the type of obtained deficiency. Specifically, Wang et al. [27] used hydrothermal route to prepare WO_3 nanorods with different concentration of oxygen vacancies by varying the amount of added citric acid. It is interesting that this approach also can be used to create W vacancies. For example, it was demonstrated that to realize it, it is enough to include fluorine into the list of used chemicals [28].

(c) *Vapor Phase Techniques*. It is possible to fabricate oxygen-deficient WO_3 *via* both physical and chemical vapor-based techniques such as reactive sputtering, atomic layer deposition, etc. The control over chemical composition during fabrication process usually is proceeded *via* regulating the partial pressure of pre-

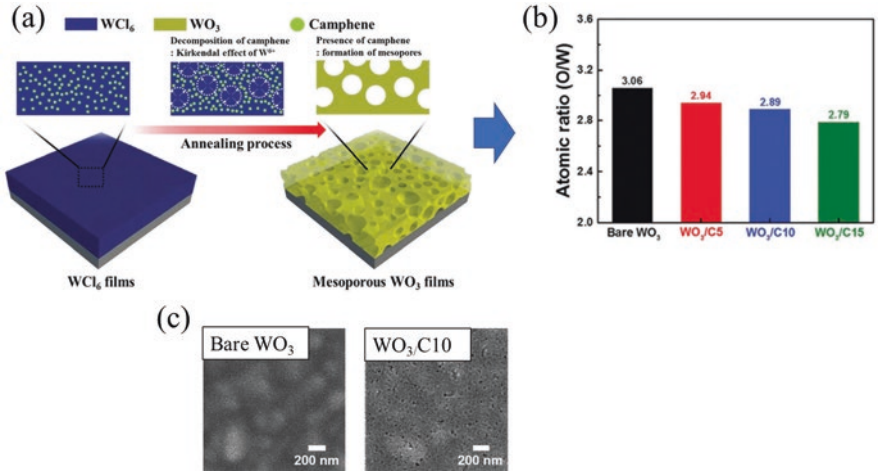

Fig. 9.3 (**a**) A schematic of the formation mechanism for the mesoporous WO_3 films prepared by the camphene-assisted sol-gel method. (**b**) The atomic ratio of O/W obtained from the samples. Numbers after "C" represent weight ratios of the added camphene. (**c**) SEM images of bare WO_3 and WO_3/C10. (Adapted from Ref. [26] with permission from *The Royal Chemical Society*. Copyright 2017)

cursors, lowering or increasing their dose, and playing with temperatures inside the reaction chambers. The main type of defect which is detected in resulted WO_3 is oxygen vacancies that could be partially explained by utilizing vacuum or low-pressure environment during fabrication step.

Post-synthesis Treatment

(a) *Annealing in Reducing Atmospheres*. Given that WO_3 represents binary oxide, it is possible in analogy with other related materials such as TiO_2 and ZnO to use annealing at elevated temperatures in reducing atmosphere such as H_2, Ar, and N_2 to create oxygen deficiency. Its level and distribution within the surface and bulk compositions can be controlled by the duration and temperatures of this treatment as well as other related parameters. Theoretically, this approach also enables to introduce W vacancies in WO_3 by using oxygen-rich atmosphere; yet up to present, there is no report about its successful realization.

(b) *Bombardment with High-Energy Particles*. Using plasma treatment or ion irradiation is also considered to be a highly effective approach to fill WO_3 with both O and W vacancies as reactive nature of this processing usually results in partial etching of the surface. In this regard, it has to be noticed that the presence of former defect is often determined having several times higher concentration than that of the latter one, and thus in relative units, the obtained structures are often identified as oxygen-deficient. The level of non-stoichiometry can be effectively tuned by playing with conditions of this treatment. As an illustration, Zheng et al. [29] revealed that by increasing the irradiation fluences of Ar^+ ions, more intense release of O atoms from the surface of WO_3 was observed.

(c) *Chemical Reduction*. Using chemical to reduce the presence of oxygen in WO_3 is also considered to be a highly attractive approach. Apart from generally recognized advantages, it also allows to reach the desired chemical compositions *via* extremely short period of time. For instance, Liu et al. [30] utilized $TiCl_3$ solutions with different concentrations as the reductant, and it was discovered that the presence of oxygen vacancies in WO_3 was proportional to the increase of its concentration. It is worth noticing that the whole process of dipping has taken only 25 s.

9.4.3.3 Properties of Defective WO_3

Structural Properties *Firstly*, the presence of oxygen vacancies results in deterioration of the crystallinity level in WO_3 due to appearance of distortion and disordered localized areas [31]; very similar phenomenon was also observed in other binary oxide materials discussed in the previous chapters. *Secondly*, the more O atoms are escaped from WO_3, the larger expansion in the parameters of crystal lattice [29] can be observed due to structural relaxation as the length of W-W and W-O bonding should be newly adjusted. This process often is accompanied by gradually reduced crystallinity size, generation of additional pores, and consequently increased specific surface area [27]. Appearance of oxygen vacancies also often is accompanied by generation of reduced W^{5+} or W^{4+} centers due to localization of an excess electrons. It is interesting that the presence of W vacancies in WO_3 also results in larger interatomic distance [28].

Optical Properties It was discovered that formation of oxygen-deficient WO_3 leads to critical enhancement of optical properties compared with its fully stoichiometric counterpart. *Firstly*, the absorption edge becomes shifted toward longer wavelength which means that larger portion of visible light can be utilized (Fig. 9.4a. It is accompanied by change of WO_3 color from traditional yellow to blue [31], green [32], or even black [33] (Fig. 9.4b) as it depends on numerous parameters such as concentration and distribution of oxygen vacancies, methods used to introduce then, quality of the original chemical composition, etc. *Secondly*, it is also often the case that band gap of defective WO_3 remained relatively the same, while the absorption in visible and even near-infrared wavelengths increases sufficiently. It is of interest that this mechanism often is connected to the appearance of both O or W vacancies [27, 28].

Electronic Properties It is still debatable how the presence of oxygen vacancies (V_O) influences the electronic configuration of the band gap as well as transposition characteristics of electrons given that two contradictory views exist in literature based on theoretical calculations. On one hand, Wang et al. [34] suggested that "oxygen vacancy acts as a shallow donor, stable only in the 2+ charge state; other charge states are not stable for Fermi levels within the band gap, at least with respect to free carriers in the conduction band." As opposite, Gerosa et al. [35] proposed

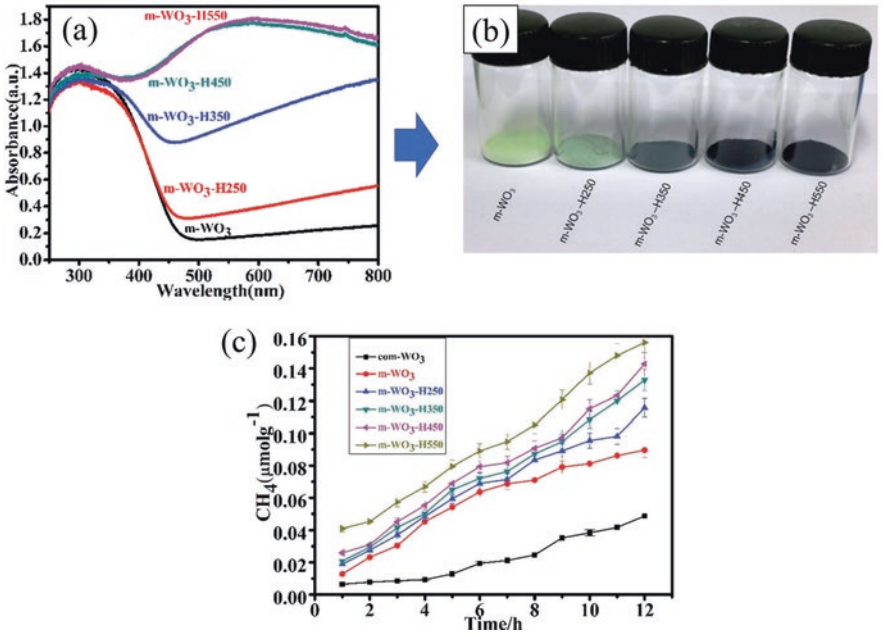

Fig. 9.4 (**a**) UV-visible diffuse reflectance spectra and (**b**) photographs of mesoporous WO_3 (m-WO_3) before and after hydrogenation at different temperatures. (**c**) Generation of CH_4 over commercial WO_3 (com-WO_3), m-WO_3, and hydrogenated m-WO_3 catalysts under visible-light irradiation. (Reprinted from Ref. [33] with permission from *The Royal Chemical Society*. Copyright 2017)

that oxygen vacancies can be presented in all three available charge states, namely, 0, +1, and +2, and their stabilities are depended on the geometrical positioning of this defect with respect to the crystal axis. Particularly, it was stated that their orientations toward *b*- and *c*-axis lead to presence of V_O (+1) as most thermodynamically favorable formation, while orientation along *a*-axis results in domination of neutral V_O. Accordingly, this defect was identified to have shallow and deep characteristics following these charge states given the positions of its transitions levels within the band gap. To add more confusion, both assumptions were claimed to have perfect correlation with the experimental studies. As a final remark, one should notice that W vacancies serve as deep acceptors given how far their transition levels are from valence band and their most stable charge state is −6 which corresponds to Fermi level located very close to conduction band [36].

Electrical Properties Oxygen vacancies enable to greatly increase the conductivity of WO_3 given that they can serve as shallow and also possibly as deep donors, thus providing electrons not only to conduction band but also in perspective to take the role of compensating centers annihilating acceptor-like defects and impurities, respectively. Thus, they can reduce recombination rate of charge carriers and

enhance their overall transportation characteristics as to make them become much easier and faster to be transferred toward surface without much loss in bulk. Furthermore, it has to be noticed that decreased size of crystallites results in shortening the range of mean free pass for charge carriers which is interpreted as lower chances to meet their counterpart. In turn, too high presence of oxygen vacancies might bring negative impact as they can be transformed into trap centers catching both electrons and holes and thus annihilating them.

9.4.3.4 Photocatalytic Application of Defective WO_3

Defective WO_3 filled with oxygen vacancies were identified to have greatly enhanced performance toward realization of solar light activated photocatalysis since many drawbacks associated with its fully stoichiometric counterpart could be properly addressed by playing with chemical composition and the degree of changing the stoichiometry. Given that this material has a great affordability, is environmentally friendly, and also possesses other important and desirable characteristic, it might be considered as a highly attractive candidate for potential adaptation toward wide applications. Overall, the following photocatalytic processing is influenced the most by employment of defect engineering

Photocatalytic and Photoelectrochemical Water Splitting As the position of conduction band cannot satisfy the redox potential of hydrogen evolution reaction, this material is mostly applied in the role of photoanode, thus proceeding the oxidation reaction. In this regard, the presence of oxygen deficiency played a crucial role in increasing its efficiency *via* improving the transportation characteristics of charge carriers, lowering the recombination rate, and also extending the sensitivity toward the visible light. It is also considered to be a highly effective approach for stabilizing this material *via* increasing its resistivity toward re-oxidation and reducing the formation of harmful peroxo-species that causes the corrosion. For example, Wang et al. [37] revealed that photocurrent density of fully stoichiometric WO_3 was identified to be 0.1 mA cm^{-2} at 1.0 V vs Ag/AgCl, and it dropped about 65% within the first 2 min of testing and then decreased slowly reaching 80% lost after 2 h. In contrast, the photocurrent density for the WO_{3-x} sample reached a maximum value of 0.88 mA cm^{-2} at 1.0 V vs Ag/AgCl, while it lost only 17% within the first 2 min of testing and then showed a great stability without decay under the irradiation for at least 7 h.

Light-Induced Water Purifications Oxygen-deficient WO_3 is determined to be an excellent photocatalysts to remove various organic pollutants from water as it shows highly increased performance thus allowing transforming it into very attractive compound to be utilized. For instance, Boruah et al. [38] prepared WO_{3-x} via a single-step plasma discharge process that occurred in deionized water and applied it for degradation of methylene blue under simulated solar light. It was discovered that bulk and nanoscaled fully stoichiometric WO_3 which was taken as standards to

compare the photocatalytic activities demonstrated that only 50% and 62% of MB were decomposed after 200 min of irradiation, respectively. In turn, application of WO_{3-x} under similar conditions resulted in efficiency rate of 77%.

Photoconversion of CO_2 The position of valence and conduction bands allows WO_3 to successfully photoreduce CO_2. Yet, this processing is limited mostly by the production of CH_3OH and CH_4 fuels as redox potentials of reactions that can be used to obtain other carbon-based compounds laid beyond the range of WO_3 band gap with respect to vacuum level. Nevertheless, introduction of oxygen vacancies can greatly contribute to the improved performance given the changes in geometrical and electrical structures which cause their presence. For example, Wang et al. [33] investigated the photoconversion of CO_2 under irradiation with visible light using mesoporous defective WO_3 prepared *via* template-supported hydrothermal method and accompanied by consequent thermal annealing in pure hydrogen for 30 min at different temperatures. It was discovered that treatment at 550 °C resulted in the highest yield of CH_4 which was ~4.3 times higher than that of fully stoichiometric sample (Fig. 9.4c). It is interesting that utilizing a heating at 250 °C during the photocatalytic reaction resulted in additional appearance of CH_3OH as the detected secondary products and also led to much higher overall yield of this processing. In turn, Li et al. [31] revealed that the presence of oxygen vacancies in WO_3 induced great thermal and chemical stabilities as it was demonstrated that conversion of CO_2 under UV light at temperatures of 60 °C can be proceeded for five consecutive recycles without any significant degradation of performance rate.

9.4.4 Case Example III: CuO and Cu_2O

9.4.4.1 CuO and Cu_2O: Fundamentals

Cupric Oxide (CuO) Cupric oxide (CuO) is a p-type semiconductor which has indirect band gap of 1.2–2.0 eV depending on its size and the method of fabrication. Thus, it enables to absorb significant part of visible and even near-infrared spectra which makes its color to be almost black. In this regard, the positions of conductions and valence bands might follow the changes in the dimensions of this materials, and it was revealed that under certain conditions they separately satisfy both redox potentials of various highly demanding reactions including water splitting or CO_2 photoconversions. It allows to use CuO as oxidation or reduction agent. Yet, given that existence as nanoscale compound within defined range of sizes usually results in appearance of lower and upper edges of band gap lied at nearly ~−4.95–5.50 eV and ~−3.25–4.05 eV [39, 40], respectively; with respect to the vacuum, the former scenario has certain difficulties to be realized practically given that it is mostly referred to formation of massive and bulk-related or ultra-small nanostructures [41, 42]. Thus, it is generally accepted that this material has higher applicability as photocathode governing the reduction reactions as a part of heterojunction or as co-

catalyst rather than photoanode. Contrary to the usual rock-salt structure of other 3D transition-metal monoxides, the CuO crystal lattice is monoclinic with C2/c symmetry; Cu atom is coordinated by four coplanar O atoms forming an almost rectangular parallelogram, while O coordination polyhedron has four Cu atoms at the corners of a distorted tetrahedron [43]. The advantages of using CuO as photocatalysts in addition to the above mentioned are the following: large surface areas, good electrochemical activity, superior conductivity, and accessibility. As for disadvantages, it is mostly referred to unacceptable stability, high recombination rate, and low charge collection.

Cuprous Oxide (Cu_2O) Cuprous oxide (Cu_2O) has a direct band gap of ~2.2 eV which extends its absorption to the far end of visible spectra and makes its color reddish. The positions of conduction and valence bands perfectly satisfy the redox potentials of water splitting and CO_2 conversions allowing to perform them without using additional materials or co-catalysts. CuO_2 has a cubic crystal structure belonging to the *pn3* space group, and its lattice is constructed by two intertwined Cu face-centered cubic and O body-centered cubic sublattice [44]. It is different from CuO by having lower conductivity and higher mobility of charge carriers [45]. In turn, both materials have very similar low quantum efficiency as a result of high recombination rate and also possess poor stability and high photocorrosion in aqueous solutions that lead to gradual reduction to metallic Cu.

As p-type conductivities of both oxides are mostly governed by the presence of copper vacancies, it is believed that proper adjustment of their concentration and distribution with regard to changes in geometrical and electronic structures can extend their applicability in photocatalytic processing. In addition, it is suggested that introduction of other defects such as oxygen vacancies might also have a positive impact. Overall, more detailed explanation regarding the employment of this strategy is provided below.

9.4.4.2 How to Create Defects

Introduction of defects into CuO and Cu_2O can be proceed *via* both synthesis and post-synthesis approached; yet the former one might be considered as more preferential choice as there is always a possibility that additional processing of already prepared structures might result in their unexpected partial or full decompositions given low stabilities.

Synthesis Approaches

(a) *Thermal Decompositions of Certain Chemical Composition*. Specially prepared chemicals can be subjected to additional thermal treatment process in order to convert them into defective CuO or Cu_2O. The temperature of this processing and other related parameters define the exact level of non-stoichiometry. For example, it was reported that annealing of metal-organic gel realized *via* mixing of $CuSO_4{\cdot}5H_2O$ and 1,3,5-tris(4,-carboxyphenyl) could be used to introduce Cu

vacancies into CuO depending on the applied temperature [46]. Similar also could be said about using CuI dipped in aqueous sodium hydroxide (NaOH) solution as its consequent thermal treatment at 250–350 °C results in formation of Cu_xO with Cu/O ratio ranging from 2.5 to 0.87 [47].

(b) *Hydrothermal/Solvothermal Method*. It is also possible to prepare defective CuO or Cu_2O *via* placing defined mixture of chemicals into Teflon autoclave accompanied by mixing with aqueous or non-aqueous solution and heating it for a certain period of time. The most important particularity of this process is that it mostly leads to processing of oxygen deficiency. For instance, Lu et al. [48] demonstrated that treating CuCP powder dissolved in methanol and placed into microwave oven overnight resulted in appearance of Cu/Cu_2O filled with oxygen vacancies. It is of interest that they could be annihilated via consequent thermal treatment in air at 500–600 °C.

(c) *Vapor Synthesis Methods*. Physical and chemical vapor depositions (PVD and CVD, respectively) could be used to prepare CuO and Cu_2O filled with certain types of defects as changing in the parameters of chemicals that are used as oxygen or copper precursors, conditions within the reaction chamber, etc. influences crucially the level of introduced stoichiometry and variation of chemical composition in the final product. Particularly, Chua et al. [49] investigated Cu_2O prepared *via* CVD process and revealed that, *firstly*, the presence of Cu vacancies was regarded as dominated type of defects and, *secondly*, their impact on properties of this materials could be partially shadowed by playing with the deposition temperature as it has clear correlation with the introduction of oxygen vacancies and, thus, resulted in partially restoring the balance of both chemicals.

(d) *Thermal Oxidation*. It is possible to control the presence of defects in both oxides obtained *via* oxidation of Cu by adjusting the conditions of this process such as temperature, duration, heating rate, etc. As an illustration, Cheon et al. [50] utilized thermal rapid treatment in Ar at 800 °C to convert Cu into Cu_2O containing both copper and oxygen vacancies.

(e) *Thermal Reduction*. The opposite process, i.e., reduction of Cu_2O into CuO filled with various defect can also be realized as well. Utilized atmosphere during it, i.e., whether oxygen-reach or oxygen-poor conditions were applied, determines the appearance of certain type of vacancies [51]. Furthermore, adjusting the temperature and duration of this process can assist in controlling their concentration and distribution.

9.4.4.3 Properties of Defective CuO and Cu_2O

Structural Properties Theoretical estimation predicted that removal of copper and oxygen atoms results in very slight relaxation of near-neighbor atoms [52, 53]; thus, it is hard to see any changes in lattice distance if only a massive level of deficiency is formed. The absence of peak shift during X-ray diffraction confirms it [50]. In addition, it has to be noticed that in analogy with any other binary materials

discussed in previous chapters, the presence of vacancies usually is accompanied by appearance of lattice distortion and development of disordered composition which leads to degradation of crystallinity as it is evident from the reduced intensity of XRD peaks.

Optical Properties Cu-based oxides demonstrate great sensitivity to the visible and even near-infrared light, thus allowing to absorb most of solar spectra. In this regard, tuning of their optical characteristics via presence of defects deserves much less attention contrary to other binary oxide compounds. Nevertheless, it was reported that oxygen-defective Cu_2O exhibits higher absorption in visible spectra compared with more stoichiometric samples, while the width of band gap remained to be relatively similar [48]. In turn, the presence of Cu vacancies allows to secure the lowest boundary of reported band gap range in CuO equaled to 1.2 eV [46].

Electronic Properties As CuO and Cu_2O are determined to be p-type materials, their charge carrier concentration has clear dependency on the presence of acceptor-like defect that is usually present in the form of cation vacancies and formation of associated trap states. The following particularities are defined regarding this processing. For simplicity, the discussion here is limited by accessing only Cu_2O as it has higher applicability toward various photocatalytic reactions due to larger band gap, and also it is possible to access its electronic structures by density functional calculation while CuO limits this perspective as it has $3d^9$ configuration [54]. *Firstly*, the existence of copper vacancy in terms of its configuration is determined to have two types of geometry: simple one, which corresponds to removing of Cu and relaxing the positions of remained atoms, and split one ascribed as removing of Cu atom accompanied by displacing one of its non-O-linked partners halfway toward the vacancy site and then also adjusting the positions of remained atoms [52]. Their appearances are relatively equaled from thermodynamically point of view even though the latter one requires to have additional step. *Secondly*, theoretical simulations stated that both of these vacancies have the lowest formation energies regardless to the applied conditions compared with other acceptor-like intrinsic defects such as oxygen interstitials [55]. It is different from that of CuO, where under O-poor conditions, appearance of oxygen deficiency is the most favorable [51]. *Thirdly*, it was revealed that (0/-1) transition levels of simple and split copper vacancies were determined to locate at 0.28 and 0.47 eV above valence band maximum [56], which allow to refer the former one with certain assumption as shallow donors that have the possibility to contribute into the origin of the p-type conductivity. It is interesting that Paul et al. [57] confirmed experimentally the existence of trap states at these distances. *Fourthly*, transition levels of oxygen interstitials have the positions close to the middle of band gap, and thus these defects are considered to be deep acceptors that serve as compensation centers. It is necessary to say several words about donor-like defects. Density functional theory calculation revealed that the presence of oxygen vacancies in Cu_2O is restricted by existence only in the neutral form [58]; thus, it is unable to influence the p-type conductivity. Yet, the analysis via PL spectroscopy revealed that they can exhibit +1 and +2 charge states which

have transitions at 1.52 and 1.67 eV, respectively [49]. The following discrepancy could be explained using work of Ricca et al. [53]. It was demonstrated that the presence of V_O in neutral form is the most stable formation, except for Fermi energies resided just above the valence band maximum, where +2 becomes the favored charge state for them with a thermodynamic transition level (+2/+1) located as 0.20 eV. Thus, at strong p-type conditions, this defect can take the role of hole killer.

Electrical Properties As CuO and Cu_2O are p-type materials, it is obvious that the presence of acceptor-like defects such as copper vacancies and oxygen interstitials that have shallow and deep trap states in the band gap, respectively, would influence greatly on increasing the concentration of relevant charge carriers. Thus, in perspective, it might cause the improved recombination rate and more efficient transportation characteristics. Yet, the introduction of copper vacancies should be proceeded with certain caution as it reduces the overall metallization of these materials and thus potentially transforms them into more insulating states. For its part, the presence of oxygen vacancies given their donor-like nature might serve oppositely as they result in suppressing of p-type behavior [51] (Fig. 9.5a, b). Yet, these defects also enable to diminish the electron transport serving as trap centers for them [53]. Thought, it is not always the case as it is likely referred only to V_O that existed in +2 or +1 charge states. In turn, their neutral form under correctly applied strategy might benefit significantly to effective separation of electron-hole pairs and occurrence of rapid charge transfer [59].

9.4.4.4 Photocatalytic Application of Defective CuO and Cu_2O

Photocatalytic and Photoelectrochemical Water Splitting Due to difference in the band gap positioning with respect to redox potentials of water splitting, these materials are applied very contrastingly in this reaction. Yet, regardless to this, introduction of defects contributes greatly to improving their performance. For example, Lu et al. [48] revealed that oxygen-deficient Cu_2O combined with Cu and nitrogen-doped nanostructured carbon demonstrated highly enhanced efficiency and stability toward hydrogen production under visible light than that of its counterpart with higher stoichiometry. In turn, the presence of Cu vacancies in CuO and its employment as photocathode resulted in detection of the highest current reported for this material up to date equaled to -1.8 mA cm^{-2} at 0.1 V_{SHE} using $NaSO_4$ as electrolyte [51] (Fig. 9.5c). It is interesting that addition of $K_2S_2O_8$ added as electron scavenger during the photocurrent measurement increases the performance further.

Light-Induced Water Purification Defective CuO and Cu_2O are determined to be excellent photocatalysts to remove various organic pollutants from water as they show highly increased outcome. For example, Zaman et al. [60] revealed that introduction of oxygen deficiency into CuO contributes to its impressive efficiency toward the degradation of methylene orange and rhodamine B compared with more stoichiometric sample. It was stated that the presence of oxygen vacancies results in

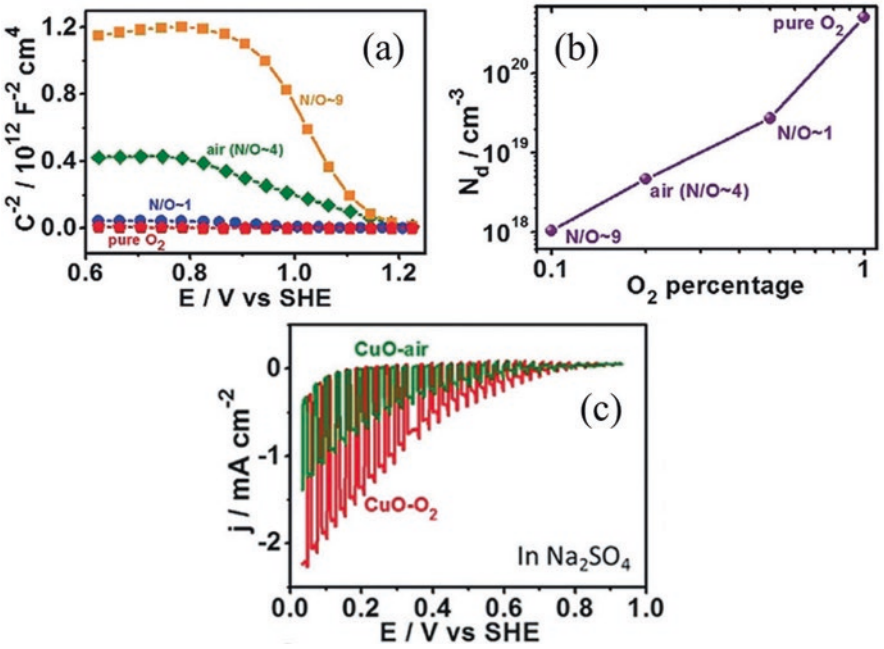

Fig. 9.5 (**a**) The Mott–Schottky curves and (**b**) the calculated carrier concentration of CuO prepared in gas atmospheres with different N_2/O_2 (N/O) ratios. The more oxygen is presented in ambient, the more copper-deficient is CuO. Calculated carriers are mostly identified to have acceptor-like character. (**c**) The photocurrent-potential curves of CuO-O_2 (red) and CuO-air (green) in 0.5 m Na_2SO_4 aqueous solution. (Reprinted from Ref. [51] with permission from *John Wiley and Sons*. Copyright 2017)

increased presence of hydroxyl ions that play the role of active species which interact with organic dyes causing their annihilation.

CO_2 Photoreduction DFT calculation revealed that introduction of copper vacancies in Cu_2O leads to turning the adsorption energy of CO_2 into positive [61] which means that the surface becomes less attractive for their occupancy. In turn, introduction of oxygen vacancies does not significantly influence this processing if only to provide very slight improvement, indicating that activation and optimization of CO_2 molecules with and without them is, in fact, the same. Thus, formation of defective Cu_2O or CuO and their application in CO_2 photoreduction would not influence much on advancements of this reaction if only to reduce its effectiveness given their p-type characteristics and dominating presence of copper deficiency. Thus, it is no surprise to find absence of available studies in literature regarding this topic.

9.4.5 *Case Example IV: α-Fe_2O_3*

9.4.5.1 α-Fe_2O_3: Fundamentals

Iron oxide (Fe_2O_3) is a transition metal oxide that has several crystalline polymorphs among which hematite α-phase is considered to be the most stable state at ambient conditions. Its crystal lattice belongs to rhombohedrally centered hexagonal structure consisting of iron atoms surrounded by six oxygen atoms. This periodical arrangement is attributed to R3c space group, and its symmetry is identified to be C_{3V} [62]. Great potential of α-Fe_2O_3 toward its application in photocatalytic processing is attributed to the presence of some unique characteristics and features such as non-toxicity, low cost, affordability, impressive stability and resistivity toward various chemical media, easy recovery, and, most importantly, relatively narrow band gap equaled to 2.0–2.2 eV that allows to reach absorption of visible light with wavelength up to infrared region. Following it, the color of this materials is evidenced as brown, reddish, or one of their shades. In turn, the positions of conduction band limit its capability to activate overall water splitting or CO_2 conversion reactions allowing only to perform oxidation step as its minimum is positioned far below their reduction redox potentials. In this regard, α-Fe_2O_3 is preferred to be used in the role of photoanode. Thus, its functionality has a lot of similarity to that of WO_3 mentioned above.

However, to the deepest regret, despite the great advantages that make the usage of this material become highly attractive, the energy conversion efficiency of α-Fe_2O_3 is still cannot be considered as satisfactory and, in fact, is very low and far from expected. The main drawbacks to cause it are referred to inefficient charge migration and transfer caused by number of reasons such as very short distance of hole diffusion, extremely high recombination rate, and poor mobility of carriers which means that only holes generated in the proximity of catalyst/electrolyte interface could be utilized, while a major part of them is lost through combining with photo-generated electrons [63]. To properly address the sluggish kinetics of α-Fe_2O_3, it is suggested that introduction of certain and very specific defects accompanied by accurate modification of internal composition might be used. One should notice that the main consideration in this section is given to oxygen vacancies as their appearance has the most prominent and recognizable impact on properties of this materials.

9.4.5.2 How to Create Defects

Given the easiness in preparation of oxygen-deficient α-Fe_2O_3, there are numerous methods available in literatures including various synthesis procedure and post-synthesis treatments which can be used to realize this strategy. As it is impossible to cover all of them in detail, only several particulate approaches, the ones that have absence of extreme complexness and receive the most recognitions are briefly

described here as to provide general overview on current achievements and trend regarding this topic.

Synthesis Approaches

(a) *Thermal Oxidation*. It is considered to be one of the simplest and most accessible method to produce defective α-Fe_2O_3. To be clear, annealing of Fe foil in oxidizing atmosphere results in its transformation into α-Fe_2O_3. Following it, control over the conditions of this processing such as temperature, pressure of flowing gaseous ambient, duration, etc. can allow very precisely the adjustment of the level of oxygen deficiency.

(b) *Vapor Synthesis*. Given that α-Fe_2O_3 represents binary oxide, in analogy to other similar materials, it is possible to synthesize it *via* physical or chemical vapor deposition techniques. Thus, playing with parameters of this processing such as pressure of oxygen source, temperature inside reaction chamber, etc. can be considered as an efficient tool to control its stoichiometry. Particularly, Noh et al. [64] reported that high-density oxygen-deficient α-Fe_2O_3 with the dominant (110) crystal plane was developed by employing aerosol-assisted chemical vapor deposition and using nitrogen gas as reaction environment. In turn, lower concentration of oxygen vacancies was detected when purified air was used instead.

(c) *Hydrothermal/Solvothermal Methods*. It is also possible to create oxygen-deficient α-Fe_2O_3 via placing defined mixture of chemicals into Teflon autoclave accompanied by aqueous or non-aqueous solution and heating it for a certain period of time. For instance, Zeng et al. [65] used $FeCl_3 \cdot 6H_2O$ and urea to make the reaction solution that was treated at 140 °C for 12 h. It was followed by thermal annealing step in air for 350 °C in order to remove unreacted chemicals and remaining contaminations as well as to stabilize the structure. Finally, oxygen-deficient Fe_2O_{3-x} nanoparticles were obtained. It is also possible to use this method toward already synthesized compounds as additional treatment. Specifically, Yang et al. [66] employed aqueous solution of sodium hypophosphite to react with α-Fe_2O_3 nanorods under 100 °C for various times. It was discovered that the highest presence of oxygen vacancies was achieved after this process was extended to 180 min.

Post-synthesis Treatment

(a) *Thermal Treatment in Reducing Atmosphere*. It is also possible to use thermal treatment in various reducing atmosphere to introduce oxygen vacancies in α-Fe_2O_3. Changes in the temperatures, duration of this processing, etc. could be tuned to precisely adjust the required stoichiometry and chemical composition. It is necessary to notice that the presence of oxygen in the utilized gaseous ambient is highly necessary as its complete absence might lead to possibility of transforming α-Fe_2O_3 into other forms of iron oxides such as Fe_3O_4. As an illustration, Makimizu et al. [67] demonstrated that annealing of α-Fe_2O_3 film at 400 °C for 40 min in 0.03% O_2-Ar atmospheres resulted in appearance of oxygen vacancies. Due to the nature of this processing, their localization was discovered to occur mostly in the bulk, while the surface was empty from its

presence. In turn, using pure argon as a flowing ambient during this treatment caused partial transformation of α-Fe_2O_3 into Fe_3O_4.

(b) *Chemical Reduction*. The formation of defects in α-Fe_2O_3 also can be conducted via chemical reduction process which realization usually is proceeded through interaction with certain chemicals (usually $NaBH_4$). During this reaction, certain part of oxygen atoms is effectively evacuated from crystal lattice of α-Fe_2O_3 leaving behind vacancies. The time of this treatment, concentration of immersed solution, and conditions of the surrounding such as temperatures and ambience influence crucially on the level of obtained non-stoichiometry.

9.4.5.3 Properties of Defective α-Fe_2O_3

Structural Properties Development of defective α-Fe_2O_3 often results in degrading its structural characteristics as it leads to flattering the surface and removal of certain particulate morphological features. For instance, Noh et al. [64] revealed that introduction of oxygen vacancies could be correlated with lowering root-mean square roughness from initial 54.2 to 49.5 nm. On its part, Makimizu et al. [67] prepared α-Fe_2O_3 that contained nanoporous composition and demonstrated that thermal treatment in oxygen-poor atmosphere causes partial disappearance of these features. It is interest that utilizing of air during this process keeps the morphology (Fig. 9.6a–c). Furthermore, the presence of defects also increases the polycrystallinity of α-Fe_2O_3 as they initiate the appearance of crystals grown in multiply directions [64].

Optical Properties Depending on the level of introduced adjustments in chemical composition and variation of stoichiometry as well as the nature and form of original nanostructure, introduction of oxygen vacancies can influence significantly on the changes in optical properties of α-Fe_2O_3. Particularly, it might lead to increased sensitivity toward irradiation of light with visible and UV spectrum and/or also enable to cause the shift of absorption edge toward higher wavelength. For instance, Feng et al. [68] investigated α-Fe_2O_3 nanoblades before and after thermally activated reduction in vacuum. It was revealed that width of band gap proceeded the decrease from ~2.12 to ~2.06 eV accompanied by enhanced capability to catch more photons with energies laid in the range of 600–800 nm.

Electronic Properties Oxygen vacancies in the α-Fe_2O_3 mostly exist in the charge states of 0, +1 and +2, and their appearances are accompanied by the crucial changes of electronic band structure. According to Lee and Han [69], the (0/+1) and (+1/+2) transition levels are located at ~0.98 and 1.08 eV from the valence band. These defects create corresponding energy states in a manner similar to that observed in oxygen-deficient ZnO [70]. Following the DFT calculation performed by Banerjee et al. [71], it was revealed that for the neutral V_O, it appears at 0.864 eV above the valence band and is fully occupied, while for V_O (+1), there exist two energy states,

and only one of them located at 1.095 eV is filled only partially. Finally, V_O (+2) leads to development of unoccupied state very close to conduction band.

To fully access this information, it is necessary to mention that formation energy of this defect increases following the decrease in the charge state thus making V_O (+2) to be the most thermodynamically favorable at both O-rich and Fe-rich conditions [70]. Even though their transition levels are located too far from conduction band, at certain conditions they enable to assist in transportation of electrons toward it. Yet, given that α-Fe_2O_3 represents n-type conductivity, the position of Fermi level is a priory supposed to be close to conduction band which means that neutral V_O should be the dominated species. Due to absence of any unoccupied states correlated with these defects, they serve as compensation centers. In turn, it was suggested that iron interstitials might be identified as source of electrons in α-Fe_2O_3 since their (0/+1) transition level locates at 1.62 eV from valence band [69].

Electrical Properties Given that oxygen vacancies have donor-like characteristics and considering the n-type conductivity of α-Fe_2O_3, it is obvious that proper management of their presence could lead to enhanced electrical characteristics of this material via increasing the concentration of relevant charge carriers and consequently reducing their recombination (Fig. 9.6d). Numerous studies confirm the applicability of this model [65, 72]. Yet, too much V_O is not good as in this case their role as trapping centers might become dominated. It is of interest that it is possible to fabricate p-type-conductive a-Fe_2O_3 nanowires by using oxygen vacancy arranged in very high order [73]. This is a very unexpected discovery given that these defects rather are considered as "hole killers" than their origin [70]. Nevertheless, it was proposed that this phenomenon could be referred to formation of an inversion layer caused by strong surface absorption of oxygen and water molecules near the surface" [73].

9.4.5.4 Photocatalytic Application of Defective α-Fe_2O_3

Photocatalytic and Photoelectrochemical Water Splitting Given the position of its band gap with respect to redox potentials of water splitting, α-Fe_2O_3 only can be used as photoanode to perform oxidation reaction. Theoretical estimations predicted that its application in this role is supposed to bring solar-to-hydrogen efficiency over ~15%, while in reality, however, it is typically much lower. In this regard, the presence of oxygen vacancies allows to enhance the performance making it approach closer to the desired level. For example, Makimizu et al. [67] demonstrated that defective α-Fe_2O_3 enables to reach 0.5 mA/cm^2 at 1.5 V vs. RHE during photoelectrochemical measurement under illumination with simulated solar light which was 20 times higher than that of fully stoichiometric sample (Fig. 9.6e). In turn, excellent stability was also recorded *via* long-term tests.

Light-Induced Water Purification Oxygen-deficient α-Fe_2O_3 also shows enhancement performance toward degrading various dyes and pollutants from water. Feng et al. [68] investigated degradation of RhB by α-Fe_2O_3 nanoblades with

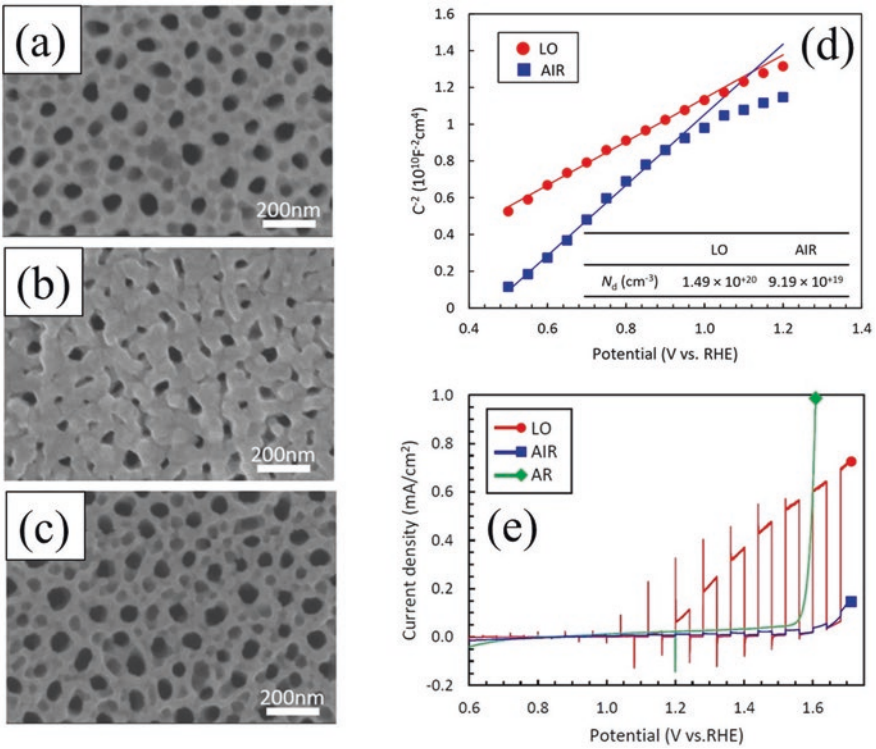

Fig. 9.6 Surface SEM images of α-Fe_2O_3 anodized layers (**a**) before annealing and after annealing at 400 °C for 40 min in (**b**) 0.03% O_2-Ar and (**c**) air ambient. (**d**) Mott-Schottky plots measured under dark condition for anodized layers of α-Fe_2O_3 after annealing in 0.03% O_2-Ar and air ambient. The inset is donor density estimated from the slope. (**e**) Photocurrent-potential (J-V) curves with chopped light (AM 1.5 G, 100 mW/cm^2) measured in 1.0m KOH electrolyte for anodized layers after annealing at 400 °C under air (AIR), 0.03% O_2-Ar (LO), and pure Ar (AR). The latter sample is taken for comparison as its structure demonstrates the presence of Fe_3O_4. (Reprinted from Ref. [67]. Copyright 2019, *John Wiley and Sons*. Available under Creative Commons Attribution 4.0 International License (CC BY 4.0), https://creativecommons.org/licenses/by/4.0/)

reduced and stoichiometric chemical compositions using visible light irradiation. It was discovered that application of former compound resulted in ~100% efficiency after 150 min, while the latter one recombined only ~80% of this dye even if the time of testing was specially extended to 180 min. It is noticed that after ten cycles, the degradation rate of reduced α-Fe_2O_3 nanoblades was almost constant.

CO_2 Photoconversion Similar to water splitting, α-Fe_2O_3 only can be used to promote oxidation reaction. In this regard, the presence of V_O might increase its outcome and consequently contribute greatly to the enhancement of overall CO_2 photoconversion rate. Yet, given that defect engineering is a relatively new topic and its application to α-Fe_2O_3 currently is under investigation, currently, there is no

available studies that describe this topic, and it is believed that they would appear in the future in order to provide more lights on the particularities of this processing.

9.4.6 Case Example V: Nb_2O_5

9.4.6.1 Nb_2O_5: Fundamentals

Niobium pentoxide (Nb_2O_5) is a typical n-type semiconductor that has a great potential to be used as very promising photocatalyst given its various attractive characteristics such as excellent chemical and thermal stabilities, abundance and affordability, non-toxicity, eco-friendliness, etc. Its structure is formed from NbO_6 octahedral and has many polymorphs out of which TT-Nb_2O_5 (pseudohexagonal), T-Nb_2O_5 (orthorhombic), and H-Nb_2O_5 (monoclinic) are the most common phases [74]. Their formations could be achieved from amorphous composition via thermal treatment with temperatures varying from 500 to 1000 °C. Out of them, H and TT phases have the highest and lowest thermodynamic stabilities, respectively [75]. Following the available reports in literature, the band gap of this materials is generalized to be within the range of ~3.1–3.9 eV depending on the crystallinity and morphology even though in certain cases it might reach even the value of 5.3 eV [76]. Thus, its color is identified as white. The positions of conduction and valence bands satisfy both redox potentials of water splitting and CO_2 reduction reactions which means that it can be used to realize these processing without applying additional compounds and elements. Yet, in analogy to another wide-band gap semiconductor such as TiO_2 or ZnO, Nb_2O_5 fails to achieve a considerable photoactivity owing to its low specific surface area, fast recombination rate of charge carriers, and, most importantly, inability to fully utilize solar light as its absorption edge is located as wavelengths of ~300–350 nm. In this regard, there is a belief that application of defect engineering can drastically change it and would greatly increase the applicability of this material. In this section, the main discussion is attributed to oxygen vacancies rather than other defects as their presence influences crucially the most desired characteristics.

9.4.6.2 How to Create Defects

Synthesis Procedure

(a) *Hydrothermal/Solvothermal Method*. It is well known that application of highly non-equilibrium conditions during this processing leads to very critical variations in chemical composition of target material, and level of these changes can be precisely adjusted by playing with natures and characteristics of utilized chemicals and their concentrations or *via* applying different temperatures and duration of heating step, etc. For example, Salim et al. [77] used Nb metal dissolved in distilled water as reactive media to prepare "nanoflake-like morphol-

ogy films" by immersing FTO substrate into it and applying consequent thermally activated treatment at 150 °C for 75 h. It was revealed that increasing the concentration of this solution from 1.5 to 2.5 mg/l resulted in changing of Nb/O ratio from 0.24 and 2.04, respectively, which could be interpreted with some reservations as appearance of niobium and oxygen deficiencies, respectively.

(b) *Vapor Synthesis*. Similar to other binary oxide materials, it is possible to prepare defective Nb_2O_5 via application of physical or chemical vapor deposition techniques. Playing with characteristics of oxygen precursors, pressure inside the reaction chamber, orientation of the substrate, etc. could influence crucially on the changes in chemical composition or stoichiometry of this material. As an illustration, Fernandes et al. [78] applied reactive sputtering to prepare Nb_2O_5 thin film and determined that lowering the flow rate of oxygen from 10 to 3 sccm resulted in significant increase in V_O presence. In turn, it was discovered that application of atomic layer deposition as thermal and plasma-enhanced processes under very similar conditions led to formation of Nb_2O_5 with oxygen and Nb vacancies, respectively [79]. It is interest that adjusting the temperature of substrate by increasing or decreasing it could be used to further tune the level of stoichiometry.

Post-synthesis Techniques

(a) *Annealing in Reducing Atmosphere or Using Reducing Agent*. As Nb_2O_5 has a high similarity to TiO_2 and ZnO since all of them represents wide band gap semiconductors that contain oxygen, the changes in its stoichiometry and chemical composition could be easily realized by applying thermal treatment in reducing atmosphere or vacuum [80]. Another approach is to use reducing agent such as Al that enables to make reaction with Nb_2O_5 once the temperature of the surrounding increase thus assisting in escaping of oxygen atoms from latter [81].

(b) *Electro-deoxidation*. Xu et al. [82] demonstrated that direct reduction of solid Nb_2O_5 could be realized *via* electrochemical processing by using it as cathode and applying the temperature of 1073 K. It was revealed that addition of carbon, calcium carbonate, and calcium oxide with certain concentrations could greatly increase the rate at which oxygen atoms are going to diffuse out from the surface. Furthermore, it was also discovered that more precise control of deficiency level could be achieved by adjusting the duration of this processing.

9.4.6.3 Properties of Defective Nb_2O_5

Structural Properties The presence of oxygen vacancies in Nb_2O_5 results in decreasing bond order of the niobia polyhedra and appearance of disordered structure which reduces the quality of crystal lattice [81]. Yet, even though, it has very limited influence on adjusting the interplanar spacing or altering the directions of crystalline axes. Furthermore, morphology or dimension of defective Nb_2O_5 nano-

structures undergoes minor changes compared with their fully stoichiometric counterparts as average crystallite size is remained to be relatively similar or decrease very slightly [83]. It is drastically different from that of other binary materials.

Optical Properties Formation of defective Nb_2O_5 causes almost no influence on the width of band gap. In turn, absorption in visible and infrared spectra greatly increases [81] which is accompanied by changes in its color from white to black (Fig. 9.7a).

Electronic Properties Currently, there is not so much known about electronic structure of oxygen-deficient Nb_2O_5 given that investigation of this material in terms of its application as photocatalyst begin very recently. For the present, the following facts are determined. *Firstly*, the existence of oxygen vacancies in Nb_2O_5 usually is considered only on terms of neutral, +1, and +2 charge states that are ascribed in a manner very close to that used for TiO_2 or ZnO. Thus, these defects are considered to have donor-like characteristics. *Secondly*, it was determined that the latter two types of V_O have the most preferential appearances in Nb_2O_5 [84, 85]. Possibly, it could be associated with their lowest formation energies. Both defects can have their predominance over each other as it depends on the parameters of their introduction. *Thirdly*, accessing the report of Greener et al. [86], one might suggest that V_O (+1) enables to create energy level positioned near conduction band and thus is likely regarded as shallow. Accordingly, this defect can originate and contribute to the origin and strengthening of natural n-type conductivity in this material that is often observed in literature [84]. In turn, V_O (+2) might be responsible for energy level located deeper in band gap [86] and have a potential to serve as compensation center. Finally, it was stated that activation energies of 0.1 and 0.5–1.0 eV are likely required to excite the first and second electrons, respectively, thus resulting in complete ionization of oxygen vacancy in Nb_2O_5 [87].

Electrical Properties Given that oxygen vacancies are donors in Nb_2O_5, it is very obvious that their introduction results in highly increase conductivity which evolution follows the level of deficiency [86]. For instance, Baik et al. [80] measured electron density of Nb_2O_5 nanotube arrays before and after applying hydrogen treatment and discovered its increase for nearly three orders of magnitude. Thus, Nb_2O_5 filled with oxygen vacancies enables to show enhanced charge transfer and reduced recombination rate [81].

9.4.6.4 Photocatalytic Application of Defective Nb_2O_5

Photocatalytic and Photoelectrochemical Water Splitting Oxygen-deficient Nb_2O_5 could demonstrate highly improve performance toward photocatalytic water splitting given that changes in chemical composition and non-stoichiometry greatly increase some of its characteristics. Particularly, Znao et al. [81] reported that Nb_2O_5 filled with V_O steadily produced hydrogen gas at a rate of 274.8 μmol h^{-1} g^{-1} under

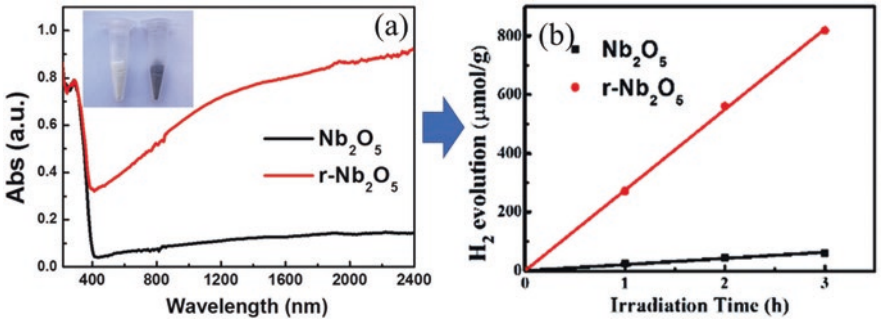

Fig. 9.7 (**a**) Absorption spectra of Nb_2O_5 and r-Nb_2O_5 samples. Inset: photograph of Nb_2O_5 (white) and r-Nb_2O_5 (black). (**b**) Solar-light-driven photocatalytic water splitting for H2 generation over Nb_2O_5 and r-Nb_2O_5 samples. r-Nb_2O_5 was obtained after reduction process via interaction with aluminum. (Reprinted from Ref. [81] with permission from *The Royal Chemical Society*. Copyright 2016)

full-sunlight irradiation spectra. It is 13 times higher compared with that of stoichiometric Nb_2O_5 (21.1 μmol h^{-1} g^{-1}) (Fig. 9.7b). In turn, it was also revealed that photocurrent density could be advanced as well via application of this strategy [80].

Light-Induced Water Purification Removal of organic pollutant or dye from water by using defective Nb_2O_5 results in very high efficiencies and stability which make it to be conserved as attractive candidate to realize this processing. For example, Kumari et al. [83] reported photocatalytic degradation of methylene blue under UV and visible lights using Nb_2O_5 particles and revealed that the presence of oxygen vacancies greatly increases the performance of this processing.

CO_2 Photoreduction There are not so many available reports regarding conversion of CO_2 by using Nb_2O_5 given that this material only recently becomes recognizable as promising photocatalyst. In this regard, the application of defect engineering to modify its composition and structure in order to boost the efficiency of this process is reserved for the future. Given that oxygen vacancies can extend optical and electronic properties, it is believed that their presence in Nb_2O_5 might influence crucially on the overall performance toward successful conversion of CO_2.

9.5 Final Remarks on Defective Nanostructured Semiconductors

Various materials and compounds have enormous potential and great perspectives to be utilized for activation and optimization of certain photocatalytic and photoelectrochemical reactions. Yet, despite their exceptional attractiveness and theoretically predicted effectiveness, often they cannot be properly applied due to existence

of specific drawbacks that limit and even diminish their performances. In this regard, proper employment of defect engineering can adequately address most of their problems as it enables to introduce changes within internal structure or chemical composition that could lead to appearance of some highly advanced properties or extending further already existed features. Thus, modified materials could show strongly enhanced efficiencies and stabilities toward realization of these processing thus making step closer to the desired goal of developing a photocatalyst that could satisfy the strictest requirements for its industrially supported implementation.

However, application of this approach cannot proceed without proper understanding regarding nature and certain particularities of these defects as it would greatly assist in correctly identifying how to achieve the desired advancement via already established roadmap and strategy. Overall, the following issues should take prioritized consideration. *Firstly*, defects create energy levels within band gap that can identify their role as acceptor or donor which has shallow or deep characteristics. It is especially important since these levels enable changes of electronic configuration as Fermi energy becomes shifted and positions of both conduction and valence bands also might be affected. *Secondly*, formation energies of these defects are necessary to be known. It allows to reach understanding which one of them is expected to have dominated appearance after applying certain conditions during synthesis or post-synthesis treatment. *Thirdly*, it is also important to realize at which concentration the presence of defects would start to have harmful effect by degrading characteristics and properties of materials. Thus, given the above, it is evident that without addressing these inquiries, the application of defect engineering toward further development of proper photocatalyst would have to follow "trial and error pathways" as the choice of experimental parameters would not be supported by any basis of knowledge. Taking the above-mentioned Nb_2O_5 as example, there is strong need to determine the formation energies and transition levels associated with oxygen vacancies as it is unknown under which conditions they might become transformed into fully neutral charge states which limit their contribution to the strengthening of n-type conductivity. Thus, more efforts are required to make this topic become highly assessable without any limitation to the nature and type of material to which it is applied. To be clear, for the present moment, the available knowledge simply is not enough to provide satisfied answers even for well-known photocatalysis.

References

1. E. Kuna, D. Mrdenovic, M. Jönsson-Niedziółka, P. Pieta, I.S. Pieta, Bimetallic nanocatalysts supported on graphitic carbon nitride for sustainable energy development: The shape-structure-activity relation. Nanoscale Adv. **3**, 1342–1351 (2021). https://doi.org/10.1039/D0NA01063D
2. A. Wang, C. Wang, L. Fu, W. Wong-Ng, Y. Lan, Recent advances of graphitic carbon nitride-based structures and applications in catalyst, sensing, imaging, and LEDs. Nano-Micro Lett. **9**, 47 (2017). https://doi.org/10.1007/s40820-017-0148-2

3. K. Parvez, Chapter 1 – Two-dimensional nanomaterials: Crystal structure and synthesis, in *Biomedical Applications of Graphene and 2D Nanomaterials*, ed. by M. Nurunnabi, J. R. McCarthy, (Elsevier, 2019), pp. 1–25. https://doi.org/10.1016/B978-0-12-815889-0.00001-5
4. J. Jiang, L. Ou-yang, L. Zhu, A. Zheng, J. Zou, X. Yi, H. Tang, Dependence of electronic structure of g-C_3N_4 on the layer number of its nanosheets: A study by Raman spectroscopy coupled with first-principles calculations. Carbon **80**, 213–221 (2014). https://doi.org/10.1016/j.carbon.2014.08.059
5. J. Wen, J. Xie, X. Chen, X. Li, A review on g-C_3N_4-based photocatalysts. Appl. Surf. Sci. **391**, 72–123 (2017). https://doi.org/10.1016/j.apsusc.2016.07.030
6. F. Su, S.C. Mathew, G. Lipner, X. Fu, M. Antonietti, S. Blechert, X. Wang, mpg-C_3N_4-catalyzed selective oxidation of alcohols using O_2 and visible light. J. Am. Chem. Soc. **132**, 16299–16301 (2010). https://doi.org/10.1021/ja102866p
7. J. Chen, Z. Hong, Y. Chen, B. Lin, B. Gao, One-step synthesis of sulfur-doped and nitrogen-deficient g-C_3N_4 photocatalyst for enhanced hydrogen evolution under visible light. Mater. Lett. **145**, 129–132 (2015). https://doi.org/10.1016/j.matlet.2015.01.073
8. J. Ding, W. Xu, H. Wan, D. Yuan, C. Chen, L. Wang, G. Guan, W.-L. Dai, Nitrogen vacancy engineered graphitic C_3N_4-based polymers for photocatalytic oxidation of aromatic alcohols to aldehydes. Appl. Catal. B **221**, 626–634 (2018). https://doi.org/10.1016/j.apcatb.2017.09.048
9. L. Kong, X. Mu, X. Fan, R. Li, Y. Zhang, P. Song, F. Ma, M. Sun, Site-selected N vacancy of g-C_3N_4 for photocatalysis and physical mechanism. Appl. Mater. Today **13**, 329–338 (2018). https://doi.org/10.1016/j.apmt.2018.10.003
10. W. Lin, K. Lu, S. Zhou, J. Wang, F. Mu, Y. Wang, Y. Wu, Y. Kong, Defects remodeling of g-C_3N_4 nanosheets by fluorine-containing solvothermal treatment to enhance their photocatalytic activities. Appl. Surf. Sci. **474**, 194–202 (2019). https://doi.org/10.1016/j.apsusc.2018.03.140
11. Y. Kang, Y. Yang, L.-C. Yin, X. Kang, G. Liu, H.-M. Cheng, An amorphous carbon nitride photocatalyst with greatly extended visible-light-responsive range for photocatalytic hydrogen generation. Adv. Mater. **27**, 4572–4577 (2015). https://doi.org/10.1002/adma.201501939
12. P. Yang, J. Zhao, W. Qiao, L. Li, Z. Zhu, Ammonia-induced robust photocatalytic hydrogen evolution of graphitic carbon nitride. Nanoscale **7**, 18887–18890 (2015). https://doi.org/10.1039/C5NR05570A
13. R.C. Pawar, S. Kang, J.H. Park, J. Kim, S. Ahn, C.S. Lee, Room-temperature synthesis of nanoporous 1D microrods of graphitic carbon nitride (g-C_3N_4) with highly enhanced photocatalytic activity and stability. Sci. Rep. **6**, 31147 (2016). https://doi.org/10.1038/srep31147
14. X. Qu, S. Hu, P. Li, Z. Li, H. Wang, H. Ma, W. Li, The effect of embedding N vacancies into g-C_3N_4 on the photocatalytic H_2O_2 production ability *via* H_2 plasma treatment. Diam. Relat. Mater. **86**, 159–166 (2018). https://doi.org/10.1016/j.diamond.2018.04.027
15. X. Li, J. Zhang, F. Zhou, H. Zhang, J. Bai, Y. Wang, H. Wang, Preparation of N-vacancy-doped g-C_3N_4 with outstanding photocatalytic H_2O_2 production ability by dielectric barrier discharge plasma treatment. Chinese J. Catal. **39**, 1090–1098 (2018). https://doi.org/10.1016/S1872-2067(18)63046-3
16. J.-Y. Tang, X.Y. Kong, B.-J. Ng, Y.-H. Chew, A.R. Mohamed, S.-P. Chai, Midgap-state-mediated two-step photoexcitation in nitrogen defect-modified g-C_3N_4 atomic layers for superior photocatalytic CO_2 reduction. Cat. Sci. Technol. **9**, 2335–2343 (2019). https://doi.org/10.1039/C9CY00449A
17. J. Li, W. Ma, J. Chen, N. An, Y. Zhao, D. Wang, Z. Mao, Carbon vacancies improved photocatalytic hydrogen generation of g-C_3N_4 photocatalyst *via* magnesium vapor etching. Int. J. Hydrog. Energy **45**, 13939–13946 (2020). https://doi.org/10.1016/j.ijhydene.2020.03.067
18. M. Shen, L. Zhang, M. Wang, J. Tian, X. Jin, L. Guo, L. Wang, J. Shi, Carbon-vacancy modified graphitic carbon nitride: Enhanced CO_2 photocatalytic reduction performance and mechanism probing. J. Mater. Chem. A **7**, 1556–1563 (2019). https://doi.org/10.1039/C8TA09302D
19. W. Tu, Y. Xu, J. Wang, B. Zhang, T. Zhou, S. Yin, S. Wu, C. Li, Y. Huang, Y. Zhou, Z. Zou, J. Robertson, M. Kraft, R. Xu, Investigating the role of tunable nitrogen vacancies in graphitic

carbon nitride nanosheets for efficient visible-light-driven H_2 evolution and CO_2 reduction. ACS Sustain. Chem. Eng. **5**, 7260–7268 (2017). https://doi.org/10.1021/acssuschemeng.7b01477
20. Y. Li, W. Ho, K. Lv, B. Zhu, S.C. Lee, Carbon vacancy-induced enhancement of the visible light-driven photocatalytic oxidation of NO over g-C_3N_4 nanosheets. Appl. Surf. Sci. **430**, 380–389 (2018). https://doi.org/10.1016/j.apsusc.2017.06.054
21. S. Zhang, C. Hu, H. Ji, L. Zhang, F. Li, Facile synthesis of nitrogen-deficient mesoporous graphitic carbon nitride for highly efficient photocatalytic performance. Appl. Surf. Sci. **478**, 304–312 (2019). https://doi.org/10.1016/j.apsusc.2019.01.270
22. X. Liang, G. Wang, X. Dong, G. Wang, H. Ma, X. Zhang, Graphitic carbon nitride with carbon vacancies for photocatalytic degradation of bisphenol A. ACS Appl. Nano Mater. **2**, 517–524 (2019). https://doi.org/10.1021/acsanm.8b02089
23. X. Li, Y. Sun, J. Xu, Y. Shao, J. Wu, X. Xu, Y. Pan, H. Ju, J. Zhu, Y. Xie, Selective visible-light-driven photocatalytic CO_2 reduction to CH_4 mediated by atomically thin $CuIn_5S_8$ layers. Nat. Energy **4**, 690–699 (2019). https://doi.org/10.1038/s41560-019-0431-1
24. C.C. Mardare, A.W. Hassel, Review on the versatility of tungsten oxide coatings. Phys. Status Solidi (a) **216**, 1900047 (2019). https://doi.org/10.1002/pssa.201900047
25. J.C. Murillo-Sierra, A. Hernández-Ramírez, L. Hinojosa-Reyes, J.L. Guzmán-Mar, A review on the development of visible light-responsive WO_3-based photocatalysts for environmental applications. Chem. Eng. J. Adv. **5**, 100070 (2021). https://doi.org/10.1016/j.ceja.2020.100070
26. B.-R. Koo, H.-J. Ahn, Fast-switching electrochromic properties of mesoporous WO_3 films with oxygen vacancy defects. Nanoscale **9**, 17788–17793 (2017). https://doi.org/10.1039/C7NR06796H
27. J. Wang, Z. Chen, G. Zhai, Y. Men, Boosting photocatalytic activity of WO_3 nanorods with tailored surface oxygen vacancies for selective alcohol oxidations. Appl. Surf. Sci. **462**, 760–771 (2018). https://doi.org/10.1016/j.apsusc.2018.08.181
28. L. Yang, Q. Xu, F. Teng, D. Yu, Y. Yang, W. Gu, Y. Teng, J. Xu, Y. Guo, An initiative, simple vacancy remedy method and the effect on photochemical properties. Appl. Catal. B **202**, 355–363 (2017). https://doi.org/10.1016/j.apcatb.2016.09.036
29. X. Zheng, L. Wu, F. Ren, Oxygen vacancy enhanced room temperature ferromagnetism in Ar^+ ion irradiated WO_3 films. Ceram. Int. **47**, 5091–5098 (2021). https://doi.org/10.1016/j.ceramint.2020.10.087
30. Y. Liu, Y. Yang, Q. Liu, H. He, W. Liu, D. Meng, Y. Li, W. Li, J. Li, Films of WO_3 plate-like arrays with oxygen vacancies proportionally controlled via rapid chemical reduction. Int. J. Hydrog. Energy **43**, 208–218 (2018). https://doi.org/10.1016/j.ijhydene.2017.11.094
31. Y. Li, C. Wang, H. Zheng, F. Wan, F. Yu, X. Zhang, Y. Liu, Surface oxygen vacancies on WO_3 contributed to enhanced photothermo-synergistic effect. Appl. Surf. Sci. **391**, 654–661 (2017). https://doi.org/10.1016/j.apsusc.2016.07.042
32. K. Kriti, P. Kaur, S. Kaur, D. Arora, K. Asokan, D.P. Singh, Influence of defect structure on colour tunability and magneto optical behaviour of WO_3 nanoforms. RSC Adv. **9**, 20536–20548 (2019). https://doi.org/10.1039/C9RA01901D
33. L. Wang, Y. Wang, Y. Cheng, Z. Liu, Q. Guo, M.N. Ha, Z. Zhao, Hydrogen-treated mesoporous WO_3 as a reducing agent of CO_2 to fuels (CH_4 and CH_3OH) with enhanced photothermal catalytic performance. J. Mater. Chem. A **4**, 5314–5322 (2016). https://doi.org/10.1039/C5TA10180H
34. W. Wang, A. Janotti, C.G.V. de Walle, Role of oxygen vacancies in crystalline WO_3. J. Mater. Chem. C **4**, 6641–6648 (2016). https://doi.org/10.1039/C6TC01643J
35. M. Gerosa, C. Di Valentin, G. Onida, C.E. Bottani, G. Pacchioni, Anisotropic effects of oxygen vacancies on electrochromic properties and conductivity of γ-monoclinic WO_3. J. Phys. Chem. C **120**, 11716–11726 (2016). https://doi.org/10.1021/acs.jpcc.6b02707
36. J. Zhu, M. Vasilopoulou, D. Davazoglou, S. Kennou, A. Chroneos, U. Schwingenschlögl, Intrinsic defects and H doping in WO_3. Sci. Rep. **7**, 40882 (2017). https://doi.org/10.1038/srep40882

37. G. Wang, Y. Ling, H. Wang, X. Yang, C. Wang, J.Z. Zhang, Y. Li, Hydrogen-treated WO_3 nanoflakes show enhanced photostability. Energy Environ. Sci. **5**, 6180–6187 (2012). https://doi.org/10.1039/C2EE03158B
38. P.J. Boruah, R.R. Khanikar, H. Bailung, Synthesis and characterization of oxygen vacancy induced narrow bandgap tungsten oxide (WO_{3-x}) nanoparticles by plasma discharge in liquid and its photocatalytic activity. Plasma Chem. Plasma Process. **40**, 1019–1036 (2020). https://doi.org/10.1007/s11090-020-10073-3
39. Y. Yang, S. Niu, D. Han, T. Liu, G. Wang, Y. Li, Progress in developing metal oxide nanomaterials for photoelectrochemical water splitting. Adv. Energy Mater. **7**, 1700555 (2017). https://doi.org/10.1002/aenm.201700555
40. B.B. Sapkota, S.R. Mishra, A simple ball milling method for the preparation of p-CuO/n-ZnO nanocomposite photocatalysts with high photocatalytic activity. J. Nanosci. Nanotechnol. **13**, 6588–6596 (2013). https://doi.org/10.1166/jnn.2013.7544
41. X. Du, J. Huang, Y. Feng, Y. Ding, Flower-like 3D CuO microsphere acting as photocatalytic water oxidation catalyst. Chinese J. Catal. **37**, 123–134 (2016). https://doi.org/10.1016/S1872-2067(15)61012-9
42. T. Velusamy, A. Liguori, M. Macias-Montero, D.B. Padmanaban, D. Carolan, M. Gherardi, V. Colombo, P. Maguire, V. Svrcek, D. Mariotti, Ultra-small CuO nanoparticles with tailored energy-band diagram synthesized by a hybrid plasma-liquid process. Plasma Process. Polym. **14**, 1600224 (2017). https://doi.org/10.1002/ppap.201600224
43. D. Su, X. Xie, S. Dou, G. Wang, CuO single crystal with exposed {001} facets - a highly efficient material for gas sensing and Li-ion battery applications. Sci. Rep. **4**, 5753 (2014). https://doi.org/10.1038/srep05753
44. M. Soldemo, J.H. Stenlid, Z. Besharat, M. Ghadami Yazdi, A. Önsten, C. Leygraf, M. Göthelid, T. Brinck, J. Weissenrieder, The surface structure of Cu_2O (100). J. Phys. Chem. C **120**, 4373–4381 (2016). https://doi.org/10.1021/acs.jpcc.5b11350
45. A.H. Jayatissa, K. Guo, A.C. Jayasuriya, Fabrication of cuprous and cupric oxide thin films by heat treatment. Appl. Surf. Sci. **255**, 9474–9479 (2009). https://doi.org/10.1016/j.apsusc.2009.07.072
46. C.P. Yang, Q. Wu, Z.W. Jiang, X. Wang, C.Z. Huang, Y.F. Li, Cu vacancies enhanced photoelectrochemical activity of metal-organic gel-derived CuO for the detection of l-cysteine. Talanta **228**, 122261 (2021). https://doi.org/10.1016/j.talanta.2021.122261
47. A. Aktar, S. Ahmmed, J. Hossain, A.B.M. Ismail, Solution-processed synthesis of copper oxide (Cu_xO) thin films for efficient photocatalytic solar water splitting. ACS Omega **5**, 25125–25134 (2020). https://doi.org/10.1021/acsomega.0c02754
48. L. Lu, X. Xu, J. Yan, F.-N. Shi, Y. Huo, Oxygen vacancy rich Cu_2O based composite material with nitrogen doped carbon as matrix for photocatalytic H_2 production and organic pollutant removal. Dalton Trans. **47**, 2031–2038 (2018). https://doi.org/10.1039/C7DT03835F
49. D. Chua, S.B. Kim, K. Li, R. Gordon, Low temperature chemical vapor deposition of cuprous oxide thin films using a copper(i) amidinate precursor. ACS Appl. Energy Mater. **2**, 7750–7756 (2019). https://doi.org/10.1021/acsaem.9b01683
50. M. Cheon, B. Jung, S.J. Kim, J.I. Jang, S.Y. Jeong, High-quality epitaxial Cu_2O films with (111)-terminated plateau grains obtained from single-crystal Cu (111) thin films by rapid thermal oxidation. J. Alloy Compd. **801**, 536–541 (2019). https://doi.org/10.1016/j.jallcom.2019.06.152
51. Z. Wang, L. Zhang, T.U. Schülli, Y. Bai, S.A. Monny, A. Du, L. Wang, Identifying copper vacancies and their role in the CuO based photocathode for water splitting. Angew. Chem. Int. Ed. **131**, 17768–17773 (2019). https://doi.org/10.1002/ange.201909182
52. A.F. Wright, J.S. Nelson, Theory of the copper vacancy in cuprous oxide. J. Appl. Phys. **92**, 5849–5851 (2002). https://doi.org/10.1063/1.1516620
53. C. Ricca, L. Grad, M. Hengsberger, J. Osterwalder, U. Aschauer, Importance of surface oxygen vacancies for ultrafast hot carrier relaxation and transport in Cu_2O, ArXiv:2103.03167 [Cond-Mat.Mtrl-Sci] (2021). http://arxiv.org/abs/2103.03167

54. M. Nolan, S.D. Elliott, The p-type conduction mechanism in Cu_2O: A first principles study. Phys. Chem. Chem. Phys. **8**, 5350–5358 (2006). https://doi.org/10.1039/B611969G
55. D.O. Scanlon, B.J. Morgan, G.W. Watson, Modeling the polaronic nature of p-type defects in Cu_2O: The failure of GGA and GGA+U. J. Chem. Phys. **131**, 124703 (2009). https://doi.org/10.1063/1.3231869
56. D.O. Scanlon, B.J. Morgan, G.W. Watson, A. Walsh, Acceptor levels in p-type Cu_2O rationalizing theory and experiment. Phys. Rev. Lett. **103**, 096405 (2009). https://doi.org/10.1103/PhysRevLett.103.096405
57. G.K. Paul, Y. Nawa, H. Sato, T. Sakurai, K. Akimoto, Defects in Cu_2O studied by deep level transient spectroscopy. Appl. Phys. Lett. **88**, 141901 (2006). https://doi.org/10.1063/1.2175492
58. H. Raebiger, S. Lany, A. Zunger, Origins of the p-type nature and cation deficiency in Cu_2O and related materials. Phys. Rev. B **76**, 045209 (2007). https://doi.org/10.1103/PhysRevB.76.045209
59. J. Xu, X. Xiao, J. Zhang, J. Liu, J. Ni, H. Xue, H. Pang, Oxygen vacancies enhancing electrocatalysis performance of porous copper oxide. Part. Part. Syst. Charact. **34**, 1600420 (2017). https://doi.org/10.1002/ppsc.201600420
60. S. Zaman, A. Zainelabdin, G. Amin, O. Nur, M. Willander, Efficient catalytic effect of CuO nanostructures on the degradation of organic dyes. J. Phys. Chem. Solids **73**, 1320–1325 (2012). https://doi.org/10.1016/j.jpcs.2012.07.005
61. L.I. Bendavid, E.A. Carter, CO_2 adsorption on $Cu_2O(111)$: A DFT+U and DFT-D study. J. Phys. Chem. C **117**, 26048–26059 (2013). https://doi.org/10.1021/jp407468t
62. D.E. Fouad, C. Zhang, H. El-Didamony, L. Yingnan, T.D. Mekuria, A.H. Shah, Improved size, morphology and crystallinity of hematite (α-Fe_2O_3) nanoparticles synthesized via the precipitation route using ferric sulfate precursor. Results Phys. **12**, 1253–1261 (2019). https://doi.org/10.1016/j.rinp.2019.01.005
63. C. Chen, F. Duan, S. Zhao, W. Wang, F. Yang, W. Nuansing, B. Zhang, Y. Qin, M. Knez, Porous Fe_2O_3 nanotubes with α-γ phase junction for enhanced charge separation and photocatalytic property produced by molecular layer deposition. Appl. Catal. B **248**, 218–225 (2019). https://doi.org/10.1016/j.apcatb.2019.02.029
64. M.F.M. Noh, H. Ullah, N.A. Arzaee, A.A. Halim, M.A.F.A. Rahim, N.A. Mohamed, J. Safaei, S.N.F.M. Nasir, G. Wang, M.A.M. Teridi, Rapid fabrication of oxygen defective α-$Fe_2O_3(110)$ for enhanced photoelectrochemical activities. Dalton Trans. **49**, 12037–12048 (2020). https://doi.org/10.1039/D0DT00406E
65. P. Zeng, Y. Zhao, Y. Lin, X. Wang, J. Li, W. Wang, Z. Fang, Enhancement of electrochemical performance by the oxygen vacancies in hematite as anode material for lithium-ion batteries. Nanoscale Res. Lett. **12**, 13 (2017). https://doi.org/10.1186/s11671-016-1783-0
66. Q. Yang, J. Du, J. Li, Y. Wu, Y. Zhou, Y. Yang, D. Yang, H. He, Thermodynamic and kinetic influence of oxygen vacancies on the solar water oxidation reaction of α-Fe_2O_3 photoanodes. ACS Appl. Mater. Interfaces **12**, 11625–11634 (2020). https://doi.org/10.1021/acsami.9b21622
67. Y. Makimizu, N.T. Nguyen, J. Tucek, H.-J. Ahn, J. Yoo, M. Poornajar, I. Hwang, S. Kment, P. Schmuki, Activation of α-Fe_2O_3 for photoelectrochemical water splitting strongly enhanced by low temperature annealing in low oxygen containing ambient. Chem. Eur. J. **26**, 2685–2692 (2020). https://doi.org/10.1002/chem.201904430
68. H. Feng, Y. Wang, C. Wang, F. Diao, W. Zhu, P. Mu, L. Yuan, G. Zhou, F. Rosei, Defect-induced enhanced photocatalytic activities of reduced α -Fe_2O_3 nanoblades. Nanotechnology **27**, 295703 (2016). https://doi.org/10.1088/0957-4484/27/29/295703
69. J. Lee, S. Han, Thermodynamics of native point defects in α-Fe_2O_3: An ab initio study. Phys. Chem. Chem. Phys. **15**, 18906–18914 (2013). https://doi.org/10.1039/C3CP53311E
70. A. Janotti, C.G. Van de Walle, Oxygen vacancies in ZnO. Appl. Phys. Lett. **87**, 122102 (2005). https://doi.org/10.1063/1.2053360
71. A. Banerjee, A.A. Kohnert, E.F. Holby, B.P. Uberuaga, Critical assessment of the thermodynamics of vacancy formation in Fe_2O_3 using hybrid density functional theory. J. Phys. Chem. C **124**, 23988–24000 (2020). https://doi.org/10.1021/acs.jpcc.0c07522

72. M. Forster, R.J. Potter, Y. Ling, Y. Yang, D.R. Klug, Y. Li, A.J. Cowan, Oxygen deficient α-Fe_2O_3 photoelectrodes: A balance between enhanced electrical properties and trap-mediated losses. Chem. Sci. **6**, 4009–4016 (2015). https://doi.org/10.1039/C5SC00423C
73. Y.-C. Lee, Y.-L. Chueh, C.-H. Hsieh, M.-T. Chang, L.-J. Chou, Z.L. Wang, Y.-W. Lan, C.-D. Chen, H. Kurata, S. Isoda, p-Type α-Fe_2O_3 nanowires and their n-type transition in a reductive ambient. Small **3**, 1356–1361 (2007). https://doi.org/10.1002/smll.200700004
74. Y. Zhao, X. Zhou, L. Ye, S.C.E. Tsang, Nanostructured Nb_2O_5 catalysts. Nano Rev. **3**, 17631 (2012). https://doi.org/10.3402/nano.v3i0.17631
75. K. Su, H. Liu, Z. Gao, P. Fornasiero, F. Wang, Nb_2O_5-based Photocatalysts. Adv. Sci. **8**, 2003156 (2021). https://doi.org/10.1002/advs.202003156
76. R.A. Rani, A.S. Zoolfakar, A.P. O'Mullane, M.W. Austin, K. Kalantar-Zadeh, Thin films and nanostructures of niobium pentoxide: Fundamental properties, synthesis methods and applications. J. Mater. Chem. A **2**, 15683–15703 (2014). https://doi.org/10.1039/C4TA02561J
77. E.T. Salim, R.A. Ismail, H.T. Halbos, Growth of Nb_2O_5 film using hydrothermal method: Effect of Nb concentration on physical properties. Mater. Res. Express **6**, 116429 (2019)
78. S.L. Fernandes, L.J. Affonço, R.A. Junior, J.H. da Silva, E. Longo, C.F. de O Graeff, Niobium oxide films deposited by reactive sputtering: Effect of oxygen flow rate. J. Vis. Exp. **151**, e59929 (2019). https://doi.org/10.3791/59929
79. S.B. Basuvalingam, B. Macco, H.C.M. Knoops, J. Melskens, W.M.M. (Erwin) Kessels, A.A. Bol, Comparison of thermal and plasma-enhanced atomic layer deposition of niobium oxide thin films. J. Vac. Sci. Technol. A **36**, 041503 (2018). https://doi.org/10.1116/1.5034097
80. J.-S. Baik, G. Yun, M. Balamurugan, S.K. Lee, J.-H. Kim, K.-S. Ahn, S.H. Kang, Hydrogen treated niobium oxide nanotube arrays for photoelectrochemical water oxidation. J. Electrochem. Soc. **163**, H1165 (2016). https://doi.org/10.1149/2.1091614jes
81. W. Zhao, W. Zhao, G. Zhu, T. Lin, F. Xu, F. Huang, Black Nb_2O_5 nanorods with improved solar absorption and enhanced photocatalytic activity. Dalton Trans. **45**, 3888–3894 (2016). https://doi.org/10.1039/C5DT04578A
82. Q. Xu, L.-Q. Deng, Y. Wu, T. Ma, A study of cathode improvement for electro-deoxidation of Nb_2O_5 in a eutectic $CaCl_2$-NaCl melt at 1073K. J. Alloy Compd. **396**, 288–294 (2005). https://doi.org/10.1016/j.jallcom.2005.01.002
83. N. Kumari, K. Gaurav, S.K. Samdarshi, A.S. Bhattacharyya, S. Paul, B. Rajbongshi, K. Mohanty, Dependence of photoactivity of niobium pentoxide (Nb_2O_5) on crystalline phase and electrokinetic potential of the hydrocolloid. Sol. Energy Mater. Sol. Cells **208**, 110408 (2020). https://doi.org/10.1016/j.solmat.2020.110408
84. T. Kikuchi, M. Goto, Oxygen vacancies in $Nb_{22}O_{54-x}$, $Nb_{25}O_{62-x}$, and $Nb_{28}O_{70-x}$. J. Solid State Chem. **16**, 363–371 (1976). https://doi.org/10.1016/0022-4596(76)90052-9
85. P. Kofstad, Comment on the defect structure of α-Nb_2O_5. J. Less Common Met. **14**, 153–156 (1968). https://doi.org/10.1016/0022-5088(68)90215-4
86. E.H. Greener, D.H. Whitmore, M.E. Fine, Electrical conductivity of near-stoichiometric α-Nb_2O_5. J. Chem. Phys. **34**, 1017–1023 (1961). https://doi.org/10.1063/1.1731627
87. E.H. Greener, The electrical conductivity of non-stoichiometric niobium-pentoxide and non-ohmic phenomena in niobium-pentoxide and titanium-dioxide, PhD thesis, Northwestern University, 1960

Chapter 10
Extrinsic Defects in Nanostructured Semiconductors

10.1 Introduction

The development of extrinsic deficiency in defined materials is usually correlated with the presence of foreign atoms or their complexes within its structure as a result of intentional doping with certain element. Under proper management, it enables to proceed very specific and desired changes in the geometrical and electronic configurations thus leading to extension and progression of their properties and features accompanied by consequent improvement of photocatalytic and photoelectrochemical performances. In fact, by its functionality, these defects have very high resemblance to the impact which is associated with the presence of vacancies with only difference is that tuning of their characteristics provides better flexibility and adaptivity toward advancement of host material given that numerous elements along with their different concentrations can be chosen as a source of doping. Overall, the following particularities and specifications are associated with them. *Firstly*, residence of foreign atoms in crystal lattice is classified to have substitutional (replacing the original atoms in periodical array) or interstitials (filling an occupied space out of atomic periodical arrays) localization. To determine, which one of them has the dominance for each given case, various factors including experimental conditions associated with their introduction and consequent manipulation, type of dopants and also host material, etc. should be considered. *Secondly*, formation of interstitial defect occurs instantly *via* diffusion process, and their existence is generally referred to the appearance of atoms with small radii such as hydrogen, carbon, and nitrogen. For its side, to create substitutional defect, it is necessary to make the atomic site in the crystal lattice empty, and only then the foreign atom can proceed there. Thus, it is a more complex process if only vacancy is available in advance. In turn, radii of substitutional atoms have less restrictions and limitations as surrounding near-neighbors undergo inward or outward relaxation in order to adjust new arrangement. Thus, introduction of metal and many non-metal elements is usually

V. Gurylev, *Nanostructured Photocatalyst via Defect Engineering*,
https://doi.org/10.1007/978-3-030-81911-8_10

proceeded *via* formation of these defects as thermodynamically they provide more favorable configuration. *Thirdly*, taking n-type TiO_2 or ZnO as examples, doping with metal atoms which have more or less valence electrons than those ones that are going to be replaced often is used to strengthen their original conductivity or to advance its transitions into p-type, respectively. This process is usually accompanied by the appearance of donor or acceptor levels within the band gap. It is interest to notice that as doping process can be highly localized, it is possible to create neighboring domains filled with both, positive and negative, charge carriers within similar material thus resulting in formation of homojunction. *Fourthly*, introduction of foreign atoms is often accompanied by the development of vacancies as they are necessary to compensate differences in charge state or assist in reconstruction of crystal lattice in order to reduce newly appeared stress due changes in dimension of crystal lattice. In this case, intrinsic and extrinsic defects can be combined to create complexes or chemical chains. *Fifthly*, it is also possible to make co-doping, i.e., atoms of two or more elements become simultaneously incorporated into target materials. In this case, each of them takes specific role in enhancing very particulate characteristics or their synergy can be used to proceed overall improvement. At the same time, under incorrect management, it also might lead to opposite results when both elements negatively influence each other resulting in partial or even complete shadowing of their positive influence, and thus it brings more harm. *Sixthly*, as doping technically is related to the incorporation of foreign atoms, it is important to consider the parameter of solubility that define whether they accumulate on surface or are supposed to "sink" deeper into the bulk and in which form. Simply to say, instead of being gradually penetrated into crystal lattice and spreading uniformly there, the dopant can avoid any interaction with crystal lattice of host materials thus becoming available as isolated formation or leading to appearance of new phase or compound that is absolutely different to that of the original one.

10.2 Advantages and Disadvantages of Using Extrinsic Deficiency

Every material that is used for photocatalytic processing along with strong characteristics which determine its utilization and relevance also possesses certain very undesirable drawbacks and limitations preventing it from demonstrating expectedly awaiting or theoretically predicted high performance thus greatly reducing the level of its applicability and consequent attractiveness. In this regard, introduction of extrinsic deficiency can be considered as one of the most effective approaches to address this problem as proper management and adjustment of foreign atoms in crystal lattice of host material can be used to greatly reduce its associated negative impact and oppositely lead to strengthening of required properties. Overall, the following advantages are usually recognized due to employment of this strategy. *Firstly,* the absorption of light becomes greatly enhanced. It is usually proceeded *via*

development of new energy levels within the band gap, narrowing its width through appearance of band tail or mixing of conduction or valance bands with mentioned levels, thus making them shift down or up, respectively, or by developing porous compositions that can assist in effective trapping of photons, thus reducing chances of their successful escape. *Secondly*, doping with proper element can be used to adjust and tune the alignment of band gap, thus making it to be suitable for redox potentials of defined photocatalytic reactions and enabling their activation. In this case, initially inactive materials can be transformed into feasible candidate to perform them. As an illustration, recent finding revealed that introduction of cations with d^{10} or $d^{10}s^2$ electronic configurations into certain semiconductors can lead to development of occupied *d* or *s* states into valence band, thus making its top edge to be shifted up [1]. *Thirdly*, it is also possible to regulate processes associated with presence and transportation of charge carrier, thus leading to their improved separation rate and extended transportation characteristics. In addition, as foreign atoms can take the role of acceptor and donors with shallow or deep features, they can provide more precise control over changes in strength and type of conductivity than the one that is achieved by using intrinsic deficiency. For instance, occurrence of p-type doping in ZnO can be proceeded simply by doping it with nitrogen or arsenic. Newly created holes could be effectively preserved, stabilized, and also reproduced with much higher level of reproducibility compared with those obtained *via* formation of zinc deficiency. Furthermore, as there are numerous elements that can be used to tune the electrical and electronic properties and each of them has its own benefits, it allows to easily fit the given conditions and requirements and provides higher flexibility in reaching the desired characteristics *via* most effective pathway.

Definitely, extrinsic deficiency cannot be considered an absolutely ideal approach. In fact, it suffers from several very crucial disadvantages and serious drawbacks which limit its employment and force researchers to apply numerous efforts in order to avoid and overpass them. As an illustration, filling of mentioned above wide band gap materials such as TiO_2 or ZnO with atoms from metallic compounds or elements can cause the following harmful effects and consequences. *Firstly*, introduced elements might have low solubility in them that leads to appearance of additional unexpected phases or formation of ternary component. *Secondly*, it is also often the case that thermal stability of host material greatly reduces; thus it becomes less resistant to the rising temperature of surrounding or other changes. *Thirdly*, as TiO_2, for example, can be presented in the form of rutile, anatase, and brookite, doping can bring unpredicted and destructive alterations in standard protocol of phase transformation [2] (Fig. 10.1). Another problem is that out of optimal concentration and distribution, metal doping has great possibility to initiate the increase of recombination rate and also negatively influence the overall electronic configurations. In turn, the presence of atoms from non-metallic elements can often lead only to short-term increase in efficiency of photocatalytic reactions as they cannot be preserved under light irradiation and tend to escape from surface. Additionally, their introduction requires the application of high-temperature and prolong treatment step that might crucially influence the composition and structures of host material.

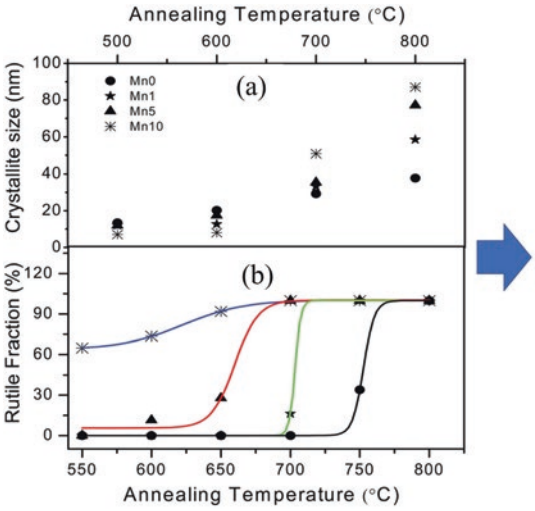

(c)

Atom% of Mn dopant	A to R Transformation temperature (°C)
0	750
1	700
5	600
10	550

Fig. 10.1 (**a**) Variation of crystallite size with the annealing temperature and (**b**) rutile content at different annealing temperatures for Mn-doped and pure TiO_2. Number after "Mn" means its atomic %. (**c**) The effect of the Mn dopant on the initiating anatase to rutile (A to R) phase-transformation process. (Adapted from Ref. [2] with permission from *PCCP Owner Societies*. Copyright 2018)

It is also necessary to mention that doping is considered to be a resource-dependent process, and its utilization potentially leads to the risks associated with progressive resource exhaustion and unavailability of critical elements. Moreover, introduction of foreign atoms into target materials might greatly increase the complexness of experimental procedure, thus making it become multistaged. It is also often the case that currently available equipment only allows doping with single and defined component, thus limiting its practical employment. To overcome it, additional changes are necessary to be implemented. Consequently, it results in higher production cost and associated difficulty to adopt this strategy for widespread. Nevertheless, benefits of using extrinsic deficiency in terms of demonstrated photocatalytic performance and future perspectives overweigh these disadvantages and thus make it to find great applicability among researchers.

10.3 Case Study I: TiO_2

10.3.1 Brief Overview

Titanium oxide is the most investigated and utilized material for photocatalytic processing given that it possesses various unique characteristics such as low cost, thermal and chemical stability, non-toxicity, and suitable positions of conductions and valence bands that enable to cover redox potentials of most of currently available

reactions including such a demanding one as water splitting and CO_2 reduction. Thus, its practicability is considered to be very attractive and have been pushing forward for the last several decades. However, successful realization of this scenario is hindered by several crucial well-known drawbacks associated with this material which need to be overcome. At first, due to wide band gap, its activation could only be proceeded under irradiation with UV light that is accounted for only about 4% of the solar spectra. In addition, extremely high recombination rate greatly reduces the availability of photo-induced electron holes and seriously affects their transportation to the surface, thus limiting participation in oxidation or reduction reactions. Another problem of TiO_2 is raised from its poor affinity toward organic pollutants, thus resulting in their reduced adsorption. In this regard, doping with metal or nonmetal elements can be used to enhance usability of this materials toward photocatalytic processing, thus making its performance approaching the required levels as remarkable advancement of its various properties can be achieved. Yet, it is necessary to be extremely careful with this strategy as under improper and inaccurate management it might result in absolutely opposite and very undesirable outcome and bring more harm than benefits.

10.3.2 Metal Doping

Over the past several decades, metal-doped TiO_2 (e.g., Mo, W, La, Nb, Co, Ni, Cr, Zn, V, Fe) has been widely studied for application in various photocatalytic processing as the presence of these elements can highly increase its certain very specific features allowing to address major drawbacks and deliver higher performance. The main parameters that determine and navigate the introduction of these changes include the character and concentration of dopants as well as the nature of applied experimental processing that is used to introduce them. *Firstly*, it is well known that TiO_2 represents n-type semiconductor with Ti having oxidation state of +4. Thus, it means that doping with penta- or hexa-valence elements is considered to be one of the most optimal choice to advance transportation characteristics of charge carriers and consequently enhance their recombination rate *via* increasing the overall concentration of electrons thus shifting-up the positions of Fermi level. *Secondly*, appearance of impurity levels close to conduction band also could be observed, and their precise positioning is fully dependent on the particularities of each introduced element. Thus, the width of band gap potentially could be regarded as decreased since electrons could travel from valence to conduction band by capturing photons with lower energies which could be associated with possible shift of absorption edge toward visible light. *Thirdly*, these dopants can take the additional role of electron or holes trap centers which also contribute to extending the overall lifetimes of charge carriers. Definitely, in order to realize it, very specific concentration of utilized element should be chosen as its too high value might result in overpassing the solubility limits and appearance of additional undesirable phases that have a highly negative impact, while too low value is not enough to make any detectable changes.

In turn, employment of metals that have tri-valent or two-valent configurations for doping of TiO_2 has been generally considered for only rare exceptions as less attractive strategy given that their presence generally reduces the availability of electrons. It is out of question that they also can participate in trapping of charge carriers in a similar way as it was mentioned above; yet the efficiency and applicability of this process is less pronounce given that it only results in comparably negligible enhancement in photoactivity.

The presence of both acceptor- and donor-like metal-doping usually leads to generation of oxygen vacancies and Ti interstitials in TiO_2 as their existence serves to compensate changes in geometrical and especially electronic configurations since it is often the case that due to large atomic radii, the doped element can accommodate in crystal lattice only with certain difficulties causing an increase in internal stress. However, despite these changes, it is of particulate interest that the crystallite size and overall surface area of metal-doped TiO_2 remain relatively invariable. As a final word, it is necessary to notice that these defects whether as single compound or in synergy with introduced foreign atoms often take major roles in photocatalytic processing.

10.3.3 Non-metal Doping

Doping with non-metal elements such as nitrogen (N), fluorine (F), carbon (C), and boron (B) is considered to be a highly attractive approach to extend the photocatalytic performance of TiO_2 beyond current limitations as their presence greatly influences the enhancement of its various characteristics. Following their small atomic radii and relatively high solubility level, they can easily penetrate and diffuse into crystal lattice filling the positions at interstitials or substitutional sites as it is controlled by adjusting and tuning the parameters of utilized experimental procedures. The particulate type of geometrical arrangement determines whether changes in the electronic configurations due to introduced atoms are governed by its donor- or acceptor-like characteristics, respectively, i.e., *via* seizing elections or oppositely, donating them to the neighboring atoms, and creating Ti^{3+} species. This process is accompanied by the formation of corresponding impurity and defect states within different approximation from valence or conduction bands, and precise identification of this localization in band gap is highly dependent on the nature of doped element and its position within crystal lattice. For example, it was revealed that in substitutional mode, B gives states high in the band gap, while N can develop them just above the top of the valence band [3]. In turn, oxygen vacancies are also formed as to keep electronic and geometrical balance, and their presence also causes the appearance of associated mid-gap states that were specified to exist within 0.18–0.30 eV from the minimum of conduction band [4].

Thus, it is evident that this approach provides extremely high flexibility on reaching required adjustment of band gap structure. To be clear, it can be applied to introduce more crucial and evident changes compared with that achieved *via* metal-doping processing. As an illustration, Zhou et al. [5] reported that the presence of nitrogen atoms into TiO_2 spherical-like particles enables to switch their color from white to black as width of band gap was narrowed to ~1.5 eV. Thus, the optical sensitivity was extended up to infrared light. In the same time, due to decreased sizes of crystallites, the specific surface area was greatly enhanced. Furthermore, it also led to reduced recombination rate of charge carriers as electron and holes were separately trapped by the oxygen vacancy and doped nitrogen atoms leading to extension of their lifetimes.

10.3.4 Photocatalytic Application of Doped TiO_2

Under proper management and with very accurate tuning, utilization of metal- and non-metal-doped TiO_2 to perform photocatalytic processing such as hydrogen production, CO_2 reduction, degradation of various harmful dyes, nitrogen fixation, etc. can result in very promising outcome as it leads to highly enhanced efficiency and prolonged stability which is usually associated with increased absorption in visible light and the presence of additional energy states in the band gap that assist in transportation of charge carriers to the surface and also contribute to their reduced recombination rate. For example, Gao et al. [6] reported that introduction of Mg atoms into TiO_2 ultrathin hollow spheres could activate the realization of overall water splitting reaction under simulated sunlight. The yield of obtained hydrogen and oxygen followed the concentration of dopant and reached maximum at its presence of ~0.5% (Fig. 10.2a, b). In turn, Akple et al. [7] investigated the influence of nitrogen doping on the capability of TiO_2 microsheets to decompose CO_2 under irradiation with visible light. It was determined that their presence greatly advance electrical and optical characteristics leading to increased rate of generated CH_3OH determined as a secondary product of reduction reaction which was much higher than that of commercial TiO_2 (Fig. 10.2c, d). Furthermore, co-doping strategy that is used to combine the presence of metal and non-metal atoms is also often considered as an effective approach given that correct choice of elements that is applied for it can cause the appearance of strong synergy between their attractive features and also lead to elimination of certain undesirable drawbacks that are associated with their presence as a single compound in TiO_2. As an illustration, Zhuang et al. [8] demonstrated that application of Sn,N/co-doped TiO_2 resulted in highly enhanced yield of hydrogen production via photocatalytic water splitting compared with that of TiO_2 filled with only N or Sn. It was revealed that formation of both Ti-O-Sn and Ti-O-N linkages greatly affects the electronic structure of this material as edge of valence band was shifted up thus leading to more efficient utilization of light.

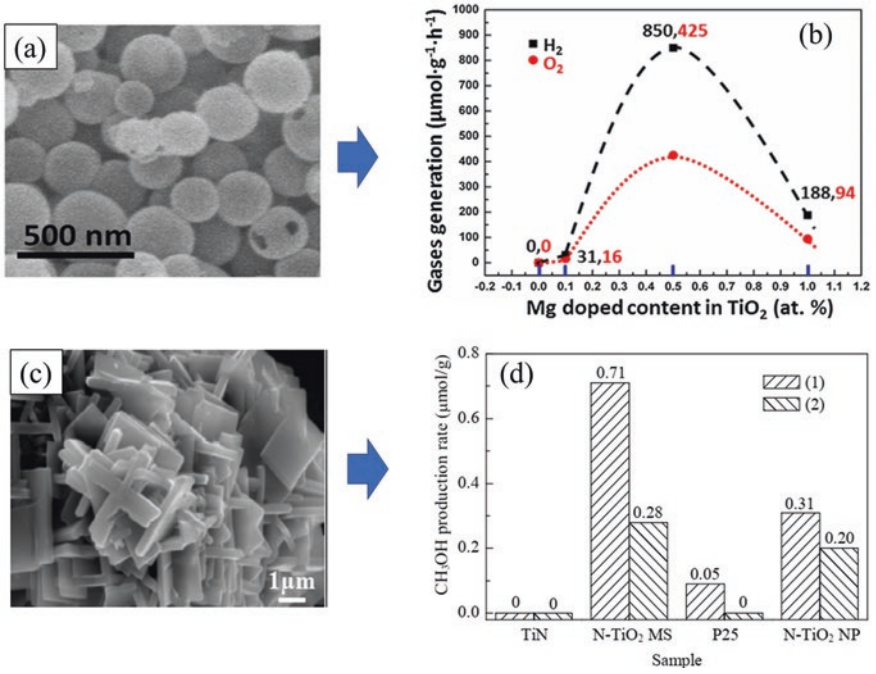

Fig. 10.2 (**a**) SEM image of 0.5% Mg-TiO_2 hollow spheres. (**b**) Gas generation rates of Mg-TiO_2 hollow sphere with 0%, 0.1%, 0.5%, 1% Mg doping during photocatalytic overall water splitting. (Adapted from Ref. [6] with permission from *Elsevier*. Copyright 2016) (**c**) SEM images of as-prepared N-TiO_2 microsheets (MS). (**d**) Comparison of CH_3OH production rates over TiN, N-TiO_2 MS, commercial TiO_2 (P25), and N-TiO_2 nanoparticles (NP) under full spectrum light irradiation (1) and visible light irradiation (2) for 2 h. (Adapted from Ref. [7] with permission from *Elsevier*. Copyright 2015)

10.4 Case Study II: ZnO

10.4.1 Brief Overview

Among various materials that are considered to have great potential to be used in photocatalytic processing, ZnO by usability and popularity is defined to be one of the most applied and investigated metal oxides. Its attractiveness is associated with the presence of various unique characteristics and properties such as excellent chemical and photochemical stabilities, non-toxicity, low cost, environmental friendliness large exciton binding energy (60 meV), etc. Furthermore, compared to well-known and widely studied TiO_2, it possesses better optical absorption spectrum and also the production cost much lower which makes it to be more favorable choice. These advantages, however, are shadowed by very poor optical characteristics as the presence of wide band gap allows to utilize only UV light that contributes very little to the solar energy. As a result, the activation of ZnO to proceed

photocatalysis cannot be realized under irradiation with visible or near-infrared lights. Another problem of this material is that recombination of electron-hole pairs is too high, and thus it limits their successful transportation toward surface where they can initiate the redox reactions with absorbed molecules. In this regard, introduction of extrinsic deficiency that is available in the form of metal and non-metal doping can be used to address these problems and to convert ZnO into efficient and practical material that enables to show the desired level of performance regardless its morphological or structural particulates as main changes are proceeded within its crystal lattice and chemical composition. These improvements can be defined and implemented with very precise accuracy given that wide number of elements along with their concentrations could be employed as dopants. However, this approach should be considered with great caution as often without proper management instead of expected advancements it might bring more harm. For example, as ZnO usually possesses very large number of various intrinsic defects, the presence of certain foreign atoms might lead to their extreme excess thus transforming them into recombination centers.

10.4.2 Metal Doping

Similar to TiO_2, metal doping of ZnO could result in highly enhanced separation rate of charge carriers as introduced atoms usually serve the role of trapped centers that extend the individual lifetimes of electrons or holes. Furthermore, they often do not change the positions of band gap with respect to vacuum level as it only results in appearance of donor or acceptor-like transitions levels within it [9] which could be used by electrons as a step to travel from valence to conduction band. In this regard, their transfer becomes possible by absorbing photons only with energies laid in the range of visible light. As for more concrete discussion, it is commonly accepted that doping with transition metals such as Fe, Cu, Co, and Mn is considered to be the most optimal choice to modify ZnO given that they have relatively similar atomic radii compared with that of Zn^{2+} allowing them to diffuse easily within crystal lattice. Thus, it causes highly negligible distortion of surrounding near-neighbors. However, due to the existence of charge compensation effect, or following the rearrangement of geometrical configuration as to minimize changes in internal energy, appearance of oxygen or zinc vacancies often cannot be avoided. Another advantage of utilizing these elements is that they have very accessible level of solubility in ZnO which means that formation of any non-desirable phases can be effectively avoided or its impact is reduced. It is also well documented that the presence of transmission metals in ZnO also causes crucial enhancement of specific surface area as the sizes of crystallites become reduced [10]. In turn, doping with rear earth metals such as Ce, Eu, and La is less effective and requires more efforts to be successful. *Firstly*, their availability is limited by very low saturated concentration; thus it might initiate the appearance of third phases in ZnO, such as formation of La_2O_3 during La-doping [11]. Given that band gap of this compound reaches

~5.3 eV [12], instead of desirable enhancement of optical characteristics, one may expect their worsening. *Secondly*, the difference in ionic size compared with that of Zn^{2+} makes their incorporation and consequent travel within crystal lattice more difficult, and it results in a huge distortion of structural and morphological features which also contribute negatively on advancement of some important properties.

As a final remark, one should notice that out of all other metals that are not included into two mentioned above groups, doping with Al is also demonstrated to be the most attractive approach as it activates the development of remarkable conductivity and appearance of impressive chemical stability [9]. The only problem that negatively influences practical adoption of this compound is its sensitivity to moisture [13] and that it requires to have complete absence of disorder locations as to ensure good carrier mobility [14]. Given that ZnO usually is rich in vacancies, it is considered to be a challenging issue.

10.4.3 Non-metal Doping

Non-metal doping of ZnO is associated with many interest and unique phenomenon that occurred within its crystal lattice as it allows to tune and adjust certain and very defined characteristics of this material. Overall, the following particularities are determined. *Firstly*, in analogy to TiO_2, introduced foreign atoms also can reside in interstitials or substitutional positions whether as individual compound or in the form of defect complex that occurred via interaction and consequent association with atoms and various imperfections of surrounding crystal lattice, and it crucially influences the nature and localization of corresponding energy levels within band gap as they might have donor or acceptor-like characteristics. It is, however, the case that they mostly occurred in a lower part of band gap as it happened, for example, during introduction of nitrogen atoms which existence as substitutional or interstitial defects leads to appearances of these levels at a distance of ~0.3 and ~1.4 eV, respectively, above the top of valence band [9]. *Secondly*, due to broken thermodynamic equilibrium, the formation of various intrinsic defects such as oxygen vacancies, Zn interstitials, etc. can hardly be avoided during doping as their presence allows to minimize changes of internal energy. Furthermore, under proper concentration and distribution, they can assist in enhancing the separation of charge carriers by taking the role of their traps and also contributing to overall increase of conductivity or advancement of charge transportation characteristics. *Thirdly*, substitutional doping of certain non-metal elements also can occur *via* residing at Zn vacant positions and compare with other materials, such as replacement of metal atoms has very high probability to occur and thus has very crucial influence. For example, Tan et al. [15] demonstrated that during introduction of carbon, this type of defect has the lowest formation energy among others once oxygen-rich

conditions were applied. Furthermore, it was also revealed that as a single compound, it represents donor-like characteristics; yet, once it becomes associated with oxygen interstitial, the transformation into acceptor-type defect was observed. *Fourthly*, the presence of non-metal compound in the atomic or molecular form as one can observe in case of nitrogen doping influences greatly on its capability to strengthen natural n-type conductivity of ZnO or serve a source of n → p transitions [16]. However, contrary to such a crucial change in electronic configuration, it is necessary to notice that structural characteristics after doping usually remain the same or undergo negative impact [17]. Thus, it is obvious that changes in morphology cannot contribute to the enhancement of photocatalytic activity and in fact, oppositely, degrade it.

10.4.4 Photocatalytic Application of Doped ZnO

There is a general concern and agreement that introduction of various metal and non-metal compounds into ZnO whether during synthesis or as a result of post-synthesis treatment usually results in highly enhanced photoactivity in terms of water purification, hydrogen production, CO_2 reduction, or other related reactions. It is mostly attributed to enhance optical and electrical properties as, *firstly*, due to existence of energy levels within the band gap, the sensitivity toward irradiation with visible light increases and, *secondly*, recombination rate of photoinduced electron holes reduces greatly while their transfer to the surface where they can react with adsorbed molecules becomes more efficient. Yet, this outcome cannot be considered as ultimate and always happened as only application of very carefully utilized experimental conditions could guarantee it since there always exists a possibility that doped elements due to their very controversial and easily changeable nature could also bring harm. For example, Kobayashi et al. [18] prepared ZnO nanorods doped with nitrogen by using zinc-ammine complex solution followed by consequent thermal annealing at 300–700 °C and utilized them for photoelectrochemical water splitting under light with wavelength over 420 nm (Fig. 10.3a). It was observed that at low temperature of treatment, N atoms serve as donors contributing greatly to enhancing concentration of charge carriers (Fig. 10.3b), and also various related characteristics and thus greatly improving the performance. In turn, at more harsh conditions, the nature of these atoms becomes transformed into acceptors, and thus, their presence resulted in very dramatic decrease of available electrons and overall degrading of photoefficiency even though more advanced optical properties were achieved (Fig. 10.3c).

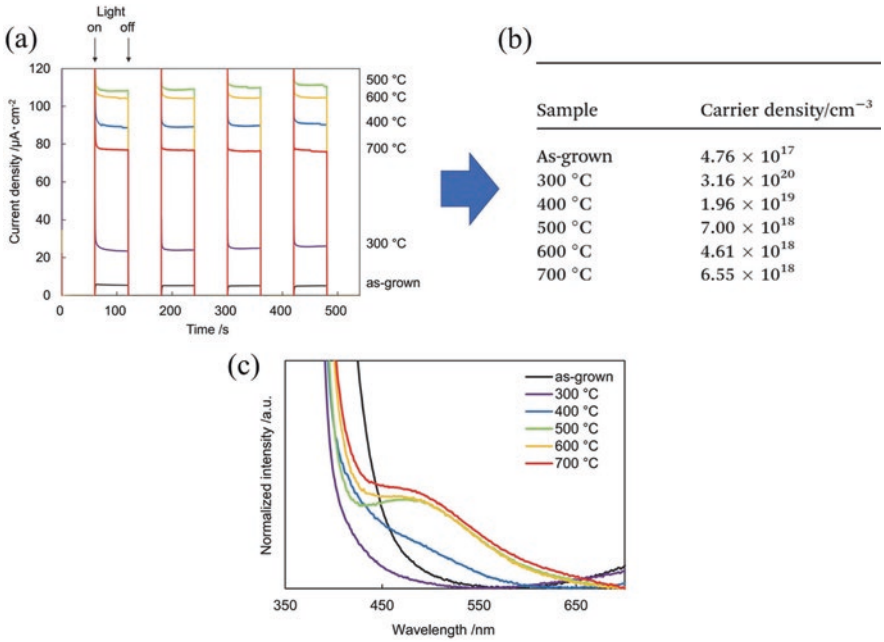

Fig. 10.3 (**a**) Electrochemical current-time measurements recorded on N:ZnO nanorod array (NRA) with light on/off cycles at 0.8 V using >422 nm illumination. (**b**) Calculated carrier densities and (**c**) diffuse reflectance spectra of N:ZnO NRAs with and without treatment at different temperatures. (Adapted from Ref. [18]. Copyright 2018, *The Royal Society of Chemistry*. Available under Creative Commons Attribution-Non Commercial 3.0 Unported License, https://creativecommons.org/licenses/by-nc/3.0/)

10.5 Case Study III: Ta_2O_5

10.5.1 Brief Overview

Among various materials and compounds currently available for photocatalytic processing, tantalum peroxide (Ta_2O_5) deserves special attention due to perfect chemical and thermal stabilities accompanied by high dielectric constant. Furthermore, compared with well-known and widely investigated TiO_2, the position of its conduction band is located ~0.3 eV more negative with respect to vacuum level which defines the existence of improved kinetic toward realization of reduction reaction and also influences greatly on the capability to produce more superoxide radicals. Yet, these positive features are easily shadowed by the presence of extremely wide band gap equaled to ~4.0 eV which limits the absorption of visible light and thus

leads to critically low number of available photoinduced electron holes that can interact with adsorbed molecule. Furthermore, the presence of high recombination rate further reduces their concentration as not all of them are able to reach the surface which means that significant part of them becomes annihilated in bulk. In that sense, it is suggested that introduction of foreign atoms can effectively address these problems as their presence could proceed the formation of additional intermediate levels within band gap thus greatly increasing the utilization of photons with lower energies. This process usually is accompanied by increase in the transport characteristics of charge carriers as introduced atoms often serve as individual trapping centers for them. Overall, more thorough discussion regarding applicability of metal and non-metal elements as a source of doping in Ta_2O_5 is provided below.

10.5.2 Metal Doping

Metal doping of Ta_2O_5 is a less popular approach compared with that of using non-metal elements. Currently, only several elements such as Fe, Na, K, and Cu [19–21] have been investigated in detail as to show the influence of their incorporation on the evolution of various characteristics with regard to consequent photocatalytic application. Overall, the following particularities are defined for this strategy. *Firstly*, the presence of metal atoms generally leads to increase of crystallites or pore sizes if mesoporous stricture is used and thus results in overall degradation of specific surface area [19, 20]. *Secondly*, changes in the optical sensitivity depend on the choice of doped elements as it can lead to positive and negative outcome. For example, introduction of Na results in increased width of band gap [20], while utilization of Fe causes an absolutely opposite consequence as absorption edge shifted to ~500 nm [19]. It is necessary to notice that both phenomena are concentration-dependent, i.e., the more foreign atoms are introduced into Ta_2O_5, the more obvious is the change in band gap width. In turn, reverse trend was observed in case of Cu doping with consideration that changes in other parameters also might influence it [21]. *Thirdly*, it is often the case that the presence of certain metals such as Gd [22] or Ti [23] might result in increased resistivity of Ta_2O_5 or degraded J-V characteristics which also could be interpreted as transportation of charge carriers results in less effect. Thus, one should become extremely aware when choosing proper elements to be combined with Ta_2O_5. It might be concluded that this phenomenon has certain correlation with the existence of Ta in Ta_2O_5 in the state of +5. In this regard, application of metal-doping strategy to strengthening natural n-type conductivity via increasing the concentration of electrons and their mobility can be challengeable given that only element with valence of 6 or higher are preferential to be used. Yet, it is not always the case as, in perspective, the presence of metals with other valances also can contribute to the enhancement of electrical characteristics.

10.5.3 Non-metal Doping

Non-metal anion doping, which is associated with using N, F, and S or other related elements, is one of the most popular ways to address most crucial drawbacks of Ta_2O_5 as their presence has very critical influence on the changes in electronic configuration. Thus, it governs the transportation of charge carriers and also determines wavelength range of light that can be utilized. Among them, nitrogen is considered to be the best and most popular choice since its 2p states and ionic radius are close to those of oxygen [24]. Several particularities can be defined with regard to application of this element. *Firstly*, its residence at substitutional site results in appearance of unoccupied energy level below conduction band. In turn, when nitrogen is presented in the form of interstitial defect, there is additional occupied level localized above valence band [25]. Both of them influence greatly on the narrowing of band gap and consequent appearance of visible light absorption. It becomes evident by changing the color of Ta_2O_5 from white to orange [24]. *Secondly*, theoretical calculation revealed that residing of nitrogen at former positions is thermodynamically a more favorable configuration [25]. *Thirdly*, its presence enables to switch the conductivity of Ta_2O_5 from n- to p-type [26] which contributes greatly to enhancing the transfer of electrons to the surface. *Fourthly*, nitrogen doping also results in positive shift of both valence and conduction bands that could be assigned to the appearance of generated dipole moments normal to the surface which enable to raise the electrostatic potential inside the Ta_2O_5 relative to the vacuum [25]. The change of band gap positioning with respect to vacuum level has very controversial influence on the photocatalytic activity of this materials. At one side, higher localization of conduction band minimum with respect to redox potentials of reduction reactions leads to improved kinetic. In other side, there might occur situation when maximum of valence band after shift is unable to match the redox potential for oxidation reaction, and thus to make it proceeded, the application of external bias is required [26].

As a final remark, it is necessary to notice that the presence of non-metal elements in Ta_2O_5 generally results in grave transformation of morphology as it leads to reduced crystallite size or smaller pore size which could be interpreted as increase in specific surface area [27]. Furthermore, it is often the case that these changes follow the concentration of introduced foreign atoms. Another important particularity of this approach is that large number of various intrinsic defects such as oxygen vacancies or tantalum interstitials might appear in crystal lattice of host materials in order to compensate broken thermodynamic equilibrium caused by doping [24]. In case of using metal elements, their existences are less evident given limitation of solubility.

10.5.4 Photocatalytic Application of Doped Ta_2O_5

It is out of question that the presence of foreign atoms in Ta_2O_5 in most cases can be correlated with highly improved performance toward processing of various photocatalytic reactions such as hydrogen production, CO_2 reduction, dye degradation, etc. given the enhanced absorption of visible light and more efficient charge separation characteristics which are especially evident in case of its transformation into p-type conductive material. Adjusting the parameters of synthesis or post-synthesis procedures can lead to more accurate tuning of resulted outcome as it fully depends on the concentration and distribution of doped elements. For example, An et al. [27] investigated introduction of fluorine into Ta_2O_5 shuttle-like structures composed of small nanoparticles via hydrothermal approach under different temperatures ranging from 160 to 220 °C and its application in water splitting reaction under illumination with xenon lamp. It was discovered that once the synthesis was proceeded at 180 °C, it resulted in highest performance among other samples which was attributed to the most optimal synergy between F atoms and accompanied oxygen vacancies along with reduced Ta^{4+} sites (Fig. 10.4). Yet it is important to notice that very

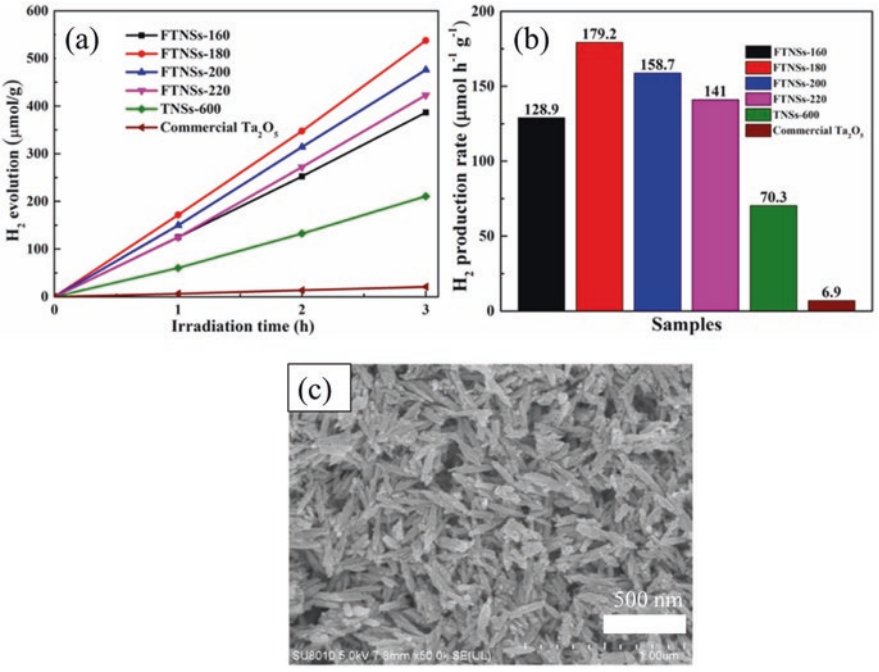

Fig. 10.4 (**a**) Photocatalytic hydrogen production and (**b**) the corresponding rate of different samples in methanol solution (20 vol%) under 300 W Xe lamp. FTNSs can be designated as fluorine-doped Ta_2O_5 nanoshuttles. Different numbers after FTNS show the temperature of hydrothermal treatment. (**c**) SEM image of FTNSs-180 °C which showed the best performance. (Adapted from Ref. [27] with permission from *Elsevier*. Copyright 2021)

accurate strategy should be applied to realize this scenario as doping with particulate elements such as nitrogen might result in inability of Ta_2O_5 to perform overall water splitting or complete CO_2 reduction procuress since the positions of valence band. In this case, it becomes too high for covering the redox potential of oxidation reaction. Thus, it only can be used as photocathode [26].

10.6 Case Study IV: Ta_3N_5

10.6.1 Brief Overview

Tantalum nitride is a very attractive and promising material to be applied in various photocatalytic reactions as in addition to its compositional simplicity, chemical inertness, and environmental compliance, it also possesses relatively narrow band gap equaled to ~2.1 eV. Thus, its activation and optimization can be easily realized by using visible light. Furthermore, the positions of conduction and valence bands with respect to redox potentials determine the ability for performing water splitting or CO_2 conversion without use of additional co-catalyst or external bias. However, it is often the case that the presence of various surface states, existence of unregistered and non-defined imperfections within crystal lattice, or availability of unexpected contaminations influences the alignment of band gap resulting in highly reduced capability to perform reduction reaction. In this regard, Ta_3N_5 is more applicable to serve as photoanode to perform more complex and thermodynamically highly demanding oxidation reaction. Yet, the efficiency of this material is still far from satisfactory, and full realization of its potentials as photocatalyst cannot be proceeded due to presence of several crucial drawbacks that greatly shade its advantages. One of them is referred to gradual appearance of self-limiting surface oxidation that existence is triggered by contact with water and activated by support of light irradiation. It leads to pinning of Fermi levels, and it dramatically suppresses the performance of Ta_3N_5. Furthermore, low carrier mobility results in greatly reduced charge separation and transport characteristics. To address them, it was reported that doping can be considered as an effective strategy.

10.6.2 Metal Doping

Due to nature of Ta_3N_5 that represents nitride compound, metal doping is considered to have the highest impact on changes of its electronic and geometrical structures. It has several very important particularities which need to be emphasized as to reach full and defined understanding of this processing. *Firstly*, in order to keep charge balance, it is often the case that introduced foreign atoms are accompanied by accumulation of oxygen in Ta_3N_5 which was evidenced, for example, during doping of

Mg or Zr [28, 29]. It resigns in nitrogen positions thus taking the role of substitutional defect (O_N). Given that corresponding energy level associated with it is located close to conduction band; thus O_N is determined to be shallow donor state that contributes greatly to enhancing the migration of electrons [30]. *Secondly*, influence on the optical properties is very individual for each particulate metal elements as it refers to existence of corresponding energy levels within band gap and consequent appearance of intrinsic defect. As an illustration, it was observed that the presence of Na, K, Rb, and Cs atoms might result in reducing the band gap for 0.2–0.3 eV and highly improved sensitivity toward irradiation with visible light [31], while introduction of Zr and Mg causes much less if any changes in UV-vis spectra [29, 30]. In turn, utilizing of W as dopant at concentration over 1% might leads to absolutely opposite outcome, e.g., worsening of absorption characteristics in both UV and visible spectrum [32]. *Thirdly*, structural properties before and after filling with foreign atoms also cannot be considered as to follow certain trends since it is fully depending on their nature. Particularly, the presence of Zr results in relatively unchanged morphology [29]. In turn, introduction of V into Ta_3N_5 nanoparticles hinders their agglomeration and clustering which was attributed to reduced sizes [33]. Consequently, the increase of specific surface area for nearly two times was observed. *Fourthly*, it is important to consider solubility of metal dopants in Ta_3N_5 as it is often the case that the only very limited concentrations can be utilized, and thus the enhancement of characteristics can be proceeded within defined range. Taking mentioned above V atoms as example, it was shown that their existence in Ta_3N_5 can produce changes only up to 2% wt [33].

10.6.3 Non-metal Doping

Non-metal doping of Ta_3N_5 is a very narrow and specialized subject as most of reports currently presented in literature about it are dedicated to the introduction and consequent manipulation over presence of oxygen atoms given their capability to bring very crucial changes in electronic and geometrical configurations. In fact, it was revealed that formation energy of oxygen substitution for nitrogen (O_N) on Ta_3N_5 is lower than that of even nitrogen vacancy [34] and, in fact, has negative value which confirms that appearance of these extrinsic defects in most cases cannot be avoided and thus should be designated as constantly available impurity. Due to existence of corresponding energy level located close to conduction band, O_N is determined to be a shallow donor, which presence usually results in enhancement of charge transportation characteristics and strengthening of intrinsic conductivity [30]. In addition, theoretical estimation predicted that O atoms have stronger ability to obtain electrons in comparison to N atoms [34]. Another benefits from introduction of oxygen into Ta_3N_5 is that it can increase the stability of this materials thus potentially leading to better resistance toward appearance of photocorrosion. Finally, the optical characteristics also might be enhanced as absorption edge can shift to longer wavelength [35]. Yet, it is possible only once the precise control over

concentration and distribution of oxygen are achieved as its excessive accumulation and consequent clustering should be avoided. Otherwise, appearance of oxygen in Ta_3N_5 might lead to various undesirable outcome including gradually increased band gap, critical suppression of photocatalytic efficiency as it was mentioned above. In far perspective, it also can cause the transformation of Ta_3N_5 into TaON or even Ta_2O_5.

10.6.4 Photocatalytic Application of Doped Ta_3N_5

As non-metal doping that is mostly represented in the form of oxygen incorporation has several critical limitations which means that its deliberate implementation cannot always guarantee positive outcome, it is very obvious that filling of Ta_3N_5 with certain and defined metal elements and consequent control over their presence such as adjusting concentration and distribution or interaction with intrinsic defects is a more evident and applicable strategy to enhance photocatalytic performance of this materials in order to effectively process highly demanding reactions that include hydrogen production, CO_2 reduction, and degradation of various harmful dyes. For example, Kado et al. [31] demonstrated that introduction of different alkaline metals such as Na, K, Rb, and Cs greatly increases the efficiency of Ta_3N_5 to initiate photoelectrochemical water splitting using simulated solar light (Fig. 10.5). This result

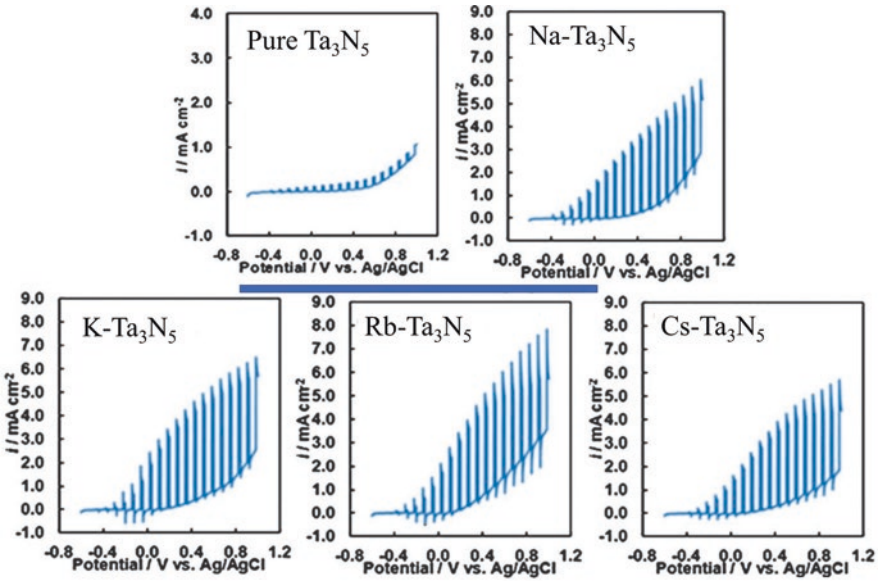

Fig. 10.5 Photoelectrochemical measurement of pure and doped Ta_3N_5 under simulated sunlight AM 1.5. (Adapted from Ref. [31] with permission from *The Royal Chemical Society*. Copyright 2012)

was explained by reduced charge transfer resistance as the conductivity was increased. It is interesting that best and lowest performances were discovered for Rb- and Cs-doped samples, respectively, which clearly demonstrated that the nature of used metal atoms is a highly important parameter. In turn, Nguyen et al. [33] investigated how the presence of V in Ta_3N_5 with different weight concentrations ranging from 1% to 3% influences the outcome of CO_2 photoconversion process activated by irradiation with visible light and estimated in terms of generated CH_4 and CO gases. It was revealed that while pristine samples showed low efficiency to perform this reaction, V doping can significantly enhance it. Following it, the highest production rate was achieved at 2% V-Ta_3N_5.

10.7 Case Study V: Fe_2O_3

10.7.1 Brief Overview

Extensive utilization of hematite (α-Fe_2O_3) in various photocatalytic reactions is mainly determined by its very attractive characteristics and features which include earth abundance, environmental friendliness, absolute non-toxicity, and chemical stability against photocorrosion in aqueous environment. Furthermore, this material possesses narrow band gap equaled to 2.0–2.2 eV which makes its absorption edge to cover very wide range of visible spectrum. Under sunlight irradiation, it allows to create large number of electron-hole pairs that can be used in activation and optimization of adsorbed molecules to proceed photocatalytic reaction thus potentially demonstrating very impressive results. For example, theoretical estimation regarding water splitting process revealed that energy conversion efficiencies should reach the value greater than 12%. However, currently, this value is hardly achievable as the presence of certain drawbacks limits the applicability of the following: *Firstly*, due to the position of band gap with respect to vacuum level, it is regarded to serve only as catalyst for oxygen evolution reaction (OER). Definitely, its outcome can be used further to successfully complete overall photoelectrochemical water splitting or CO_2 conversion processes; yet, to implement this strategy, the presence of additional compounds as a part of complex heterostructure that includes α-Fe_2O_3 or in the form of co-catalyst is required. It provides additional difficulties in using this material and its proper adaption for wide use. *Secondly*, realization of OER half-reaction in terms of absolute values is far from ideal due to presence of large overpotential that often requires the use of external bias. *Thirdly*, it is also necessary to consider low conductivity, short diffusion length of the photogenerated holes, and extremely high electron-hole recombination rates of α-Fe_2O_3 that degrade further the photocatalytic efficiency. In this regard, employment of doping strategy is determined as attractive approach to properly address most of these issues thus increasing the attractiveness and usability of α-Fe_2O_3.

10.7.2 Metal Doping

Introduction of metal atoms into α-Fe_2O_3 to advance its various characteristics including electronic configuration, change of conductivity, optical properties, etc. is considered to be a highly controversial and complex processing as it is greatly depended on the choice of utilized element, its characteristics, or method used to introduce it. Thus, under improper management, very negligible if any improvement can be obtained. Overall, the following particularities are identified. *Firstly*, it was revealed that the presence of transition metals such as V, Cr, Mn, Zn, Co, Ni, Cu, Nb, Mo, and Ti leads to very slight change of band gap ranging only ~0.1 eV [36]. In turn, the alignment of both conduction and valence bands with respect to vacuum level becomes upshifted. Relatively similar observation regarding absorption characteristics of α-Fe_2O_3 was observed during its doping with noble metals with only difference that both bands were shifted down slightly [37]. As for the electrical characteristics, the presence of metal atoms usually results in higher density of charge carrier and, thus, contributes to the improved electrical conductivity of α-Fe_2O_3 with only exceptions of Ni and Ti [36]. *Secondly*, as some metals such as Zn or Mn can have less availability of valence electrons compared with that of Fe^{3+}, they can not only take roles of p-dopants which is obvious but also enable to become the source of strengthening the n-type conductivity since it depends on their localization, i.e., whether outside or inside crystal lattice of α-Fe_2O_3. In the latter case, they are presented in the form of surface accumulation identified as chemical doping, while in former case, they are introduced as substitutional defect replacing Fe^{3+}, respectively [38]. In addition, they not only contribute to the increased concentration of relevant type of charge carriers but also can be used as trap centers selectively capturing electrons or holes and thus inhibiting the recombination via increasing their lifetimes. *Thirdly*, filling of α-Fe_2O_3 with metal atoms usually degrades its structural characteristics due to increased size of crystallites that is correlated with reduced specific surface area [37]. *Fourthly*, it is also necessary to consider the factor of solubility while discussing the doping effect since the introduced changes in various characteristics of α-Fe_2O_3 are greatly dependent on the concentration of utilized elements.

10.7.3 Non-metal Doping

Introduction of non-metal atoms can effectively address main drawbacks of α-Fe_2O_3 transforming it into highly efficient and practical photocatalyst with excellent characteristics. Surely, precise tuning is mostly dependent on the nature and concentration of utilized foreign atoms as it determines the level of expected advancement. In this context, several very crucial controversies could be observed in literature that might influence negatively on full and successful realization of this strategy. Overall, the following particularities are defined. *Firstly*, numerous experimental studies

demonstrated that optical characteristics α-Fe_2O_3 after combining with various anion elements including sulfur [39], nitrogen [40], carbon [41], or fluorine [42] are remained relatively the same or even degraded slightly which means that that the presence of these atoms cannot be used to improve absorption of light. In turn, theoretical estimations came to opposite conclusion. For example, it was predicted that S-doping enables to reduce width of band gap from original value of ~2.1 to ~1.45 eV or even lower as it depends on the dimension of α-Fe_2O_3, i.e., whether this material is available as bulk compound or thin film [43, 44]. Furthermore, it was revealed that concentration of S also plays a crucial role as the higher it is, the more evident it becomes the positive shift in absorption edge. *Secondly*, non-metal elements such as nitrogen and fluorine or sulfur can selectively introduce both acceptor- and donor-like additional level close to valence or conduction band, respectively, which causes the enhancement of charge separation and significantly reduces the recombination effect. Furthermore, in former case, it results in appearance of p-type conductivity [40, 42] and also influences band alignments which enable to approach the redox potentials of reduction reaction [45] thus making α-Fe_2O_3 potentially eligible to perform overall water splitting process and CO_2 conversion. For its part, S-doping preserves the position of conduction band [43] and only leads to upshifting of Fermi level [39]. *Thirdly*, the presence of non-metal elements in α-Fe_2O_3 has positive influence on its morphological features as the grain size becomes dramatically reduced which could be linked to increased specific surface area [41]. As for the 1-D structures, which is one of the most common forms of α-Fe_2O_3, their shapes and sizes after doping remained relatively the same or changed only slightly [39].

10.7.4 Photocatalytic Application of Doped α-Fe_2O_3

It is evident that doped α-Fe_2O_3 in most cases demonstrates improved performance toward processing of various photocatalytic and photoelectrochemical reactions such as hydrogen production, CO_2 reduction, dye degradation, etc. given more efficient transport characteristics of charge carriers and their reduced recombination rate which are often accompanied by transformation of its conductivity into p-type. Thus, higher incident photon-to-current efficiency (IPCE) can be observed even though the absorption spectra is remained the same. Due to positions of its conduction band, α-Fe_2O_3 is mostly applied as photoanode as in this role it demonstrates the best outcome. Overall, comparing metal and non-metal doping, it might become evident that under proper control over the concentration of introduced foreign atoms, the former strategy often can lead to better enhancement of efficiency using relative units or in comparison with certain standard. For instance, Zhang et al. [39] revealed that S-doped α-Fe_2O_3 nanorods array grown on a Ti plate shows a substantially increased photocurrent density of 1.42 mA cm^{-2} at 1.23 V vs RHE in 1.0 M NaOH under simulated sunlight irradiation which was 2.45 times higher than that of pristine α-Fe_2O_3 counterpart which performance reached only 0.58 mA cm^{-2}

(Fig. 10.6a). It also showed great stability (Fig. 10.6b). In addition, IPCE efficiency in the wavelength range of 350–600 nm was increased for nearly 3.5 times (Fig. 10.6c). In turn, Jang et al. [46] investigated *via* scanning electrochemical microscopy under applied potential of 0.2 V vs. Ag/AgCl how doping and co-doping with different types of metals influences the efficiency of α-Fe_2O_3. It was discovered that while α-Fe_2O_3 showed the photocurrent of only 8 ± 2 nA using irradiation with visible light, its doping with 6% Be-4% Sn resulted in very dramatical enhancement of this value as it reaches 130 ± 15 nA which was interpreted as ~15 times improvement.

10.8 Case Study VI: MoS_2 and WS_2

10.8.1 Brief Overview

Molybdenum and tungsten disulfates that are available in the form of mono- or several-layered structure are considered as attractive materials that could be applied in photocatalytic processing given their narrow band gap of ~1.9 eV and 2.0 eV,

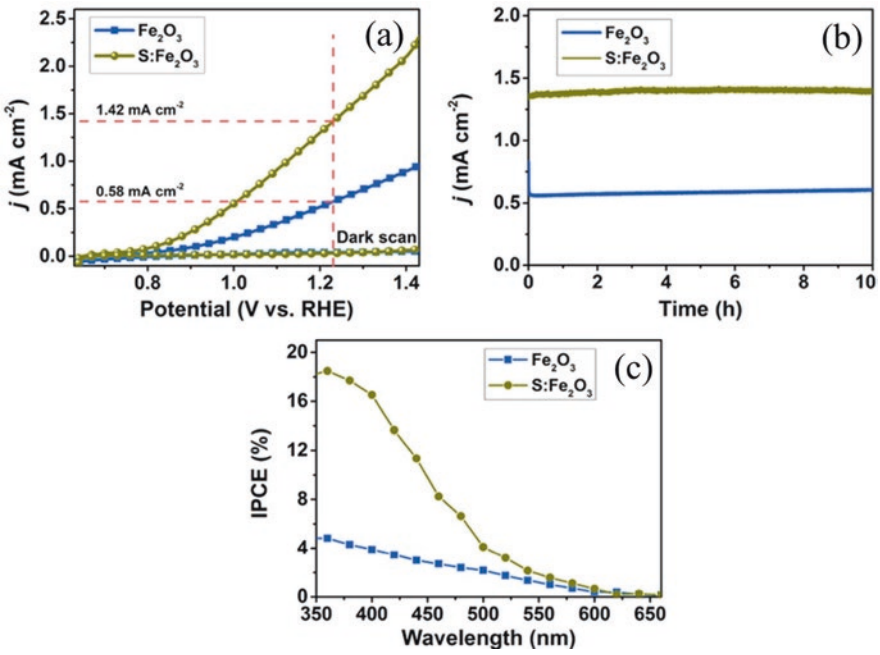

Fig. 10.6 (**a**) Linear sweep voltammetry curves of α-Fe_2O_3 and S:α-Fe_2O_3 photoanodes under AM 1.5G illumination and in the dark in 1.0 M NaOH with a scan rate of 5 mV s^{-1}. (**b**) Time-dependent current density curves measured under illumination and (**c**) IPCE at 1.23 V vs RHE. (Adapted from Ref. [39] with permission from *American Chemical Society*. Copyright 2017)

respectively, that allow to absorb visible light, suitable positions of valence and conduction bands with respect to redox potentials for oxidation and reduction reactions, and other related characteristics. However, these advantages are shadowed by extremely high recombination rate of charge carriers, low mechanical stability as their layers can be easily broken up, very minor resistance to keep electronic and geometrical configurations within the required range under unfavorable conditions, and low capability to capture the absorbed photons. It restrains full and complete realization of MoS_2 and WS_2 and degrade perspectives of their application. In this regard, employment of doping strategy can be considered as an efficient tool to properly address these drawbacks and also to achieve precise control over electrical, optical, and structural properties of these materials. Contrary to conventional semiconductors with 3-D structures that were described above, introduction of impurity atoms into these materials usually proceeded *via* the following mechanism: (i) residing at substitutional position thus replacing S or Mo/W and (ii) localization between layers which defines introduced foreign atoms as intercalation defects. Given the length limitation of ionic bonds, it was determined that non-metal dopants in MoS_2 and WS_2 usually prefer to occupy anion sites at the outer layers, while for metal dopants, the favorable position has clear dependency on their atomic sizes [47]. Elements that have relatively small radii, such as Li, Mg, and Ca, prefer to accommodate at intercalation sites due to attractive dispersion interactions, whereas for heavy dopants with larger radii, the substitutional positioning is thermodynamically more favorable as it reduces probability to create exchange repulsion between them and W or S atoms [48]. Both types of defects are discussed below in more details.

10.8.2 Metal Doping

Substitutional Doping In order to achieve highly effective substitutional doping that enables to improve the characteristics and features of MoS_2 and WS_2, transition metals are considered to be one of the most optimal choices as their sizes are very close to that of W or S which minimize the distortion of modified crystal lattice. Furthermore, their presence also allows to achieve precise control over the strength and type of conductivity. For example, Yoshimura et al. [49] reported that as Nb and Ta possess one less valence electron than Mo does, thus they are determined to be p-type dopants in MoS_2. In turn, Re and Tc take the roles of contributors to n-type conductivity, having one more valence electron than Mo. It is necessary to notice that the presence of the encapsulating chalcogenide layers effectively block the incorporation of extrinsic metal element in the post-growth treatments. Hence, it is of general concern that this type of doping can be achieved only during the fabrication process of the MoS_2 or WS_2, e.g., by adjusting the composition of precursors or via tuning the conditions of the growth environment. In this case, however, it is especially important to be very careful with concentration of introduced atoms as its

too high value may result in unexpected phase transformation [47] or the increase of band gap which eventually reduces the number of absorbed photons [49].

Intercalation Doping It is considered to be a great approach to change the electronic structure of the host materials and various interest phenomenon including unconventional superconductivity, and charge density waves were discovered via its application. During this process, when the donor (acceptor)-type intercalants are inserted between the layers of the host 2-D material, they donate (withdraw) electrons to (from) the adjacent host layers, causing their Fermi level to shift and properties to change [50]. It results in great enhancement of electrical characteristics and improved charge transport properties. However, this type of doping is rarely applied to assist in proceeding of photocatalytic reactions given that it also leads to semiconductor-to-metal translons often ascribed by consequent appearance of disordered yet highly stabilized metallic 1T phase which has evident absence of band gap and thus is absolutely transparent to light.

10.8.3 Non-metal Doping

As S atoms in MoS_2 and WS_2 are generally exposed to the outer space, non-metal doping provides much flexibility in its successful realization as it can be proceeded via not only synthesis but also post-synthesis approaches such as exposure to plasma and thermal treatment in desired atmosphere. The resulted composition usually shows enhanced electrical characteristics in terms of their concentration and mobility [47], thus potentially enabling to cause the reduced recombination rate of charge carriers. Furthermore, similar to mentioned above metal doping, the type of conductivity can also be easily adjusted. As for the optical characteristics of modified MoS_2 and WS_2, the presence of non-metal elements has very controversial influence on its change due to existence of positive and negative impacts. On one hand, incorporated foreign atoms increase the capability of these materials to capture higher number of photons and also enable to slightly shift the absorption edge toward longer wavelength [51] (Fig. 10.7a, b). On the other hand, under incorrect concentration or improper management over undesirable accumulations, their presence can potentially lead to very crucial narrowing of band gap width due to appearance of additional energy levels within it which are defined by shifting down and up the positions of conduction and valance band, respectively, with regard to vacuum level [52]. Thus, in perspective, they could no longer match the redox potentials of oxidation and reduction reactions as well as fail to satisfy the minimum value of energy required to proceed water splitting or CO_2 reduction. Non-metal doping also influences structural properties of MoS_2 and WS_2 resulting in their advancement due to development of more obvious and visible morphological features associated with appearance of exposed edges, increased mesoporosity, etc. For example, it was reported that specific surface area of the MoS_2 nanosheets before and after filling with N atoms was estimated to be 71.7 $m^2\ g^{-1}$ and 22.9 $m^2\ g^{-1}$ with pore volumes of

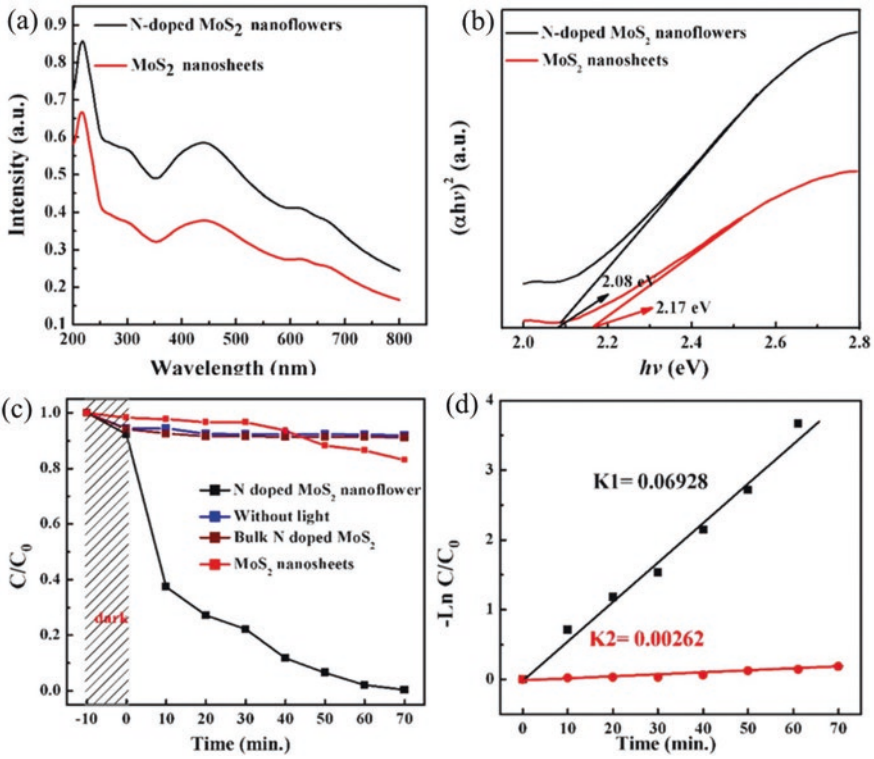

Fig. 10.7 (**a**) UV-vis DRS and (**b**) estimated band-gap energy of N-doped MoS_2 nanoflowers and MoS_2 nanosheets. (**c**) Photocatalytic degradation of RhB by different photocatalysts under visible light irradiation. (**d**) Plot of $\ln(C_0/C)$ with irradiation time for N-doped MoS_2 nanoflowers and MoS_2 nanosheets. (Adapted from Ref. [51]. Copyright 2016, *IOP Publishing*. Available under Creative Commons Attribution 3.0 License, https://creativecommons.org/licenses/by/3.0/)

0.225 and 0.101 $cm^3\ g^{-1}$, respectively [53]. Yet, the best outcome depends on reaching the optimal concentration of introduced atoms.

10.8.4 Photocatalytic Application of Doped MoS_2 and WS_2

Doping of MoS_2 and WS_2 with certain and very specific metal and non-metal elements using proper management and control can provide great enhancement of their optical, electrical, and structural characteristics that is proceeded *via* increased absorption capability, enhanced stabilization of internal composition, and more advanced electrical and electronic characteristics. Given small band of these materials which allow to consume photons with energies of visible lights, it greatly contributes toward attractiveness of their applicability in various photocatalytic reactions and allows to reach high level of performance. For example, Liu et al. [51]

reported that N-doped MoS_2 nanoflower could completely degrade 50 ml of 30 mg l^{-1} RhB in 70 min with excellent recycling and structural stability. Thus, it showed a reaction rate constant (k) as high as 0.06928 min^{-1} which was 26.4 and ~7 times higher than that of bare MoS_2 nanosheets (k = 0.00262 min^{-1}) and commercial TiO_2 (k = 0.01 min^{-1}) (Fig. 10.7c, d), respectively. In turn, Li et al. [54] investigated how the substitution of Mo with Ag in MoS_2 influences its efficiency during water splitting process using irradiation with visible light. It was revealed that pristine phase MoS_2 exhibited relatively weak photocatalytic activity, and the hydrogen production rate was 1708 μmol h^{-1} g^{-1}, while Ag-doped MoS_2 nanosheets under similar conditions demonstrated the efficiency of 2695 μmol h^{-1} g^{-1}. In addition, it also showed excellent stability during cycling testing. Similar trend with only certain limitation as well might be applied to modified WS_2. Yet, additional studies are required to confirm it.

10.9 Final Remarks on Extrinsic Deficiency

Application of extrinsic deficiency in terms of doping with metal and non-mental elements or compounds is considered to be a highly attractive and perspective approach to improve the most important characteristics of target materials in order to advance its efficiency and stability toward activation, optimization, and successful processing of specific photocatalytic and photoelectrochemical reactions such as dye degradation, water splitting, CO_2 conversion, etc. This strategy has several important advantages which define its wide utilization and applicability such as dramatic influence on geometrical and electronic configurations of target material that allows to reach precise and accurate tuning of the required and concrete features. To achieve it, wide spectrum of various parameters associated with introduced atoms can be adjusted and modified, including its nature, concentration, distribution, the choice of methods that can be adapted to proceed them, possible co-doping effect, and formation of complexes or chemically connected chains through combining with already existed intrinsic defects such as vacancies and interstitials.

However, to fully realize this strategy, it is extremely important to address the main disadvantages which influence very negatively on its continuous development and consequent employment with regard to photocatalytic application. For example, the main problem of metal doping is that each utilized element has very restricted solubility in target material beyond which their presence would often become destructive due to appearance of undesirable and unexpected phases. Definitely, this effect is less dramatic in case of using non-metal atoms. Yet, it is often the case that they suffer from low stability and thus could be easily evacuated leaving behind empty sites. Another disadvantage of doping is that the consumption of additional chemicals is always required. Thus, adoption for industrial usage might need additional efforts and spending. Finally, given the number of reports available in literature regarding it, one can come to conclusion about existence of huge contradictions toward acquiring knowledge regarding concrete and defined

influence of certain elements or their concentrations on improving characteristics of target materials. Partially, it could be explained by particularities and specifications of each investigated system especially in terms of conditions at which it was created and consequently analyzed. Yet, it is obvious that higher consistency is required to investigate doping strategy as currently it is not clear in which direction the future progress should be proceeded. Thus, to reach maximum profits from application of extrinsic deficiency within the shortest period of time, deeper understanding and more extensive investigations are in need.

References

1. H. Tong, S. Ouyang, Y. Bi, N. Umezawa, M. Oshikiri, J. Ye, Nano-photocatalytic materials: Possibilities and challenges. Adv. Mater. **24**, 229–251 (2012). https://doi.org/10.1002/adma.201102752
2. D. Banerjee, S.K. Gupta, N. Patra, S.W. Raja, N. Pathak, D. Bhattacharyya, P.K. Pujari, S.V. Thakare, S.N. Jha, Unraveling doping induced anatase–rutile phase transition in TiO_2 using electron, X-ray and gamma-ray as spectroscopic probes. Phys. Chem. Chem. Phys. **20**, 28699–28711 (2018). https://doi.org/10.1039/C8CP04310H
3. C. Di Valentin, G. Pacchioni, Trends in non-metal doping of anatase TiO_2: B, C, N and F. Catal. Today **206**, 12–18 (2013). https://doi.org/10.1016/j.cattod.2011.11.030
4. X. Pan, M.-Q. Yang, X. Fu, N. Zhang, Y.-J. Xu, Defective TiO_2 with oxygen vacancies: Synthesis, properties and photocatalytic applications. Nanoscale **5**, 3601–3614 (2013). https://doi.org/10.1039/C3NR00476G
5. L. Zhou, M. Cai, X. Zhang, N. Cui, G. Chen, G. Zou, In-situ nitrogen-doped black TiO_2 with enhanced visible-light-driven photocatalytic inactivation of Microcystis aeruginosa cells: Synthesization, performance and mechanism. Appl. Catal. B Environ. **272**, 119019 (2020). https://doi.org/10.1016/j.apcatb.2020.119019
6. L. Gao, Y. Li, J. Ren, S. Wang, R. Wang, G. Fu, Y. Hu, Passivation of defect states in anatase TiO_2 hollow spheres with Mg doping: Realizing efficient photocatalytic overall water splitting. Appl. Catal. B Environ. **202**, 127–133 (2017). https://doi.org/10.1016/j.apcatb.2016.09.018
7. M.S. Akple, J. Low, Z. Qin, S. Wageh, A.A. Al-Ghamdi, J. Yu, S. Liu, Nitrogen-doped TiO_2 microsheets with enhanced visible light photocatalytic activity for CO_2 reduction. Chinese J. Catal. **36**, 2127–2134 (2015). https://doi.org/10.1016/S1872-2067(15)60989-5
8. H. Zhuang, Y. Zhang, Z. Chu, J. Long, X. An, H. Zhang, H. Lin, Z. Zhang, X. Wang, Synergy of metal and nonmetal dopants for visible-light photocatalysis: A case-study of Sn and N co-doped TiO_2. Phys. Chem. Chem. Phys. **18**, 9636–9644 (2016). https://doi.org/10.1039/C6CP00580B
9. M. Samadi, M. Zirak, A. Naseri, E. Khorashadizade, A.Z. Moshfegh, Recent progress on doped ZnO nanostructures for visible-light photocatalysis. Thin Solid Films **605**, 2–19 (2016). https://doi.org/10.1016/j.tsf.2015.12.064
10. K.C. Barick, S. Singh, M. Aslam, D. Bahadur, Porosity and photocatalytic studies of transition metal doped ZnO nanoclusters. Micropor. Mesopor. Mater. **134**, 195–202 (2010). https://doi.org/10.1016/j.micromeso.2010.05.026
11. S. Anandan, A. Vinu, T. Mori, N. Gokulakrishnan, P. Srinivasu, V. Murugesan, K. Ariga, Photocatalytic degradation of 2,4,6-trichlorophenol using lanthanum doped ZnO in aqueous suspension. Catal. Commun. **8**, 1377–1382 (2007). https://doi.org/10.1016/j.catcom.2006.12.001
12. Y. Zhao, K. Kita, K. Kyuno, A. Toriumi, Band gap enhancement and electrical properties of La_2O_3 films doped with Y_2O_3 as high-*k* gate insulators. Appl. Phys. Lett. **94**, 042901 (2009). https://doi.org/10.1063/1.3075954

13. K.C. Cadien, L. Nolan, Chapter 10 – Chemical mechanical polishing method and practice, in *Handbook of Thin Film Deposition*, ed. by K. Seshan, D. Schepis, Fourth edn., (William Andrew Publishing, 2018), pp. 317–357. https://doi.org/10.1016/B978-0-12-812311-9.00010-4
14. A. Narjis, H. El Aakib, M. Boukendil, M. El Hasnaoui, L. Nkhaili, A. Aberkouks, A. Outzourhit, Controlling the structural properties of pure and aluminum doped zinc oxide nanoparticles by annealing. J. King Saud. Univ. Sci. **32**, 1074–1080 (2020). https://doi.org/10.1016/j.jksus.2019.10.004
15. S.T. Tan, X.W. Sun, Z.G. Yu, P. Wu, G.Q. Lo, D.L. Kwong, p-type conduction in unintentional carbon-doped ZnO thin films. Appl. Phys. Lett. **91**, 072101 (2007). https://doi.org/10.1063/1.2768917
16. V. Kumari, A. Mittal, J. Jindal, S. Yadav, N. Kumar, S-, N- and C-doped ZnO as semiconductor photocatalysts: A review. Front. Mater. Sci. **13**, 1–22 (2019). https://doi.org/10.1007/s11706-019-0453-4
17. R. Kumari, A. Sahai, N. Goswami, Effect of nitrogen doping on structural and optical properties of ZnO nanoparticles. Prog. Nat. Sci. Mater. **25**, 300–309 (2015). https://doi.org/10.1016/j.pnsc.2015.08.003
18. R. Kobayashi, T. Kishi, Y. Katayanagi, T. Yano, N. Matsushita, Fabrication of nitrogen-doped ZnO nanorod arrays by hydrothermal synthesis and ambient annealing. RSC Adv. **8**, 23599–23605 (2018). https://doi.org/10.1039/C8RA04168G
19. D. Jing, L. Guo, Hydrogen production over Fe-doped tantalum oxide from an aqueous methanol solution under the light irradiation. J. Phys. Chem. Solids **68**, 2363–2369 (2007). https://doi.org/10.1016/j.jpcs.2007.07.045
20. T. Grewe, H. Tüysüz, Alkali metals incorporated ordered mesoporous tantalum oxide with enhanced photocatalytic activity for water splitting. J. Mater. Chem. A **4**, 3007–3017 (2016). https://doi.org/10.1039/C5TA07086D
21. M. Danish, A. Pandey, M.O. Ansari, A. Jilani, Influence of ammonolysis, Cu-incorporation and film thickness on structure, optical and photocatalytic properties of Ta_2O_5 thin films fabricated via sol-gel: A comparative study. J. Mater. Sci. Mater. Electron. **28**, 6812–6822 (2017). https://doi.org/10.1007/s10854-017-6379-7
22. K.X. Shi, H.Y. Xu, Z.Q. Wang, X.N. Zhao, W.Z. Liu, J.G. Ma, Y.C. Liu, Improved performance of Ta_2O_{5-x} resistive switching memory by Gd-doping: Ultralow power operation, good data retention, and multilevel storage. Appl. Phys. Lett. **111**, 223505 (2017). https://doi.org/10.1063/1.5002571
23. E. Atanassova, D. Spassov, A. Paskaleva, M. Georgieva, J. Koprinarova, Electrical characteristics of Ti-doped Ta_2O_5 stacked capacitors. Thin Solid Films **516**, 8684–8692 (2008). https://doi.org/10.1016/j.tsf.2008.05.003
24. W.-S. Liu, S.-H. Huang, C.-F. Liu, C.-W. Hu, T.-Y. Chen, T.-P. Perng, Nitrogen doping in Ta_2O_5 and its implication for photocatalytic H_2 production. Appl. Surf. Sci. **459**, 477–482 (2018). https://doi.org/10.1016/j.apsusc.2018.07.185
25. R. Jinnouchi, A.V. Akimov, S. Shirai, R. Asahi, O.V. Prezhdo, Upward shift in conduction band of Ta_2O_5 due to surface dipoles induced by N-doping. J. Phys. Chem. C **119**, 26925–26936 (2015). https://doi.org/10.1021/acs.jpcc.5b06932
26. T.M. Suzuki, S. Saeki, K. Sekizawa, K. Kitazumi, N. Takahashi, T. Morikawa, Photoelectrochemical hydrogen production by water splitting over dual-functionally modified oxide: p-type N-doped Ta_2O_5 photocathode active under visible light irradiation. Appl. Catal. B Environ. **202**, 597–604 (2017). https://doi.org/10.1016/j.apcatb.2016.09.066
27. L. An, X. Han, Y. Li, H. Wang, C. Hou, Q. Zhang, One step synthesis of self-doped F-Ta_2O_5 nanoshuttles photocatalyst and enhanced photocatalytic hydrogen evolution. Int. J. Hydrog. Energy **46**, 3996–4006 (2021). https://doi.org/10.1016/j.ijhydene.2020.10.250
28. Y. Xie, Y. Wang, Z. Chen, X. Xu, Role of oxygen defects on the photocatalytic properties of Mg-doped mesoporous Ta_3N_5. ChemSusChem **9**, 1403–1412 (2016). https://doi.org/10.1002/cssc.201600193

29. Y. Wang, D. Zhu, X. Xu, Zr-doped mesoporous Ta_3N_5 microspheres for efficient photocatalytic water oxidation. ACS Appl. Mater. Interfaces **8**, 35407–35418 (2016). https://doi.org/10.1021/acsami.6b14230
30. L. Pei, Z. Xu, Z. Shi, H. Zhu, S. Yan, Z. Zou, Mg-doped Ta_3N_5 nanorods coated with a conformal CoOOH layer for water oxidation: Bulk and surface dual modification of photoanodes. J. Mater. Chem. A **5**, 20439–20447 (2017). https://doi.org/10.1039/C7TA06227C
31. Y. Kado, C.-Y. Lee, K. Lee, J. Müller, M. Moll, E. Spiecker, P. Schmuki, Enhanced water splitting activity of M-doped Ta_3N_5 (M = Na, K, Rb, Cs). Chem. Commun. **48**, 8685–8687 (2012). https://doi.org/10.1039/C2CC33822J
32. S. Grigorescu, B. Bärhausen, L. Wang, A. Mazare, J.E. Yoo, R. Hahn, P. Schmuki, Tungsten doping of Ta_3N_5-nanotubes for band gap narrowing and enhanced photoelectrochemical water splitting efficiency. Electrochem. Commun. **51**, 85–88 (2015). https://doi.org/10.1016/j.elecom.2014.12.019
33. T.D.C. Nguyen, T.P.L.C. Nguyen, H.T.T. Mai, V.-D. Dao, M.P. Nguyen, V.N. Nguyen, Novel photocatalytic conversion of CO_2 by vanadium-doped tantalum nitride for valuable solar fuel production. J. Catal. **352**, 67–74 (2017). https://doi.org/10.1016/j.jcat.2017.04.020
34. L. Cui, M. Wang, Y.X. Wang, Nitrogen vacancies and oxygen substitution of Ta_3N_5: First-principles investigation. J. Phys. Soc. Jpn. **83**, 114707 (2014). https://doi.org/10.7566/JPSJ.83.114707
35. J. Wang, T. Fang, L. Zhang, J. Feng, Z. Li, Z. Zou, Effects of oxygen doping on optical band gap and band edge positions of Ta_3N_5 photocatalyst: A GGA+U calculation. J. Catal. **309**, 291–299 (2014). https://doi.org/10.1016/j.jcat.2013.10.014
36. Y. Yin, X. Zhang, C. Sun, Transition-metal-doped Fe_2O_3 nanoparticles for oxygen evolution reaction. Prog. Nat. Sci. Mater. **28**, 430–436 (2018). https://doi.org/10.1016/j.pnsc.2018.07.005
37. A. Bak, S.K. Choi, H. Park, Photoelectrochemical performances of hematite (α-Fe2O3) films doped with various metals. Bull. Kor. Chem. Soc. **36**, 1487–1494 (2015). https://doi.org/10.1002/bkcs.10290
38. Z. Fan, X. Wen, S. Yang, J.G. Lu, Controlled p- and n-type doping of Fe_2O_3 nanobelt field effect transistors. Appl. Phys. Lett. **87**, 013113 (2005). https://doi.org/10.1063/1.1977203
39. R. Zhang, Y. Fang, T. Chen, F. Qu, Z. Liu, G. Du, A.M. Asiri, T. Gao, X. Sun, Enhanced photoelectrochemical water oxidation performance of Fe_2O_3 nanorods array by S doping. ACS Sustain. Chem. Eng. **5**, 7502–7506 (2017). https://doi.org/10.1021/acssuschemeng.7b01799
40. T. Morikawa, K. Kitazumi, N. Takahashi, T. Arai, T. Kajino, p-type conduction induced by N-doping in α-Fe_2O_3. Appl. Phys. Lett. **98**, 242108 (2011). https://doi.org/10.1063/1.3599852
41. M.-C. Huang, W.-S. Chang, J.-C. Lin, Y.-H. Chang, C.-C. Wu, Magnetron sputtering process of carbon-doped α-Fe_2O_3 thin films for photoelectrochemical water splitting. J. Alloys Compd. **636**, 176–182 (2015). https://doi.org/10.1016/j.jallcom.2015.02.166
42. D. Barreca, G. Carraro, A. Gasparotto, C. Maccato, C. Sada, A.P. Singh, S. Mathur, A. Mettenbörger, E. Bontempi, L.E. Depero, Columnar Fe_2O_3 arrays *via* plasma-enhanced growth: Interplay of fluorine substitution and photoelectrochemical properties. Int. J. Hydrog. Energy **38**, 14189–14199 (2013). https://doi.org/10.1016/j.ijhydene.2013.08.119
43. C. Xia, Y. Jia, M. Tao, Q. Zhang, Tuning the band gap of hematite α-Fe_2O_3 by sulfur doping. Phys. Lett. A **377**, 1943–1947 (2013). https://doi.org/10.1016/j.physleta.2013.05.026
44. J. An, P. Wanaguru, C. Xia, M. Tao, Q. Zhang, First-principles study of sulfur atom doping and adsorption on α–Fe_2O_3 (0001) film. Phys. Lett. A **380**, 3149–3154 (2016). https://doi.org/10.1016/j.physleta.2016.07.042
45. M. Mishra, D.-M. Chun, α-Fe_2O_3 as a photocatalytic material: A review. Appl. Catal. A Gen. **498**, 126–141 (2015). https://doi.org/10.1016/j.apcata.2015.03.023
46. J.S. Jang, J. Lee, H. Ye, F.-R.F. Fan, A.J. Bard, Rapid screening of effective dopants for Fe_2O_3 photocatalysts with scanning electrochemical microscopy and investigation of their photoelectrochemical properties. J. Phys. Chem. C **113**, 6719–6724 (2009). https://doi.org/10.1021/jp8109429

47. P. Luo, F. Zhuge, Q. Zhang, Y. Chen, L. Lv, Y. Huang, H. Li, T. Zhai, Doping engineering and functionalization of two-dimensional metal chalcogenides. Nanoscale Horiz. **4**, 26–51 (2018). https://doi.org/10.1039/C8NH00150B
48. J. Fan, J. Yang, A. Pham, S. Li, Origins of possible synergistic effects in the interactions between metal atoms and MoS_2/graphene heterostructures for battery applications. Phys. Chem. Chem. Phys. **20**, 18671–18677 (2018). https://doi.org/10.1039/C8CP02740D
49. A. Yoshimura, N. Koratkar, V. Meunier, Substitutional transition metal doping in MoS_2: A first-principles study. Nano Express **1**, 010008 (2020). https://doi.org/10.1088/2632-959X/ab7cb3
50. M. Rajapakse, B. Karki, U.O. Abu, S. Pishgar, M.R.K. Musa, S.M.S. Riyadh, M. Yu, G. Sumanasekera, J.B. Jasinski, Intercalation as a versatile tool for fabrication, property tuning, and phase transitions in 2D materials. Npj 2D Mater. Appl. **5**, 1–21 (2021). https://doi.org/10.1038/s41699-021-00211-6
51. P. Liu, Y. Liu, W. Ye, J. Ma, D. Gao, Flower-like N-doped MoS_2 for photocatalytic degradation of RhB by visible light irradiation. Nanotechnology **27**, 225403 (2016). https://doi.org/10.1088/0957-4484/27/22/225403
52. X. Wen, S. Yu, Y. Wang, Y. Liu, H. Wang, J. Zhao, Doping MoS_2 monolayer with nonmetal atoms to tune its electronic and magnetic properties, and chemical activity: A computational study. New J. Chem. **43**, 5766–5772 (2019). https://doi.org/10.1039/C9NJ00466A
53. R. Li, L. Yang, T. Xiong, Y. Wu, L. Cao, D. Yuan, W. Zhou, Nitrogen doped MoS_2 nanosheets synthesized via a low-temperature process as electrocatalysts with enhanced activity for hydrogen evolution reaction. J. Power Sources **356**, 133–139 (2017). https://doi.org/10.1016/j.jpowsour.2017.04.060
54. M. Li, Z. Cui, E. Li, Silver-modified MoS_2 nanosheets as a high-efficiency visible-light photocatalyst for water splitting. Ceram. Int. **45**, 14449–14456 (2019). https://doi.org/10.1016/j.ceramint.2019.04.166

Chapter 11
Comparison of Intrinsic and Extrinsic Deficiencies

11.1 Introduction

Semiconductor materials that currently are used for photocatalytic and photoelectrochemical processing cannot be considered as the most optical choice since each of them has numerous drawbacks and disadvantages associated with non-ideality of their certain features and characteristics such as inability to absorb visible light and consequently low sensitivity toward capturing photons with accessible energies, unfavorable alignment of band gap, high recombination rate and inefficient transportation characteristics of charge carriers, low thermal and chemical stabilities, unfavorable specifications of electronic or geometrical configurations, etc. that prevent them from showing best outcome. As a result, their applicability in most cases is highly limited by acquiring only low productivity or stability and thus cannot be adapted for industrial needs. In this regard, it was suggested that introduction of intrinsic or extrinsic defects that is usually proceeded though their existence as separate and individual compounds or by developing various assemblance with each other via elaborating chemically connected complexes and formations can be used to advance these materials in order to make them approach the desired level of expectation toward demonstrating required efficiencies during prolong exploitation. At a first glance, the functionality and reliability of these two strategies basically have a lot of similarity to achieving this goal. For example, wide band gap TiO_2 filled with oxygen vacancies or combined with nitrogen dopants enable to extend its absorption edge to longer wavelength thus allowing to create more photo-induced electrons and holes. In turn, their presence also can be used to advance the electrical conductivity. Thus, it is expected that enhancement level of photocatalytic performances under irradiation with sunlight could be achieved. In another glance, however, this outcome is considered as been only the tip of iceberg since practical usage of both strategies have certain difficulties and complications toward their successful and profitable realization given the presence of associated individual negative and

V. Gurylev, *Nanostructured Photocatalyst via Defect Engineering*,
https://doi.org/10.1007/978-3-030-81911-8_11

positive impacts that have connections with specific particularities of their implementation. It not only on influences greatly the progress and grade of the overall improvements that is referred to the extension of distinct property but also determines the suitability of each strategy to be readily adapted and used appropriately in concrete situation and within certain limit of resources as to achieve the best outcome.

Returning back to mentioned TiO_2, introduction of nitrogen dopants usually allows to decrease the band gap only slightly from 3.2 to ~2.5 eV [1], while development of oxygen non-stoichiometry could lead to its more dramatic narrowing that reaches down to ~1.3 eV [2] or even lower as it depends on several factors. The main reason of this contrast is laid in the sharp difference between natures of both intrinsic and extrinsic deficiencies. The former one is created as a result of deviation and transformation of thermodynamically balanced and relatively perfect crystal structure due to certain input of external energy into system, while generation of the latter one is fully referred to the introduction of foreign atoms into host material and their consequent localization within regular periodic arrangement of its lattice at substitutional or interstitial positions. Thus, it is evident that both types of defects cannot be considered as equal and fully identical in terms of their formation proceeding and consequent impact on target material. Accordingly, this chapter is going to define their differences and similarity as to understand what realistic advantages each strategy can provide with respect to each other.

11.2 Comparison in Terms of Synthesis Approaches and Post-synthesis Treatment

Introduction of intrinsic and extrinsic deficiencies and consequent manipulation over their various characteristics generally follow very similar experimental procedure as it can be realized via analogous synthesis or post-synthesis protocols. However, defined choice over concrete method and its associated parameters are dependent on certain factors and requirements toward finalizing the obtained composition or structure such as desired level of created non-ideality, whether the introduced changes are limited only by surface layer or extended deeply in bulk, lifetimes of defects and possible interaction between them, etc. Thus, in order to provide more precise tuning and accuracy, it is important to determine at which conditions the formation of each type of defects can be proceeded individually with minimum interferences and influences toward and from each other. In this regard, the discussion below is organized in such a way that several most utilized and applicable approaches are examined independently as to determine their specific particularities, eligibility, and adaptability for reaching the desired goal. It is necessary to notice that for simplicity, accessibility of intrinsic defects is limited by reviewing only vacancies.

11.2.1 Synthesis Approaches

(a) *Chemical methods*. Employment of chemical methods that include sol-gel, hydrothermal/solvothermal procedures, spray pyrolysis, etc. can be used to obtain both types of deficiencies with very accurate specifications of their consequent existences. To be more precise, doping is realized via inclusion of additional highly specific chemical or compound into reactive solution following the adjustment of its desirable concentration or weight/atomic percent as to make the residual of proceeded chemical interaction become localized in crystal lattice of target material within defined configuration, positioning, and ratio. In turn, to form vacancies, the presence of external elements during synthesis usually assists in incomplete filling of atomic positions within periodical arrangements that lead to breakage of localized thermodynamic equilibrium and further developing of defined perturbations within crystal lattice. Depending on the type of used chemicals, it is possible to make metal or non-metal doping as well as to create anion- or cation-like vacancies. For example, it was reported that fabrication of TiO_2 filled with fluorine or iron atoms via spray pyrolysis could be easily achieved by using H_2TiF_6 [3] and $Zr(C_5H_7O_2)_4$ [4], respectively, as supplements. It is followed by treatment at required temperature and atmosphere in order to initiate thermal decomposition. In turn, the presence [5] or absence [6] of propanetriol during solvothermal synthesis of ZnO along with adaptation of other parameters defines the dominated formation of zinc or oxygen vacancies, respectively.

(b) *Vapor phase methods*. Vapor phase methods are very useful to prepare various nanoscale-based structures and compositions given that they have several important advantages such as high accuracy in achieving the desirable geometry, great comfortability over utilized substrate, control of thickness, great adaptability, etc. Contrary to the above-mentioned chemical synthesis, this approach can be applied to form both intrinsic and extrinsic defects not only with various natures and concentrations but also precise localization in terms of their controlled accumulation whether in surface or bulk layers. It is proceeded usually via adjusting the parameters of utilized precursors, type of substrate, and tuning of other related parameters or through introduction of additional compounds into reaction chamber and consequent management over their interaction with atoms of target materials, respectively. Furthermore, the conditions which accompany the realization of vapor phase-supported fabrication such as presence of plasma source or temperature and pressure during deposition as well as expected characteristics of obtained product in terms of its dimension, roughness, or crystalline compositions also play a crucial role in determining the availability and distribution of generated defects. For example, atomic layer deposition (ALD) is highly applicable to create anion vacancies as it uses oxygen-poor environment inside the reaction chamber. Thus, it was demonstrated that playing with the number of cycles, i.e., the thicker or thinner is the produced film, the stoichiometry of wide band gap semiconductors such as ZnO

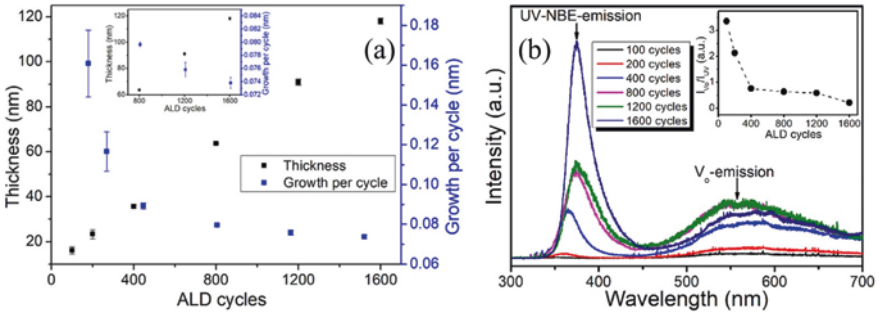

Fig. 11.1 (**a**) ZnO film thickness and growth per cycle as a function of the atomic layer deposition (ALD) cycles. Due to small range of standard deviations in growth rates for ZnO-800, ZnO-1200, and ZnO-1600 samples, the inset was used to visualize them. (**b**) Photoluminescence spectra of ZnO thin films fabricated via different atomic layer deposition (ALD) cycles. The inset shows corresponding ratios between the intensities of emissions assigned to oxygen vacancies (I_{VO}) and ultraviolet near band edge (I_{UV}). (Adapted from Ref. [7] with permission from *Elsevier*. Copyright 2020)

could be adjusted [7] (Fig. 11.1). In turn, ALD also can be used to proceed doping with both metal and non-metal elements. As an illustration, introduction of Al-based precursor during fabrication of ZnO can lead to formation of $Al_xZnO_{1-x}O$ composition [8].

(c) *Mechanical methods*. High-energy ball milling (BM) is determined to be an effective, simple, and highly accessible technique that can be applied to successfully realize the fabrication of nanoparticle-based powders with desired stoichiometries or filled with atoms of defined element. During this process, the friction and collision generated by interaction with balls usually lead to appearance of relatively high temperatures over 1000 °C within localized area of only 1 μm^2 for the duration of ~10^{-3} to 10^{-4} s [9]. Implementation of these conditions disturbs the periodic arrangement of atoms in crystal lattice and often leads to their release and consequent appearance of vacancies. In turn, when two materials are introduced, BM processing causes the development of interdiffusion between them thus leading to formation of combined composition. It happened, for instance, in study of Reddy et al. [10], where ZnO nanoparticles doped with Fe atoms were realized by mixing this material with Fe_3O_4 and consequent milling up to 40 h. It is important to notice that this method is only applied to elements and compound that are available in solid form which means that gaseous N, O, Ar, F, B, S, and C cannot be used. Finally, adjusting the parameters of this processing, such as weight concentration of utilized precursors, duration, temperature of surrounding, and the level of both intrinsic and extrinsic deficiencies, can be controlled.

11.2.2 Post-synthesis Treatment

(a) *Thermal treatment in specific atmosphere*. This method can produce both intrinsic and extrinsic defects in already synthesized materials and compounds regardless their geometry or morphological features. It is usually realized via placing them into furnace or other related setup and consequent heating up under the required gaseous ambient. To determine the level of introduced changes, its flow rate and level of purity as well as the conditions of surrounding environment including the temperature and pressure and also the time of treatment could be adjusted. Considering intrinsic defects, it is possible to induce the formation of anion or cation vacancies without much restriction and also reach precise control over their concentration and distribution. In turn, the introduction of extrinsic deficiency cannot be proceeded so easily due to certain limitations. *Firstly*, this method is mostly utilized to obtain non-metal doping given that flowing gas ambient serves as the only source of foreign atoms that could be introduced into target material. In this regard, one might confuse how to determine at which conditions, for example, nitrogen can induce the appearance of oxygen vacancies in TiO_2 or ZnO or resign within them as a part of modified crystal lattice. In fact, there is no concrete answer for this question as this differentiation depends on various factors and parameters of experimental process and specification of utilized materials that is proceeded for this treatment and thus is highly individual for each investigated system. It is only said that formation of vacancies often is processed at conditions which are less harsh than that used to achieve doping. *Secondly*, if the filling of target material with metal atoms is proceeded in advance, the application of thermal treatment can be considered as activation step to initiate their internal diffusion in order to fill more favorable position in crystal lattice and minimize overall internal energy. It is necessary to notice that metal doping still can be proceeded via this experimental setup, but in this case, additional compound, usually in solid form, should be placed into reaction chamber as to serve the source of it. In this case, flowing atmosphere take the role of transportation tool that enable the transfer of those compound toward target materials. Then, the interaction between them become activated by the type of surrounding environment and its temperature.

(b) *Plasma treatment*. Similar to the above-mentioned thermal treatment, the exposure of target material to certain plasma source enables to induce the formation of intrinsic defect in the form of anion and cation vacancies as well as to develop the realization of doping which is usually proceeded in the form of introduced non-metal atoms. Adjusting the parameters of this processing can be used to tune their various characteristics including concentration, level of distribution, and even the type with very precise accuracy and clarity. For example, application of hydrogen plasma enables to create dominant presence of oxygen [11] or zinc vacancies [12] in ZnO depending on the utilized conditions. Given their donor and acceptor-like characteristics, it might lead to the strengthening of natural n-type conductivity or initiating n → p transition, respectively. One

should notice that the main advantage of utilizing plasma treatment that determines its explicit application is that it is considered to be a surface-modified approach. Definitely, changes in structure and composition can be introduced deeper into bulk due to longer time of exposure or increasing the power of plasma source, but in this case, the appearance of etching effect which can reduce the dimension of materials and also decrease the influence of introduced defects can become a very undesirable reality. Another important particularity of this processing is that it mostly leads to non-metal doping.

11.3 Comparison in Terms of Effect and Influence on Materials Properties

It is very obvious that the presence of both intrinsic and extrinsic defects can induce not only positive but also negative influence on various features of material, thus enabling them to become improved or degraded, respectively, as it is depending on the conditions of their introduction, characteristics of consequent existence, and possible involvements in the interaction with each other. Thus, it is necessary to compare them with regard to this outcome in order to determine which strategy has higher applicability and better potentials in terms of its future employment. For the purpose of making this discussion become more ordered and to follow certain sequence for easy access, only structural, optical, electronic, and electrical properties are considered given their significant influence on the consequent applicability of material in photocatalytic processing.

11.3.1 Structural Properties

The presence of defects, whether in the form of vacancies or doped element enable to increase or decrease the lattice parameters as well as to modify surface morphology and critically affect the size of crystallites along with extension or reduction of specific area. Yet, once these impacts are compared, it become obvious that introduction of vacancies leads to more obvious changes in geometrical configuration and structural adjustment given that releasing of atoms and leaving behind an unoccupied site is supposed to result in highly crucial breakage of thermodynamic equilibrium as its near-neighbors should adjust their positions within wide range of inward or outward movement in order to reduce the impact of this lost. For example, the presence of oxygen and zinc vacancies in ZnO leads to appearance of relaxation that can reach up to 23% and 14%, respectively [13], respectively. In turn, once the dopant is incorporated into material and fills substitutional positioning, its presence would partially reduce changes in internal energy and increase the level of its

minimization as adaptation of surrounding crystal lattice only proceeds to compensate differences in sizes between it and evacuated atom. As an illustration, Duan et al. [14] discovered that introduction of N into ZnO and its residing at O site resulted in relaxation of near Zn atoms for only 2.3–2.8%. Furthermore, the appearance of these values has high dependency on the availability of dopants as its concentration should reach certain critical ratio in order to make any detectable impacts on parameters of crystal lattice. As for interstitial defect, the size of atoms that reside there is very small, and thus their correlation with modification and evolution of surface morphology is less pronounced and evident.

11.3.2 Optical Properties

The presence of intrinsic and extrinsic defects often results in greatly improved optical response of target materials. It is usually proceeded via narrowing the width of band gap due to appearance of additional energy levels which can induce shift of valence or conduction bands. Following it, increased sensitivity toward irradiation with visible and even near-infrared lights is achieved. Accordingly, the color of surface often becomes darker. Yet, as both strategies have their own particularities and specifications, it influences greatly on the origin of introduced adjustments in geometrical and electronic configurations. Thus, it is obvious that changes in optical response might have different origin and, consequently, non-similar enhancement. In this regard, comparative analysis is required in order to achieve certain understanding which type of defect has more chances to provide desirable outcome in terms of expected advancement. To increase accessibility of this discussion and to make it more relevant, wide band gap oxide semiconductors such as ZnO, TiO_2, and Ta_2O_5 are taken as a model system. Overall, several important particularities can be identified. *Firstly*, it might be said that existence of anion vacancies usually results in the highest enhancement of optical response that is associated with very crucial shift of absorption edge and increased capability to acquire more photons. As an illustration, the development of oxygen deficiency in TiO_2 makes it sensitive to the light with wavelength up to ~1000 nm [2]. For its part, doping with certain nonmetal elements such as nitrogen or carbon often causes relatively similar outcome; yet to achieve it, implementation of very accurately tuned concentration and distribution should be adapted. *Secondly*, introduction of metal compounds often leads to less obvious changes in the width of band gap and absorption characteristics and thus might be considered with certain reservations as less effective strategy for improving the optical response. For instance, Feng et al. [15] demonstrated that TiO_2 combined with Ag, Cu, Ce, and Fe enables to show only small improvement in absorption region between 400 and 580 nm which means that significant part of visible light still could not be utilized.

11.3.3 Electronic Properties

Both intrinsic and extrinsic defects can create additional energy levels within the band gap that can exist as separate discrete states or contribute to the elevating or lowering the maximum and minimum of valence and conduction bands, respectively, thus greatly assist in progressing transportation characteristics of charge carriers, and also support the enhancement of their concentrations and mobility. The main difference between these two strategies is that the latter one can demonstrate higher flexibility in generation of these levels as it can be used to realize precise adjustment of their localization toward reaching the required features simply via choosing correct element to be doped or controlling geometrical configuration of its atoms in crystal lattice of host material. Thus, it is possible to achieve the desirable level of contribution toward strengthening donor or acceptor-like behavior via compensating mechanism or directly by supplying corresponding charge carriers. Definitely, solubility and other related parameters should be considered in this case as to achieve the best outcome. For instance, introduction of non-metal elements such as nitrogen or carbon in wide band gap materials, particularly, ZnO or TiO_2, can be proceeded through their residing on substitutional or interstitial sites as it can be controlled by experimental conditions. This positioning influences critically how far corresponding energy levels are generated from valence band and also which type of defect complex contributes to its appearance. In turn, the presence of anion and cation vacancies usually is associated with their availability within only several defined charge states, some of which are regarded as unstable and thus cannot exist for a long time. It leads to certain restrictions in modifying the electronic configurations of target materials as it only can be proceeding within very limited and expected range of changes. In turn, such a predictability greatly assists in accessing them via theoretical simulations and thus implementing very precise tuning.

11.3.4 Electrical Properties

It is out of question that introduction of intrinsic and extrinsic deficiencies under proper conditions can be used to greatly improve electrical properties of target material via strengthening of its original conductivity. It is usually caused by supplying more charge carriers or rising their mobility. Comparing both strategies, it might become obvious that the latter one provides higher flexibility in reaching the desirable range of enhancements as various compounds and elements or their combinations along with different concentrations and distribution can be used to proceed the required changes. Furthermore, it is also possible to play with parameters of their introduction along with adjusting the diffusion and consequent localizations within crystal lattice. Combining together, it allows to reach clear understanding

toward suitability of each dopant for achieving the designated goal with regard to particularities and specification of target material. For example, Sahasrabudhe et al. [16] investigated filling of TiO_2 with Nb and discovered that once its mole ratio becomes 3%, the conductivity was enhanced for ~1,000,000 times, i.e., from 10^{-7} to 40 ohm^{-1} cm^{-1}. It is interesting that higher concentration of Nb resulted in reduced capability of electrons to reach the conduction band. Thus, it is evident that there is always an optimal ratio of dopants which deviation below or above it would only lead to declining the positive effect of its presence. In turn, utilization of intrinsic defects as a source of improved electrical properties results in lower range of achieved changes due to certain limitation in adjusting their features and parameters. Simply to say, anion and cation vacancies often have strictly defined donor- and acceptor-like characteristics, respectively, and thus only individual existence of each of them can be considered as favorable for concrete material following its type of conductivity. Similar to doping, in order to demonstrate the best outcome, its concentration should achieve very defined saturation point, and its overpassing would result in critical self-annihilation of charge carriers due to their excess. Thus, comparing both of these strategies, it should be mentioned that by convenience, availability, and practicability and also considering the correlation with other properties, intrinsic deficiency is more preferential choice for improving the electrical characteristics. Yet, in absolute and relative values, the best enhancement still can be achieved via properly developed correctly implemented doping process.

11.4 Comparison in Terms of Photocatalytic Efficiency

In recent years, the employment of intrinsic and extrinsic defects that are usually proceeded via introduction of specific type of vacancies or realization of doping with certain elements and compounds, respectively, has attracted numerous attentions as an effective tool to strengthening and extending important properties and features of target material as both of them lead to changes in its chemical composition and structure. Thus, increased absorption of visible and infrared lights, narrowed width of band gap, reduced recombination rate of electron-holes pairs, more advanced transportation characteristics of charge carriers, higher surface area, etc. could be achieved. It correlates well with great enhancement in efficiency and stability of various photocatalytic and photoelectrochemical reactions resulting in their successful and prolong realization. However, while comparing these strategies, it might become evident that their usage cannot lead to equal outcome in terms of demonstrated performance, and thus certain specification should be clarified as to achieve some understanding how the extension of each concrete processing can be affected by their application.

11.4.1 Photocatalytic and Photoelectrochemical Water Splitting

To realize the best possible efficiency of hydrogen production via photocatalytic reaction, it is considered that employment of doping strategy can provide more attractive consequence compared with that of utilizing intrinsic defects as it enables to play with nature of introduced elements or their concentrations and distribution in target materials thus allowing to reach the most optimal adjustment of its geometrical and electronic structures. As a result, great extension of properties and characteristics can be reached. For example, currently, one of the highest achieved hydrogen production rates was demonstrated by $Cd_{0.25}Zn_{0.75}Se$ hollow nanotubes [17] (Fig. 11.2a). Under simulated sunlight irradiation and using 5.0% CoP as cocatalyst, its value reached 36,600 μmol h^{-1} g^{-1} in artificial seawater filled with properly adjusted concentrations of Na_2S and Na_2SO_3 that served as sacrificial agents (Fig. 11.2b). In turn, changing the reactive solution into aqueous media resulted in further enhancement of production rate up to 45,000 μmol h^{-1} g^{-1} (Fig. 11.2c). Several more remarkable results were also achieved with assistance of

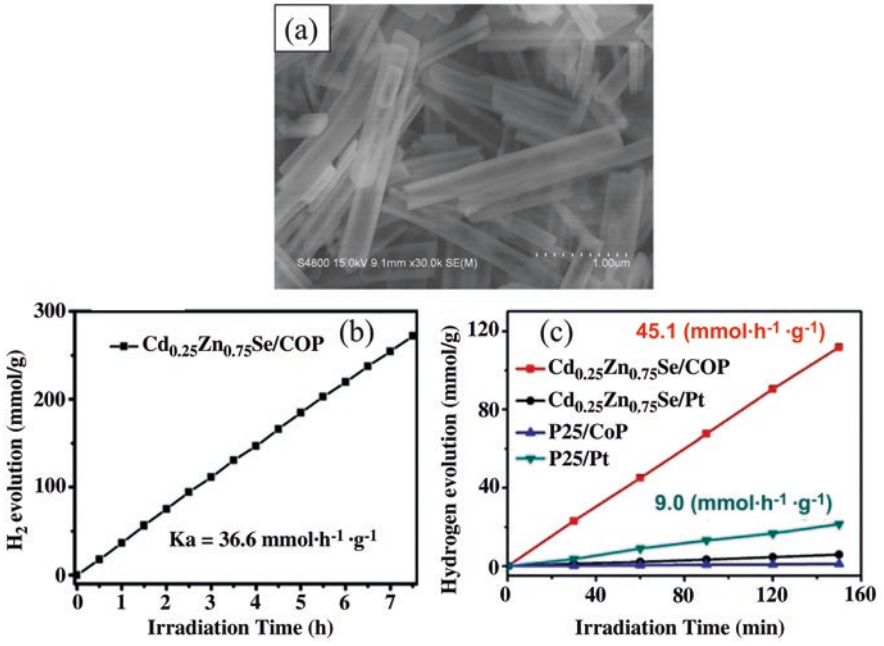

Fig. 11.2 (**a**) SEM image of $Cd_{0.25}Zn_{0.75}Se$ hollow tubes. (**b**) Photocatalytic H_2 evolution over $Cd_{0.25}Zn_{0.75}Se$/CoP under simulated solar light irradiation in artificial sea water. Other materials are taken for comparison. P25 represents commercial TiO_2 that consisted of mixed rutile and anatase phases. (**c**) H_2 production comparison by using different co-catalysts under simulated solar light irradiation in aqueous solution. (Adapted from Ref. [17] with permission from *The Royal Chemical Society*. Copyright 2017)

doping [18]. Yet, it has to be noticed that such an impressive outcome often is accompanied by application of complex setup and formation of multilayer structures. In general, introduction of foreign atoms into target materials such as filling of TiO_2 and ZnO with nitrogen or other non-metal elements leads to performance that is relatively similar to that achieved through modifying them via changing original stoichiometry or playing with chemical compositions. Yet, utilization of intrinsic deficiencies can be proceeded with higher accessibility toward more practical realization of this process as there is no necessity to use external compound if only to assist in release of atoms from crystal lattice. Thus, it has more chances to become adapted and implemented for everyday use. Furthermore, recent studies revealed that this processing also enables to create greatly productive compound that can deliver hydrogen at rate which is only slightly lower than that mentioned above [19]. Given that the topic of intrinsic deficiency has been studied very deeply for only last decade, one should consider that it is already a very impressive achievement. In this regard, there is a strong belief that its further development might have a great impact on the future extension of photocatalytic water splitting process.

11.4.2 Light-Induced Water Purification

Light-induced purification of water usually is achieved via removing of dyes by means of their degradation into certain non-hazardous compounds and elements via application of proper photocatalyst. With regard to intrinsic and extrinsic deficiencies, their introduction into target materials generally causes very dramatic increase in efficiency and stability of this processing regardless of the type of utilized dye, wavelength of irradiated light, or other related parameters and conditions. The following particularities define application of both strategies. *Firstly*, as the mechanisms of their enhancement follow relatively similar pathway, it is often very hard to define which one of them has higher preferentiality toward achieving the best outcome. For example, it was proposed that oxygen vacancies in ZnO can favor the adsorption of O_2 [20]. Its interaction with the photo-induced electrons results in the production of superoxide radical anions $O_2^{\bullet}$ that are chemically active species and promote the oxidation of nearby organic substances. In turn, doping of this semiconductor with metals such as Co [21] or Fe [22] can also increase the availability of O_2 and greatly assist in its transformation into $O_2^{\bullet}$. *Secondly*, there is no solid standard to identify how high is the degradation rate in absolute values, and also modified compounds are often tested under absolutely different conditions which makes the comparison between studies hardly achievable. As an illustration, authors of Ref. [20] investigated photocatalytic activity of ZnO via decomposition of H_2O_2 under visible light, while in Ref. [22], it was achieved by degradation of methylene blue under Xe lamp. Thus, it would be more correct to say that particularities of each investigated system and the purpose of its use determine which strategy has higher contribution to the enhancement of overall outcome.

11.4.3 Photoconversion of CO_2

Both intrinsic and extrinsic defects can bring very positive influence on the photoconversion efficiency of CO_2 not only extending the yield rate of secondary carbon products but also providing higher selectivity toward obtaining them. As the applicability of both strategies to successfully realize this processing has certain differences, it is necessary to define in which case each of them has clear preferentiality to be used. Thus, the following particularities are defined. For simplicity, only oxide semiconductor materials are taken for examination. *Firstly*, it is a well-recognized fact that the presence of oxygen vacancies or doped elements within the surface layer increases the adsorption characteristics of target materials resulting in improved binding energy of arrived CO_2 molecules and also leading to lowering the barriers for the subsequent reduction reactions. Considering functionality, convenience to use, and also the expected outcome, it might be said that utilizing the former type of defect seems a more attractive option given that their uniform distribution can be achieved much easier in comparison to introduced foreign atoms especially the ones which represents metal compounds. In addition, less efforts are required to avoid their accumulation in bulk, and it allows to eliminate several very harmful effects associated with this localization. *Secondly*, as the material doped with suitable element within very specific concentration enables to reach the most optimal level of enhancement with regard to selected properties and features, it often results in higher efficiency of CO_2 photoconversion taken in absolute values in contrast to that achieved via formation of oxygen vacancies [23]. It is a very expected outcome given that this strategy provides higher flexibility in tuning and adjusting the features of material. *Thirdly*, it is well known that selectivity of this processing is dependent on the density of available electrons. In this regard, it is suggested that the presence of intrinsic deficiencies enables to assist in acquiring more impressive results to produce only defined carbon by-product compared with that of doping. It is justified by the fact that in average, excluding the most advance and outstanding results, the former strategy can often lead to higher presence of defined charge carriers or their higher accessibility. It is especially a very attractive perspective given the simplicity and relative easiness associated with achieving required changes in chemical composition or stoichiometry. For instance, Yang et al. [24] reported that Bi_2MoO_6 filled with oxygen vacancies enables to deliver CH_4 with selectivity up to 96.7% using irradiation with visible light which was much higher than that of its stoichiometric counterpart (Fig. 11.3a). Recycling test demonstrated that this material also exhibited good stability (Fig. 11.3b). In turn, filling with foreign atoms also can lead to appearance of certain selectivity, which, however, often is limited by detecting two or more carbon by-products. Particularly, Liu et al. [25] showed that utilization of Ni-doped $ZnCo_2O_4$ to photoreduce CO_2 resulted in simultaneous generation of CO and CH_4. Yet, it is a very subjective and preliminary conclusion, and more efforts are required to clarify and confirm it. Finally, it should be noticed that higher performance toward CO_2 photoreduction might be realized by concurrent existence of both, intrinsic and extrinsic, deficiencies as their successful synergy

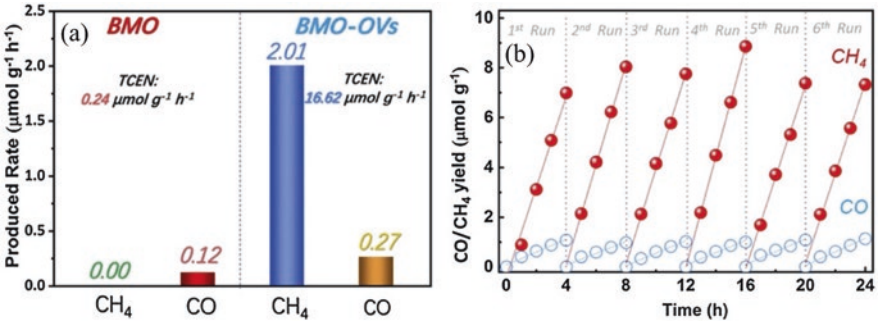

Fig. 11.3 (**a**) Production rate for CO_2 photoreduction over Bi_2MoO_6 without and with oxygen vacancies designated as BMoO and BMoO-OVs, respectively. (**b**) Typical time course of the amount of CO/CH_4 generated over BMoO-OVs under visible-light irradiation. (Adapted from Ref. [24] with permission from *Elsevier*. Copyright 2019)

under proper conditions can be used to enhance the most crucial advantages associated with each of them with regard to increased production rate and selectivity [26]. It is especially an attractive strategy given that introduction of foreign atoms into certain semiconductors often enables to cause the accompanied formation of intrinsic defects such as, for example, Ti^{3+} or oxygen vacancies in TiO_2. Thus, it is possible to feed two birds with one scone, i.e., create desirable compound within only single experimental step.

References

1. S.A. Ansari, M.M. Khan, M.O. Ansari, M.H. Cho, Nitrogen-doped titanium dioxide (N-doped TiO_2) for visible light photocatalysis. New J. Chem. **40**, 3000–3009 (2016). https://doi.org/10.1039/C5NJ03478G
2. J. Chen, Y. Fu, F. Sun, Z. Hu, X. Wang, T. Zhang, F. Zhang, X. Wu, H. Chen, G. Cheng, R. Zheng, Oxygen vacancies and phase tuning of self-supported black TiO_{2-X} nanotube arrays for enhanced sodium storage. Chem. Eng. J. **400**, 125784 (2020). https://doi.org/10.1016/j.cej.2020.125784
3. D. Li, H. Haneda, S. Hishita, N. Ohashi, N.K. Labhsetwar, Fluorine-doped TiO_2 powders prepared by spray pyrolysis and their improved photocatalytic activity for decomposition of gas-phase acetaldehyde. J. Fluor. Chem. **126**, 69–77 (2005). https://doi.org/10.1016/j.jfluchem.2004.10.044
4. A. Juma, I. Oja Acik, A.T. Oluwabi, A. Mere, V. Mikli, M. Danilson, M. Krunks, Zirconium doped TiO_2 thin films deposited by chemical spray pyrolysis. Appl. Surf. Sci. **387**, 539–545 (2016). https://doi.org/10.1016/j.apsusc.2016.06.093
5. T. Ghoshal, S. Biswas, M. Paul, S.K. De, Synthesis of ZnO nanoparticles by solvothermal method and their ammonia sensing properties. J. Nanosci. Nanotechnol. **9**, 5973–5980 (2009). https://doi.org/10.1166/jnn.2009.1290
6. L. Pan, S. Wang, W. Mi, J. Song, J.-J. Zou, L. Wang, X. Zhang, Undoped ZnO abundant with metal vacancies. Nano Energy **9**, 71–79 (2014). https://doi.org/10.1016/j.nanoen.2014.06.029

7. Y. Wang, K.-M. Kang, M. Kim, H.-H. Park, Film thickness effect in c-axis oxygen vacancy-passivated ZnO prepared via atomic layer deposition by using H_2O_2. Appl. Surf. Sci. **529**, 147095 (2020). https://doi.org/10.1016/j.apsusc.2020.147095
8. A. Illiberi, R. Scherpenborg, Y. Wu, F. Roozeboom, P. Poodt, Spatial atmospheric atomic layer deposition of $Al_xZn_{1-x}O$. ACS Appl. Mater. Interfaces **5**, 13124–13128 (2013). https://doi.org/10.1021/am404137e
9. K. Ralphs, C. Hardacre, S.L. James, Application of heterogeneous catalysts prepared by mechanochemical synthesis. Chem. Soc. Rev. **42**, 7701–7718 (2013). https://doi.org/10.1039/C3CS60066A
10. I.N. Reddy, C.V. Reddy, M. Sreedhar, J. Shim, M. Cho, D. Kim, Effect of ball milling on optical properties and visible photocatalytic activity of Fe doped ZnO nanoparticles. Mater. Sci. Eng. B-Solid State Mater. Adv. Technol. **240**, 33–40 (2019). https://doi.org/10.1016/j.mseb.2019.01.002
11. T. Gu, E.-T. Hu, S. Guo, Y. Wu, J. Wang, Z.-Y. Wang, K.-H. Yu, W. Wei, Y.-X. Zheng, S.-Y. Wang, L.-Y. Chen, Ellipsometric study on optical properties of hydrogen plasma-treated aluminum-doped ZnO thin film. Vacuum **163**, 69–74 (2019). https://doi.org/10.1016/j.vacuum.2019.02.006
12. V. Gurylev, A. Useinov, P.Y. Hsieh, C.Y. Su, T.P. Perng, Hydrogenated ZnO thin film with p-type surface conductivity from plasma treatment. J. Phys. D. Appl. Phys. **50**, 24LT02 (2017). https://doi.org/10.1088/1361-6463/aa6e91
13. A. Janotti, C.G. Van de Walle, Native point defects in ZnO. Phys. Rev. B **76**, 165202 (2007). https://doi.org/10.1103/PhysRevB.76.165202
14. X.M. Duan, C. Stampfl, M.M.M. Bilek, D.R. McKenzie, Codoping of aluminum and gallium with nitrogen in ZnO: A comparative first-principles investigation. Phys. Rev. B **79**, 235208 (2009). https://doi.org/10.1103/PhysRevB.79.235208
15. H. Feng, M.-H. Zhang, L.E. Yu, Hydrothermal synthesis and photocatalytic performance of metal-ions doped TiO_2. Appl. Catal. A Gen. **413–414**, 238–244 (2012). https://doi.org/10.1016/j.apcata.2011.11.014
16. G. Sahasrabudhe, J. Krizan, S.L. Bergman, R.J. Cava, J. Schwartz, Million-fold increase of the conductivity in TiO_2 rutile through 3% niobium incorporation. Chem. Mater. **28**, 3630–3633 (2016). https://doi.org/10.1021/acs.chemmater.6b02031
17. B. Qiu, Q. Zhu, M. Xing, J. Zhang, A robust and efficient catalyst of $Cd_xZn_{1-x}Se$ motivated by CoP for photocatalytic hydrogen evolution under sunlight irradiation. Chem. Commun. **53**, 897–900 (2017). https://doi.org/10.1039/C6CC08311K
18. J. Zhang, W. Hu, S. Cao, L. Piao, Recent progress for hydrogen production by photocatalytic natural or simulated seawater splitting. Nano Res. **13**, 2313–2322 (2020). https://doi.org/10.1007/s12274-020-2880-z
19. X. Chen, L. Liu, P.Y. Yu, S.S. Mao, Increasing solar absorption for photocatalysis with black hydrogenated titanium dioxide nanocrystals. Science **331**, 746–750 (2011). https://doi.org/10.1126/science.1200448
20. M. Montero-Muñoz, J.E. Ramos-Ibarra, J.E. Rodríguez-Páez, M.D. Teodoro, G.E. Marques, A.R. Sanabria, P.C. Cajas, C.A. Páez, B. Heinrichs, J.A.H. Coaquira, Role of defects on the enhancement of the photocatalytic response of ZnO nanostructures. Appl. Surf. Sci. **448**, 646–654 (2018). https://doi.org/10.1016/j.apsusc.2018.04.105
21. M. Adeel, M. Saeed, I. Khan, M. Muneer, N. Akram, Synthesis and characterization of Co–ZnO and evaluation of its photocatalytic activity for photodegradation of methyl orange. ACS Omega **6**, 1426–1435 (2021). https://doi.org/10.1021/acsomega.0c05092
22. D. Neena, K.K. Kondamareddy, H. Bin, D. Lu, P. Kumar, R.K. Dwivedi, V.O. Pelenovich, X.-Z. Zhao, W. Gao, D. Fu, Enhanced visible light photodegradation activity of RhB/MB from aqueous solution using nanosized novel Fe-Cd co-modified ZnO. Sci. Rep. **8**, 10691 (2018). https://doi.org/10.1038/s41598-018-29025-1
23. H. Zhao, F. Pan, Y. Li, A review on the effects of TiO_2 surface point defects on CO_2 photoreduction with H_2O. J. Mater. **3**, 17–32 (2017). https://doi.org/10.1016/j.jmat.2016.12.001

24. X. Yang, S. Wang, N. Yang, W. Zhou, P. Wang, K. Jiang, S. Li, H. Song, X. Ding, H. Chen, J. Ye, Oxygen vacancies induced special CO_2 adsorption modes on Bi_2MoO_6 for highly selective conversion to CH_4. Appl. Catal. B Environ. **259**, 118088 (2019). https://doi.org/10.1016/j.apcatb.2019.118088
25. K. Liu, X. Li, L. Liang, J. Wu, X. Jiao, J. Xu, Y. Sun, Y. Xie, Ni-doped $ZnCo_2O_4$ atomic layers to boost the selectivity in solar-driven reduction of CO_2. Nano Res. **11**, 2897–2908 (2018). https://doi.org/10.1007/s12274-017-1943-2
26. D. Zhao, C. L. Dong, B. Wang, C. Chen, Y. C. Huang, Z. Diao,S. Li, L. Guo, S. Shen, Synergy of dopants and defects in graphitic carbon nitride with exceptionally modulated band structures for efficient photocatalytic oxygen evolution, Adv. Mater. **31**, e1903545 (2019). https://doi.org/10.1002/adma.201903545

Index

V. Gurylev, *Nanostructured Photocatalyst via Defect Engineering*,
https://doi.org/10.1007/978-3-030-81911-8